UNIVERSITY OF CALIFORNIA

Santa Barbara

Synthesis of f-Element Multiple Bonds: Providing Insight into Covalency

A dissertation submitted in partial satisfaction of the

requirements for the degree Doctor of Philosophy

in Chemistry

by

Selena L. Staun

Committee in charge:

Professor Trevor W. Hayton Chair

Professor Gabriel Ménard

Professor Peter C. Ford

Professor Steven Buratto

June 2021

The dissertation of Selena L. Staun is approved.

_____

Professor Gabriel Ménard

_____

Professor Peter C. Ford

_____

Professor Steven Buratto

_____

Professor Trevor W. Hayton, Committee Chair

May 2021

Synthesis of f-Element Multiple Bonds: Providing Insight into Covalency

Acknowledgements

I would like to start by thanking my very first mentor, Dr. Allen Oliver from the University of Notre Dame, whom I met my junior year of high school. I was required to find a chemist in my community who would work on a science project with me for my Independent Research class and he happily agreed. At the time I did not find it odd that Dr. Oliver and I borrowed lab space and chemicals from the floor above us, or that my project specialized in X-ray crystallography, but of course this all makes sense to me now that I fully understand what a crystallographer does. I am beyond grateful for him taking on a high school student and working with me for two years. His support has been never ending.

I would like to thank my undergraduate research advisor, Prof. Suzanne Bart, who welcomed me into her lab my sophomore year at Purdue University and introduced me to her mission of f-block domination. I spent two years working in her lab with uranium and found that I enjoyed being there more than anywhere else on campus. I will be forever grateful, ever true, to my first female role model in science, who continues to support me along my endeavors well past my undergraduate graduation. Furthermore, I would like to thank my graduate mentor in the Bart group, John "JKat" Kiernicki, who continues to congratulate me on my success to this day.

I would not be here at UCSB if it was not for Dr. Oliver suggesting it when I mentioned I wanted to go to Califormia for graduate school (I had no idea UCSB existed beforehand), guidance from Dr. Suzanne Bart, and of course my PI, Prof. Trevor Hayton, who welcomed me into his lab. I would like to thank him for the chance to continue working on f-block chemistry and guiding me every step of the way. I am grateful for his support, guidance, and especially patience, throughout my studies. I am beyond grateful for the opportunities that I

gained while in the Hayton lab, which allowed me to leave the lab nest and work at Los Alamos National Laboratory for almost a full year. Thank you for letting me fly! Overall, it has been an enjoyable experience. I'm also thankful for my thesis committee, Prof. Gabriel Ménard, Prof. Peter Ford and Prof. Steven Buratto, who helped me reach the end successfully.

To the labmates who preceded me, I have to thank Dr. Mikiyas Assefa for training me how to use a glovebox and how to fix what became broken. I am extremely grateful for Dr. Danil Smiles, who answered my many short emails in great length and description. I would like to thank the one person who joined the rad-lab after me, Greggory Kent. I have thoroughly enjoyed our time together and being dramatic when necessary. I am amazed at how much candy he consumed each week and I hope someday he won't be so tired.

I'd also like thank my mentors during my time at Los Alamos National Laboratory, Dr. Andrew Gaunt and Dr. Aaron Tondreau. Andy trusted me working alone in the transuranic glovebox sooner than I would have thought, but always reminded me to never put a hole in the glove. I enjoyed Andy's outlook on life and hearing many stories about Trevor. A big thank you to Aaron for taking me in under his wing last minute. I'd also like to thank Dr. Lauren Stevens, Dr. Conrad Goodwin, and Dr. Brennan Billow, who were post-docs at the lab while I was there. Their company made my time at the national lab very memorable.

Lastly, and definently most importantly, I want to thank my family, who cheered me on every step of this journey from the Midwest. The daily FaceTime talks and yearly visits kept me going. Dear mom, you are always telling me to write a book…here it is! Thank you especially to Everett Berry, who started this journey as my boyfriend, became my fiancé, and will soon be my husband! This shall be my last great work as a Staun. I love you all!

Vita of Selena L. Staun

May 2021

Education:

Doctor of Philosophy in Chemistry

University of California Santa Barbara (May 2021 expected)

Advisor: Professor Trevor W. Hayton

Dissertation: "Synthesis of f-Element Multiple Bonds: Providing Insight into Covalency"

Bachelor of Science (Honors), Chemistry

Purdue University (May 2016)

Advisor: Professor Suzanne C. Bart

Professional Employment:

- Graduate Student Researcher - UC Santa Barbara, Dept. of Chemistry (07/16 - Present)
- Graduate Student Researcher - Los Alamos National Laboratory (06/18 - 08/18, 07/19 - 03/20)
- Teaching Assistant - Dept. of Chemistry, UCSB (09/16 - 06/20)
- Undergraduate Reseacher – Dept. of Chemistry, Purdue University (01/14 - 05/16)

Publications:

- **Staun, S. L.**, Smiles, D. E., Stevens, L. M., Goodwin, C. A.P., Billow, B. S., Scott, B. L., Wu, G., Tondreau, A. M., Gaunt, A. J., Hayton, T. W. Extending the Nonaqueous Chemistry of Neptunium: Synthesis and Structural Characterization of $[Np(NR_2)_3Cl]$, $[Np(NR_2)_3Cl]^-$, and $[Np\{N(R)(SiMe_2CH_2)\}_2(NR_2)]^-$ ($R = SiMe_3$), *Inorganic Chemistry*, **2021**, *60* (4), 2740-2748.
- Sergentu, DC., Kent, G. T., **Staun, S. L.**, Yu, X., Cho, H. Autschbach, J., Hayton, T. W. Probing the Electronic Structure of a Thorium Nitride Complex by Solid-State ^{15}N NMR Spectroscopy, *Inorganic Chemistry*, **2020**, *59*, 10138-10145.

- **Staun, S. L.**, Kent, G. T., Wu, G., Hayton, T. W. Reactivity of $[Ce(NR_2)_3]$ ($R = SiMe_3$) with Prospective Carbon-Atom Transfer Reagents. *Organometallics*, **2020**, *39*, 2375-2382.
- **Staun, S. L.**, Sergentu, D-C., Wu, G., Autschbach, J., Hayton, T. W. Use of ^{15}N NMR spectroscopy to probe covalency in a thorium nitride. *Chemical Science*, **2019**, *10*, 6431-6436.
- Kiernicki, J. J., **Staun, S. L.**, Zeller, M., Bart, S. C. A Uranium(IV) Triamide Species with Brønsted Basic Ligand Character: Metal-Ligand Cooperativity in the f Block. *Organometallics*, **2017**, *36(3)*, 665-672.
- **Staun, S. L.** Synthesis and Characterization of a Series of Uranium(IV) Species: Investigating Coordination With a Redox Innocent Triamine Ligand. *Journal of Purdue Undergraduate Research*, **2016**, *6*, 56-63.
- **Staun, S. L**., Oliver, A. G. Crystal structure of benzene-1,3,5-tricarboxylic acid-4-pyridone (1/3). *Acta Crystallographica*, **2015**, *E71*, 1283-1286.
- **Staun, S. L**., Oliver, A. G. Crystal structure of 4-hydroxypyridin-1-ium 3,5-dicarboxybenzoate. *Acta Crystallographica*, **2015**, *E71*, 861-863.
- **Staun, S. L**., Oliver, A. G. 4-Pyridone-terephthalic acid-water (2/1/2) and bis(3-hyrdoxypyridinium) terephthalate. *Acta Crystallographica*, **2012**, *C68*, 84-87.

Awards:

- First place in the 2020 Innovations in Nuclear Technology R&D Awards, U.S. DOE 2020
- Graduate Division Dissertation Fellowship, UC Santa Barbara 2020
- Science Graduate Student Research (SCGSR) 2018 S2 Program at Los Alamos National Laboratory, U.S. DOE 2019 – 2020
- Outstanding Poster Presentation Chemistry, Los Alamos National Laboratory 2018, 2019
- G. T. Seaborg Institute Summer Research Fellowship, Los Alamos National Laboratory 2018, 2019
- Outstanding Service Award, UC Santa Barbara 2016 – 2017 & 2017 – 2018

- Chair's Fellowship for Excellence, UC Santa Barbara 2016 - 2017
- Honorable Mention, NSF Graduate Research Fellowship Program (GRFP) 2016

Major Field: Synthetic Inorganic Chemistry

Studies in Organometallic Lanthanide and Actinide Chemistry

Abstract

Synthesis of f-Element Multiple Bonds: Providing Insight into Covalency

by

Selena L. Staun

Herein, I report the synthesis, characterization, and reactivity of the *N*-(isocyanoimine)triphenylphosphine ($CNNPPh_3$) adduct of $[Ce(NR_2)_3]$ ($R = SiMe_3$): namely, $[(NR_2)_3Ce(CNNPPh_3)]$. Photolysis of $[(NR_2)_3Ce(CNNPPh_3)]$ with a 380 nm LED source for 1 month results in clean formation of $[(NR_2)_3Ce(NCNPPh_3)]$, *via* reorganization of the nitrilimine ligand to its carbodiimide isomer.

Reaction of $U(N(SiMe_2)_3)$ ($R = SiMe_3$) with 2 equiv *tert*-butyl isocyanide proceeded to oxidize the uranium center and reduce the ligand to synthesize, $[U(NR_2)_3(CN)(CN^tBu)]$, in pentane, suggesting that the C-N triple bond in the *tert*-butyl isocyanide ligand was not strong enough to withstand the reaction conditions. Utilizing the sp2 bond in 2,6-Dimethylphenyl isocyanide (CNXyl, Xyl = $2,6\text{-}Me_2C_6H_3$), reaction of $U(NR_2)_3$ with 2 equiv 2,6-Dimethylphenyl isocyanide resulted in the isolation of $[U(NR_2)_3(CNXyl)_2]$, as well as $[U\{N(R)SiC(=CH_2)N(Xyl)\}(NR_2)_2]$, formed by $[U\{N(R)(SiMe_2)CH_2\}(NR_2)_2]$, a decomposition product of $U(NR_2)_3$, reacting with 1 equiv of 2,6-Dimethylphenyl isocyanide. Reduction reactivity of $[U(NR_2)_3(CNXyl)_2]$ was also explored and is discussed.

Herein, I report the synthesis and characterization of three novel actinide imido complexes, [K(18-crown-6)][U(NTs)(NR_2)$_3$] ($R = SiMe_3$), [Li(12-crown-4)$_2$][Th($NCPh_3$)(NR_2)$_3$], and [K(18-crown-6)][Th(NTs)(NR_2)$_3$], where the corresponding amide salts, [Li($NHCPh_3$)(THF)] or KNHTs ($Ts = MeC_6H_4SO_2$) were used to protonate the

actinide metallacycle, [An(*C*H_2SiMe_2*N*SiMe_3)(NR_2)$_2$] (An = U, Th), as well as two novel actinide amido borane complexes, [Na(2,2,2-cryptand)][U(NR_2)$_3$NHBPh_3] and [K(dibenzo-18-crown-6)][Th(NR_2)$_3$NHBPh_3], through the reaction of NH_3BPh_3 with the actinide bis(metallacycle), [An{*N*(R)(SiMe_2*C*H_2)}$_2$(NR_2)]$^-$ (An = U, Th). These imido and amido complexes are ideal for synthesizing actinide nitrido species through the method of reductive deprotection, in an effort to cleave the N-C, N-S, and N-B bond.

Reaction of the thorium metallacycle, [Th{*N*(R)(SiMe_2)*C*H_2}(NR_2)$_2$] (R = SiMe_3) with 1 equiv of $NaNH_2$ in THF, in the presence of 18-crown-6, results in formation of the bridged thorium nitride complex, [Na(18-crown-6)(Et_2O)][(R_2N)$_3$Th(μ-N)(Th(NR_2)$_3$], which can be isolated in 66% yield after work-up. [Na(18-crown-6)(Et_2O)][(R_2N)$_3$Th(μ-N)(Th(NR_2)$_3$] is the first isolable molecular thorium nitride complex. Mechanistic studies suggest that the first step of the reaction is deprotonation of [Th{*N*(R)(SiMe_2)*C*H_2}(NR_2)$_2$] by $NaNH_2$, which results in formation of the thorium bis(metallacycle) complex, [Na($THF)_x$][Th{*N*(R)(SiMe_2*C*H_2)}$_2$(NR_2)], and NH_3. NH_3 then reacts with unreacted [Th{*N*(R)(SiMe_2)*C*H_2}(NR_2)$_2$], forming [Th(NR_2)$_3$(NH_2)], which protonates [Na($THF)_x$][Th{*N*(R)(SiMe_2*C*H_2)}$_2$(NR_2)] to give [Na(18-crown-6)(Et_2O)][(R_2N)$_3$Th(μ-N)(Th(NR_2)$_3$]. Consistent with hypothesis, addition of excess NH_3 to a THF solution of [Th{*N*(R)(SiMe_2)*C*H_2}(NR_2)$_2$] results in formation of [Th(NR_2)$_3$(NH_2)], which can be isolated in 51% yield after work-up. Furthermore, reaction of [K(DME)][Th{*N*(R)(SiMe_2*C*H_2)}$_2$(NR_2)] with [Th(NR_2)$_3$(NH_2)], in THF-d_8, results in clean formation of [K(18-crown-6)(THF)2][(R_2N)$_3$Th(μ-N)(Th(NR_2)$_3$], according to ^{1}H NMR spectroscopy. The electronic structures of [(R_2N)$_3$Th(μ-N)(Th(NR_2)$_3$]$^-$ and [Th(NR_2)$_3$(NH_2)] were investigated by ^{15}N NMR spectroscopy and DFT calculations. This analysis reveals that

the Th–$N_{nitride}$ bond in $[(R_2N)_3Th(\mu\text{-}N)(Th(NR_2)_3]^-$ features more covalency and a greater degree of bond multiplicity than the Th–NH_2 bond in $[Th(NR_2)_3(NH_2)]$. Similarly, this analysis indicates a greater degree of covalency in $[(R_2N)_3Th(\mu\text{-}N)(Th(NR_2)_3]^-$ vs. comparable thorium imido and oxo complexes.

Reaction of the thorium bis(metallacycle), [K(DME)][Th{*N*(R)($SiMe_2$*C*H_2)}$_2$(NR_2)] (R = $SiMe_3$) with 1 equiv of the newly synthesized uranium parent amide, $[U(NR_2)_3(NH_2)]$, in THF, in the presence of 18-crown-6, results in formation of a bridged uranium-thorium nitride complex, $[K(18\text{-crown-6})(THF)_2][(NR_2)_3U^{IV}(\mu\text{-}N)Th^{IV}(NR_2)_3]$, which can be isolated in 56% yield after work-up. $[K(18\text{-crown-6})(THF)_2][(NR_2)_3U^{IV}(\mu\text{-}N)Th^{IV}(NR_2)_3]$ is the first isolable molecular mixed actinide nitride complex. Additonally, a $\mu\text{-}CH_2$ bridging mixed actinide nitride complex, $[(K(18\text{-crown-6})_{0.5})(K(18\text{-crown-6})_{0.5}Et_2O)][(NR_2)_2U^{IV}(\mu\text{-}N)(CH_2SiMe_2NR)Th^{IV}(NR_2)_2]$, is also isolated in this reaction in 34% yield. Furthermore, $[K(18\text{-crown-6})(THF)_2][(NR_2)_3U^{IV}(\mu\text{-}N)Th^{IV}(NR_2)_3]$ is oxidized by 0.5 equiv of I_2 to a mixed-valent U^V/Th^{IV} bridged nitride, $[(NR_2)_3U^V(\mu\text{-}N)Th^{IV}(NR_2)_3]$, which can be isolated in 42% yield after work-up. The structural assignments have been supported by means of ^{15}N-isotopic labeling, electronic absorption spectroscopy, magnetometry, electronic structure calculations, and elemental analyses.

Reaction of 3 equiv of $NaNR_2$ (R = $SiMe_3$) with $NpCl_4(DME)_2$ in THF afforded the Np(IV) silylamide complex, $[Np(NR_2)_3Cl]$, in good yield. Reaction of $[Np(NR_2)_3Cl]$ with 1.5 equiv of KC_8 in THF, in the presence of 1 equiv of dibenzo-18-crown-6, resulted in formation of $[\{K(DB\text{-}18\text{-}C\text{-}6)(THF)\}_3(\mu_3\text{-}Cl)][Np(NR_2)_3Cl]_2$, also in good yield. Complex $[\{K(DB\text{-}18\text{-}C\text{-}6)(THF)\}_3(\mu_3\text{-}Cl)][Np(NR_2)_3Cl]_2$ represents the first structurally characterized Np(III) amide. Finally, reaction of $NpCl_4(DME)_2$ with 5 equiv of $NaNR_2$ and 1 equiv of dibenzo-18-

crown-6 afforded the Np(IV) bis(metallacycle), [{Na(DB-18-C-6)(Et_2O)$_{0.62}$(κ^1-DME)$_{0.38}$}$_2$(μ-DME)][Np{*N*(R)($SiMe_2$*C*H_2)}$_2$(NR_2)]$_2$, in moderate yield. Complex [{Na(DB-18-C-6)(Et_2O)$_{0.62}$(κ^1-DME)$_{0.38}$}$_2$(μ-DME)][Np{*N*(R)($SiMe_2$*C*H_2)}$_2$(NR_2)]$_2$ was characterized by ^{1}H NMR spectroscopy and X-ray crystallography and represents a rare example of a structurally characterized neptunium–hydrocarbyl complex. To support these studies, I also synthesized the uranium analogues, namely, [K(2,2,2-cryptand)][U(NR_2)$_3$Cl], [K(DB-18-C-6)(THF)$_2$][U(NR_2)$_3$Cl], [Na(DME)$_3$][U{*N*(R)($SiMe_2$*C*H_2)}$_2$(NR_2)], and [{Na(DB-18-C-6)(Et_2O)$_{0.5}$(κ^1-DME)$_{0.5}$}$_2$(μ-DME)][U{*N*(R)($SiMe_2$*C*H_2)}$_2$(NR_2)]$_2$. Complexes were characterized by a number of techniques, including NMR spectroscopy and X-ray crystallography.

Table of Contents

List of Figures

List of Schemes

List of Tables

List of Abbreviations

°	degree
°C	degree Celsius
ε	extinction coefficient *or* bond critical point ellipticity
Δ	heat *or* difference
δ	chemical shift, ppm
η^n	hapticity of order n
κ^n	denticity of order n
μ	micro or denotes bridging atom
ν	stretching frequency, cm^{-1}
ρ	bond critical point electron density
Å	angstrom, 10^{-10} m
Ad	adamantyl
An	actinide
Ar	aryl
av.	average
$BArF^{24}$	$B(C_6H_3\text{-}3,5\text{-}CF_3)_4$
BCP	bond critical point
BDE	bond dissociation energy
br	broad
Bu	butyl
C_6D_6	Benzene-d_6
calcd.	calculated
$^{13}C\{^1H\}$	carbon-13 proton decoupled
ca.	circa
CCD	charge coupled device
$CNNPPh_3$	*N*-(isocyanoimine)triphenylphosphine
Cp^*	$\eta^5\text{-}C_5Me_5$
Cp^*_2Co	decamethyl cobaltocene
Cp	$\eta^5\text{-}C_5H_5$
cm^{-1}	wavenumber
CV	cyclic voltammetry
d	doublet *or* day(s)
d_n	deuterated in *n* positions
deg	degree
DB-18-C-6	dibenzo-18-crown-6
DFT	density functional theory
DI	delocalization index

Dipp	2,6-diisopropylphenyl
DMAP	4-(Dimethylamino)pyridine
DME	1,2-dimethoxyethane
$E_{1/2}$	average wave potential, $(E_{p,a} + E_{p,c})/2$
$E_{p,a}$	anodic half-wave potential
$E_{p,c}$	cathodic half-wave potential
e^-	electron
EPR	electron paramagnetic resonance
equiv	equivalent
Et_2O	diethyl ether
Et	ethyl
$^{19}F\{^1H\}$	fluorine-19 proton decoupled
Fc	ferrocene
Ft	feet
FTIR	Fourier transform infrared
FWHM	full width at half maximum
g	gram(s)
GOF	goodness of fit
H	enthalpy *or* bond critical point energy density
^1H	hydrogen-1
$^1H\{^{31}P\}$	hydrogen-1 phosphorus decoupled
h	hour(s)
HOMO	Highest Occupied Molecular Orbital
Hz	Hertz
$i_{p,a}$	anodic half-wave current
$i_{p,c}$	cathodic half-wave current
^{i}Pr	isopropyl
IR	infrared
J	NMR coupling constant
K	Kelvin
k	kilo
L	liter *or* ligand
LANL	Los Alamos National Laboratory
LED	Light Emitting Diode
$^7Li\{^1H\}$	lithium-7 proton decoupled
Ln	Lathanide
LUMO	Lowest Unoccupied Molecular Orbital
M	Molar
m	meter *or* multiplet *or* medium
m	meta

Me	methyl
min	minute(s)
mL	milliliter(s)
mmol	millimole(s)
mol	mole(s)
NBO	natural bond order
^{n}Bu	n-butyl
$^{15}N\{^{1}H\}$	nitrogen-15 proton decoupled
NH_4Cl	ammonium chloride
NHC	*N*-heterocyclic carbene
NIR	near infrared
nm	nanometer(s)
NMR	nuclear magnetic resonance
NR_2	$N(SiMe_3)_2$
o	ortho
ORTEP	Oak Ridge Thermal Ellipsoid Program
OTf	triflate, $[CF_3SO_3]^-$
p	para
$^{31}P\{^{1}H\}$	phosphorus-31 proton decoupled
Ph	phenyl
ppm	parts per million
py	pyridine
PUREX	Plutonium Uranium Redox Extraction
q	quartet
QTAIM	Quantum Theory of Atoms-in-Molecules
R	alkyl
redox	reduction-oxidation
RT	room temperature
$^{77}Se\{^{1}H\}$	Selenium-77 proton decoupled
$^{29}Si\{^{1}H\}$	Silicon-29 proton decoupled
s	singlet *or* strong *or* second(s)
sh	shoulder
SO	spin-orbit
SQUID	superconducting quantum interference device
$^{125}Te\{^{1}H\}$	Tellurium-125 proton decoupled
t	triplet
T	Tesla
^{t}Bu	*tert*-butyl
TBP	tri-n-butyl phosphate
THF	tetrahydrofuran

Ts	$MeC_6H_4SO_2$
μ_B	Bohr magneton
UV	ultraviolet
V	Volt
vis	visible
VT	variable temperature
w	Weak
W	watt
XAS	X-ray Absorption Spectrscopy
xs	excess
Xyl	$2,6\text{-}Me_2C_6H_3$

“Nevertheless, she persisted.”

Chapter 1. Introduction

1.1 Nuclear Power and Handling Nuclear Waste

Since the public disclosure of the Manhattan Project, following World War II, the world became familiar with uranium and plutonium, increasing the interest in their fundamental chemical and material properties, as well as finding other applications for these elements.[1-8] Today, nuclear power is of interest because of its appeal as a non-fossil fuel source of energy, as climate change becomes a real problem that needs to be combatted fast.[9] Nuclear power remains a popular alternative for many countries, as new reactors continue to be built alongside those in full operation.[10] The demand of nuclear power differs from country to country, for example, nuclear power accounts for approximately 20% of all the electricity generated in the United States, whereas it is closer to 71% in France.[10] Despite nuclear power's appeal as a non-fossil fuel alternative, there remains strong opposition to its use due to safety concerns related to working the power plants, as well as dealing with the generated waste.

The processing and storage of the nuclear waste are some of the biggest challenges associated with nuclear energy.[11] Over time, the fuel in the nuclear reactors must be replaced as the lanthanide portion "eats" neutrons, which are required for nuclear fission to occur.[12, 13] The used fuel that comes out of the reactors is deemed spent nuclear fuel and is comprised of mostly uranium (95.6%), stable fission products (2.9%), such as lanthanides and transition metals, and the minor actinides that are formed by neutron capture by uranium and plutonium in nuclear reactors.[12] Even though the minor actinides make up 0.1% of the spent nuclear fuel, they account for much of the long-term radiotoxicity.[14] Therefore, removal of these elements is necessary for reducing the hazards associated with spent nuclear fuel and the ability to reprocess and reuse these components within the fuel cycle is also favorable.

One route taken to handle this spent fuel is called the 'once-through' cycle (Scheme 1.1a). This route initially separates the spent nuclear fuel to reduce the volume before its storage and

final placement.[15] For example, the majority of spent nuclear fuel rods from nuclear reactors are stored in stainless steeled lined pools, inside metal boxes with walls that contain neutron-absorbing boron to prevent criticality.[16] After 5 years, the fuel rods are moved above ground into dry casks.[16] All other radioactive waste is stored in large drums, sealed, and placed underground throughout the United States in dumps that are dug like a conventional mine.[17] Over time, leaks and salt build ups are minor risks that can occur, but much larger risks involving a sealed drum exploding and contaminating the underground area have occurred and are extremely risky and costly to clean up.[18]

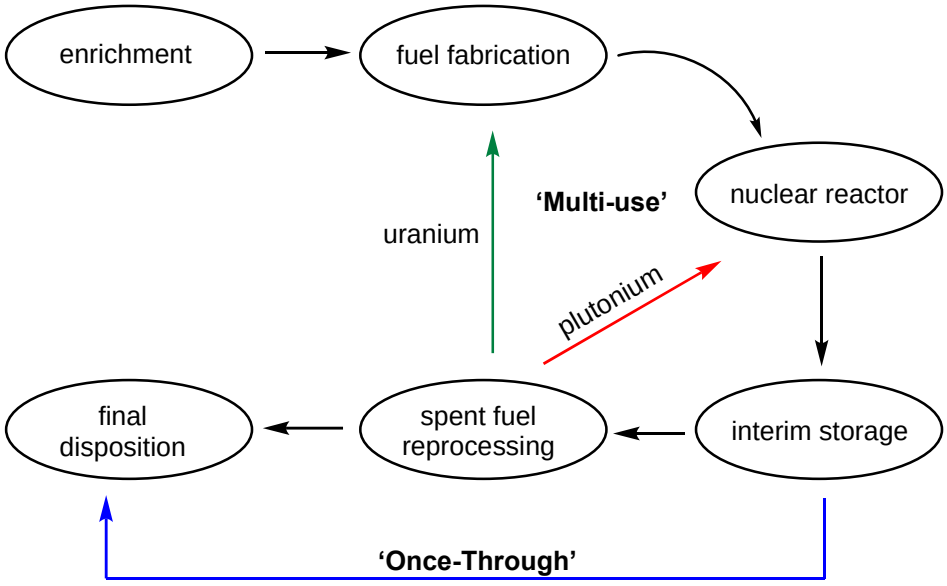

Scheme 1.1. Two fuel cycle routes: (a) 'once-through' or (b) 'multi-use'. Adapted from Ref. 15.

Alternatively, the second route taken to handle spent fuel is called the 'multi-use' cycle (Scheme 1.1b). This route also involves an initial separation of waste, but the spent fuel is then reprocessed, recycling uranium and plutonium back into the nuclear fuel process.[15] This process is called PUREX, Plutonium Uranium Redox Extraction, and has been used internationally the past 60 years. This process reprocesses nuclear fuel by utilizing the

differences in redox chemistry to fully separate plutonium and uranium from the fission products (lanthanides) and heavier actinides (minor actinides) initially, and then plutonium from uranium.[19] The hard oxygen donor ligand, tri-n-butyl phosphate (TBP), is used in this process and is efficient at separating uranium and plutonium from the minor actinides and fission products, but binds similarly with the fission products and minor actinides, creating a challenging separation between these two portions (Scheme 1.2).[20, 21]

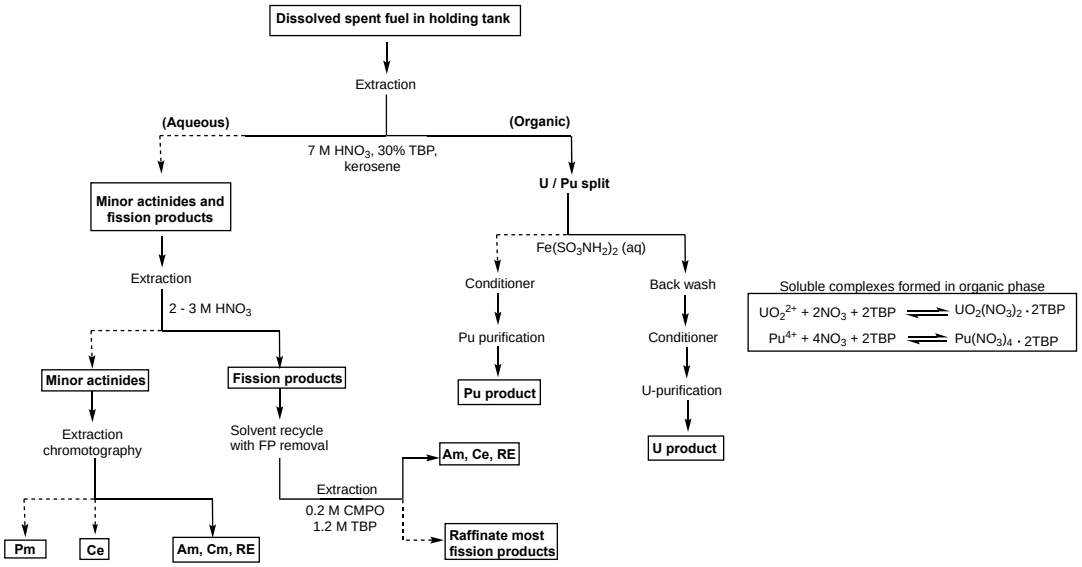

Scheme 1.2. Spent nuclear fuel reprocessing flowchart with a focus on the aqueous phase extraction process. Adapted from Ref 19.

It is desirable to fully separate the minor actinides from the lanthanides because the minor actinides, such as americium, can be converted into short-lived fission products versus being stored long-term and decaying into the long-lived alpha emitter, neptunium. However, this lack of separation occurs because of the similar charge and chemical behaviors of the minor actinides and lanthanides, causing a competition with TBP.

Since this separation is advantageous to solve, research has been done to synthesize complexation agents that will bind with the actinides versus the lanthanides as a way to afford

better separation.[13, 20, 22-24] One study done by Zhu and co-workers looked at the separation factor for Am^{3+} versus Eu^{3+} for bis(2,2,4-trimethylpentyl)dithiophosphinic acid.[25] By changing the hard oxygen donor, TBP, with a soft donor ligand, such as sulfur, and the geometry of the ligand scaffold, separation between americium and europium increased from 20 factors to 100,000 factors (Figure 1.1).[25-28] While more research needs to be done in this area, the results of this study suggest that the actinides are better at forming more covalent bonds with soft donor ligands versus the lanthanides.

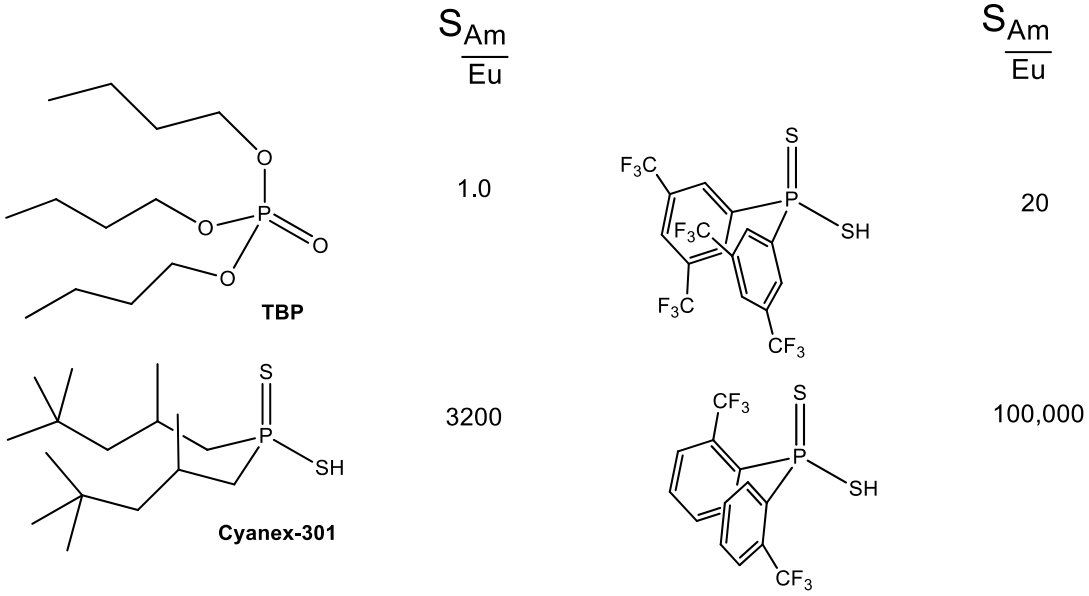

Figure 1.1. The typical hard-oxygen donor ligand, TBP, versus dithiophoscphinic acid extractants and their separation factors for Am^{3+}/Eu^{3+}. Data taken from Refs 25-28.

1.2 f-orbital Bonding and Covalency in Actinide-Ligand Bonding

For a long time the actinides have been considered hard metal ions, in which their chemistry can be predicted by their charge and ionic radii.[29, 30] Moreover, the f-block has shown to have similar ionic radii between the lanthanides and actinides, affording similar chemistry between these elements.[31] However, as more research is done with these elements, there is data that suggests the actinides can bond differently than the lanthanides, affording

different reactivity due to covalency in the actinides and how the 5f orbitals participate in bonding more than the 4f orbitals.[32-37] Additionally, it has been observed that the 5f orbitals can spread further radially, unlike the 4f orbitals which are considered core-like orbitals, and may contribute in bonding alongside the other valence orbitals (Scheme 1.3).[29, 38]

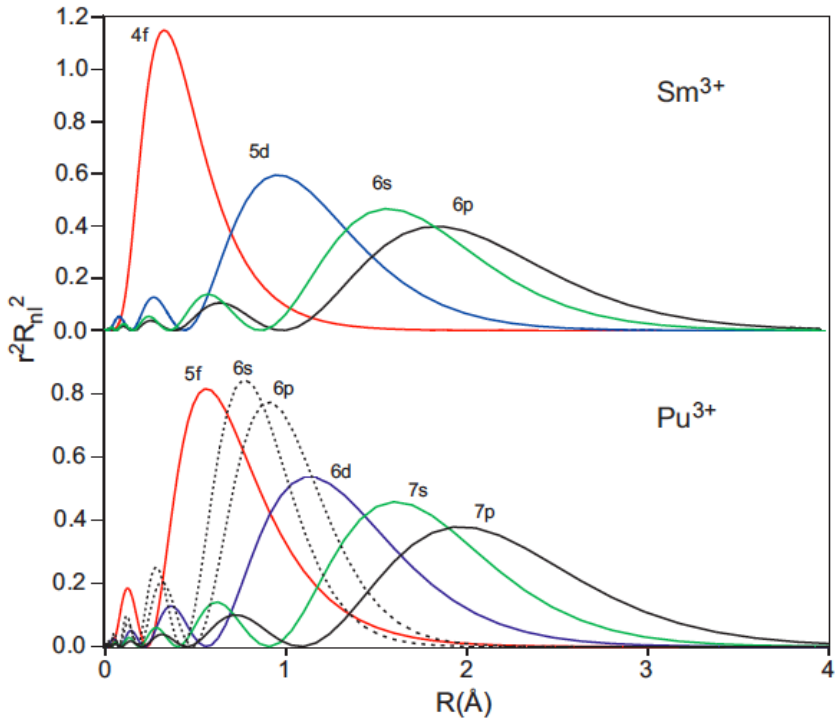

Scheme 1.3. Radial distribution seen in 4f (Sm^{3+}) versus 5f (Pu^{3+}) orbitals. Taken from Ref 36.

Due to increasing interest in studying the f-block elements, the participation of the 5f orbitals in bonding is supported by growing evidence.[39-43] There are several techniques and methods that can be used to measure covalency in actinide ligand bonding.[44-48] The technique X-ray absorption spectroscopy (XAS) has been shown to be useful in measuring the orbital particaption of metal-ligand bonds[49-52] and has been used on several actinide complexes.[40, 41, 43, 53] One study, done by Kozimor and co-workers, studied the bonding of several metal-chloride complexes, such as $[UCl_6]^{2-}$, using Cl K-edge XAS and discovered that both the 6d

and 5f orbitals participate in bonding.[41, 43] Although these results showed the covalency involved, the amount of covalency was not very large for the metal-halide bond. Furthermore, work done by Shuh and co-workers revealed that both the 5f and 6d orbitals participate in the bonding of $[(C_8H_8)_2An]$ (An = Th and U), using C K-edge XAS, which shows the range of this technique.[40] However, XAS beam time can be difficult to get and this technique does not work on every type of compound.

Most of these experimental analyses are accompanied with computational methods, such as Density Functional Theory (DFT). For example, Hayton and co-workers reported the synthesis and characterization of a thorium(IV) phosphorano-stabilized carbene, $[Th(CHPPh_3)(NR_2)_3]$ (R = $SiMe_3$).[54] This diamagnetic compound, with an NMR active nucleus, ^{13}C, directly bound to the metal center, allowed its electronic structure to be investigated by NMR spectroscopy in combination with DFT. The results show that Th-C bonding not only displayed a substantial amount of covalency, but the 5f orbitals played a large role to this bonding. DFT has also been used extensively as a standalone method to probe actinide-ligand bonding as well.[55-58] For example, Liddle and co-workers reported the synthesis and characterization of the terminal U(V) nitride complex, $[U(N)(Tren^{TIPS})][Na(12\text{-crown-4})_2]$ ($Tren^{TIPS}$ = $[N(CH_2CH_2NSiPr^i_3)_3]^{3-}$ and Pr^i = $CH(CH_3)_2$), and analyzed the U-N bond using DFT.[59] This analysis determined that there was significant amount of uranium character in both the σ and π bonds, suggesting a large amount of covalency. Moreover, the vast majority of the uranium contributions present in the U-N triple bond were found to be from the 5f orbitals versus the 6d, where the σ bond contained 44% 5f and 47% 6d orbital character and the two π bonds each contained 72% 5f and 28% 6d character. These results show the advantages of using computational techniques, alone or in combination with NMR

spectroscopy, to measure the amount of covalency in actinide-ligand bonding and to better understand the role covalency plays in the f-orbitals, as well as the importance of studying multiple-ligand bonded complexes.

1.3 Metal-Ligand Multiple Bonds

Throughout inorganic chemistry, metal-ligand multiple bonded ligands, which include oxos, imidos, nitridos, and carbenes, to name a few, are involved in many fundamental roles.[60] For example, metal nitrogen multiple bonded ligands, such as imidos and nitridos, likely play a role in the process of nitrogen fixation. The Haber-Bosch process accounts for 1-2% of all energy intake in the world does this process on an industrial scale.[61] Whereas in nature, nitrogen fixation is carried out by nitrogenase,[62, 63] in which the synthesis of imido and nitrido moieties are thought to be involved.[64, 65] To gain insight into this mechanistic pathway, synthetic complexes that can catalytically reduce dinitrogen have also been explored.[66-69] The reaction of [(HIPTN$_3$N)Mo] (HIPT = 3,5-(2,4,6-^{i}Pr$_3$C$_6$H$_2$)$_2$-C$_6$H$_3$) with N_2 to generate NH_3 was studied by Schrock and co-workers, where imido and nitrido complexes were isolated as intermediates and fully characterizaed.[70-73]

Fischer and co-workers reported the first examples of metal carbene complexes in the 1960s, which featured a heteroatom stabilized carbene moiety.[74-76] Numerous examples have now been reported, including N-heterocyclic carbenes,[77-84] featuring heteroatom stabilization, and alkylidenes, which do not.[85-87] These complexes have been applied in many reactions,[88-91] such as their use in olefin metathesis,[92-95] which earned a Nobel Prize.[96-98]

Although f-element-ligand multiple bonded complexes have not been studied as thoroughly as their main block counterparts, increasing interest over the past several decades has helped this field start to grow.[99-101] Now the synthesis of actinide oxo,[102-118] imido,[119-144]

chalcogenide,[145-155] and nitrido complexes,[156-162] among others,[54, 163-175] are much more common. Among these complexes are the first uranium carbene complexes, $[Cp_3U(CHP(Me)_2R)]$ (R = Ph[166] and Me[165]), reported by Gilje and co-workers, and the first uranium nitride complex, $[\{K(dme)(calix[4]tetrapyrrole)U\}_2(\mu\text{-}NK)_2][K(dme)_4]$, reported by Gamboratta and co-workers in 2002.[176] The latter complex inspired the synthesis of many bridging and terminal uranium nitride complexes.[59, 156, 157, 177-186] Additionally, Boncella and co-workers reported the synthesis of several uranium bis-imido complexes,[123, 127, 128] as well as the first transuranic bis-imido complex $[Np(NDipp)_2(^tBubipy)_2(Cl)]$ (Dipp = 2,6-$^iPr_2C_6H_3$).[121]

Despite the progress in this field, thorium nitrides remains rare,[187] as a handful of thorium nitrides have been identified in matrix isolation studies, but are only stable at cryogenic temperatures.[188-190] Moreover, the majority of actinide carbenes feature a phosphorous substituent that helps stabilize the actinide-carbene interaction rather than a Schrock-type carbene, which involves a true double bond through the equal distribution of electrons on the metal and carbon centers, has yet to by synthesized with an actinide.[80, 82, 169, 171, 172, 191] Lastly, in comparison to U and Th chemistry, contemporary knowledge of the physicochemical properties of Np and Pu has not kept pace, despite the central role of these minor actinide in the nuclear fuel cycle.[99, 100, 192-194] The coordination chemistry of Np and Pu has started to expand with the recent development of several new transuranic starting materials,[121, 195-201] providing the ground work for novel transuranic chemistry to take place that was not accessible before.

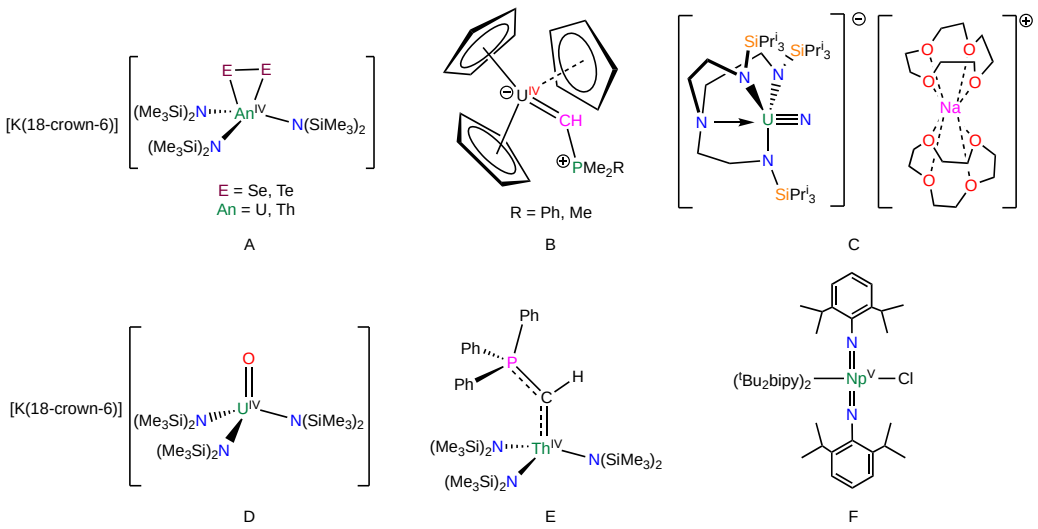

Figure 1.2. Examples of complexes with actinide-ligand multiple bonds. A, Refs. 145, 146; B, Refs. 165, 166; C, Ref. 59; D, Ref. 107; E, Ref. 54; F, Ref. 121.

1.4 General Remarks

This goal of this research is to gain better understanding of f-element, metal-ligand bonding through the synthesis of complexes containing lanthanide and actinide ligand multiple bonds, with a particular focus upon f-element carbenes, imidos, and nitridos.

Chapter 2 describes the use of a nitrilimine source with cerium tris(amide) in efforts to afford a cerium(IV) carbene. The cerium nitrilimine adduct was photolyzed for 30 days and monitored *via* ^{1}H and ^{31}P NMR spectroscopy, whereupon rearrangement of the nitrilimine ligand is observed and confirmed by X-ray crystallography.

Chapter 3 details the use of isocyanide ligands with low valent uranium tris(amide) as a method to afford adducts that can undergo ligand reduction in order to oxidize the metal center in efforts to synthesize a uranium carbene. The reducing agents used and the reactions that were followed is discussed. X-ray crystallography and NMR spectroscopy are used to study these complexes.

Chapter 4 describes methods of synthesizing uranium and thorium imido and amido complexes using different protecting groups and ammonia-triphenylborane, including reductive deprotection of these moieties *via* addition of external reducing agents and Lewis bases. These complexes are characterized both by NMR spectroscopy and X-ray crystallography. The differing reactivity observed is also discussed.

Chapter 5 details the use of sodium amide as a nitride source to synthesize the first isolable thorium nitride. The synthesis of a novel thorium parent amide is also discussed. Labeling experiments using ^{15}N sources are detailed within and NMR spectroscopy, X-ray crystallography, and DFT analysis is performed to probe the electronic structure of these complexes and a discussion of the thorium ligand bonding is included.

Chapter 6 describes a method of synthesizing a uranium(IV) parent amide, a uranium(IV)-thorium(IV) bridged nitride, and a uranium(V)-thorium(IV) bridged nitride. Labeling experiments using an ^{15}N source are also detailed. X-ray crystallography, IR spectroscopy, UV-vis/NIR spectroscopy, and NMR spectroscopy are all used to probe the electronic structure of these complexes, as well as EPR Spectroscopy on the uranium(V)-thorium(IV) nitride, and a discussion of the actinide ligand bonding is included.

Chapter 7 details the reactivity of the 1,2-dimethoxyethane (DME) solvent adducts of neptunium(IV) tetrachloride with 3, 4, and 5 equiv of $NaNR_2$ ($R = SiMe_3$). Reduction experiments to a Np(III) complex are also discussed. NMR spectroscopy, X-ray crystallography, and UV-vis/NIR spectroscopy are all used to study the electronic structure of these complexes.

1.5 References

1. Ibers, J., Neglected neptunium. *Nature Chem.* **2010,** *2* (11), 996-996.
2. Levine, C. A.; Seaborg, G. T., The occurrence of plutonium in nature. *J. Am. Chem. Soc.* **1951,** *73* (7), 3278-3283.
3. Rhodes, R., *The making of the atomic bomb*. Simon and Schuster: 2012.
4. SEABORG, G. T., The Chemical and Radioactive Properties of the Heavy Elements. In *Modern Alchemy*, pp 20-23.
5. Seaborg, G. T., Forty Years of Plutonium Chemistry: The Beginnings. In *Plutonium Chemistry*, AMERICAN CHEMICAL SOCIETY: Vol. 216, pp 1-22.
6. Seaborg, G. T., The Transuranium Elements. *Science* **1946,** *104* (2704), 379-386.
7. Seaborg, G. T.; Segrè, E., *The transuranium elements*. Atomic Energy Commission: 1946.
8. Weigel, F.; Katz, J. J.; Seaborg, G. T., *Plutonium*. Chapman and Hall: United Kingdom, 1986.
9. *IAEA: 2018.*
10. IEA, *World Energy Outlook 2019*. OECD Publishing.
11. OECD, *Actinide and Fission Product Partitioning and Transmutation*. OECD Publishing.
12. Choppin, G. L., J.-O.; Rydberg, J.; Ekberg, C. , *Radiochem. Nucl. Chem.* **2013**, 685.
13. Hill, C., CRC Press: Ion exchange and Solvent Extraction, 2009; p 119.
14. Madic, C.; Lecomte, M.; Baron, P.; Boullis, B., Separation of long-lived radionuclides from high active nuclear waste. *Comptes Rendus Physique* **2002,** *3* (7-8), 797-811.
15. EIA The Nuclear Fuel Cycle.
16. NRC, Radioactive Waste. **2017**.
17. Crowley, K. D.; Ahearne, J. F., Managing the Environmental Legacy of US Nuclear-Weapons Production: Although the waste from America's arms buildup will never be" cleaned up," human and environmental risks can be reduced and managed. *American Scientist* **2002,** *90* (6), 514-523.
18. Vartabedian, R. Nuclear accident in New Mexico ranks among the costliest in U.S. history 2016.
19. NEA Spent Nuclear Fuel Reproccessing Flowsheet.
20. Nash, K. L., A review of the basic chemistry and recent developments in trivalent f-elements separations. *Solvent Extr. Ion Exch.* **1993,** *11* (4), 729-768.
21. Wenzel, U. B., C. L.; Herz, D.; Ritter, G., *Actinide Separations* **1980,** *117*.
22. Dam, H. H.; Reinhoudt, D. N.; Verboom, W., *Chem. Soc. Rev.* **2007,** *36*, 367.
23. Ionova, G.; Ionov, S.; Rabbe, C.; Hill, C.; Madic, C.; Guillaumont, R.; Krupa, J. C., *Solvent Extr. Ion Exch.* **2001,** *19*, 391.
24. Kolarik, Z., *Chem. Rev.* **2008,** *108*, 4208.
25. Zhu, Y.; Chen, J.; Choppin, G. R., *Solvent Extr. Ion Exch.* **1996,** *14*, 543.
26. Hill, C.; Madic, C.; Baron, P.; Ozawa, M.; Tanaka, Y., *J. Alloys Compd.* **1998,** *271-273*, 159.
27. Klaehn, J. R.; Peterman, D. R.; Harrup, M. K.; Tillotson, R. D.; Klaehn, J. R.; Harrup, M. K.; Luther, T. A.; Law, J. D., *Inorg. Chim. Acta* **2008,** *361*, 2522.
28. Peterman, D. R.; Greenhalgh, M. R.; Tillotson, R. D.; Klaehn, J. R.; Harrup, M. K.; Luther, T. A.; Law, J. D., *Sep. Sci. Technol* **2010,** *45*, 1711.

29. Kaltsoyannis, N.; Scott, P., *The f elements*. Oxford University Press: New York: 1999.
30. Katz, J. J.; Morss, L. R.; Seaborg, G. T., *The Chemistry of the Actinide Elements*. 2nd ed.; 1986.
31. Choppin, G. R., *J. Less-Common Met.* **1983,** *93*, 323.
32. Choppin, G. R., Covalency in f-element bonds. *J. Alloys Compd.* **2002,** *344* (1-2), 55-59.
33. Ingram, K. I.; Tassell, M. J.; Gaunt, A. J.; Kaltsoyannis, N., Covalency in the f Element− Chalcogen Bond. Computational Studies of $M[N(EPR_2)_2]_3$ (M= La, Ce, Pr, Pm, Eu, U, Np, Pu, Am, Cm; E = O, S, Se, Te; R = H, ^{i}Pr, Ph). *Inorg. Chem.* **2008,** *47* (17), 7824-7833.
34. Ingram, K. I. M.; Kaltsoyannis, N.; Gaunt, A. J.; Neu, M. P., Covalency in the f-element–chalcogen bond: computational studies of $[M(N(EPH_2)_2)_3]$(M= La, U, Pu; E= O, S, Se, Te). *J. Alloys Compd.* **2007,** *444*, 369-375.
35. Jones, M. B.; Gaunt, A. J.; Gordon, J. C.; Kaltsoyannis, N.; Neu, M. P.; Scott, B. L., Uncovering f-element bonding differences and electronic structure in a series of 1 : 3 and 1 : 4 complexes with a diselenophosphinate ligand. *Chem. Sci.* **2013,** *4* (3), 1189-1203.
36. Neidig, M. l. L.; Clark, D. L.; Martin, R. L., Covalency in f-element complexes. *Coord. Chem. Rev.* **2013,** *257* (2), 394-406.
37. Gaunt, A. J.; Reilly, S. D.; Enriquez, A. E.; Scott, B. L.; Ibers, J. A.; Sekar, P.; Ingram, K. I. M.; Kaltsoyannis, N.; Neu, M. P., Experimental and Theoretical Comparison of Actinide and Lanthanide Bonding in $M[N(EPR_2)_2]_3$ Complexes (M= U, Pu, La, Ce; E= S, Se, Te; R= Ph, *i*Pr, H). *Inorg. Chem.* **2008,** *47* (1), 29-41.
38. Schreckenbach, G.; Hay, P. J.; Martin, R. L., *J. Comput. Chem.* **1999,** *20*, 70.
39. Seaman, L. A.; Wu, G.; Edelstein, N.; Lukens, W. W.; Magnani, N.; Hayton, T. W., Probing the 5f Orbital Contribution to the Bonding in a U(V) Ketimide Complex. *J. Am. Chem. Soc.* **2012,** *134* (10), 4931-4940.
40. Minasian, S. G.; Keith, J. M.; Batista, E. R.; Boland, K. S.; Clark, D. L.; Kozimor, S. A.; Martin, R. L.; Shuh, D. K.; Tyliszezak, T., *Chem. Sci.* **2014,** *5*, 351.
41. Minasian, S. G.; Keith, J. M.; Batista, E. R.; Boland, K. S.; Clark, D. L.; Conradson, S. D.; Kozimor, S. A.; Martin, R. L.; Schwarz, D. E.; Shuh, D. K.; Wagner, G. L.; Wilkerson, M. P.; Wolfsberg, L. E.; Yang, P., Determining Relative f and d Orbital Contributions to M–Cl Covalency in MCl_6^{2-} (M = Ti, Zr, Hf, U) and $UOCl_5^{-}$ Using Cl K-Edge X-ray Absorption Spectroscopy and Time-Dependent Density Functional Theory. *J. Am. Chem. Soc.* **2012,** *134* (12), 5586-5597.
42. Lukens, W. W.; Edelstein, N. M.; Magnani, N.; Hayton, T. W.; Fortier, S.; Seaman, L. A., *J. Am. Chem. Soc.* **2013,** *135*, 10742.
43. Kozimor, S. A.; Yang, P.; Batista, E. R.; Boland, K. S.; Burns, C. J.; Clark, D. L.; Conradson, S. D.; Martin, R. L.; Wilkerson, M. P.; Wolfsberg, L. E., Trends in Covalency for d- and f-Element Metallocene Dichlorides Identified Using Chlorine K-Edge X-ray Absorption Spectroscopy and Time-Dependent Density Functional Theory. *J. Am. Chem. Soc.* **2009,** *131* (34), 12125-12136.
44. Pepper, M.; Bursten, B. E., *Chem. Rev.* **1991,** *91*, 719.
45. Kaltsoyannis, N., *Chem. Soc. Rev.* **2003,** *32*, 9.
46. Green, J. C.; de Simone, M.; Coreno, M.; Jones, A.; Pritchard, H. M. I.; McGrady, G. S., *Inorg. Chem.* **2005,** *44*, 7781.

47. Clark, J. P.; Green, J. C., *J. Chem. Soc. Dalton Trans* **1977,** (505).
48. Brennan, J. G.; Green, J. C.; Redfern, C. M., *J. Am. Chem. Soc.* **1989,** *111*, 2373.
49. Solomon, E. I.; Hedman, B.; Hodgson, K. O.; Dey, A.; Szilagyi, R. K., *Coord. Chem. Rev.* **2005,** *249*, 97.
50. Löble, M. W.; Keith, J. M.; Altman, A. B.; Stieber, S. C. E.; Batista, E. R.; Boland, K. S.; Conradson, S. D.; Clark, D. L.; Lezama Pacheco, J.; Kozimor, S. A.; Martin, R. L.; Minasian, S. G.; Olson, A. C.; Scott, B. L.; Shuh, D. K.; Tyliszezak, T.; Wilkerson, M. P.; Zehnder, R. A., *J. Am. Chem. Soc.* **2015,** *137*, 2506.
51. Daly, S. R.; Keith, J. M.; Batista, E. R.; Boland, K. S.; Clark, D. L.; Kozimor, S. A.; Martin, R. L., *J. Am. Chem. Soc.* **2012,** *134*, 14408.
52. Altman, A. B.; Pacold, J. I.; Lukens, W. W.; Minasian, S. G., *Dalton Trans.* **2016,** *45*, 9948.
53. Kozimor, S. A.; Yang, P.; Batista, E. R.; Boland, K. S.; Burns, C. J.; Christensen, C. N.; Clark, D. L.; Conradson, S. D.; Hay, P. J.; Lezama, J. S.; Martin, R. L.; Schwarz, D. E.; Wilkerson, M. P.; Wolfsberg, L. E., *Inorg. Chem.* **2008,** *47*, 5365.
54. Smiles, D. E.; Wu, G.; Hrobárik, P.; Hayton, T. W., Synthesis, Thermochemistry, Bonding, and ^{13}C NMR Chemical Shift Analysis of a Phosphorano-Stabilized Carbene of Thorium. *Organometallics* **2017,** *36* (23), 4519-4524.
55. Tassell, M. J.; Kaltsoyannis, N., *Dalton Trans.* **2010,** *39*, 6719.
56. Kirker, I.; Kaltsoyannis, N., Does covalency *really* increase across the 5f series? A comparison of molecular orbital, natural population, spin and electron density analyses of AnCp $_3$ (An = Th–Cm; Cp = η^5-C_5H_5). *Dalton Trans.* **2011,** *40* (1), 124-131.
57. Kaltsoyannis, N., Does covalency increase or decrease across the actinide series? Implications for minor actinide partitioning. *Inorg. Chem.* **2013,** *52* (7), 3407-3413.
58. Huang, Q.-R.; Kingham, J. R.; Kaltsoyannis, N., *Dalton Trans.* **2015,** *44*, 2554.
59. King, D. M.; Tuna, F.; McInnes, E. J. L.; McMaster, J.; Lewis, W.; Blake, A. J.; Liddle, S. T., Synthesis and Structure of a Terminal Uranium Nitride Complex. *Science* **2012,** *337* (6095), 717.
60. Nugent, W. A.; Mayer, J. M., *Metal-Ligand Mulitple Bonds*. John Wiley & Sons: New York, NY: 1988.
61. Smil, V., *Enriching the Earth: Fritz Haber, Carl Bosch, and the Transformation of World Food Production*. MIT Press: Cambridge, MA, 2004.
62. Einsle, O.; Tezcan, F. A.; Andrade, S. L. A.; Schmid, B.; Yoshida, M.; Howard, J. B.; Rees, D. C., *Science* **2002,** *297*, 1696.
63. Lancaster, K. M.; Roemelt, M.; Ettenhuber, P.; Hu, Y.; Ribbe, M. W.; Neese, F.; Bergmann, U.; DeBeer, S., *Science* **2011,** *334*, 974.
64. Hoffman, B. M.; Lukoyanov, D.; Yang, Z.-Y.; Dean, D. R.; Seefeldt, L. C., *Chem. Rev.* **2014,** *114*, 4041.
65. Seefeldt, L. C.; Hoffman, B. M.; Dean, D. R., *Annu. Rev. Biochem.* **2009,** *78*, 701.
66. McWilliams, S. F.; Holland, P. L., *Acc. Chem. Res.* **2015,** *48*, 2059.
67. Rittle, J.; Peters, J. C., *J. Am. Chem. Soc.* **2016,** *138*, 4243.
68. Schrock, R. R., *Acc. Chem. Res.* **2005,** *38*, 955.
69. Hohenberger, J.; Ray, K.; Meyer, K., *Nat. Commun.* **2012,** *3*, 720.
70. Yandulov, D. V.; Schrock, R. R., *J. Am. Chem. Soc.* **2002,** *124*, 6252.
71. Yandulov, D. V.; Schrock, R. R., *Science* **2003,** *301*, 76.
72. Yandulov, D. V.; Schrock, R. R., *Inorg. Chem.* **2005,** *44*, 1103.

73. Yandulov, D. V.; Schrock, R. R.; Rheingold, A. L.; Ceccarelli, C.; Davis, W. M., *Inorg. Chem.* **2003,** *42*, 796.
74. Fischer, E. O., *Pure Appl. Chem.* **1970,** *24*, 407.
75. Fischer, E. O.; Maasböl, A., *Angew. Chem. Int. Ed.* **1964,** *3*, 580.
76. Mills, O. S.; Redhouse, A. D., *Angew. Chem. Int. Ed.* **1965,** *4*, 1082.
77. Diez-Gonzalez, S.; Nolan, S. P., *Annu. Rep. Prog. Chem., Sect. B: Org. Chem.* **2005,** *101*, 171.
78. Öfele, K. J., *Organomet. Chem.* **1968,** *12*, 42.
79. Wanzlick, H. W.; Schönherr, H. J., *Angew. Chem. Int. Ed.* **1968,** *7*, 141.
80. Mills, D. P.; Cooper, O. J.; Tuna, F.; McInnes, E. J. L.; Davies, E. S.; McMaster, J.; Moro, F.; Lewis, W.; Blake, A. J.; Liddle, S. T., *J. Am. Chem. Soc.* **2012,** *134*, 10047.
81. Tourneux, J.-C.; Berthet, J.-C.; Thuery, P.; Mezailles, P.; Le Floch, P.; Ephritikhine, M., *Dalton Trans.* **2010,** *39*, 2494.
82. Cooper, O. J.; Mills, D. P.; McMaster, J.; Moro, F.; Davies, E. S.; Lewis, W.; Blake, A. J.; Liddle, S. T., *Angew. Chem. Int. Ed.* **2011,** *50*, 2383.
83. Matson, E. M.; Fanwick, P. E.; Bart, S. C., *Eur. J. Inorg. Chem.* **2012**, 5471.
84. Gardner, B. M.; Patel, D.; Lewis, W.; Blake, A. J.; Liddle, S. T., *Angew. Chem. Int. Ed.* **2011,** *50*, 10440.
85. Nguyen, S. T.; Grubbs, R. H.; Ziller, J. W., *J. Am. Chem. Soc.* **1993,** *115*, 9858.
86. Nguyen, S. T.; Johnson, L. K.; Grubbs, R. H.; Ziller, J. W., *J. Am. Chem. Soc.* **1992,** *114*, 3974.
87. Schrock, R. R., *J. Am. Chem. Soc.* **1974,** *96*, 6796.
88. Dötz, K. H.; Stendel, J., *Chem. Rev.* **2009,** *109*, 3227.
89. Doyle, M. P., *Chem. Rev.* **1986,** *86*, 919.
90. Kaufhold, S.; Petermann, L.; Staehle, R.; Rau, S., *Coord. Chem. Rev.* **2015,** *304-305*, 73.
91. Velazquez, H. D.; Verpoort, F., *Chem. Soc. Rev.* **2012,** *41*, 7032.
92. Cardin, D. J.; Cetinkaya, B.; Lappert, M. F., *Chem. Rev.* **1972,** *72*, 545.
93. Dötz, K. H., *Metal Carbenes in Organic Synthesis*. Springer Berlin Heidelberg: Berlin, Heidelberg, 2004.
94. Tebbe, F. N.; Parshall, G. W.; Reddy, G. S., *J. Am. Chem. Soc.* **1978,** *100*, 3611.
95. Vougioukalakis, G. C.; Grubbs, R. H., *Chem. Rev.* **2010,** *110*, 1746.
96. Chauvin, Y., *Angew. Chem. Int. Ed.* **2006,** *45*, 3740.
97. Grubbs, R. H., *Angew. Chem. Int. Ed.* **2006,** *45*, 3760.
98. Schrock, R. R., *Angew. Chem. Int. Ed.* **2006,** *45*, 3748.
99. Hayton, T. W., Metal–ligand multiple bonding in uranium: structure and reactivity. *Dalton Trans.* **2010,** *39* (5), 1145-1158.
100. Hayton, T. W., Recent developments in actinide–ligand multiple bonding. *Chem. Commun.* **2013,** *49* (29), 2956-2973.
101. Zi, G., Organothorium complexes containing terminal metal-ligand multiple bonds. *Sci. China Chem.* **2014,** *57* (8), 1064-1072.
102. Bart, S. C.; Anthon, C.; Heinemann, F. W.; Bill, E.; Edelstein, N. M.; Meyer, K., Carbon dioxide activation with sterically pressured mid-and high-valent uranium complexes. *J. Am. Chem. Soc.* **2008,** *130* (37), 12536-12546.

103. Fortier, S.; Brown, J. L.; Kaltsoyannis, N.; Wu, G.; Hayton, T. W., Synthesis, Molecular and Electronic Structure of $U^{V}(O)[N(SiMe_3)_2]_3$. *Inorg. Chem.* **2012,** *51* (3), 1625-1633.
104. Fortier, S.; Kaltsoyannis, N.; Wu, G.; Hayton, T. W., Probing the reactivity and electronic structure of a uranium (V) terminal oxo complex. *J. Am. Chem. Soc.* **2011,** *133* (36), 14224-14227.
105. Ren, W.; Zi, G.; Fang, D.-C.; Walter, M. D., Thorium oxo and sulfido metallocenes: synthesis, structure, reactivity, and computational studies. *J. Am. Chem. Soc.* **2011,** *133* (33), 13183-13196.
106. Zi, G.; Jia, L.; Werkema, E. L.; Walter, M. D.; Gottfriedsen, J. P.; Andersen, R. A., Preparation and Reactions of Base-Free Bis(1,2,4-tri-*tert*-butylcyclopentadienyl)uranium Oxide, Cp'_2UO. *Organometallics* **2005,** *24* (17), 4251-4264.
107. Smiles, D. E.; Wu, G.; Hayton, T. W., Synthesis of Uranium–Ligand Multiple Bonds by Cleavage of a Trityl Protecting Group. *J. Am. Chem. Soc.* **2014,** *136* (1), 96-99.
108. Evans, W. J.; Kozimor, S. A.; Ziller, J. W., *Polyhedron* **2004,** *23*, 2689.
109. Williams, V. C.; Muller, M.; Leech, M. A.; Denning, R. G.; Green, M. L. H., *Inorg. Chem.* **2000,** *39*, 2538.
110. Brown, D. R.; Denning, R. G., *Inorg. Chem.* **1996,** *35*, 6158.
111. Kraft, S. J.; Walensky, J. R.; Fanwick, P. E.; Hall, M. B.; Bart, S. C., *Inorg. Chem.* **2010,** *49*, 7620.
112. Lam, O. P.; Bart, S. C.; Kameo, H.; Heinemann, F. W.; Meyer, K., *Chem. Commun.* **2010,** *46*, 3137.
113. Castro, L.; Lam, O. P.; Bart, S. C.; Meyer, K.; Maron, L., *Organometallics* **2010,** *29*, 5504.
114. Schmidt, A.-C.; Nizovtsev, A. V.; Scheurer, A.; Heinemann, F. W.; Meyer, K., *Chem. Commun.* **2012,** *48*, 8634.
115. Kosog, B.; La Pierre, H. S.; Heinemann, F. W.; Liddle, S. T.; Meyer, K., *J. Am. Chem. Soc.* **2012,** *134*, 5284.
116. Kosog, B.; La Pierre, H. S.; Denecke, M. A.; Heinemann, F. W.; Meyer, K., *Inorg. Chem.* **2012,** *51*, 7940.
117. Brown, J. L.; Fortier, S.; Lewis, R. A.; Wu, G.; Hayton, T. W., *J. Am. Chem. Soc.* **2012,** *134*, 15468.
118. Gong, Y.; Wang, X.; Andrews, L.; Schlader, T.; Riedel, S., *Inorg. Chem.* **2012,** *51*, 6983.
119. Anderson, N. H.; Odoh, S. O.; Yao, Y.; Williams, U. J.; Schaefer, B. A.; Kiernicki, J. J.; Lewis, A. J.; Goshert, M. D.; Fanwick, P. E.; Schelter, E. J., Harnessing redox activity for the formation of uranium tris (imido) compounds. *Nature* **2014,** *6* (10), 919-926.
120. Bell, N. L.; Maron, L.; Arnold, P. L., Thorium Mono- and Bis(imido) Complexes Made by Reprotonation of *cyclo*-Metalated Amides. *J. Am. Chem. Soc.* **2015,** *137* (33), 10492-10495.
121. Brown, J. L.; Batista, E. R.; Boncella, J. M.; Gaunt, A. J.; Reilly, S. D.; Scott, B. L.; Tomson, N. C., A Linear *trans*-Bis(imido) Neptunium(V) Actinyl Analog: $Np^{V}(NDipp)_2(^{t}Bu_2bipy)_2Cl$ (Dipp = 2,6-$^{i}Pr_2C_6H_3$). *J. Am. Chem. Soc.* **2015,** *137* (30), 9583-9586.

122. Haskel, A.; Straub, T.; Eisen, M. S., Organoactinide-Catalyzed Intermolecular Hydroamination of Terminal Alkynes. *Organometallics* **1996,** *15* (18), 3773-3775.
123. Hayton, T. W.; Boncella, J. M.; Scott, B. L.; Palmer, P. D.; Batista, E. R.; Hay, P. J., Synthesis of imido analogs of the uranyl ion. *Science* **2005,** *310* (5756), 1941-1943.
124. King, D. M.; McMaster, J.; Tuna, F.; McInnes, E. J.; Lewis, W.; Blake, A. J.; Liddle, S. T., Synthesis and Characterization of an f-Block Terminal Parent Imido [U=NH] Complex: A Masked Uranium(IV) Nitride. *J. Am. Chem. Soc.* **2014,** *136* (15), 5619-5622.
125. Ren, W.; Zi, G.; Walter, M. D., Synthesis, Structure, and Reactivity of a Thorium Metallocene Containing a 2,2′-Bipyridyl Ligand. *Organometallics* **2012,** *31* (2), 672-679.
126. Jilek, R. E.; Spencer, L. P.; Lewis, R. A.; Scott, B. L.; Hayton, T. W.; Boncella, J. M., *J. Am. Chem. Soc.* **2012,** *134*, 9876.
127. Hayton, T. W.; Boncella, J. M.; Scott, B. L.; Batista, E. R., *J. Am. Chem. Soc.* **2006,** *128*, 12622.
128. Hayton, T. W.; Boncella, J. M.; Scott, B. L.; Batista, E. R.; Hay, P. J., *J. Am. Chem. Soc.* **2006,** *128*, 10549.
129. Spencer, L. P.; Schelter, E. J.; Yang, P.; Gdula, R. L.; Scott, B. L.; Thompson, J. D.; Kiplinger, J. L.; Batista, E. R.; Boncella, J. M., *Angew. Chem. Int. Ed.* **2009,** *121*, 3853.
130. Spencer, L. P.; Yang, P.; Scott, B. L.; Batista, E. R.; Boncella, J. M., *J. Am. Chem. Soc.* **2008,** *130*, 2930.
131. Jilek, R. E.; Spencer, L. P.; Kuiper, D. L.; Scott, B. L.; Williams, U. J.; Kikkawa, J. M.; Schelter, E. J.; Boncella, J. M., *Inorg. Chem.* **2011,** *50*, 4235.
132. Seaman, L. A.; Fortier, S.; Wu, G.; Hayton, T. W., *Inorg. Chem.* **2011,** *50*, 636.
133. Swartz II, D. L.; Spencer, L. P.; Scott, B. L.; Odom, A. L.; Boncella, J. M., *Dalton Trans.* **2010,** *39*, 6841.
134. Spencer, L. P.; Yang, P.; Scott, B. L.; Batista, E. R.; Boncella, J. M., *C. R. Chim.* **2010,** *13*, 758.
135. Evans, W. J.; Traina, C. A.; Ziller, J. W., *J. Am. Chem. Soc.* **2009,** *131*, 17473.
136. Lam, O. P.; Franke, S. M.; Nakai, H.; Heinemann, F. W.; Hieringer, W.; Meyer, K., *Inorg. Chem.* **2012,** *51* (6190).
137. Lam, O. P.; Heinemann, F. W.; Meyer, K., *C. R. Chim.* **2010,** *13*, 803.
138. Castro-Rodriguez, I.; Olsen, K.; Gantzel, P.; Meyer, K., *J. Am. Chem. Soc.* **2003,** *125*, 4565.
139. Castro-Rodriguez, I.; Meyer, K., *Chem. Commun.* **2006**, 1353.
140. Ren, W.; Zi, G.; Fang, D.-C.; Walter, M. D., *Chem. -Eur. J.* **2011,** *17*, 12669.
141. Straub, T.; Haskel, A.; Neyroud, T. G.; Kapon, M.; Botoshansky, M.; Eisen, M. S., *Organometallics* **2001,** *20*, 5017.
142. Matson, E. M.; Crestani, M. G.; Fanwick, P. E.; Bart, S. C., *Dalton Trans.* **2012,** *41*, 7952.
143. Evans, W. J.; Walensky, J. R.; Ziller, J. W.; Rheingold, A. L., *Organometallics* **2009,** *28*, 3350.
144. Brennan, J. G.; Andersen, R. A., *J. Am. Chem. Soc.* **1985,** *107*, 514.
145. Smiles, D. E.; Wu, G.; Hayton, T. W., Synthesis of Terminal Monochalcogenide and Dichalcogenide Complexes of Uranium Using Polychalcogenides, $[E_n]^{2-}$ (E = Te, n = 2; E = Se, n = 4), as Chalcogen Atom Transfer Reagents. *Inorg. Chem.* **2014,** *53* (19), 10240-10247.

146. Smiles, D. E.; Wu, G.; Hrobárik, P.; Hayton, T. W., Use of ^{77}Se and ^{125}Te NMR Spectroscopy to Probe Covalency of the Actinide-Chalcogen Bonding in $[Th(E_n)\{N(SiMe_3)_2\}_3]^-$ (E = Se, Te; *n* = 1, 2) and Their Oxo-Uranium(VI) Congeners. *J. Am. Chem. Soc.* **2016,** *138* (3), 814-825.
147. Smiles, D. E.; Wu, G.; Kaltsoyannis, N.; Hayton, T. W., Thorium–ligand multiple bonds *via* reductive deprotection of a trityl group. *Chem. Sci.* **2015,** *6* (7), 3891-3899.
148. Smiles, D. E.; Wu, G.; Hayton, T. W., Reactivity of $[U(CH_2SiMe_2NSiMe_3)(NR_2)_2]$ (R = $SiMe_3$) with elemental chalcogens: towards a better understanding of chalcogen atom transfer in the actinides. *New J. Chem.* **2015,** *39* (10), 7563-7566.
149. Brennan, J. G.; Andersen, R. A.; Zalkin, A., *Inorg. Chem.* **1986,** *25*, 1761.
150. Gaunt, A. J.; Scott, B. L.; Neu, M. P., *Inorg. Chem.* **2006,** *45*, 7401.
151. Avens, L. R.; Barnhart, D. M.; Burns, C. J.; McKee, S. D.; Smith, W. H., *Inorg. Chem.* **1994,** *33*, 4245.
152. Spencer, L. P.; Yang, P.; Scott, B. L.; Batista, E. R.; Boncella, J. M., *Inorg. Chem.* **2009,** *48*, 11615.
153. Lam, O. P.; Heinemann, F. W.; Meyer, K., *Chem. Sci.* **2011,** *2*, 1538.
154. Lam, O. P.; Franke, S. M.; Heinemann, F. W.; Meyer, K., *J. Am. Chem. Soc.* **2012,** *134*, 16877.
155. Brown, J. L.; Wu, G.; Hayton, T. W., *Organometallics* **2013,** *2013*, 1193.
156. Fortier, S.; Wu, G.; Hayton, T. W., Synthesis of a Nitrido-Substituted Analogue of the Uranyl Ion, $[N{=}U{=}O]^+$. *J. Am. Chem. Soc.* **2010,** *132* (20), 6888-9.
157. Fox, A. R.; Arnold, P. L.; Cummins, C. C., Uranium-Nitrogen Multiple Bonding: Isostructural Anionic, Neutral, and Cationic Uranium Nitride Complexes Featuring a Linear U=N=U Core. *J. Am. Chem. Soc.* **2010,** *132* (10), 3250-1.
158. King, D. M.; Liddle, S. T., Progress in molecular uranium-nitride chemistry. *Coord. Chem. Rev.* **2014,** *266-267*, 2-15.
159. King, D. M.; Tuna, F.; McInnes, E. J.; McMaster, J.; Lewis, W.; Blake, A. J.; Liddle, S. T., Synthesis and structure of a terminal uranium nitride complex. *Science* **2012,** *337* (6095), 717-720.
160. King, D. M.; Tuna, F.; McInnes, E. J. L.; McMaster, J.; Lewis, W.; Blake, A. J.; Liddle, S. T., Isolation and characterization of a uranium(VI)–nitride triple bond. *Nat. Chem.* **2013,** *5* (6), 482-488.
161. Mindiola, D. J.; Tsai, Y.-C.; Hara, R.; Chen, Q.; Meyer, K.; Cummins, C. C., *Chem. Commun.* **2001**, 125.
162. Fortier, S.; Wu, G.; Hayton, T. W., *Dalton Trans.* **2010,** *39*, 352.
163. Brown, J. L.; Fortier, S.; Lewis, R. A.; Wu, G.; Hayton, T. W., A Complete Family of Terminal Uranium Chalcogenides, [U(E)(N{SiMe3}2)3]− (E = O, S, Se, Te). *J. Am. Chem. Soc.* **2012,** *134* (37), 15468-15475.
164. Cantat, T.; Arliguie, T.; Noël, A.; Thuéry, P.; Ephritikhine, M.; Floch, P. L.; Mézailles, N., The U=C Double Bond: Synthesis and Study of Uranium Nucleophilic Carbene Complexes. *J. Am. Chem.Soc.* **2009,** *131* (3), 963-972.
165. Cramer, R. E.; Bruck, M. A.; Edelmann, F.; Afzal, D.; Gilje, J. W.; Schmidbaur, H., Synthesis and structure of $Cp_3U{=}CHPMe_3$: A compound with a U-C multiple bond. *Chem. Ber.* **1988,** *121* (3), 417-420.

166. Cramer, R. E.; Maynard, R. B.; Paw, J. C.; Gilje, J. W., A uranium-carbon multiple bond. Crystal and molecular structure of (η^5-$C_5H_5)_3UCHP(CH_3)_2(C_6H_5)$. *J. Am. Chem. Soc.* **1981,** *103* (12), 3589-3590.
167. Cramer, R. E.; Maynard, R. B.; Paw, J. C.; Gilje, J. W., Crystal and Molecular Structure of ($\eta^5C_5H_5)_3U$=$CHP(CH_3)_2(C_6H_5)$. A Compound with a Uranium-Carbon Multiple Bond. *Organometallics* **1983,** *2* (10), 1336-1340.
168. Fortier, S.; Walensky, J. R.; Wu, G.; Hayton, T. W., Synthesis of a Phosphorano-Stabilized U(IV)-Carbene via One-Electron Oxidation of a U(III)-Ylide Adduct. *J. Am. Chem. Soc.* **2011,** *133* (18), 6894-6897.
169. Ma, G.; Ferguson, M. J.; McDonald, R.; Cavell, R. G., Actinide Metals with Multiple Bonds to Carbon: Synthesis, Characterization, and Reactivity of U(IV) and Th(IV) Bis(iminophosphorano)methandiide Pincer Carbene Complexes. *Inorg. Chem.* **2011,** *50* (14), 6500-6508.
170. Ren, W.; Deng, X.; Zi, G.; Fang, D.-C., The Th=C double bond: an experimental and computational study of thorium poly-carbene complexes. *Dalton Trans.* **2011,** *40* (38), 9662-9664.
171. Tourneux, J.-C.; Berthet, J.-C.; Cantat, T.; Thuéry, P.; Mézailles, N.; Ephritikhine, M., Exploring the Uranyl Organometallic Chemistry: From Single to Double Uranium−Carbon Bonds. *J. Am. Chem. Soc.* **2011,** *133* (16), 6162-6165.
172. Tourneux, J.-C.; Berthet, J.-C.; Cantat, T.; Thuéry, P.; Mézailles, N.; Le Floch, P.; Ephritikhine, M., Uranium(IV) Nucleophilic Carbene Complexes. *Organometallics* **2011,** *30* (11), 2957-2971.
173. Ventelon, L.; Lescop, C.; Arliguie, T.; Leverd, P. C.; Lance, M.; Nierlich, M.; Ephritikhine, M., *Chem. Commun.* **1999**, 659.
174. Gardner, B. M.; Balázs, G.; Scheer, M.; Tuna, F.; McInnes, E. J. L.; McMaster, J.; Lewis, W.; Blake, A. J.; Liddle, S. T., *Angew. Chem. Int. Ed.* **2014,** *53*, 4484.
175. Smiles, D. E.; Wu, G.; Hayton, T. W., Synthesis, Electrochemistry, and Reactivity of the Actinide Trisulfides [K(18-crown-6)][An(η^3-$S_3)(NR_2)_3$] (An = U, Th; R = $SiMe_3$). *Inorg. Chem.* **2016,** *55* (18), 9150-9153.
176. Korobkov, I.; Gambarotta, S.; Yap, G. P. A., A Highly Reactive Uranium Complex Supported by the Calix[4]tetrapyrrole Tetraanion Affording Dinitrogen Cleavage, Solvent Deoxygenation, and Polysilanol Depolymerization. *Angew. Chem. Int. Ed.* **2002,** *41* (18), 3433-3436.
177. Chatelain, L.; Scopelliti, R.; Mazzanti, M., Synthesis and Structure of Nitride-Bridged Uranium(III) Complexes. *J. Am. Chem. Soc.* **2016,** *138* (6), 1784-1787.
178. Cleaves, P. A.; Kefalidis, C. E.; Gardner, B. M.; Tuna, F.; McInnes, E. J. L.; Lewis, W.; Maron, L.; Liddle, S. T., Terminal Uranium(V/VI) Nitride Activation of Carbon Dioxide and Carbon Disulfide: Factors Governing Diverse and Well-Defined Cleavage and Redox Reactions. *Chem. Eur. J.* **2017,** *23* (12), 2950-2959.
179. Cleaves, P. A.; King, D. M.; Kefalidis, C. E.; Maron, L.; Tuna, F.; McInnes, E. J. L.; McMaster, J.; Lewis, W.; Blake, A. J.; Liddle, S. T., Two-Electron Reductive Carbonylation of Terminal Uranium(V) and Uranium(VI) Nitrides to Cyanate by Carbon Monoxide. *Angew. Chem. Int. Ed.* **2014,** *53* (39), 10412-10415.
180. Evans, W. J.; Kozimor, S. A.; Ziller, J. W., Molecular Octa-Uranium Rings with Alternating Nitride and Azide Bridges. *Science* **2005,** *309* (5742), 1835.

181. Falcone, M.; Chatelain, L.; Mazzanti, M., Nucleophilic Reactivity of a Nitride-Bridged Diuranium(IV) Complex: CO_2 and CS_2 Functionalization. *Angew. Chem. Int. Ed.* **2016,** *55* (12), 4074-4078.
182. Falcone, M.; Chatelain, L.; Scopelliti, R.; Mazzanti, M., CO Cleavage and CO Functionalization under Mild Conditions by a Multimetallic CsU_2 Nitride Complex. *CHIMIA* **2017,** *71* (4), 209-212.
183. Falcone, M.; Chatelain, L.; Scopelliti, R.; Živković, I.; Mazzanti, M., Nitrogen reduction and functionalization by a multimetallic uranium nitride complex. *Nature* **2017,** *547*, 332.
184. Falcone, M.; Kefalidis, C. E.; Scopelliti, R.; Maron, L.; Mazzanti, M., Facile CO Cleavage by a Multimetallic CsU_2 Nitride Complex. *Angew. Chem. Int. Ed.* **2016,** *55* (40), 12290-12294.
185. Falcone, M.; Poon, L. N.; Fadaei Tirani, F.; Mazzanti, M., Reversible Dihydrogen Activation and Hydride Transfer by a Uranium Nitride Complex. *Angew. Chem. Int. Ed.* **2018,** *57* (14), 3697-3700.
186. King, D. M.; Cleaves, P. A.; Wooles, A. J.; Gardner, B. M.; Chilton, N. F.; Tuna, F.; Lewis, W.; McInnes, E. J. L.; Liddle, S. T., Molecular and electronic structure of terminal and alkali metal-capped uranium(V) nitride complexes. *Nat. Commun.* **2016,** *7*, 13773.
187. Du, J.; King, D. M.; Chatelain, L.; Lu, E.; Tuna, F.; McInnes, E. J. L.; Wooles, A. J.; Maron, L.; Liddle, S. T., Thorium- and uranium-azide reductions: a transient dithorium-nitride *versus* isolable diuranium-nitrides. *Chem. Sci.* **2019,** *10*, 3738-3745.
188. Green, D. W.; Reedy, G. T., Identification of matrix-isolated thorium nitride and the thorium-dinitrogen complex. *J. Mol. Spectrosc.* **1979,** *74* (3), 423-434.
189. Kushto, G. P.; Souter, P. F.; Andrews, L., An infrared spectroscopic and quasirelativistic theoretical study of the coordination and activation of dinitrogen by thorium and uranium atoms. *J. Chem. Phys.* **1998,** *108* (17), 7121-7130.
190. Vlaisavljevich, B.; Andrews, L.; Wang, X.; Gong, Y.; Kushto, G. P.; Bursten, B. E., Detection and Electronic Structure of Naked Actinide Complexes: Rhombic-Ring $(AnN)_2$ Molecules Stabilized by Delocalized π-Bonding. *J. Am. Chem. Soc.* **2016,** *138* (3), 893-905.
191. Su, W.; Pan, S.; Sun, X.; Wang, S.; Zhao, L.; Frenking, G.; Zhu, C., Double dative bond between divalent carbon(0) and uranium. *Nat. Commun.* **2018,** *9* (1), 4997.
192. Arnold, P. L.; Dutkiewicz, M. S.; Walter, O., Organometallic Neptunium Chemistry. *Chem. Rev.* **2017,** *117* (17), 11460-11475.
193. Jones, M. B.; Gaunt, A. J., Recent developments in synthesis and structural chemistry of nonaqueous actinide complexes. *Chem. Rev.* **2013,** *113* (2), 1137-1198.
194. Liddle, S. T., The Renaissance of Non-Aqueous Uranium Chemistry. *Angew. Chem. Int. Ed.* **2015,** *54* (30), 8604-8641.
195. Gaunt, A. J.; Reilly, S. D.; Enriquez, A. E.; Hayton, T. W.; Boncella, J. M.; Scott, B. L.; Neu, M. P., Low-Valent Molecular Plutonium Halide Complexes. *Inorg. Chem.* **2008,** *47* (18), 8412-8419.
196. Gaunt, A. J.; Reilly, S. D.; Hayton, T. W.; Scott, B. L.; Neu, M. P., An entry route into non-aqueous plutonyl coordination chemistry. *Chem. Commun.* **2007,** (16), 1659-1661.

197. Brown, J. L.; Gaunt, A. J.; King, D. M.; Liddle, S. T.; Reilly, S. D.; Scott, B. L.; Wooles, A. J., Neptunium and plutonium complexes with a sterically encumbered triamidoamine (TREN) scaffold. *Chem. Commun.* **2016,** *52* (31), 5428-5431.
198. Fichter, S.; Kaufmann, S.; Kaden, P.; Brunner, T. S.; Stumpf, T.; Roesky, P. W.; März, J., Enantiomerically Pure Tetravalent Neptunium Amidinates: Synthesis and Characterization. *Chem. Eur. J.* **2020,** *26* (41), 8867-8870.
199. Myers, A. J.; Tarlton, M. L.; Kelley, S. P.; Lukens, W. W.; Walensky, J. R., Synthesis and Utility of Neptunium(III) Hydrocarbyl Complex. *Angew. Chem. Int. Ed.* **2019,** *58* (42), 14891-14895.
200. Pattenaude, S. A.; Anderson, N. H.; Bart, S. C.; Gaunt, A. J.; Scott, B. L., Non-aqueous neptunium and plutonium redox behaviour in THF – access to a rare Np(III) synthetic precursor. *Chem. Commun.* **2018,** *54* (48), 6113-6116.
201. Reilly, S. D.; Brown, J. L.; Scott, B. L.; Gaunt, A. J., Synthesis and characterization of $NpCl_4(DME)_2$ and $PuCl_4(DME)_2$ neutral transuranic An(IV) starting materials. *Dalton Trans.* **2014,** *43* (4), 1498-1501.

Chapter 2. Cerium Photolysis

Portions of this work were published in:

Greggory T. Kent, Selena L. Staun, Guang Wu, and Trevor W. Hayton

Organometallics **2020**, *39*, 2375-2382

2.1 Introduction

While cerium *N*-heterocyclic carbene (NHC) complexes are now relatively common,[1-4] cerium complexes containing Schrock- or Fischer-type carbenes are essentially unknown. Likewise, cerium carbides and alkylidynes are also unknown. That said, some progress has been made toward the generation of Ce-C multiple bonds in recent years. For example, Liddle and co-workers have reported the synthesis of the cerium methanediide complexes, $[Ce(BIPM^{TMS})(ODipp)_2]$ (Scheme 2.1, **A**) and $[Ce(BIPM^{TMS})_2]$ (Scheme 2.1, **B**) ($BIPM^{TMS}$ = $[C(PPh_2NR)_2]^{2-}$, R = $SiMe_3$; Dipp = 2,6-diisopropylphenyl).[5-8] More recently, Zhu and co-workers ligated the carbodiphosphorane, $C(PPh_3)_2$, to Ce(III),[9, 10] forming $[BrCe(CDP)_2][BPh_4]_2$ (Scheme 2.1, **C**). DFT calculations revealed that the Ce-C bond in this complex consisted of a strong σ-interaction and a weak π-interaction.

Scheme 2.1. Previously reported complexes containing cerium-carbon multiple bonds. A, Ref. 5; B, Ref. 6; C, Ref. 9.

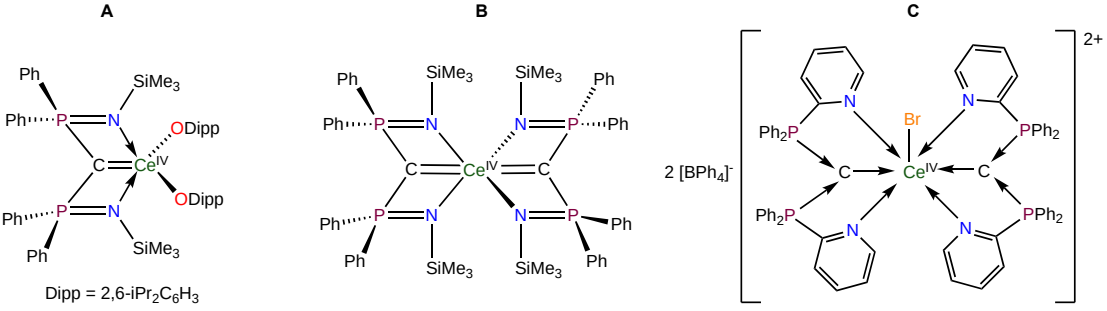

In the past few years, a number of carbon-atom transfers reagents have been identified, which could, in principle, be employed to generate an elusive Ce-C multiple bond. For example, Cummins and co-workers demonstrated that 7-isocyano-7-azadibenzonorbornadiene ($CN_2C_{14}H_{10}$) could be used in a C-atom transfer reaction to synthesize the ruthenium carbide complex, $[RuCl_2(C)(PCy_3)_2]$, *via* loss of N_2 and anthracene (Scheme 2.2a).[11] In addition, Smith and co-workers demonstrated that

bis(diisopropylamino)cyclopropenylidene (BAC) can transfer a carbon atom to the iron(IV) nitride, [{PhB(^{i}Pr$_2$Im)$_3$}Fe(N)] (^{i}Pr$_2$Im = 1,2-diisopropylimidazolylidene), resulting in formation of a cyanide complex concomitant with loss of bis(diisopropylamino)acetylene (Scheme 2.2b).[12]

Scheme 2.2. Previous examples of carbon-atom transfer.

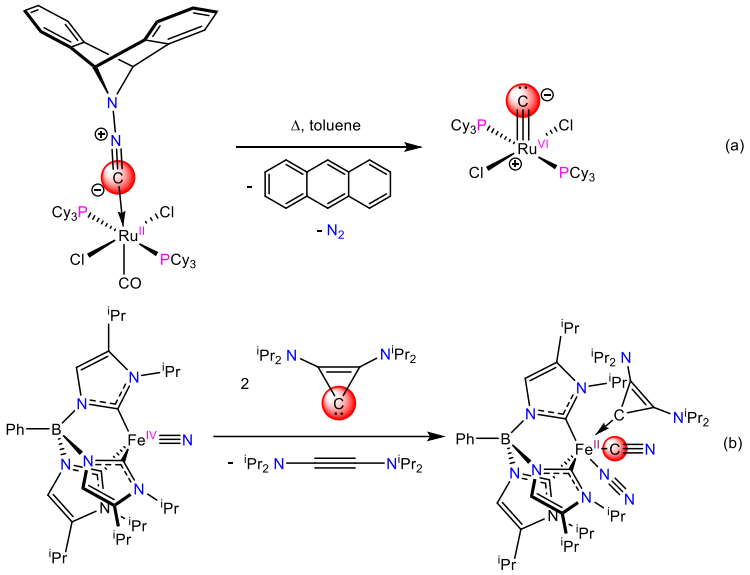

Generally speaking, the use of these carbon-atom transfer reagents requires a reducing metal complex to effect C-atom transfer.[12, 13] Cerium(III) is not usually considered to be a good reductant, as it prefers the 3+ oxidation state;[14, 15] however, it has recently been shown that photolysis of cerium(III) results in the generation of a substantially more reducing metal center.[16] For example, Schelter and co-workers reported that photolysis of [Ce(NR$_2$)$_3$] (R = SiMe$_3$) resulted in formation of a relatively long-lived excited state.[17, 18] This excited state species is strongly reducing, and can elicit homolytic cleavage of the C-Cl bond in PhCH$_2$Cl, resulting in formation of [Ce(Cl)(NR$_2$)$_3$] and bibenzyl (Scheme 2.3).[17]

Scheme 2.3. Reduction of $PhCH_2Cl$ through photolysis. Taken from Ref 17.

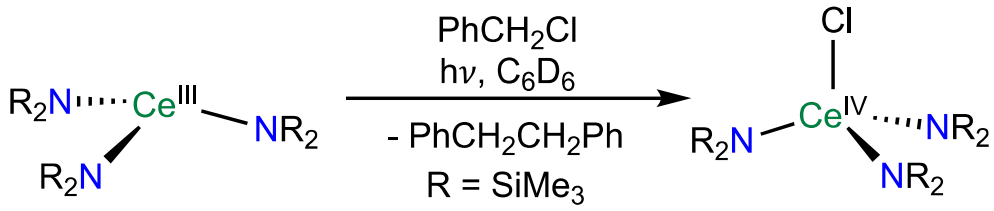

Since then, Ce(III) has been shown to facilitate a variety of photo-mediated transformations, including aryl coupling and borylation reactions.[18-21] In addition, our group reported that photolysis of a cerium nitrate complex, [Li(2,2,2-cryptand)][Ce(κ^2-O_2NO)(NR_2)$_3$], resulted in formation of the terminal Ce=O complex, [Li(2,2,2-cryptand)][Ce(O)(NR_2)$_3$], *via* formal loss of NO_2.[22] Motivated by these past results, I hypothesized that ligation of a carbon-atom transfer reagent to cerium(III), followed by photolysis, could induce either partial or complete carbon atom transfer and allow access to novel Ce(IV) organometallics.

Herein, I describe the ligation of the prospective carbon-atom transfer reagent, *N*-(isocyanoimine)triphenylphosphine ($CNNPPh_3$), a much more easily synthesized relative of 7-isocyano-7-azadibenzonorbornadiene, to the well-known Ce(III) tris(amide) complex, [Ce(NR_2)$_3$], along with an investigation of its photolytic chemistry. While carbon-atom transfer from $CNNPPh_3$ is nominally a $4e^-$ redox process,[11, 12] and each Ce(III) center can provide only one electron, I envisioned that cooperative reactivity of multiple Ce(III) centers could give rise to unique carbide-containing complexes or clusters.

2.2 Results and Discussion

2.2.1 Synthesis and Characterization of [$(NR_2)_3Ce(CNNPPh_3)$] (R = $SiMe_3$) (2.1)

Reaction of $CNNPPh_3$ with [$Ce(NR_2)_3$] (R = $SiMe_3$) in benzene-d_6 affords the Ce(III) isocyanoimine adduct, [$(NR_2)_3Ce(CNNPPh_3)$] (**2.1**), which can be isolated as pale yellow plates in 51% yield after work-up (Scheme 2.4). The ^{1}H NMR spectrum of the isolated material in benzene-d_6 features a broad resonance at -0.55 ppm, which is assignable to the $SiMe_3$ environment (Figure A2.2). In addition, resonances at 2.88, 5.43, and 6.00 ppm, are assignable to the *o*-, *m*-, and *p*-aryl protons of the three phenyl groups, respectively. The $^{31}P\{^1H\}$ NMR spectrum displays a sharp resonance at 8.59 ppm (Figure A2.3), which is shifted upfield from the signal observed for free $CNNPPh_3$ (25.7 ppm in benzene-d_6, Figure A2.14). Finally, **2.1** features a sharp ν_{CN} mode at 2117 cm^{-1} in its IR spectrum (Figure A2.15), which is substantially blue-shifted from that observed for the free ligand (ν_{CN} = 2067 cm^{-1}).[23]

Scheme 2.4. Synthesis of Ce(III) carbene complex **2.1**.

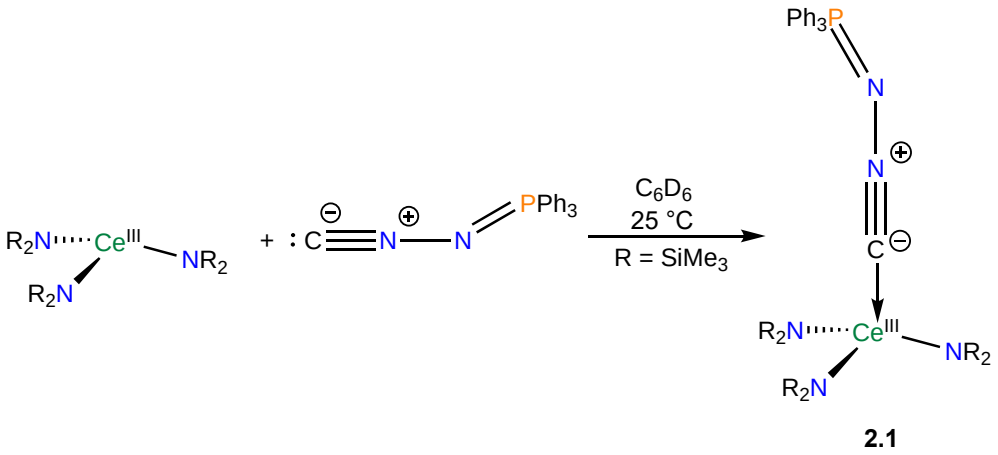

2.1

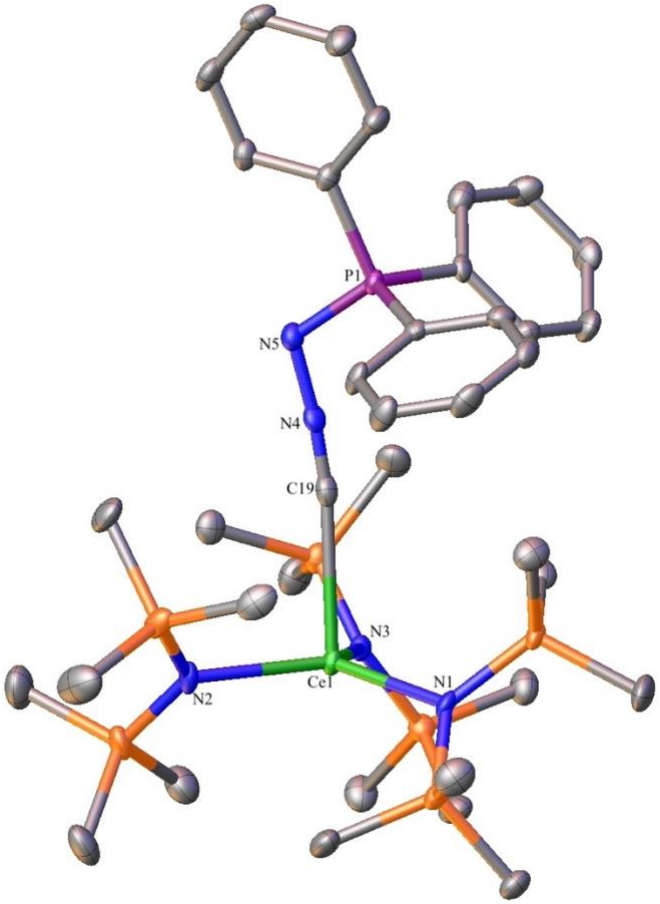

Figure 2.1. Solid-state molecular structure of **2.1**, shown with 50% probability ellipsoids. Hydrogen atoms removed for clarity. Selected bond lengths (Å) and angles (°): Ce1-N1 = 2.369(4), Ce1-N2 = 2.360(4), Ce1-N3 = 2.355(4), Ce1-C19 = 2.669(5), C19-N4 = 1.152(6), N4-N5 = 1.343(5), N5-P1 = 1.624(4), N1-Ce1-N2 = 116.7(1), N1-Ce1-N3 = 119.5(1), N2-Ce1-N3 = 121.1(1).

The connectivity of complex **2.1** was verified by X-ray crystallography (Figure 2.1). Complex **2.1** crystallizes in the triclinic space group *P*-1 and features a pseudo-tetrahedral geometry about the cerium center. Its Ce-N_{amide} distances (av. Ce-N = 2.36 Å) are consistent with the Ce-N distances reported for other Ce(III) amide complexes.[22, 24-27] Moreover, its Ce-C distance (Ce1-C19 = 2.669(5) Å) is slightly shorter than those seen in previously reported Ce(III)-isocyanide and Ce(III)-NHC complexes. For example, the Ce(III) isocyanide

complexes, [(CpMe)$_3$Ce(CN^{t}Bu)] and [Cp'$_3$Ce(CN^{t}Bu)] (Cp' = 1,3-(Me$_3$Si)$_2$C$_5$H$_3$) feature Ce-C bond lengths of 2.79(3) and 2.87(3) Å, respectively.[28] For further comparison, the Ce(III)-NHC complexes, [Cp*$_2$CeI(C$_3$Me$_4$N$_2$)] and [(C$_5$H$_4$^{t}Bu)$_3$Ce(C$_3$Me$_4$N$_2$)] feature Ce-C distances of 2.724(4) Å and 2.797(4) Å, respectively.[4] Finally, the C-N (1.152(6) Å) and N-N (1.343(5) Å) distances in **2.1** are similar to those observed in the free ligand (C-N = 1.153(4) Å; N-N = 1.345(4) Å),[29] as well as a previously isolated Cr(0) complex, [(OC)$_5$Cr(CNNPPh$_3$)] (C-N = 1.150(4) Å; N-N = 1.346(3) Å),[29] suggesting minimal disruption of the nitrilimine fragment upon coordination to Ce(III).

The UV-vis spectrum of **2.1** in Et$_2$O features a broad absorption at 397 nm (ε = 562 M^{-1}cm^{-1}) (Figure 2.2), and is similar to that reported for [Ce(NR$_2$)$_3$].[17] I have assigned the absorption to a metal-based 4f $\rightarrow$ 5d$_z^2$ transition, by analogy with the assignments reported for [Ce(NR$_2$)$_3$] and other CeX$_3$-type complexes.[20, 21, 30] For comparison, the 4f $\rightarrow$ 5d$_z^2$ and 4f $\rightarrow$ 5d$_{xz/yz}$ transitions for [Ce(NR$_2$)$_3$] occur at 413 nm and 341 nm, respectively. I attribute the *ca*. 16 nm blue shift observed for the 4f $\rightarrow$ 5d$_z^2$ transition in **2.1** to an increase in energy of the 5d$_z^2$ orbital due to electron donation by the CNNPPh$_3$ ligand.

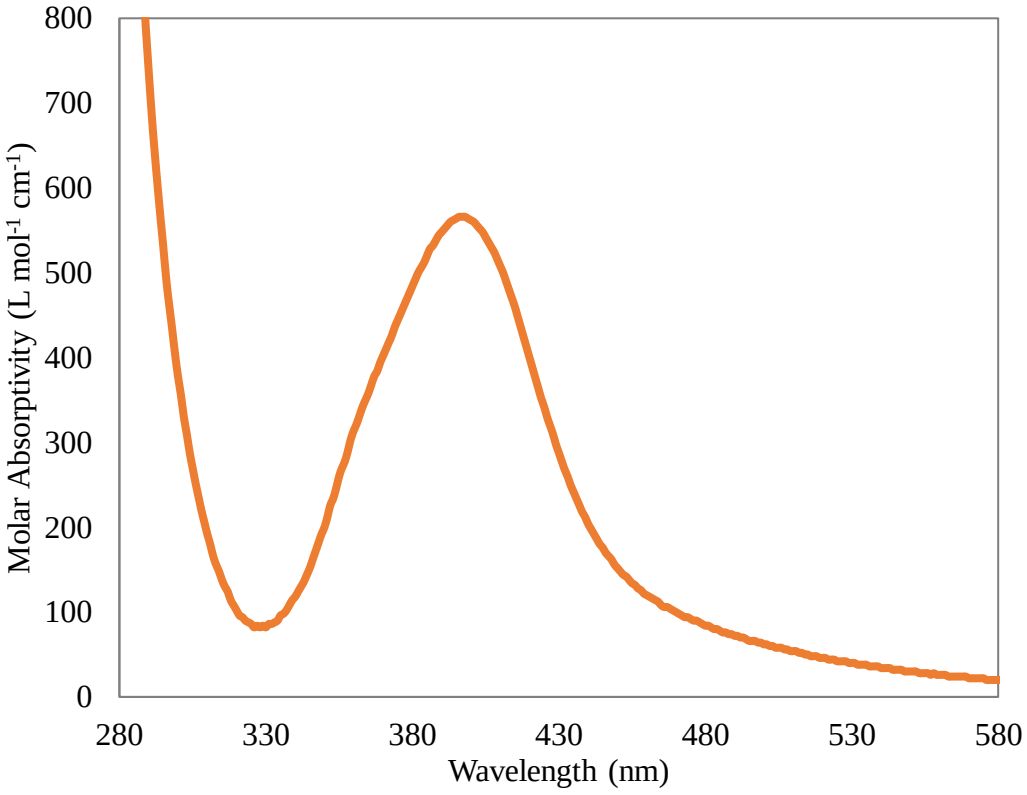

Figure 2.2. UV-vis spectra of complex **2.1** (0.31 mM, λ_{max} = 397 nm, ε = 562 L·mol^{-1}·cm^{-1}) in diethyl ether.

2.2.2 Synthesis and Characterization of [(NR$_2$)$_3$Ce(NCNPPh$_3$)] (2.2).

Given the similar optical properties of **2.1** and [Ce(NR$_2$)$_3$], I hypothesized that photolysis of **2.1** would also generate a highly reducing photo-excited state, which could initiate a C-atom or nitrilimine transfer to the Ce center. To this end, photolysis of a benzene-d_6 solution of **2.1** at 380 nm resulted in a very gradual color change from yellow to orange (eqn (2.1)). Complete conversion was achieved after 1 month of photolysis. A ^{1}H NMR spectrum of this sample revealed the presence of a new SiMe$_3$ resonance at -0.36 ppm, as well as new phenyl resonances at 3.11, 5.53, and 6.05 ppm, which correspond to the *o*-, *m*-, and *p*-aryl protons, respectively (Figure A2.4). These resonances as assignable to the carbodiimide complex,

[$(NR_2)_3Ce(NCNPPh_3)$] (**2.2**). Moreover, the $^{31}P\{^1H\}$ NMR spectrum of this sample features a new resonance at 7.26 ppm, which is assignable to complex **2.2**. Also present in this spectrum are minor resonances at -26.37 and 22.4 ppm, which are assignable to an unidentified product and free $CNNPPh_3$, respectively (Figure 2.4). In addition, I observe a minor resonance at -1.26 ppm, which I have tentatively assigned to the Ce(IV) phosphiniminato complex, [$(NR_2)Ce(NPPh_3)_3$] (**2.3**) (See **1.2.3** for more details).

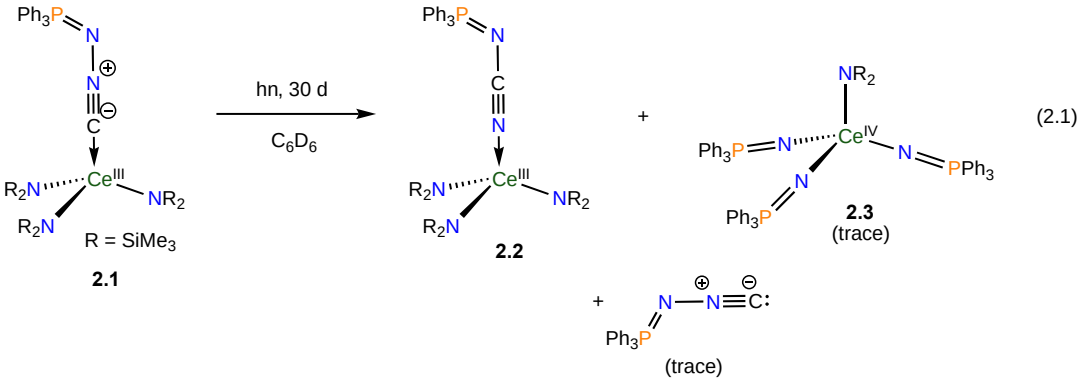

Work-up of the reaction mixture resulted in the isolation of pale-yellow blocks of **2.2**, which could be isolated in 52% crystalline yield. Complex **2.2** crystallizes in the triclinic space group *P*-1 and features a pseudo-tetrahedral geometry about the cerium center (Figure 2.3). The Ce-$N_{nitrile}$ distance (Ce1-N4 = 2.50(2) Å) in **2.2** is notably shorter that the Ce-C distance in **2.1**. This decrease likely reflects the greater electronegativity of nitrogen, which makes it a better donor to the highly electropositive Ce^{3+} center. For comparison, the Ce(III) benzonitrile complex, [$Ce\{CH(SiMe_3)_2\}_3(NCPh)$], features a Ce-N distance of 2.607(4) Å, while [$Cp^*_3Ce(NC^tBu)_2$] features an average Ce-N distance of 2.64 Å.[31, 32] The N-C (1.159(3) Å) and C-N (1.297(3) Å) distances in **2.2** are similar to those observed in the free ligand (N-C = 1.151(9) Å; C-N = 1.301(7) Å), as well as a previously isolated Pd(II) complex, [$PdCl_2(NCNPPh_3)_2$] (N-C = 1.151(4) Å; C-N = 1.292(4) Å).[33, 34] These values are indistinguishable from the N-C and N-N distances observed for **2.1**, demonstrating that X-ray

crystallography cannot be used to discriminate between the nitrilimine and carbodiimide fragments. However, the IR spectrum of **2.2** features intense ν_{CN} modes at 2150 cm^{-1} and 2177 cm^{-1} (Figures A2.16-A2.17). Their positions and relative intensities are consistent with those reported for other (*N*-cyanoimino)triphenylphosphine complexes.[29, 34]

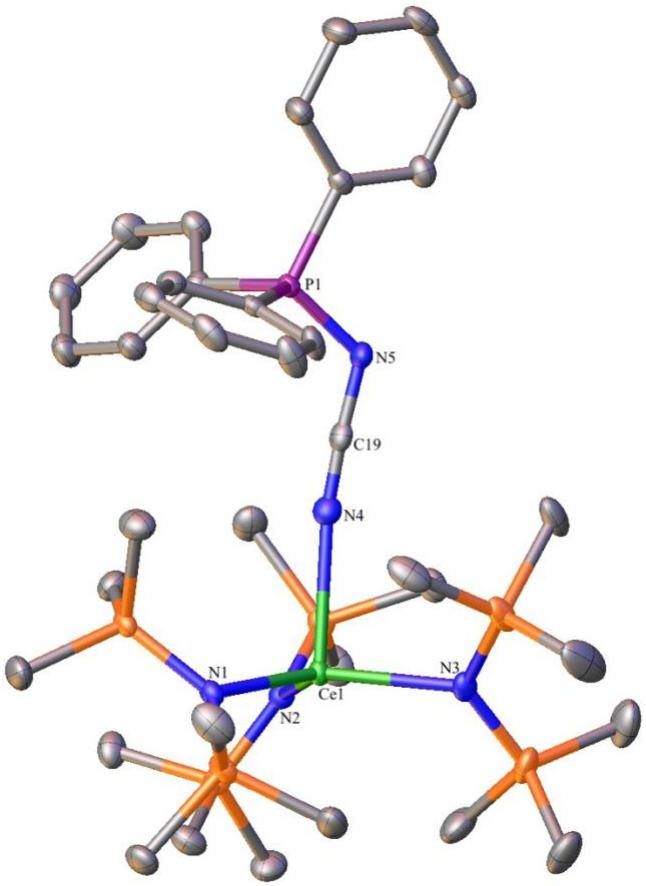

Figure 2.3. Solid-state molecular structure of **2.2**, shown with 50% probability ellipsoids. Hydrogen atoms removed for clarity. Selected bond lengths (Å) and angles (°): Ce1-N1 = 2.371(2), Ce1-N2 = 2.366(2), Ce1-N3 = 2.362(2), Ce1-N4 = 2.50(2), N4-C19 = 1.159(3), C19-N5 = 1.297(3), N5-P1 = 1.62(2), N1-Ce1-N2 = 118.69(6), N1-Ce1-N3 = 116.48(6), N2-Ce1-N3 = 120.14(6), N4-Ce1-N1 = 101.56(6), N4-Ce1-N2 = 96.76(6), N4-Ce1-N3 = 93.41(6).

Complex **2.2** can also be generated upon thermolysis of a C_6D_6 solution of **2.1** at 42 ºC for 3 d; however, under these conditions the reaction is not as selective. In particular, I observe the formation of increased amounts of complex **2.3**, according to the $^{31}P\{^1H\}$ NMR spectrum (Figure A2.9). Finally, control experiments reveal that free $CNNPPh_3$ is stable to both the photolytic and thermolytic conditions employed in this study (Figures A2.10-A2.13), demonstrating the need for Ce(III) to effect the isomerization. For comparison, both the photochemical and thermal isomerization of metal-bound nitrilimines are known,[29, 35-38] although there are only a few examples reported for the f-elements. In particular, Liddle and co-workers observed that the uranium nitrilimine complex, $[U(tren^{TMS})\{\mu\text{-}N(SiMe_3)NC\}]_2$ ($tren^{TMS}$ = $N(CH_2CH_2NSiMe_3)_3$], cleanly converted to the nitrile complex, $[U\{N(CH_2CH_2NSiMe_3)_2(\mu\text{-}CH_2CH_2NC{\equiv}N)\}\{N(SiMe_3)_2\}]_2$ upon photolysis.[39] Clearly, N-N bond cleavage and isomerization is the preferred route of reactivity for $CNNPPh_3$, unlike Cummins' 7-isocyano-7-azadibenzonorbornadiene, which likely has a substantially larger thermodynamic driving force for C-atom transfer.[11]

2.2.3 Synthesis and Characterization of $[(NR_2)Ce(NPPh_3)_3]$ (2.3).

In one instance, during an attempted crystallization of **2.2**, I also observed the deposition of a few yellow-orange blocks, which were subsequently identified as the Ce(IV) phosphiniminato complex, $[(NR_2)Ce(NPPh_3)_3]$ (**2.3**), by X-ray crystallography (Figure 2.4). Complex **2.3** crystallizes in the orthorhombic space group *P*bca and features a pseudo-tetrahedral geometry about the cerium center. The $Ce\text{-}N_{amide}$ distance is 2.39(2) Å, which is comparable with the $Ce\text{-}N_{amide}$ distances reported for other Ce amide complexes.[22, 24-27] Not surprisingly, the $Ce\text{-}N_{phosphiniminato}$ bonds in **2.3** are much shorter (av. Ce-N = 2.12 Å), reflecting the stronger donating ability of the phosphiniminato ligand. In addition, complex

2.3 features an average N-P distance of 1.57 Å. For comparison, the recently reported homoleptic Ce(IV) phosphiminato complex [Ce(NP(pip)$_3$)$_4$] (pip = piperidinyl, NC_5H_{10}) features average Ce-N and N-P distances of 2.20 Å and 1.42 Å, respectively.[40] Only a few crystals of complex **2.3** could be isolated, so it was not characterized further.

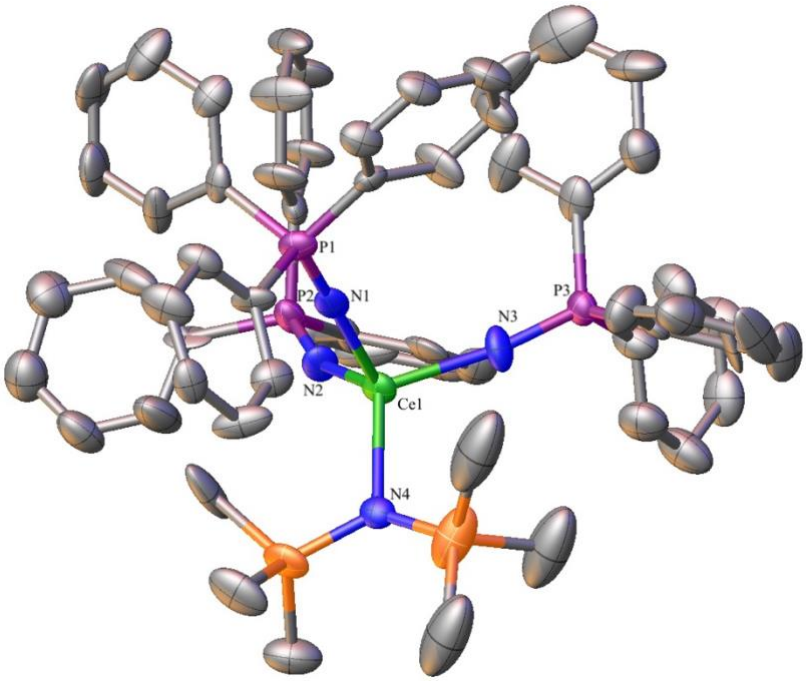

Figure 2.4. Solid-state molecular structure of **2.3**, shown with 50% probability ellipsoids. Hydrogen atoms removed for clarity. Selected bond lengths (Å) and angles (°): Ce1-N4 = 2.39(2), Ce-N1 = 2.131(16), Ce-N2 = 2.100(17), Ce-N3 = 2.120(16), N1-P1 = 1.582(17), N2-P2 = 1.564(16), N3-P3 = 1.552(17), N2-Ce-N4 = 125.9(6).

2.3 Summary

In summary, I have explored the coordination chemistry of [Ce(NR$_2$)$_3$] with the prospective C-atom transfer reagent, *N*-(isocyanoimine)triphenylphosphine (CNNPPh$_3$). Photolysis of the resulting adducts, [(NR$_2$)$_3$Ce(CNNPPh$_3$)] (**2.1**), does not result in the originally envisioned carbon-atom transfer, but instead results in ligand rearrangement,

namely, [$(NR_2)_3Ce(NCNPPh_3)$] (**2.2**), the product of nitrilimine rearrangement to its carbodiimide isomer. While ultimately unsuccessful in my efforts to generate a cerium carbide or carbene, this work expands the scope of Ce(III)-mediated photochemistry, which is an emerging area of photocatalysis.

2.4 Acknowledgements

This work was supported by the National Science Foundation (CHE 1764345). NMR spectra were collected on instruments supported by an NIH Shared Instrumentation Grant (SIG, 1S10OD012077-01A1). I would like to thank Greggory Kent (UCSB) for his collaboration on this work.

2.5 Experimental

2.5.1 General Methods

All reactions and subsequent manipulations were performed under anaerobic and anhydrous conditions under an atmosphere of nitrogen. Hexanes, Et_2O, and toluene were dried using a Vacuum Atmospheres DRI-SOLV Solvent Purification system and stored over 3Å sieves for 24 h prior to use. THF was dried by distillation from sodium/benzophenone, and stored over 3Å sieves for 24 h prior to use. Benzene-d_6 and THF-d_8 were dried over 3Å molecular sieves for 24 h prior to use. [$Ce(N(SiMe_3)_2)_3$] and $CNNPPh_3$ were synthesized according to the previously reported procedures.[22, 41] All other reagents were purchased from commercial suppliers and used as received.

NMR spectra were recorded on an Agilent Technologies 400-MR DD2 400 MHz Spectrometer or a Varian UNITY INOVA 500 spectrometer. ^{1}H NMR spectra were referenced to external tetramethylsilane (TMS) using the residual protio solvent peaks as internal

standards. $^{13}C\{^{1}H\}$ and $^{31}P\{^{1}H\}$ NMR spectra were referenced indirectly with the ^{1}H resonance of TMS at 0.0 ppm, according to IUPAC standard,[42, 43] using the residual solvent peaks as internal standards. Lumcrissy 12V flexible LED Lightstrips, emitting at 380 nm, and Waveform lighting 12V flexible LED Lighstrips, emitting at 365 nm, were used for photolyses. IR spectra were recorded on a Nicolet 6700 FT-IR spectrometer with a NXR FT Raman Module. Electronic absorption spectra were recorded on a Shimadzu UV3600 UV-NIR Spectrometer. Elemental analyses were performed by the Micro-Analytical Facility at the University of California, Berkeley.

2.5.2 Synthesis and Characterization of $[(NR_2)_3Ce(CNNPPh_3)]$ (2.1).

To a stirring, cold (-25 °C), deep yellow solution of $[Ce(N(SiMe_3)_2)_3]$ (218.3 mg, 0.351 mmol) in toluene (3 mL) was added a cold (-25 °C) orange solution of $CNNPPh_3$ (108.2 mg, 0.358 mmol) in toluene (3 mL). The reaction mixture was allowed to warm to room temperature with stirring. After 30 min, the volatiles were removed *in vacuo* to provide a brown orange solid. The solid was then extracted into diethyl ether (6 mL) and the resulting brown orange solution was filtered through a Celite column supported on glass wool (0.5 × 2 cm). The volatiles were then removed *in vacuo* to provide a gold powder. This solid was extracted into diethyl ether (6 mL) and the resulting yellow solution was filtered through a Celite column supported on glass wool (0.5 × 2 cm). The filtrate was concentrated *in vacuo* to 2 mL, layered with pentane (6 mL), and stored at -25 °C for 24 h, which resulted in the deposition of yellow plates. The solid was isolated by decanting the supernatant and then dried *in vacuo* to yield **2.1** as yellow plates (106.6 mg, 37 % yield). The supernatant was filtered through a Celite column supported on glass wool (0.5 × 2 cm). The filtrate was concentrated

in vacuo to 2 mL, layered with pentane (6 mL), and stored at -25 °C for 24 h. This resulted in the deposition of a second crop of yellow crystalline solid (62.7 mg). Total yield: 0.1693 g, 51% yield. Anal. Calcd for $C_{37}H_{69}CeN_5PSi_6$: C, 48.11; H, 7.53; N, 7.58. Found: C, 47.79; H, 7.46; N, 7.58. ^{1}H NMR (400 MHz, 25 °C, C_6D_6): δ -0.55 (s, 54H, SiC*H*$_3$), 2.88 (br s, 6H, *o*-C_6H_5), 5.43 (s, 6H, *m*-C_6H_5), 6.00 (s, 3H, *p*-C_6H_5). ^{31}P{^{1}H} NMR (162 MHz, 25 °C, C_6D_6): δ 8.59 (s, 1P). UV-Vis/NIR (Et_2O, 0.31 mM, 25 °C, L·mol^{-1}·cm^{-1}): 397 nm (ε = 562). IR (KBr pellet, cm^{-1}): 825 (m), 989 (s), 1117 (s, ν_{PN}), 1136 (m), 1146 (s), 1246 (s), 1439 (s), 1485 (s), 1591 (s), 1828 (w), 1901 (w), 1967 (w), 2117 (s, ν_{CN}), 2170 (w), 2181 (w), 2893 (s), 2951 (s), 3059 (m).

2.5.3 Synthesis and Characterization of [(NR$_2$)$_3$Ce(NCNPPh$_3$)] (2.2) and [(NR$_2$)Ce(NPPh$_3$)$_3$] (2.3).

An NMR tube fitted with a J-Young valve was charged with a dark-orange solution of **2.1** (83.8 mg, 0.091 mmol) in C_6D_6 (1 mL). ^{1}H and ^{31}P NMR spectrum were then recorded (Figures S6-S7). ^{1}H NMR (400 MHz, 25 °C, C_6D_6): δ -0.46 (s, 54H, SiC*H*$_3$), 2.98 (br s, 6H, *o*-C_6H_5), 5.47 (s, 6H, *m*-C_6H_5), 6.03 (s, 3H, *p*-C_6H_5). ^{31}P{^{1}H} NMR (162 MHz, 25 °C, C_6D_6): δ 8.84 (s, 1P). The NMR tube was then placed an aluminum foil-wrapped beaker with a 4 ft (0.7 W/ft) 380 nm LED strip lining the inside. The internal temperature of the beaker was determined to be 32 °C during photolysis. The photolysis was monitored intermittently by ^{1}H and ^{31}P NMR spectroscopy. After 32 d, the reaction had achieved 99% conversion, according to the ^{31}P{^{1}H} NMR spectrum. ^{31}P{^{1}H} NMR (162 MHz, 25 °C, C_6D_6): δ 22.4 (s, 1P, CNNPPh$_3$) 7.26 (s, 1P, **2.2**), -1.26 (s, 3P, **2.3**), -26.37 (s, unknown). The NMR tube was brought back into the box, where the solution was transferred to a 20 mL scintillation vial and the volatiles were removed *in vacuo* to afford a dark orange solid. The solid was then extracted

into pentane (3 mL) and the resulting orange suspension was filtered through a Celite column supported on glass wool (0.5 × 2 cm). The filtrate was transferred to a 4 mL vial, which was placed inside a 20 mL scintillation vial and iso-octane (2 mL) was added to the outer vial. Storage of this two-vial system at -25 °C for 24 h resulted in the deposition of a pale orange crystalline needles. The solid was isolated by decanting the supernatant and then dried *in vacuo* to yield **2.2** (32.0 mg, 38 % yield). The supernatant was transferred to a new 4 mL vial, which was placed inside a 20 mL scintillation vial and iso-octane (2 mL) was added to the outer vial. Storage of this two-vial system at -25 °C for 24 h resulted in the deposition of more pale orange crystals of **2.2** (11.3 mg, 14% yield). Total yield: 0.0433 g, 52% yield. In one instance, a few crystals of [$(NR_2)Ce(NPPh_3)_3$] (**2.3**) were also isolated from the reaction mixture, but this material could not be fully characterized. Anal. Calcd for $C_{37}H_{69}CeN_5PSi_6$: C, 48.11; H, 7.53; N, 7.58. Found: C, 48.22; H, 7.61; N, 7.59. ^{1}H NMR (400 MHz, 25 °C, C_6D_6): δ -0.36 (s, 54H, SiC*H*$_3$), 3.11 (br s, 6H, *o*-C$_6$*H*$_5$), 5.53 (s, 6H, *m*-C$_6$*H*$_5$), 6.05 (s, 3H, *p*-C$_6$*H*$_5$). ^{31}P{^{1}H} NMR (162 MHz, 25 °C, C_6D_6): δ 7.26 (s, 1P). IR (KBr pellet, cm^{-1}): 1003 (m), 1119 (s), 1240 (m), 1319 (m), 1439 (s), 1485 (s), 1591 (s), 1666 (m), 1774 (m), 1821 (m), 1901(m), 1971 (m), 2150 (m, ν_{NC}), 2177 (m, ν_{NC}), 2891 (w), 2941 (w), 2985 (s), 3498 (w), 3629 (m), 3697 (m), 3761 (m).

2.5.4 Thermolysis of [$(NR_2)_3Ce(CNNPPh_3)$] (2.1).

An NMR tube fitted with a J-Young valve was charged with a dark-orange solution of **2.1** (12.1 mg, 0.013 mmol) in C_6D_6 (1 mL). ^{1}H and ^{31}P NMR spectra was then recorded (Figures A2.8-A2.9). ^{1}H NMR (400 MHz, 25 °C, C_6D_6): δ -0.46 (s, 54H, SiC*H*$_3$), 2.98 (br s, 6H, *o*-C$_6$*H*$_5$), 5.47 (s, 6H, *m*-C$_6$*H*$_5$), 6.03 (s, 3H, *p*-C$_6$*H*$_5$). ^{31}P{^{1}H} NMR (162 MHz, 25 °C, C_6D_6): δ 8.84 (s, 1P). The NMR tube was then placed in an oil bath at 42 °C and heated for 72 h,

whereupon the ^{1}H and ^{31}P{^{1}H} NMR spectra were re-recorded. This spectrum revealed trace amounts of **2.1**, along with formation of complexes **2.2** and **2.3**, in a 5:1 ratio, respectively, as determined *via* integration of the ^{1}H NMR spectrum. ^{1}H NMR (400 MHz, 25 °C, C_6D_6): δ -0.36 (s, 54H, SiC*H*$_3$, **2.2**), 0.38 (s, 18H, N(SiC*H*$_3$)$_2$, **2.3**), 3.11 (br s, 6H, *o*-C$_6$*H*$_5$, **2.2**), 5.53 (s, 6H, *m*-C$_6$*H*$_5$, **2.2**), 6.05 (s, 3H, *p*-C$_6$*H*$_5$, **2.2**), 7.00-7.07 (m, 27H *m*, *p*-C$_6$*H*$_5$, **2.3**), 7.70-7.77 (m, 18H *o*-C$_6$*H*$_5$, **2.3**). ^{31}P{^{1}H} NMR (162 MHz, 25 °C, C_6D_6): δ 7.26 (s, 1P, **2.2**), -1.30 (s, 3P, **2.3**).

2.5.5 Photolysis of CNNPPh$_3$.

An NMR tube fitted with a J-Young valve was charged with a dark-orange solution of CNNPPh$_3$ (8.0 mg, 0.026 mmol) in THF-d_8 (1 mL). ^{1}H and ^{31}P NMR spectra were then recorded (Figures A2.10-A2.11). ^{1}H NMR (400 MHz, 25 °C, C_6D_6): δ 7.5-7.75 (m, 15H, P(C$_6$*H*$_5$)$_3$). ^{31}P{^{1}H} NMR (162 MHz, 25 °C, C_6D_6): δ 25.14 (s, 1P). The NMR tube was then placed in an aluminum foil-wrapped beaker with a 4 ft (0.7 W/ft) 380 nm LED strip lining the inside. After 5 d, the ^{1}H and ^{31}P NMR spectra were rerecorded, which revealed no change to the sample.

2.5.6 Thermolysis of CNNPPh$_3$.

An NMR tube fitted with a J-Young valve was charged with a dark-orange solution of CNNPPh$_3$ (8.0 mg, 0.026 mmol) in THF-d_8 (1 mL). ^{1}H and ^{31}P NMR spectra were then recorded (Figures A2.12-A2.13). ^{1}H NMR (400 MHz, 25 °C, C_6D_6): δ 7.5-7.75 (m, 15H, P(C$_6$*H*$_5$)$_3$). ^{31}P{^{1}H} NMR (162 MHz, 25 °C, C_6D_6): δ 25.14 (s, 1P). The NMR tube was then heated to 42 °C. After 48 h, the ^{1}H and ^{31}P NMR spectra were rerecorded, which revealed no change to the sample.

2.5.7 X-ray Crystallography

Data for **2.1**, **2.2**, and **2.3** were collected on a Bruker KAPPA APEX II diffractometer equipped with an APEX II CCD detector using a TRIUMPH monochromator with a Mo Kα X-ray source (α = 0.71073 Å). The crystals were mounted on a cryoloop under Paratone-N oil. Complexes **2.1** and **2.2** were collected at 100(2) K, **2.3** was collected at 110(2) K, using an Oxford nitrogen gas cryostream. Data were collected using ω scans with 0.5° frame widths. Frame exposures of 15, 10, and 5 seconds were used for **2.1**, **2.2**, and **2.3**, respectively. Data collection and cell parameter determinations were conducted using the SMART program.[44] Integration of the data frames and final cell parameter refinements were performed using SAINT software.[45] Absorption corrections of the data were carried out using the multi-scan method SADABS for **2.1**-**2.3**.[46] Subsequent calculations were carried out using SHELXTL.[47] Structure determination was done using direct or Patterson methods and difference Fourier techniques. All hydrogen atom positions were idealized, and rode on the atom of attachment. Structure solution, refinement, graphics, and creation of publication materials were performed using SHELXTL.[47] Further crystallographic details can be found in Table 2.1. Complexes **2.1**-**2.3** have been deposited in the Cambridge Structural Database (**1**: CCDC 1991069; **2.2**: 1991071; **2.3**: 1991072).

Table 2.1. X-ray Crystallographic Data for **2.1**, **2.2**, and **2.3**.

	2.1	**2.2**	**2.3**
empirical formula	$C_{37}H_{69}CeN_5PSi_6$	$C_{37}H_{69}CeN_5PSi_6$	$C_{60}H_{63}CeN_4P_3Si_2$
crystal habit, color	Plate, Pale yellow	Block, Pale yellow	Block, Orange
crystal size (mm)	0.25 × 0.2 × 0.1	0.3 × 0.3 × 0.1	0.25 × 0.2 × 0.1
space group	$P\bar{1}$	$P\bar{1}$	*P*bca
volume ($Å^3$)	2493.0(18)	2504.6(9)	11120(6)
a (Å)	11.908(5)	11.907(3)	21.131(7)
b (Å)	13.968(6)	14.022(3)	20.920(7)
c (Å)	16.134(7)	16.150(3)	25.156(7)
α (deg)	68.410(9)	68.391(5)	90
β (deg)	87.750(10)	87.591(5)	90
γ (deg)	88.219(10)	88.340(5)	90
Z	2	2	8
formula weight (g/mol)	923.60	923.60	1129.35
density (calculated) (Mg/m^3)	1.230	1.225	1.349
absorption coefficient (mm^{-1})	1.118	1.113	0.990
F_{000}	966	966	4656
total no. reflections	11219	27479	42603
unique reflections	7763	11065	9433
Final R Indices ($I > 2\sigma(I)$]	$R_1 = 0.0415$ $wR_2 = 0.0881$	$R_1 = 0.0268$ $wR_2 = 0.0620$	$R_1 = 0.1287$ $wR_2 = 0.2940$
largest diff. peak and hole ($e^- A^{-3}$)	1.023 and -0.901	0.656 and -0.355	3.477 and -1.422
GOF	1.006	1.038	1.146

2.6 Appendix

2.6.1 Synthesis and Characterization of $(PPh_3N)(NR_2)_2UCNU(NR_2)_3$ (2.4) and $(Ph_3PN)(NR_2)_2UCN\mu NCU(NR_2)_2(NPPh_3)$ (R = $SiMe_3$) (2.5)

Similar to the synthesis of the Ce(III) isocyanoimine adduct, $[(NR_2)_3Ce(CNNPPh_3)]$ (**2.1**), an analogous uranium complex was sought after. Thus, reaction of 0.5 equiv of CNNPPh3 with uranium tris(amide), in THF, affords the uranium phosphiniminato complex $(PPh_3N)(NR_2)_2UCNU(NR_2)_3$ (**2.4**) as dark green plates in 5% yield (Scheme A2.1). However, when the reaction was done in toluene, the uranium(IV) phosphiniminato dimer $(Ph_3PN)(NR_2)_2UCN\mu NCU(NR_2)_2(NPPh_3)$ (**2.5**) was isolated as brown needles in 2% yield (Scheme A2.1). Complete characterization of these species was not done due to low yields and inadequate reproducibility and is only included here for completeness.

Scheme A2.1. Synthesis of **2.4** and **2.5**.

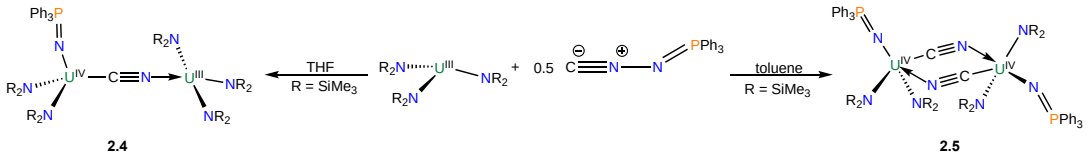

The proposed mechanism of **2.4** begins with homolytic bond cleavage of the N-N bond, then oxidative addition to a uranium(V) trigonal bipyramidal intermediate that is bulky and unstable, where unreacted uranium tris(amide) reacts with the intermediate and forms **2.4** with one equiv of amine radical (Scheme A2.2).

Scheme A2.2. Proposed mechanism to **2.4.**

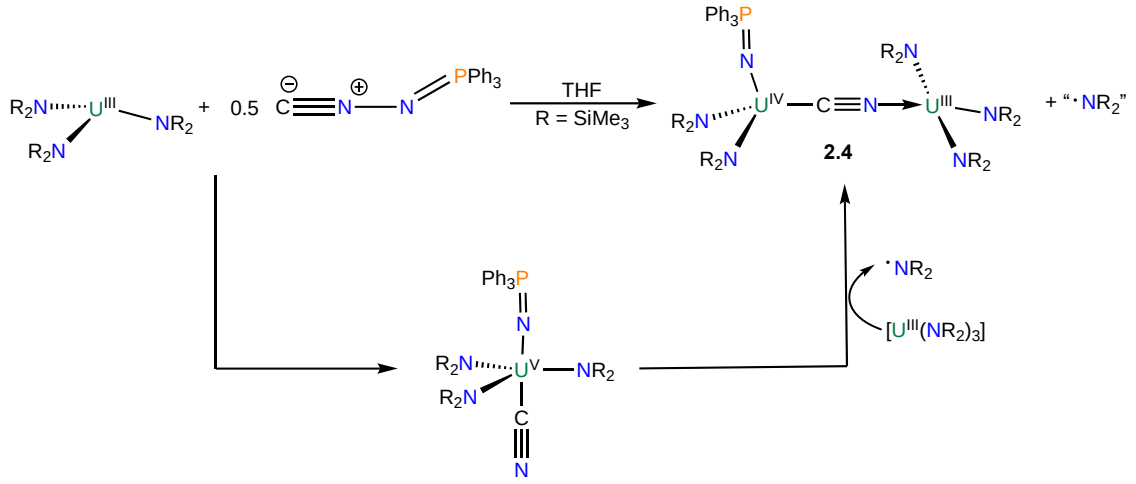

Similarly, when this reaction is done in toluene, homolytic bond cleavage of the N-N bond happens, then oxidative addition to an unstable and bulky uranium(V) trigonal bipyramidal intermediate, where the uranium complex dimerizes into **2.5** with 2 equiv of amine radical (Scheme A2.3).

Scheme A2.3 Proposed mechanism to **2.5**.

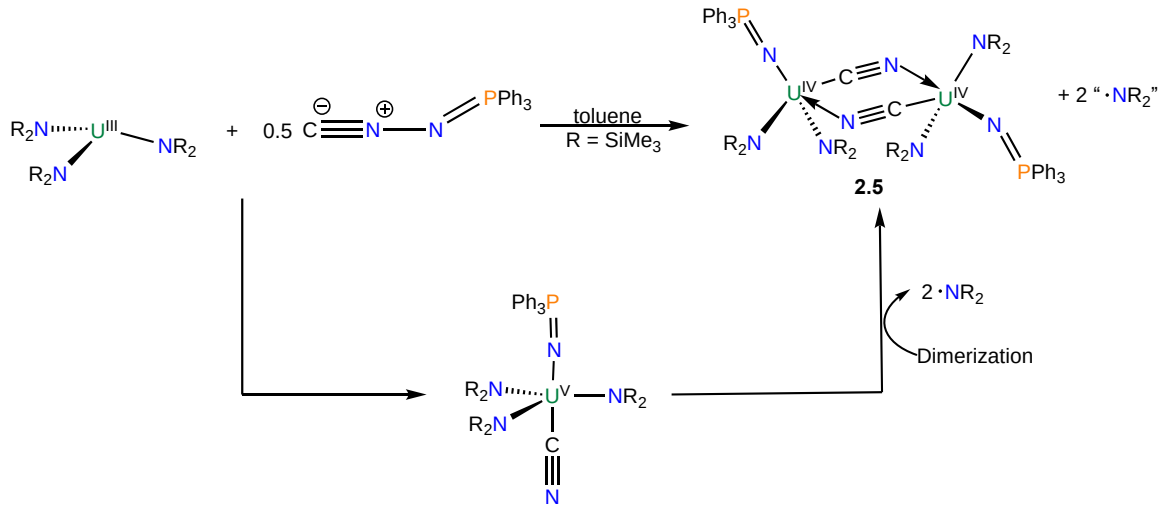

Both $(PPh_3N)(NR_2)_2UCNU(NR_2)_3$ (**2.4**) and $(Ph_3PN)(NR_2)_2UCN\mu NCU(NR_2)_2(NPPh_3)$ (**2.5**) crystallize in the monoclinic space group P21/n (Figure A2.1). Most interestingly are the rare imido-like bonds found in **2.4** (U2-N7) and **2.5** (U1-N4) with the short bond length of

2.056(10) Å and 2.100(4) Å, respectively. Both complexes also feature a C-N functional group that bridges the uranium metal centers, where C49-N8 (1.143(15) Å) found in **2.4** is slightly longer than the C-N bonds bridging the dimer of **2.5**, N2-C13 (1.139(7) Å). It should be noted that atoms C49 and N8 are in a 50:50 position and can be interchanged.

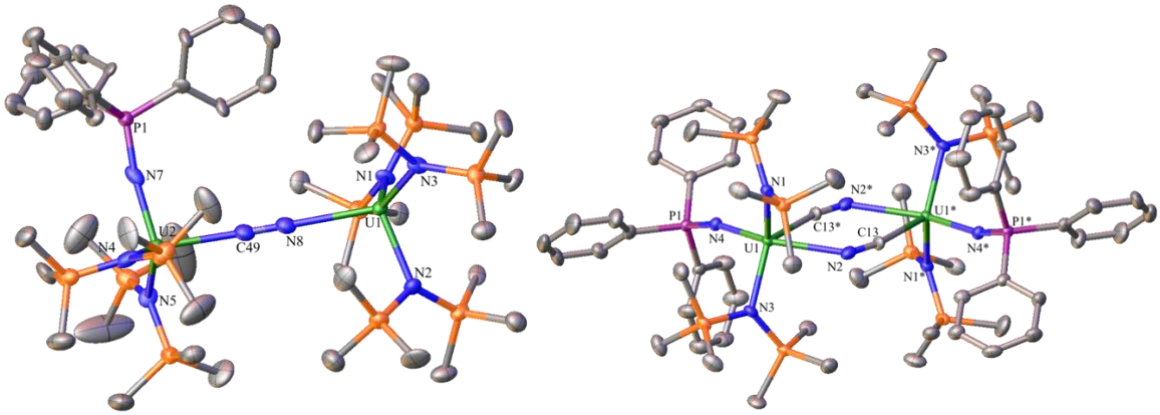

Figure A2.1. Solid-state molecular structures of **2.4** (left) and **2.5** (right), shown with 50% probability ellipsoids. Hydrogen atoms removed for clarity. Selected bond lengths (Å) and angles (°) of 2.4: U1-N8 = 2.614(12), C49-N8 = 1.143(15), U-$N_{silylsmido}$ (av.) = 2.354, U2-N7 = 2.056(10), N7-P1 = 1.575(10), C49-N8-U1 = 176.8(10). Selected bond lengths (Å) and angles (°) of 2.5: N2-C13 = 1.139(7), U1-N2 = 2.578(5), U-$N_{silylsmido}$ (av.) = 2.268, U1-N4 = 2.100(4), N4-P1 = 1.564(4), C13-U1-N2 = 70.32(16).

X-ray Crystallography

Data for **2.4**, and **2.5** were collected on a Bruker KAPPA APEX II diffractometer equipped with an APEX II CCD detector using a TRIUMPH monochromator with a Mo Kα X-ray source (α = 0.71073 Å). The crystals were mounted on a cryoloop under Paratone-N oil. Complex **2.5** was collected at 100(2) K and **2.4** was collected at 109(2) K, using an Oxford nitrogen gas cryostream. Data were collected using ω scans with 0.5° frame widths. Frame exposures of 10, 2, and 5 seconds were used for **2.4** and **2.5** respectively. Data collection and cell parameter determinations were conducted using the SMART program.[44] Integration of the data frames and final cell parameter refinements were performed using SAINT software.[45] Absorption corrections of the data were carried out using the multi-scan method SADABS for **2.4**-**2.5**.[46] Subsequent calculations were carried out using SHELXTL.[47] Structure determination was done using direct or Patterson methods and difference Fourier techniques. All hydrogen atom positions were idealized, and rode on the atom of attachment. Structure solution, refinement, graphics, and creation of publication materials were performed using SHELXTL.[47] Further crystallographic details can be found in Table A2.1.

Table A2.1. X-ray Crystallographic Data for **2.4** and **2.5**.

	2.4	**2.5**
empirical formula	$C_{49}H_{105}U_2N_7PSi_{10}$	$C_{67}H_{114}U_2N_8P_2Si_8$
crystal habit, color	Plate, Dark green	Needle, Brown
crystal size (mm)	0.25 × 0.2 × 0.1	0.25 × 0.25 × 0.15
space group	*P21/n*	*P21/n*
volume ($Å^3$)	7039(2)	4164.8(14)
a (Å)	20.396(3)	11.877(2)
b (Å)	12.178(3)	18.774(3)
c (Å)	28.787(7)	18.934(4)
α (deg)	90	90
β (deg)	100.102(12)	99.449(4)
γ (deg)	90	90
Z	4	2
formula weight (g/mol)	1580.32	1794.38
density (calculated) (Mg/m^3)	1.491	1.431
absorption coefficient (mm^{-1})	4.823	4.077
F_{000}	28528	18358
total no. reflections	11219	27479
unique reflections	13025	9182
Final R Indices	$R_1 = 0.0674$	$R_1 = 0.0408$
($I > 2\sigma(I)$]	$wR_2 = 0.1261$	$wR_2 = 0.0956$
largest diff. peak and hole ($e^- A^{-3}$)	2.981 and -2.462	5.771 and -1.160
GOF	1.003	1.026

2.6.2 NMR Spectra

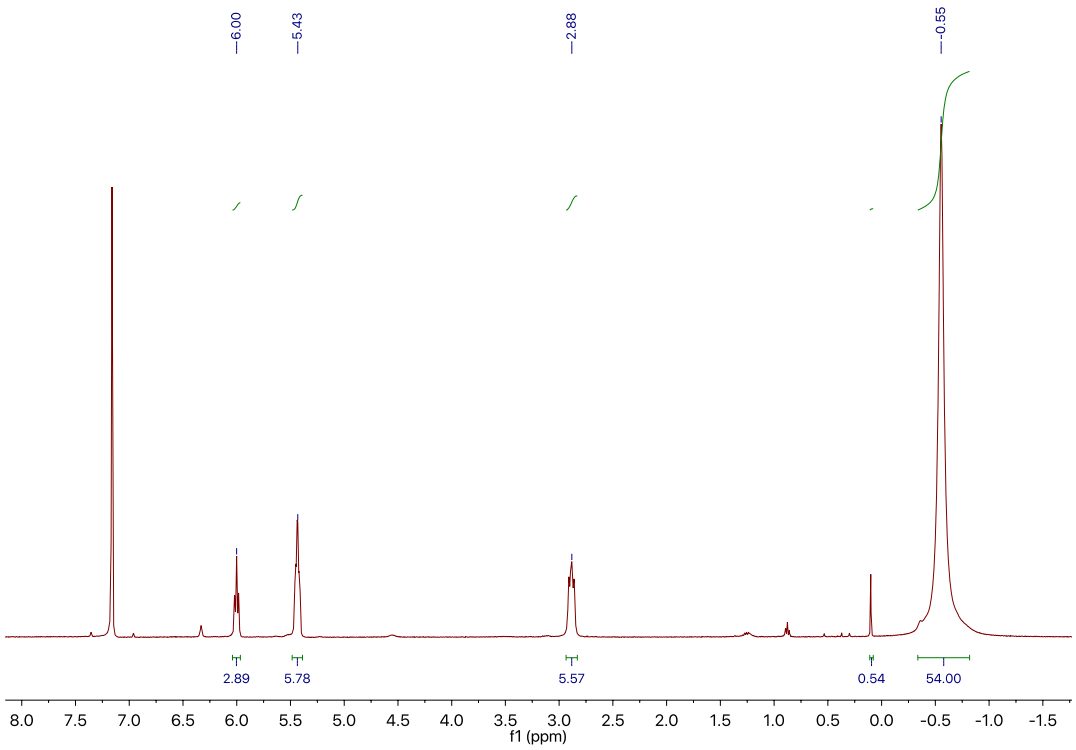

Figure A2.2. ^{1}H NMR spectrum of $[(NR_2)_3Ce(CNNPPh_3)]$ (**2.1**) in C_6D_6.

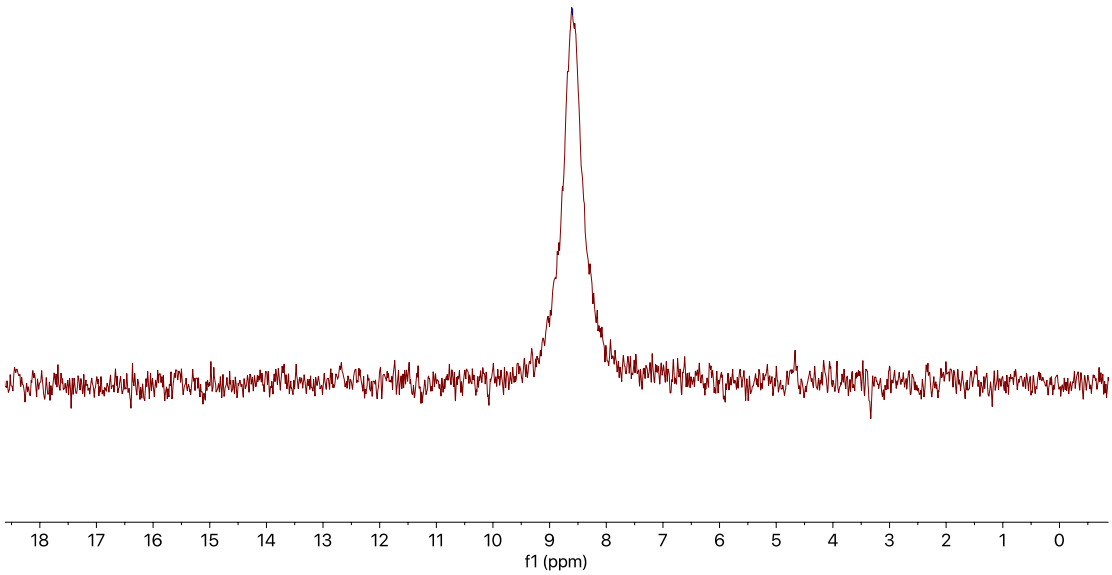

Figure A2.3. $^{31}P\{^{1}H\}$ NMR spectrum of $[(NR_2)_3Ce(CNNPPh_3)]$ (**2.1**) in C_6D_6.

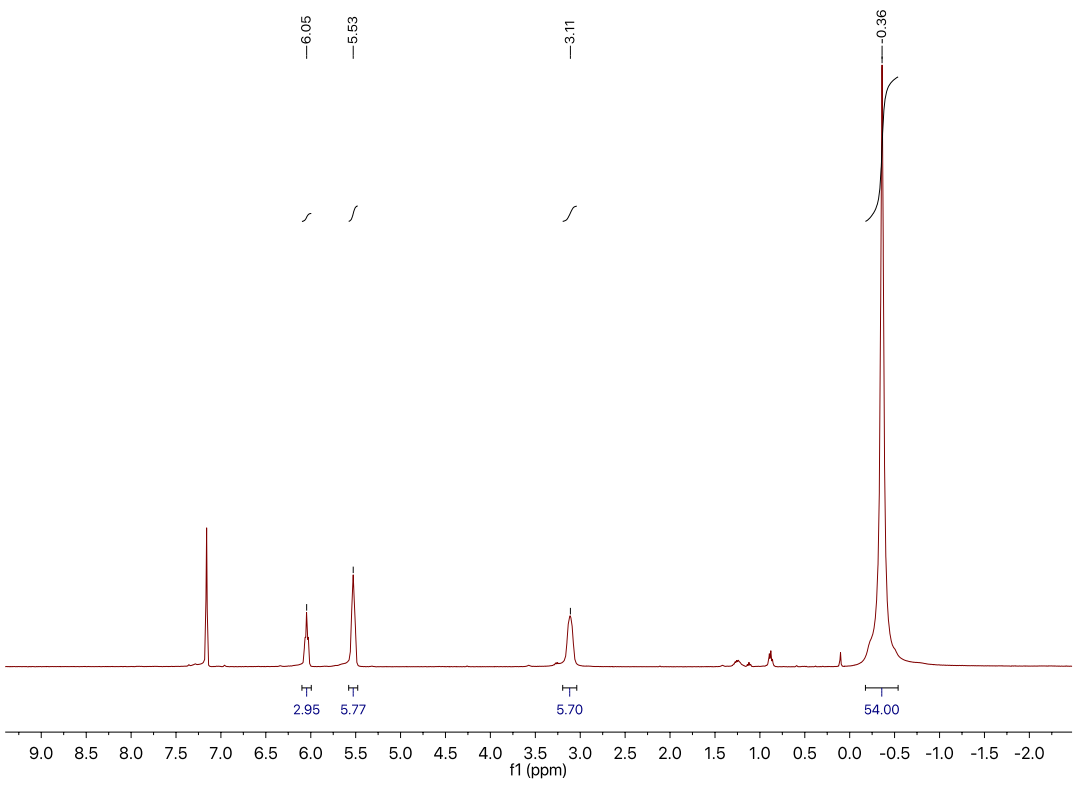

Figure A2.4. ^{1}H NMR spectrum of $[(NR_2)_3Ce(NCNPPh_3)]$ (**2.2**) in C_6D_6.

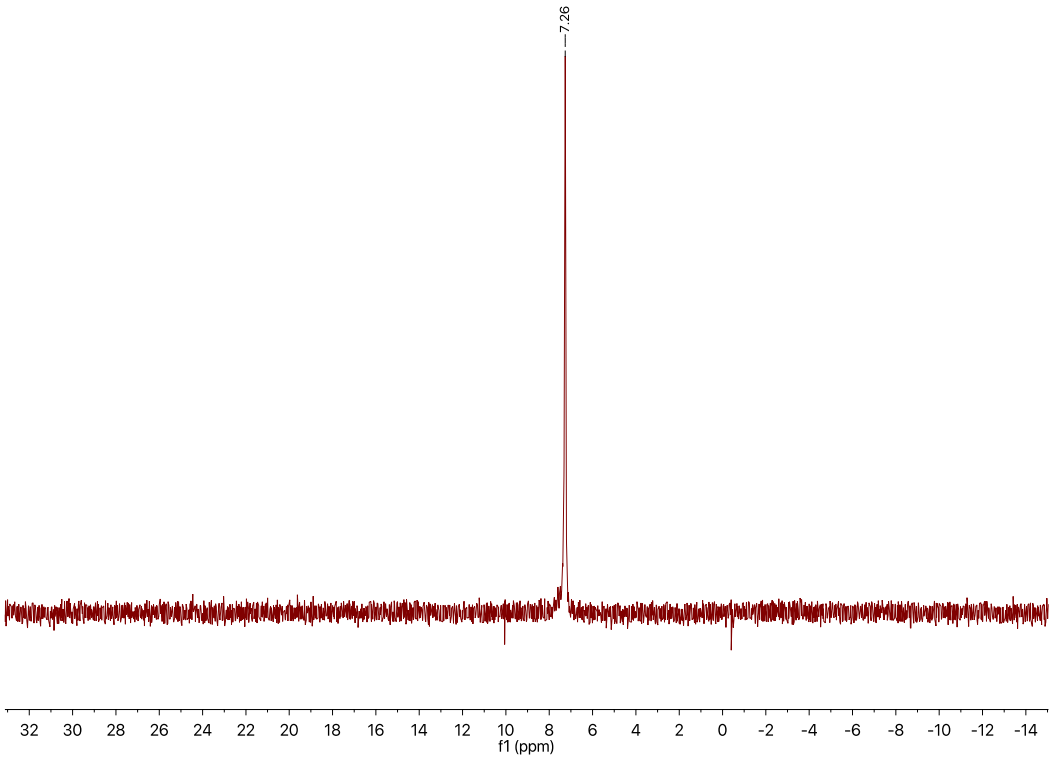

Figure A2.5. $^{31}P\{^{1}H\}$ NMR spectrum of $[(NR_2)_3Ce(NCNPPh_3)]$ (**2.2**) in C_6D_6.

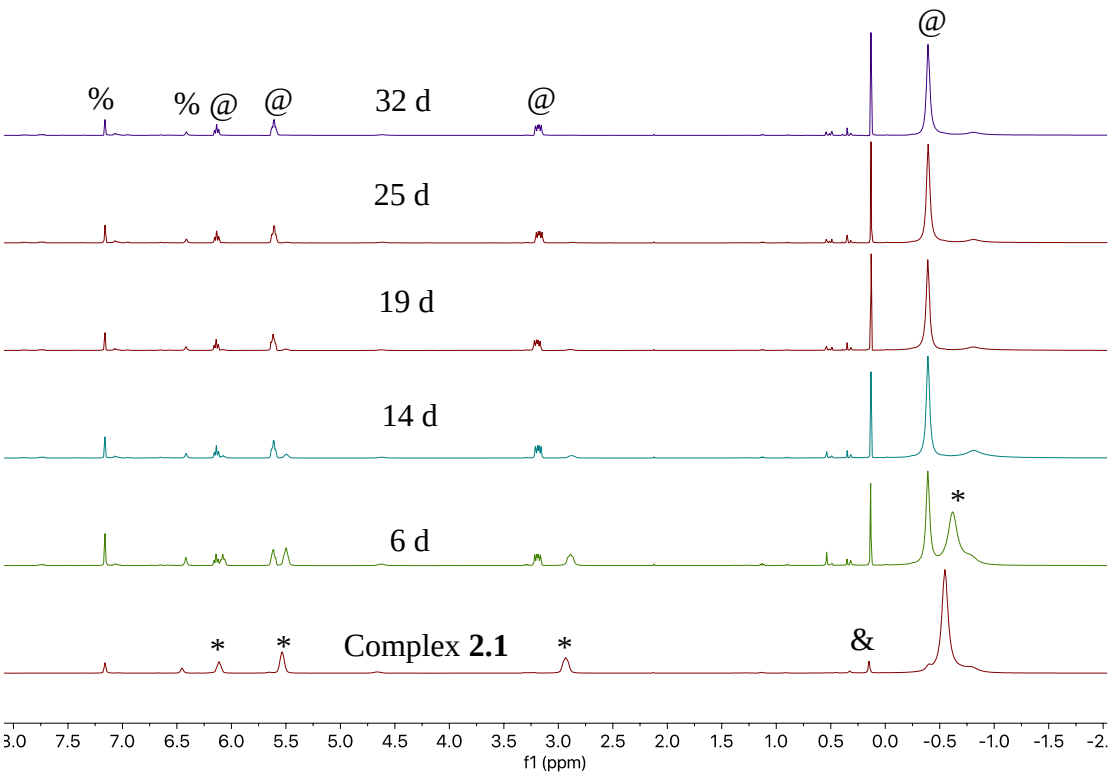

Figure A2.6. ^{1}H NMR spectra of the photolysis of **2.1** in C_6D_6 over 32 days. (*) indicates **2.1**, (@) indicates **2.2**, (&) indicates $HN(SiMe_3)_2$, and (%) indicates free $CNNPPh_3$.

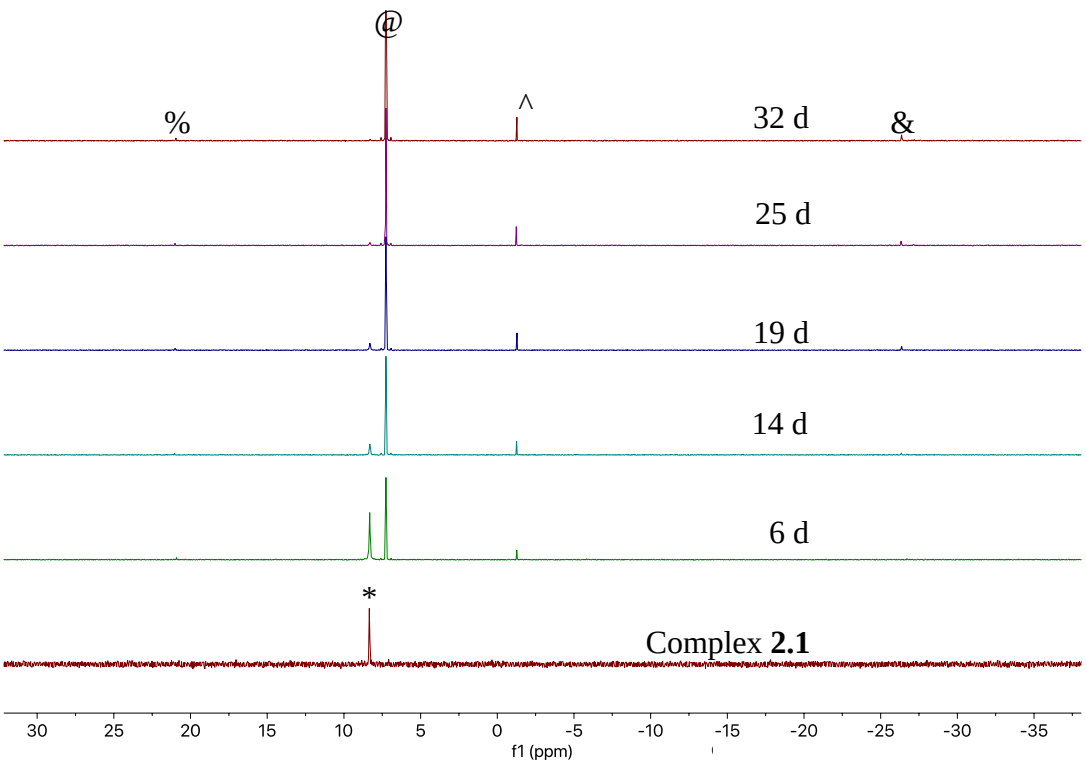

Figure A2.7. $^{31}P\{^{1}H\}$ NMR spectra of the photolysis of **2.1** in C_6D_6 over 32 days. (*) indicates **2.1**, (@) indicates **2.2**, (^) indicates a resonance tentatively assigned to **2.3**, (&) indicates an unidentified byproduct, and (%) indicates free $CNNPPh_3$.

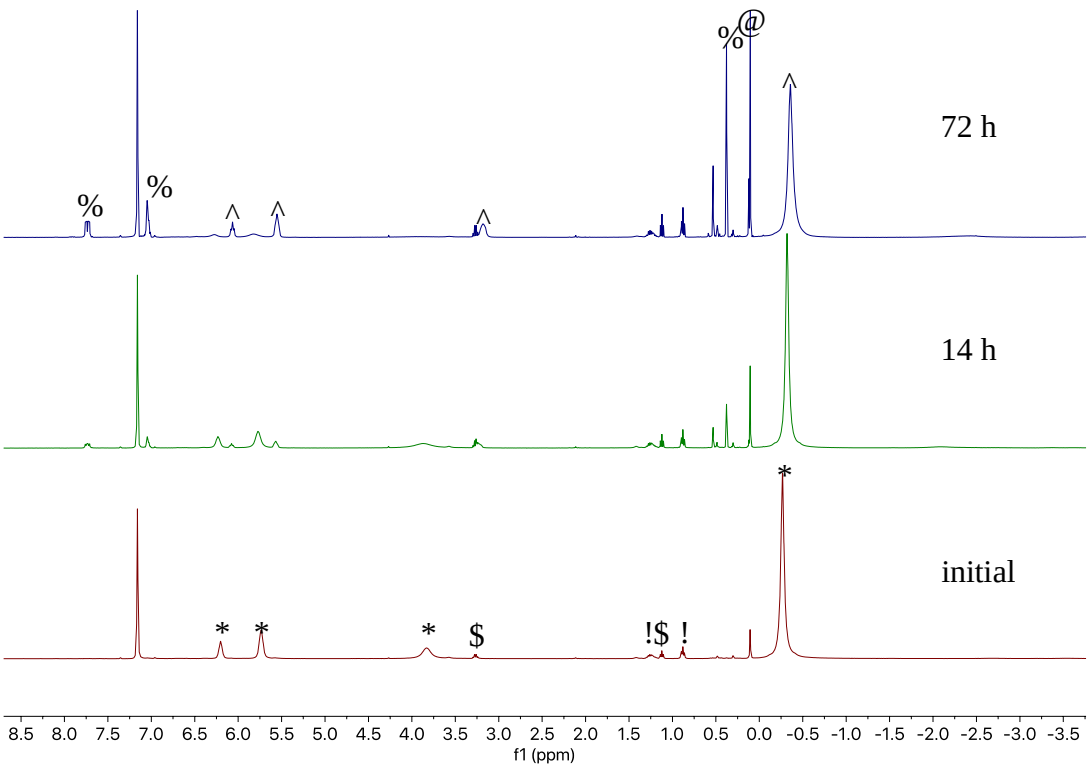

Figure A2.8. ^{1}H NMR spectra of the thermolysis of **2.1** at 42 ºC in C_6D_6. (*) indicates **2.1**, (^) indicates **2.2**, (%) indicates **2.3**, (@) indicates free $HN(SiMe_3)_2$, (!) indicates hexanes, and ($) indicates diethyl ether.

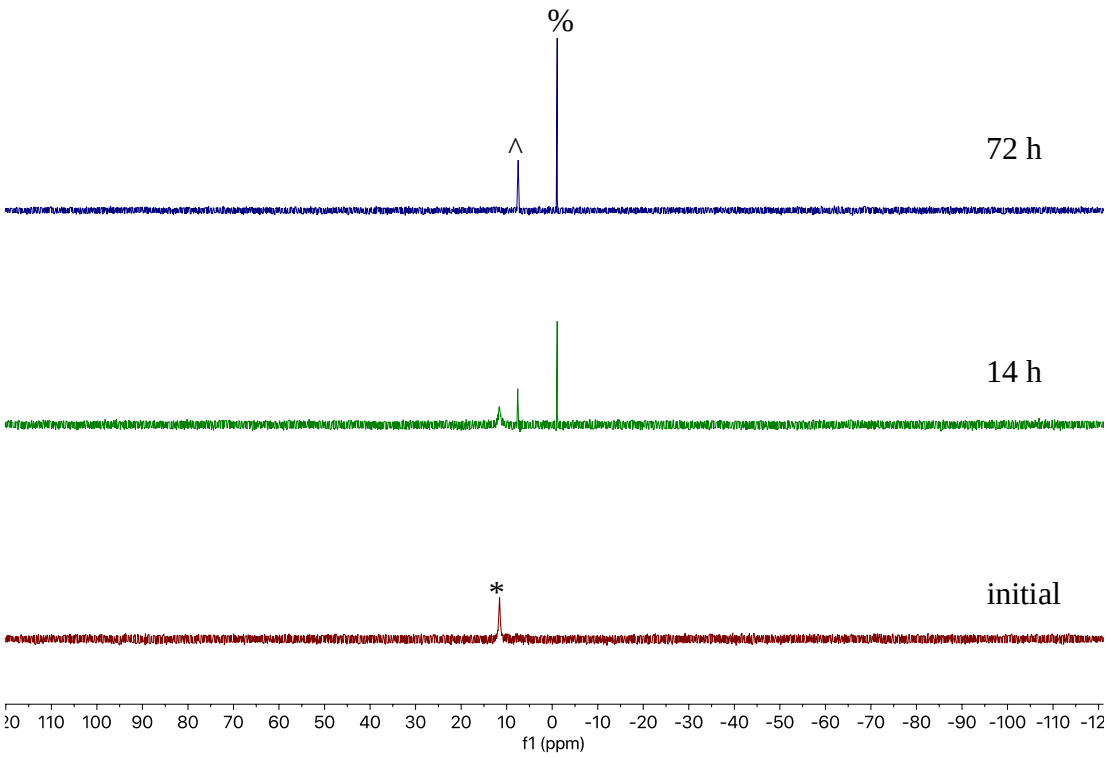

Figure A2.9. $^{31}P\{^{1}H\}$ NMR spectra of the thermolysis of **2.1** at 42 ºC in C_6D_6. (*) indicates **2.1**, (^) indicates **2.2**, (%) indicates **2.3**.

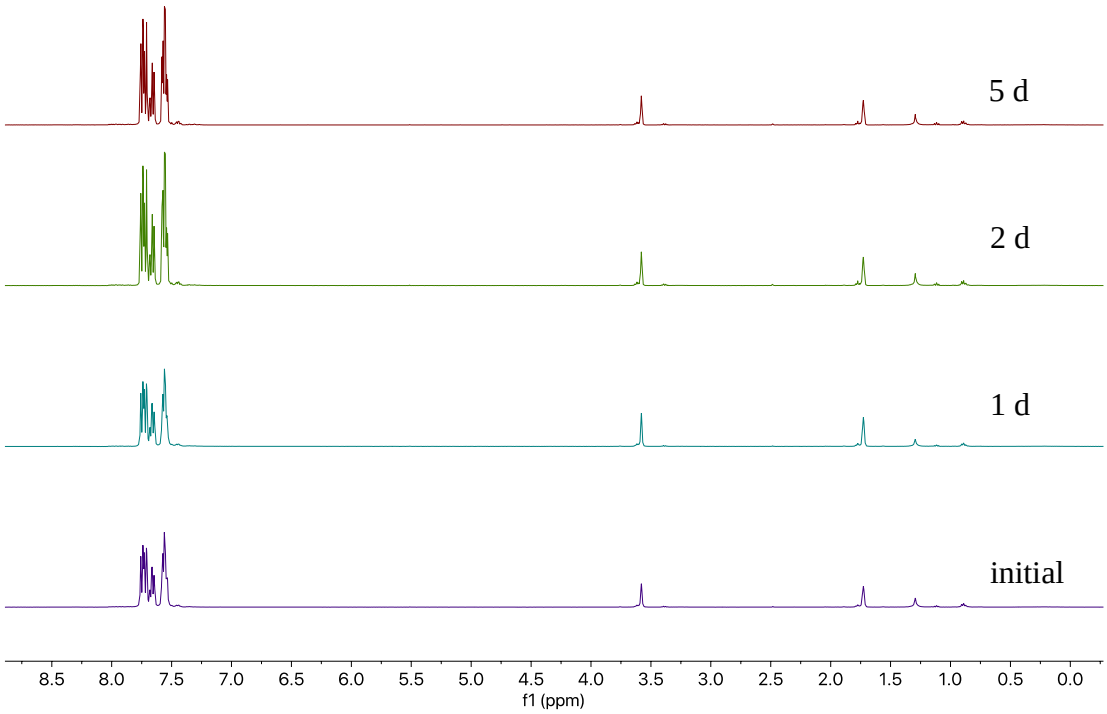

Figure A2.10. ^{1}H NMR spectra of the photolysis of $CNNPPh_3$ at 380 nm for 5 d in THF-d_8.

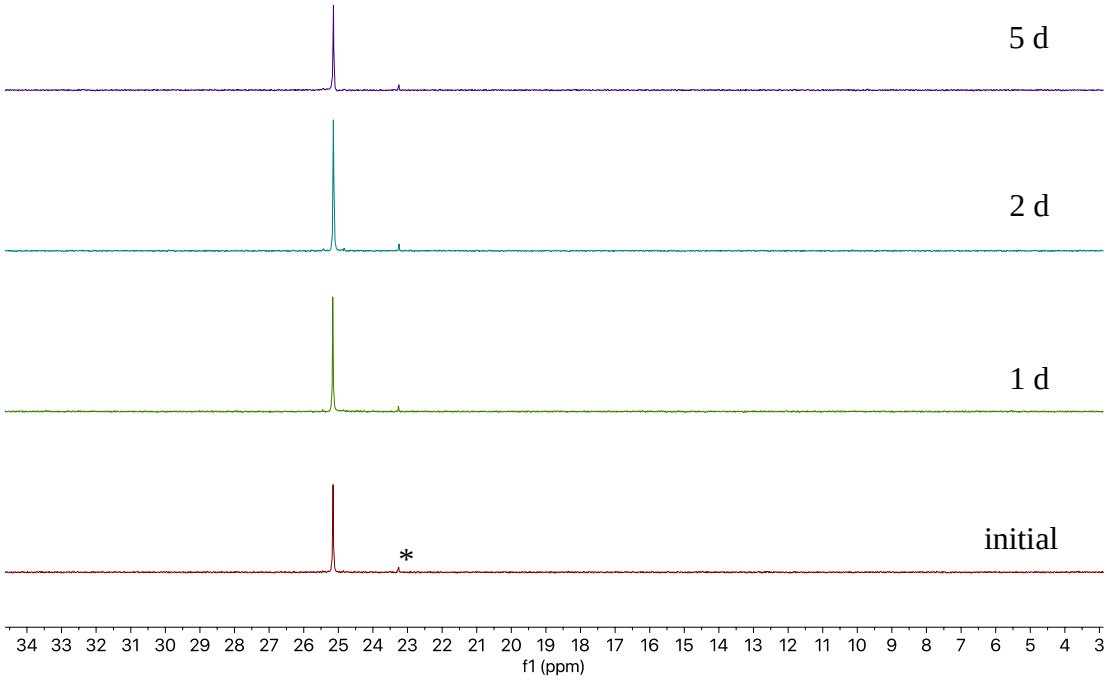

Figure A2.11. $^{31}P\{^{1}H\}$ NMR spectra of the photolysis of $CNNPPh_3$ at 380 nm over 5 d in THF-d_8. (*) indicates the presence of triphenylphosphine oxide, a by-product of the $CNNPPh_3$ synthesis.

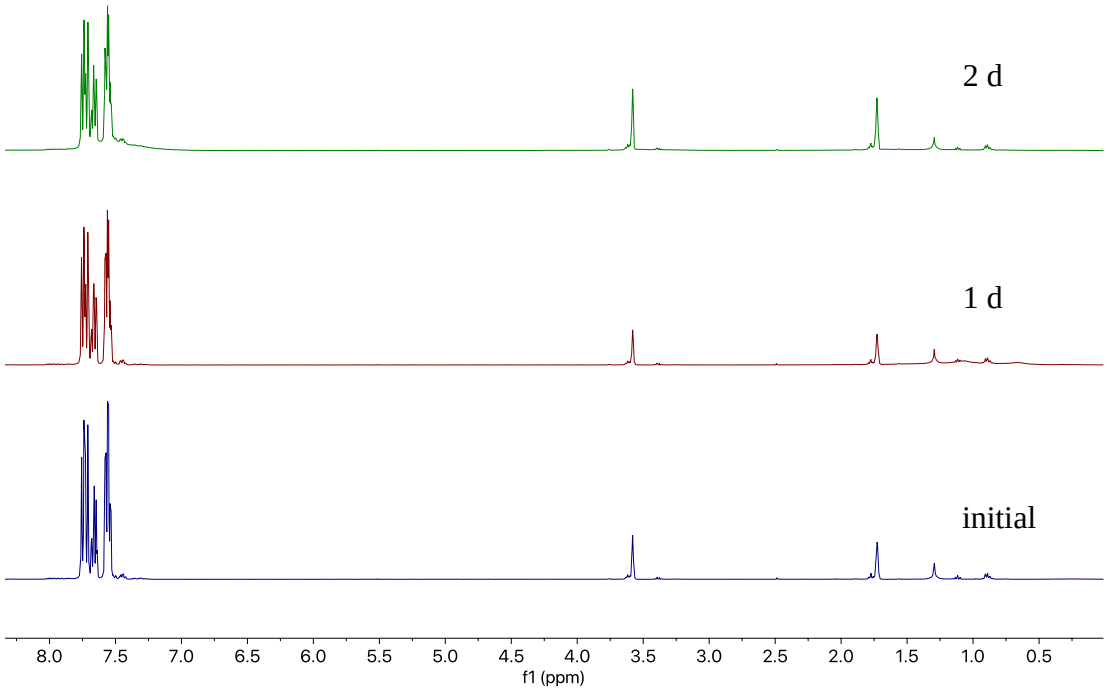

Figure A2.12. ^{1}H NMR spectra of the thermolysis of CNNPPh$_3$ at 42 ºC in THF-d_8.

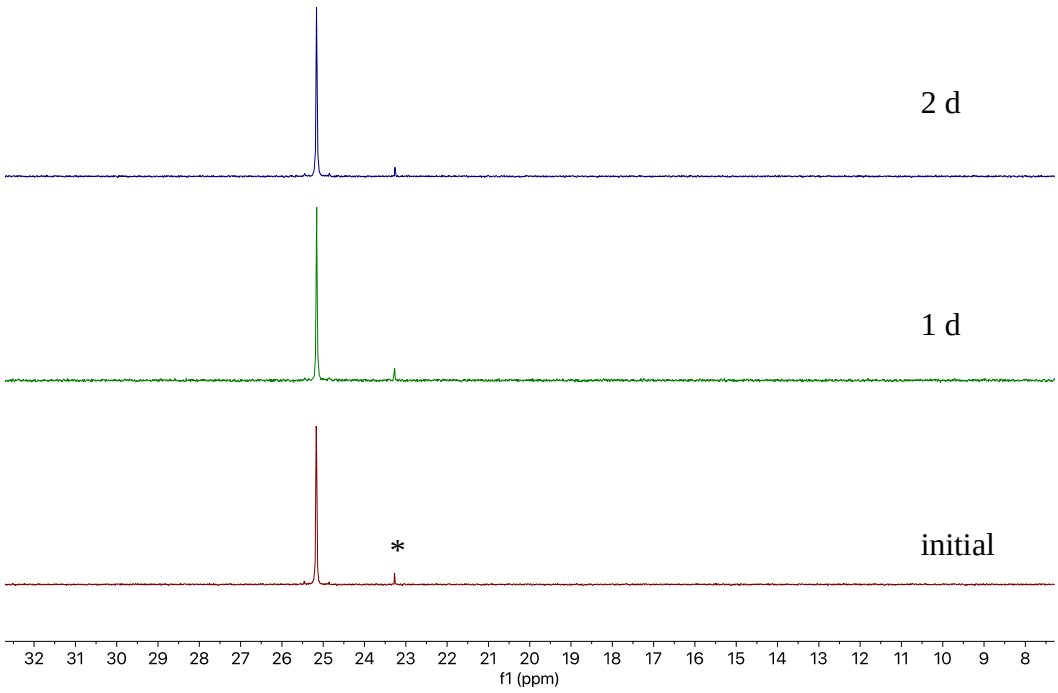

Figure A2.13. $^{31}P\{^{1}H\}$ NMR spectra of the thermolysis of $CNNPPh_3$ at 42 ºC in THF-d_8. (*) indicates the presence of triphenylphosphine oxide, a by-product of the $CNNPPh_3$ synthesis.

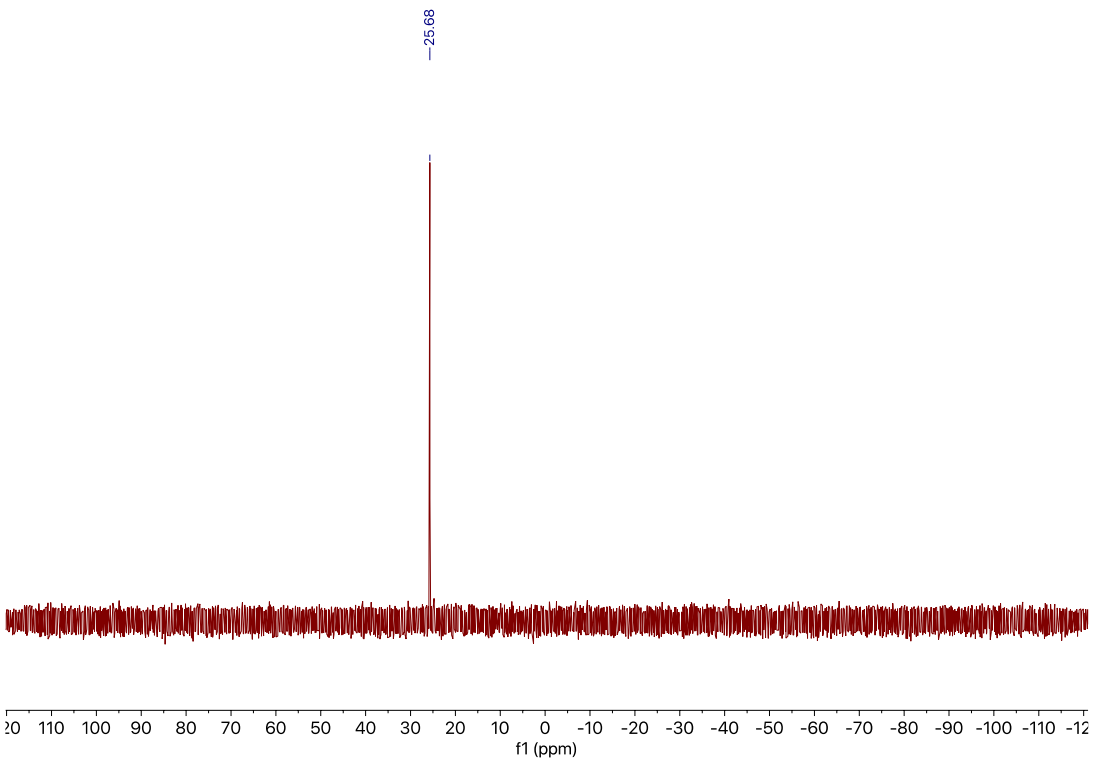

Figure A2.14. $^{31}P\{^{1}H\}$ NMR spectrum of free $CNNPPh_3$ in C_6D_6.

2.6.3 IR Spectra

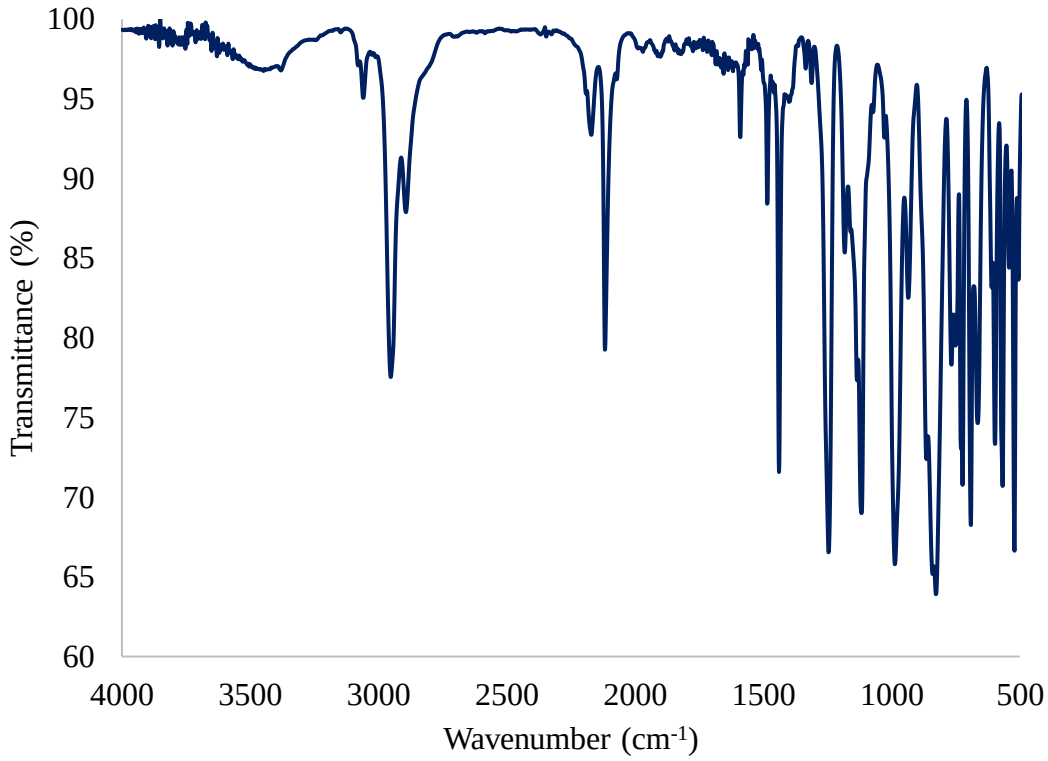

Figure A2.15. IR spectrum of $[(NR_2)_3Ce(CNNPPh_3)]$ (**2.1**) (KBr pellet).

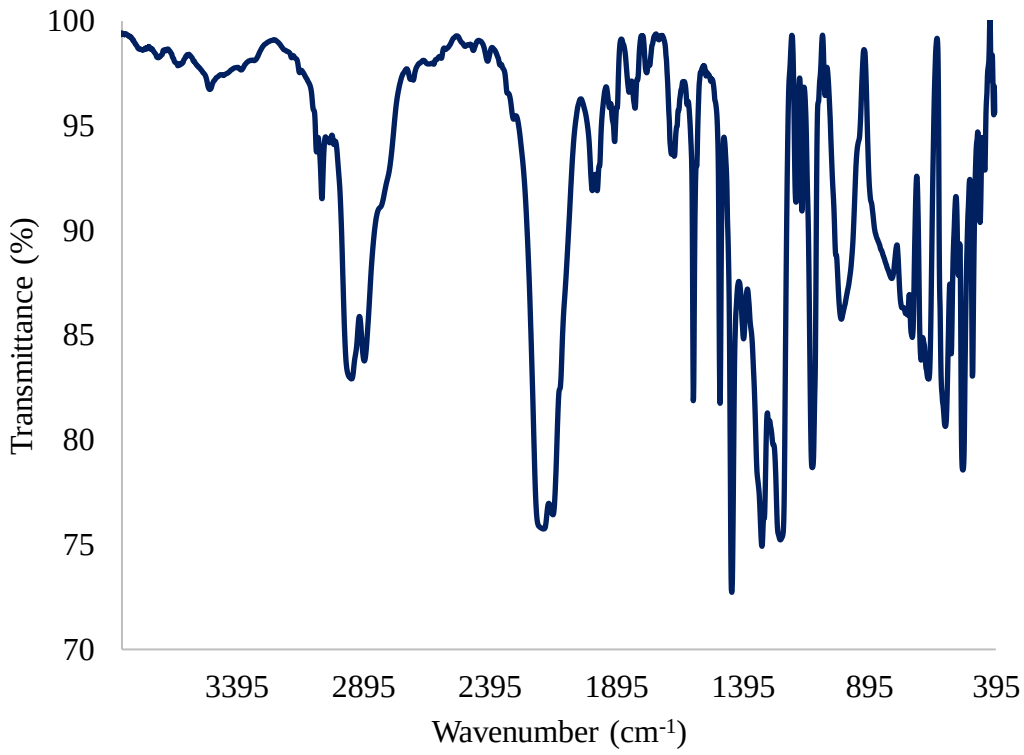

Figure A2.16. IR spectrum of [$(NR_2)_3Ce(NCNPPh_3)$] (**2.2**) (KBr pellet).

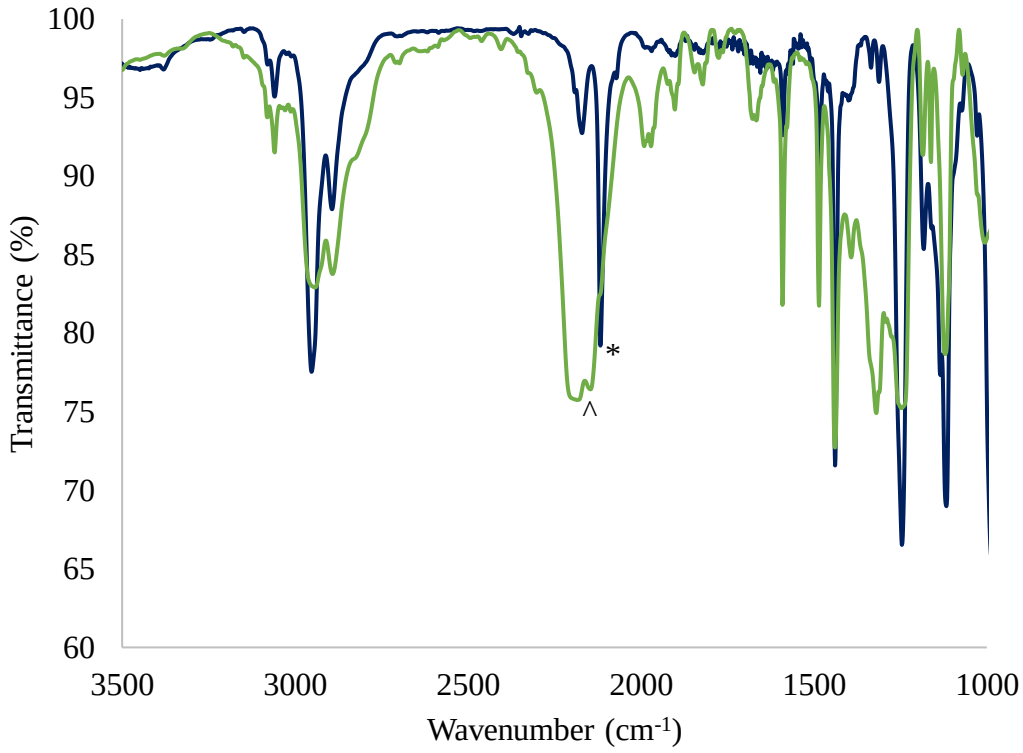

Figure A2.17. Overlay of the IR spectra recorded for **2.1** and **2.2** (*) denotes the ν(CN) stretch for **2.1** and (^) denotes the ν(NC) stretches for **2.2**.

2.7 References

1. Casely, I. J.; Liddle, S. T.; Blake, A. J.; Wilson, C.; Arnold, P. L., Tetravalent cerium carbene complexes. *Chem. Commun.* **2007,** (47), 5037-5039.
2. Liddle, S. T.; Arnold, P. L., Synthesis of Heteroleptic Cerium(III) Anionic Amido-Tethered N-Heterocyclic Carbene Complexes. *Organometallics* **2005,** *24* (11), 2597-2605.
3. Arnold, P. L.; Casely, I. J., F-Block N-Heterocyclic Carbene Complexes. *Chem. Rev.* **2009,** *109* (8), 3599-3611.
4. Mehdoui, T.; Berthet, J.-C.; Thuéry, P.; Ephritikhine, M., The remarkable efficiency of N-heterocyclic carbenes in lanthanide(III)/actinide(III) differentiation. *Chem. Commun.* **2005,** (22), 2860-2862.
5. Gregson, M.; Lu, E.; McMaster, J.; Lewis, W.; Blake, A. J.; Liddle, S. T., A Cerium(IV)–Carbon Multiple Bond. *Angew. Chem. Int. Ed.* **2013,** *52* (49), 13016-13019.
6. Gregson, M.; Lu, E.; Mills, D. P.; Tuna, F.; McInnes, E. J. L.; Hennig, C.; Scheinost, A. C.; McMaster, J.; Lewis, W.; Blake, A. J.; Kerridge, A.; Liddle, S. T., The inverse-trans-influence in tetravalent lanthanide and actinide bis(carbene) complexes. *Nat. Commun.* **2017,** *8* (1), 14137.
7. Marshall, G.; Wooles, A. J.; Mills, D. P.; Lewis, W.; Blake, A. J.; Liddle, S. T., Synthesis and Characterisation of Lanthanide N-Trimethylsilyl and -Mesityl Functionalised Bis(iminophosphorano)methanides and -Methanediides. *Inorganics* **2013,** *1* (1), 46-69.
8. Wooles, A. J.; Mills, D. P.; Lewis, W.; Blake, A. J.; Liddle, S. T., Lanthanide tri-benzyl complexes: structural variations and useful precursors to phosphorus-stabilised lanthanide carbenes. *Dalton Trans.* **2010,** *39* (2), 500-510.
9. Su, W.; Pan, S.; Sun, X.; Zhao, L.; Frenking, G.; Zhu, C., Cerium–carbon dative interactions supported by carbodiphosphorane. *Dalton Trans.* **2019,** *48* (42), 16108-16114.
10. Su, W.; Pan, S.; Sun, X.; Wang, S.; Zhao, L.; Frenking, G.; Zhu, C., Double dative bond between divalent carbon(0) and uranium. *Nat. Commun.* **2018,** *9* (1), 4997.
11. Joost, M.; Nava, M.; Transue, W. J.; Cummins, C. C., An exploding N-isocyanide reagent formally composed of anthracene, dinitrogen and a carbon atom. *Chem. Commun.* **2017,** *53* (83), 11500-11503.
12. Martinez, J. L.; Lin, H.-J.; Lee, W.-T.; Pink, M.; Chen, C.-H.; Gao, X.; Dickie, D. A.; Smith, J. M., Cyanide Ligand Assembly by Carbon Atom Transfer to an Iron Nitride. *J. Am. Chem. Soc.* **2017,** *139* (40), 14037-14040.
13. List, A. K.; Hillhouse, G. L.; Rheingold, A. L., Carbon suboxide as a C_1 reagent. Sequential cleavage of CO from C_3O_2 at a metal center to give $WCl_2(CO)(PMePh_2)_2[C,C':\eta^2\text{-}C(O)CPMePh_2]$ and $WCl_2(CO)(PMePh_2)_2(\equiv CPMePh_2)$. *Organometallics* **1989,** *8* (8), 2010-2016.
14. Cotton, S., *Lanthanide and Actinide Chemistry*. John Wiley and Sons: West Sussex, U.K., 2006.
15. Piro, N. A.; Robinson, J. R.; Walsh, P. J.; Schelter, E. J., The electrochemical behavior of cerium(III/IV) complexes: Thermodynamics, kinetics and applications in synthesis. *Coord. Chem. Rev.* **2014,** *260*, 21-36.
16. Qiao, Y.; Schelter, E. J., Lanthanide Photocatalysis. *Acc. Chem. Res.* **2018,** *51* (11), 2926-2936.
17. Yin, H.; Carroll, P. J.; Anna, J. M.; Schelter, E. J., Luminescent Ce(III) Complexes as Stoichiometric and Catalytic Photoreductants for Halogen Atom Abstraction Reactions. *J. Am. Chem. Soc.* **2015,** *137* (29), 9234-9237.

18. Yin, H.; Jin, Y.; Hertzog, J. E.; Mullane, K. C.; Carroll, P. J.; Manor, B. C.; Anna, J. M.; Schelter, E. J., The Hexachlorocerate(III) Anion: A Potent, Benchtop Stable, and Readily Available Ultraviolet A Photosensitizer for Aryl Chlorides. *J. Am. Chem. Soc.* **2016,** *138* (50), 16266-16273.
19. Qiao, Y.; Yang, Q.; Schelter, E. J., Photoinduced Miyaura Borylation by a Rare-Earth-Metal Photoreductant: The Hexachlorocerate(III) Anion. *Angew. Chem. Int. Ed.* **2018,** *57* (34), 10999-11003.
20. Yin, H.; Carroll, P. J.; Manor, B. C.; Anna, J. M.; Schelter, E. J., Cerium Photosensitizers: Structure–Function Relationships and Applications in Photocatalytic Aryl Coupling Reactions. *J. Am. Chem. Soc.* **2016,** *138* (18), 5984-5993.
21. Qiao, Y.; Cheisson, T.; Manor, B. C.; Carroll, P. J.; Schelter, E. J., A strategy to improve the performance of cerium(III) photocatalysts. *Chem. Commun.* **2019,** *55* (28), 4067-4070.
22. Assefa, M. K.; Wu, G.; Hayton, T. W., Synthesis of a terminal Ce(iv) oxo complex by photolysis of a Ce(iii) nitrate complex. *Chem. Sci.* **2017,** *8* (11), 7873-7878.
23. Weinberger, B.; Fehlhammer, W. P., N-Isocyanoiminotriphenylphosphorane: Synthesis, Coordination Chemistry, and Reactions at the Metal. *Angew. Chem. Int. Ed.* **1980,** *19* (6), 480-481.
24. Daniel, S. D.; Lehn, J.-S. M.; Korp, J. D.; Hoffman, D. M., Syntheses and X-ray structures of cerium amide complexes. *Polyhedron* **2006,** *25* (2), 205-210.
25. Hitchcock, P. B.; Hulkes, A. G.; Lappert, M. F., Oxidation in Nonclassical Organolanthanide Chemistry: Synthesis, Characterization, and X-ray Crystal Structures of Cerium(III) and -(IV) Amides. *Inorg. Chem.* **2004,** *43* (3), 1031-1038.
26. Hitchcock, P. B.; Lappert, M. F.; Protchenko, A. V., Facile formation of a homoleptic Ce(IV) amide *via* aerobic oxidation. *Chem. Commun.* **2006,** (33), 3546-3548.
27. Schneider, D.; Spallek, T.; Maichle-Mössmer, C.; Törnroos, K. W.; Anwander, R., Cerium tetrakis(diisopropylamide) – a useful precursor for cerium(IV) chemistry. *Chem. Commun.* **2014,** *50* (94), 14763-14766.
28. Stults, S. D.; Andersen, R. A.; Zalkin, A., Structural studies on cyclopentadienyl compounds of trivalent cerium: tetrameric (MeC5H4)3Ce and monomeric (Me3SiC5H4)3Ce and [(Me3Si)2C5H3]3Ce and their coordination chemistry. *Organometallics* **1990,** *9* (1), 115-122.
29. Stolzenberg, H.; Weinberger, B.; Fehlhammer, W. P.; Pühlhofer, F. G.; Weiss, R., Free and Metal-Coordinated (N-Isocyanimino)triphenylphosphorane: X-ray Structures and Selected Reactions. *Eur. J. Inorg. Chem.* **2005,** *2005* (21), 4263-4271.
30. Qiao, Y.; Sergentu, D.-C.; Yin, H.; Zabula, A. V.; Cheisson, T.; McSkimming, A.; Manor, B. C.; Carroll, P. J.; Anna, J. M.; Autschbach, J.; Schelter, E. J., Understanding and Controlling the Emission Brightness and Color of Molecular Cerium Luminophores. *J. Am. Chem. Soc.* **2018,** *140* (13), 4588-4595.
31. Avent, A. G.; Caro, C. F.; Hitchcock, P. B.; Lappert, M. F.; Li, Z.; Wei, X.-H., Synthetic and structural experiments on yttrium, cerium and magnesium trimethylsilylmethyls and their reaction products with nitriles; with a note on two cerium β-diketiminates. *Dalton Trans.* **2004,** (10), 1567-1577.
32. Evans, W. J.; Mueller, T. J.; Ziller, J. W., Lanthanide versus Actinide Reactivity in the Formation of Sterically Crowded [$(C_5Me_5)_3MLn$] Nitrile and Isocyanide Complexes. *Chem. Eur. J.* **2010,** *16* (3), 964-975.

33. Kaiser, J.; Hartung, H.; Richter, R., Strukturuntersuchungen an Pseudochalkogen-Phosphor-Verbindungen. II. Kristall- und MolekülStruktur von Triphenylphosphonio-cyanamid. *Z. Anorg. Allg. Chem.* **1980,** *469* (1), 188-196.
34. C. Barco, I.; R. Falvello, L.; Fernández, S.; Navarro, R.; P. Urriolabeitia, E., Synthesis and characterization of palladium(II) complexes with the α-stabilized phosphoylide ligand Ph3P=C(H)CONMe2. *J. Chem. Soc., Dalton Trans.* **1998,** (10), 1699-1706.
35. Bégué, D.; Santos-Silva, H.; Dargelos, A.; Wentrup, C., Imidoylnitrenes R′C(=NR)–N, Nitrile Imines, 1*H*-Diazirines, and Carbodiimides: Interconversions and Rearrangements, Structures, and Energies at DFT and CASPT2 Levels of Theory. *J. Phys. Chem. A* **2017,** *121* (43), 8227-8235.
36. Leue, C.; Reau, R.; Neumann, B.; Stammler, H.-G.; Jutzi, P.; Bertrand, G., Preparation of mono-and bis (germyl) nitrilimines from germylenes and stannyl diazo derivatives. *Organometallics* **1994,** *13* (2), 436-438.
37. Bégué, D.; Qiao, G. G. H.; Wentrup, C., Nitrile Imines: Matrix Isolation, IR Spectra, Structures, and Rearrangement to Carbodiimides. *J. Am. Chem. Soc.* **2012,** *134* (11), 5339-5350.
38. Nunes, C. M.; Araujo-Andrade, C.; Fausto, R.; Reva, I., Generation and Characterization of a 4π-Electron Three-Membered Ring 1*H*-Diazirine: An Elusive Intermediate in Nitrile Imine–Carbodiimide Isomerization. *J. Org. Chem.* **2014,** *79* (8), 3641-3646.
39. Gardner, B. M.; Patel, D.; Lewis, W.; Blake, A. J.; Liddle, S. T., Photochemically Promoted Bond-Cleavage and -Capture in a Diazomethane Derivative of a Triamidoamine Uranium(IV) Complex. *Angew. Chem. Int. Ed.* **2011,** *50* (44), 10440-10443.
40. Rice, N. T.; Su, J.; Gompa, T. P.; Russo, D. R.; Telser, J.; Palatinus, L.; Bacsa, J.; Yang, P.; Batista, E. R.; La Pierre, H. S., Homoleptic Imidophosphorane Stabilization of Tetravalent Cerium. *Inorg. Chem.* **2019,** *58* (8), 5289-5304.
41. Stolzenberg, H.; Weinberger, B.; Fehlhammer, W. P.; Pühlhofer, F. G.; Weiss, R., Free and Metal-Coordinated (*N*-Isocyanimino) triphenylphosphorane: X-ray Structures and Selected Reactions. *Eur. J. Inorg. Chem.* **2005,** *2005* (21), 4263-4271.
42. Harris, R. K.; Becker, E. D.; Cabral de Menezes, S. M.; Goodfellow, R.; Granger, P., NMR nomenclature: nuclear spin properties and conventions for chemical shifts. IUPAC Recommendations 2001. International Union of Pure and Applied Chemistry. Physical Chemistry Division. Commission on Molecular Structure and Spectroscopy. *Magn. Reson. Chem.* **2002,** *40* (7), 489-505.
43. Harris, R. K.; Becker, E. D.; De Menezes, S. M. C.; Granger, P.; Hoffman, R. E.; Zilm, K. W., Further Conventions for NMR Shielding and Chemical Shifts (IUPAC Recommendations 2008). *Magn. Reson. Chem.* **2008,** *46* (6), 582-598.
44. *SMART* Apex II, Version 5.632.; Bruker AXS, Inc.: Madison, WI, 2005.
45. *SAINT Software User's Guide*, Version 7.34a ed.; Bruker AXS Inc.: Madison, WI, 2005.
46. *SADABS*, Sheldrick, G.M.; University of Göttingen, Germany: 2005.
47. *SHELXTL*, Version 6.12 ed.; Bruker AXS Inc.: Madison, WI, 2005.

Chapter 3. Reductive Coupling of Isocyanides Using Low-Valent Uranium(III)

3.1 Introduction

As f-element metal-ligand multiple bond chemistry continues to grow,[1-7] the study of these complexes has allowed chemists to reveal fundamentally important insights into covalency and f orbital participation in bonding, as well as uncover novel modes of reactivity.[8-15] These advancements have been demonstrated through the synthesis of novel f-element carbene complexes (Scheme 3.1, **A**-**G**),[16-23] which are of interest for their potential use in catalysis and for their diverse reactivity.[2, 15, 24, 25]

Scheme 3.1. Previously reported f-element carbene complexes. A, Ref. 17 and 18; B, Ref. 16; C, Ref. 19; D, Ref. 22; E, Ref. 20; F, Ref. 23; G, Ref. 21.

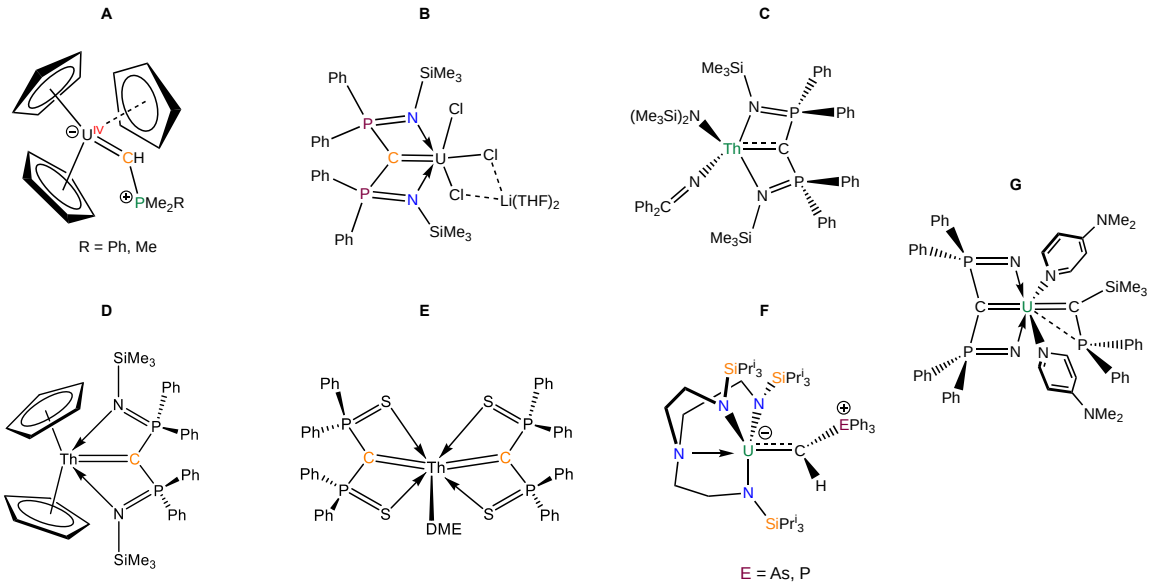

After the first uranium carbene complexes were reported by Gilje and co-workers in the 1980s (Scheme 3.1, **A**),[17, 18] many other actinide carbenes have been reported that feature the same stabilization technique involving phosphorus. This feature has not only allowed organometallic chemists to isolate a wide variety of uranium carbenes, but to access carbenes with different oxidation states of uranium, such as the pentavalent uranium carbene **B**.[16]

Liddle and co-workers have contributed greatly in synthesizing uranium carbenes (Scheme 3.1, **B**, **F**, **G**), which include a series of silyl-phosphino-carbene complexes that feature a 3-center P-C-U linkage that contains a dominant U=C double bond component **G**,[21] and most recently were able to extend the stabilization found by phosphorus to arsonium, in which a arsonium-ylide was used to stabilize the uranium(IV) arsonium-carbene **F**.[23] Compared to uranium, fewer examples involving thorium have been reported, including compounds **C**-**E**.[19, 20, 22] These complexes each feature short Th=C bonds and **E** is notably the first thorium poly-carbene complex reported.[20]

Despite this progress, a "Schrock-type" actinide carbene complex has remained elusive as all the actinide carbenes synthesized thus far feature at least one phosphorus substituent attached to the α-carbon.[1, 2, 16-20, 25-30] In a Schrock-type carbene, the metal atom forms a strong π-backbond to the C atom because the C atom has a lone pair from its empty p orbital that contributes in bonding with the filled metal d orbital (Scheme 3.2a).[31-33] Most of the stabilization on the carbene center is provided by the metal fragment and this type of metal-carbon interaction is described as a covalent double bond.[31, 33] Whereas in a methanediide carbene, such as bis(phosphoranimino)methandiide ($[C(Ph_2P{=}NSiMe_3)_2)]^{2-}$),[34] the metal d orbital contributes very little in bonding, forming a weak π-backbond with the C atom that is sometimes denoted as a dative interaction. Rather, two electrons are donated from the lone pairs at carbon while the phosphorus substituents bonded to carbon help stabilize the metal-carbon interaction (Scheme 3.2b).[27, 31-36] In this type of carbene, the stabilization of the center carbon is provided by the substituents on the carbon atom.[31] For example, one advantage of using a phosphorus substituent to stabilize the U=C interaction is that it allows the α-carbon

atom to delocalize the large negative charge density on the adjacent heteroatom since the U-C π bond is highly polarized in these complexes.[2, 26, 27, 36, 37]

Scheme 3.2. Dominant orbital interactions and bonding in (a) Schrock-type and (b) methanediide-type carbene complexes. Adapted from Refs. 32 and 36.

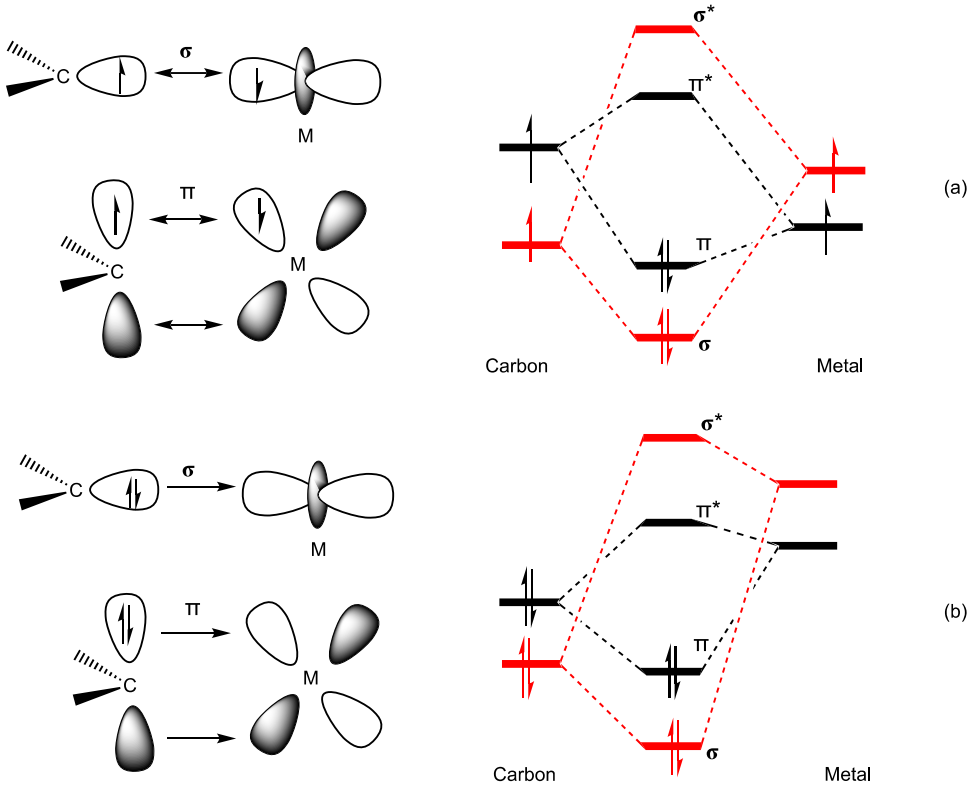

Inspired by work published by Figueroa and co-workers[38] (Scheme 3.3a), I sought to synthesize a "true" uranium carbene complex using the low-valent, highly reducing U(III) tris(amide), $U(NR_2)_3$ (R = $SiMe_3$), first reported by Andersen in 1979.[39, 40] This uranium precursor has shown to be useful in facilitating small molecule reactivity.[41, 42] I hypothesize that the reaction of uranium tris(amide) with an isocyanide ligand will form an adduct, in which I plan to reduce the isocyanide group by the addition of an electrophile, such as TMSCl, whereupon the uranium center would become oxidized en route to a carbene (Scheme 3.3b).

Scheme 3.3. (a) Previously reported synthesis by Figueroa and co-workers to a terminal iron carbyne. Ref 38. (b) Proposed synthetic route to a uranium carbene complex through an isocyanide adduct.

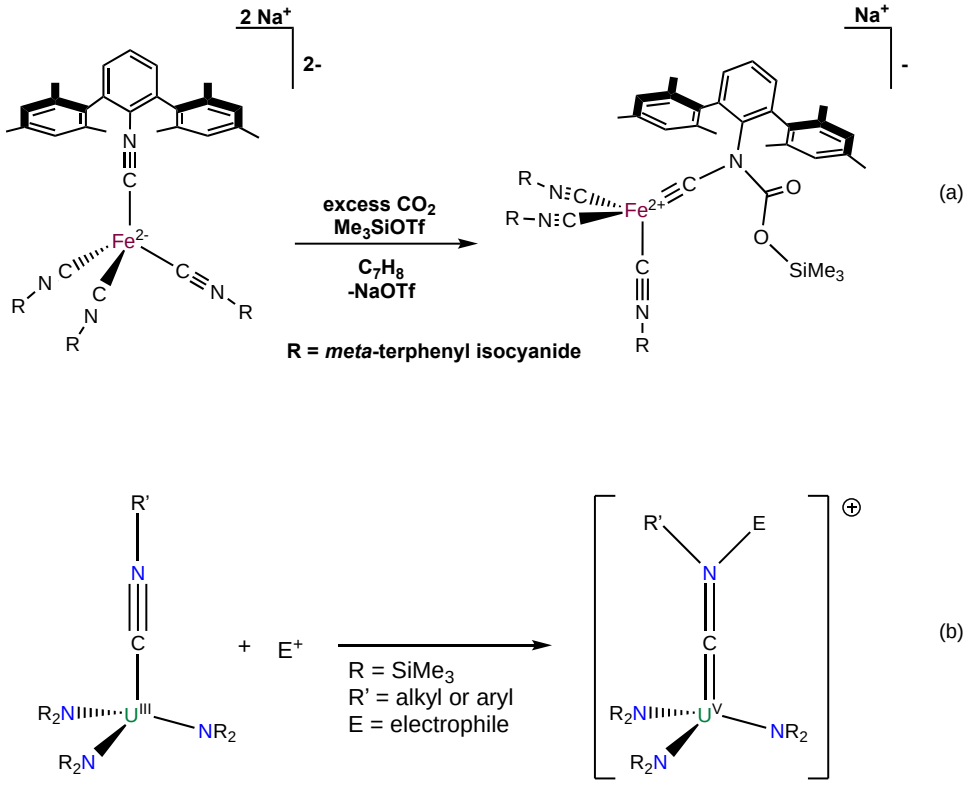

Herein, I report the reactions of the low valent U(III) tris(amide) $U(NR_2)_3$ (R = $SiMe_3$) with isocyanides containing either an alkyl or aryl substituent. In efforts to form an adduct using *tert*-butyl isocyanide, $U(NR_2)_3$ proves to be too reducing, resulting in the isolation of $[U(NR_2)_3(CN)(CN^tBu)]$ (R = $SiMe_3$) (**3.1**), which suggests one *tert*-butyl isocyanide ligand is reduced, ejecting a *tert*-butyl radical, while the metal center becomes oxidized. Moving towards a stronger C-N bond, the use of 2,6-dimethylphenyl isocyanide (CNXyl, Xyl = 2,6-$Me_2C_6H_3$) results in the isolation of $[U(NR_2)_3(CNXyl)_2]$ (**3.3**), as well as $[U\{N(R)SiC(=CH_2)N(Xyl)\}(NR_2)_2]$ (**3.4**). The reduction of **3.3** was also explored using KC_8 and Cp^*_2Co and is discussed in detail.

3.2 Results and Discussion

3.2.1 Synthesis and Characterization of [U(NR$_2$)$_3$(CN)(CN^{t}Bu)] (3.1)

Addition of 2 equiv of *tert*-butyl isocyanide to a cold (-25 °C) pentane solution of uranium tris(amide), U(NR$_2$)$_3$ (R = SiMe$_3$), results in a color change from purple to orange, concomitant with the deposition of a light green precipitate, over 24 h. The reaction mixture is filtered, and the insoluble green precipitate is collected on the Celite column as the soluble orange solution is isolated. The green solid on the filter is extracted with THF and is layered with pentane. Upon cooling (-25 °C) for 24 h, green crystalline blocks can be isolated from the THF fraction in 32% yield and identified as [U(NR$_2$)$_3$(CN)(CN^{t}Bu)] (**3.1**), while orange crystalline plates were isolated from the pentane solution in 29% yield and identified by ^{1}H NMR spectroscopy as the known complex, [U{*N*(R)SiC(=CH$_2$)*N*(^{t}Bu)}(NR$_2$)$_2$] (**3.2**),[43] which has been previously reported by Andersen and co-workers (eqn (3.1)). Complex **3.2** is formed from the isocyanide ligand reacting with the decomposition product of uranium tris(amide), the known uranium metallacycle, [U{*N*(R)(SiMe$_2$)*C*H$_2$}(NR$_2$)$_2$].[43]

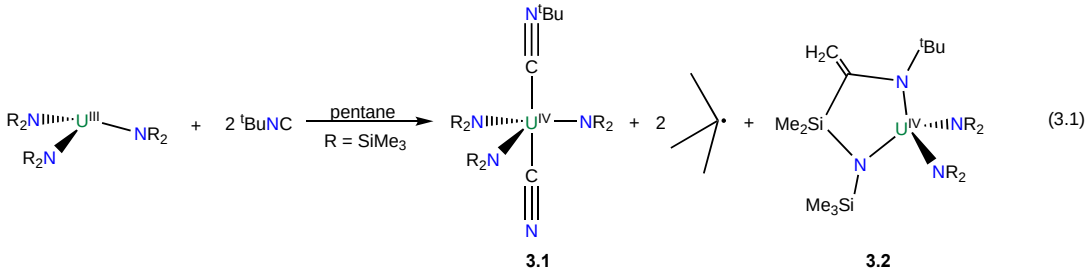

(3.1)

Complex **3.1** is insoluble in THF-d_8 and must be warmed (50 °C) for 2 h in an oil bath to fully dissolve. The ^{1}H NMR spectrum of **3.1** in THF-d_8 features broad resonances at -7.24 ppm (9H), assigned to the *tert*-butyl group, and at 2.15 ppm (54H), assigned to the SiMe$_3$ groups (Figure 3.1). The ratio of these two peaks is consistent with the presence of only one ^{t}Bu group in the final product.

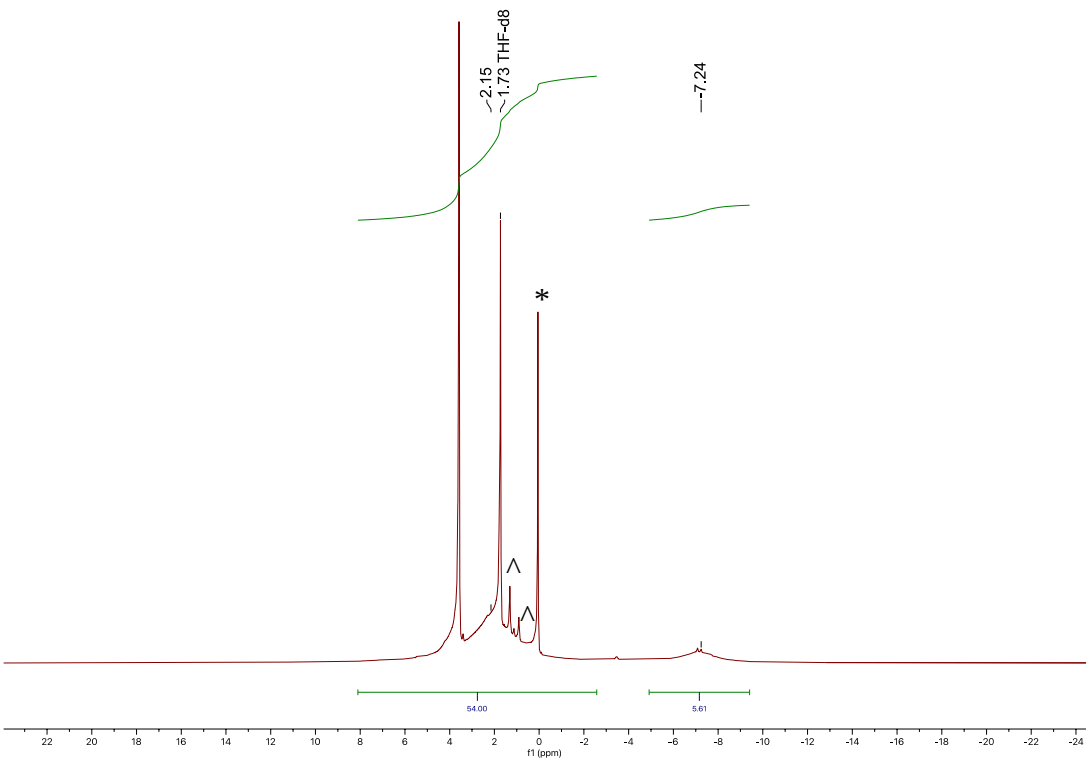

Figure 3.1. ^{1}H NMR spectrum of **3.1** in THF-d_8. (*) indicates $HN(SiMe_3)_2$ and (^) indicates pentane.

The connectivity of complex **3.1** was verified by X-ray crystallography (Figure 3.2). Complex **3.1** crystallizes in the trigonal space group $P\bar{3}_1c$. In the solid-state, the *tert*-butyl isocyanide ligand and cyanide ligand are disordered over two positions in a 50:50 ratio, which somewhat lowers the precision of the resulting metrical parameters. It features a trigonal bipyramidal coordination geometry about the uranium center with one isocyanide and one cyanide ligand in the axial positions and three $SiMe_3$ ligands in the equatorial positions. The U-C(isocyanide) distance (2.63(2) Å) in **3.1** is consistent with other U(IV) *tert*-butyl isocyanide complexes[44, 45] and is statistically identical to what is reported for a series of Th(IV) *tert*-butyl isocyanide complexes, $[(C_5Me_5)_2Th(CN^tBu)(\eta^2\text{-}N,C)\text{-}(^tBuNC{=}PMes)]$ and $[(C_5Me_5)_2Th(CN^tBu)(\eta^2\text{-}N,C)\text{-}(^tBuNC{=}AsTipp)]$ (Tipp = 2,4,6-^{i}Pr$_3$C$_6$H$_2$, Mes = 2,4,6-

$Me_3C_6H_2$), which are 2.643(6) Å and 2.638(6) Å,[46] respectively. Furthermore, the C-N bond distance (1.03(3) Å) seen in **3.1** is much shorter than reported for $[U(Cp^*_2)_2(NMe_2)(CN^tBu)_2][BPh_4]$ (Cp^* = η-C_5Me_5) (1.14(1), 1.16(1) Å)[44] and in the Th complexes $[(C_5Me_5)_2Th(CN^tBu)(\eta^2$-*N*,*C*)-(^{t}BuNC=PMes)] and $[(C_5Me_5)_2Th(CN^tBu)(\eta^2$-*N*,*C*)-(^{t}BuNC=AsTipp)] (1.131(8) Å and 1.128(7) Å, respectively),[46] suggesting that this is most likely an artifact from the disorder in this complex. Lastly, the U-$N_{silylamide}$ distances (av. 2.225 Å) are consistent with those found in other U(IV) silylamide complexes.[47-49]

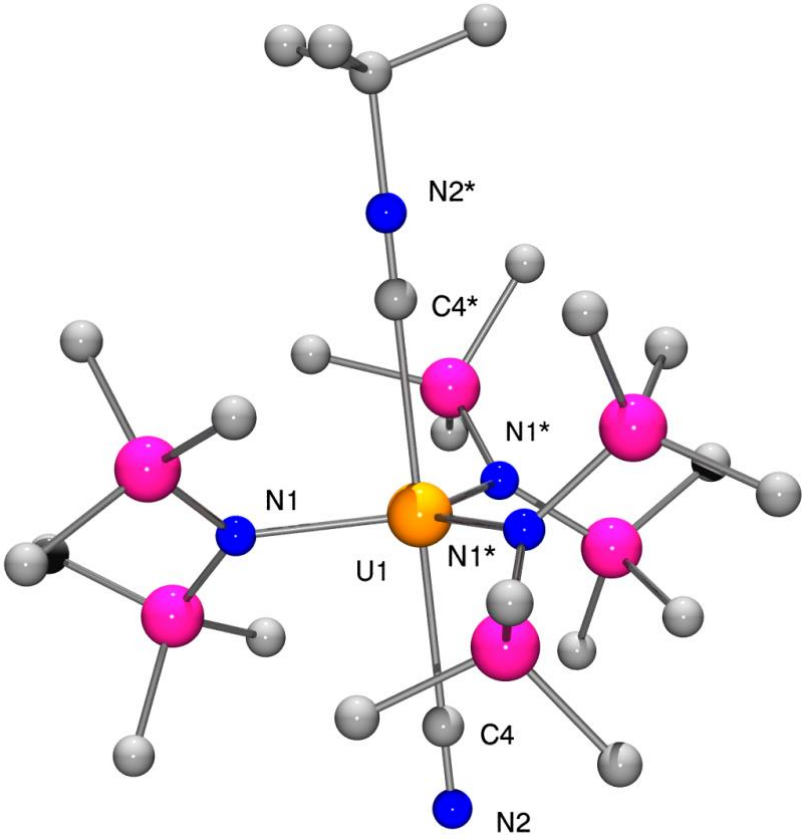

Figure 3.2. Solid-state molecular structure of **3.1**, shown with 50% probability ellipsoids. Hydrogen atoms and solvent molecules removed for clarity. Selected bond lengths (Å) and angles (°): U1-C4 = 2.63(2), C4-N2 = 1.03(3), av. U1-N_{amide} = 2.225, NC-U-CN^tBu = 180.

Complex **3.1** is insoluble in pentane and benzene, but is slightly soluble in Et_2O and THF when warmed. In addition, the IR spectrum of **3.1** features a prominent ν_{CNtBu} stretch at 2189 cm^{-1}, which is higher than that of free ^{t}BuNC (2134 cm^{-1}), and a prominent ν_{CN} stretch at 2056 cm^{-1} (Figure 3.3). For comparison, similar ν_{CNtBu} stretches have been observed in other U(IV) *tert*-butyl isocyanide complexes, such as $[U(Cp^*_2)_2(NMe_2)(CN^tBu)_2][BPh_4]$ (ν_{CN} = 2181 cm^{-1}),[44] $[(Cp^{iPr4})_2U(CN^tBu)_4][B(C_6F_5)_4]_2$ (ν_{CN} = 2176 cm^{-1}),[45] and $[(Cp^{iPr4})_2U(I)(CN^tBu)_2][B(C_6F_5)_4]_2$ (ν_{CN} = 2182 cm^{-1}), as well as in a series of Th(IV) complexes reported by Walensky and co-workers,[46] $[(C_5Me_5)_2Th(CN^tBu)(\eta^2\text{-}N,C)\text{-}(^t$BuNC=PTipp)], $[(C_5Me_5)_2Th(CN^tBu)(\eta^2\text{-}N,C)\text{-}(^t$BuNC=PMes)], and $[(C_5Me_5)_2Th(CN^tBu)(\eta^2\text{-}N,C)\text{-}(^t$BuNC=AsTipp)], which reported ν_{CN} stretches at 2181, 2186, and 2182 cm^{-1}, respectively. For further comparison, the ν_{CN} stretch overserved in **3.1** agrees well with other actinide cyanide complexes.[50-54] In particular, Ephritikhine and co-workers report ν_{CN} stretches for $[U(NR_2)_3(CN)]$ and $[M][U(NR_2)_3(CN)_2]$ (M = NEt_4 or $K(THF)_4$) at 2044 cm^{-1}, 2058 cm^{-1}, and 2078 cm^{-1}, respectively.[52]

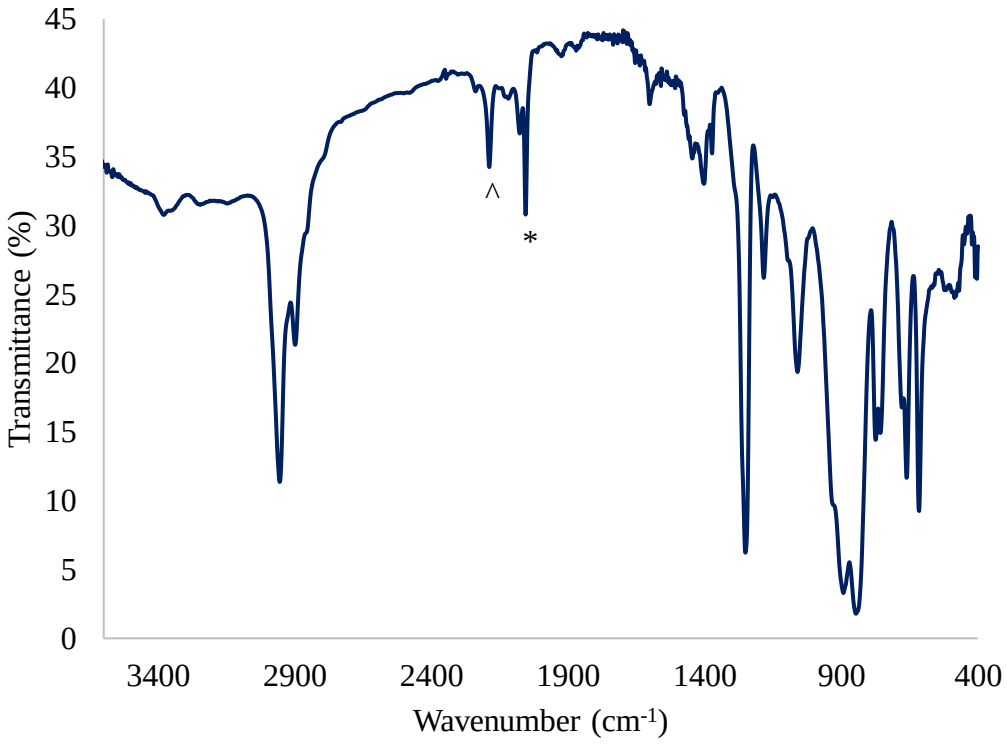

Figure 3.3. IR spectrum of **3.1** (KBr pellet). (*) indicates the ν_{CN} stretch and (^) indicates the ν_{CNtBu} stretch.

To explain the formation of **3.1** I hypothesize that uranium tris(amide) reduces the *tert*-butyl isocyanide ligand, which results in formation of *tert*-butyl radical while oxidizing the uranium center. While I was unable to observe the presence of isobutylene or isobutene in the in-situ ^{1}H NMR spectrum, which are the expected products of *tert*-butyl radical generation, I note that the U(III) alkyl isocyanide adducts, $[(C_5Me_4H)_3U(CN(alkyl))]$ (alkyl = Me, *i*Pr, *t*Bu), have been reported to be unstable in solution and decompose readily to produce the U(IV) cyanide, $[(C_5Me_4H)_3U(CN)]$, where the rate of decomposition is alkyl dependent.[55] This type of conversion has been well studied in organometallic d- and f-element chemistry.[56, 57] Accordingly, I hypothesized that switching from an alkyl isocyanide ligand (sp^3 CN bonding) to an aryl isocyanide that has stronger sp^2 CN bonding, such as 2,6-dimethylphenyl isocyanide

(CNXyl, Xyl = 2,6-$Me_2C_6H_3$), would not undergo this unwanted decomposition pathway. It has also been reported that aromatic isocyanide complexes display reasonable thermal stability, which further supports this change.[56]

3.2.2 Synthesis and Characterization of $U(NR_2)_3(CNXyl)_2$ (Xyl = 2,6-$Me_2C_6H_3$) (3.3)

Reaction of 2 equiv of CNXyl with $U(NR_2)_3$ in pentane results in formation of $[U(NR_2)_3(CNXyl)_2]$ (**3.3**) , which could be isolated as a dark green crystalline material after work-up in a concentrated pentane solution and stored at -25 °C for 24 h in 50% yield (eqn (3.2)). Orange crystals were also isolated in 15% yield and characterized as $[U\{N(R)SiC(=CH_2)N(Xyl)(NR_2)_2]$ (**3.4**), which is formed from the isocyanide ligand reacting with the decomposition product of uranium tris(amide), the known uranium metallacycle, $[U\{N(R)(SiMe_2)CH_2\}(NR_2)_2]$.[43] More detail about **3.4** is described in section **3.2.3**.

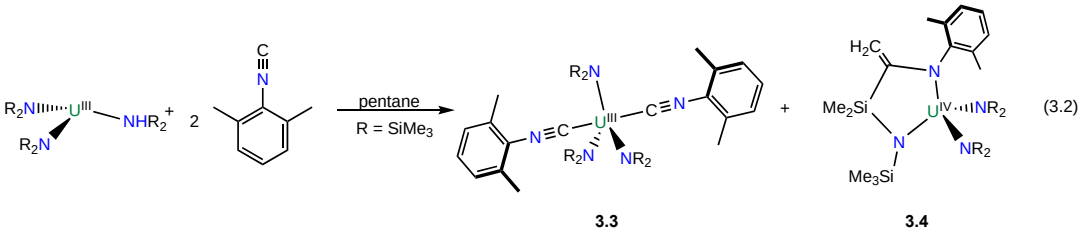

The ^{1}H NMR spectrum of **3.3** in C_6D_6 features resonances at -5.68 ppm (12H), assigned to the methyl groups on the phenyl rings, -5.25 ppm (54H), assigned to the $SiMe_3$ groups, 2.62 ppm (4H), assigned to the *m*- protons on the phenyl ring, and at 7.75 ppm (2H), assigned to the *p*-phenyl protons (Figure 3.4). There is also a very small amount of **3.4** present in the sample, as revealed by a singlet at -25.50 ppm in the spectrum.

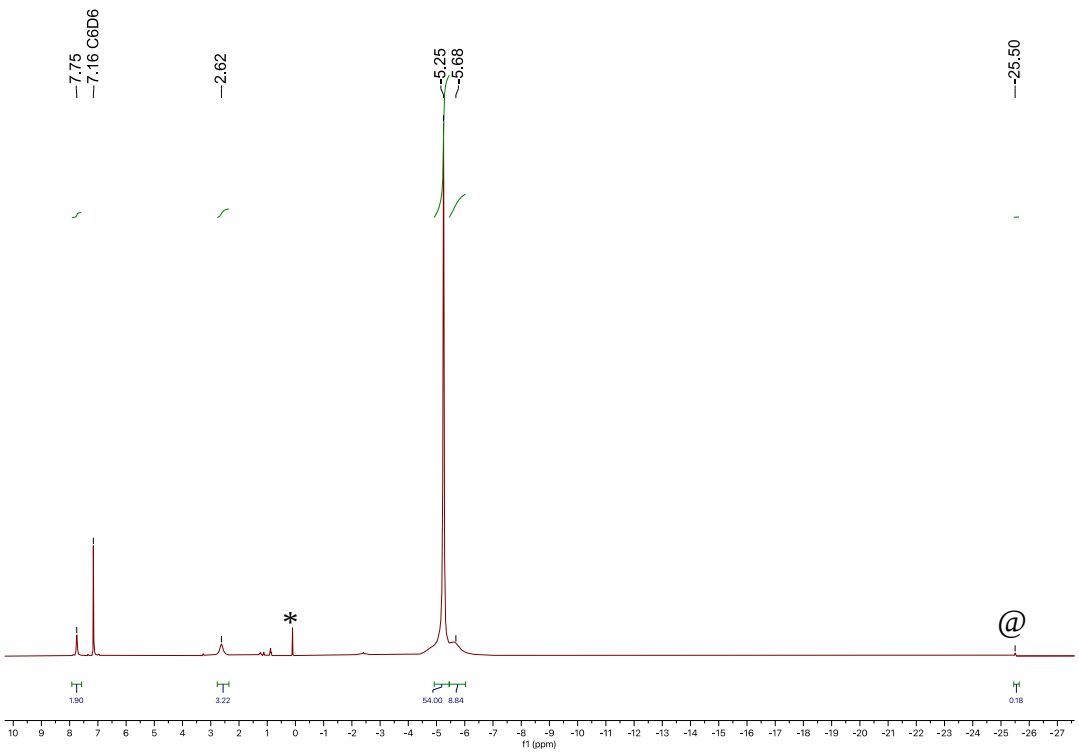

Figure 3.4. ^{1}H NMR spectrum of **3.3** in C_6D_6. (*) indicates the presence of $HN(SiMe_3)_2$ and (@) indicates the presence of **3.4**.

The connectivity of complex **3.3** was verified by X-ray crystallography (Figure 3.5). Complex **3.3** crystalizes in the monoclinic space group *P2₁/n*. In the solid-state, the isocyanide ligands are *trans* disposed and the three silylamide ligands are located on equatorial sites in an idealized trigonal bipyramid geometry about the U center. The U-C bond distances (2.725(6) and 2.733(6) Å) are much longer than reported distances seen in $[(Me_4C_5H)_3U(CNC_6H_4\text{-}p\text{-}OMe)]$ (2.464(4) Å),[55] $[UBr\{C_5H_3[SiMe_3]_2\}_2][CNtBu]_2$ (2.662(8), 2.697(7) Å),[58] and $[U(C_5H_3(R)_2)_2Cl(CN(C_6H_3Me_2))_2]$ (2.681(9), 2.654(9) Å).[59] The U-C-N linkage is almost linear (av. 173.5°), which compares well to other U(III) isocyanide complexes.[55, 58] The C-N bond distances (1.162(6) and 1.157(6) Å) are also similar to those

in other U(III) isocynaides.[55, 58] Lastly, the average U-$N_{silylamide}$ bond length is 2.368 Å, which is consistent with those reported for other U(III) amide complexes.[7, 39, 60]

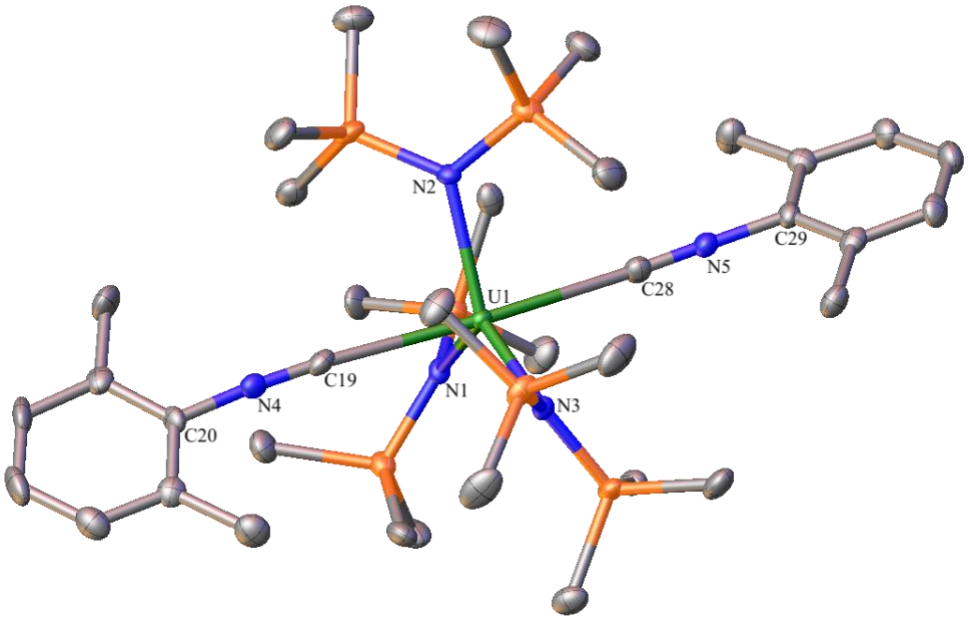

Figure 3.5. Solid-state structure of **3.3**, shown with 50% probability ellipsoids. Hydrogen atoms have been removed for clarity. Selected bond lengths (Å) and angles (°): av. U1-N_{amide} = 2.368, C19-U1-C28 = 176.30(15), U1-C28 = 2.733(6), C28-N5 = 1.162(6), N5-C29 = 1.405(6), U1-C19 = 2.725(6), C19-N4 = 1.157(6), N4-C20 = 1.390(7), U1-C19-N4 = 174.9(3), U1-C28-N5 = 172.1(4).

Complex **3.3** is soluble in pentane, Et_2O, and benzene, but reacts with THF, as indicated by a color change from blue-green to maroon Complex **3.3** is stable at room temperature in a benezene-d_6 solution for up to 8 h; however, a color change from green to yellow was observed after 24 h, and the complex is completely decomposed after 48 h. In addition, the IR spectrum of **3.3** features a prominent ν_{CN} stretch at 2131 cm^{-1} (Figure 3.6), which is higher than that seen in free Xyl isocyanide (ν_{CNXyl} = 2114 cm^{-1}).[55] For comparison, this higher energy stretch is closer to what was observed in the Ce(III) compound, [$(MeC_5H_4)_3Ce(CNXyl)$] (ν_{CNXyl} =

2150 cm^{-1}),[55] than what has been reported for U(III) CNXyl complexes $[(MeC_5H_4)_3U(CNXyl)]$, $[(MeC_5H_4)_3U(CNXyl)_2]$, and $[(C_5Me_4H)_3U(CNXyl)]$, which are 50-60 cm^{-1} lower in frequency than free Xyl isocyanide.[55]

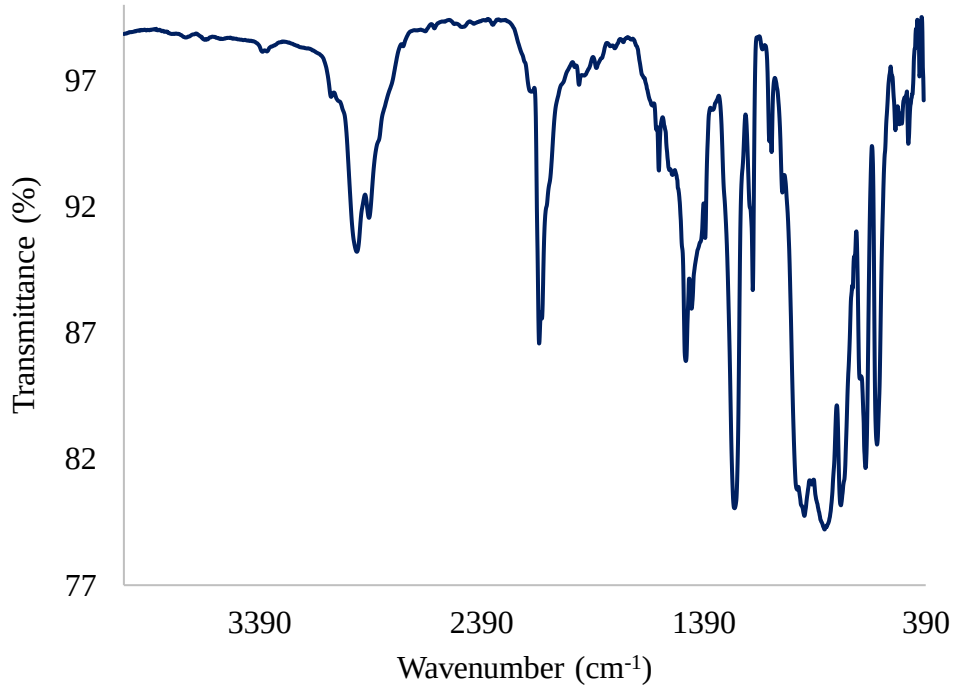

Figure 3.6. IR spectrum of **3.3** (KBr pellet).

3.2.3 Synthesis and Characterization of $[U\{N(R)SiC(=CH_2)N(Xyl)\}(NR_2)_2]$ (3.4)

Complex **3.4** was synthesized directly by reacting 1 equiv of 2,6-dimethylphenyl isocyanide with the known uranium metallacycle, $[U\{N(R)(SiMe_2)CH_2\}(NR_2)_2]$,[43] in pentane. Work-up in a concentrated pentane solution yields **3.4** in 93% yield (eqn (3.3)) as orange crystals. This type of insertion is known, as observed in **3.2**, reported by Andersen and co-workers in 1981.[43]

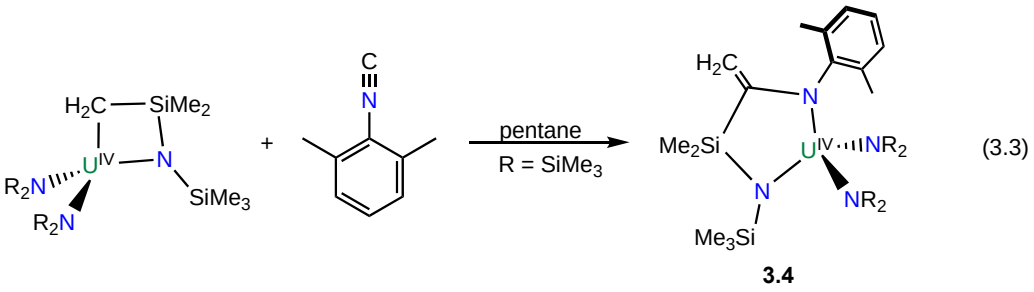

The ^{1}H NMR spectrum of **3.4** in C_6D_6 features a broad resonance at -62.62 ppm (9H), assignable to the $SiMe_3$ group, a sharp singlet at -25.31 ppm (36H), assignable to the $SiMe_3$ groups, two singlets at -2.94 ppm (3H) and -1.19 ppm (3H) assignable to inequivalent methyl groups off the aryl substituent, two singlets at 1.99 ppm (1H) and 2.24 ppm (1H) assignable to the inequivalent protons from the methylene group, and a triplet at 8.22 ppm (3H) assignable to the inequivalent *m*- and *p*-protons on the aryl ring, and one broad peak at 88.20 ppm (6H) assignable to the $SiMe_2$ group (Figure 3.7). However, these assignments are tentative, and there are several broad resonances that cannot definitely be accounted for.

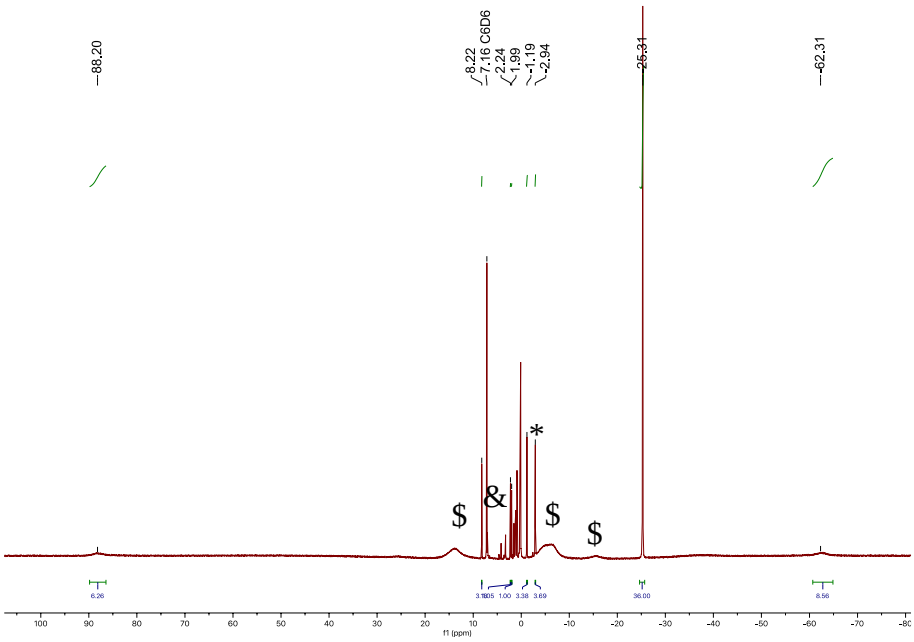

Figure 3.7. ^{1}H NMR spectrum of **3.4** in C_6D_6. (*) indicates $HN(SiMe_3)_2$, (&) indicates Et_2O, pentane, hexanes, and ($) indicates unidentified peak.

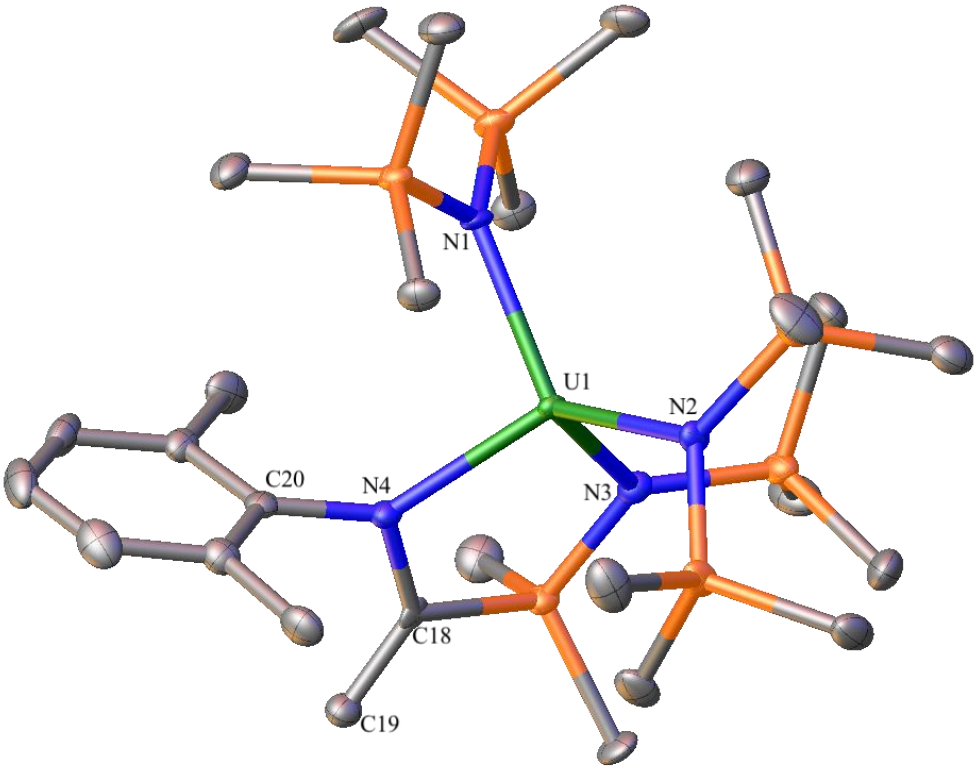

Figure 3.8. Solid-state structure of **3.4**, shown with 50% probability ellipsoids. Hydrogen atoms and solvent molecules have been removed for clarity. Selected bond lengths (Å) and angles (°): av. U-N_{amide} = 2.260, U1-N4 = 2.252(5), N4-C20 = 1.449(8), C18-C19 = 1.335(10), N4-U1-N3 = 89.5(2).

The connectivity of complex **3.4** was verified by X-ray crystallography (Figure 3.8). Complex **3.4** crystalizes in the triclinic space group *P-1*. In the solid-state, the U center features four-coordinate geometry. The C18-C19 bond is 1.335(10) Å, suggesting a double bond, the U1-N4 bond is 2.252(5) Å, suggesting a single bond, while the U-N_{amide} bond lengths average 2.260 Å, which is consistent with those reported for other U(IV) amide complexes.[47-49] This structure is very similar to Andersen's reported complex, [U{*N*(R)SiC(=CH_2)*N*(^{t}Bu)}(NR_2)$_2$],[43] which was seen in the formation of **3.1**, however no crystallographic data was reported. However, the IR spectra of **3.4** ($\nu_{C=C}$ = 1533 cm^{-1}) (Figure

3.9) compares well to Andersen and co-workers *tert*-butyl analogue, which reports a C=C stretch at 1537 cm^{-1}.[43] Furthermore, the Th *tert*-butyl analogue reports a similar C=C stretch at 1535 cm^{-1}.[43]

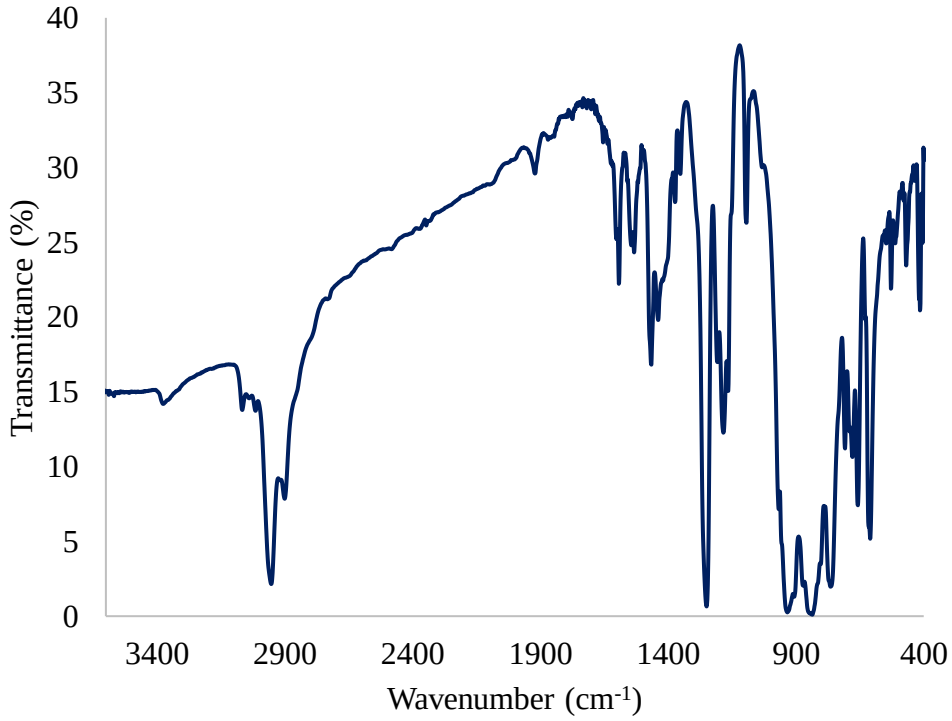

Figure 3.9. IR spectrum of **3.4** (KBr pellet).

3.2.4 Reactions of $U(NR_2)_3(CNXyl)_2$ (3.3) with TMSCl

In an attempt to synthesize a carbene in a similar route reported by Figueroa and co-workers,[38] the reaction of **3.3** with the electrophile TMSCl, in a benzene-d_6 solution, was monitored *via* ^{1}H NMR spectroscopy. Over the course of 3 d, a color change from dark blue-green to dark brown-yellow occurs, while the resonances assigned to **3.3** decreased in intensity and a broad resonance at ca. -2 ppm grew in intensity. Upon work-up, yellow crystals were isolated in low yield upon cooling (-25 °C) after 24 h, which were run on the X-ray spectrometer. The yellow crystals had a unit cell that matched $U(NR_2)_3Cl_2$.[61]

In another attempt to form a carbene, **3.3** was initially reduced with 1 equiv of KC_8 before the addition of TMSCl. Thus, KC_8 was added to a dark blue-green Et_2O solution of **3.3**, which resulted in a color change to dark yellow. After 30 min, the reaction mixture was filtered and TMSCl was added, which resulted in a color change to golden yellow. A ^1H NMR spectrum of the crude material in benzene-d_6 displayed one broad resonance at -2.41 ppm, assignable to the $SiMe_3$ environment of the known complex $U(NR_2)_3Cl$.[52]

From these results, I concluded that the use of TMSCl results in the oxidation at the metal center from U(III) to U(V) or U(IV), shown by the isolation of $U(NR_2)_3Cl_2$ and $U(NR_2)_3Cl$ (eqn (3.4)), respectively, but is unable to aid in the formation of the desired uranium carbene.

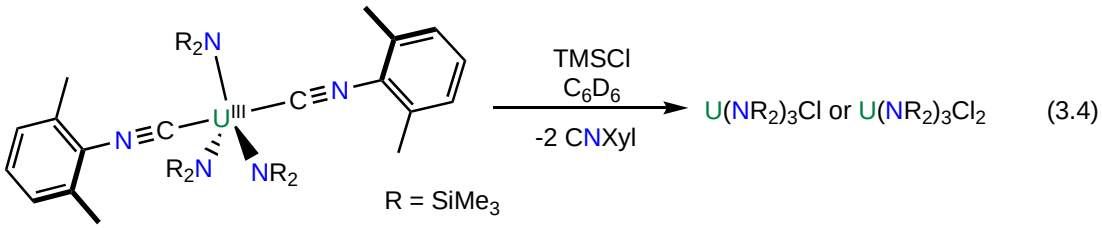

3.3

3.2.5 Reduction reactions of $U(NR_2)_3(CNXyl)_2$ (3.3) with KC_8 and $[Cp^*_2Co]^+$ and the Synthesis and Characterization of $[Cp^*_2Co][\{\eta^2\text{-}C,N\text{-}(Xyl)NCN(Xyl)\}U(NR_2)_3]$ (3.5)

I also sought to reduce the isocyanide ligand in complex **3.3** with KC_8 and Cp^*_2Co. The use of KC_8 in Et_2O led to intractable dark yellow material, but ^1H NMR spectroscopy of the crude reaction mixture, in benzene-d_6, showed the presence of a new broad paramagnetic resonance at ca. -11 ppm. Complexing agents such as 18-crown-6, dibenzo-18-crown-6, and 2,2,2-cryptand were added to reactions with KC_8 in an attempt to isolate X-ray quality material, but these reagents did not suffice. Gratifyingly, the reaction of **3.3** with 1 equiv of Cp^*_2Co in benzene affords insoluble dark emerald crystalline material of the U(IV) acetylene

diamide complex [Cp*$_2$Co][{η^2-*C*,*N*-(Xyl)NCN(Xyl)}U(NR$_2$)$_3$] (**3.5**), after 24 h in 40% yield (eq (3.5)).

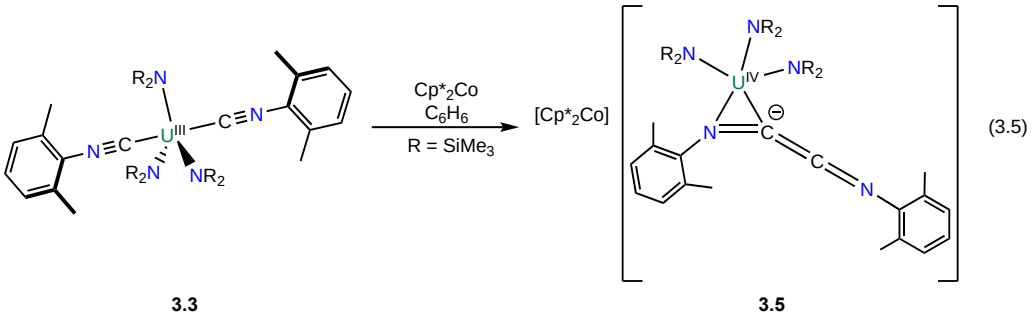

3.3 **3.5**

Complex **3.5** is formally generated by reducing the two CNXyl ligands by 2 electrons, where 1 electron comes from the uranium center, as the uranium center is oxidized from 3+ to 4+, and the other electron comes from decamethylcobaltocene. Other examples, all transition metal complexes that mostly contain molybdenum, have shown this ligand being protonated, as shown by work reported by Lippard and co-workers in Scheme 3.4, **A**-**B**,[62, 63] whereas **3.5** is not only the example of this ligand bound to an actinide, but also the first example of this ligand to be un-protonated.[64, 65]

Scheme 3.4. Previously reported protonation of the isocyanide ligand. A, Ref. 62; B, Ref. 63.

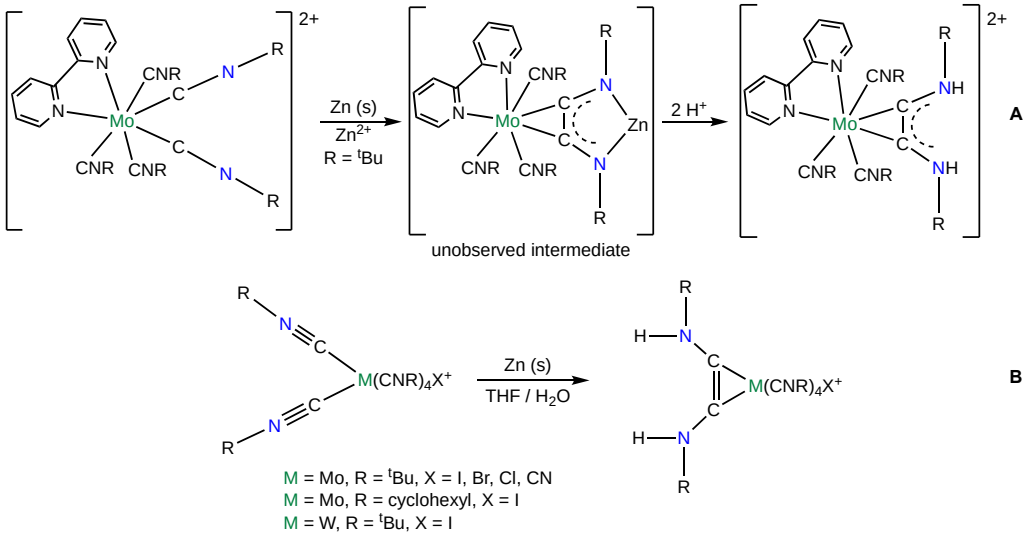

Furthermore, similar reactivity has been shown with CO, which is iso-electronic to isocyanide, as shown by the products formed *via* CO coupling in Scheme 3.5, **A**-**C**.[66-69] These complexes feature an acetylenediolate linkage, $[OCCO]^{2-}$, with the metal center. Similarly, two examples are reported in which isocyanide ligands have been coupled in a C-C bond formation with $[NCCN]^{2-}$ linkages bridging two metal centers, as shown in Scheme 3.5, **C**-**D**.[70-72] Moreover, the uranium-centered N-C binding mode found in **3.5** is unique versus previously coupled isocyanides, which feature a η^2-*C*,*C* bonding mode, as shown in Scheme 3.4 and Scheme 3.5, **C**-**D**.[62-65, 70-79]

Scheme 3.5. Previously reported coupling with CO and isocyanide. A, Ref. 66; B, Ref. 67; C, Refs. 68, 69; D, Ref. 72; E, Refs. 70, 71.

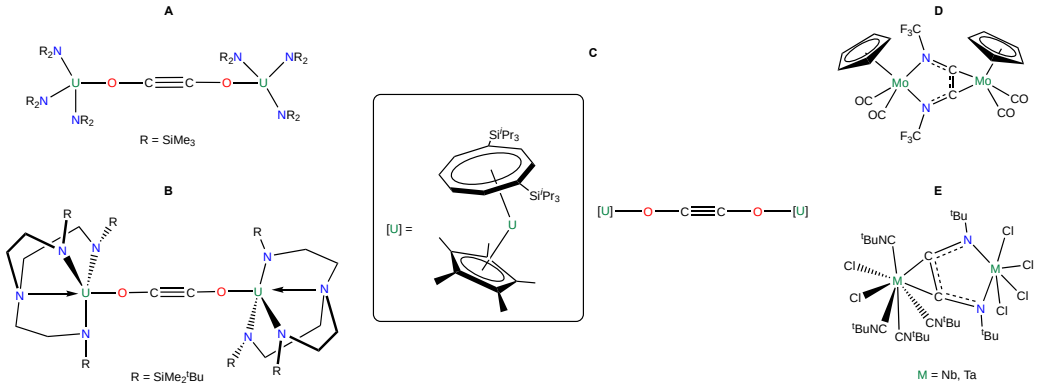

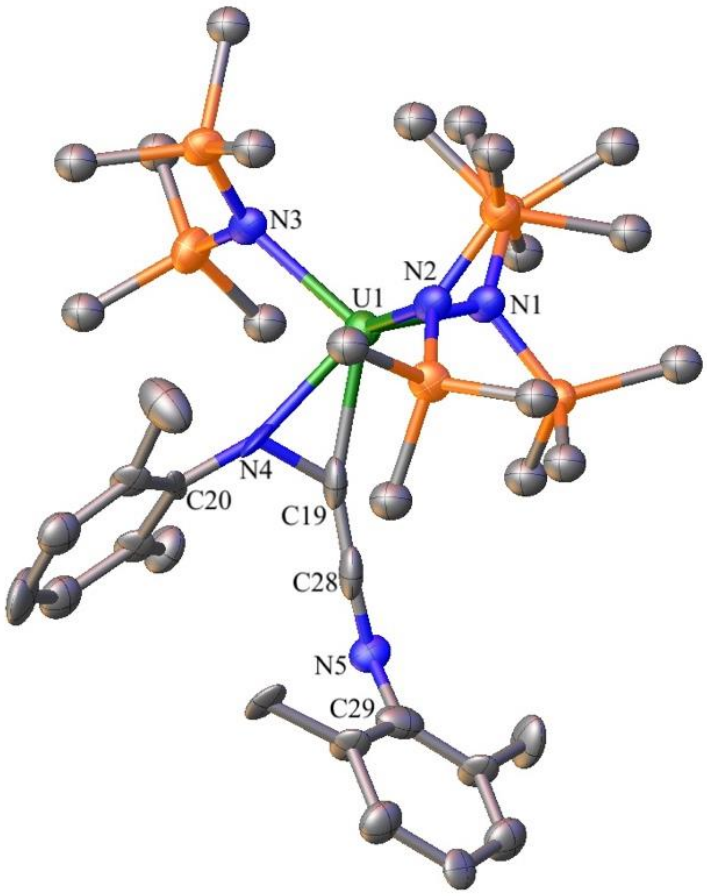

Figure 3.10. Solid-state structure of **3.5**, shown with 50% probability ellipsoids. $[Cp^*_2Co]^+$ counterion, hydrogen atoms, and benzene molecules removed for clarity. Selected bond lengths (Å) and angles (°): av. $U\text{-}N_{amide}$ = 2.31, U1-N4 = 2.24(3), N4-C20 = 1.40(4), N4-C19 = 1.42(4), C19-C28 = 1.35(5), C28-N5 = 1.28(4), N5-C29 = 1.37(4).

The connectivity of complex **3.5** was verified by X-ray crystallography (Figure 3.10). Complex **3.5** crystalizes in the tetragonal space group *P42bc*. In the solid-state, the U center features five-coordinate geometry. The two C-N bond lengths on the CNXyl ligand (N4-C19 = 1.42(4) Å, N5-C28 = 1.28(4) Å) are longer than in **3.3** (N4-C19 = 1.157(6) Å, N5-C28 = 1.162(6) Å) suggesting they are no longer triple bonds but double bonds due to the ligands

new binding mode with the uranium center. The U-N_{amide} bond lengths average 2.31 Å, which is consistent with those reported for other U(IV) amide complexes,[47-49] including **3.3**.

The ^{1}H NMR spectrum of **3.5** in THF-d_8 shows a similar spectrum to what was observed in the reactions with KC_8, which suggest the same product was being formed. The spectrum consists of a broad resonance upfield at -11.43 ppm, assigned to the $SiMe_3$ groups, a sharp peak at 1.10 ppm, assigned to the methyl environments on the Xyl groups, a broad singlet at 5.22 ppm, assigned to the methyl groups of the $[Cp^*_2Co]^+$ counterion, and two singlets at 23.15 and 30.47 ppm, assigned to the *p*- and *m*- groups of the Xyl groups, respectively (Figure 3.11). Interestingly, an initial THF-d_8 solution of **3.5** is green, but turns royal blue over several hours, where a follow-up ^{1}H NMR in THF-d_8 no longer shows the major product, suggesting reactivity of **3.5** with THF or decomposition.

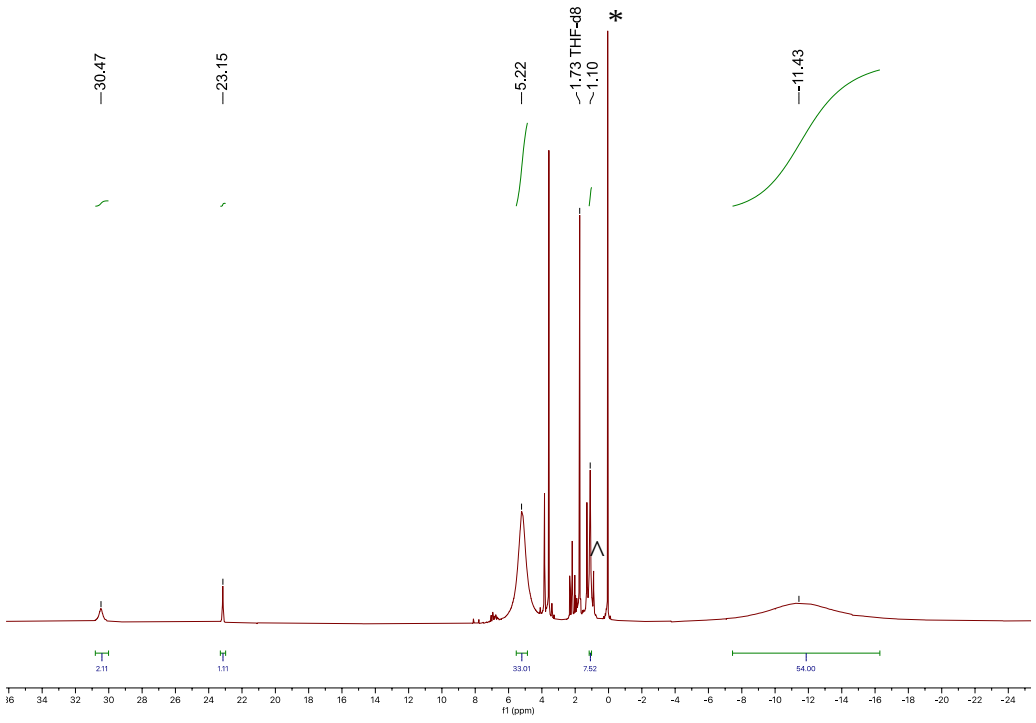

Figure 3.11. ^{1}H NMR spectrum of **3.5** in THF-d_8. (*) indicates $HN(SiMe_3)_2$ and (^) indicates pentane.

In addition, the IR spectrum of **3.5** features a prominent ν_{CN} stretch at 1913 cm^{-1}, which is significantly red shifted from the ν_{CN} stretch in **3.3** at 2131 cm^{-1} and that seen in free Xyl isocyanide (ν_{CNXyl} = 2114 cm^{-1})[55] (Figure 3.12).

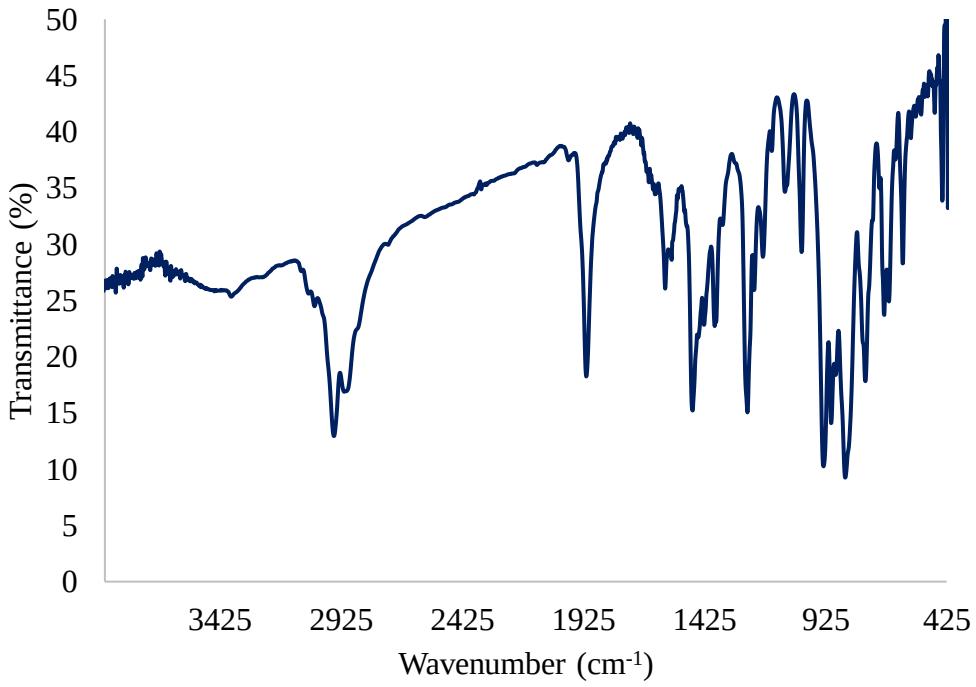

Figure 3.12. IR spectrum of **3.5** (KBr pellet).

3.3 Summary

I have synthesized and characterized new uranium isocyanide complexes using *tert*-butyl isocyanide and 2,6-dimethylphenyl isocyanide. In the former case, *tert*-butyl isocyanide was too oxidized, causing a redox reaction to occur, where the uranium center was oxidized, and the ligand was reduced to form complex **3.1**. In order to explain the aforementioned redox reaction, I hypothesize that the low valent U(III) starting material reduces the *tert*-butyl isocyanide to form a *tert*-butyl radical, resulting in the oxidation of the metal center from U 3+ to U 4+. I tried to observe this redox reaction *via* in-situ ^{1}H NMR spectroscopy, but was unable to observe the expected products, isobutylene and isobutene, if the reaction was indeed

making a *tert*-butyl radical. Therefore, I can only propose a hypothetical mechanistic pathway to **3.1**. However, it has been previously reported that alkyl isocyanide adducts are unstable in solution and decompose quickly to form cyanide,[56] suggesting that *t*Bu is a poor ligand choice for this reaction.

Moving away from alkyl substituents, I hypothesized that switching to an aryl isocyanide substituent, which has stronger sp^2 CN bonding, such as 2,6-dimethylphenyl isocyanide (CNXyl, Xyl = 2,6-$Me_2C_6H_3$), would not undergo this unwanted decomposition pathway. Upon reaction of uranium tris(amide) with 2 equiv CNXyl, complex **3.3** was synthesized, thus proving my hypothesis correct. However, I noticed that a minor side product was always formed in low yield, which was isolated and characterized as **3.4**. This side product is formed from 1 equiv of the CNXyl reacting with the decomposition product of uranium tris(amide) starting material, [U{*N*(R)(SiMe$_2$)*C*H$_2$}(NR$_2$)$_2$], which is usually around in small quantities making the isolation of pure **3.3** very difficult. Complex **3.4** was synthesized directly and fully characterized. A similar decomposition product was isolated en route to **3.1**, where 1 equiv of the *tert*-butyl isocyanide ligand reacted with [U{*N*(R)(SiMe$_2$)*C*H$_2$}(NR$_2$)$_2$] to form **3.2**, which has been previously reported by Andersen and co-workers.[43]

With a stable U(III) isocyanide adduct in hand, I attempted to synthesize a carbene *via* the route reported by Figueroa and co-workers,[38] by reacting **3.3** with an electrophile. Although, reactions of **3.3** with TMSCl resulted in the desired oxidation of the uranium center, as indicated by X-ray crystallography and ^{1}H NMR spectroscopy of the isolated material, I was unable to synthesize the desired uranium carbene. These results suggested that the addition of an electrophile would not be fruitful, so I sought to explore possible reducing agents, such as KC_8 and Cp*$_2$Co. Although initial reduction reactions with KC_8 suggested a reaction was

occurring, indicated by a color change, no tractable material was isolated. However, ^{1}H NMR spectroscopy of the crude material showed support for the formation of a new product due to the presence of a new upfield paramagnetic resonance.

Efforts to reduce complex **3.3** using the reducing agent Cp^*_2Co led to formation of a U(IV) acetylene diamide complex, **3.5**. Moreover, the ^{1}H NMR spectrum of **3.5** aligns well with what was previously observed in ^{1}H NMR spectrums of the crude material isolated in the reactions with KC_8, suggesting that **3.5** is the only product being synthesized between **3.3** and a reducing agent.

Although **3.5** was not the intended carbene product, I was able to show that the CNXyl ligand can be reduced as the metal center is oxidized. Going forward, this method of carbene formation will likely not work with the actinides. However, complex **3.5** is the first example that shows reductive coupling of isocyanide with an actinide and displays a novel binding mode, N-C metal centered versus C-C, which has not been observed previously.

3.4 Acknowledgements

This work was supported by the U.S. Department of Energy, Office of Basic Energy Sciences, Chemical Sciences, Biosciences, and Geosciences Division, under Contract DE-SC0001861.

3.5 Experimental

3.5.1 General Methods

All reactions and subsequent manipulations were performed under anaerobic and anhydrous conditions under an atmosphere of nitrogen. Hexanes, Et_2O, and pentane, were dried using a Vacuum Atmospheres DRI-SOLV Solvent Purification system and stored over

3Å sieves for 24 h prior to use. THF was dried by distillation from sodium/benzophenone, and stored over 3Å sieves for 24 h prior to use. Benzene-d_6 and THF-d_8 were dried over 3Å molecular sieves for 24 h prior to use. U(N(SiMe$_2$)$_3$) and [U{*N*(R)(SiMe$_2$)*C*H$_2$}(NR$_2$)$_2$] were synthesized according to the previously reported procedure.[39, 43] Cp*$_2$Co was recrystalixed from hexanes before use. All other reagents were purchased from commercial suppliers and used as received.

NMR spectra were recorded on an Agilent Technologies 400-MR DD2 400 MHz Spectrometer, a Varian UNITY INOVA 500 spectrometer, or a Varian Unity Inova 600 MHz spectrometer. ^{1}H NMR spectra were referenced to external tetramethylsilane (TMS) using the residual protio solvent peaks as internal standards. IR spectra were recorded on a Nicolet 6700 FT-IR spectrometer with a NXR FT Raman Module. Electronic absorption spectra were recorded on a Shimadzu UV3600 UV-NIR Spectrometer. Elemental analyses were performed by the Micro-Analytical Facility at the University of California, Berkeley.

3.5.2 Synthesis and Characterization of [U(NR$_2$)$_3$(CN)(CN^{t}Bu)] (R = SiMe$_3$) (3.1)

To a stirring, cold (-25 °C), purple solution of U(N(SiMe$_2$)$_3$) (36.8 mg, 0.0517 mmol) in pentane (2 mL) was added a solution of *tert*-butyl isocyanide (12 μL, 0.00851 mg, 0.102 mmol). The dark green reaction mixture was allowed to warm to room temperature with stirring. After 6 h, the reaction mixture became an orange solution with a lime green precipitate. The reaction mixture was filtered through a Celite column supported on glass wool (0.5 × 2 cm) and the orange pentane solution was concentrated *in vacuo* to 2 mL. Storage at -25 °C for 24 h resulted in the deposition of orange crystalline material, which was isolated by decanting the supernatant and then dried *in vacuo* to yield the known product, [U{*N*(R)SiC(=CH$_2$)*N*(^{t}Bu)}(NR$_2$)$_2$] (**3.2**), which was confirmed by ^{1}H NMR spectroscopy.[43]

The lime green solid on the Celite column was extracted into THF and the lime green solution was layered with pentane. Storage at -25 °C for 24 h resulted in the deposition of **3.1** as a green crystalline solid (0.042 g, 32% yield). Anal. Calcd for $C_{24}H_{63}N_5Si_6U$: C, 34.80; H, 7.67; N, 8.45. Found: C, 29.14; H, 6.90; N, 7.07. ^{1}H NMR (400 MHz, 25 °C, THF-d_8): δ -7.24 (br s, 9H, CN^t*Bu*), 2.15 (br s, 54H, SiC*H*$_3$). IR (KBr pellet, cm^{-1}): 480 (m), 615 (s), 619 (s), 756 (m), 843 (w), 1059 (m), 1184 (s), 1248 (s), 1400 (w), 1601 (m), 2056 (s, ν_{CN}), 2189 (s, ν_{CNtBu}), 2897 (w), 2951 (w), 3348 (m).

3.5.3 Synthesis and Characterization of U(NR$_2$)$_3$(CNXyl)$_2$ (Xyl = 2,6-Me$_2$C$_6$H$_3$) (3.3)

To a stirring, cold (-25 °C), purple solution of U(N(SiMe$_2$)$_3$) (163.3 mg, 0.2271 mmol) in pentane (2 mL) was added a cold (-25 °C) pentane solution of 2,6-Dimethylphenyl isocyanide (CNXyl) (60.1 mg, 0.458 mmol). The dark blue-green reaction mixture was allowed to warm to room temperature with stirring. After 30 min, the reaction mixture was filtered through a Celite column supported on glass wool (0.5 × 2 cm) and concentrated *in vacuo* to 2 mL. Storage at -25 °C for 24 h resulted in the deposition of dark green crystalline material, which was isolated by decanting the supernatant and then dried *in vacuo* to yield **3.3** (94.2 mg). The supernatant was transferred to a new 20 mL vial. Storage at -25 °C for 24 h resulted in the deposition of more dark green crystalline solid (15.2 mg). Total yield: 0.109 g, 50% yield. Anal. Calcd for $C_{36}H_{72}N_5Si_6U$: C, 44.05; H, 7.39; N, 7.14. Found: C, 44.25; H, 7.24; N, 6.92. ^{1}H NMR (400 MHz, 25 °C, C_6D_6): δ -25.50 (s, **2**), -5.68 (br s, 12H, phenyl-C*H*$_3$), -5.25 (s, 54H, SiC*H*$_3$), 2.62 (s, 4H, phenyl-*m*), 7.75 (s, 2H, phenyl-*p*). IR (KBr pellet, cm^{-1}): 469 (m), 606 (s), 660 (s), 768 (w), 835 (w), 933 (w), 1167 (s), 1248 (m), 1470 (w), 2131 (m, ν_{CNXyl}), 2895 (w), 2951 (w).

3.5.4 Synthesis and Characterization of [U{*N*(R)(SiC(=CH$_2$)*N*(Xyl)}(NR$_2$)$_2$] (3.4)

To a stirring, cold (-25 °C), orange solution of [U{*N*(R)(SiMe$_2$)*C*H$_2$}(NR$_2$)$_2$] (36.2 mg, 0.0504 mmol) in pentane (2 mL) was added a cold (-25 °C) pentane (2 mL) solution of 2,6-Dimethylphenyl isocyanide (7.20 mg, 0.0549 mmol). After 20 min, the solution was filtered through a Celite column supported on glass wool (0.5 × 2 cm) and concentrated *in vacuo* to 1 mL. Storage at -25 °C for 24 h resulted in the deposition of orange crystalline material, which was isolated by decanting the supernatant and then dried *in vacuo* to yield **3.4**. Total yield: 0.0398 g, 93% yield. Anal. Calcd for $C_{27}H_{62}N_4Si_6U$: C, 38.181; H, 7.36; N, 6.60. Found: C, 38.17; H, 7.36; N, 6.47. ^{1}H NMR (400 MHz, 25 °C, C_6D_6): δ -62.90 (br s, 3H, phenyl-C*H*$_3$), -25.31 (s, 18H, SiC*H*$_3$), -5.98 (br s, 18H, SiC*H*$_3$), -2.94 (s, 2H, C*H*$_2$), -1.19 (s, 2H, phenyl-*m*), 8.22 (s, 1H, phenyl-*p*), 13.84 (br s, 6H, SiC*H*$_3$), 88.20 (br s, 3H, phenyl-C*H*$_3$). IR (KBr pellet, cm^{-1}): 415 (s), 607 (s), 762 (w), 835 (w), 930 (w), 1093 (s), 1184 (m), 1248 (s), 1437 (m), 1479 (m), 1533 (s, $\nu_{C=C}$), 1593 (s), 2899 (w), 2953 (w).

3.5.5 Synthesis and Characterization of [Cp*$_2$Co][{η^2-*C*,*N*-(Xyl)NCN(Xyl)}U(NR$_2$)$_3$] (3.5)

To a teal benzene solution (1 mL) of **3.3** (18.9 mg, 0.0193 mmol) was added Cp*$_2$Co (6.3 mg, 0.0192 mmol) as a crystalline solid. After 24 h, dark crystalline material precipitated out of an amber solution and was isolated by decanting off the supernatant and then dried *in vacuo* to yield **3.5**. Total yield: 0.010 g, 40% yield. Anal. Calcd for $C_{56}H_{102}CoN_5Si_6U$: C, 51.31; H, 7.84; N, 5.34. Found: C, 52.25; H, 7.69; N, 5.15. ^{1}H NMR (400 MHz, 25 °C, THF-*d*$_8$): δ -11.43 (br s, 54H, SiC*H*$_3$), 1.10 (s, 6H, phenyl-C*H*$_3$), 5.22 (br s, 30H, Cp*$_2$Co), 23.15 (s, 1H, phenyl-*p*), 30.47 (s, 2H, phenyl-*m*). IR (KBr pellet, cm^{-1}): 606 (s), 663 (s), 683 (s), 760 (m),

845 (w), 931 (w), 1022 (s), 1032 (s), 1182 (s), 1246 (m), 1375 (m), 1473 (w), 1587 (m), 1913 (m, ν_{CN}), 2900 (w), 2953 (w).

3.5.6 X-ray Crystallography

Data for **3.1**, **3.3**, **3.4** and **3.5** were collected on a Bruker KAPPA APEX II diffractometer equipped with an APEX II CCD detector using a TRIUMPH monochromator with a Mo Kα X-ray source (α = 0.71073 Å). The crystals were mounted on a cryoloop under Paratone-N oil. Complex **3.1**, **3.3**, and **3.5** were collected at 100(2) K and complex **3.4** was collected at 104(2) K, using an Oxford nitrogen gas cryostream. Data were collected using ω scans with 0.5° frame widths. Frame exposures of 20, 5, 10, and 30 seconds were used for **3.1**, **3.3**, **3.4**, and **3.5** respectively. Data collection and cell parameter determinations were conducted using the SMART program.[80] Integration of the data frames and final cell parameter refinements were performed using SAINT software.[81] Absorption corrections of the data were carried out using the multi-scan method SADABS for **3.1**, **3.3**-**3.5**.[82] Subsequent calculations were carried out using SHELXTL or Olex2.[83-85] Structure determination was done using direct or Patterson methods and difference Fourier techniques. All hydrogen atom positions were idealized, and rode on the atom of attachment. Structure solution, refinement, graphics, and creation of publication materials were performed using SHELXTL.[83] Further crystallographic details can be found in Table 3.1 and 3.2.

Table 3.1. X-ray Crystallographic Data for **3.1**, **3.3**, and **3.4**.

	3.1	**3.3**	**3.4**
empirical formula	$C_{28}H_{72}N_5Si_6U$	$C_{36}H_{72}N_5Si_6U$	$C_{29.5}H_{62}N_4Si_6U$
crystal habit, color	Block, Green	Plate, Dark Green	Plate, Orange
crystal size (mm)	0.15 × 0.15 × 0.1	0.15 × 0.1 × 0.1	0.2 × 0.1 × 0.05
space group	$P\bar{3}_1c$	$P2_1/n$	$P\text{-}1$
volume (Å^3)	2161.5(10)	4779(5)	2122.1(14)
a (Å)	14.151(3)	13.020(9)	11.654(4)
b (Å)	14.151(3)	18.767(10)	11.887(4)
c (Å)	12.464(2)	19.560(10)	16.836(7)
α (deg)	90	90	69.983(17)
β (deg)	90	90.61(2)	78.421(15)
γ (deg)	120	90	78.000(17)
Z	2	4	2
formula weight (g/mol)	885.47	981.55	879.40
density (calculated) (Mg/m^3)	1.360	1.364	1.376
absorption coefficient (mm^{-1})	3.944	3.575	4.017
F_{000}	902	1996	886
total no. reflections	11128	23675	12528
unique reflections	1258	10438	8607
Final R Indices (I >2σ(I)]	R_1 = 0.0664 wR_2 = 0.1595	R_1 = 0.0373 wR_2 = 0.0658	R_1 = 0.0474 wR_2 = 0.1149
largest diff. peak and hole (e$^-$ A^{-3})	1.120 and -0.512	0.853 and -0.703	5.077 and -2.810
GOF	1.133	0.998	1.017

Table 3.2. X-ray Crystallographic Data for **3.5**.

	3.5
empirical formula	$C_{59}H_{105}CoN_5Si_6U$
crystal habit, color	Plate, Brown
crystal size (mm)	0.15 × 0.15 × 0.05
space group	$P42bc$
volume ($Å^3$)	13679(18)
a (Å)	24.163(13)
b (Å)	24.163(13)
c (Å)	23.430(17)
α (deg)	90
β (deg)	90
γ (deg)	90
Z	8
formula weight (g/mol)	1349.97
density (calculated) (Mg/m^3)	1.311
absorption coefficient (mm^{-1})	2.749
F_{000}	5576
total no. reflections	81528
unique reflections	11253
Final R Indices ($I > 2\sigma(I)$)]	$R_1 = 0.1020$ $wR_2 = 0.2279$
largest diff. peak and hole ($e^- A^{-3}$)	2.338 and -0.859
GOF	1.128

3.6 References

1. Hayton, T. W., Metal–ligand multiple bonding in uranium: structure and reactivity. *Dalton Trans.* **2010,** *39* (5), 1145-1158.
2. Hayton, T. W., Recent developments in actinide–ligand multiple bonding. *Chem. Commun.* **2013,** *49* (29), 2956-2973.
3. Jones, M. B.; Gaunt, A. J., Recent Developments in Synthesis and Structural Chemistry of Nonaqueous Actinide Complexes. *Chem. Rev.* **2013,** *113* (2), 1137-1198.
4. King, D. M.; Liddle, S. T., Progress in molecular uranium-nitride chemistry. *Coord. Chem. Rev.* **2014,** *266-267*, 2-15.
5. Liddle, S. T., The Renaissance of Non-Aqueous Uranium Chemistry. *Angew. Chem. Int. Ed.* **2015,** *54* (30), 8604-8641.
6. Patel, D.; Liddle, S. T., f-Element-metal bond chemistry. *Prog. Inorg. Chem.* **2012,** *32* (1), 1.
7. Staun, S. L.; Stevens, L. M.; Smiles, D. E.; Goodwin, C. A. P.; Billow, B. S.; Scott, B. L.; Wu, G.; Tondreau, A. M.; Gaunt, A. J.; Hayton, T. W., Expanding the Nonaqueous Chemistry of Neptunium: Synthesis and Structural Characterization of $[Np(NR_2)_3Cl]$, $[Np(NR_2)_3Cl]^-$, and $[Np\{N(R)(SiMe_2CH_2)_2(NR_2)]^-$ (R = $SiMe_3$). *Inorg. Chem.* **2021,** *60* (4), 2740-2748.
8. Chatelain, L.; Scopelliti, R.; Mazzanti, M., Synthesis and Structure of Nitride-Bridged Uranium(III) Complexes. *J. Am. Chem. Soc.* **2016,** *138* (6), 1784-1787.
9. Falcone, M.; Barluzzi, L.; Andrez, J.; Fadaei Tirani, F.; Zivkovic, I.; Fabrizio, A.; Corminboeuf, C.; Severin, K.; Mazzanti, M., The role of bridging ligands in dinitrogen reduction and functionalization by uranium multimetallic complexes. *Nat. Chem.* **2019,** *11* (2), 154-160.
10. Falcone, M.; Chatelain, L.; Mazzanti, M., Nucleophilic Reactivity of a Nitride-Bridged Diuranium(IV) Complex: CO_2 and CS_2 Functionalization. *Angew. Chem. Int. Ed.* **2016,** *55* (12), 4074-4078.
11. Falcone, M.; Chatelain, L.; Scopelliti, R.; Mazzanti, M., CO Cleavage and CO Functionalization under Mild Conditions by a Multimetallic CsU_2 Nitride Complex. *CHIMIA* **2017,** *71* (4), 209-212.
12. Falcone, M.; Kefalidis, C. E.; Scopelliti, R.; Maron, L.; Mazzanti, M., Facile CO Cleavage by a Multimetallic CsU_2 Nitride Complex. *Angew. Chem. Int. Ed.* **2016,** *55* (40), 12290-12294.
13. Falcone, M.; Poon, L. N.; Fadaei Tirani, F.; Mazzanti, M., Reversible Dihydrogen Activation and Hydride Transfer by a Uranium Nitride Complex. *Angew. Chem. Int. Ed.* **2018,** *57* (14), 3697-3700.
14. Mullane, K. C.; Ryu, H.; Cheisson, T.; Grant, L. N.; Park, J. Y.; Manor, B. C.; Carroll, P. J.; Baik, M.-H.; Mindiola, D. J.; Schelter, E. J., C–H Bond Addition across a Transient Uranium–Nitrido Moiety and Formation of a Parent Uranium Imido Complex. *J. Am. Chem. Soc.* **2018,** *140* (36), 11335-11340.
15. Thomson, R. K.; Cantat, T.; Scott, B. L.; Morris, D. E.; Batista, E. R.; Kiplinger, J. L., Uranium azide photolysis results in C–H bond activation and provides evidence for a terminal uranium nitride. *Nat. Chem.* **2010,** *2*, 723.
16. Cooper, O. J.; Mills, D. P.; McMaster, J.; Moro, F.; Davies, E. S.; Lewis, W.; Blake, A. J.; Liddle, S. T., Uranium–Carbon Multiple Bonding: Facile Access to the

Pentavalent Uranium Carbene [U{C(PPh$_2$NSiMe$_3$)$_2$}(Cl)$_2$(I)] and Comparison of U^{V}=C and U^{IV}=C Bonds. *Angew. Chem. Int. Ed.* **2011,** *123* (10), 2431-2434.
17. Cramer, R. E.; Bruck, M. A.; Edelmann, F.; Afzal, D.; Gilje, J. W.; Schmidbaur, H., Synthesis and structure of Cp$_3$U=CHPMe$_3$: A compound with a U-C multiple bond. *Chem. Ber.* **1988,** *121* (3), 417-420.
18. Cramer, R. E.; Maynard, R. B.; Paw, J. C.; Gilje, J. W., A uranium-carbon multiple bond. Crystal and molecular structure of (η^5-C$_5$H$_5$)$_3$UCHP(CH$_3$)$_2$(C$_6$H$_5$). *J. Am. Chem. Soc.* **1981,** *103* (12), 3589-3590.
19. Ma, G.; Ferguson, M. J.; McDonald, R.; Cavell, R. G., Actinide Metals with Multiple Bonds to Carbon: Synthesis, Characterization, and Reactivity of U(IV) and Th(IV) Bis(iminophosphorano)methandiide Pincer Carbene Complexes. *Inorg. Chem.* **2011,** *50* (14), 6500-6508.
20. Ren, W.; Deng, X.; Zi, G.; Fang, D.-C., The Th=C double bond: an experimental and computational study of thorium poly-carbene complexes. *Dalton Trans.* **2011,** *40* (38), 9662-9664.
21. Lu, E.; Boronski, J. T.; Gregson, M.; Wooles, A. J.; Liddle, S. T., Silyl-Phosphino-Carbene Complexes of Uranium(IV). *Angew. Chem. Int. Ed.* **2018,** *57* (19), 5506-5511.
22. Rungthanaphatsophon, P.; Rosal, I. d.; Ward, R. J.; Vilanova, S. P.; Kelley, S. P.; Maron, L.; Walensky, J. R., Formation of an α-Diimine from Isocyanide Coupling Using Thorium(IV) and Uranium(IV) Phosphido–Methyl Complexes. *Organometallics* **2019,** *38* (8), 1733-1740.
23. Seed, J. A.; Sharpe, H. R.; Futcher, H. J.; Wooles, A. J.; Liddle, S. T., Nature of the Arsonium-Ylide Ph$_3$As=CH$_2$ and a Uranium(IV) Arsonium–Carbene Complex. *Angew. Chem. Int. Ed.* **2020,** *59* (37), 15870-15874.
24. Fox, A. R.; Bart, S. C.; Meyer, K.; Cummins, C. C., Towards uranium catalysts. *Nature* **2008,** *455* (7211), 341-349.
25. Mills, D. P.; Cooper, O. J.; Tuna, F.; McInnes, E. J. L.; Davies, E. S.; McMaster, J.; Moro, F.; Lewis, W.; Blake, A. J.; Liddle, S. T., Synthesis of a Uranium(VI)-Carbene: Reductive Formation of Uranyl(V)-Methanides, Oxidative Preparation of a [R$_2$C=U=O]$^{2+}$ Analogue of the [O=U=O]$^{2+}$ Uranyl Ion (R = Ph$_2$PNSiMe$_3$), and Comparison of the Nature of U^{IV}=C, U^{V}=C, and U^{VI}=C Double Bonds. *J. Am. Chem. Soc.* **2012,** *134* (24), 10047-10054.
26. Ephritikhine, M., Uranium carbene compounds. *Comptes Rendus Chimie* **2013,** *16* (4), 391-405.
27. Fortier, S.; Walensky, J. R.; Wu, G.; Hayton, T. W., Synthesis of a Phosphorano-Stabilized U(IV)-Carbene via One-Electron Oxidation of a U(III)-Ylide Adduct. *J. Am. Chem. Soc.* **2011,** *133* (18), 6894-6897.
28. Tourneux, J.-C.; Berthet, J.-C.; Cantat, T.; Thuéry, P.; Mézailles, N.; Ephritikhine, M., Exploring the Uranyl Organometallic Chemistry: From Single to Double Uranium−Carbon Bonds. *J. Am. Chem. Soc.* **2011,** *133* (16), 6162-6165.
29. Tourneux, J.-C.; Berthet, J.-C.; Cantat, T.; Thuéry, P.; Mézailles, N.; Le Floch, P.; Ephritikhine, M., Uranium(IV) Nucleophilic Carbene Complexes. *Organometallics* **2011,** *30* (11), 2957-2971.
30. Tourneux, J.-C.; Berthet, J.-C.; Thuéry, P.; Mézailles, N.; Le Floch, P.; Ephritikhine, M., Easy access to uranium nucleophilic carbene complexes. *Dalton Trans.* **2010,** *39* (10), 2494-2496.

31. Cantat, T.; Mézailles, N.; Auffrant, A.; Le Floch, P., Bis-phosphorus stabilised carbene complexes. *Dalton Trans.* **2008,** (15), 1957-1972.
32. Cantat, T.; Ricard, L.; Mézailles, N.; Le Floch, P., Synthesis, Reactivity, and DFT Studies of S−C−S Zirconium(IV) Complexes. *Organometallics* **2006,** *25* (26), 6030-6038.
33. Liddle, S. T.; Mills, D. P.; Wooles, A. J., Early metal bis(phosphorus-stabilised)carbene chemistry. *Chem. Soc. Rev.* **2011,** *40* (5), 2164-2176.
34. Jones, N. D.; Cavell, R. G., Phosphorus-substituted carbene complexes: Chelates, pincers and spirocycles. *J. Organometallic Chem.* **2005,** *690* (24), 5485-5496.
35. Becker, J.; Gessner, V. H., Synthesis and Electronic Structure of Carbene Complexes Based on a Sulfonyl-Substituted Dilithio Methandiide. *Organometallics* **2014,** *33* (5), 1310-1317.
36. Cantat, T.; Arliguie, T.; Noël, A.; Thuéry, P.; Ephritikhine, M.; Floch, P. L.; Mézailles, N., The U=C Double Bond: Synthesis and Study of Uranium Nucleophilic Carbene Complexes. *J. Am. Chem. Soc.* **2009,** *131* (3), 963-972.
37. Tatsumi, K.; Nakamura, A., Electronic structures of tris(cyclopentadienyl)uranium(IV)-ligand complexes. *J. Organomet. Chem.* **1984,** *272* (2), 141-154.
38. Mokhtarzadeh, C. C.; Moore, C. E.; Rheingold, A. L.; Figueroa, J. S., Terminal Iron Carbyne Complexes Derived from Arrested CO_2 Reductive Disproportionation. *Angew. Chem.* **2017,** *129* (36), 11034-11039.
39. Andersen, R. A., Tris((hexamethyldisilyl)amido)uranium(III): preparation and coordination chemistry. *Inorg. Chem.* **1979,** *18* (6), 1507-1509.
40. Avens, L. R.; Bott, S. G.; Clark, D. L.; Sattelberger, A. P.; Watkin, J. G.; Zwick, B. D., A Convenient Entry into Trivalent Actinide Chemistry: Synthesis and Characterization of $AnI_3(THF)_4$ and $An[N(SiMe_3)_2]_3$ (An = U, Np, Pu). *Inorg. Chem.* **1994,** *33* (10), 2248-2256.
41. Arnold, P. L., Uranium-mediated activation of small molecules. *Chem. Commun.* **2011,** *47* (32), 9005-9010.
42. Lam, O. P.; Meyer, K., Uranium-mediated carbon dioxide activation and functionalization. *Polyhedron* **2012,** *32* (1), 1-9.
43. Simpson, S. J.; Andersen, R. A., Actinide-Carbon Bonds: Insertion Reactions of Carbon Monoxide, *tert*-Butyl Isocyanide, and t*ert*-Butyl Cyanide into $[(Me_3Si)_2N]_2MCH_2Si(Me)_2NSiMe_3$. *J. Am. Chem. Soc.* **1981,** *103* (14), 4063-4066.
44. Boisson, C.; Berthet, J. C.; Lance, M.; Nierlich, M.; Ephritikhine, M., Reactivity of the cationic uranium amide compound $[U(\eta\text{-}C_5Me_5)_2(NMe_2)(OC_4H_8)][BPh_4]$. *J. Organomet. Chem.* **1997,** *548* (1), 9-16.
45. Boreen, M. A.; Groß, O. A.; Hohloch, S.; Arnold, J., Isocyanide adducts of tri- and tetravalent uranium metallocenes supported by tetra(isopropyl)cyclopentadienyl ligands. *Dalton Trans.* **2020,** *49* (34), 11971-11977.
46. Behrle, A. C.; Walensky, J. R., Insertion of ^{t}BuNC into thorium–phosphorus and thorium–arsenic bonds: phosphaazaallene and arsaazaallene moieties in f element chemistry. *Dalton Trans.* **2016,** *45* (24), 10042-10049.
47. Smiles, D. E.; Wu, G.; Hayton, T. W., Synthesis of Uranium–Ligand Multiple Bonds by Cleavage of a Trityl Protecting Group. *J. Am. Chem. Soc.* **2014,** *136* (1), 96-99.
48. Smiles, D. E.; Wu, G.; Hayton, T. W., Synthesis of Terminal Monochalcogenide and Dichalcogenide Complexes of Uranium Using Polychalcogenides, $[E_n]^{2-}$ (E = Te, n = 2;

E = Se, *n* = 4), as Chalcogen Atom Transfer Reagents. *Inorg. Chem.* **2014,** *53* (19), 10240-10247.
49. Smiles, D. E.; Wu, G.; Hayton, T. W., Synthesis, Electrochemistry, and Reactivity of the Actinide Trisulfides [K(18-crown-6)][An(η^3-S_3)(NR_2)$_3$] (An = U, Th; R = $SiMe_3$). *Inorg. Chem.* **2016,** *55* (18), 9150-9153.
50. Berthet, J.-C.; Thuéry, P.; Ephritikhine, M., The first actinyl cyanide. *Chem. Commun.* **2007,** (6), 604-606.
51. Hervé, A.; Bouzidi, Y.; Berthet, J.-C.; Belkhiri, L.; Thuéry, P.; Boucekkine, A.; Ephritikhine, M., U–CN versus Ce–NC Coordination in Trivalent Complexes Derived from M[N(SiMe3)2]3 (M = Ce, U). *Inorg. Chem.* **2014,** *53* (13), 6995-7013.
52. Hervé, A.; Bouzidi, Y.; Berthet, J.-C.; Belkhiri, L.; Thuéry, P.; Boucekkine, A.; Ephritikhine, M., U^{III}–CN versus U^{IV}–NC Coordination in Tris(silylamide) Complexes. *Inorg. Chem.* **2015,** *54* (5), 2474-2490.
53. Hervé, A.; Thuéry, P.; Ephritikhine, M.; Berthet, J.-C., Structural Diversity in Cyanido Thorocene Complexes. *Organometallics* **2014,** *33* (8), 2088-2098.
54. Maynadié, J.; Barros, N.; Berthet, J.-C.; Thuéry, P.; Maron, L.; Ephritikhine, M., The Crucial Role of the f Electrons in the Bent or Linear Configuration of Uranium Cyanido Metallocenes. *Angew. Chem. Int. Ed.* **2007,** *46* (12), 2010-2012.
55. del Mar Conejo, M.; Parry, J. S.; Carmona, E.; Schultz, M.; Brennann, J. G.; Beshouri, S. M.; Andersen, R. A.; Rogers, R. D.; Coles, S.; Hursthouse, M. B., Carbon Monoxide and Isocyanide Complexes of Trivalent Uranium Metallocenes. *Chem. Euro. J.* **1999,** *5* (10), 3000-3009.
56. Evans, W. J.; Mueller, T. J.; Ziller, J. W., Lanthanide versus Actinide Reactivity in the Formation of Sterically Crowded [$(C_5Me_5)_3ML_n$] Nitrile and Isocyanide Complexes. *Chem. Euro. J.* **2010,** *16* (3), 964-975.
57. Van der Sluys, W. G.; Sattelberger, A. P., Uranium Alkoxide Chemistry. 3. *tert*-Butyl Isocyanide Adducts of Tris(2,6-di-*tert*-butylphenoxy)uranium(III). *Inorg. Chem.* **1989,** *28* (12), 2496-2498.
58. Beshouri, S. M.; Zalkin, A., Bis[η^5-bis(trimethylsilyl)cyclopentadienyl]bromouranium(III) Bis(*tert*-butyl isocyanide). *Acta Cryst.* **1989,** *C45* (8), 1221-1222.
59. Zalkin, A.; Beshouri, S. M., Bis[bis(trimethylsilyl)cyclopentadienyl](chloro)uranium(III)Bis(2, 6-dimethylphenylisocyanide). *Acta Cryst.* **1989,** *C45* (7), 1080-1082.
60. Mansell, S. M.; Perandones, B. F.; Arnold, P. L., New U^{III} and U^{IV} silylamides and an improved synthesis of $NaN(SiMe_2R)_2$ (R = Me, Ph). *J. Organometallic Chem.* **2010,** *695* (25), 2814-2821.
61. Lewis, A. J.; Nakamaru-Ogiso, E.; Kikkawa, J. M.; Carroll, P. J.; Schelter, E. J., Pentavalent uranium *trans*-dihalides and -pseudohalides. *Chem. Commun.* **2012,** *48* (41), 4977-4979.
62. Giandomenico, C. M.; Lam, C. T.; Lippard, S. J., Reductive Coupling of Coordinated Alkyl Isocyanides in Seven-Coordinate Molybdenum(II) and Tungsten(II) Complexes. Removal of the Coupled Ligand as an Oxamide. *J. Am. Chem. Soc.* **1982,** *104* (5), 1263-1271.

63. Warner, S.; Lippard, S. J., Reductive coupling of isocyanide ligands in seven-coordinate molybdenum(II) mixed isocyanide bipyridine complexes. *Organometallics* **1986,** *5* (8), 1716-1725.
64. Carnahan, E. M.; Rardin, R. L.; Bott, S. G.; Lippard, S. J., Synthesis and characterization of seven-coordinate tantalum(I) and niobium(I) complexes with cis carbonyl and alkyl isocyanide ligands. *Inorg. Chem.* **1992,** *31* (25), 5193-5201.
65. Rehder, D.; Böttcher, C.; Collazo, C.; Hedelt, R.; Schmidt, H., Isocyanide–Group 5 complexes and metal-centred C–C coupling. *J. Organomet. Chem.* **1999,** *585* (2), 294-307.
66. Arnold, P. L.; Turner, Z. R.; Bellabarba, R. M.; Tooze, R. P., Carbon monoxide coupling and functionalisation at a simple uranium coordination complex. *Chem. Sci.* **2011,** *2* (1), 77-79.
67. Gardner, B. M.; Stewart, J. C.; Davis, A. L.; McMaster, J.; Lewis, W.; Blake, A. J.; Liddle, S. T., Homologation and functionalization of carbon monoxide by a recyclable uranium complex. *PNAS* **2012,** *109* (24), 9265-9270.
68. Frey, A. S.; Cloke, F. G. N.; Coles, M. P.; Maron, L.; Davin, T., Facile Conversion of CO/H_2 into Methoxide at a Uranium(III) Center. *Angew. Chem.* **2011,** *123* (30), 7013-7015.
69. Frey, A. S.; Cloke, F. G. N.; Hitchcock, P. B.; Day, I. J.; Green, J. C.; Aitken, G., Mechanistic Studies on the Reductive Cyclooligomerisation of CO by U(III) Mixed Sandwich Complexes; the Molecular Structure of $[(U(\eta\text{-}C_8H_6\{Si^iPr_3\text{-}1,4\}_2)(\eta\text{-}Cp^*)]_2(\mu\text{-}\eta^1\text{:}\eta^1\text{-}C_2O_2)$. *J. Am. Chem. Soc.* **2008,** *130* (42), 13816-13817.
70. Cotton, F. A.; Duraj, S. A.; Roth, W. J., Reactions of dinuclear niobium(III) and tantalum(III) compounds with alkyl isocyanides to give dinuclear products with dimerized isocyanides. *J. Am. Chem. Soc.* **1984,** *106* (23), 6987-6993.
71. Cotton, F. A.; Roth, W. J., Reactions of tert-butyl isocyanide with a binuclear niobium(III) compound. *J. Am. Chem. Soc.* **1983,** *105* (11), 3734-3735.
72. Lentz, D.; Brüdgam, I.; Hartl, H., *Angew. Chem. Int. Ed. Engl.* **1984,** *23* (7), 525-526.
73. Carnahan, E. M. L., S. J., *Dalton Trans.* **1991**, 699.
74. Dewan, J. C.; Giandomenico, C. M.; Lippard, S. J., Dealkylation and Reductive Coupling of *tert*-Butyl Isocyanide Ligands in Heptakis(*tert*-Butyl isocyanide)molybdenum (II). Structure of Seven-Coordinate Cyanotetrakis (*tert*-Butyl isocyanide)((*N*, *N*'-di-*tert*-butyldiamino)acetylene)molybdenum(II) Tetraphenylborate. *Inorg. Chem.* **1981,** *20* (12), 4069-4074.
75. Filipppou, A. C. G., W. J., *Organomet. Chem.* **1990,** *393*, C10.
76. Lam, C. T. C., P. W.; Lippard, S. J., *J. Am. Chem. Soc.* **1977,** *99*, 617.
77. Vrtis, R. N.; Rao, C. P.; Warner, S.; Lippard, S. J., Carbynes generated from metal carbonyl and isocyanide complexes; intermediates in the reductive coupling of carbonyl and CNR ligands. *J. Am. Chem. Soc.* **1988,** *110* (8), 2669-2670.
78. Vrtis, R. N. L., S. J., *Isr. J. Chem.* **1990,** *30*, 331.
79. Vrtis, R. N. L., S.; Rao, C. P.; Bott, S. G.; Lippard, S. J., *Organometallics* **1991,** *10*, 275.
80. *SMART* Apex II, Version 5.632.; Bruker AXS, Inc.: Madison, WI, 2005.
81. *SAINT Software User's Guide*, Version 7.34a ed.; Bruker AXS Inc.: Madison, WI, 2005.
82. *SADABS*, Sheldrick, G.M.; University of Göttingen, Germany: 2005.

83. *SHELXTL*, Version 6.12 ed.; Bruker AXS Inc.: Madison, WI, 2005.
84. Olex2 1.2 (compiled 2014.06.27 svn.r2953 for OlexSys, GUI svn. r4855).
85. Dolomanov, O.; Bourhis, L.; Gildea, R.; Howard, J.; Puschmann, H., *J. Appl. Cryst* **2009,** *42*, 339-341.

Chapter 4. Reductive Deprotection of Actinide Imido and Amido (An = Th, U) Complexes to Access a Nitrido Complex

4.1 Introduction

The utility of actinide-ligand multiple bonds to the study of covalency and f-orbital participation in bonding has spurred intense growth in this area.[1-8] The last decade has seen reports of a wide variety of compounds with actinide-ligand multiple bonds, including oxos,[9-12] imidos,[13-15] and nitridos,[16-20] to highlight a few. Notably, almost all of these reported complexes are of uranium, and despite the success had with uranium, examples with other actinides, such as thorium, remain relatively rare.[21]

Scheme 4.1. Previously reported complexes containing thorium-ligand multiple bonds. A, Ref. 22; B, Ref. 23; C, Ref. 25; D, Ref. 29; E, Ref. 30, F, Ref. 19.

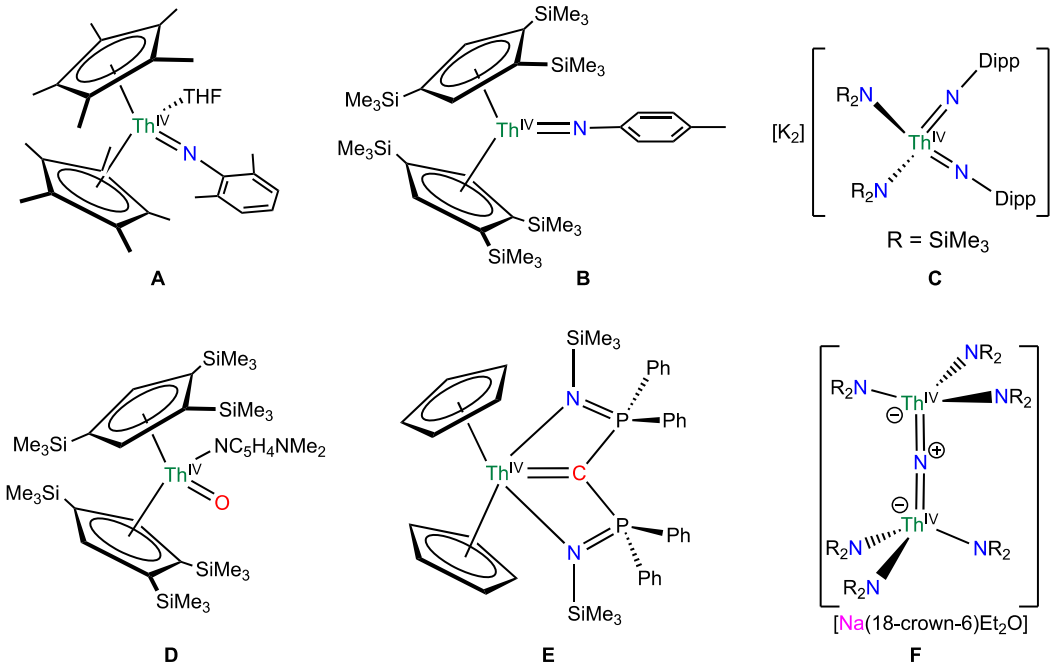

That said, there are a few examples that have been reported, some of which are shown in Scheme 4.1. The first thorium imido species, $[Cp^*_2Th(NAr)(THF)]$ (Ar = 2,6-dimethylphenyl), was reported by Eisen and co-workers in 1996, and was synthesized *via* the reaction of $[Cp^*_2Th(Me)_2]$ with 2,6-dimethylaniline.[22] In 2012, Zi and co-workers reported the synthesis of a series of terminal imido complexes, $[(\eta^5\text{-}1,2,4\text{-}{}^tBu_3C_5H_2)_2Th(NR)]$ (R = *p*-

tolyl, Ph_3C, Me_3Si),[23] and in 2015, Arnold and co-workers reported the synthesis of mono-, [K][Th(NDipp)$(NR_2)_3$], and bis-imido, [K_2][Th$(NDipp)_2(NR_2)_2$] (R = $SiMe_3$, Dipp = 2,6-$^iPr_2C_6H_3$) complexes of thorium *via* protonation of the thorium metallacycles [Th($CH_2SiMe_2NSiMe_3$)$(NR_2)_2$][24] and [K][Th($CH_2SiMe_2NSiMe_3$)$_2(NR_2)_2$], respectively, with KNHDipp.[25] Most recently, in 2019, Schelter and co-workers reported a series of thorium-imido complexes that were formed by deprotonation of a thorium anilide, [Th($NHAr^F$)(TriNOx)] (Ar^F = $C_8H_4F_6$, TriNOx = tris(2-*tert*-butylhydroxylaminato)benzylamine), using the strong bases $LiCH_2(SiMe_3)$ and potassium benzyl to form [$Li(THF)_2$][Th=NAr^F(TriNOx)] and [K(2.2.2-cryptand)][Th=NAr^F(TriNOx)], respectively.[26]

A handful of thorium chalcogen complexes have been reported, many of which were synthesized by the Hayton group. Work from our laboratory includes the synthesis of a series of thorium chalcogen complexes, [K(18-crown-6)][Th(E)$(NR_2)_3$] (E = O, S, Se, Te, R = $SiMe_3$).[27, 28] Additionally, another thorium terminal oxo, [(η^5-1,2,4-$^tBu_3C_5H_2$)$_2$Th(O)(dmap)] (dmap = dimethylaminopyridine) was reported by Zi and co-workers in 2011.[29] This complex was isolated from the reaction of [(η^5-1,2,4-$^tBu_3C_5H_2$)$_2$Th(NR)] (R = *p*-tolyl) with Ph_2CO.

Several thorium carbene complexes have also been reported.[30-32] This includes the first examples reported by Cavell and co-workers in 2011, which utilized a bis(iminophosphorano) methanediide ligand [$C(Ph_2P{=}NSiMe_3)_2]^{2-}$.[31] Also in 2011, Zi and co-workers reported the synthesis of bis and tris carbene complexes of thorium, utilizing the structurally similar bis(thiophosphorano) methanediide ligand [$C(Ph_2P{=}S)_2)]^{2-}$.[32] Liddle and co-workers reported the synthesis of several thorium carbenes, again utilizing chelating ligands with an NCN

binding motif.[30] Moreover, Hayton and co-workers reported the phosphorano-stabilized thorium carbene, $[Th(CHPPh_3)(NR_2)_3]$ (R = $SiMe_3$) in 2017.[33]

Lastly, I recently reported the synthesis of the first isolable molecular thorium nitride using $NaNH_2$ as a nitride source.[19] Moreover, Liddle and co-workers reported the isolation of a bridged Th(IV) parent imido complex, $[\{Th(Tren^{DMBS})\}_2(\mu\text{-}NH)]$ ($Tren^{DMBS}$ = $\{N(CH_2CH_2NSiMe_2{}^tBu)_3\}^{-3}$), which was thought to form *via* an unobserved bridging nitride intermediate.[34] However, this intermediate was thought to be extremely basic on account of its highly polarized Th-$N_{nitride}$ bonds and spontaneously deprotonated the solvent, forming the bridged parent imido. Despite the above-mentioned progress, a terminal nitride of Th remains elusive.

The scarcity of complexes with thorium-ligand multiple bonds can be ascribed to both the difficulty installing these types of moieties in thorium based systems and the energetics of the thorium valence orbitals, especially compared to uranium. Specifically, it is believed that the higher energy of the 5f orbitals of thorium weakens any metal-ligand π-bonding that may arise, making it harder to form a multiple bond.[35] Another challenge is the absence of nearly any metal based redox chemistry associated with thorium.[36-38] Many pathways developed for the synthesis of uranium-ligand multiple bonds utilize oxidative atom transfer, which cannot occur in an analogous thorium system due to its lack of redox chemistry. For example, Burns and co-workers synthesized the uranium terminal oxo complex, $[Cp^*_2U(OAr)(O)]$ *via* reaction of $[Cp^*_2U(OAr)(THF)]$ with pyridine-*N*-oxide.[39] Similarly, Liddle and co-workers reported that reaction of $[U(Tren^{TIPS})]$ with NaN_3 and 12-crown-4 affords the first uranium terminal nitride, $[Na(12\text{-}crown\text{-}4)_2][U(N)(Tren^{TIPS})]$.[18] Both reactions proceed *via* a $2e^-$ oxidation of U(III) to U(V). These reactions demonstrate the diversity of products that are

inaccessible due to the inability of thorium to undergo much redox chemistry. Although, Zi and co-workers reacted [(η^5-1,2,4-^{t}Bu$_3$C$_5$H$_2$)$_2$Th(bipy)], which contains a dianionic bipy ligand, with azides RN$_3$ (R = *p*-tolyl, Ph$_3$C, Me$_3$Si) to afford the corresponding thorium imido complexes [(η^5-1,2,4-^{t}Bu$_3$C$_5$H$_2$)$_2$Th(NR)].[40]

Given the limited progress made toward the synthesis of thorium imidos, it is obvious that new methods are needed for installing thorium-ligand multiple bonds. In this regard the reductive deprotection protocol, which was developed in the Hayton group and requires no oxidation state change, has been shown to be ideal for actinide based multiply bonded systems (Scheme 4.2).

Scheme 4.2. Reductive deprotection toward a terminal oxo and sulfide. Refs. 27 and 46.

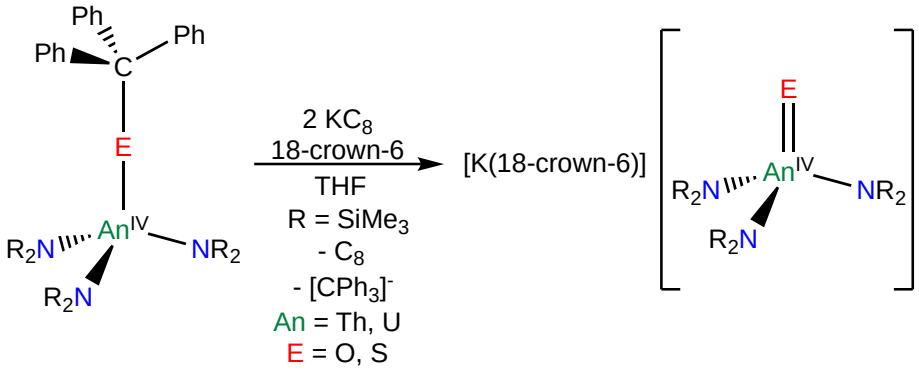

For reference, it has been shown that a trityl protecting group can be used to install functional groups not only in organic systems, but in inorganic systems as well, including those containing uranium, thorium, copper, nickel, and zinc.[28, 41-44] The use of a triphenylmethyl protecting group to install terminal chalcogenide moieties and access complexes with uranium and thorium multiple bonds has been reported.[28, 44] Removal of this protecting group is accomplished *via* both homolytic and heterolytic C-E bond cleavage, the latter of which utilizes an external reducing agent.

Schelter and co-workers recently reported the synthesis of the U(IV) triphenylmethylimido complex, $[K(THF)_3][U(NCPh_3)(NR_2)_3]$, *via* the reduction of the analogous U(V) imido complex with excess KC_8.[45] Cleavage of the trityl group and formation of a nitride were not reported, which is likely due in part to the strength of the C-N bond of the imido ligand, similar to what was seen for the related U(IV) triphenylmethylamide complex.[44] Based upon these results, I hypothesized that use of a different protecting group, with a weaker E-N bond, could afford access to the desired nitrido complex *via* the reductive deprotection protocol. In this regard, use of a *p*-toluenesulfonyl (Ts = $MeC_6H_4SO_2$) or tosyl protecting group was pursued, as a S-N bond should be weaker than the corresponding C-N bond.[46] Moreover, Arnold and co-workers reported the synthesis of thorium imido complexes $[K(18\text{-crown-}6)][Th(NR')(NR_2)_3]$ (R' = 2,6-$^{i}Pr_2C_6H_3$, 2,4,6-$Me_3C_6H_3$, 2,6-$Ph_2C_6H_3$) *via* protonation of the Th(IV) metallacycle $[Th(CH_2SiMe_2NSiMe_3)(NR_2)_2]$ with the corresponding amide salt KNHR,[25] which would provide facile access to the desired nitrido precursors.

This chapter details the synthesis of three novel actinide multiple bonded imido complexes synthesized through protonation of $[An(CH_2SiMe_2NSiMe_3)(NR_2)_2]$ (An = U, Th) with the corresponding amide salts, $[Li(NHCPh_3)(THF)]$ and KNHTs (Ts = $MeC_6H_4SO_2$). In addition, I describe the reactivity of $[An\{N(R)(SiMe_2CH_2)\}_2(NR_2)]^-$ (An = U, Th) with NH_3BPh_3 in an effort to synthesize novel actinide amido borane complexes. These new imido and amido complexes are prospective candidates for reductive deprotection to afford an An nitrido complex and these efforts are discussed within.

4.2 Results and Discussion

4.2.1 Synthesis and Characterization of [Li(12-crown-4)$_2$][Th(NCPh$_3$)(NR$_2$)$_3$] (4.1)

Reaction of [Li(NHCPh$_3$)(THF)][44] with [Th(*C*H$_2$SiMe$_2$*N*SiMe$_3$)(NR$_2$)$_2$] in THF along with 2 equiv of 12-crown-4 affords the Th(IV) imido complex, [Li(12-crown-4)$_2$][Th(NCPh$_3$)(NR$_2$)$_3$] (**4.1**), which can be isolated as colorless crystals in 75% yield, after crystallization from diethyl ether (Scheme 4.3).

Scheme 4.3. Synthesis of **4.1**, **4.2**, and **4.3**.

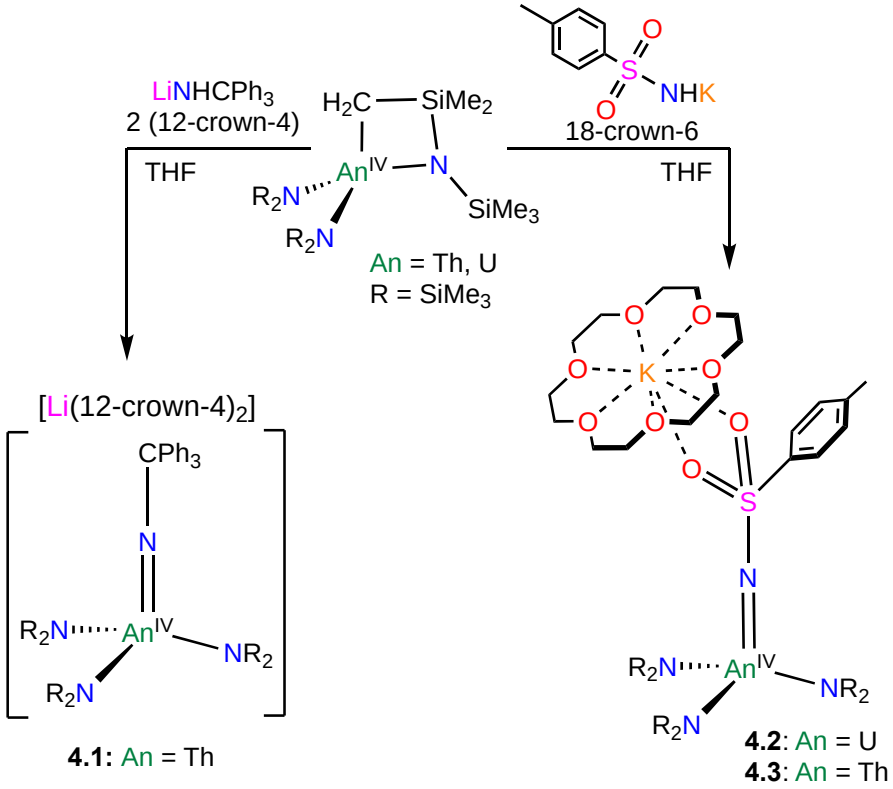

The connectivity of complex **4.1** was verified by X-ray crystallography (Figure 4.1, Table 4.1). Complex **4.1** crystallizes in the triclinic space group $P\bar{1}$ with two molecules in the asymmetric unit. Its Th-N$_{imido}$ distances (av. 2.036 Å) are comparable to those of other Th(IV) imido complexes.[22, 23, 25] For example, the Th-imido distance in **4.1** aligns well with the Th-N$_{imido}$ distances reported for complexes reported by Ren and co-workers, [η^5-1,2,4-

$(Me_3C)_3C_5H_2]Th{=}NR$ (R = CPh_3, Th1-N1 = 2.034(2); R = $SiMe_3$, Th-N1 = 2.035(3)),[23] but is shorter than the Th-N_{imido} bond reported by Arnold and co-workers, [K(18-crown-6)][Th(NR')$(NR_2)_3$] (R' = 2,6-$^{i}Pr_2C_6H_3$, 2,4,6-$Me_3C_6H_3$, 2,6-$Ph_2C_6H_3$) (Th1-N1 = 2.072(3) Å).[25] Furthermore the Th-N_{imido} and Th-N_{amide} (av. 2.45 Å) bond lengths are longer than corresponding bond lengths of $[K(THF)_3][U(NCPh_3)(NR_2)_3]$ (U-N_{imido} = 1.993(1), U-N_{amide} (av.) = 2.387 Å) consistent with the increased ionic radius of Th^{4+} versus U^{4+}.[45, 47]

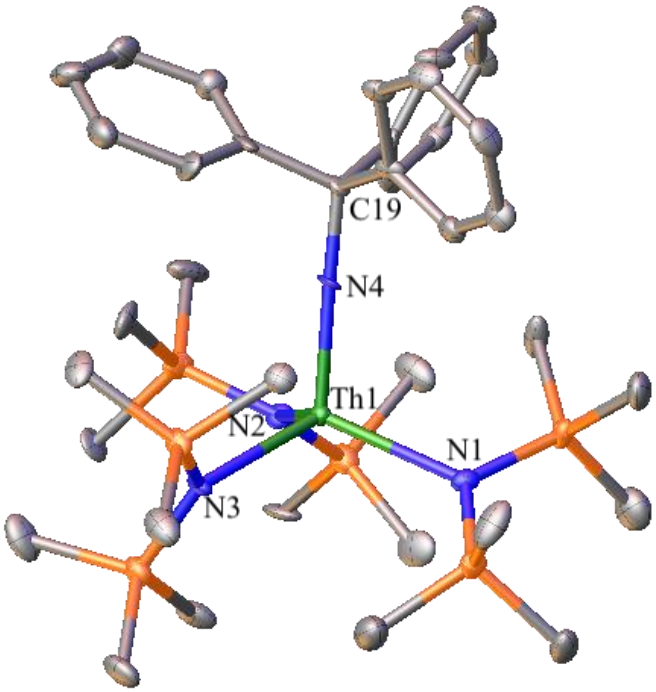

Figure 4.1. Solid-state molecular structure of $[Th(NCPh_3)(NR_2)_3]$ (**4.1**), shown with 50% probability ellipsoids. $[Li(12\text{-crown-}4)_2]^+$, one molecule of **4.1**, and hydrogen atoms removed for clarity. Selected bond lengths (Å) and angles (°): Th1-N4 = 2.030(8), Th2-N8 = 2.041(8), av. Th-N_{amide} = 2.45, av. C-N_{imido} = 1.45, av. N-Th-N = 109.5, av. Th-N-C = 178.3.

The ^{1}H NMR spectrum of complex **4.1** in benzene-d_6 features two sharp singlets at 0.58 and 3.15 ppm, attributable to the methyl groups in the silylamide ligands and the methylene

groups of the 12-crown-4 moieties, respectively (Figure A4.5). Three additional resonances at 7.05, 7.26, and 7.91 ppm, consisting of two triplets and a doublet, are observed and are assignable to the *p*-, *m*-, and *o*-aryl proton environments of the triphenylmethyl ligand, respectively. In addition, the $^{7}Li\{^{1}H\}$ spectrum of **4.1**, in benzene-d_6, exhibits a single resonance at -1.64 ppm (Figure A4.6).

4.2.2 Synthesis and Characterization of [K(18-crown-6)][U(NTs)(NR$_2$)$_3$] (4.2) and [K(18-crown-6)][Th(NTs)(NR$_2$)$_3$] (4.3)

Reaction of 1 equiv of KNHTs (Ts = $MeC_6H_4SO_2$)[48] with the U(IV) metallacycle, [U(*C*H_2SiMe_2*N*SiMe_3)(NR_2)$_2$], in the presence of 18-crown-6, in THF, affords the U(IV) imido complex, [K(18-crown-6)][U(NTs)(NR_2)$_3$] (**4.2**), as a tan powder in 61% yield (Scheme 4.3**).** Similarly, addition of KNHTs[48] to a THF solution of [Th(*C*H_2SiMe_2*N*SiMe_3)(NR_2)$_2$] and 18-crown-6 affords the Th(IV) imido, [K(18-crown-6)][Th(NTs)(NR_2)$_3$] (**4.3**), as a pale orange powder in 70% yield upon workup (Scheme 4.3**)**

Crystals suitable for X-ray diffraction of **4.2** were grown from a concentrated pentane solution stored at -25 °C for 24 h, whereas a solution of Et_2O/pentane (2:4), stored at -25 °C for 24 h, led to suitable crystals of **4.3** for X-ray diffraction. Complexes **4.2** and **4.3** are isostructural: they crystallize in the triclinic space group $P\bar{1}$ and feature pseudotetrahedral geometry about the metal center (av. N-An-N = 109.1°, An = U, Th) (Figure 4.2). The U-N_{imido} bond distance (U1-N4 = 2.084(3) Å) of complex **4.2** is longer those of other U(IV) imido complexes, including that of [K(THF)$_3$][U(NCPh$_3$)(NR_2)$_3$] (U-N_{imido} = 1.9926(14) Å).[45] The Th-N_{imido} (2.149(7) Å) bond distance of **4.3** is slightly longer than those of other structurally characterized Th(IV) imido complexes,[22, 23, 25] but still considerably shorter than the Th-N_{amide} (av. = 2.36 Å) bond distances. In addition, the Th-N_{imido} and the Th-N_{amide} bond

distances of **4.3** are longer than the corresponding bond lengths of the analogous uranium complex **4.2** (see Table 4.1), consistent with the increased ionic radius of Th^{4+} versus U^{4+}.[47]

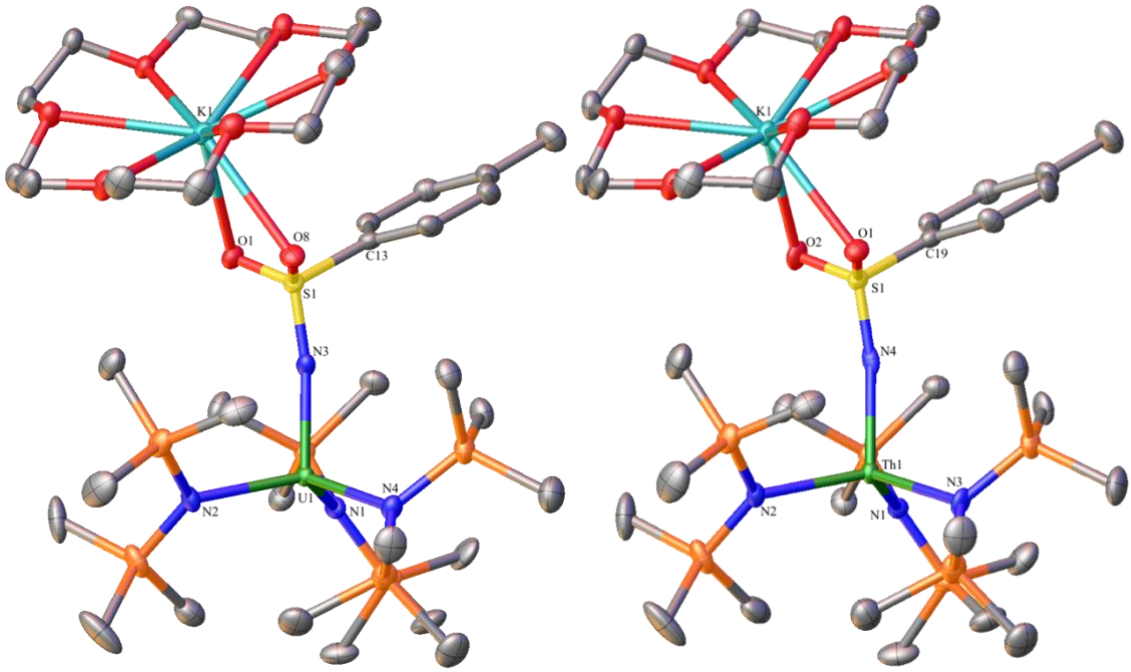

Figure 4.2. Solid-state molecular structures of [K(18-crown-6)][U(NTs)$(NR_2)_3$] (**4.2**) (left) and [K(18-crown-6)][Th(NTs)$(NR_2)_3$] (**4.3**) (right), shown with 50% probability ellipsoids. Hydrogen atoms removed for clarity. Selected bond lengths (Å) and angles (°) for **4.2**: U1-N4 = 2.088(5), av. U-N_{amide} = 2.29, N4-S1 = 1.545(6), av. N-U-N = 109.1, U1-N4-S1 = 169.6(3). Selected bond lengths (Å) and angles (°) for **4.3**: Th1-N4 = 2.149(7), av. Th-N_{amide} = 2.36, N4-S1 = 1.543(8), av. N-Th-N = 109.1, Th1-N4-S1 = 168.2(4).

The ^{1}H NMR spectrum of complex **4.2**, in benzene-d_6, features two resonances at -2.79 and 2.83 ppm, assignable to the methyl groups of the silylamide ligands and the methylene groups of the 18-crown-6 moiety. Three additional resonances are observed at 0.74, 4.24, and 4.96 ppm, in a 3:2:2 ratio, attributable to the methyl group and two distinct aryl environments of the tosyl moiety, respectively (Figure A4.8). Additionally, the ^{1}H NMR spectrum of

complex **4.3** exhibits five resonances in benzene-d_6, in a 54:3:24:2:2 ratio (Figure A4.10). These resonances consist of two singlets at 0.63 ppm and 3.18 ppm, assignable to the methyl groups of the silylamide ligands and the methylene groups of the 18-crown-6 moiety, as well as, one singlet and two doublets at 2.13, 7.06, and 8.15 ppm, assignable to the methyl group and two distinct aryl proton environments of the tosyl moiety.

Table 4.1 Comparison of select bond lengths (Å) and angles (°) in complexes **4.1** – **4.3** and $[K(THF)_3][U(NCPh_3)(NR_2)_3]$.[45]

	4.1 (L = C)	$[K(THF)_3][U(NCPh_3)(NR_2)_3]$ (L =C)	**4.2** (L = S)	**4.3** (L = S)
An = N_{imido}	2.030(8)	1.9926(14)	2.088(5)	2.149(7)
N-L	1.45	-	1.545(6)	1.543(8)
An-N_{amide} (av.)	2.45	2.39	2.29	2.36
An-N_{imido}-L	178.3	169.82(12)	169.6(3)	168.2(4)
An-N_{amide} (av.)	109.5	-	109.1	109.1

4.2.3 Synthesis and Characterization of $[Na(2,2,2\text{-cryptand})][U(NR_2)_3NHBPh_3]$ (4.4) and $[K(DB\text{-}18\text{-}C\text{-}6)(THF)_2][Th(NR_2)_3NHBPh_3]$ (4.5)

Reaction of 1 equiv of NH_3BPh_3 with the U(IV) bis(metallacycle), $[Na(DME)_3][U\{N(R)(SiMe_2CH_2)\}_2(NR_2)]$,[49] in the presence of 2,2,2-cryptand, in toluene, affords the U(IV) amido borate complex, $[Na(2,2,2\text{-cryptand})][U(NR_2)_3NHBPh_3]$ (**4.4**), as an orange crystalline powder in 24% yield (Scheme 4.4). A related complex, where the Na cation is bound to DME, THF, and the phenyl ring has also been isolated, $[U(NR_2)_3NHBPh_3][Na(DME)(THF)]$ (**4.6**) (see Table 4.2 and Figure 4.5 for more details).

It should be noted that the formation of **4.4** was initially monitored by ^{1}H NMR spectroscopy for 24 h in a THF-d_8 solution, whereupon new resonances increased in intensity, assignable to **4.4**, while resonances assignable to uranium bis(metallacycle) and free NH_3BPh_3 environments decreased in intensity, as expected. However, not all of the bis(metallacycle) complex is consumed, even after prolong reaction times. From these observations, I hypothesize that NH_3BPh_3 initially reacts with uranium bis(metallacycle) to form the newly synthesized complex **4.4** but this new product proceeds to react with unreacted NH_3BPh_3 and decomposes, leaving uranium bis(metallacycle) and trace amounts of NH_3BPh_3 partially unreacted in solution. This hypothesis helps explain why **4.4** is isolated in low yield. Moreover, **4.4** has similar solubility to the uranium bis(metallacycle), and the crystallization procedure produces a mixture.

Similarly, addition of NH_3BPh_3 to a THF solution of [K(DME)][Th{*N*(R)(SiMe$_2$*C*H$_2$)}$_2$(NR$_2$)][25] and dibenzo-18-crown-6 (DB-18-C-6) affords the Th(IV) amido borane, [K(DB-18-C-6)(THF)$_2$][Th(NR$_2$)$_3$NHBPh$_3$] (**4.5**), as colorless crystals in 62% yield upon work-up (Scheme 4.4). The use of 2,2,2-cryptand as the complexing agent results in formation of [K(2,2,2-cryptand)][Th(NR$_2$)$_3$NHBPh$_3$] (**4.7**), but this reaction was inconsistent at producing tractable material (see Table 4.2 and Figure 4.6 for more details).

Scheme 4.4. Synthesis of **4.4** and **4.5**.

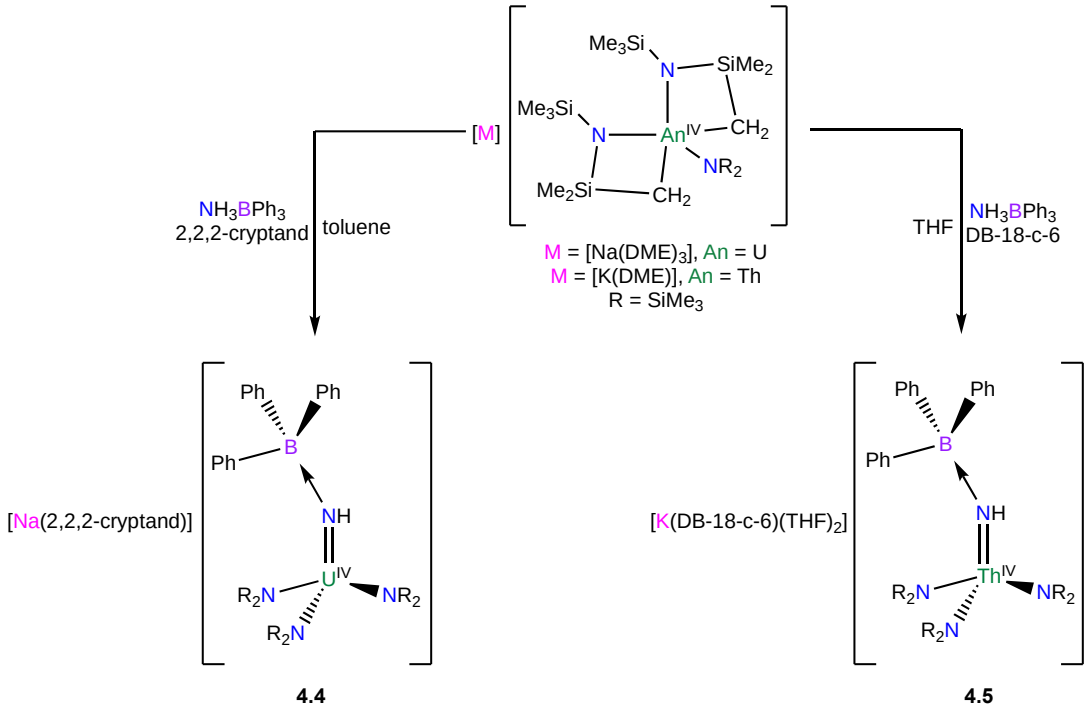

Crystals suitable for X-ray diffraction of **4.4** were grown from a solution of Et_2O/pentane (2:4) stored at -25 °C for 24 h, whereas a solution of THF/pentane (2:4), stored at -25 °C for 24 h, led to suitable crystals of **4.5** for X-ray diffraction. Complex **4.4** crystallizes in the monoclinic space group $P2_1/c$ and **4.5** crystallizes in the triclinic space group $P\bar{1}$. Both feature pseudotetrahedral geometry about the metal center (av. N-An-N = 109.2° (**4.4**), 109.4° (**4.5**)) (Figure 4.3). The U-N_{imido} bond distance (2.127(3) Å) of complex **4.4** and the Th-N_{imido} bond distance (2.205(3) Å) in **4.5**, are much longer compared to other Th-imido bond distances reported in the literature. For example, Zi and co-workers report a short Th=N bond length (2.034(2) Å) in [Cp*$_2$ThN(THF)Ar] (Cp* = C_5Me_5, Ar = 2,6-$Me_2C_6H_3$),[23] while Eisen and co-workers report a Th=N bond distance of 2.045(8) Å in [$Cp_2ThNCPh_3$] (Cp = η^5-1,2,4-$^tBu_3C_5H_2$),[22] and Arnold and co-workers report an imido complex, [K(18-crown-6)][Th(NR_2)$_3$NAr] (Ar = 2,6-$^i Pr_2C_6H_3$), that features a Th=N bond distance of 2.072(3) Å.[25]

The elongation in **4.4** and **4.5** is attributed to the dative bond between nitrogen and triphenyl borane. Compared to free NH_3BPh_3 (N-B = 1.639(2) Å),[50] **4.4** (1.599(5) Å) and **4.5** (1.583(5) Å) have a shorter N-B bond distance, but a longer N-B bond distance compared to a previously reported Hf amido borate complex, $Cp_2Hf\{NHBH(C_6F_5)_2\}$ (1.509(10) Å).[51] It is important to note that no actinide amido boranes have been reported to date.

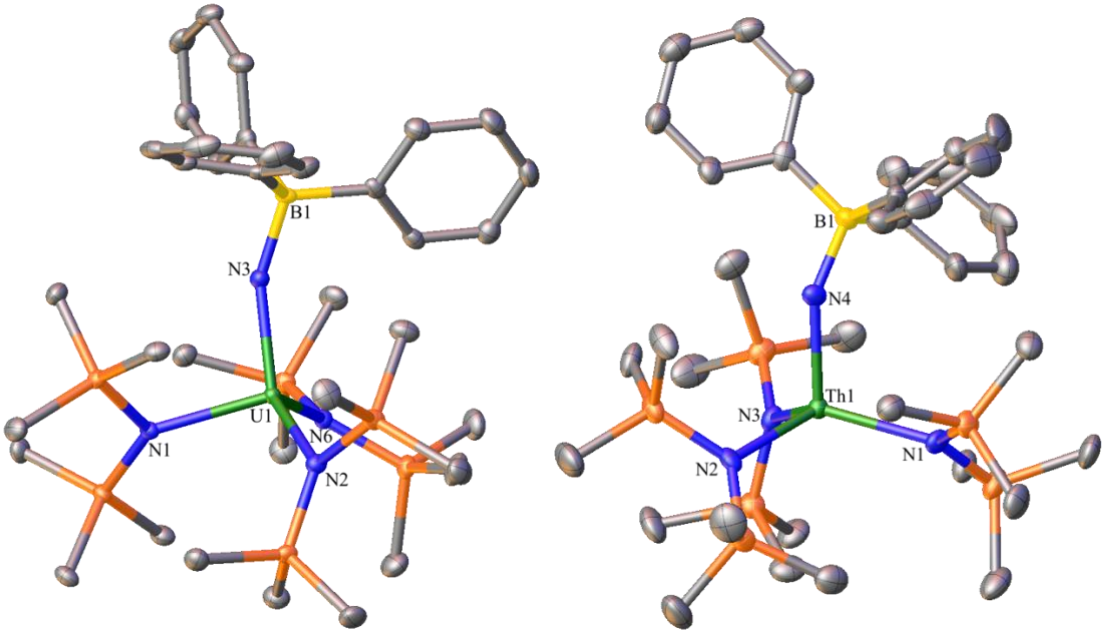

Figure 4.3. Solid-state molecular structures of **4.4** and **4.5**, shown with 50% probability ellipsoids. $[Na(2,2,2\text{-cryptand})]^+$ and $[K(\text{dibenzo-18-crown-6})]^+$ counterions removed for clarity, respectively, as well as hydrogen atoms. Selected bond lengths (Å) and angles (°) for **4.4**: U1-N3 = 2.127(3), av. U-N_{amide} (av.) = 2.32, N3-B1 = 1.599(5), av. N-U-N = 109.2, U1-N3-B1 = 154.0(2). Selected bond lengths (Å) and angles (°) for **4.5**: Th1-N4 = 2.205(3), av. Th-N_{amide} = 2.37, N4-B1 = 1.583(5), av. N-Th-N = 109.4, Th1-N4-B1 = 148.8(2).

Table 4.2 Comparison of select bond lengths (Å) and angles (°) in complexes **4.4** – **4.7** and free NH_3BPh_3.[50]

	4.4 An = U	**4.5** An = Th	**4.6** An = U	**4.7** An = Th	NH_3BPh_3
An-N_{imido}	2.127(3)	2.205(3)	2.140(4)	2.187(6)	-
An–N_{amide}	2.301(3) 2.325(3) 2.327(3)	2.366(3) 2.375(3) 2.362(3)	2.314(4) 2.315(4) 2.303(4)	2.373(6) 2.401(6) 2.359(6)	-
N-B	1.599(5)	1.583(5)	1.577(7)	1.558(11)	1.639(2)
An-N-B	154.0(2)	148.8(2)	149.1(3)	146.5(5)	-
An-N_{amide} (av.)	109.2	109.4	109.6	113.9	-

The ^{1}H NMR spectrum of complex **4.4**, in THF-d_8, features a sharp resonance at -5.63 ppm, assignable to the methyl groups of the silylamide ligands. Three resonances are obeserved at 2.49, 3.42, and 3.46 ppm, in a 12:12:12 ratio, assignable to the three distinct methyl environments of 2,2,2-cryptand. Additionally, three resonances are observed at 7.54, 8.10, and 10.36 ppm, in a 3:6:6 ratio, attributable to the distinct aryl environments of the phenyl rings (Figure A4.12). The N-H proton was not observed. Additionaly, the uranium bis(metallacycle), is also present in this sample, in a 0.5:1 ratio, for reasons discussed above.

The ^{1}H NMR spectrum of complex **4.5** exhibits eight resonances in THF-d_8, in a 54:8:1:8:6:6:8:3 ratio (Figure A4.14). These resonances consist of a sharp resonance observed at 0.21 ppm, assignable to the methyl groups of the silylamide ligands. Two singlets at 3.84

ppm and 4.14 ppm, as well as a broad peak at 6.96 ppm, assignable to the methyl groups and aryl environments of the dibenzo-18-crown-6 moiety, a broad peak at 4.35 ppm, attributable to the N-H proton, as well as three resonances at 6.76, 6.90, and 7.39 ppm, assignable to the three distinct proton environments of the phenyl rings.

4.2.4 Attempted Deprotection Reactions of [Li(12-crown-4)$_2$][Th(NCPh$_3$)(NR$_2$)$_3$] (4.1) with KC$_8$

Reaction of **4.1** with 1 equiv of KC$_8$ and 18-crown-6 in THF resulted in formation of a red solution. Work-up in diethyl ether resulted in the deposition of a few small crystals of [K(18-crown-6)NR$_2$] (Scheme 4.5). A ^{1}H NMR spectrum of the red residue in pyridine-d_5 was compared to a ^{1}H NMR spectrum of a mxiture of 18-crown-6 and KNR$_2$ in pyridine-d_5. The spectra shared two identical sharp peaks at 0.63 and 3.45 ppm, confirming the formation of the anion in the reaction with **4.1**. Upon repitition of the reduction method, crystals formed in low yield from diethyl ether and the solid-state molecular structure was [K(18-crown-6)(12-crown-4)][Th(NCPh$_3$)(NR$_2$)$_3$] (Scheme 4.5). Based on the observed color change, the isolation of KNR$_2$ crystals, and the formation of the potassium salt of [Th(NCPh$_3$)(NR$_2$)$_3$]$^-$, I hypothesize that some reduction is occurring, but the resulting product(s) are unstable and decompose.

Scheme 4.5. Reaction of **4.1** with KC$_8$.

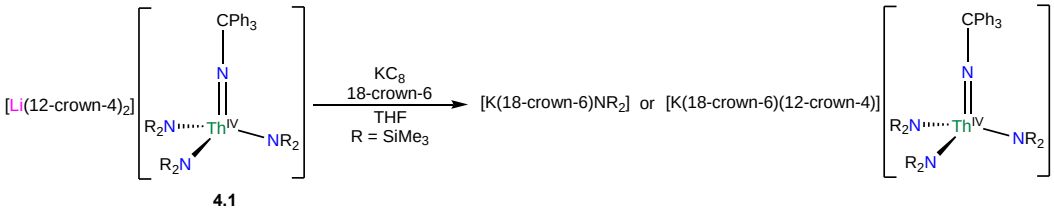

Interestingly, the use of excess KC$_8$ (8 equiv) led to formation of a blue/purple solution, which quickly turned to the familiar red solution. I hypothesize the blue/purple solution is a

Th(III) complex. Unfurtunately, work-up of these reaction mixtures did not result in any isolable product.

4.2.5 Attempted Deprotection Reactions of [K(18-crown-6)][U(NTs)(NR_2)$_3$] (4.2)

Based upon the results discussed in **4.2.4**, I rationalized that complex **4.2** could undergo the desired reduction better in part to the different protecting group. Reaction of **4.2** with 2 equiv of KC_8 and 18-crown-6 in THF was stirred for 1 h, which resulted in a yellow solution upon work-up in diethyl ether. The solution was stored at -25 °C for 24 h, where yellow, crystalline blocks were grown of the metallacycle, [K(18-crown-6)]$_2$[U{*N*(R)(SiMe$_2$*C*H$_2$)}(NR$_2$)(NTs)]$_2$ (**4.8**), isolated in 24% yield, in which two methyl groups undergo deprotonation by [NR$_2$]$^-$ to form a μ-CH$_2$ linkage and the loss of 2 equiv of HNR$_2$ (Scheme 4.6). The preliminary ^{1}H NMR spectrum of the yellow benzene-*d*$_6$ solution of **4.8** is shown in Figure A4.17, but further synthetic work is likely required to confidently make all of the assignments.

Scheme 4.6. Synthesis to **4.8**.

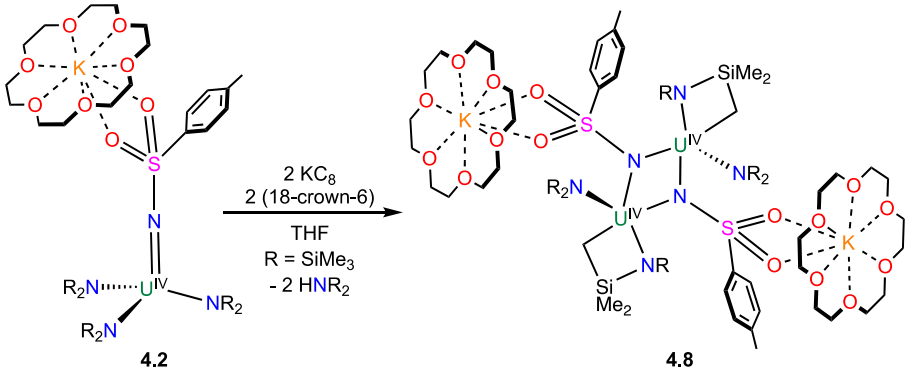

Complex **4.8** crystallizes in the triclinic space group $P\bar{1}$ as a dimer (Figure 4.4). Compared to **4.2** (2.088(5) Å), the U-N$_{imido}$ distance (2.356(10) Å) is elongated by 0.268 Å. Moreover, the N-S bond has decreased (1.516(10) Å) from what is reported in **4.2** (1.545(6) Å) by 0.029

Å and the U-N-S bond angle (149.1(7)°) has also decreased by 20.5° compared to **4.2** (169.6(3)°).

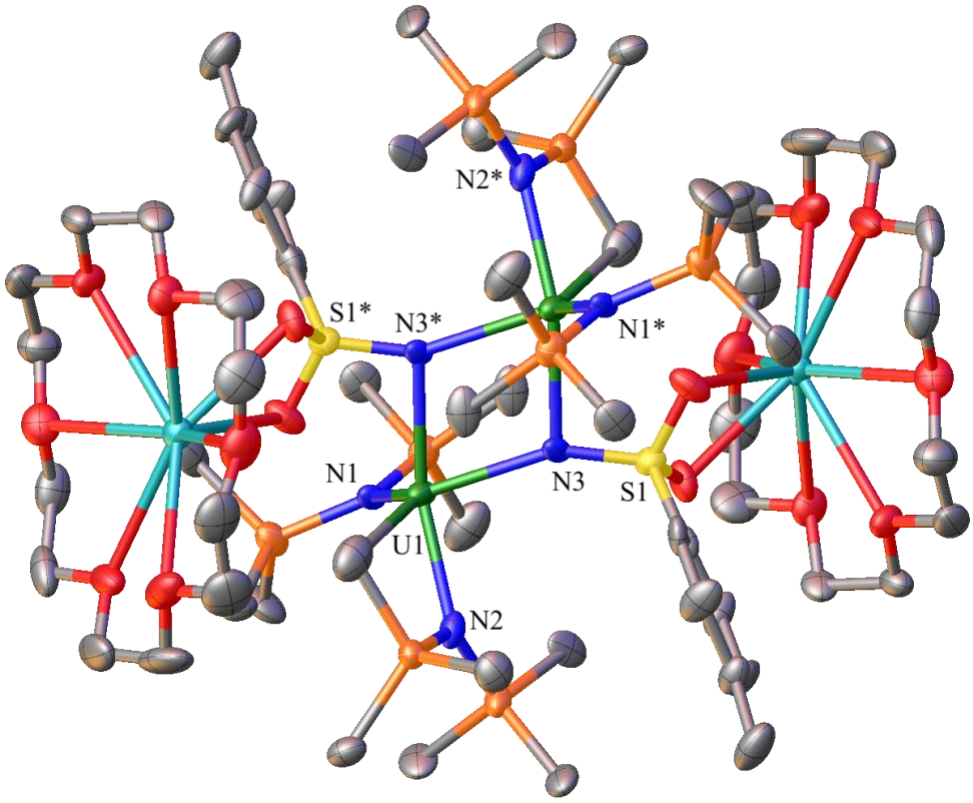

Figure 4.4. Solid-state molecular structure of **4.8**, shown with 50% probability ellipsoids. Hydrogen atoms and solvent molecules removed for clarity. Selected bond lengths (Å) and angles (°): U1-N3 = 2.356(10), U1-C7 = 2.651(15), av. U-N_{amide} = 2.31, N5-S2 = 1.516(10), U2-N5-S2 = 149.1(7).

Upon repetition of the reduction method, without the addition of 18-crown-6, a color change to a dark brown solution occurred and work-up in a diethyl ether/pentane (2:4) mixture led to a small amount of brown crystals of **4.8** after being stored at -25 °C for 24 h. These results suggest that the anticipated deprotection was not successful since **4.8** was the only product repeatedly isolated. This failure of the deprotection was further confirmed by the ^{1}H

NMR spectrum, which did not show the expected diamagnetic resonances of the tosyl by-product, [K(18-crown-6)][SO_2Ts].

Other reducing agents were used as well in a series of NMR spectroscopic monitoring reactions. The ^{1}H NMR spectrum of **4.2** with 2 equiv of Cp*$_2$Co in benzene-d_6 showed no change in the spectrum after 4 h, despite a color change to yellow. Additionally, the ^{1}H NMR spectrum of **4.2** with 1 equiv of TMSCl in benzene-d_6 showed no change after 30 min even though a color change to yellow occurred, along with formation of a fine off-white precipitate. Lastly, thermolysis of a benzene-d_6 solution of **4.2** at 70 °C was monitored by ^{1}H NMR spectroscopy for 24 h, but only decomposition was seen after 24 h, as revlealed by formation of free amine.

4.2.6 Attempted Deprotection Reactions of [K(18-crown-6)][Th(NTs)(NR$_2$)$_3$] (4.3)

Reaction of **4.3** with 2 equiv of KC_8 and 18-crown-6 in THF resulted in a color change from faint orange to colorless. Work-up of the reaction mixture in diethyl ether led to the crystallization of [K(18-crown-6)][NR_2] as colorless blocks in low yield (Scheme 4.7). Their identy was was confirmed by a unit cell match with authentic material.[52]

Scheme 4.7. Reaction of **4.3** with KC_8.

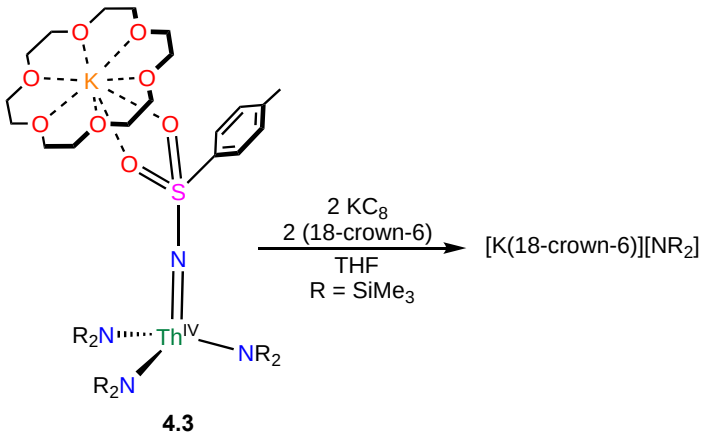

Furthermore, a crude ^{1}H NMR spectrum of the colorless material in benzene-d_6 was compared to a ^{1}H NMR spectrum of a mixture of 18-crown-6 and KNR_2 in benzene-d_6, where the spectra shared two identical sharp peaks at 0.60 and 3.17 ppm, confirming the formation of potassium amide. Other reducing agents were used as well in a series of NMR spectroscopic monitoring reactions. For example, the ^{1}H NMR spectrum of **4.3** with 2 equiv of Cp^*_2Co in benzene-d_6, showed no change over 3 h. Similarly, a DME solution of 2 equiv of Na/Nathaphlene was added dropwise to a benzene-d_6 solution of **4.3**, where the green solution disappeared upon addition. However, the ^{1}H NMR spectrum showed no immediate change, but two new peaks are present at 0.60 ppm and 3.33 ppm, which match well with the resonances assigned to sodium amide (0.57 ppm and 3.35 ppm), suggesting the same reactivity that was seen with KC_8 is occuring. After many attempts of reducing complex **4.3**, these results suggest that the N-S bond is too strong to break *via* the reductive deprotection method.

4.2.7 Reactions of NH_3BPh_3 with Lewis Bases

Initial efforts to probe the cleavage of the N-B bond were done using the free ligand, NH_3BPh_3. A range of Lewis bases, such as PPh_3, Et_3NH, trityl amine, PCy_3, PMe_3, DABCO, and KF/2,2,2-cryptand, were tested through ^{1}H NMR spectroscopy monitoring reactions. None of these reagents showed any reaction with NH_3BPh_3, but the use of excess (10 equiv) 4-(Dimethylamino)pyridine (DMAP) in THF-d_8 showed promising results as new phenyl peaks grew in, presumed to be the BPh_3DMAP adduct, as resonances assigned to free NH_3BPh_3 decreased over 24 h. Moveover a resonance assignable to free NH_3 is observed at 0.40 ppm within 5 min (Scheme 4.8 inset, Figure A4.18). With these results in hand, I explored the reaction of DMAP (10 equiv) with complexes **4.4** and **4.5**.

4.2.8 Reactions of [Na(2,2,2-cryptand)][U(NR$_2$)$_3$NHBPh$_3$] (4.4) and [K(DB-18-C-6)(THF)$_2$][Th(NR$_2$)$_3$NHBPh$_3$] (4.5) with DMAP

Addition of excess DMAP (10 equiv) to THF-d_8 solutions of **4.4** or **4.5** were monitored over 48 h using ^{1}H NMR spectroscopy, whereupon the resonances assignable to the original SiMe$_3$ and phenyl resonances have completely disappeared, but no new SiMe$_3$ resonance were clearly observed as expected, while new resonances in the phenyl region grew in intensity. Regarding the phenyl region, the 28 h and 22 h spectra from the reaction with **4.4** and **4.5**, respectively, showed that both reactions were forming the same product, as indicated by resonances at 6.8 ppm, 7.2 ppm, and 7.4 ppm, which are tentatively assigned to the BPh$_3$DMAP adduct (Figure A4.19). Moreover, when the 28 h and 22 h spectra from the reactions with **4.4** and **4.5**, respectively, are overlayed with the spectrum from the reaction of NH$_3$BPH$_3$ + 10 equiv DMAP after 48 h, the peaks in the phenyl region matched well with what I tentatively assigned to the BPh$_3$DMAP adduct formed from the control experiment (Figure A4.20). Therefore, I hypoythesize that a new actinide containing complex is forming, but is unstable and quickly decomposing in-situ, which is supported by the formation of the BPH$_3$DMAP adduct and increase in free amine (Scheme 4.8). Furthermore, the reaction solutions deepened in color, where **4.4** became a darker orange and **4.5** turned more yellow.

Scheme 4.8. Attempted deprotection with DMAP.

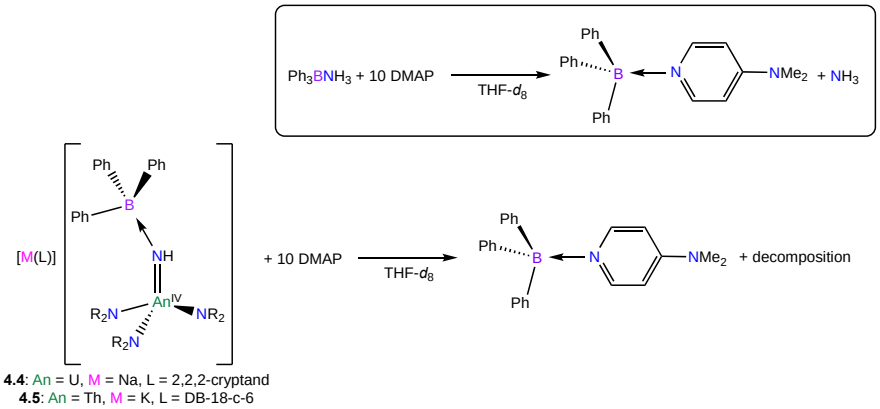

Furthemore, efforts to cleave the N-B bond in **4.4** was done using 0.5 equiv of iodine, which led to the formation of the uranium bridged nitride U(IV/V), [{$(R_2N)_3U$}$_2$(μ-N)] (**4.9**), previously reported by Mazzanti and co-workers,[53] in 19% yield. The brown needles were dissolved in THF-d_8 and the ^{1}H NMR spectrum matched that reported in the literature.[53] To account for the formation of **4.9**, I suggest that **4.4** is intially oxidized to U(V), which proceeds to react with another equivalent of **4.4**, forming **4.9**, while losing BPh_3 and [Na(2,2,2-cryptand)][Ph_3BNH_2] (Scheme 4.9).

Scheme 4.9. Proposed mechanism to **4.9**.

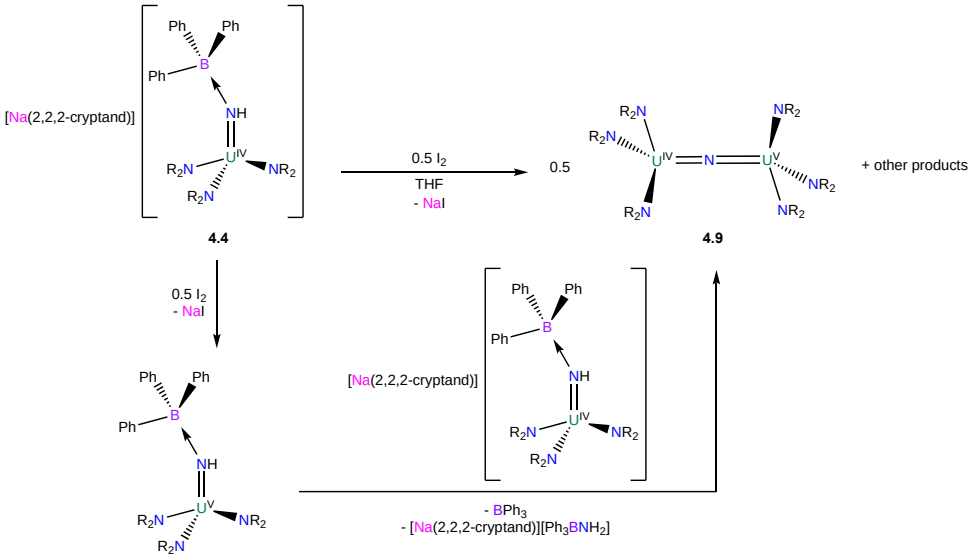

4.2.9 Reactions of [Na(2,2,2-cryptand)][$U(NR_2)_3NHBPh_3$] (4.4) and [K(DB-18-C-6)$(THF)_2$][$Th(NR_2)_3NHBPh_3$] (4.5) with $KN(SiMe_3)_2$

I also probed the reactivity of **4.4** and **4.5** with strong bases, in an effort to form the [$An(NR_2)_3NBPh_3$]$^{2-}$ dianion. Reaction of KNR_2 in a THF-d_8 solution of **4.4** or **4.5** was monitored over 48 h using ^{1}H NMR spectroscopy. Regarding the reaction with **4.4** (Figure A4.21), the original $SiMe_3$ and phenyl resonances completely disappear over 3 h, while a mulititude of new resonances grow in intensity, suggesting that more than one product is

forming. Regarding the reaction of **4.5** (Figure A4.22), new peaks start to grow in intensity over 48 h that can be assigned to Th bis(metallacycle),[25] while the $SiMe_3$ environment assigned to **4.5** starts to slowly decrease in intensity, suggesting decomposition of **4.5** into the Th bis(metallacycle). Overall, these data suggest that the $[An(NR_2)_3NBPh_3]^{2-}$ dianion is unstable (Scheme 4.10).

Scheme 4.10. Reaction of **4.4** and **4.5** with a strong base.

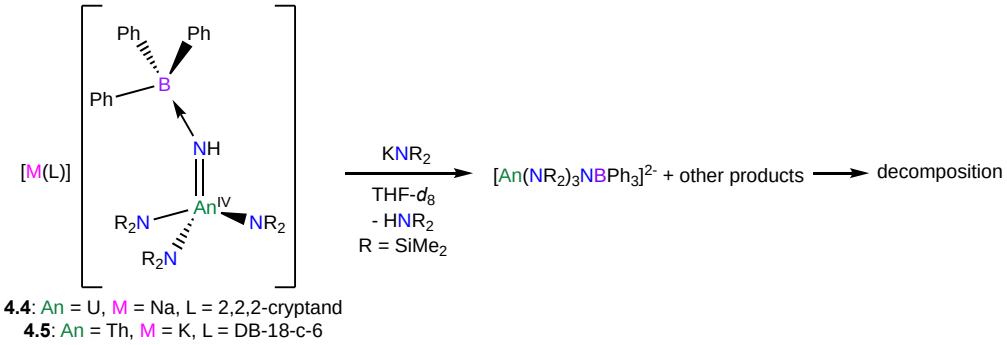

4.4: An = U, M = Na, L = 2,2,2-cryptand
4.5: An = Th, M = K, L = DB-18-c-6

4.3 Summary

In summary, $[Li(12\text{-crown-}4)_2][Th(NCPh_3)(NR_2)_3]$ (**4.1**), $[K(18\text{-crown-}6)][U(NTs)(NR_2)_3]$ (**4.2**), and $[K(18\text{-crown-}6)][Th(NTs)(NR_2)_3]$ (**4.3**) were synthesized through the protonation of the metallacycle, $[An(CH_2SiMe_2NSiMe_3)(NR_2)_2]$ (An = U, Th), with the corresponding amide salt, $[Li(NHCPh_3)(THF)]$, KNHTs (Ts = $MeC_6H_4SO_2$), and $[Na(2,2,2\text{-cryptand})][U(NR_2)_3NHBPh_3]$ (**4.4**) and $[K(DB\text{-}18\text{-}C\text{-}6)(THF)_2][Th(NR_2)_3NHBPh_3]$ (**4.5**) were synthesized by reaction of bis(metallacycle), $[An\{N(R)(SiMe_2CH_2)\}_2(NR_2)]^-$, with NH_3BPh_3. This work, in combination with the past work of Arnold and co-workers, demonstrates that protonation of the An-C bond in $[An(CH_2SiMe_2NSiMe_3)(NR_2)_2]$ and $[An\{N(R)(SiMe_2CH_2)\}_2(NR_2)]^-$ represents a reliable method of making Th=N multiple bonds. Moreover, complexes **4.2** and **4.3** are the first examples of tosylsubstituted imido complexes involving the actinides, while **4.4** - **4.7** being

the first examples of amido borane complexes of the actinides. Furthermore, the imido and amido complexes were fully characterized, helping to specifically expand the scope of Th multiple bond chemistry. These complexes were hypothesized to be ideal for reductive deprotection in order to access an actinide nitrido. However, the trityl protecting group proved to have too strong of a N-C bond, so I switched to the *p*-toluenesulfonyl (Ts = $MeC_6H_4SO_2$) or tosyl protecting group, which I predicted would have a weaker N-S bond than the corresponding N-C bond for the desired reduction. Moreover, I predicted the weak, dative N-B bond formed with the use of NH_3BPh_3 would be easier to cleave than the N-C and N-S bonds. Unfortunately, upon reduction, no cleavage of the N-C, N-S, or N-B bond was achieved. Therefore, new leaving groups are worth trying that have weaker bonds than previously used. Despite not reaching a terminal nitride, this research shows insight to actinide metal-ligand bonding and lays the groundwork for extending imido and amido chemistry to the transuranics.

4.4 Acknowledgements

This work was supported by the U.S. Department of Energy, Office of Basic Energy Sciences, Chemical Sciences, Biosciences, and Geosciences Division, under Contract DE-SC0001861.

I would also like to thank Dr. Danil Smiles (UCSB and group alumni) for the preliminary work done in this area of research. His insights and advice on this chemistry were extremely detailed and helpful.

4.5 Experimental

4.5.1 General Methods

All reactions and subsequent manipulations were performed under anaerobic and anhydrous conditions under an atmosphere of nitrogen. Hexanes, Et_2O, and toluene were dried using a Vacuum Atmospheres DRI-SOLV Solvent Purification system and stored over 3Å sieves for 24 h prior to use. THF was dried by distillation from sodium/benzophenone, and stored over 3Å sieves for 24 h prior to use. Benzene-d_6 and THF-d_8 were dried over 3Å molecular sieves for 24 h prior to use. [An(CH$_2$SiMe$_2$$N$SiMe$_3$)(NR$_2$)$_2$] (An = U, Th), [Li(NHCPh$_3$)(THF)], KNHTs (Ts = MeC$_6$H$_4$SO$_2$), [K(DME)][Th{N(R)(SiMe$_2$$CH_2$)}$_2$(NR$_2$)], and [Na(DME)$_3$][U{$N$(R)(SiMe$_2$$CH_2$)}$_2$(NR$_2$)] were synthesized according to the previously reported procedures.[25, 44, 48, 49, 54, 55] All other reagents were purchased from commercial suppliers and used as received.

NMR spectra were recorded on an Agilent Technologies 400-MR DD2 400 MHz Spectrometer or a Varian UNITY INOVA 500 spectrometer. ^{1}H and ^{13}C{^{1}H} NMR spectra were referenced to external tetramethylsilane (TMS) using the residual protio solvent peaks as internal standards. ^{7}Li{^{1}H} NMR spectra were referenced to external LiCl in D_2O. ^{11}B NMR spectra were referenced externally to Et_2O•BF_3. IR spectra were recorded on a Nicolet 6700 FT-IR spectrometer with a NXR FT Raman Module. Electronic absorption spectra were recorded on a Shimadzu UV3600 UV-NIR Spectrometer. Elemental analyses were performed by the Micro-Analytical Facility at the University of California, Berkeley.

4.5.2 Synthesis and Characterization of [Li(12-crown-4)$_2$][Th(NCPh$_3$)(NR$_2$)$_3$] (4.1)

To a stirring, cold (-25 °C), pale yellow solution of [Th(*C*H$_2$SiMe$_2$*N*SiMe$_3$)(NR$_2$)$_2$] (49.9 mg, 0.070 mmol) in THF (3 mL) was added a cold (-25 °C) solution of [LiNHCPh$_3$(THF)] (24.0 mg, 0.071 mmol) in THF (3 mL) and a cold (-25 °C) solution of 12-crown-4 (22.67 μL, 0.140 mmol) in THF (3 mL). The reaction mixture was allowed to warm to room temperature with stirring. After 1 h, the volatiles were removed *in vacuo* to provide a colorless/white solid. The solid was then extracted into diethyl ether (6 mL) and the resulting colorless/white solution was filtered through a Celite column supported on glass wool (0.5 × 2 cm). The filtrate was concentrated *in vacuo* to 2 mL and stored at -25 °C for 24 h, which resulted in the deposition of colorless crystals. The solid was isolated by decanting the supernatant and then dried *in vacuo* to yield **4.1** as white powder (70.3 mg, 75 % yield). Anal. Calcd for $C_{53}H_{101}LiN_4O_8Si_6Th$: C, 47.87; H, 7.66; N, 4.21. Found: C, 47.59; H, 7.45; N, 4.12. ^{1}H NMR (400 MHz, 25 °C, C_6D_6): δ -0.58 (s, 54H, SiC*H*$_3$), 3.15 (s, 32H, Li(*C*$_8$H$_{16}$O$_4$)$_2$), 7.05 (s, 3H, *o*-C$_6$*H*$_5$), 7.26 (s, 6H, *m*-C$_6$*H*$_5$), 7.91 (s, 6H, *p*-C$_6$*H*$_5$). ^{7}Li{^{1}H} NMR (59 MHz, 25 °C, C_6D_6): δ -1.64 (s, 1Li). ^{13}C{^{1}H} NMR (100 MHz, 25 °C, C_6D_6): δ 6.00 (s, Si*C*H$_3$), 67.35 (s, Li(*C*$_8$H$_{16}$O$_4$)$_2$), 127.19 (hep, C$_6$*H*$_5$), 155.35 (s, N*C*Ph$_3$). IR (KBr pellet, cm^{-1}): 405 (s), 461 (sh, s), 472 (s), 484 (s), 592 (s), 596 (s), 660 (s), 754 (s), 769 (s), 827 (w), 953 (w), 982 (s), 1097 (w), 1246 (m), 1292 (s), 1444 (m), 1495 (s), 1927 (m), 2941 (w), 2987 (m), 3431 (w).

4.5.3 Synthesis and Characterization of K(18-crown-6)][U(NTs)(NR$_2$)$_3$] (4.2)

To a stirring, cold (-25 °C), pale yellow solution of [Th(*C*H$_2$SiMe$_2$*N*SiMe$_3$)(NR$_2$)$_2$] (150.3 mg, 0.209 mmol) in THF (2 mL) was added a cold (-25 °C) solution of KNHTs (44.2 mg, 0.209 mmol) in THF (2 mL) and a cold (-25 °C) solution of 18-crown-6 (55.3 mg, 0.209

mmol). After stirring for 4 h the volatiles were removed *in vacuo* to yield a light brown powder. The powder was then extracted into pentane (5 mL) and the solution was filtered through a Celite column supported on glass wool (0.5 × 2 cm). The filtrate was concentrated *in vacuo* to 2 mL and storage of this solution for 24 h at -25 °C resulted in the deposition of X-ray quality crystals. The crystals were isolated by decanting the supernatant and then dried *in vacuo* to afford **4.2**. Yield: 0.1510 g, 61% yield. Anal. Calcd for $C_{37}H_{85}KN_4O_8SSi_6U$: C, 37.29; H, 7.19; N, 4.70. Found: C, 36.95; H, 7.05; N, 4.52. ^{1}H NMR (400 MHz, 25 °C, C_6D_6): δ -2.79 (s, 54H, SiC*H*$_3$), 0.74 (s, 3H, *p*-C*H*$_3$), 2.83 (br s, 24H, $C_{12}H_{24}O_6$), 4.24 (d, 2H, *o*-C_6H_5), 4.96 (d, 2H, *m*-C_6H_5). ^{13}C{^{1}H} NMR (100 MHz, 25 °C, C_6D_6): δ -26.47 (s, Si*C*H$_3$), 19.26 (s, *C*H$_3$), 69.29 (s, $C_{12}H_{24}O_6$), 121.98 (s, C_6H_5), 127.34 (s, C_6H_5), 136.55 (s, C_6H_5), 168.77 (s, C_6H_5). IR (KBr pellet, cm^{-1}): 401 (s), 530 (sh, s), 557 (s), 607 (s), 663 (m), 673 (m), 833 (w), 1107 (w), 1246 (m), 1261 (s), 1454 (s), 1504 (s), 1925 (w), 2893 (w), 2904 (w), 3381 (w).

4.5.4 Synthesis and Characterization of [K(18-crown-6)][Th(NTs)(NR$_2$)$_3$] (4.3)

To a stirring, cold (-25 °C), pale yellow solution of [Th(*C*H$_2$SiMe$_2$*N*SiMe$_3$)(NR$_2$)$_2$] (108.1 mg, 0.152 mmol) in THF (2 mL) was added a cold (-25 °C) solution of KNHTs (32.6 mg, 0.154 mmol) in THF (2 mL) and a cold (-25 °C) solution of 18-crown-6 (40.1 mg, 0.152 mmol) in THF (2 mL). After stirring for 1h, the volatiles were removed *in vacuo* to yield an off-white solid. The solid was then extracted into diethyl ether (5 mL) and the solution was filtered through a Celite column supported on glass wool (0.5 × 2 cm), concentrated *in vacuo* to 2 mL and layered onto pentane (4 mL). Storage of this solution for 24 h at -25 °C resulted in the deposition of X-ray quality colorless crystals. The crystals were isolated by decanting the supernatant and then dried *in vacuo* to afford **4.3**. Yield: 0.1262 g, 70% yield. Anal. Calcd

for $C_{37}H_{85}KN_4O_8SSi_6Th$: C, 37.48; H, 7.23; N, 4.72. Found: C, 37.71; H, 6.91; N, 4.34. ^{1}H NMR (400 MHz, 25 °C, C_6D_6): δ -0.63 (s, 54H, SiC*H*$_3$), 2.13 (s, 3H, *p*-C*H*$_3$), 3.18 (s, 24H, $C_{12}H_{24}O_6$), 7.06 (d, 2H, *o*-C_6H_5) 8.15 (d, 2H, *m*-C_6H_5). ^{13}C{^{1}H} NMR (100 MHz, 25 °C, C_6D_6): δ 4.38 (s, *C*$_6$H$_5$), 4.82 (s, Si*C*H$_3$), 20.81 (s, *C*H$_3$), 69.64 (s, *C*$_{12}$H$_{24}$O$_6$), 127.07 (s, *C*$_6$H$_5$), 136.75 (s, *C*$_6$H$_5$), 149.43 (s, *C*$_6$H$_5$). IR (KBr pellet, cm^{-1}): 407 (s), 534 (s), 563 (s), 606 (s), 673 (s), 685 (sh, s), 771 (s), 839 (m), 962 (m), 1111 (m), 1149 (s), 1250 (m), 1352 (s), 1454 (m), 1597 (w), 1907 (w), 2883 (w), 3406 (w).

4.5.5 Synthesis and Characterization of [Na(2,2,2-cryptand)][U(NR$_2$)$_3$NHBPh$_3$] (4.4)

To a stirring, cold (-25 °C), green solution of [Na(DME)$_3$][U{*N*(R)(SiMe$_2$*C*H$_2$)}$_2$(NR$_2$)] (57.2 mg, 0.0566 mmol) in toluene (2 mL) was added a cold (-25 °C) toluene suspension of NH$_3$BPh$_3$ (0.0155 mg, 0.0598 mmol) and a cold (-25 °C) toluene solution of 2,2,2-cryptand (0.0220 mg, 0.0584 mmol). The green reaction mixture gradually became orange as it was allowed to warm to room temperature with stirring. After 4 h, the reaction mixture was filtered through a Celite column supported on glass wool (0.5 × 2 cm) and the toluene solution was dried *in vacuo*. The resulting solid was extracted into Et$_2$O, where upon the solution was filtered through a Celite column supported on glass wool (0.5 × 2 cm) and concentrated *in vacuo* to 2 mL and layered with pentane. Storage at -25 °C for 24 h resulted in the deposition of orange crystalline material, which was isolated by decanting the supernatant and then dried *in vacuo* to yield **4.4** (.0187 g, 24% yield). Anal. Calcd for $NaC_{54}H_{106}BN_6O_6Si_6U$: C, 47.14; H, 7.77; N, 6.11. Found: C, 45.52; H, 7.85; N, 6.66. ^{1}H NMR (400 MHz, 25 °C, THF-*d*$_8$): δ -5.63 (s, 54H, SiC*H*$_3$), 2.49 (s, 12H, cryptand), 3.42 (s, 12H, cryptand), 3.46 (s, 12H, cryptand), 7.54 (s, 3H, phenyl-*p*, C*H*), 8.10 (s, 6H, phenyl-*o*, C*H*), 10.36 (s, 6H, phenyl-*m*, C*H*). IR (KBr

pellet, cm^{-1}): 523 (s), 592 (s), 661 (s), 704 (s), 706 (m), 843 (m), 931 (m), 1105 (m), 1142 (m), 1250 (m), 1269 (m), 1356 (s), 1431 (m), 2818 (w), 2889 (w), 2954 (w), 2997 (w).

4.5.6 Synthesis and Characterization of $[K(DB\text{-}18\text{-}C\text{-}6)(THF)_2][Th(NR_2)_3NHBPh_3]$ (4.5)

To a stirring, cold (-25 °C), pale yellow solution of $[K(DME)][Th\{N(R)(SiMe_2CH_2)\}_2(NR_2)]$ (66.9 mg, 0.0796 mmol) in THF (2 mL) was added a cold (-25 °C) THF solution of NH_3BPh_3 (0.0207 mg, 0.0799 mmol) and a cold (-25 °C) THF solution of dibenzo-18-crown-6 (DB-18-C-6) (0.0287 mg, 0.0796 mmol). After 4 h, the reaction mixture was filtered through a Celite column supported on glass wool (0.5 × 2 cm) and the THF solution was concentrated *in vacuo* to 2 mL and layered with pentane. Storage at -25 °C for 24 h resulted in the deposition of colorless crystalline material, which was isolated by decanting the supernatant and then dried *in vacuo* to yield **4.5** (.0749 g, 62% yield). Anal. Calcd for $KC_{56}H_{94}BN_4O_6Si_6Th$: C, 49.10; H, 6.92; N, 4.09. Found: C, 50.83; H, 7.12; N, 3.53. ^{1}H NMR (400 MHz, 25 °C, THF-d_8): δ 0.21 (s, 54H, SiCH_3), 3.84 (s, 8H, CH_2, DB-18-C-6), 4.14 (s, 8H, CH_2, DB-18-C-6), 4.35 (br s, 1H, N*H*), 6.76 (m, 6H, phenyl-*o*, C*H*), 6.90 (m, 6H, phenyl-*m*, C*H*), 6.96 (m, 8H, *o, m* C*H*, DB-18-C-6), 7.39 (s, 3H, phenyl-*p*, C*H*). ^{13}C{^{1}H} NMR (100 MHz, 25 °C, THF-d_8): δ 6.84 (s, NSi*C*H$_3$), 15.22 (s), 24.05 (s), 27.22 (s), 69.03 (d, DB-18-C-6), 71.06 (s, DB-18-C-6), 113.13 (s, DB-18-C-6), 123.18 (d, DB-18-C-6), 124.30 (s), 127.02 (d), 136.62 (d), 148.82 (s, DB-18-C-6). ^{11}B NMR (32.08 MHz, 25 °C, THF-d_8): δ 0.95. IR (KBr pellet, cm^{-1}): 573(s), 706 (s), 708 (m), 847 (m), 889 (m), 943 (m), 1061 (s), 1124 (s), 1215 (s), 1248 (s), 1284 (s), 1319 (s), 1454 (s), 1504 (s), 1597 (s), 2873 (w), 2931 (w), 3037 (w).

4.5.7 X-ray Crystallography

Data for **4.1**, **4.2**, **4.3**, **4.4, 4.5**, and **4.7** were collected on a Bruker KAPPA APEX II diffractometer equipped with an APEX II CCD detector using a TRIUMPH monochromator with a Mo Kα X-ray source (α = 0.71073 Å), while data for **4.6** was collectd on a Bruker AXS SMART APEX II diffractormeter. The crystals were mounted on a cryoloop under Paratone-N oil. Complexes **4.1**, **4.2**, **4.5**, **4.6**, and **4.7** were collected at 100(2) K, **4.4** was collected at 103(2)K, and **4.3** was collected at 101(2) K, using an Oxford nitrogen gas cryostream. Data were collected using ω scans with 0.5° frame widths. Frame exposures of 10, 10, 15, 10, 10, 10, and 15 seconds were used for **4.1**, **4.2**, **4.3**, **4.4**, **4.5**, **4.6**, **4.7**, respectively. Data collection and cell parameter determinations were conducted using the SMART program.[56] Integration of the data frames and final cell parameter refinements were performed using SAINT software.[57] Absorption corrections of the data were carried out using the multi-scan method SADABS for **4.1**-**4.7**.[58] Subsequent calculations were carried out using SHELXTL[59] or GUI Olex2 software package.[60, 61] Structure determination was done using direct or Patterson methods and difference Fourier techniques. All hydrogen atom positions were idealized, and rode on the atom of attachment. Structure solution, refinement, graphics, and creation of publication materials were performed using SHELXTL[59] or Olex2.[60, 61]

Table 4.3. X-ray Crystallographic Data for **4.1**, **4.2**, and **4.3**.

	4.1	**4.2**	**4.3**
Empirical formula	$C_{53}H_{100.5}LiN_4O_8Si_6Th$	$C_{37}H_{85}KN_4O_8SSi_6U$	$C_{37}H_{85}KN_4O_8SSi_6Th$
crystal habit, color	Block, Colorless	Block, Colorless	Block, Colorless
crystal size (mm)	0.2 × 0.15 × 0.15	0.2 × 0.15 × 0.15	0.2 × 0.15 × 0.1
space group	*P*bca	$P\bar{1}$	$P\bar{1}$
volume (Å^3)	26238(3)	2868.4(12)	2888.9(8)
a (Å)	24.8732(18)	12.085(3)	12.0418(18)
b (Å)	22.7061(16)	14.933(4)	15.092(2)
c (Å)	46.458(3)	16.514(4)	16.523(3)
α (deg)	90	94.036(4)	94.258(3)
β (deg)	90	90.318(4)	90.083(3)
γ (deg)	90	105.162(4)	105.224(3)
Z	16	2	2
formula weight (g/mol)	1329.39	1191.81	1185.82
density (calculated) (Mg/m^3)	1.346	1.380	1.363
absorption coefficient (mm^{-1})	2.431	3.107	2.856
F_{000}	11000	1220	1216
total no. reflections	110422	29864	22420
unique reflections	26829	12141	12089
Final R Indices (I >2σ(I)]	R_1 = 0.0783 wR_2 = 0.1693	R_1 = 0.0379 wR_2 = 0.0516	R_1 = 0.0405 wR_2 = 0.0567
largest diff. peak and hole (e$^-$ A^{-3})	3.524 and -1.667	0.0876 and -1.159	1.972 and -0.999
GOF	1.222	1.064	1.273

Table 4.4. X-ray Crystallographic Data for **4.4**, **4.5**, **4.6**, and **4.7**.

	4.4	**4.5**	**4.6**	**4.7**
empirical formula	$C_{54}H_{105}BN_6O_6Si_6U$	$C_{70.5}H_{123}BKN_4O_9Si_6Th$	$C_{44}H_{88}BN_4NaO_3Si_6U$	$C_{54}H_{105}BKN_6O_6Si_6Th$
crystal habit, color	Needle, Orange	Block, Colorless	Block, Light Orange	Block, colorless
crystal size (mm)	0.3 × 0.2 × 0.1	0.2 × 0.1 × 0.1	0.24 × 0.18 ×0.18	0.20 × 0.15 ×0.10
space group	*P2₁/c*	*P-1*	*P1₂1/n₁*	*P2₁/c*
volume (Å^3)	6694.5(5)	4268.3(11)	5656(5)	6925.1(7)
a (Å)	16.9815(7)	15.602(2)	18.216(10)	22.4704(13)
b (Å)	21.8765(9)	17.427(3)	16.495(9)	16.8165(11)
c (Å)	18.0272(7)	17.828(3)	18.889(11)	19.0085(11)
α (deg)	90	104.155(3)	90	90
β (deg)	91.5710(10)	110.721(3)	94.749(7)	105.394(4)
γ (deg)	90	97.498(3)	90	90
Z	4	2	4	4
Formula weight (g/mol)	1374.80	1621.21	1161.55	1384.92
density (calculated) (Mg/m^3)	1.364	1.261	1.364	1.328
Absorption coefficient (mm^{-1})	2.586	1.929	3.042	2.363
F_{000}	2844	1688	2384	2868
total no.reflections	35255	40549	58792	45746
unique reflections	13632	21836	11569	14203
Final R Indices (I >2σ(I)]	R_1 = 0.0323 wR_2 = 0.0739	R_1 = 0.0377 wR_2 = 0.1021	R_1 = 0.0471 wR_2 = 0.0762	R_1 = 0.0574 wR_2 =0.1304
Largest diff. peak and hole (e$^-$ A^{-3})	6.226 and -1.004	2.663 and -0.941	1.548 and -1.639	2.801 and -1.788
GOF	0.974	0.953	1.019	0.966

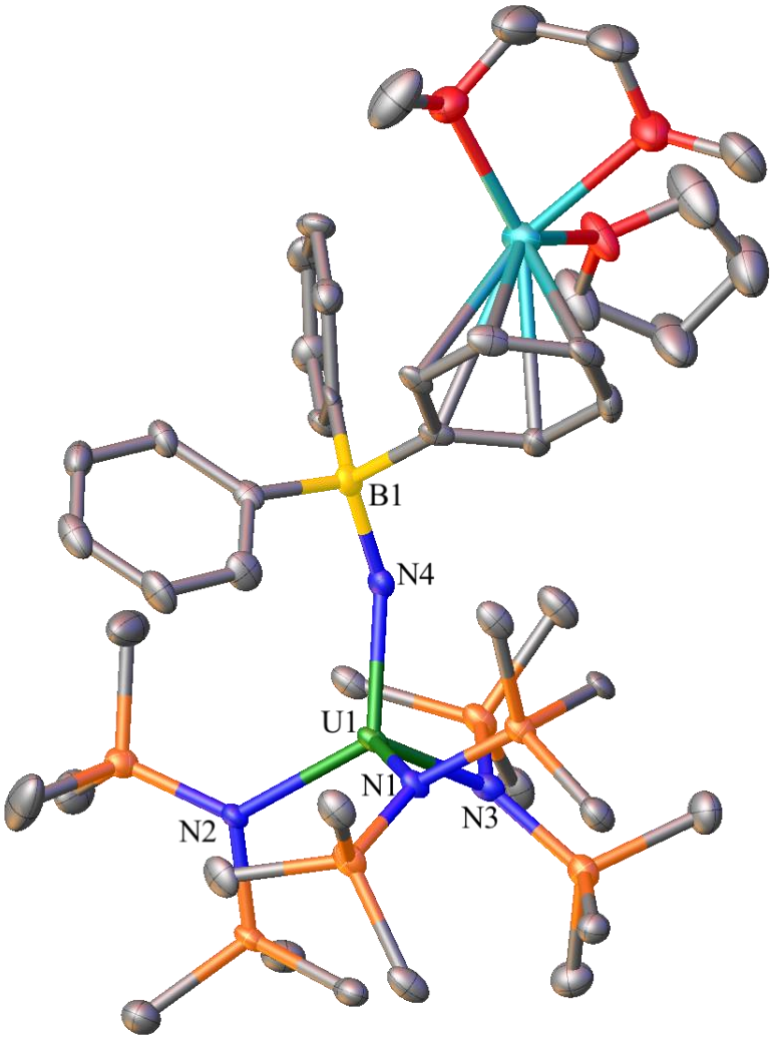

Figure 4.5. Solid-state molecular structure of **4.6**, shown with 50% probability ellipsoids. Hydrogen atoms removed for clarity. Selected bond lengths (Å) and angles (°): U1-N4 = 2.140(4), U-$N_{silylamido}$ (av.) = 2.31, N4-B1 = 1.577(7), N-U-N (av.) = 109.6, U1-N4-B1 = 149.1(3).

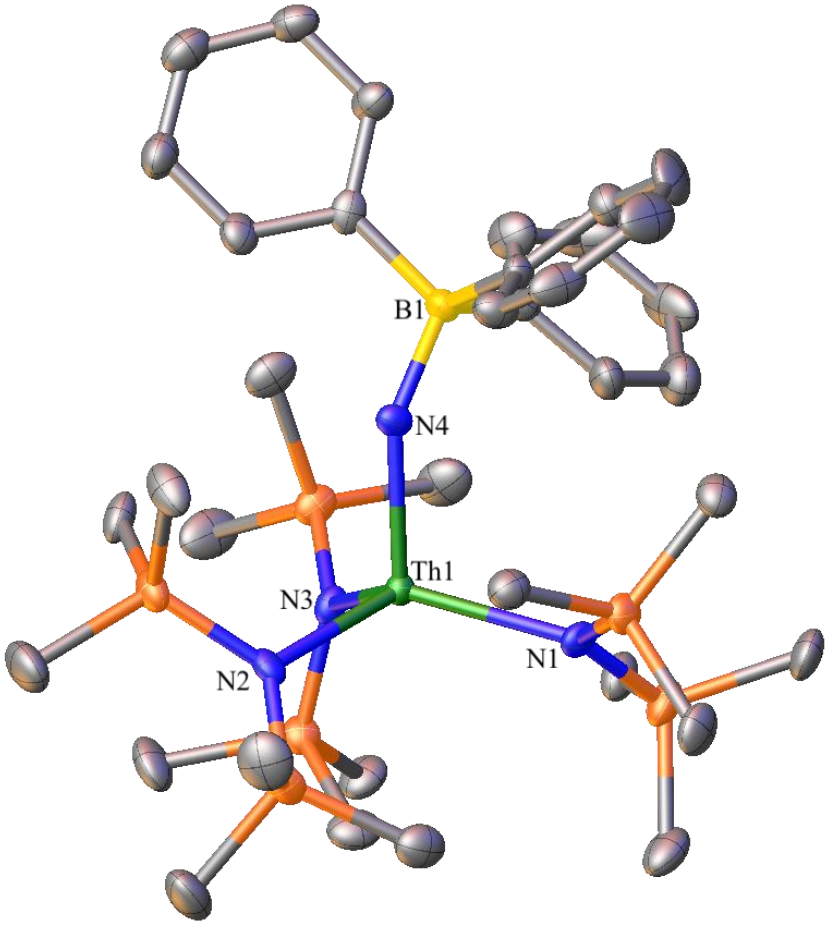

Figure 4.6. Solid-state molecular structure of **4.7**, shown with 50% probability ellipsoids. $[K(2,2,2\text{-cryptand})]^+$ counterion and hydrogen atoms removed for clarity. Selected bond lengths (Å) and angles (°): Th1-N4 = 2.187(6), Th-$N_{silylamido}$ (av.) = 2.38, N4-B1 = 1.588(11), N-U-N (av.) = 113.9, Th1-N4-B1 = 146.5(5).

4.6 Appendix

4.6.1 Synthesis and Characterization of $U(NR_2)_3C_8H_4NO_3UNR$ (R = $SiMe_3$) (4.10)

I sought to synthesize a new uranium amide complex by using N-hydroxyphthalimide, $C_8H_5NO_3$, that could then be subjected to the reductive deprotection protocol to synthesize a uranium terminal oxo complex. Thus, reaction of N-hydroxyphthalimide to uranium metallacycle, $[U(CH_2SiMe_2NSiMe_3)(NR_2)_2]$, in THF, results in the dimer $U(NR_2)_3C_8H_4NO_3UNR$ (**4.10**), as orange needles from concentrated pentane. Complex **4.10** crystallizes in the monoclinic space group C2/c, and its solid-state molecular structure is shown in Figure A4.1. The U2-O3 bond distance (2.329(7) Å) is much shorter than U2-O2 (2.429(7) Å), suggesting the later to be a dative bond. The N5-O3 bond distance (1.365(9) Å) in **4.12** is slightly shorter than that reported in N-hydroxyphthalimide (1.374(5) Å).[62]

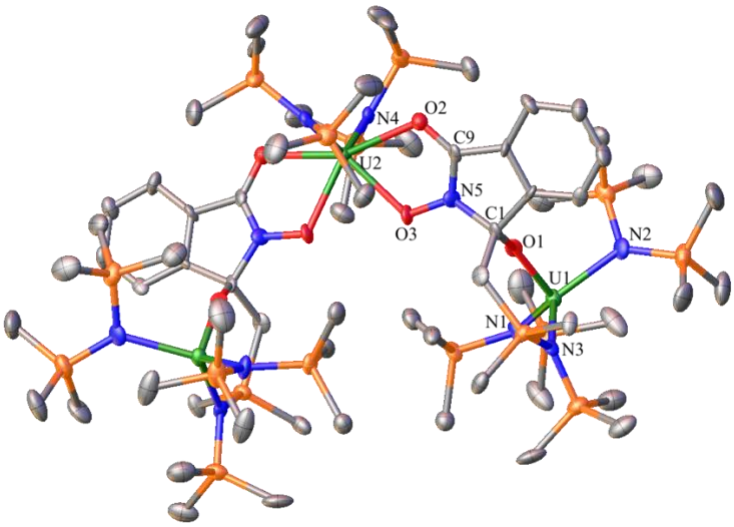

Figure A4.1. Solid-state molecular structure of **4.10**, shown with 50% probability ellipsoids. Hydrogen atoms removed for clarity. Selected bond lengths (Å) and angles (°): U2 – O2 = 2.429(6), U2 – O3 = 2.329(7), U1-$N_{silylamido}$ (av.) = 2.259, U1 – O1 = 2.059(7), U2 – N4 = 2.230(8), O3 – N5 = 1.365(9), N-U-N (av.) = 117.2.

4.6.2 Synthesis of $C_8H_4NO_3K$ (4.11)

After the results of using N-hydroxyphthalimide, I sought to synthesize a ligand that would better facilitate the desired chemistry and thought switching the proton in the original ligand with potassium would promote a better leaving group with the loss of KCl. Thus, reaction of N-hydroxyphthalimide with potassium bis(trimethylsilyl)amide, in THF, results in the loss of free amine and the deprotonated complex $C_8H_4NO_3K$ (**4.11**), as a dark purple powder (Scheme 4.11). Attempts to crystallize **4.11** proved difficult and I was unable to recrystallize due to the extremely low solubility in pyridine, DME, CH_2Cl_2, DMSO, and acetonitrile.

Scheme 4.11. Synthesis of **4.11**.

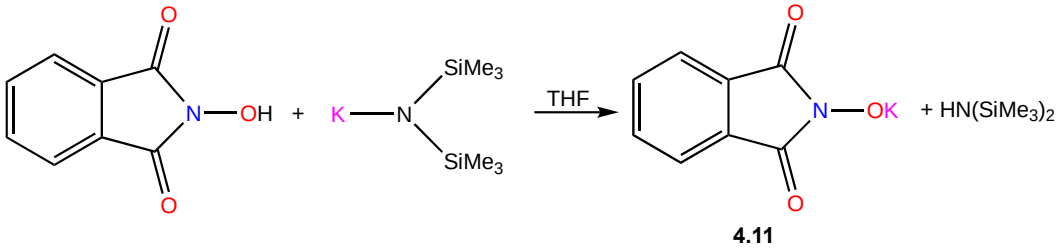

4.11

The ^{1}H NMR spectrum in dimethyl sulfoxide-d_6 shows two resonances in a 1:1 ratio at 7.27 ppm and 7.42 ppm, assignable to the two environments of the phenyl ring, phenyl-*p* and phenyl-*m*, respectively (Figure A4.2).

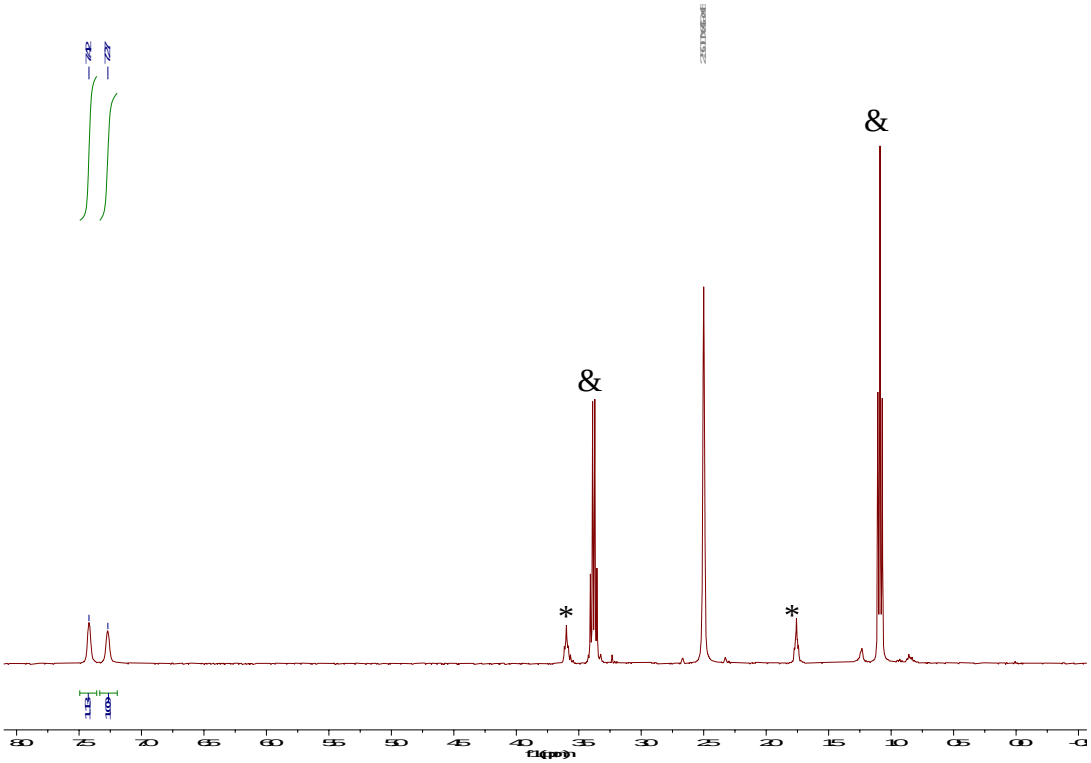

Figure A4.2 ^{1}H NMR of **4.11** in dimethyl sulfoxide-d_6. (*) indicates THF and (&) indicates diethyl ether.

4.6.3 Synthesis and Characterization of $Th(NR_2)_3C_8H_4NO_3$ (R = $SiMe_3$) (4.12)

With **4.11** in hand, I explored using it in efforts to synthesize a thorium amide complex that could be subjected to the reductive deprotection protocol to synthesize a thorium terminal oxo complex. Therefore, reaction of **4.11** to $Th(NR_2)_3Cl$ (R = $SiMe_3$), in THF, results in $Th(NR_2)_3C_8H_4NO_3$ (**4.12**), as yellow blocks after crystallization in diethyl ether in 40% yield (Scheme 4.12). The ^{1}H NMR spectrum (Figure A4.3) in benzene-d_6 has three resonances in a 54:2:2 ratio at 0.47 ppm, 6.64 ppm, and 7.07 ppm, assignable to the $SiMe_3$ groups, phenyl-*p*, and phenyl-*m*, respectively.

Scheme 4.12. Synthesis of **4.12**.

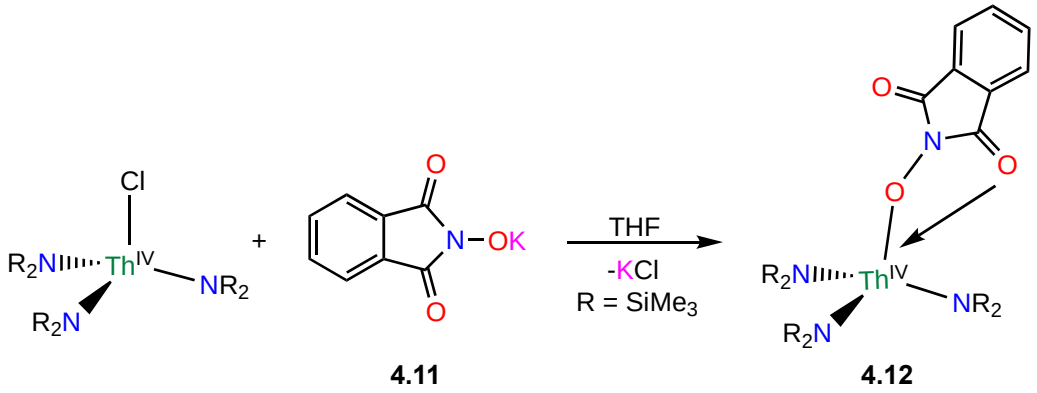

4.11 **4.12**

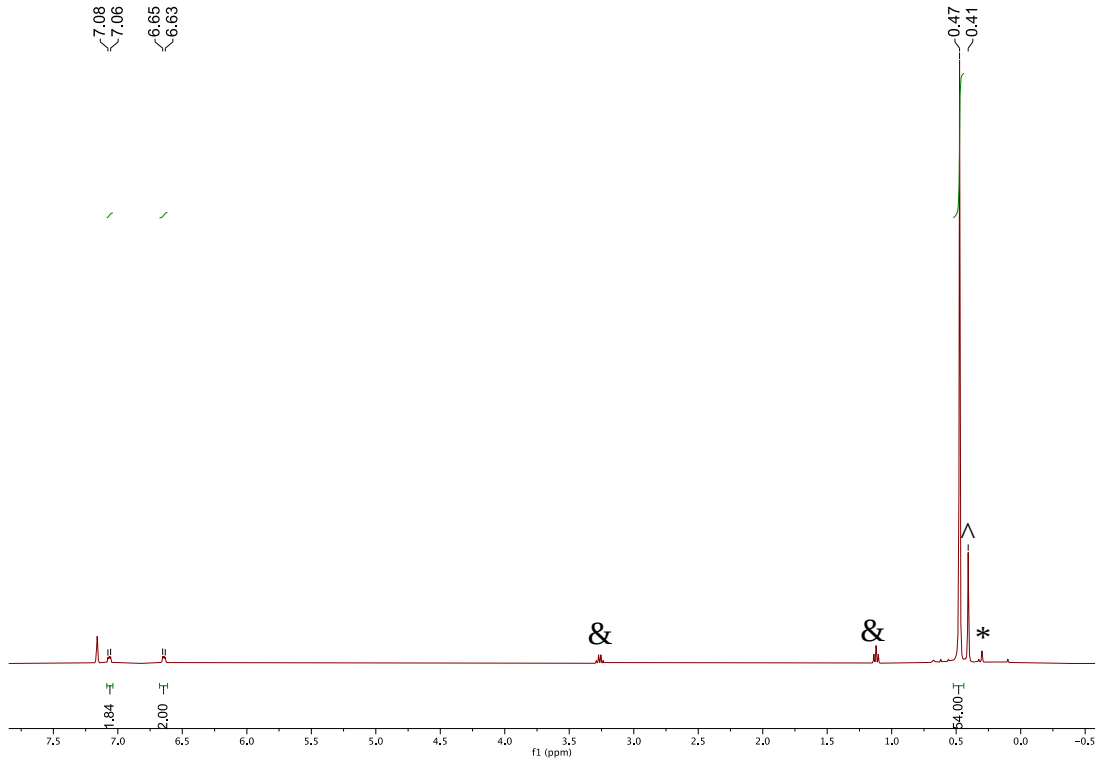

Figure A4.3 ^{1}H NMR of **4.12** in benzene-d_6. (*) indicates $HN(SiMe_3)_2$, (^) indicates free $Th(NR_2)_3Cl$, and (&) indicates diethyl ether.

Complex **4.12** crystallizes in the monoclinic space group P2/n with two molecules in the asymmetric unit, and its solid-state molecular structure is shown in Figure A4.4. The Th2-O4 bond distance (2.307(7) Å) is much shorter than Th2-O6 (2.662(7) Å), suggesting the later to

be a dative bond. The N5-O4 bond distance (1.3549(11) Å) in **4.12** is slightly shorter than that reported in N-hydroxyphthalimide (1.374(5) Å) and **4.10**.[62] Furthermore, the Th-$N_{silylamido}$ (av. = 2.323 Å) bond lengths are longer than corresponding bond lengths of **4.10** (U-$N_{silylamido}$ (av. = 2.259 Å) consistent with the increased ionic radius of Th^{4+} versus U^{4+}.[47]

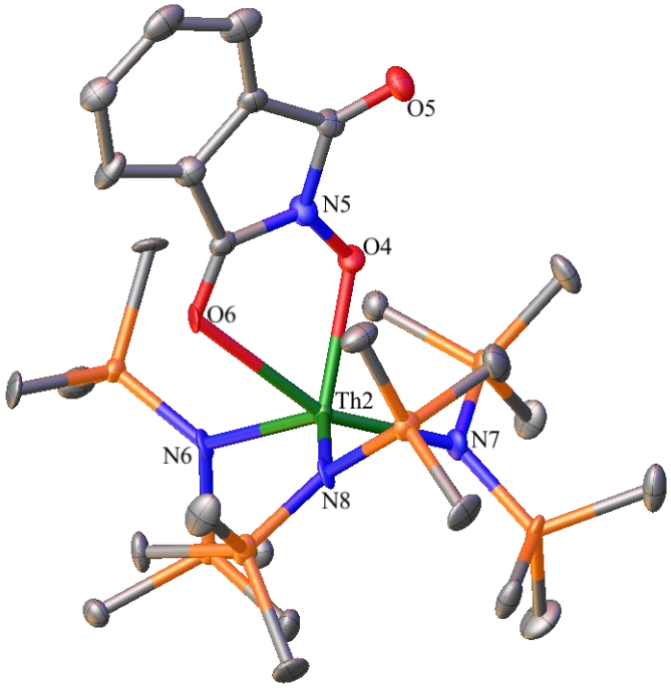

Figure A4.4. Solid-state molecular structure of **4.12**, shown with 50% probability ellipsoids. One $Th(NR_2)_3C_8H_4NO_3$ molecule and hydrogen atoms removed for clarity. Selected bond lengths (Å) and angles (°): Th2 – O4 = 2.307(7), Th2 – O6 = 2.662(7), Th-$N_{silylamido}$ (av.) = 2.323, O4 – N5 = 1.3549(11), N-Th2-N (av.) = 113.53, Th2-O4-N5 = 118.0(6).

4.6.4 NMR Spectra

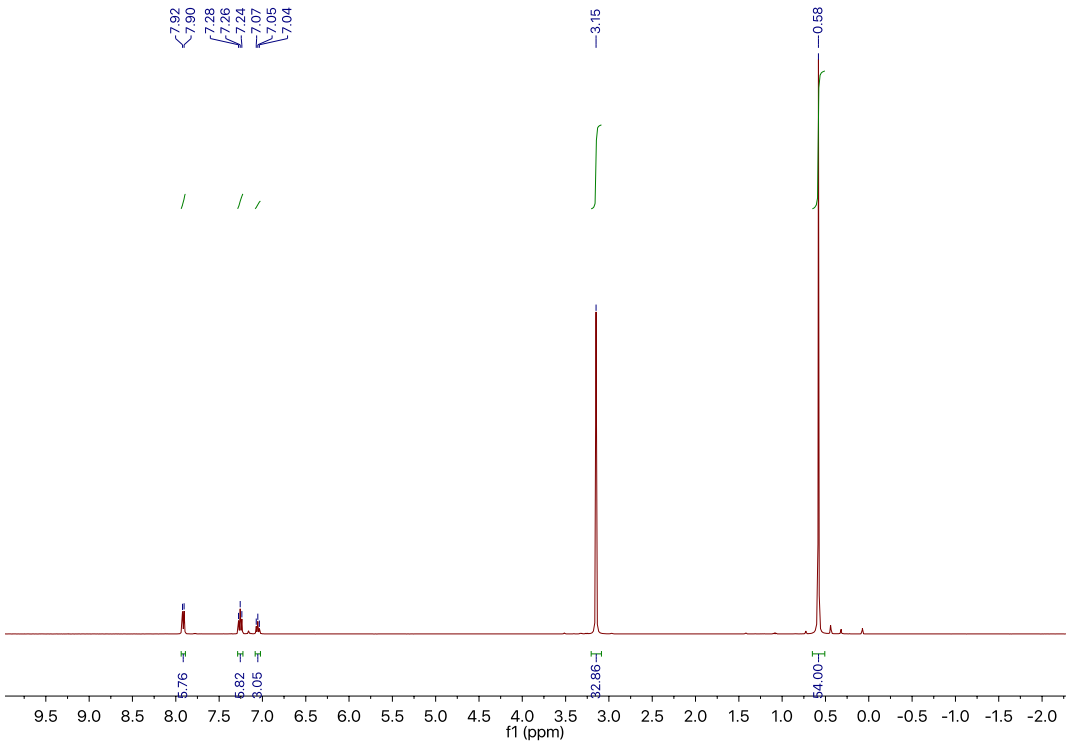

Figure A4.5. ^{1}H NMR spectrum of $[Li(12\text{-crown-4})_2][Th(NCPh_3)(NR_2)_3]$ (**4.1**) in C_6D_6.

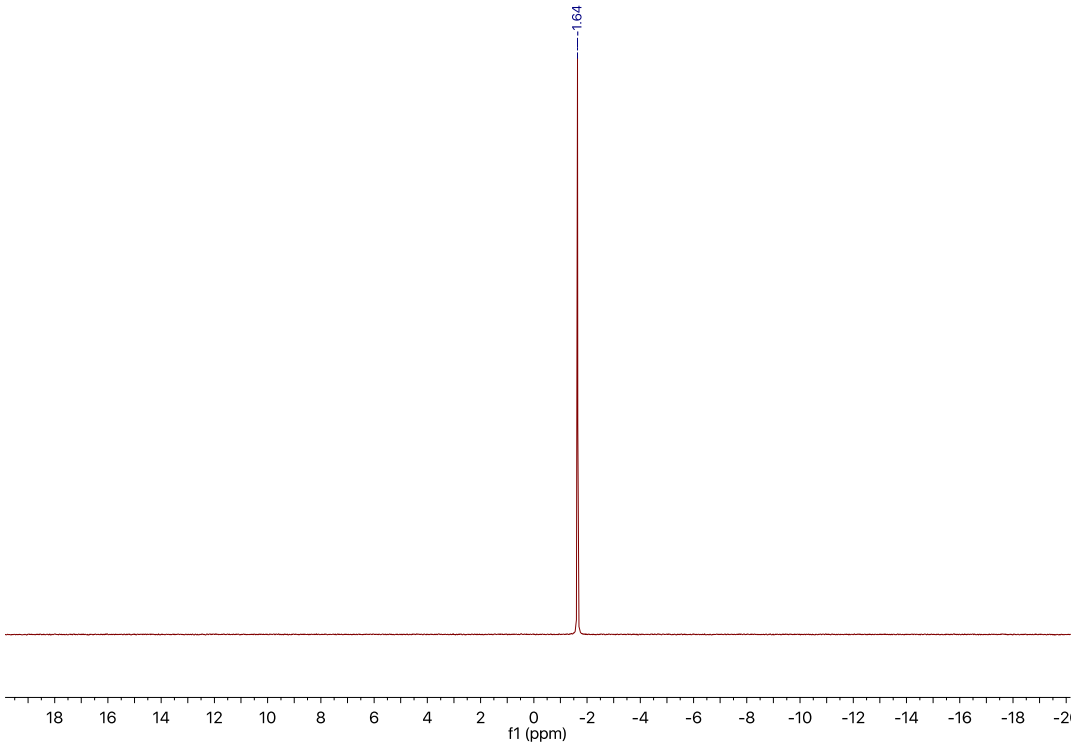

Figure A4.6. $^{7}Li\{^{1}H\}$ NMR spectrum of $[Li(12\text{-crown-4})_2][Th(NCPh_3)(NR_2)_3]$ (**4.1**) in C_6D_6.

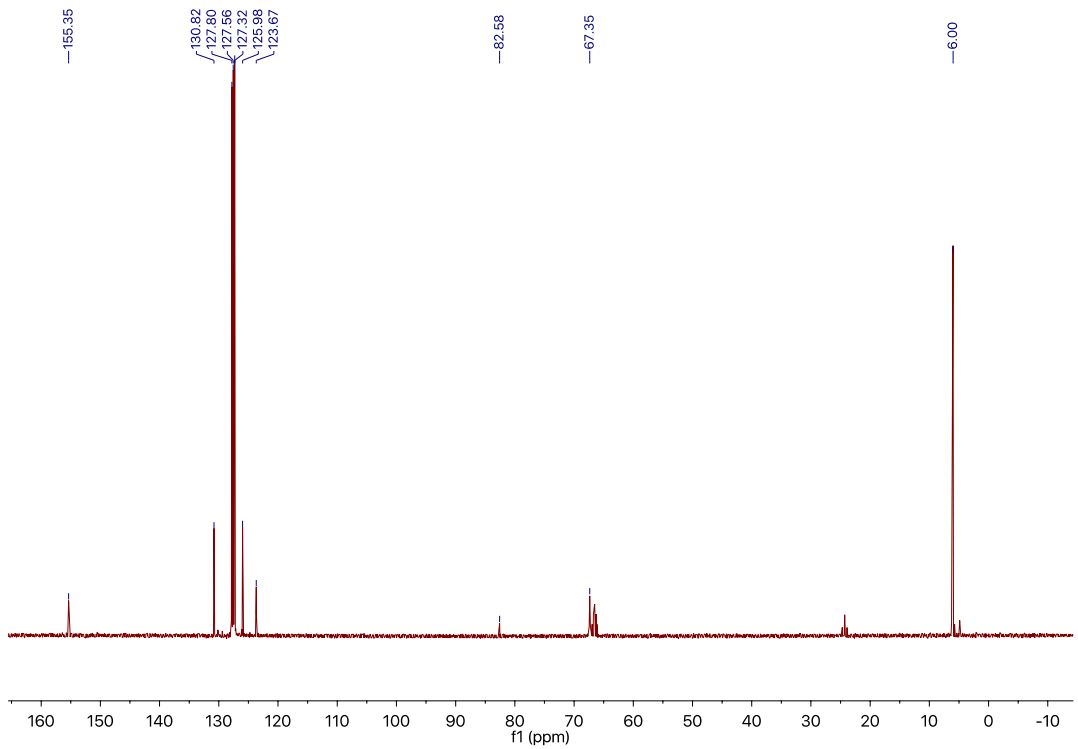

Figure A4.7. $^{13}C\{^{1}H\}$ NMR spectrum of $[Li(12\text{-crown-4})_2][Th(NCPh_3)(NR_2)_3]$ (**4.1**) in C_6D_6.

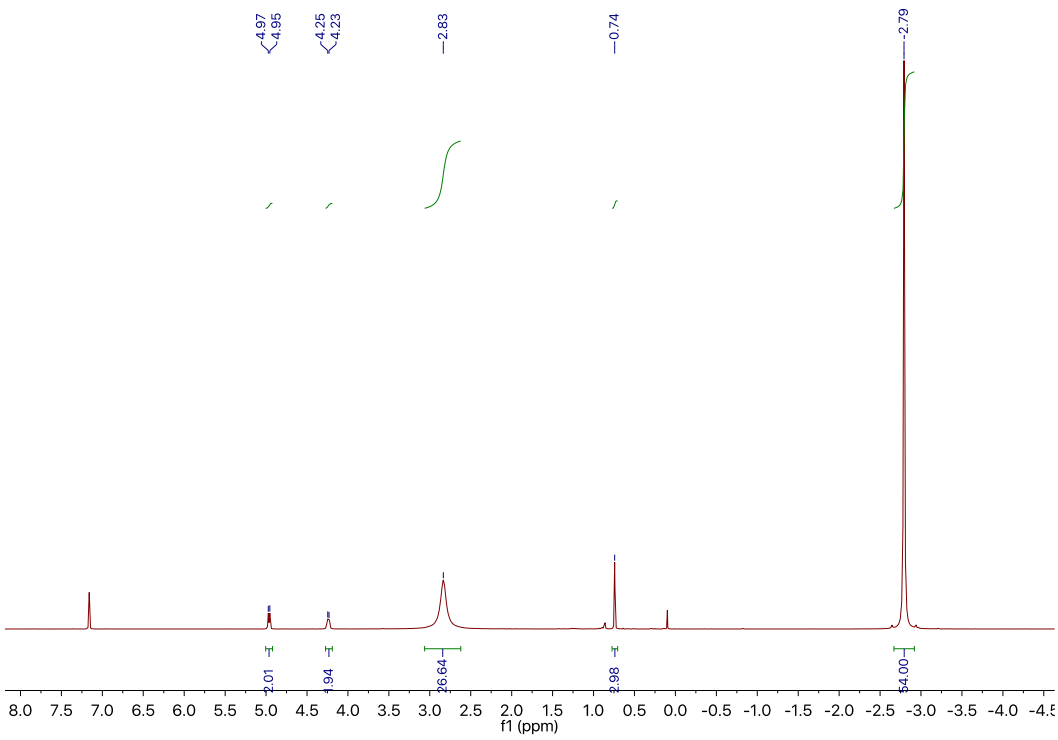

Figure A4.8. ^{1}H NMR spectrum of [K(18-crown-6)][U(NTs)(NR$_2$)$_3$] (**4.2**) in C_6D_6.

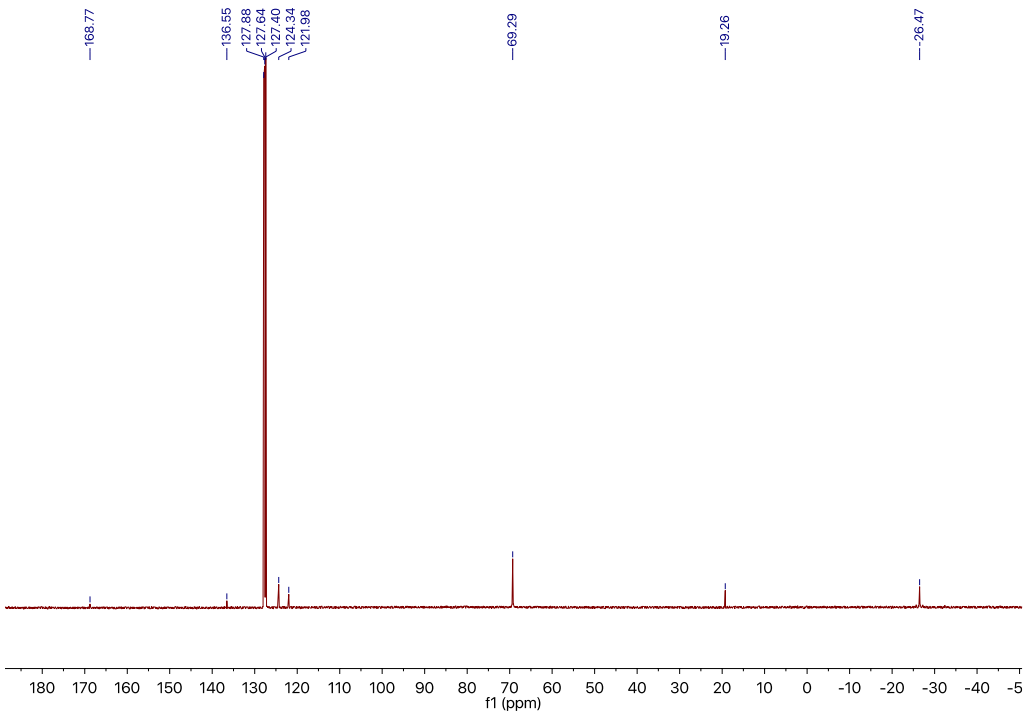

Figure A4.9. $^{13}C\{^{1}H\}$ NMR spectrum of [K(18-crown-6)][U(NTs)$(NR_2)_3$] (**4.2**) in C_6D_6.

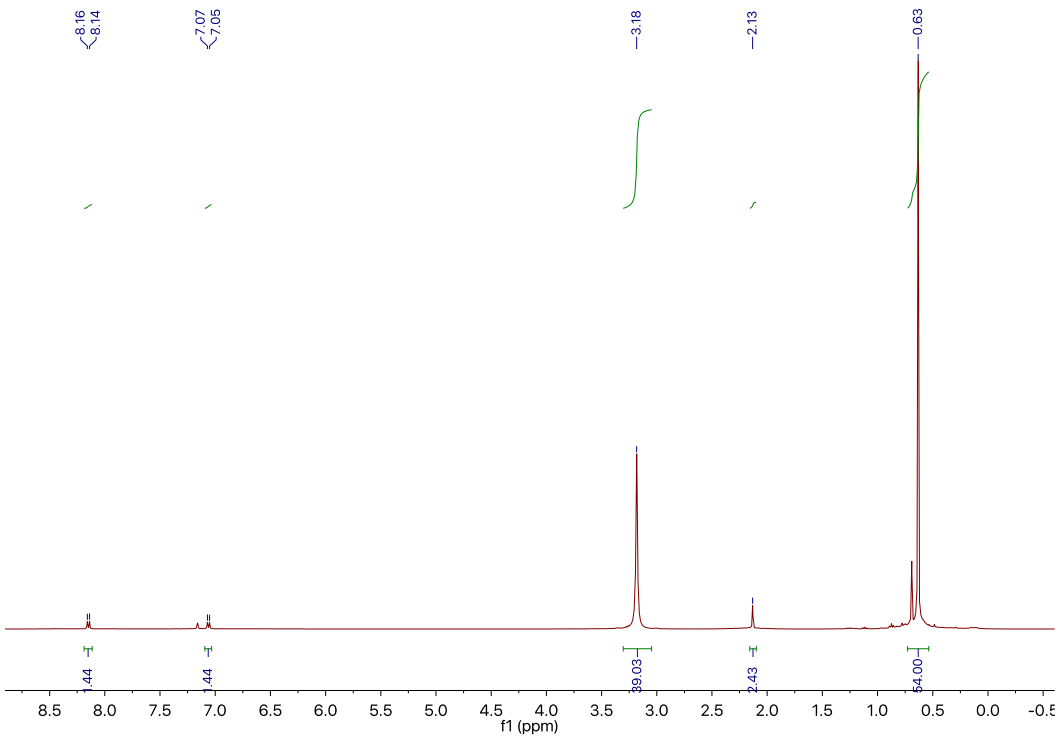

Figure A4.10. ^{1}H NMR spectrum of [K(18-crown-6)][Th(NTs)(NR$_2$)$_3$] (**4.3**) in C_6D_6.

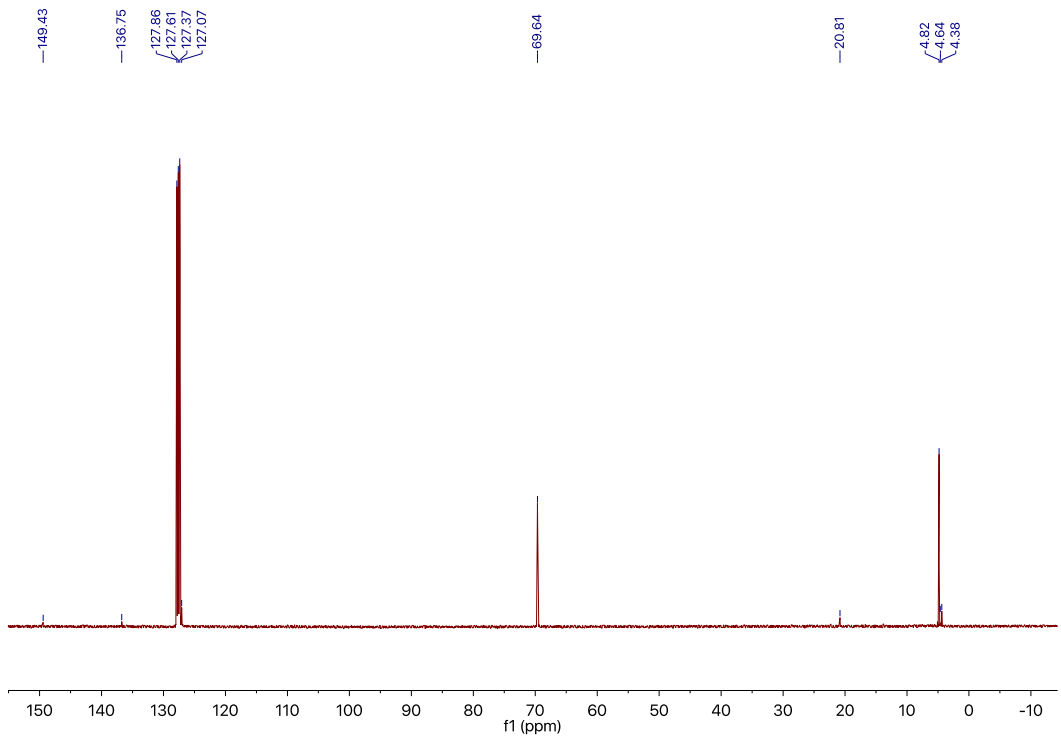

Figure A4.11. $^{13}C\{^{1}H\}$ NMR spectrum of [K(18-crown-6)][Th(NTs)$(NR_2)_3$] (**4.3**) in C_6D_6.

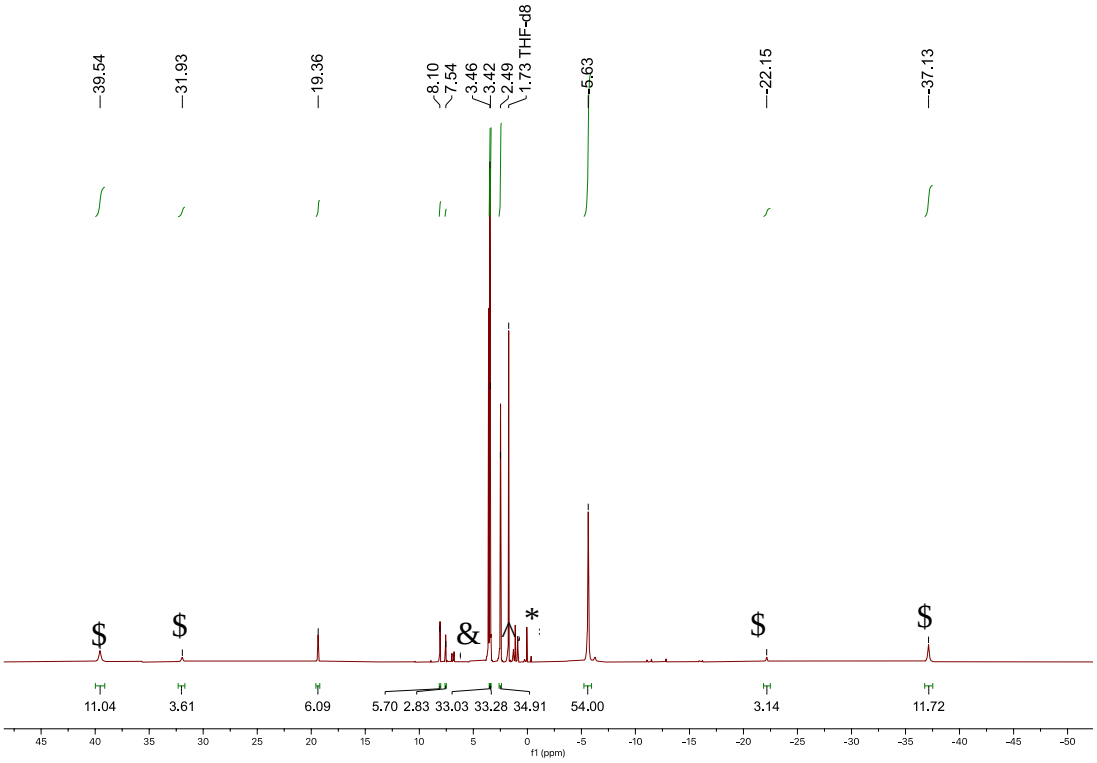

Figure A4.12. ^{1}H NMR spectrum of [Na(2,2,2-cryptand)][U(NR$_2$)$_3$NHBPh$_3$] (**4.4**) in THF-d_8. (*) indicates HN(SiMe$_3$)$_2$, (&) indicates the presence of an unidentified product, (^) indicates pentane and ($) indicates [Na(DME)$_3$][U{*N*(R)(SiMe$_2$*C*H$_2$)}$_2$(NR$_2$)][49].

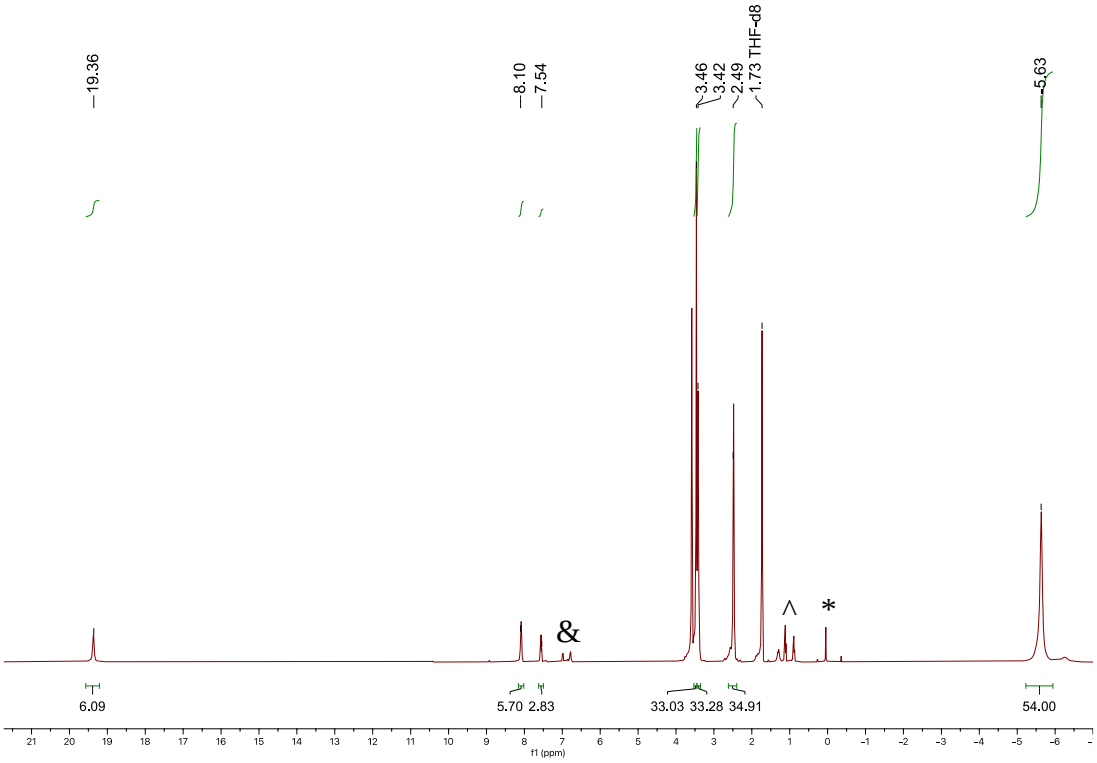

Figure A4.13. Partial ^{1}H NMR spectrum of [Na(2,2,2-cryptand)][U(NR$_2$)$_3$NHBPh$_3$] (**4.4**) in THF-d_8. (*) indicates HN(SiMe$_3$)$_2$, (&) indicates the presence of an unidentified product, and (^) indicates pentane.

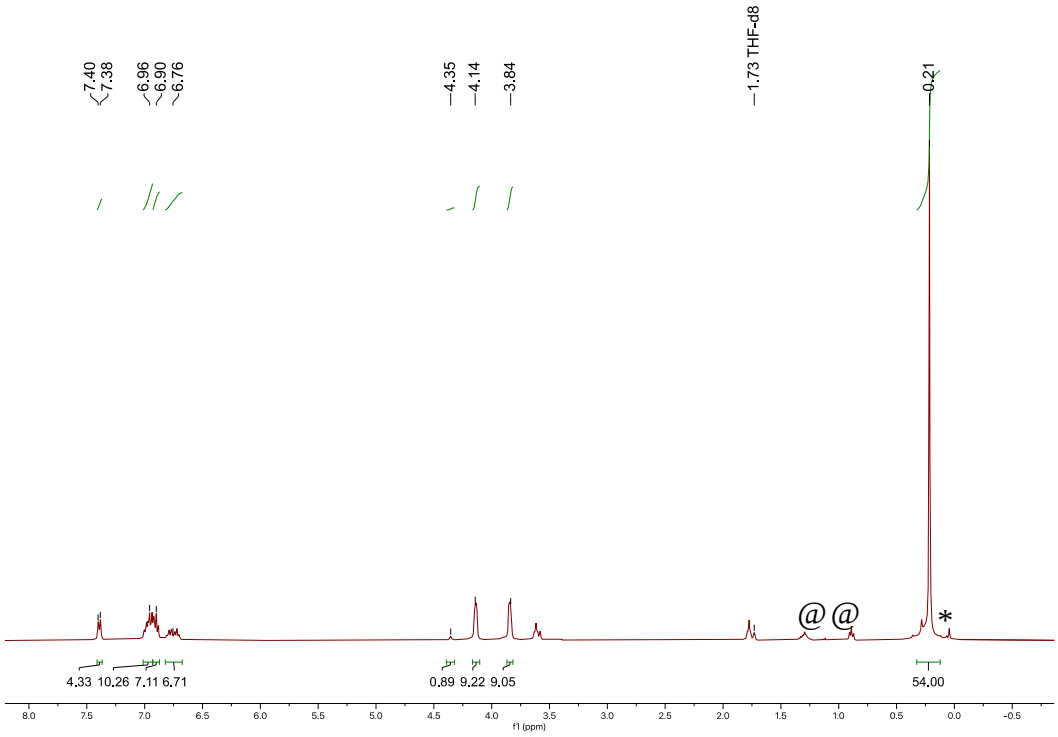

Figure A4.14. ^{1}H NMR spectrum of [K(DB-18-C-6)][Th(NR$_2$)$_3$NHBPh$_3$] (**4.5**) in THF-d_8. (*) indicates the presence of HN(SiMe$_3$)$_2$ and (@) indicates the presence of pentane.

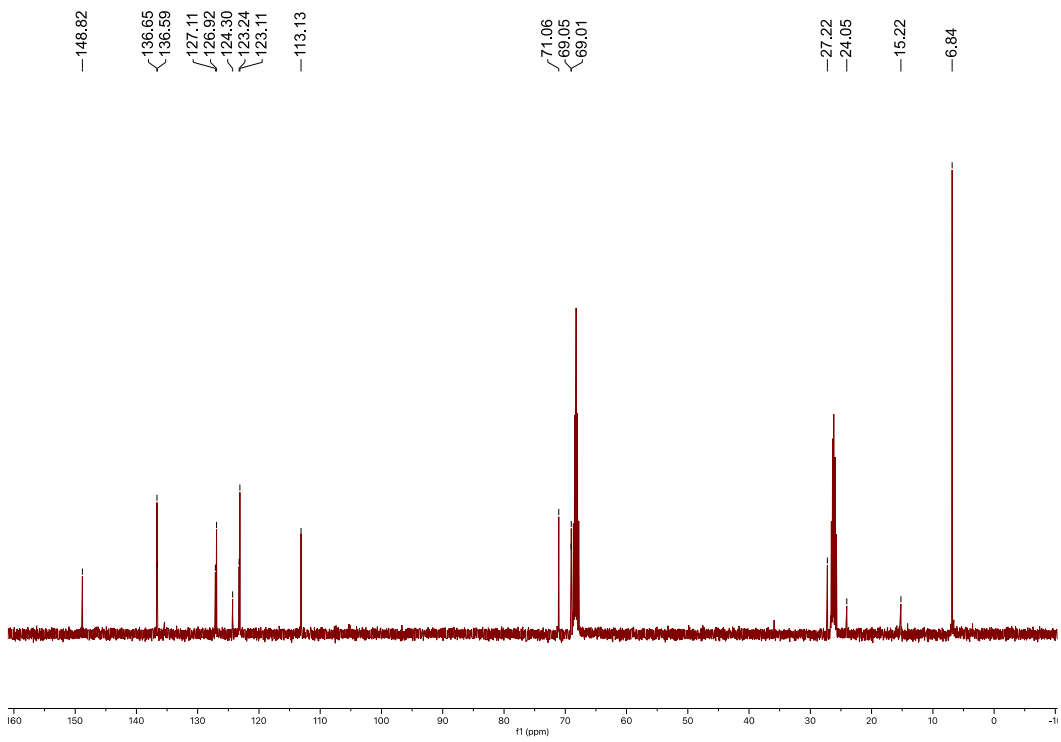

Figure A4.15. $^{13}C\{^{1}H\}$ NMR spectrum of [K(DB-18-C-6)][Th$(NR_2)_3$NHBPh_3] (**4.5**) in THF-d_8.

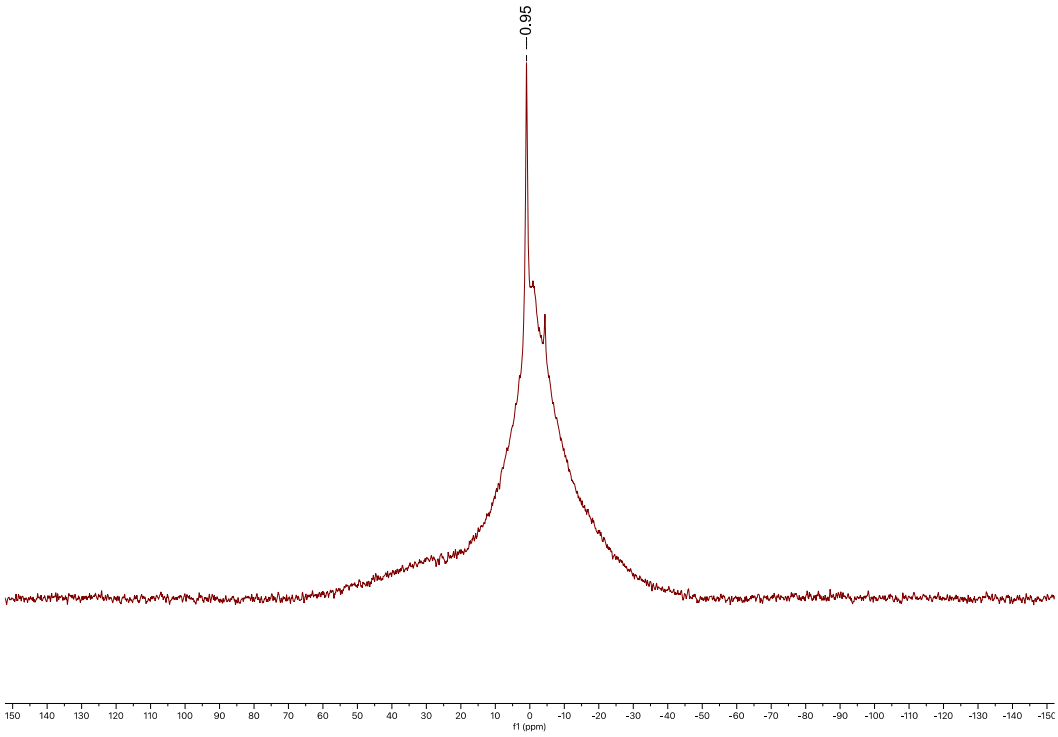

Figure A4.16. ^{11}B NMR spectrum of [K(DB-18-C-6)][Th(NR$_2$)$_3$NHBPh$_3$] (**4.5**) in THF-d_8.

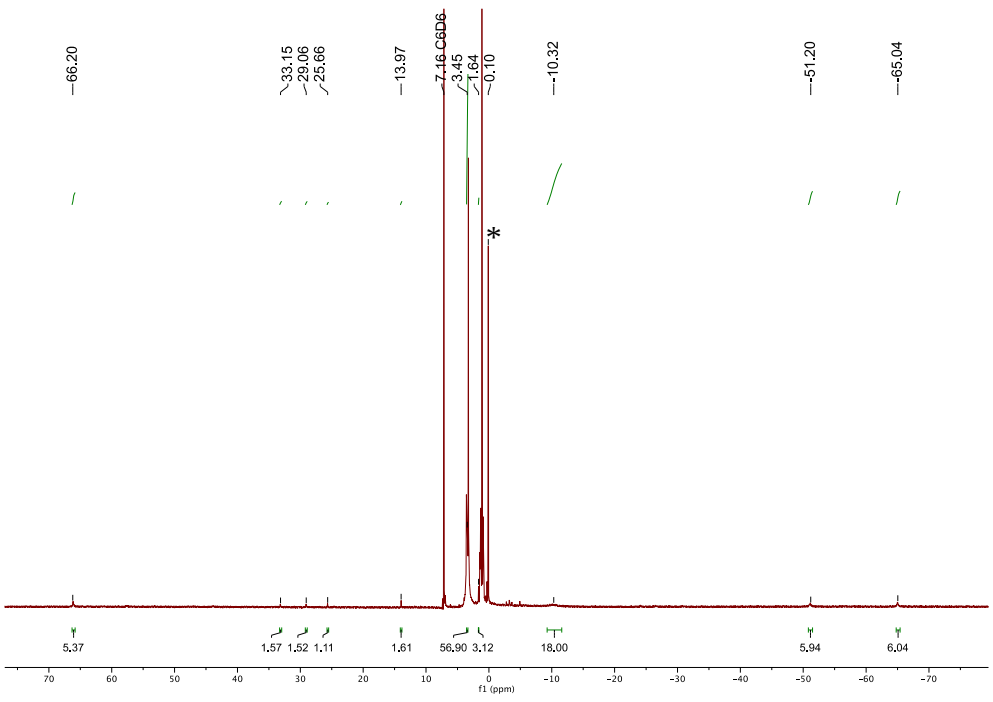

Figure A4.17. ^{1}H NMR spectrum of **4.8** in C_6D_6. (*) indicates the presence of $HN(SiMe_3)_2$.

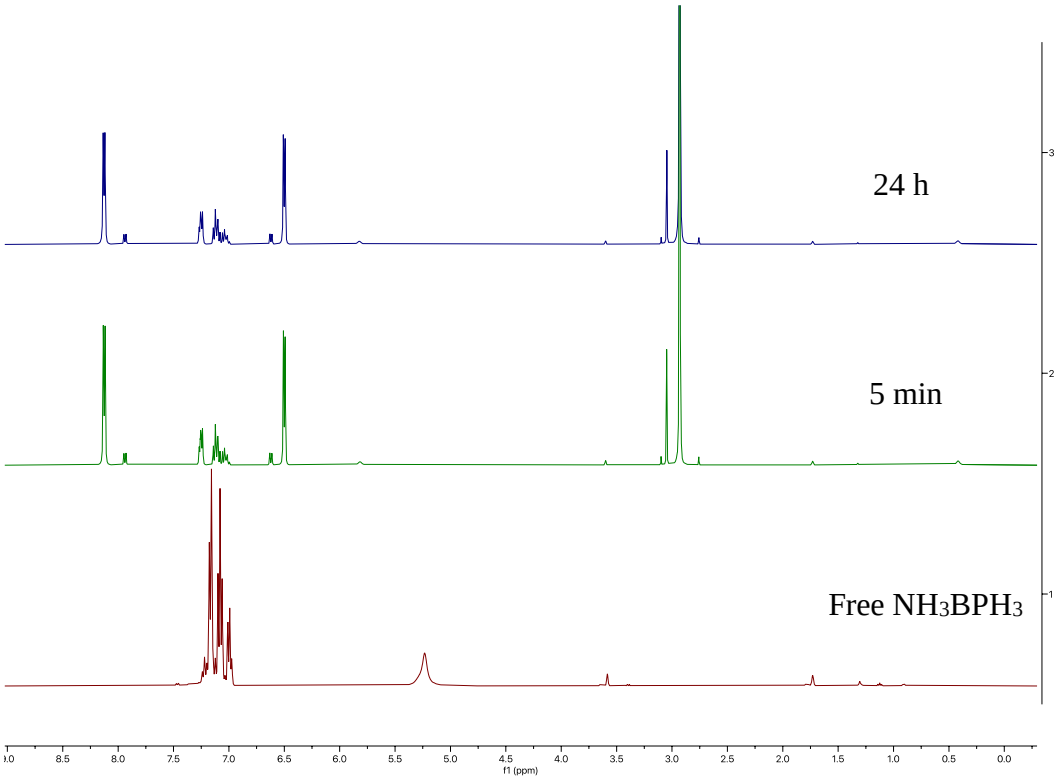

Figure A4.18. In-situ ^{1}H NMR spectrum of NH_3BPh_3 with 10 equiv DMAP in THF-d_8.

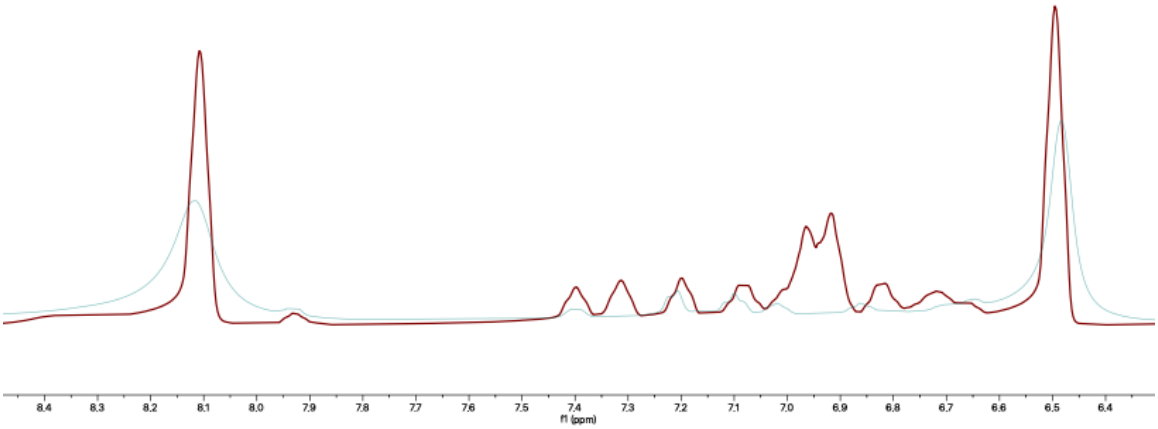

Figure A4.19. In-situ ^{1}H NMR spectrum of **4.4** (green) and **4.5** (red) with 10 equiv DMAP in THF-d_8 at 28 h and 22 h, respectively.

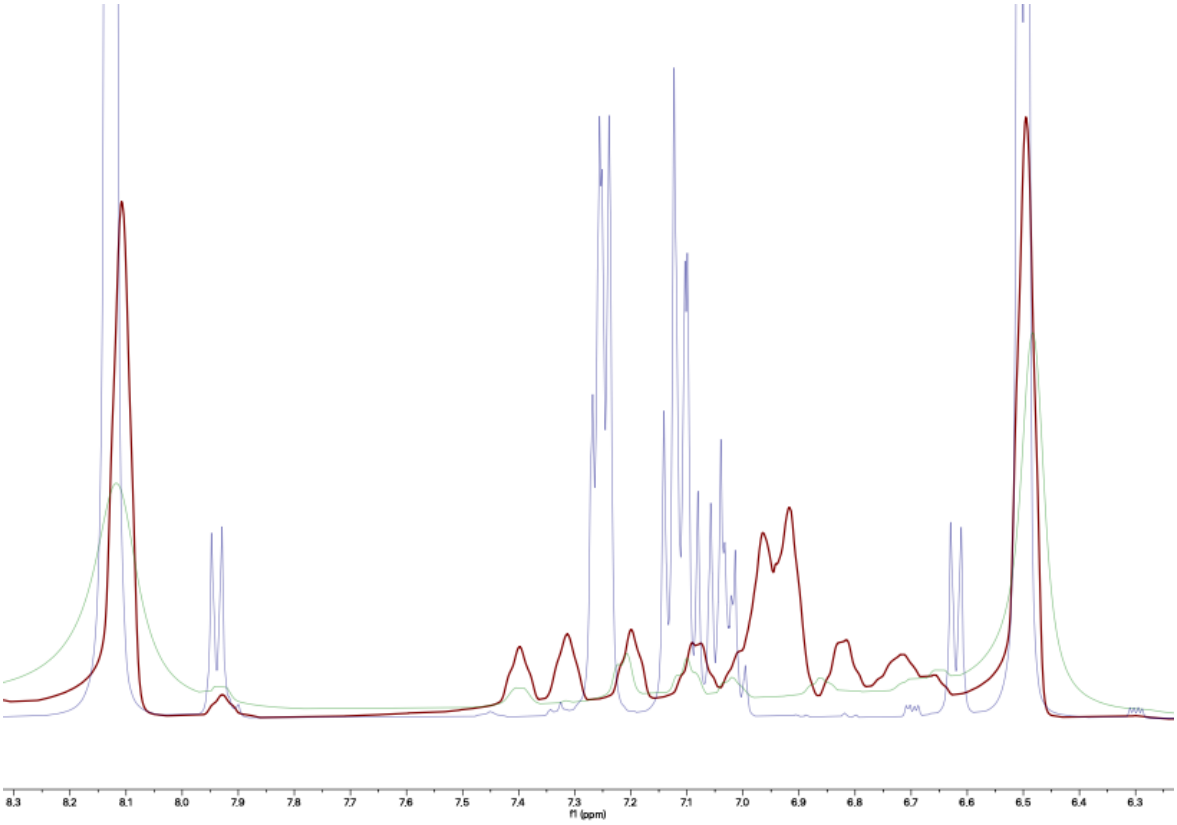

Figure A4.20. In-situ ^{1}H NMR spectrum of **4.4** (green), **4.5** (red), and NH_3BPH_3 (purple) with 10 equiv DMAP in THF-d_8 at 28 h, 22 h, and 48 h respectively.

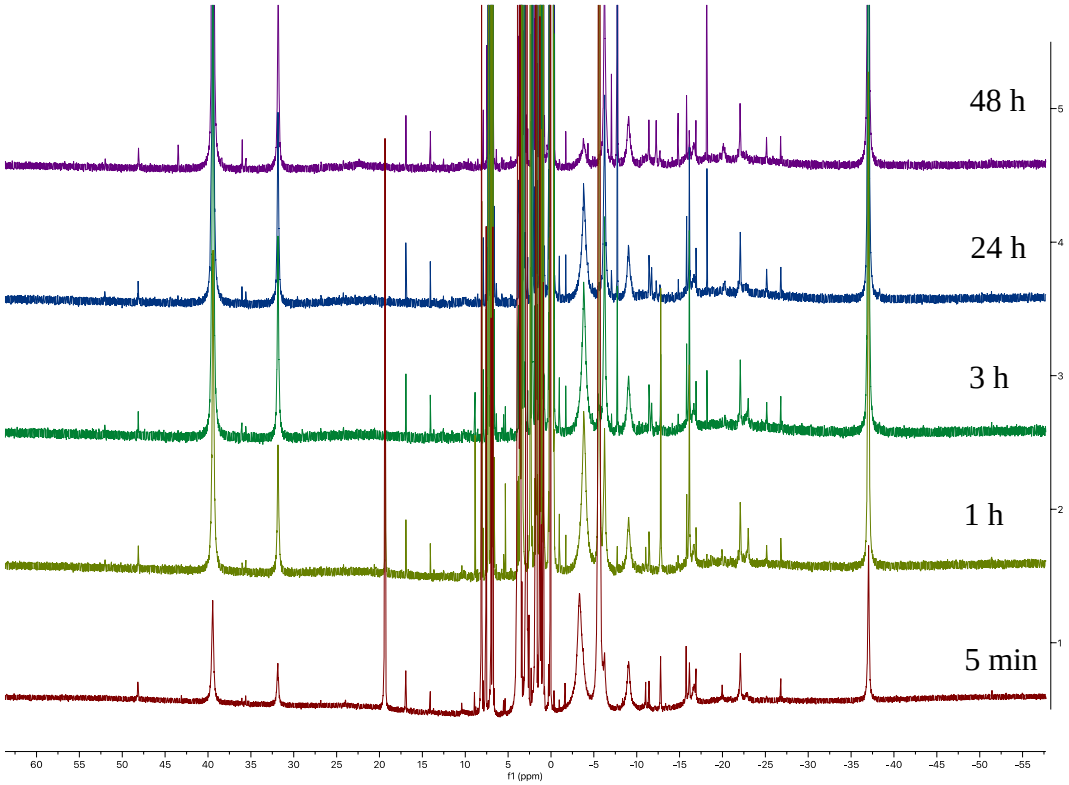

Figure A4.21. In-situ ^{1}H NMR spectrum of **4.4** with 1 equiv $K(NSiMe_3)_2$ in THF-d_8 over 48 h.

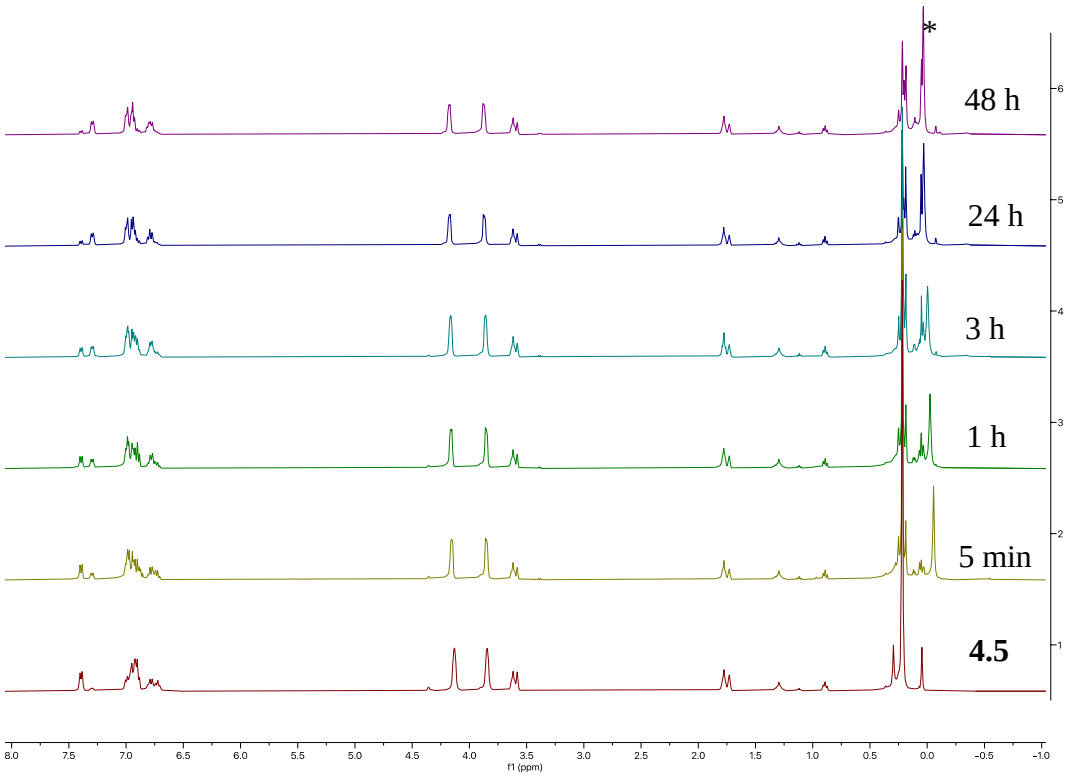

Figure A4.22. In-situ ^{1}H NMR spectrum of **4.5** with 1 equiv K(NSiMe$_3$)$_2$ in THF-d_8 over 48 h. (*) indicates the presence of [Th{*N*(R)(SiMe$_2$*C*H$_2$)}$_2$(NR$_2$)]$^-$.

4.6.5 IR Spectra

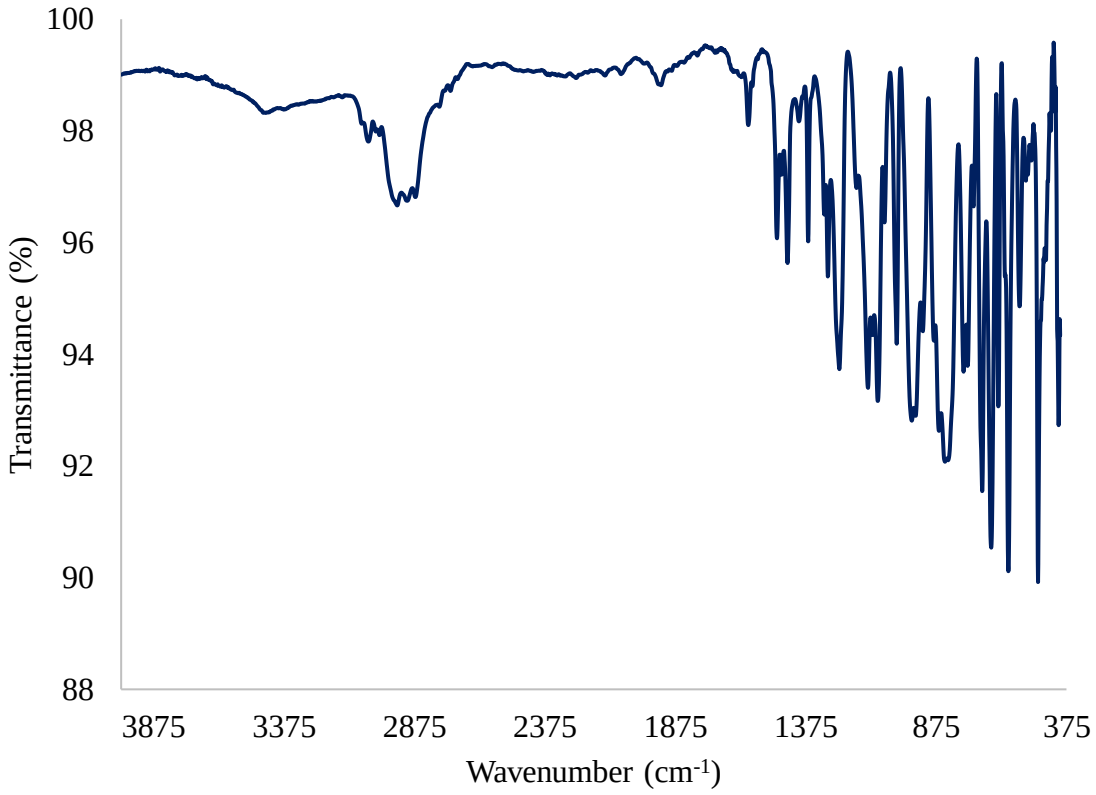

Figure A4.23. IR spectrum of $[Li(12\text{-crown-4})_2][Th(NCPh_3)(NR_2)_3]$ (**4.1**) (KBr pellet).

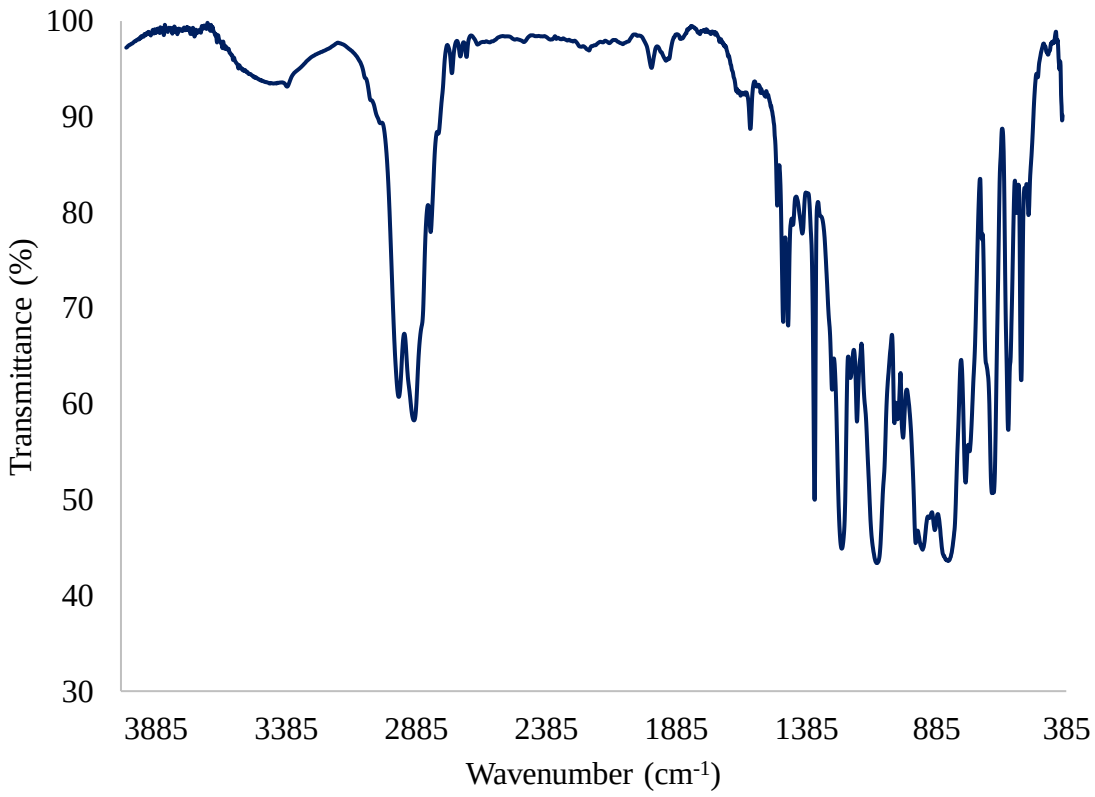

Figure A4.24. IR spectrum of [K(18-crown-6)][U(NTs)(NR$_2$)$_3$] (**4.2**) (KBr pellet).

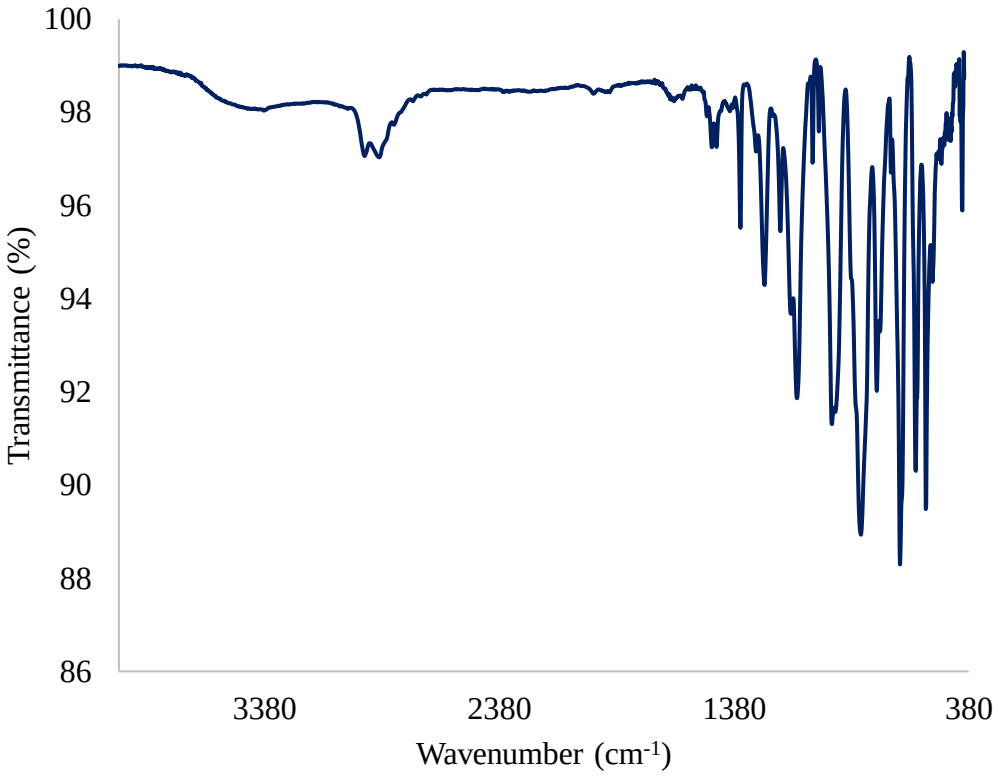

Figure A4.25. IR spectrum of [K(18-crown-6)][Th(NTs)(NR_2)$_3$] (**4.3**) (KBr pellet).

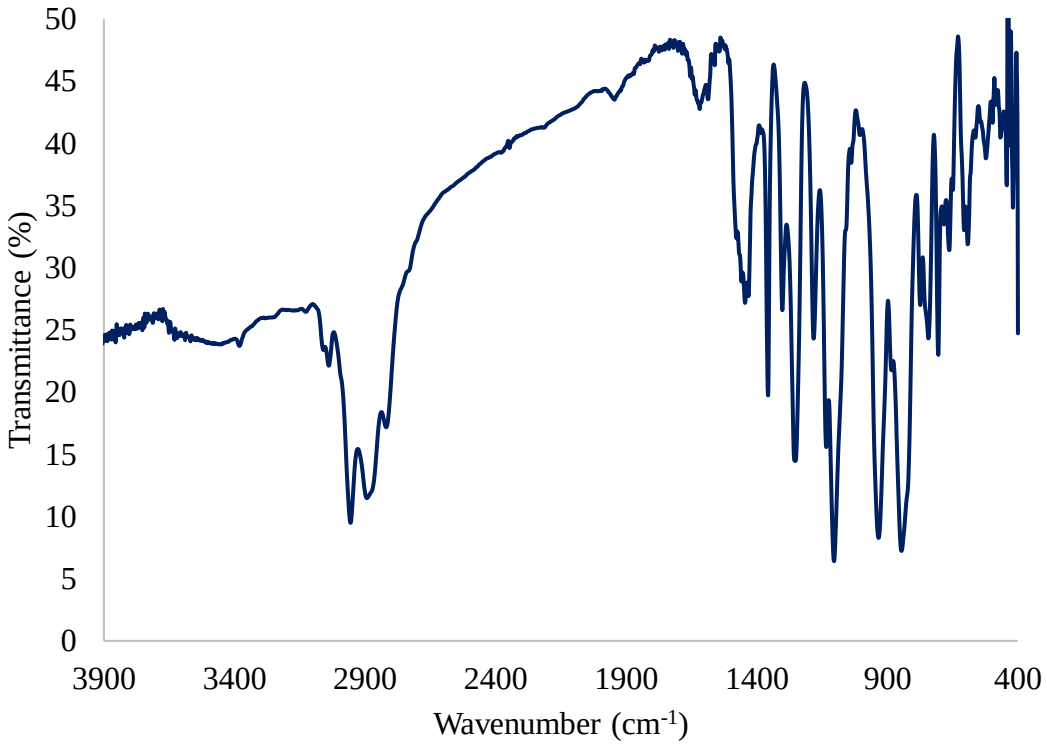

Figure A4.26. IR spectrum of [Na(2,2,2-cryptand)][U(NR$_2$)$_3$NHBPh$_3$] (**4.4**) (KBr pellet).

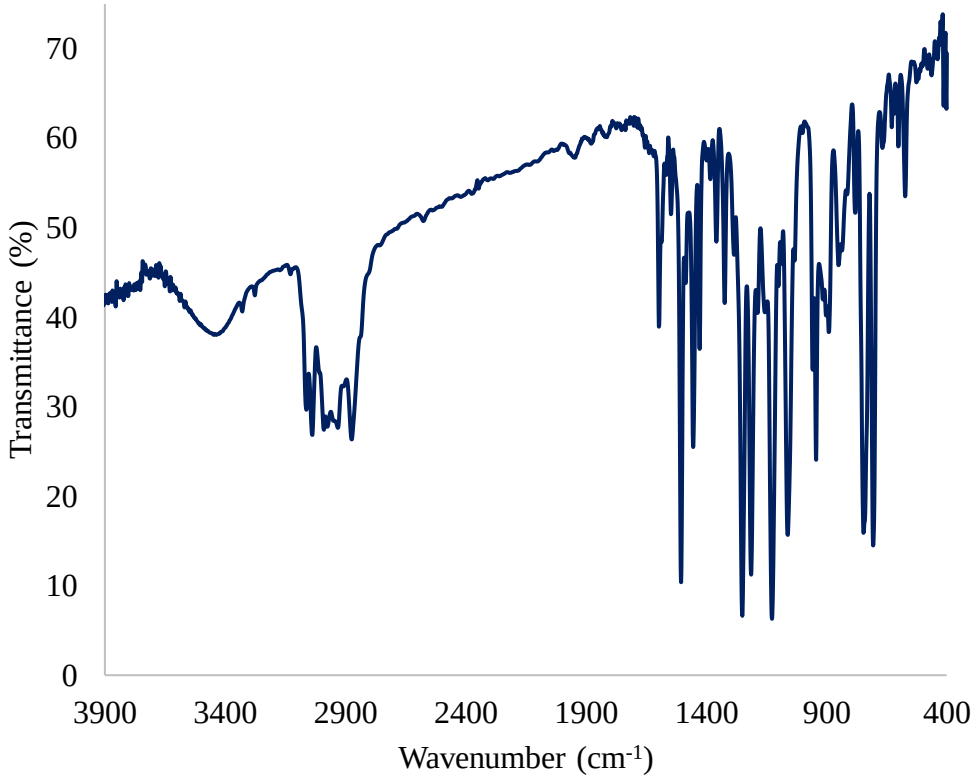

Figure A4.27. IR spectrum of [K(DB-18-C-6)][Th(NR_2)$_3$NHBPh_3] (**4.5**) (KBr pellet).

4.7 References

1. Hayton, T. W., Metal–ligand multiple bonding in uranium: structure and reactivity. *Dalton Trans.* **2010,** *39* (5), 1145-1158.
2. Hayton, T. W., Recent developments in actinide–ligand multiple bonding. *Chem. Commun.* **2013,** *49* (29), 2956-2973.
3. Ingram, K. I.; Tassell, M. J.; Gaunt, A. J.; Kaltsoyannis, N., Covalency in the f Element− Chalcogen Bond. Computational Studies of $M[N(EPR_2)_2]_3$ (M= La, Ce, Pr, Pm, Eu, U, Np, Pu, Am, Cm; E = O, S, Se, Te; R = H, ^{i}Pr, Ph). *Inorg. Chem.* **2008,** *47* (17), 7824-7833.
4. Jensen, M. P.; Bond, A. H., Comparison of covalency in the complexes of trivalent actinide and lanthanide cations. *J. Am. Chem. Soc.* **2002,** *124* (33), 9870-9877.
5. Kaltsoyannis, N., Does covalency increase or decrease across the actinide series? Implications for minor actinide partitioning. *Inorg. Chem.* **2013,** *52* (7), 3407-3413.
6. Kirker, I.; Kaltsoyannis, N., Does covalency *really* increase across the 5f series? A comparison of molecular orbital, natural population, spin and electron density analyses of $AnCp_3$ (An = Th–Cm; Cp = η^5-C_5H_5). *Dalton Trans.* **2011,** *40* (1), 124-131.
7. Minasian, S. G.; Krinsky, J. L.; Arnold, J., Evaluating f-Element Bonding from Structure and Thermodynamics. *Chem. Euro. J.* **2011,** *17* (44), 12234-12245.
8. Neidig, M. l. L.; Clark, D. L.; Martin, R. L., Covalency in f-element complexes. *Coord. Chem. Rev.* **2013,** *257* (2), 394-406.
9. Bart, S. C.; Anthon, C.; Heinemann, F. W.; Bill, E.; Edelstein, N. M.; Meyer, K., Carbon dioxide activation with sterically pressured mid-and high-valent uranium complexes. *J. Am. Chem. Soc.* **2008,** *130* (37), 12536-12546.
10. Fortier, S.; Brown, J. L.; Kaltsoyannis, N.; Wu, G.; Hayton, T. W., Synthesis, Molecular and Electronic Structure of $U^{V}(O)[N(SiMe_3)_2]_3$. *Inorg. Chem.* **2012,** *51* (3), 1625-1633.
11. Fortier, S.; Kaltsoyannis, N.; Wu, G.; Hayton, T. W., Probing the reactivity and electronic structure of a uranium (V) terminal oxo complex. *J. Am. Chem. Soc.* **2011,** *133* (36), 14224-14227.
12. Zi, G.; Jia, L.; Werkema, E. L.; Walter, M. D.; Gottfriedsen, J. P.; Andersen, R. A., Preparation and Reactions of Base-Free Bis(1,2,4-tri-*tert*-butylcyclopentadienyl)uranium Oxide, Cp'_2UO. *Organometallics* **2005,** *24* (17), 4251-4264.
13. Anderson, N. H.; Odoh, S. O.; Yao, Y.; Williams, U. J.; Schaefer, B. A.; Kiernicki, J. J.; Lewis, A. J.; Goshert, M. D.; Fanwick, P. E.; Schelter, E. J., Harnessing redox activity for the formation of uranium tris (imido) compounds. *Nature* **2014,** *6* (10), 919-926.
14. Hayton, T. W.; Boncella, J. M.; Scott, B. L.; Palmer, P. D.; Batista, E. R.; Hay, P. J., Synthesis of imido analogs of the uranyl ion. *Science* **2005,** *310* (5756), 1941-1943.
15. King, D. M.; McMaster, J.; Tuna, F.; McInnes, E. J.; Lewis, W.; Blake, A. J.; Liddle, S. T., Synthesis and Characterization of an f-Block Terminal Parent Imido [U=NH] Complex: A Masked Uranium(IV) Nitride. *J. Am. Chem. Soc.* **2014,** *136* (15), 5619-5622.
16. Fortier, S.; Wu, G.; Hayton, T. W., Synthesis of a Nitrido-Substituted Analogue of the Uranyl Ion, $[N=U=O]^{+}$. *J. Am. Chem. Soc.* **2010,** *132* (20), 6888-9.
17. Fox, A. R.; Arnold, P. L.; Cummins, C. C., Uranium-Nitrogen Multiple Bonding: Isostructural Anionic, Neutral, and Cationic Uranium Nitride Complexes Featuring a Linear U=N=U Core. *J. Am. Chem. Soc.* **2010,** *132* (10), 3250-1.

18. King, D. M.; Tuna, F.; McInnes, E. J.; McMaster, J.; Lewis, W.; Blake, A. J.; Liddle, S. T., Synthesis and structure of a terminal uranium nitride complex. *Science* **2012,** *337* (6095), 717-720.
19. Staun, S. L.; Sergentu, D.-C.; Wu, G.; Autschbach, J.; Hayton, T. W., Use of ^{15}N NMR spectroscopy to probe covalency in a thorium nitride. *Chem. Sci.* **2019,** *10* (26), 6431-6436.
20. King, D. M.; Liddle, S. T., Progress in molecular uranium-nitride chemistry. *Coord. Chem. Rev.* **2014,** *266-267*, 2-15.
21. Zi, G., Organothorium complexes containing terminal metal-ligand multiple bonds. *Sci. China Chem.* **2014,** *57* (8), 1064-1072.
22. Haskel, A.; Straub, T.; Eisen, M. S., Organoactinide-Catalyzed Intermolecular Hydroamination of Terminal Alkynes. *Organometallics* **1996,** *15* (18), 3773-3775.
23. Ren, W.; Zi, G.; Walter, M. D., Synthesis, Structure, and Reactivity of a Thorium Metallocene Containing a 2,2′-Bipyridyl Ligand. *Organometallics* **2012,** *31* (2), 672-679.
24. Simpson, S. J.; Turner, H. W.; Andersen, R. A., Hydrogen-Deuterium Exchange: Perdeuteriohydridotris (hexamethyldisilylamido)- thorium(IV) and -uranium(IV). *J. Am. Chem. Soc.* **1979,** *101* (26), 7728-7729.
25. Bell, N. L.; Maron, L.; Arnold, P. L., Thorium Mono- and Bis(imido) Complexes Made by Reprotonation of *cyclo*-Metalated Amides. *J. Am. Chem. Soc.* **2015,** *137* (33), 10492-10495.
26. Cheisson, T.; Kersey, K. D.; Mahieu, N.; McSkimming, A.; Gau, M. R.; Carroll, P. J.; Schelter, E. J., Multiple Bonding in Lanthanides and Actinides: Direct Comparison of Covalency in Thorium(IV)- and Cerium(IV)-Imido Complexes. *J. Am. Chem. Soc.* **2019,** *141* (23), 9185-9190.
27. Smiles, D. E.; Wu, G.; Hrobárik, P.; Hayton, T. W., Use of ^{77}Se and ^{125}Te NMR Spectroscopy to Probe Covalency of the Actinide-Chalcogen Bonding in $[Th(E_n)\{N(SiMe_3)_2\}_3]^-$ (E = Se, Te; *n* = 1, 2) and Their Oxo-Uranium(VI) Congeners. *J. Am. Chem. Soc.* **2016,** *138* (3), 814-825.
28. Smiles, D. E.; Wu, G.; Kaltsoyannis, N.; Hayton, T. W., Thorium–ligand multiple bonds *via* reductive deprotection of a trityl group. *Chem. Sci.* **2015,** *6* (7), 3891-3899.
29. Ren, W.; Zi, G.; Fang, D.-C.; Walter, M. D., Thorium oxo and sulfido metallocenes: synthesis, structure, reactivity, and computational studies. *J. Am. Chem. Soc.* **2011,** *133* (33), 13183-13196.
30. Lu, E.; Lewis, W.; Blake, A. J.; Liddle, S. T., The Ketimide Ligand is Not Just an Inert Spectator: Heteroallene Insertion Reactivity of an Actinide–Ketimide Linkage in a Thorium Carbene Amide Ketimide Complex. *Angew. Chem. Int. Ed.* **2014,** *53* (35), 9356-9359.
31. Ma, G.; Ferguson, M. J.; McDonald, R.; Cavell, R. G., Actinide Metals with Multiple Bonds to Carbon: Synthesis, Characterization, and Reactivity of U(IV) and Th(IV) Bis(iminophosphorano)methandiide Pincer Carbene Complexes. *Inorg. Chem.* **2011,** *50* (14), 6500-6508.
32. Ren, W.; Deng, X.; Zi, G.; Fang, D.-C., The Th=C double bond: an experimental and computational study of thorium poly-carbene complexes. *Dalton Trans.* **2011,** *40* (38), 9662-9664.

33. Smiles, D. E.; Wu, G.; Hrobárik, P.; Hayton, T. W., Synthesis, Thermochemistry, Bonding, and ^{13}C NMR Chemical Shift Analysis of a Phosphorano-Stabilized Carbene of Thorium. *Organometallics* **2017,** *36* (23), 4519-4524.
34. Du, J.; King, D. M.; Chatelain, L.; Lu, E.; Tuna, F.; McInnes, E. J. L.; Wooles, A. J.; Maron, L.; Liddle, S. T., Thorium- and uranium-azide reductions: a transient dithorium-nitride *versus* isolable diuranium-nitrides. *Chem. Sci.* **2019,** *10*, 3738-3745.
35. Bursten, B. E.; Strittmatter, R. J., Cyclopentadienyl—Actinide Complexes: Bonding and Electronic Structure. *Angew. Chem. Int. Ed.* **1991,** *30* (9), 1069-1085.
36. Blake, P. C.; Edelstein, N. M.; Hitchcock, P. B.; Kot, W. K.; Lappert, M. F.; Shalimoff, G. V.; Tian, S., Synthesis, properties and structures of the tris(cyclopentadienyl)thorium(III) complexes [Th{η^5-$C_5H_3(SiMe_2R)_2$-1,3}$_3$] (R=Me or ^{t}Bu). *J. Organomet. Chem.* **2001,** *636* (1), 124-129.
37. Nugent, L.; Baybarz, R.; Burnett, J.; Ryan, J., Electron-transfer and f-d absorption bands of some lanthanide and actinide complexes and the standard (II-III) oxidation potential for each member of the lanthanide and actinide series. *J. Phys. Chem.* **1973,** *77* (12), 1528-1539.
38. Ortu, F.; Formanuik, A.; Innes, J. R.; Mills, D. P., New vistas in the molecular chemistry of thorium: low oxidation state complexes. *Dalton Trans.* **2016,** *45* (18), 7537-7549.
39. Arney, D. S.; Burns, C. J., Synthesis and structure of high-valent organouranium complexes containing terminal monooxo functional groups. *J. Am. Chem. Soc.* **1993,** *115* (21), 9840-9841.
40. Ren, W.; Song, H.; Zi, G.; Walter, M. D., A bipyridyl thorium metallocene: synthesis, structure and reactivity. *Dalton Trans.* **2012,** *41* (19), 5965-5973.
41. Cho, J.; Van Heuvelen, K. M.; Yap, G. P. A.; Brunold, T. C.; Riordan, C. G., New Synthetic Routes to a Disulfidodinickel(II) Complex: Characterization and Reactivity of a $Ni_2(\mu$-η^2:η^2-$S_2)$ Core. *Inorg. Chem.* **2008,** *47* (10), 3931-3933.
42. Fujisawa, K.; Moro-Oka, Y.; Kitajima, N., Formation of a μ-η^2:η^2-disulfide dinuclear copper(II) complex by thermal decomposition of a thiolate complex *via* C–S bond cleavage. *Chem. Commun.* **1994,** (5), 623-624.
43. Kawaguchi, H.; Tatsumi, K., Synthesis of (Pentamethylcyclopentadienyl)tantalum Sulfido Complexes via C−S Bond Cleavage of Triphenylmethanethiolate and Formation of a Novel Trithioborato Ligand. *Organometallics* **1997,** *16* (3), 307-309.
44. Smiles, D. E.; Wu, G.; Hayton, T. W., Synthesis of Uranium–Ligand Multiple Bonds by Cleavage of a Trityl Protecting Group. *J. Am. Chem. Soc.* **2014,** *136* (1), 96-99.
45. Mullane, K. C.; Lewis, A. J.; Yin, H.; Carroll, P. J.; Schelter, E. J., Anomalous One-Electron Processes in the Chemistry of Uranium Nitrogen Multiple Bonds. *Inorg. Chem.* **2014,** *53* (17), 9129-9139.
46. Luo, Y.-R., *Handbook of bond dissociation energies in organic compounds*. CRC press: 2002.
47. Shannon, R., Acta Crystallogr., Sect. A: Cryst. Phys., Diffr., Theor. Gen. Crystallogr. **1976,** (32), 751-767.
48. Breugst, M.; Tokuyasu, T.; Mayr, H., Nucleophilic reactivities of imide and amide anions. *J. Org. Chem.* **2010,** *75* (15), 5250-5258.
49. Staun, S. L.; Stevens, L. M.; Smiles, D. E.; Goodwin, C. A. P.; Billow, B. S.; Scott, B. L.; Wu, G.; Tondreau, A. M.; Gaunt, A. J.; Hayton, T. W., Expanding the

Nonaqueous Chemistry of Neptunium: Synthesis and Structural Characterization of [Np(NR_2)$_3$Cl], [Np(NR_2)$_3$Cl]$^-$, and [Np{*N*(R)(SiMe_2*C*H_2)$_2$(NR_2)]$^-$ (R = SiMe_3). *Inorg. Chem.* **2021,** *60* (4), 2740-2748.
50. Dąbrowski, M.; Durka, K.; Luliński, S.; Serwatowski, J.; Warkocka, J., Ammonia-triphenyl-borane. *Acta Cryst. E* **2011,** *67* (Pt 11), o3098-o3098.
51. Jacobs, E. A.; Fuller, A.-M.; Lancaster, S. J.; Wright, J. A., The hafnium-mediated NH activation of an amido-borane. *Chem. Comm.* **2011,** *47* (20), 5870-5872.
52. Evans, W. J.; Rego, D. B.; Ziller, J. W., Lanthanum and Alkali Metal Coordination Chemistry of the Bis(dimethylphenylsilyl)amide Ligand. *Inorg. Chem.* **2006,** *45* (8), 3437-3443.
53. Palumbo, C. T.; Barluzzi, L.; Scopelliti, R.; Zivkovic, I.; Fabrizio, A.; Corminboeuf, C.; Mazzanti, M., Tuning the structure, reactivity and magnetic communication of nitride-bridged uranium complexes with the ancillary ligands. *Chem. Sci.* **2019,** *10* (38), 8840-8849.
54. Cantat, T.; Scott, B. L.; Kiplinger, J. L., Convenient access to the anhydrous thorium tetrachloride complexes $ThCl_4(DME)_2$, $ThCl_4$(1,4-dioxane)$_2$ and $ThCl_4(THF)_{3.5}$ using commercially available and inexpensive starting materials. *Chem. Commun.* **2010,** *46* (6), 919-21.
55. Simpson, S. J.; Turner, H. W.; Andersen, R. A., Preparation and hydrogen-deuterium exchange of alkyl and hydride bis(trimethylsilyl)amido derivatives of the actinide elements. *Inorg. Chem.* **1981,** *20* (9), 2991-2995.
56. *SMART* Apex II, Version 5.632.; Bruker AXS, Inc.: Madison, WI, 2005.
57. *SAINT Software User's Guide*, Version 7.34a ed.; Bruker AXS Inc.: Madison, WI, 2005.
58. *SADABS*, Sheldrick, G.M.; University of Göttingen, Germany: 2005.
59. *SHELXTL PC*, Version 6.12 ed.; Bruker AXS Inc.:Madison, WI, 2005.
60. Olex2 1.2 (compiled 2014.06.27 svn.r2953 for OlexSys, GUI svn. r4855).
61. Dolomanov, O.; Bourhis, L.; Gildea, R.; Howard, J.; Puschmann, H., *J. Appl. Cryst* **2009,** *42*, 339-341.
62. Miao, F.-M.; Wang, J.-L.; Miao, X.-S., N-Hydroxyphthalimide. *Acta Cryst Section C* **1995,** *51* (4), 712-713.

Chapter 5. Use of ^{15}N NMR Spectroscopy to Probe Covalency in a Thorium Nitride and Amide

Portions of this work were published in:

Selena L. Staun, Dumitru-Claudiu Sergentu, Guang Wu, Jochen Autschbach, and Trevor W. Hayton

Chem. Sci., **2019**, *10*, 6431-6436

5.1 Introduction

The past decade has seen a remarkable expansion of the chemistry of actinide-ligand multiple bonds.[1-6] This is exemplified especially well by the chemistry of molecular uranium nitrides.[6] Since the synthesis of the first molecular uranium nitride in 2002,[7] many bridging and terminal uranium nitride complexes have been reported.[2, 8-21] The study of these complexes has allowed actinide chemists to reveal fundamentally important insights into 5f covalency, as well as uncover novel modes of reactivity.[12, 15-18, 22-24]

In contrast, no isolable molecular thorium nitride complexes are known.[25] A handful of thorium nitrides have been identified in matrix isolation studies, such as ThN, NThN, and NThO, but these are only stable at cryogenic temperatures.[26-28] Recently, Liddle and co-workers reported the isolation of the bridged Th(IV) parent imido complex, $[\{Th(Tren^{DMBS})\}_2(\mu\text{-}NH)]$ ($Tren^{DMBS}$ = $\{N(CH_2CH_2NSiMe_2{}^tBu)_3\}^{3-}$), which was thought to form *via* an unobserved Th nitride intermediate, $[\{Th(Tren^{DMBS})\}_2(\mu\text{-}N)]^-$.[25] It was postulated that the nitride ligand in this intermediate was exceptionally basic on account of its highly polarized Th-$N_{nitride}$ bonds. As a result, it spontaneously deprotonated the solvent, forming the bridged parent imido. These results prompted the authors to suggest that the Th=N=Th unit may be intrinsically more reactive than the more covalent U=N=U unit. Significantly, further work in this area would allow us to evaluate this hypothesis in more detail, as well as permit a better evaluation of the bonding within this functional group.

Herein, I report the synthesis of the first isolable molecular thorium nitride complex, $[Na(18\text{-crown-}6)(Et_2O)][(R_2N)_3Th(\mu\text{-}N)(Th(NR_2)_3]$ (R = $SiMe_3$). In addition, I report its characterization by ^{15}N NMR spectroscopy and DFT calculations, which has allowed me to evaluate the degree of 5f covalency within the Th=N=Th unit. To provide context, I have also

synthesized the parent amide complex, [Th(NR_2)$_3$(NH_2)]. This material was also characterized by ^{15}N NMR spectroscopy and DFT calculations.

5.2 Results and Discussion

5.2.1 Synthesis and Characterization of [Na(18-crown-6)(Et_2O)][(R_2N)$_3$Th(μ-N)(Th(NR_2)$_3$] (R = $SiMe_3$) ([Na][5.1]).

Addition of 1 equiv of $NaNH_2$ to a cold (-25 °C) solution of the thorium metallacycle,[29] [Th{*N*(R)($SiMe_2$)*C*H_2}(NR_2)$_2$] (R = $SiMe_3$), in tetrahydrofuran (THF), followed by addition of 1 equiv of 18-crown-6, afforded the bridged nitride complex, [Na(18-crown-6)(Et_2O)][(R_2N)$_3$Th(μ-N)(Th(NR_2)$_3$] (**[Na][5.1]**), after stirring for 24 h. This material could be isolated as colorless plates in 66% yield after work-up (eqn (5.1)). The reaction of [Th{*N*(R)($SiMe_2$)*C*H_2}(NR_2)$_2$] with 0.5 equiv of both $NaNH_2$ and 18-crown-6 also generates **[Na][5.1]**, but with reduced yields (30%). The isolation of **[Na][5.1]** contrasts with the recent results of Liddle and co-workers, who attempted to isolate a bridged thorium nitride complex by reduction of a Th azide precursor, but isolated the bridged parent imido complex, [{Th(Tren^{DMBS})}$_2$(μ-NH)], instead.[25]

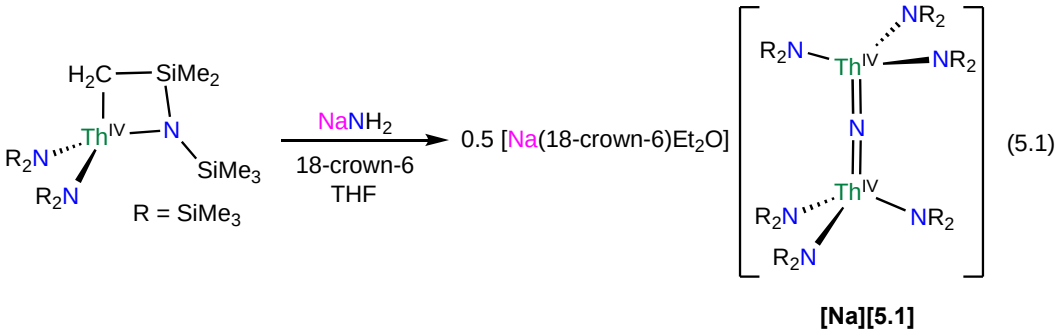

The connectivity of complex **[Na][5.1]** was verified by X-ray crystallography (Figure 5.1). Complex **[Na][5.1]** crystallizes in the monoclinic space group $P2_1/c$. In the solid-state, each Th center features a pseudo-tetrahedral coordination geometry. In addition, the Th-N-Th

linkage is linear (179(1)°), while its Th-$N_{nitride}$ bond lengths (Th1-N1 = 2.14(2), Th2-N1 = 2.11(2) Å) are much shorter than its Th-$N_{silylamido}$ bond lengths (av. 2.41 Å), suggesting multiple bond character in the former. A $[Na(18\text{-crown-}6)(Et_2O)]^+$ counterion is also present in the unit cell. The potassium analog, $[K(18\text{-crown-}6)(THF)_2][(R_2N)_3Th(\mu\text{-}N)(Th(NR_2)_3]$ (**[K][5.1]**), has also been structurally characterized. It features nearly identical metrical parameters to those of **[Na][5.1]** (Figure 5.4 for full details).

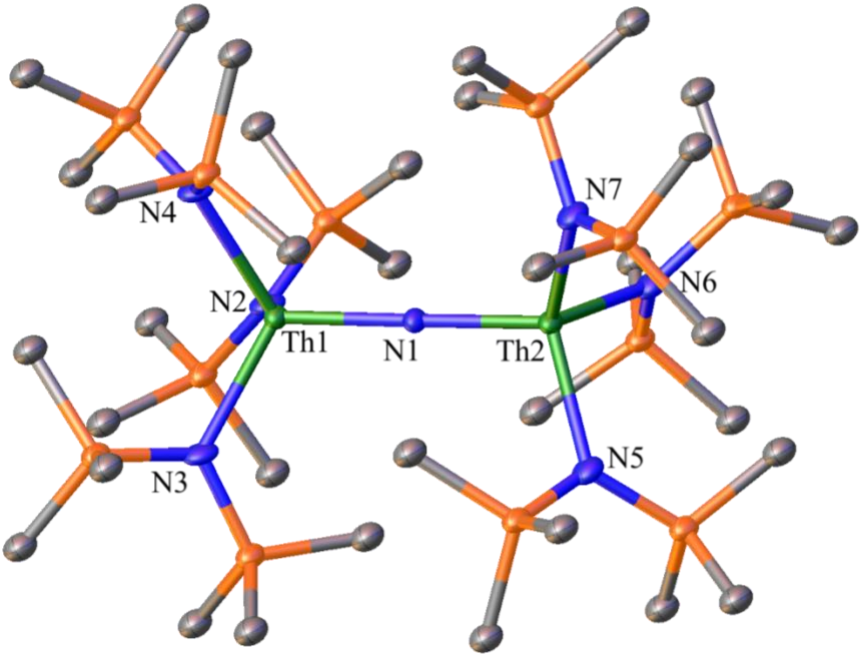

Figure 5.1. Solid-state molecular structure of **[Na][5.1]**, shown with 50% probability ellipsoids. Hydrogen atoms and $[Na(18\text{-crown-}6)(Et_2O)]^+$ counterion removed for clarity. Selected bond lengths (Å) and angles (°): Th1-N1 = 2.14(2), Th2-N1 = 2.11(2), Th1-N1-Th2 = 179(1), av. Th1-N_{amido} = 2.41, av. Th2-N_{amido} = 2.41, av. N_{amido}-Th1-N_{amido} = 108.3, av. N_{amido}-Th2-N_{amido} = 108.7.

Complex **[Na][5.1]** is the first nitrido complex reported for thorium. However, several thorium imido complexes have been structurally characterized.[30-36] Generally, these complexes feature shorter Th-N bonds than those of **[Na][5.1]**. For example, $[Cp^*_2Th(N\text{-}2,6\text{-}$

$Me_2C_6H_3$)(THF)] features a Th-N distance of 2.045(8) Å,[32] while [K(18-crown-6)][Th(=NDipp)$(NR_2)_3$] (Dipp = 2,6-^{i}Pr$_2$C$_6$H$_3$) features a Th-N distance of 2.072(3) Å.[30] For further comparison, the bridged U(IV) nitride, [Na][(μ-N)(U[*t*-Bu]Ar)$_3$)$_2$] (Ar = 3,5-$Me_2C_6H_3$), also features a linear U=N=U linkage (175.1(2)°), but shorter An-N bond distances (2.080(4) Å and 2.077(4) Å),[9] consistent with the smaller ionic radius of uranium. Similar metric parameters are observed in [Cs][{U(OSi(O^{t}Bu)$_3$)$_3$}$_2$(μ-N)] (U-N-U = 170.2(3)°; U1-N1 = 2.058(5) Å; U2-N1 = 2.079(5) Å).[12]

The ^{1}H NMR spectrum of **[Na][5.1]** in THF-d_8 features a sharp singlet at 0.36 ppm, assignable to the $SiMe_3$ groups, along with a broad resonance at 3.62 ppm, assignable to the 18-crown-6 moiety (Figure A5.1). Complex **[Na][5.1]** is insoluble in pentane and benzene, but is quite soluble in Et_2O and THF. It is stable as a THF-d_8 solution at room temperature for at least 24 h, showing minimal signs of decomposition over this time. Finally, the IR spectrum of **[Na][5.1]** features a mode at 742 cm^{-1}, which corresponds to the principal Th-N-Th asymmetric stretch (Figure A5.14). For comparison, this mode was calculated to occur at 758 cm^{-1} (Figure A5.29, see **5.6.3** for calculation details).

5.2.2 NMR scale reaction of [Th{*N*(R)(SiMe$_2$)*C*H$_2$}(NR$_2$)$_2$] with NaNH$_2$.

To better understand the mechanism of formation of **[Na][5.1]** I monitored the reaction of [Th{*N*(R)(SiMe$_2$)*C*H$_2$}(NR$_2$)$_2$] with $NaNH_2$ and 18-crown-6, in THF-d_8, by ^{1}H NMR spectroscopy (Figure A5.12). A ^{1}H NMR spectrum of this mixture after 7 h revealed an intense new resonance at 0.36 ppm, which is assignable to **[Na][5.1]**. Interestingly, this spectrum also features minor resonances at 0.30 and 0.18 ppm, which are assignable to the terminal parent amide complex, [Th$(NR_2)_3(NH_2)$] (**5.2**), and the bis(metallacycle) complex, [Na(THF)$_x$][Th{*N*(R)(SiMe$_2$*C*H$_2$)}$_2$(NR$_2$)],[30] respectively. The assignment for the latter

species was made by comparison with the ^{1}H NMR spectrum of the known bis(metallacycle) complex, [K(DME)][Th{*N*(R)(SiMe$_2$*C*H$_2$)}$_2$(NR$_2$)].[30] After 32 h, the resonance assignable to **[Na][5.1]** has grown in intensity, while the resonances assignable to [Th{*N*(R)(SiMe$_2$)*C*H$_2$}(NR$_2$)$_2$] and **5.2** have completely disappeared, and only trace amounts of [Na(THF)$_x$][Th{*N*(R)(SiMe$_2$*C*H$_2$)}$_2$(NR$_2$)] are still present in solution. To explain these observations, I suggest that the first step of the reaction is deprotonation of [Th{*N*(R)(SiMe$_2$)*C*H$_2$}(NR$_2$)$_2$] by NaNH$_2$, forming [Na(THF)$_x$][Th{*N*(R)(SiMe$_2$*C*H$_2$)}$_2$(NR$_2$)] and NH$_3$ (Scheme 5.1). NH$_3$ then reacts with unreacted [Th{*N*(R)(SiMe$_2$)*C*H$_2$}(NR$_2$)$_2$], forming **5.2**, which then protonates [Na(THF)$_x$][Th{*N*(R)(SiMe$_2$*C*H$_2$)}$_2$(NR$_2$)] to give **[Na][5.1]**.

Scheme 5.1. Proposed mechanism of formation of **[Na][5.1]**.

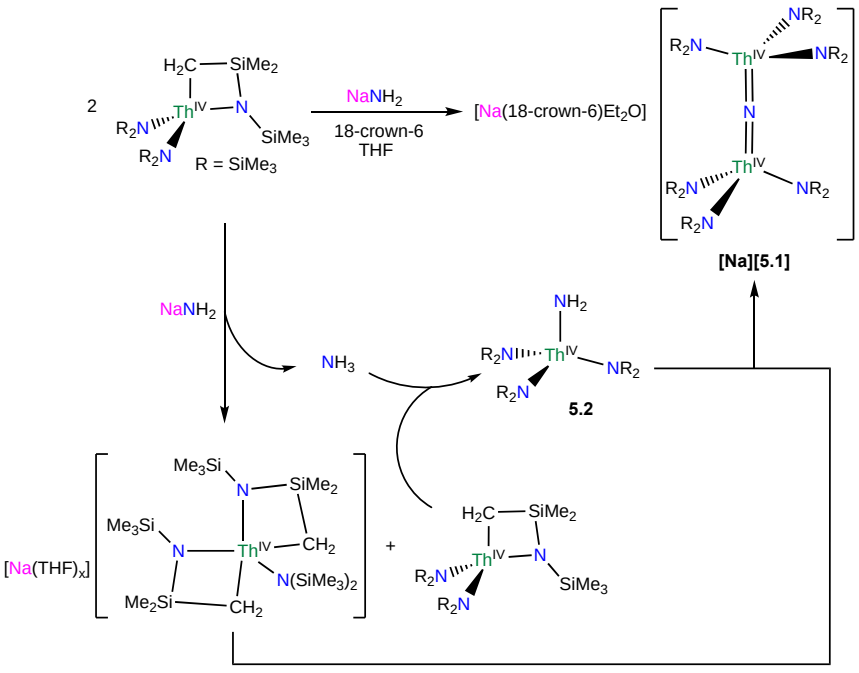

5.2.3 Synthesis and Characterization of [Th(NR$_2$)$_3$(NH$_2$)] (R = SiMe$_3$) (5.2)

To test this hypothesis I explored the reaction of [Th{*N*(R)(SiMe$_2$)*C*H$_2$}(NR$_2$)$_2$] with NH$_3$. Thus, addition of 3 equiv of NH$_3$, as a 0.4 M solution in THF, to a THF solution of [Th{*N*(R)(SiMe$_2$)*C*H$_2$}(NR$_2$)$_2$] results in rapid formation of **5.2**, which can be isolated in 51% yield after work-up (eqn (5.2)).

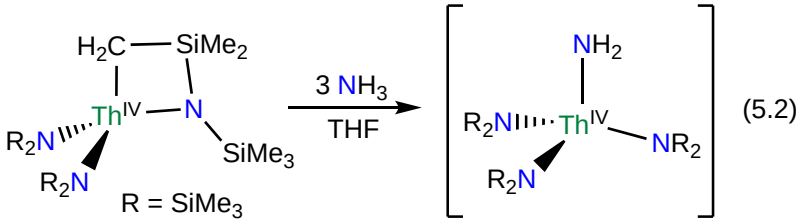

(5.2)

5.2

The ^{1}H NMR spectrum of **5.2** in C$_6$D$_6$ features a sharp resonance at 0.37 ppm (54H), assignable to the SiMe$_3$ groups. In addition, a 1:1:1 triplet (2H, J_{NH} = 45.8 Hz) at 3.67 ppm is assignable to the -NH$_2$ resonance (Figure A5.3). For comparison, the J_{NH} values for the isostructural group(IV) complexes, [M(NR$_2$)$_3$(NH$_2$)] (M = Zr, Hf), were found to be 45.6 Hz (Zr) and 46.0 Hz (Hf).[37] Interestingly, the only other known thorium NH$_2$ complex, [K(DME)$_4$][(DME)Th(NH$_2$)(diphenolate)$_2$]; featured a broad singlet at 2.0 ppm in its ^{1}H NMR spectrum, which was assignable to the -NH$_2$ group.[38]

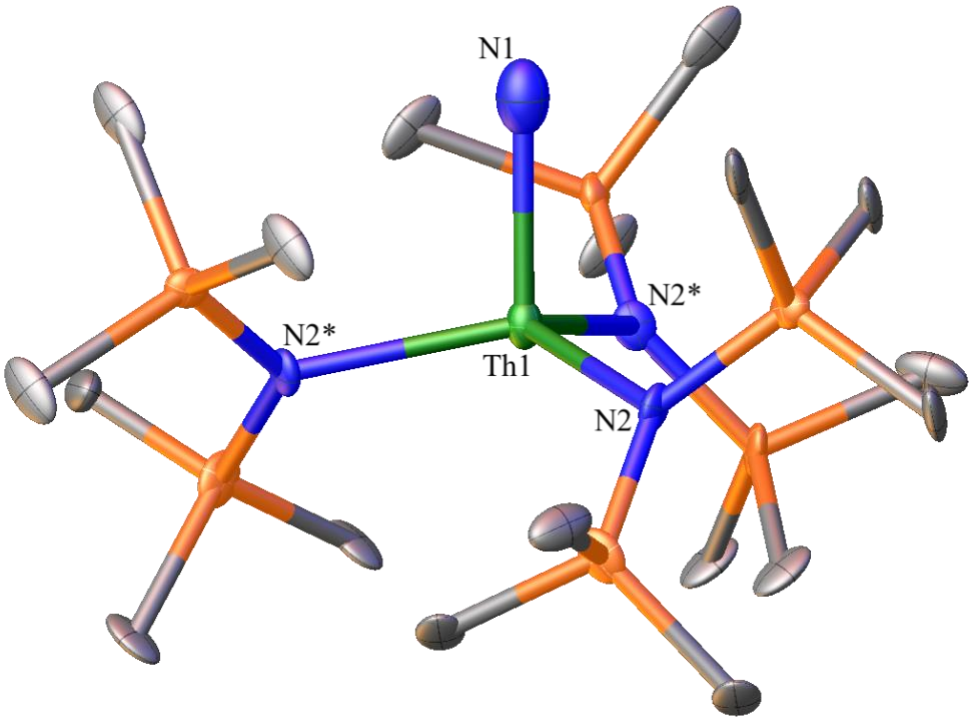

Figure 5.2. Solid-state molecular structure of **5.2**, shown with 50% probability ellipsoids. Hydrogen atoms removed for clarity. Selected bond lengths (Å) and angles (°): Th1-N1 =2.24(6), Th1-N2 = 2.36(2), N1-Th1-N2 = 100.7(3), N2-Th1-N2* = 116.7(2).

The connectivity of complex **5.2** was verified by X-ray crystallography (Figure 5.2). Complex **5.2** crystallizes in the trigonal space group R-3c. In the solid-state, complex **5.2** is disordered over two positions in a 50:50 ratio, which somewhat lowers the precision of the resulting metrical parameters. It features a pseudo-tetrahedral geometry about the thorium center. Due to the large ESDs, the Th-NH_2 distance (2.24(6) Å) in **5.2** is statistically identical to its Th-$N_{silylamido}$ distances (2.36(2) Å).[30, 39] The other Th-NH_2 complex has a similar Th-NH_2 bond length (2.2431(6) Å).[38] For further comparison, the uranium(IV) terminal amide complexes, [U(NH_2)($Tren^{TIPS}$)] ($Tren^{TIPS}$ = {$N(CH_2CH_2NSi^iPr_3)_3$}$^{3-}$) and [{η^5-1,2,4-

$C_5H_2{}^tBu_3\}_2U(NH_2)_2$], feature U-$NH_2$ bond lengths of 2.228(4) and av. 2.19 Å (av.), respectively.[40, 41]

Complex **5.2** is highly soluble in pentane, benzene, Et_2O and THF. Furthermore, **5.2** is stable as a C_6D_6 solution for over 36 h with minimal signs of decomposition. In addition, the IR spectrum of **5.2** features a prominent N-H stretching mode at 3321 cm^{-1} (Figure A5.20), providing further support for my formulation. For comparison, this mode is observed at 3342 cm^{-1} (Zr) and 3364 cm^{-1} (Hf) for [$M(NR_2)_3(NH_2)$] (M = Zr, Hf).[37]

5.2.4 NMR scale reaction of [K(DME)][Th{*N*(R)(SiMe$_2$*C*H$_2$)}$_2$(NR$_2$)] with [Th(NR$_2$)$_3$(NH$_2$)] (5.2).

To further test my proposed mechanistic hypothesis, I monitored the reaction of [K(DME)][Th{*N*(R)(SiMe$_2$*C*H$_2$)}$_2$(NR$_2$)][30] with **5.2** in THF-d_8, in the presence of 1 equiv of 18-crown-6, by ^{1}H NMR spectroscopy (eqn (5.3)). A ^{1}H NMR spectrum of this solution, after standing at room temperature for 4 h, reveals a new resonance at 0.36 ppm, which is assignable to **[K][5.1]** (Figure A5.13). After 3 d, the peak assignable to the nitride has increased in intensity, while resonances assignable to complex **5.2** and [K(DME)][Th{*N*(R)(SiMe$_2$*C*H$_2$)}$_2$(NR$_2$)] have decreased in intensity. These three complexes are present in a ratio of 1:3:6.7 in the 3 d spectrum. Overall, this result supports the proposed mechanism (Scheme 5.1), but it is important to note that formation of **[5.1]**$^-$ under these conditions is much slower than its rate of formation under the conditions described in eqn (5.1), suggesting that this experiment does not perfectly duplicate the original reaction conditions.

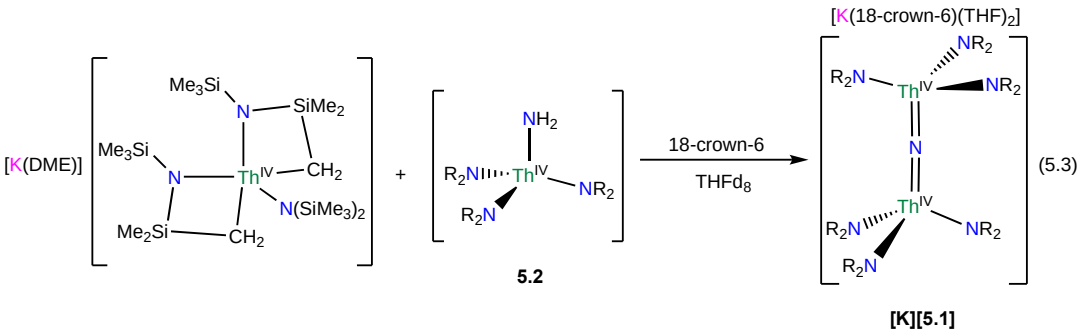

5.2.5 Synthesis and Characterization of [K(18-crown-6)(THF)$_2$][(R$_2$N)$_3$Th(μ-^{15}N)(Th(NR$_2$)$_3$] ([K][5.1-^{15}N])

To facilitate my covalency analysis I endeavored to synthesize **[5.1-^{15}N]$^-$**. Given the proposed intermediacy of [Na(THF)$_x$][Th{*N*(R)(SiMe$_2$*C*H$_2$)}$_2$(NR$_2$)] in the formation of **[Na][5.1]**, I rationalized that reaction of NH$_4$Cl with 2 equiv of [Th{*N*(R)(SiMe$_2$*C*H$_2$)}$_2$(NR$_2$)]$^-$ would generate the nitride complex. Thus, addition of 1 equiv of finely ground ^{15}NH$_4$Cl to a pale yellow THF solution containing 2 equiv of [K(DME)][Th{*N*(R)(SiMe$_2$*C*H$_2$)}$_2$(NR$_2$)],[30] followed by addition of 1 equiv of 18-crown-6, results in formation of [K(18-crown-6)(THF)$_2$][(R$_2$N)$_3$Th(μ-^{15}N)(Th(NR$_2$)$_3$] (**[K][5.1-^{15}N]**), which can be isolated as a white powder in 13% yield after work-up (eqn (5.4)).

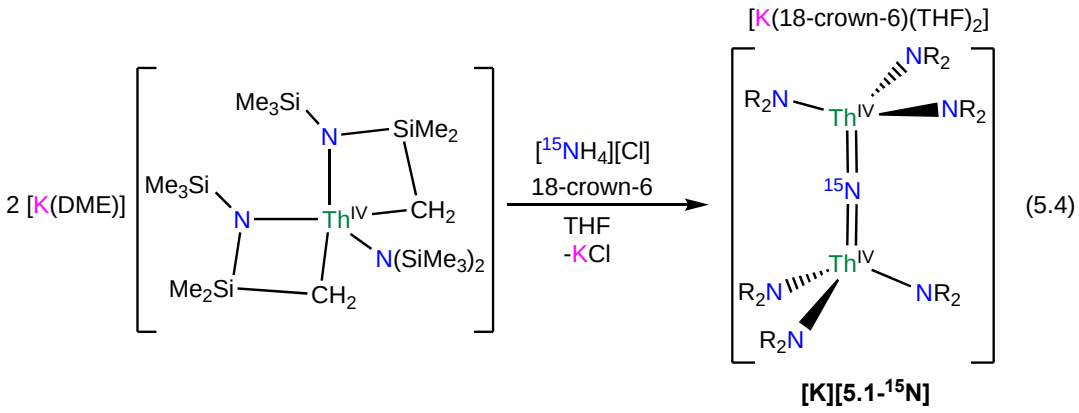

The low yield of **[K][5.1-^{15}N]** under these conditions can be partly ascribed to unselective protonation of [K(DME)][Th{*N*(R)(SiMe$_2$*C*H$_2$)}$_2$(NR$_2$)] by ^{15}NH$_4$Cl, which results in the

formation of copious amounts of HNR_2 (observed in the *in situ* ^{1}H NMR spectrum), and results in the presence of unreacted [K(DME)][Th{*N*(R)(SiMe$_2$*C*H$_2$)}$_2$(NR$_2$)] in the final reaction mixture. The unreacted [K(DME)][Th{*N*(R)(SiMe$_2$*C*H$_2$)}$_2$(NR$_2$)] can be conveniently removed from the nitride product by rinsing with toluene. The ^{1}H NMR spectrum of **[K][5.1-^{15}N]** in THF-d_8 matches those recorded for both **[Na][5.1]** and **[K][5.1]** (Figure A5.7), where a singlet at 0.36 ppm can be assigned to the $SiMe_3$ groups and a resonance at 3.63 ppm can be assigned to 18-crown-6. Furthermore, the ^{15}N{^{1}H} NMR spectrum of **[K][5.1-^{15}N]** (referenced to CH_3NO_2) reveals a sharp singlet at 298.8 ppm. No other resonances are observed in this spectrum. This is the first observation of an ^{15}N chemical shift for an actinide nitride. For comparison, the group 4 nitride complexes [{(η^5-C$_5$H$_2$-1,2,4-Me$_3$)$_2$Hf}$_2$(μ-N)(NCO)(DMAP)] and [{Cp*TiCl$_2$}(μ-N){Cp*TiCl(NH$_3$)}] feature ^{15}N resonances at 567.19 ppm and 431.6 ppm, respectively, for their bridging nitride ligands.[42, 43] Finally, the IR spectrum of **[K][5.1-^{15}N]** features a stretch at 735 cm^{-1}, which corresponds to the principal Th-N-Th asymmetric stretch (Figure A5.16), and is redshifted by 7 cm^{-1} from that observed for **[Na][5.1]**.

Furthermore, building on these results, a solid-state ^{15}N NMR powder spectrum was collected on **[K][5.1-^{15}N]** by my collaborators at University at Buffalo and represents the first reported solid-state ^{15}N NMR data for an actinide complex.[44]

5.2.6 Synthesis and Characterization of [Th(NR$_2$)$_3$(^{15}NH$_2$)] (5.2-^{15}N)

Access to **5.2-^{15}N** was achieved by reaction of [Th{*N*(R)(SiMe$_2$)*C*H$_2$}(NR$_2$)$_2$] with 1 equiv of $^{15}NH_3$ gas in THF. Synthesized in this manner, colorless crystals of **5.2-^{15}N** could be isolated in 85% yield after work-up. Similar to **5.2**, the ^{1}H NMR spectrum in benzene-d_6 shows a singlet at 0.36 ppm (54H), assignable to the $SiMe_3$ groups. In addition, a 1:1 doublet (2H,

J_{NH} = 62.3 Hz) at 3.67 ppm is assignable to the -NH_2 resonance (Figure A5.9). The ^{15}N NMR spectrum of **5.2-^{15}N** (referenced to CH_3NO_2) reveals a sharp resonance at −198.4 ppm (Figure A5.11). For comparison, the previously reported thorium amide ^{15}N NMR spectrum featured a sharp triplet centered at 155.01 ppm (J = 57.2 Hz).[38] It is not readily apparent why this chemical shift is so different from that recorded for complex **5.2-^{15}N**. Furthermore, building on these results, a solid-state ^{15}N NMR powder spectrum was collected on **5.2-^{15}N** by my collaborators at University at Buffalo.[44] Finally, the IR spectrum of **5.2-^{15}N** features an N-H stretch at 3317 cm^{-1}, and a Th-NH_2 stretch at 482 cm^{-1} (Figure A5.21). The identity of the latter stretch was confirmed by comparison with the calculated IR spectrum (Figure A5.30), where it is predicted to occur at 508 cm^{-1}.

5.2.7 Electronic Structure Analysis of [5.1]$^-$ and 5.2

My collaborators, Jochen Autschbach and Dumitru-Claudiu Sergentu (University at Buffalo), analyzed the electronic structures of **[5.1]**$^-$ and **5.2** with DFT. Using the B3LYP functional, I observe excellent agreement between the calculated and experimentally determined structural parameters for both complexes. For example, the calculated Th-$N_{nitride}$ and Th-$N_{silylamide}$ bond lengths for **[5.1]**$^-$ are within 0.02 Å of the distances found in the solid state. Similarly, the calculated Th-N_{amide} and Th-$N_{silylamide}$ bond lengths in **5.2** are within 0.02 Å of those found in its crystal structure.

An NBO/NLMO analysis of **[5.1]**$^-$ reveals that the Th-N-Th interaction consists of two orthogonal 3c-2e π bonds and two predominantly 2c-2e σ bonds that feature some three-center character (Figure 5.3), suggestive of overall Th=N double bond character. The covalency in the Th-$N_{nitride}$ bonds in **[5.1]**$^-$ is greater than that observed for the related Th imido,

$[Th(NAr)(NR_2)_3]^-$ (Ar = 2,6-^{i}Pr$_2$C$_6$H$_3$),[30] and Th oxo, $[Th(O)(NR_2)_3]^-$,[45] with a greater magnitude of 5f orbital involvement. For example, the Th-N π interaction in **[5.1]$^-$** features 16% Th character (58% 6d, 42% 5f) (Table 5.1), whereas $[Th(NAr)(NR_2)_3]^-$ and $[Th(O)(NR_2)_3]^-$ feature 0% and 12% Th character (65% 6d, 35% 5f), respectively, in their Th-E π bonds. For further comparison, the degree of covalency in **[5.1]$^-$** is comparable to that observed for the thorium sulfide, $[Th(S)(NR_2)_3]^-$, which features 17% Th character (61% 6d, 38% 5f) in its Th-S π interaction.[45] The Wiberg bond index of the Th-$N_{nitride}$ bond is 0.94, which is greater than that calculated for $[Th(NAr)(NR_2)_3]^-$ (0.88).[30] Overall, these combined computational metrics indicate a greater degree of covalency in **[5.1]$^-$** vs. the comparable imido and oxo complexes. Similar observations have been made for uranium(V) nitride and oxo complexes.[21, 40, 46]

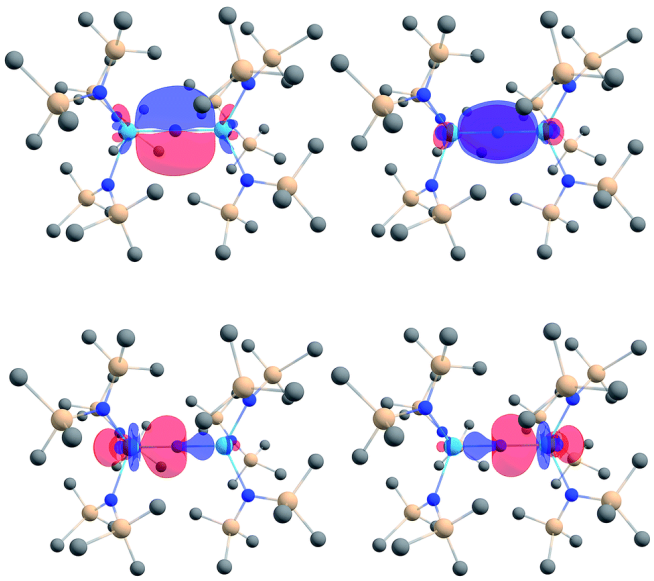

Figure 5.3. Th−N (2σ+2π) bonding NLMOs in $[(NR_2)_3Th(\mu\text{-}N)Th(NR_2)_3]^-$ (isosurface plots ±0.03 au; hydrogen atoms are omitted for clarity). Color code for atoms: Th, light blue; N, blue; Si, beige; C, gray.

Table 5.1. % compositions of the Th-N Bonding NLMOs in $[(NR_2)_3Th(\mu\text{-}N)Th(NR_2)_3]^-$

Orbital	**% N**			**% Th**				
	Total N	2s	2p	Total Th	7s	7p	6d	5f
σ	87	51	49	10	3	6	67	24
				3*	2	10	30	58
π	84	0	100	16	0	0	58	42

*The σ-bonding orbitals have some three-center character, each with 10 vs. 3% weight from the two Th centers.

For complex **5.2**, an NBO/NLMO analysis reveals that the Th-N interaction consists of 2c-2e π bond and a 2c-2e σ bond (Figure A5.27). Not surprisingly, the degree of covalency within the $Th\text{-}N_{amide}$ bond in **5.2** is less than that observed for the Th=N=Th bonds of **[5.1]**$^-$. Specifically, the σ bond in **5.2** features 7% Th character (63% 6d, 21% 5f, 5% 7p, 11% 7s) and the π bond features 10% Th character (59% 6d, 41% 5f). Accordingly, the Wiberg bond index of the $Th\text{-}N_{amide}$ bond (0.65) is substantially less than that observed for the $Th\text{-}N_{nitride}$ bonds in **[5.1]**$^-$.

5.2.8 Chemical Shift Analysis of [5.1]$^-$ and 5.2.

To assess the accuracy of my computational approach, Jochen Autschbach and Dumitru-Claudiu Sergentu (University at Buffalo) calculated the ^{15}N chemical shift of the nitride ligand in the known group(IV) nitride complex, $[\{Cp^*TiCl_2\}(\mu\text{-}N)\{Cp^*TiCl(NH_3)\}]$.[43] The ^{15}N chemical shift of the nitride ligand for the B3LYP-optimized structure was calculated to be 406.8 / 421.8 ppm using the PBE0 / B3LYP functionals and the scalar relativistic (SR) all-

electron ZORA Hamiltonian, respectively. For comparison, the experimentally determined chemical shift is 431.6 ppm.[43] Even better agreement was achieved by performing the calculation with two-component ZORA, i.e., including the spin-orbit (SO) coupling variationally. At this level, the calculated chemical shift (414.5 / 430.5 ppm) is in very good agreement with experiment.

With these results in hand, the ^{15}N NMR chemical shifts for the nitride and NH_2 ligands in **[5.1]**$^-$ and **5.2** were calculated using the PBE0 functional. Jochen Autschbach and Dumitru-Claudiu Sergentu (University at Buffalo), and others, have found that this functional works better than B3LYP for NMR shift calculations in actinide-containing molecules.[47] For **[5.1]**$^-$, the calculated ^{15}N chemical shift without spin orbit effects (ZORA-SR) is 226 ppm – substantially upfield from the experimental result (298.8 ppm). Considerably better agreement is obtained when SO coupling is taken into account, with a calculated ^{15}N shift of 305 ppm. The 79 ppm downfield shift induced by SO coupling is evidence of 5f character in the Th-$N_{nitride}$ bonds. For **5.2**, the calculated ^{15}N chemical shift without SO effects is –254 ppm. Upon inclusion of SO coupling, the shift changes to –210 ppm, which is much closer to the measured value (–198.4 ppm). The smaller downfield shift induced by SO coupling in **5.2** ($\Delta\delta$ = 44 ppm) is consistent with the reduced covalency, and reduced bond multiplicity, of the Th-N_{amide} bond. Perhaps most importantly, the good agreement between the experimental and calculated shifts for both **[5.1]**$^-$ and **5.2** gives credence to the NBO analysis presented in **5.2.7**.

5.3 Summary

I have synthesized and characterized the first isolable molecular thorium nitride complex, $[(NR_2)_3Th(\mu\text{-}N)Th(NR_2)_3]^-$. This complex is thermally stable, in contrast to the bridged thorium nitride recently proposed by Liddle and co-workers.[25] The origin of this stability

difference is not known, but it may be related to the lack of a *trans* donor ligand in $[(NR_2)_3Th(\mu\text{-}N)Th(NR_2)_3]^-$ vs. $[\{Th(Tren^{DMBS})\}_2(\mu\text{-}N)]^-$. Alternatively, it could relate to the different method of synthesis. ^{15}N NMR spectroscopic characterization of $[(NR_2)_3Th(\mu\text{-}N)Th(NR_2)_3]^-$, in combination with a DFT analysis, reveals the presence of 5f orbital participation within the Th=N=Th unit. In line with the reduced electronegativity of nitrogen vs. oxygen, my data suggests greater levels of covalency in $[(NR_2)_3Th(\mu\text{-}N)Th(NR_2)_3]^-$ than in the closely related oxo, $[Th(O)(NR_2)_3]^-$. However, I find comparable covalency in $[(NR_2)_3Th(\mu\text{-}N)Th(NR_2)_3]^-$ to that found in the thorium sulfide, $[Th(S)(NR_2)_3]^-$, likely on account of the greater energy-driven overlap in the latter.[48] To better contextualize my results, I also synthesized and characterized the thorium parent amide complex, $[Th(NR_2)_3(NH_2)]$. According to ^{15}N NMR spectroscopy and DFT calculations, this complex features a lesser degree of 5f covalency in its Th-NH_2 bond than that found for the bridging nitride complex, which is not surprising given its reduced bond order.

This work further solidifies the use of NMR spectroscopy as an important tool for probing the electronic structure of the actinides. Previously, ^{13}C, ^{77}Se, and ^{125}Te NMR spectroscopies had been used to evaluate covalency in An-E bonds.[39, 47, 49-52] In the case of An-C bonding, large downfield ^{13}C shifts have been consistently observed for the ^{13}C nuclei bonded directly to an actinide center. More significantly, the degree of deshielding was found to correlate with the amount of 5f covalency within the An-C bond. For example, the ^{13}C NMR shift of acetylide carbon in the U(VI) acetylide complexes, $U^{VI}(O)(C{\equiv}CC_6H_4\text{-}p\text{-}R)(NR_2)_3$ (R = NMe_2, OMe, Me, Ph, H, Cl), correlated well with two measures of covalency, the QTAIM delocalization index and the Wiberg bond order of the U-C bond.[49] Highly deshielded ^{13}C resonances are also observed for the carbene resonance in $[Th(CHPPh_3)(NR_2)_3]$ and the

methylene resonances in $[UO_2(CH_2SiMe_3)_4]^{2-}$ and $[U(CH_2SiMe_3)_6]^-$.[47, 53] My results demonstrate that ^{15}N NMR spectroscopy can also be used to evaluate covalency in actinide-ligand bonding, and like ^{13}C NMR spectroscopy, the magnitude of the downfield shift appears to correlate with the degree of 5f character in the An-N bond. Going forward, I propose to characterize other actinide nitrides by ^{15}N NMR spectroscopy. Of particular interest is the measurement of the ^{15}N chemical shift of a U(VI) nitride complex, which, on account of the high anticipated covalency, should exhibit an extreme downfield shift of its nitride resonance.

5.4 Acknowledgements

This work was supported by the U.S. Department of Energy, Office of Basic Energy Sciences, Chemical Sciences, Biosciences, and Geosciences Division, under Contract DE-SC-0001861. I would like to thank the Ménard group (UCSB) for the use of their $^{15}NH_3$ and help with the addition. I would also like to thank the collaborators on this project, Jochen Autschbach and Dumitru-Claudiu Sergentu (University at Buffalo) for their computational work and insights.

5.5 Experimental

5.5.1 General Methods

All reactions and subsequent manipulations were performed under anaerobic and anhydrous conditions under an atmosphere of nitrogen. Hexanes, Et_2O, toluene were dried using a Vacuum Atmospheres DRI-SOLV Solvent Purification system and stored over 3Å sieves for 24 h prior to use. THF was dried by distillation from sodium/benzophenone, and stored over 3Å sieves for 24 h prior to use. Benzene-d_6 and THF-d_8 were dried over 3Å molecular sieves for 24 h prior to use. $[Th(CH_2SiMe_2NSiMe_3)(NR_2)_2]$[29] (R = $SiMe_3$),

[U(*C*H$_2$SiMe$_2$*N*SiMe$_3$)(NR$_2$)$_2$],[54] and [K(DME)][Th{*N*(R)(SiMe$_2$*C*H$_2$)}$_2$(NR$_2$)][30] were synthesized according to the previously reported procedures. All other reagents were purchased from commercial suppliers and used as received.

NMR spectra were recorded on an Agilent Technologies 400-MR DD2 400 MHz Spectrometer. ^{1}H NMR spectra were referenced to external tetramethylsilane (TMS) using the residual protio solvent peaks as internal standards. ^{13}C{^{1}H} NMR spectra were referenced indirectly with the ^{1}H resonance of TMS at 0.0 ppm, according to IUPAC standard,[55, 56] using the residual solvent peaks as internal standards. ^{15}N NMR spectra were referenced to CH_3NO_2 (δ = 0.0 ppm) as external standard. IR spectra were recorded on a Nicolet 6700 FT-IR spectrometer with a NXR FT Raman Module. Elemental analyses were performed by the Micro-Analytical Facility at the University of California, Berkeley.

5.5.2 Synthesis and Characterization of [Na(18-crown-6)(Et$_2$O)][(R$_2$N)$_3$Th(μ-N)(Th(NR$_2$)$_3$] (R = SiMe$_3$) ([Na][5.1]).

To a stirring, cold (-25 °C), pale yellow solution of [Th{*N*(R)(SiMe$_2$)*C*H$_2$}(NR$_2$)$_2$] (204.1 mg, 0.287 mmol) in THF (3 mL) was added $NaNH_2$ (11.3 mg, 0.290 mmol). No obvious change was observed upon addition. To this mixture was added a cold (-25 °C) solution of 18-crown-6 (75.5 mg, 0.286 mmol) in THF (2 mL). The reaction mixture was allowed to warm to room temperature with stirring. After 24 h, the volatiles were removed *in vacuo* from the cloudy, pale yellow suspension to provide an off-white solid. The solid was then extracted into diethyl ether (6 mL) and the resulting pale-yellow, cloudy suspension was filtered through a Celite column supported on glass wool (0.5 × 2 cm). The filtrate was concentrated *in vacuo* to 2 mL, layered with pentane (4 mL), and stored at -25 °C for 24 h, which resulted in the deposition of colorless crystalline solid. The solid was isolated by decanting the supernatant

and then dried *in vacuo* to yield **[Na][5.1]** (106.6 mg). The supernatant was dried *in vacuo*, and the resulting off white solid was dissolved in diethyl ether (4 mL) and filtered through a Celite column supported on glass wool (0.5 × 2 cm). The filtrate was concentrated *in vacuo* to 2 mL, layered with pentane (6 mL), and stored at -25 °C for 24 h, which resulted in the deposition of more colorless crystalline solid (62.7 mg). Total yield: 169.3 mg, 66% yield. Anal. Calcd for $C_{48}H_{132}NaN_7O_6Si_{12}Th_2 \cdot C_4H_{10}O$: C, 34.66; H, 7.94; N, 5.44. Anal. Calcd for $C_{48}H_{132}NaN_7O_6Si_{12}Th_2$: C, 33.37; H, 7.70; N, 5.68. Found: C, 33.17; H, 7.77; N, 5.81. ^{1}H NMR (400 MHz, 25 °C, THF-d_8): δ 0.36 (s, 108H, NSiCH_3), 3.62 (s, 24H, 18-crown-6). $^{13}C\{^1H\}$ NMR (100 MHz, 25 °C, THF-d_8): δ 8.21 (s, NSiCH$_3$), 71.80 (s, 18-crown-6). IR (KBr pellet, cm^{-1}): 411 (s), 415 (m, sh), 422 (s), 430 (s), 438 (s), 451 (m, sh), 457 (s), 465 (s), 480 (w), 494 (m), 505 (m), 538 (s), 569 (s), 596 (s), 604 (s, sh), 656 (m, sh), 661 (s), 681 (s, sh), 692 (m, sh), 733 (m, sh), 742 (s, asym ν_{ThNTh}), 756 (s), 773 (s), 820 (m, sh), 829 (m), 843 (m, sh), 860 (s), 885 (m, sh), 939 (s), 962 (s, sh), 991 (s), 1020 (m, sh), 1041 (s), 1059 (s), 1076 (m, sh), 1107 (s), 1136 (m, sh), 1155 (m, sh), 1176 (m, sh), 1219 (m, sh), 1240 (m, sh), 1248 (s), 1250 (s), 1298 (s), 1335 (s), 1354 (s), 1367 (m, sh), 1385 (s), 1412 (m), 1433 (m, sh), 1446 (m, sh), 1456 (s), 1466 (s), 1495 (s), 1930 (w), 1969 (s), 1973 (s), 2089 (s), 2337 (w), 2360 (m), 2704 (m, sh), 2723 (m, sh), 2740 (s), 2812 (m, sh), 2858 (m, sh), 2875 (m, sh), 2899 (s), 2914 (m, sh), 2949 (s), 3377 (w).

5.5.3 Synthesis and Characterization of [K(18-crown-6)(THF)$_2$][(R$_2$N)$_3$Th(μ-N)(Th(NR$_2$)$_3$] ([K][5.1]).

To a stirring, cold (-25 °C), pale yellow solution of [K(DME)][Th{N(R)(SiMe$_2$$CH_2$)}$_2$(NR$_2$)] (315.8 mg, 0.376 mmol) in THF (5 mL) was added finely ground NH_4Cl (10.3 mg, 0.193 mmol). The reaction mixture was allowed to warm to

room temperature with stirring. After 2 h, a solution of 18-crown-6 (49.7 mg, 0.188 mmol) in THF (2 mL) was added to the reaction mixture. After stirring for a further 30 min, the volatiles were removed *in vacuo* from the cloudy, pale yellow suspension to provide an off-white solid. The solid was then extracted into diethyl ether (6 mL) and the resulting pale-yellow, cloudy suspension was filtered through a Celite column supported on glass wool (0.5 × 2 cm). The filtrate was dried *in vacuo* to yield an off white powder, which was rinsed with toluene (3 × 4 mL) to separate **[K][5.1]** from unreacted [K(DME)][Th{*N*(R)(SiMe$_2$*C*H$_2$)}$_2$(NR$_2$)]. The soluble [K(DME)][Th{*N*(R)(SiMe$_2$*C*H$_2$)}$_2$(NR$_2$)] was decanted away from the solid and discarded. The remaining white microcrystalline powder was dried *in vacuo*, dissolved in a mixture of diethyl ether (4 mL) and THF (2 mL), and filtered through a Celite column supported on glass wool (0.5 × 2 cm). The colorless filtrate was concentrated *in vacuo* to 2 mL, layered with pentane (4 mL), and stored at -25 °C for 24 h, which resulted in the deposition of colorless crystalline solid. The solid was isolated by decanting the supernatant and dried *in vacuo* to yield **[K][5.1]** (15 mg, 5% yield). Anal. Calcd for $C_{48}H_{132}KN_7O_6Si_{12}Th_2 \cdot 2C_4H_8O$: C, 35.63; H, 7.90; N, 5.19. Anal. Calcd for $C_{48}H_{132}KN_7O_6Si_{12}Th_2$: C, 33.06; H, 7.63; N, 5.62. Found: C, 33.13; H, 7.54; N, 5.32. ^{1}H NMR (400 MHz, 25 °C, THF-d_8): δ 0.36 (s, 108H, NSiC*H*$_3$), 3.63 (s, 24H, 18-crown-6). ^{13}C{^{1}H} NMR (100 MHz, 25 °C, THF-d_8): δ 8.22 (s, NSi*C*H$_3$), 72.03 (s, 18-crown-6). IR (KBr pellet, cm^{-1}): 409 (s), 420 (s), 472 (w), 499 (w), 526 (s), 596 (s), 604 (s), 615 (w, sh), 656 (s), 669 (w, sh), 677 (m, sh), 694 (w, sh), 742 (s, asym ν_{ThNTh}), 752 (m, sh), 773 (s), 802 (m, sh), 820 (m, sh), 831 (w), 839 (m, sh), 864 (s), 937 (m), 962 (s), 1032 (w), 1059 (s), 1111 (s), 1132 (m, sh), 1180 (m), 1248 (s), 1252 (w, sh), 1267 (m, sh), 1282 (s), 1352 (s), 1365 (w, sh), 1396 (m), 1433 (m), 1454 (s), 1473 (s), 1848 (w), 1923 (m), 1977 (s), 2075 (m), 2141 (w), 2245

(w), 2364 (m), 2467 (m), 2598 (w), 2632 (w), 2686 (s), 2708 (s), 2744 (s), 2796 (s), 2827 (s), 2897 (s), 2947 (s).

5.5.4 Synthesis and Characterization of [K(18-crown-6)(THF)$_2$][(R$_2$N)$_3$Th(μ-^{15}N)(Th(NR$_2$)$_3$] ([K][5.1-^{15}N]).

To a stirring, cold (-25 °C), pale yellow solution of [K(DME)][Th{*N*(R)(SiMe$_2$*C*H$_2$)}$_2$(NR$_2$)] (300.7 mg, 0.358 mmol) in THF (3 mL) was added finely ground ^{15}NH$_4$Cl (9.7 mg, 0.273 mmol). The reaction mixture was allowed to warm to room temperature with stirring. After 2 h, a solution of 18-crown-6 (48.3 mg, 0.183 mmol) in THF (2 mL) was added to the reaction mixture. After stirring for 1 h further, the volatiles were removed *in vacuo* from the cloudy, pale yellow suspension to provide an off-white solid. The solid was then extracted into diethyl ether (6 mL) and the resulting pale-yellow, cloudy suspension was filtered through a Celite column supported on glass wool (0.5 × 2 cm). The filtrate was dried *in vacuo* to yield an off white powder, which was rinsed with toluene (3 × 4 mL) to separate **[K][5.1-^{15}N]** from unreacted [K(DME)][Th{*N*(R)(SiMe$_2$*C*H$_2$)}$_2$(NR$_2$)]. The soluble [K(DME)][Th{*N*(R)(SiMe$_2$*C*H$_2$)}$_2$(NR$_2$)] was decanted away from the solid and discarded. The remaining white microcrystalline powder was dried *in vacuo*, dissolved in a mixture of diethyl ether (4 mL) and THF (2 mL), and filtered through a Celite column supported on glass wool (0.5 × 2 cm). The filtrate was concentrated *in vacuo* to 2 mL, layered with pentane (4 mL), and stored at -25 °C for 24 h, which resulted in the deposition of colorless crystalline solid. The solid was isolated by decanting the supernatant and then dried *in vacuo* to yield **[K][5.1-^{15}N]** (43.2 mg, 13% yield). ^{1}H NMR (400 MHz, 25 °C, THF-*d*$_8$): δ 0.36 (s, 108H, NSiC*H*$_3$), 3.63 (s, 24H, 18-crown-6). ^{15}N{^{1}H} NMR (40 MHz, 25 °C, THF-*d*$_8$): δ 298.79 (s, (μ-N)). IR (KBr pellet, cm^{-1}): 409 (s), 422 (s), 436 (s), 442 (m), 447 (m, sh), 469

(m), 476 (m), 488 (w), 492 (m, sh), 528 (s), 592 (s), 604 (s), 613 (w, sh), 652 (s), 658 (w), 669 (m), 677 (m, sh), 690 (m, sh), 735 (s, asym ν_{ThNTh}), 756 (s), 773 (s), 820 (m, sh), 831 (w), 843 (m), 864 (s), 904 (m, sh), 943 (s), 962 (s), 1028 (s), 1059 (s), 1113 (s), 1132 (m, sh), 1182 (s), 1248 (s), 1252 (m, sh), 1269 (m, sh), 1282 (s), 1352 (s), 1363 (m, sh), 1390 (m, sh), 1400 (s), 1433 (s), 1454 (s), 1473 (s), 1925 (m), 1975 (s), 2075 (w), 2135 (w), 2251 (w), 2347 (w), 2463 (w), 2586 (w), 2638 (w), 2688 (s), 2708 (s), 2744 (s), 2796 (m), 2825 (s), 2877 (m, sh), 2897 (s), 2947 (s), 2958 (m, sh), 3130 (m, sh).592 (s), 652 (s), 733 (m), 833 (m), 945 (m), 1059 (s), 1113 (s), 1182 (s), 1248 (m), 1352 (s), 1473 (s), 2897 (w).

5.5.5 Synthesis and Characterization of [Th(NR$_2$)$_3$(NH$_2$)] (R = SiMe$_3$) (5.2).

To a stirring, cold (-25 °C), pale yellow solution of [Th{*N*(R)(SiMe$_2$)*C*H$_2$}(NR$_2$)$_2$] (97.4 mg, 0.137 mmol) in THF (2 mL) was added a THF solution of NH_3 (1.0 mL, 0.4 mmol, 0.4 M). The pale yellow reaction mixture was allowed to warm to room temperature with stirring. After 1 h, the volatiles were removed *in vacuo* to provide an off-white solid. The solid was then extracted into pentane (3 mL) and the resulting pale-yellow, cloudy suspension was filtered through a Celite column supported on glass wool (0.5 × 2 cm). The filtrate was transferred to a 4 mL vial, which was placed inside a 20 mL scintillation vial and iso-octane (2 mL) was added to the outer vial. Storage of this two-vial system at -25 °C for 7 d resulted in the deposition of a colorless crystalline solid. The solid was isolated by decanting the supernatant and then dried *in vacuo* to yield **5.2** (13.2 mg). The supernatant was transferred to a new 4 mL vial, which was placed inside a 20 mL scintillation vial and iso-octane (2 mL) was added to the outer vial. Storage of this two-vial system at -25 °C for 7 d resulted in the deposition of more colorless crystalline solid (37.9 mg). Total yield: 51.1 mg, 51% yield. Anal. Calcd for $C_{18}H_{56}N_4Si_6Th$: C, 29.65; H, 7.74; N, 7.68. Found: C, 29.78; H, 7.87; N, 7.49.

^{1}H NMR (400 MHz, 25 °C, C_6D_6): δ 0.37 (s, 54H, NSiCH_3), 3.67 (t, 2H, NH_2, J_{NH} = 45.8 Hz). ^{13}C{^{1}H} NMR (100 MHz, 25 °C, C_6D_6): δ 3.79 (s, CH$_3$). IR (KBr pellet, cm^{-1}): 415 (m, sh), 424 (s), 430 (m, sh), 455 (w), 496 (s), 607 (s), 660 (s), 671 (m, sh), 735 (m, sh), 756 (m, sh), 769 (s), 822 (m, sh), 841 (m, sh), 860 (m), 957 (s), 1038 (m, sh), 1115 (m, sh), 1126 (s), 1182 (s), 1246 (s), 1259 (m, sh), 1284 (m, sh), 1344 (m), 1358 (m, sh), 1400 (s), 1421 (m), 1439 (m), 1493 (m, sh), 1508 (s), 1560 (s), 1610 (s), 1857 (s), 1919 (s), 1994 (m), 2013 (w), 2083 (m), 2233 (w), 2347 (m), 2478 (s), 2582 (m), 2638 (m), 2791 (m, sh), 2819 (s), 2897 (s), 2926 (s), 2949 (s), 3140 (m), 3201 (m, sh), 3321 (s, ν_{NH}).

5.5.6 Synthesis and Characterization of [Th(NR$_2$)$_3$(^{15}NH$_2$)] (5.2-^{15}N).

A pale yellow solution of [Th{N(R)(SiMe$_2$)CH$_2$}(NR$_2$)$_2$] (215.7 mg, 0.303 mmol) in THF (13 mL) was added to a 20 mL Schlenk tube fitted with a rotaflow valve. The Schlenk tube was removed from the glovebox, attached to a vacuum line, the headspace was evacuated, and gaseous ^{15}NH$_3$ (1 atm, 7 mL, 0.291 mmol) was added to the Schlenk flask. The Schlenk tube was allowed to stand for 30 min, brought back into the glovebox, and the pale yellow reaction mixture was transferred to a 20 mL vial. The volatiles were removed *in vacuo* to provide a pale yellow oily solid. The solid was extracted into pentane (3 mL) and the resulting pale-yellow, cloudy suspension was filtered through a Celite column supported on glass wool (0.5 × 2 cm). The filtrate was transferred to a 4 mL vial, which was placed inside a 20 mL scintillation vial and iso-octane (2 mL) was added to the outer vial. Storage of this two-vial system at -25 °C for 7 d resulted in the deposition of colorless crystalline solid. The solid was isolated by decanting the supernatant and then dried *in vacuo* to yield **5.2-^{15}N** (188.8 mg, 85% yield). ^{1}H NMR (400 MHz, 25 °C, C_6D_6): δ 0.36 (s, 54H, NSiCH_3), 3.67 (d, 2H, NH_2, J_{NH} = 62.3 Hz). ^{1}H{^{15}N} (400 MHz, 25 °C, C_6D_6): δ 0.36 (s, 54H, NSiCH_3), 3.67 (NH_2). ^{15}N{^{1}H}

NMR (40 MHz, 25 °C, C_6D_6): δ -198.4 (s, *N*H_2). IR (KBr pellet, cm^{-1}): 407 (m, sh), 413 (s), 422 (s), 432 (m, sh), 445 (w), 482 (s, ν_{ThN}), 486 (s), 513 (m, sh), 565 (m, sh), 607 (s), 660 (s), 675 (w, sh), 735 (m, sh), 756 (m, sh), 773 (s), 812 (m, sh), 864 (w), 906 (w), 955 (w), 1014 (m, sh), 1045 (m, sh), 1115 (s), 1126 (s), 1182 (m), 1244 (s), 1259 (m, sh), 1284 (m, sh), 1340 (m, sh), 1358 (m, sh), 1400 (s), 1425 (s), 1439 (m, sh), 1468 (m, sh), 1504 (s), 1626 (m), 1632 (m, sh), 1662 (s), 1859 (s), 1919 (s), 1986 (w), 2040 (s), 2081 (m), 2231 (w), 2330 (m), 2359 (s), 2476 (s), 2640 (m), 2791 (m, sh), 2819 (s), 2897 (s), 2947 (s), 3140 (m), 3211 (w), 3317 (s, ν_{NH}), 3377 (w).

5.5.7 NMR scale reaction of [Th{*N*(R)(SiMe$_2$)*C*H$_2$}(NR$_2$)$_2$] with NaNH$_2$.

An NMR tube fitted with a J-Young valve was charged with [Th{*N*(R)(SiMe$_2$)*C*H$_2$}(NR$_2$)$_2$] (23.4 mg, 0.0329 mmol), $NaNH_2$ (1.6 mg, 0.0410 mmol), and THF-d_8 (0.5 mL). To this pale yellow solution was added a colorless solution of 18-crown-6 (8.7 mg, 0.0329 mmol) in THF-d_8 (0.5 mL). A ^{1}H NMR spectrum was then recorded (Figure A5.12). ^{1}H NMR (400 MHz, 25 °C, THF-d_8): δ 0.11 (s, 9H, NSi(C*H*$_3$)$_3$), 0.22 (s, 6H, Si(C*H*$_3$)$_2$), 0.29 (s, 36H, N(Si(C*H*$_3$)$_3$)$_2$), 0.47 (s, 2H, C*H*$_2$), 3.57 (s, 24H, 18-crown-6). The NMR tube was then attached to a wrist action tube shaker. After 150 min of shaking, a ^{1}H NMR spectrum was re-recorded. This spectrum revealed the appearance of a resonances corresponding to **[Na][5.1]** and **5.2**, concomitant with a decrease in the intensity of the resonances assignable to [Th{*N*(R)(SiMe$_2$)*C*H$_2$}(NR$_2$)$_2$]. ^{1}H NMR (400 MHz, 25 °C, THF-d_8): δ 0.11 (s, 9H, NSi(C*H*$_3$)$_3$), 0.22 (s, 6H, Si(C*H*$_3$)$_2$), 0.29 (s, 36H, N(Si(C*H*$_3$)$_3$)$_2$), 0.30 (s, 54H, NSiC*H*$_3$, **5.2**), 0.36 (s, 108H, NSiC*H*$_3$, **[Na][5.1]**), 0.47 (s, 2H, C*H*$_2$), 3.58 (s, 24H, 18-crown-6)). The NMR tube was then re-attached to a wrist action tube shaker. After 7 h and 30 min of shaking, a ^{1}H NMR spectrum was re-recorded. This spectrum revealed the appearance

of resonances assignable to [Na(THF-d_8)$_x$][Th{*N*(R)(SiMe$_2$*C*H$_2$)}$_2$(NR$_2$)], while resonances assignable to **[Na][5.1]** and **5.2** grow in intensity, and peaks assignable to [Th{*N*(R)(SiMe$_2$)*C*H$_2$}(NR$_2$)$_2$] continue to decrease in intensity. ^{1}H NMR (400 MHz, 25 °C, THF-d_8): δ -0.36 (br s, 4H, C*H*$_2$, bis(metallacycle)), 0.03 (s, 12H, N(SiC*H*$_3$)$_2$, bis(metallacycle)), 0.04 (s, NSi(C*H*$_3$)$_3$, bis(metallacycle) overlapping with HN(SiMe$_3$)$_2$), 0.11 (s, 9H, NSi(C*H*$_3$)$_3$), 0.18 (s, 18H, N(SiC*H*$_3$)$_2$, bis(metallacycle)), 0.22 (s, 6H, Si(C*H*$_3$)$_2$), 0.29 (s, 36H, N(Si(C*H*$_3$)$_3$)$_2$), 0.30 (s, 54H, NSiC*H*$_3$, **5.2**), 0.36 (s, 108H, NSiC*H*$_3$, **[Na][5.1]**), 0.47 (s, 2H, C*H*$_2$), 3.58 (s, 24H, 18-crown-6). The NMR tube was then re-attached to a wrist action tube shaker. After 32 h of shaking, the resonance assignable to **[Na][5.1]** is the most prominent peak in the spectrum, the resonances assignable to **5.2** and [Th{*N*(R)(SiMe$_2$)*C*H$_2$}(NR$_2$)$_2$] have disappeared, and only a small amount of [Na(THF-d_8)$_x$][Th{*N*(R)(SiMe$_2$*C*H$_2$)}$_2$(NR$_2$)] remains in the sample. ^{1}H NMR (400 MHz, 25 °C, THF-d_8): δ -0.36 (br s, 4H, C*H*$_2$, bis(metallacycle)), 0.03 (s, 12H, N(SiC*H*$_3$)$_2$, bis(metallacycle)), 0.04 (s, NSi(C*H*$_3$)$_3$, bis(metallacycle) overlapping with HN(SiMe$_3$)$_2$), 0.18 (s, 18H, N(SiC*H*$_3$)$_2$, bis(metallacycle)), 0.36 (s, 108H, NSiC*H*$_3$, **[Na][5.1]**), 3.60 (s, 24H, 18-crown-6).

5.5.8 NMR scale reaction of [K(DME)][Th{*N*(R)(SiMe$_2$*C*H$_2$)}$_2$(NR$_2$)] with [Th(NR$_2$)$_3$(NH$_2$)] (5.2).

A colorless solution of [K(DME)][Th{*N*(R)(SiMe$_2$*C*H$_2$)}$_2$(NR$_2$)] (4.7 mg, 0.0056 mmol) in THF-d_8 (0.5 mL) was added to an NMR tube fitted with a J-Young valve. A ^{1}H NMR spectrum was recorded (Figure A5.13). ^{1}H NMR (400 MHz, 25 °C, THF-d_8): δ -0.36 (br s, 4H, C*H*$_2$), 0.02 (s, 12H, N(SiC*H*$_3$)$_2$), 0.04 (s, 18H, NSi(C*H*$_3$)$_3$), 0.18 (s, 18H, N(Si(C*H*$_3$)$_3$)$_2$), 3.27 (s, 6H, OC*H*$_3$), 3.42 (s, 4H, OC*H*$_2$). The NMR tube was brought back into the glovebox, and a colorless solution of **5.2** (4.1 mg, 0.0056 mmol) in THF-d_8 (0.5 mL) was added to the

tube. After 15 min, a ^{1}H NMR spectrum was taken, which revealed the presences of resonances assignable to both **5.2** and bis(metallacycle). ^{1}H NMR (400 MHz, 25 °C, THF-d_8): δ -0.36 (br s, 4H, CH_2), 0.02 (s, 12H, N(SiCH_3)$_2$), 0.04 (s, 18H, NSi(CH_3)$_3$), 0.18 (s, 18H, N(Si(CH_3)$_3$)$_2$), 0.30 (s, 54H, NSiCH_3, **5.2**), 3.27 (s, 6H, OCH_3), 3.42 (s, 4H, OCH_2), 3.99 (t, 2H, NH_2, **5.2**). 18-crown-6 (2.1 mg, 0.0080 mmol) was then added to the reaction mixture as a crystalline solid. No obvious change was observed upon addition. A ^{1}H NMR spectrum was re-recorded after 4 h. This spectrum revealed the presence of small amounts of **[K][5.1]**, along with resonances assignable to both **5.2** and bis(metallacycle). ^{1}H NMR (400 MHz, 25 °C, THF-d_8): δ -0.36 (br s, 4H, CH_2), 0.02 (s, 12H, N(SiCH_3)$_2$), 0.04 (s, 18H, NSi(CH_3)$_3$), 0.18 (s, 18H, N(Si(CH_3)$_3$)$_2$), 0.30 (s, 54H, NSiCH_3, **5.2**), 0.36 (s, 108H, NSiCH_3, **[K][5.1]**), 3.27 (s, 6H, OCH_3), 3.42 (s, 4H, OCH_2), 3.99 (t, 2H, NH_2, **5.2**). A ^{1}H NMR spectrum was re-recorded after 3 d. This spectrum revealed considerable increase in the amount of **[K][5.1]** present in the sample, while resonances corresponding to **5.2** and bis(metallacycle) have decreased in intensity. The ratio of **[K][5.1]**:**5.2**:[K(DME)][Th{*N*(R)(SiMe$_2$*C*H$_2$)}$_2$(NR$_2$)] after 3 d was 1:3:6.7. ^{1}H NMR (400 MHz, 25 °C, THF-d_8): δ -0.36 (br s, 4H, CH_2), 0.02 (s, 12H, N(SiCH_3)$_2$), 0.04 (s, 18H, NSi(CH_3)$_3$), 0.18 (s, 18H, N(Si(CH_3)$_3$)$_2$), 0.30 (s, 54H, NSiCH_3, **5.2**), 0.36 (s, 108H, NSiCH_3, **[K][5.1]**), 3.27 (s, 6H, OCH_3), 3.42 (s, 4H, OCH_2), 3.99 (t, 2H, NH_2, **5.2**).

5.5.9 X-ray Crystallography

Data for **[Na][5.1]**, **5.2**, and **[K][5.1]** were collected on a Bruker KAPPA APEX II diffractometer equipped with an APEX II CCD detector using a TRIUMPH monochromator with a Mo Kα X-ray source (α = 0.71073 Å). The crystals were mounted on a cryoloop under Paratone-N oil, and all data were collected at 100(2) K using an Oxford nitrogen gas cryostream. Data were collected using ω scans with 0.5° frame widths. Frame exposures of 15, 5, and 10 seconds were used for **[Na][5.1]**, **5.2**, and **[K][5.1]**, respectively. Data collection and cell parameter determinations were conducted using the SMART program.[57] Integration of the data frames and final cell parameter refinements were performed using SAINT software.[58] Absorption corrections of the data were carried out using the multi-scan method SADABS.[59] Subsequent calculations were carried out using SHELXTL.[60] Structure determination was done using direct or Patterson methods and difference Fourier techniques. All hydrogen atom positions were idealized, and rode on the atom of attachment. Structure solution, refinement, graphics, and creation of publication materials were performed using SHELXTL.[60]

Table 5.2. X-ray Crystallographic Data for **[Na][5.1]**, **5.2**, and **[K][5.1]**.

	[Na][5.1]	**5.2**	**[K][5.1]**
empirical formula	$C_{52}H_{142}NaN_7O_7Si_{12}Th_2$	$C_{18}H_{56}N_4Si_6Th$	$C_{56}H_{148}KN_7O_8Si_{12}Th_2$
crystal habit, color	Block, Colorless	Block, Colorless	Block, Colorless
crystal size (mm)	0.2 × 0.1 × 0.05	0.25 × 0.2 × 0.15	0.15× 0.15 × 0.1
space group	*P*21/c	R-3c	*P*-1
volume ($Å^3$)	8593(16)	5029(3)	2238.6(10)
a (Å)	12.391(14)	18.497(6)	11.893(3)
b (Å)	23.18(2)	18.497(6)	14.617(4)
c (Å)	29.92(3)	16.973(4)	14.620(4)
α (deg)	90	90	74.546(15)
β (deg)	90.96(3)	90	71.051(15)
γ (deg)	90	120	71.238(14)
Z	4	6	1
formula weight (g/mol)	1801.87	729.24	1888.07
density (calculated) (Mg/m^3)	1.393	1.445	1.400
absorption coefficient (mm^{-1})	3.672	4.674	3.569
F_{000}	3672	2196	964
total no. reflections	31666	8880	22425
unique reflections	13515	930	9312
final R indices (I >2σ(I)]	R_1 = 0.1190 wR_2 = 0.1927	R_1 = 0.0714 wR_2 = 0.1843	R_1 = 0.0804 wR_2 = 0.1803
largest diff. peak and hole ($e^- A^{-3}$)	3.831 and -2.354	0.796 and -1.627	01.246 and -2.456
GOF	1.085	1.406	1.142

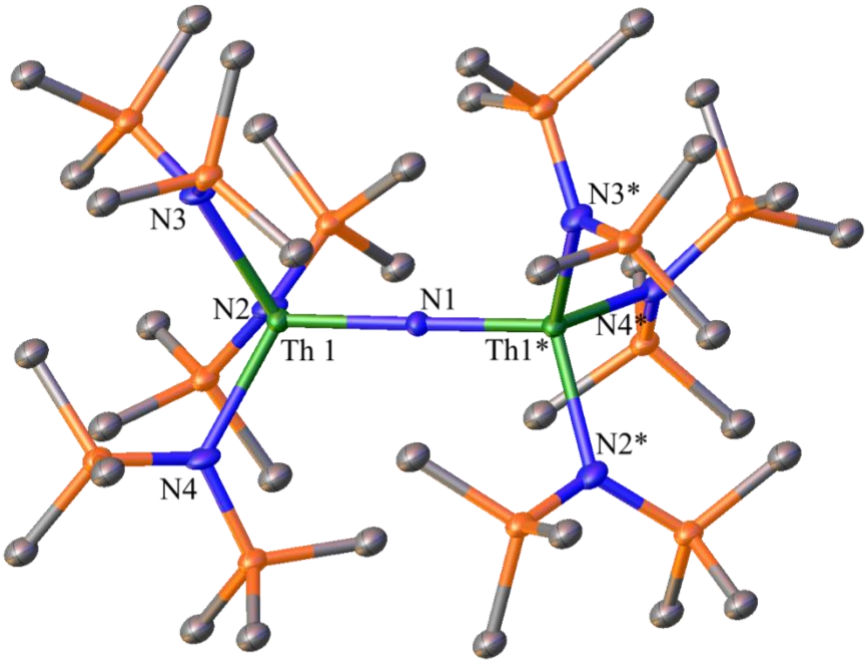

Figure 5.4. Solid-state molecular structure of **[K][5.1]**, with 50% probability ellipsoids. Hydrogen atoms and $[K(18\text{-crown-6})(THF)_2]^+$ counterion removed for clarity. Selected bond lengths (Å) and angles (°): Th1-N1 = 2.1167(7), av. Th1–N_{amido} = 2.41, Th1-N1-Th1* = 180, av. N_{amido}-Th1-N_{amido} = 109.2.

5.6 Appendix

5.6.1 Synthesis and Characterization of [Na(18-crown-6)(Et_2O)][($(R_2N)_3U(\mu$-N)(U(NR_2)$_3$] (R = $SiMe_3$) (5.5).

Given the successful results reported in **5.2.1**, I sought to extend this work onto uranium. Therefore, addition of 1 equiv of $NaNH_2$ to a cold (-25 °C) solution of the uranium metallacycle, [U{*N*(R)($SiMe_2$)*C*H_2}(NR_2)$_2$] (R = $SiMe_3$),[54] in tetrahydrofuran (THF), followed by addition of 1 equiv of 18-crown-6, afforded the bridged nitride complex, [Na(18-crown-6)(Et_2O)][($(R_2N)_3U(\mu$-N)(U(NR_2)$_3$] (**5.5**), after stirring for 24 h. This material could be isolated as brown blocks in 10% yield after work-up, along with uranium bis(metallacycle), [Na][U{*N*(R)($SiMe_2$*C*H_2)}$_2$(NR_2)],[61] in 20% yield, and the U(IV) bridged-nitrido,, [Na][($(NR_2)_2U(\mu$-N)(*C*$H_2$$SiMe_2$*N*R)U($NR_2$)$_2$],[10] in trace amount (eqn (5.5)).

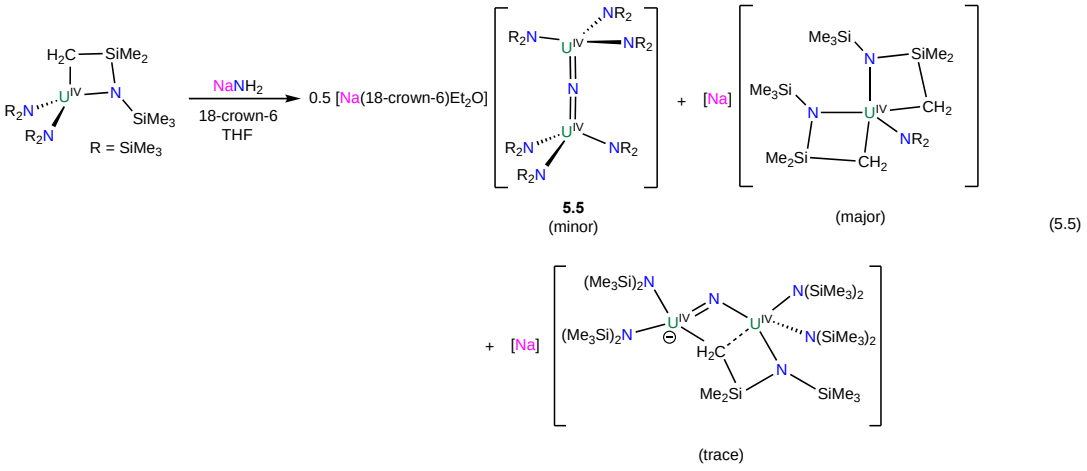

Complex **5.5** was always isolated as a mixture and in low yields, so I did not pursue this very long since I was more interested in the thorium analogue at the time. Moreover, this complex was reported by Mazzanti and co-workers in 2019 *via* a different route.[62]

These results suggest that uranium bis(metallacycle) does not readily react with acids, specifically NH_3. The proposed mechanism of **[5.1]**$^-$ (Scheme 5.1) should be analogous to the

formation of **5.5**, which suggests NH_3 and the bis(metallacycle) anion are formed in the first step of the reaction. However, the uranium bis(metallacycle) is surprisingly unreactive and does not proceed to fully react, forming **5.5** as the minor product and uranium bis(metallacycle) as the major product.

5.6.2 NMR Spectra

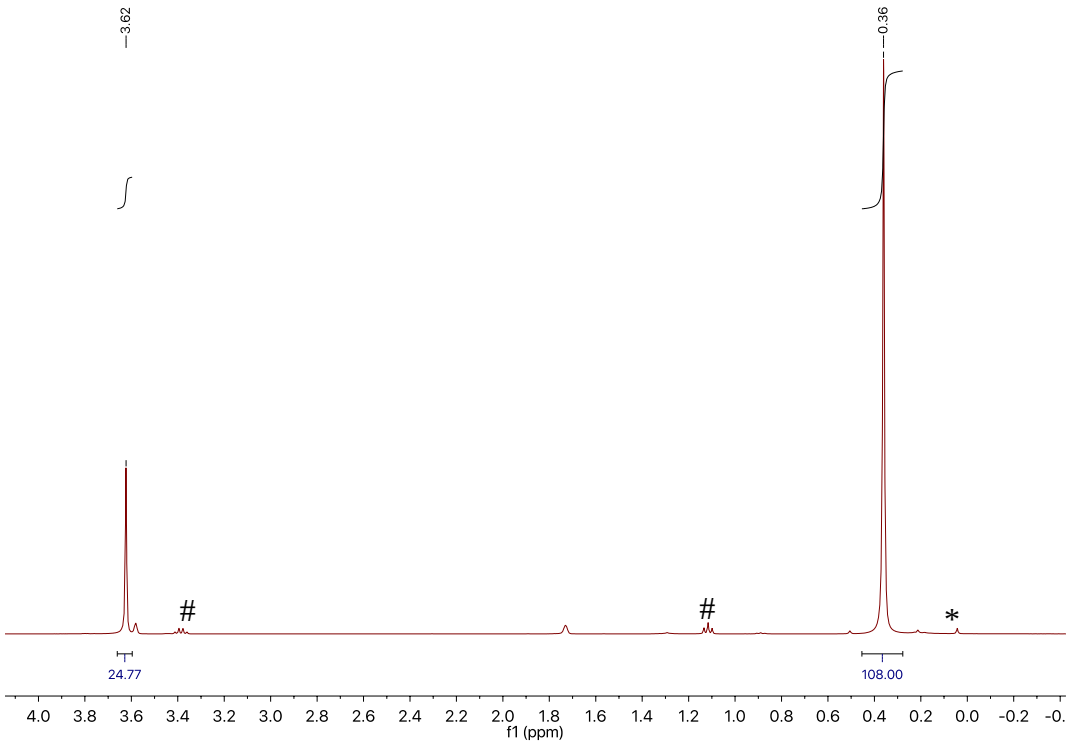

Figure A5.1. ^{1}H NMR spectrum of **[Na][5.1]** in THF-d_8. (*) indicates the presence of $HN(SiMe_3)_2$ and (#) indicates the presence of Et_2O.

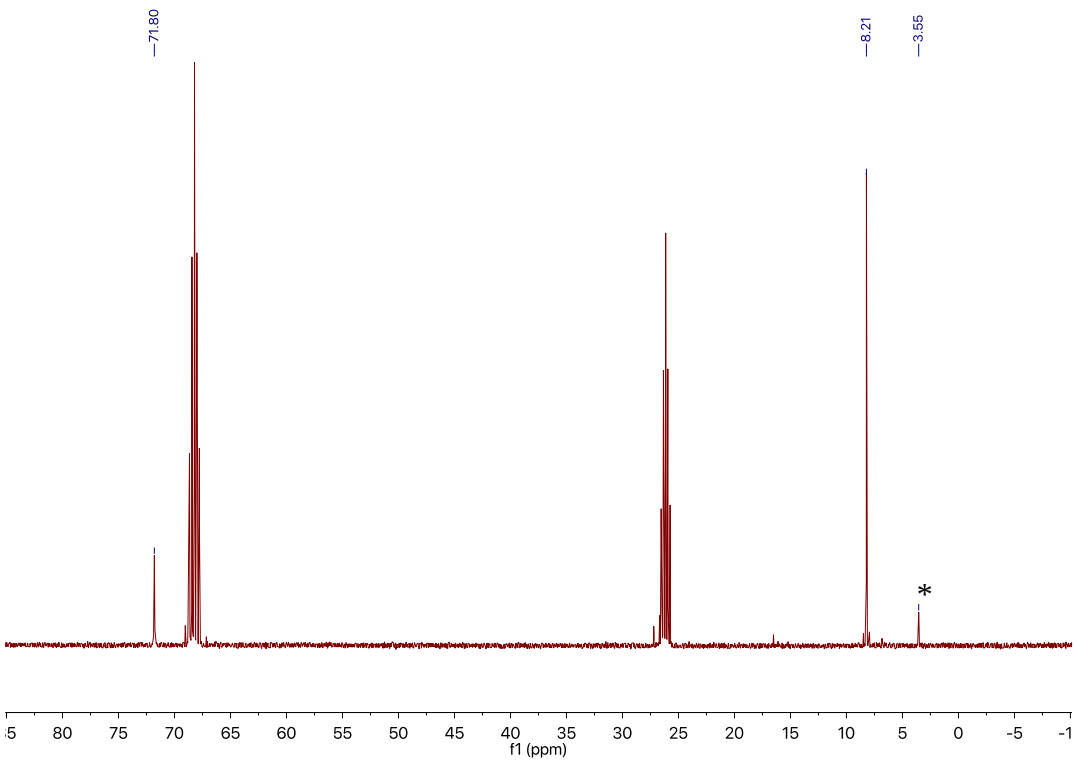

Figure A5.2. ^{13}C NMR spectrum of **[Na][5.1]** in THF-d_8. (*) indicates the presence of $HN(SiMe_3)_2$.

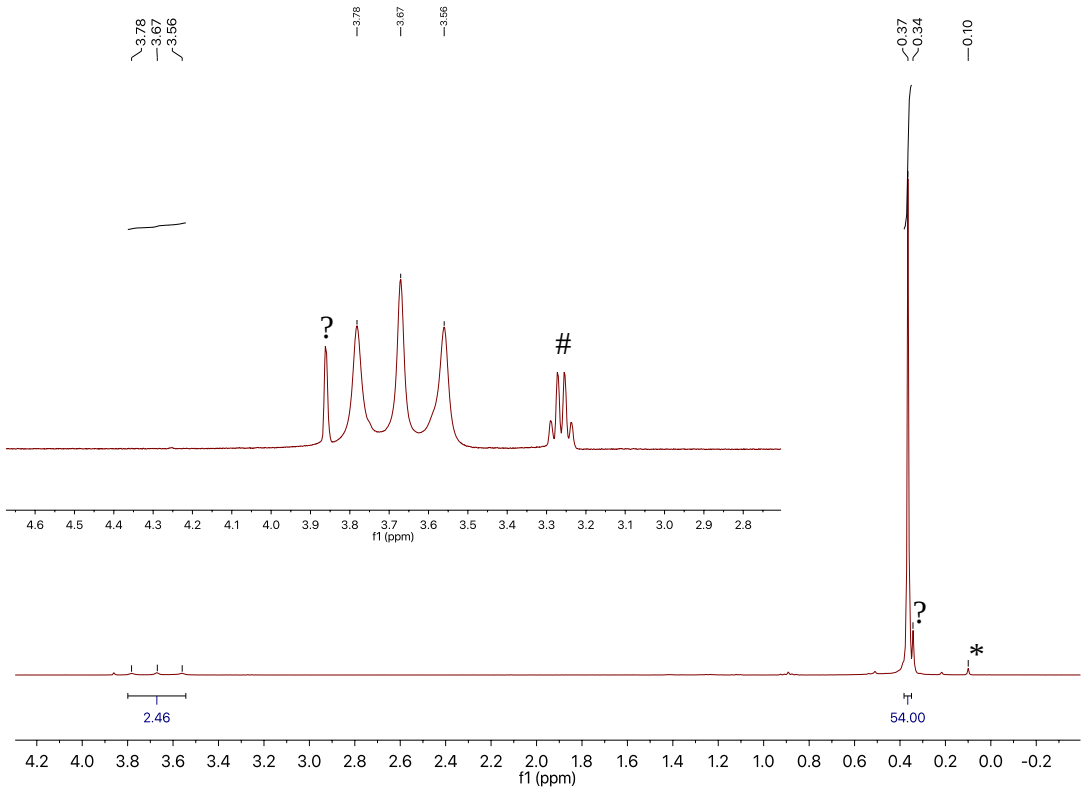

Figure A5.3. ^{1}H NMR spectrum of **5.2** in C_6D_6. The inset highlights the -NH_2 resonance. (*) indicates the presence of $HN(SiMe_3)_2$, (#) indicates the presence of Et_2O, and (?) indicates the presence of unidentified products.

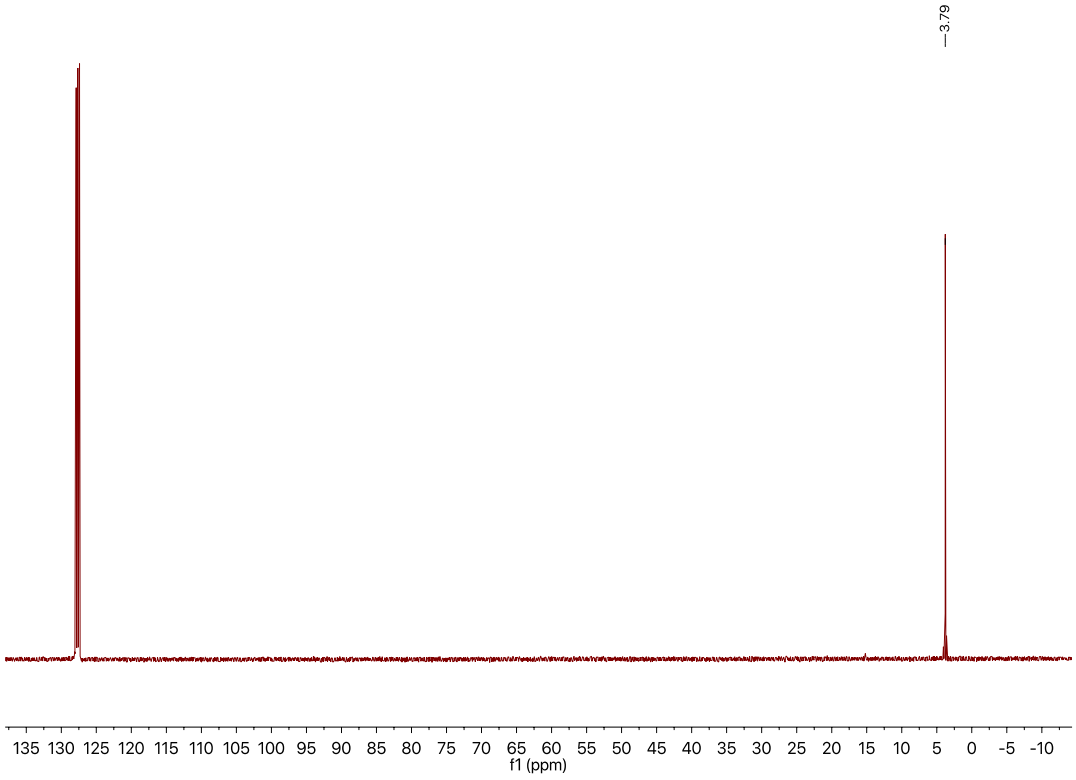

Figure A5.4. ^{13}C NMR spectrum of **5.2** in C_6D_6.

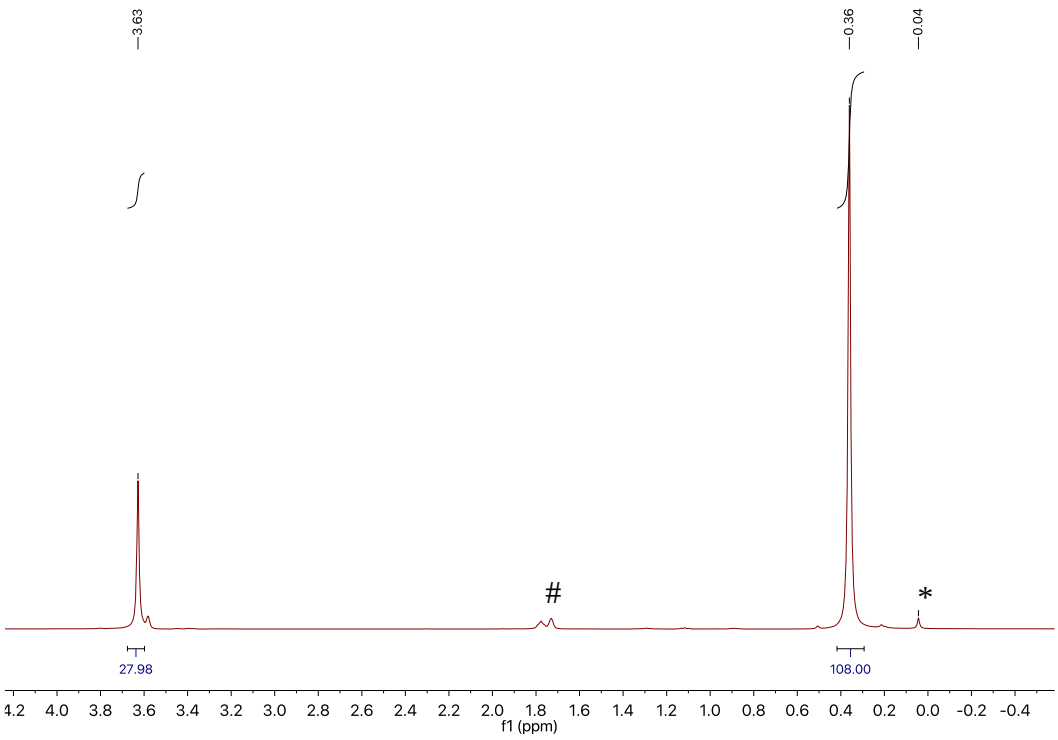

Figure A5.5. ^{1}H NMR spectrum of **[K][5.1]** in THF-d_8. (*) indicates the presence of $HN(SiMe_3)_2$ and (#) indicates the presence of THF-h_8.

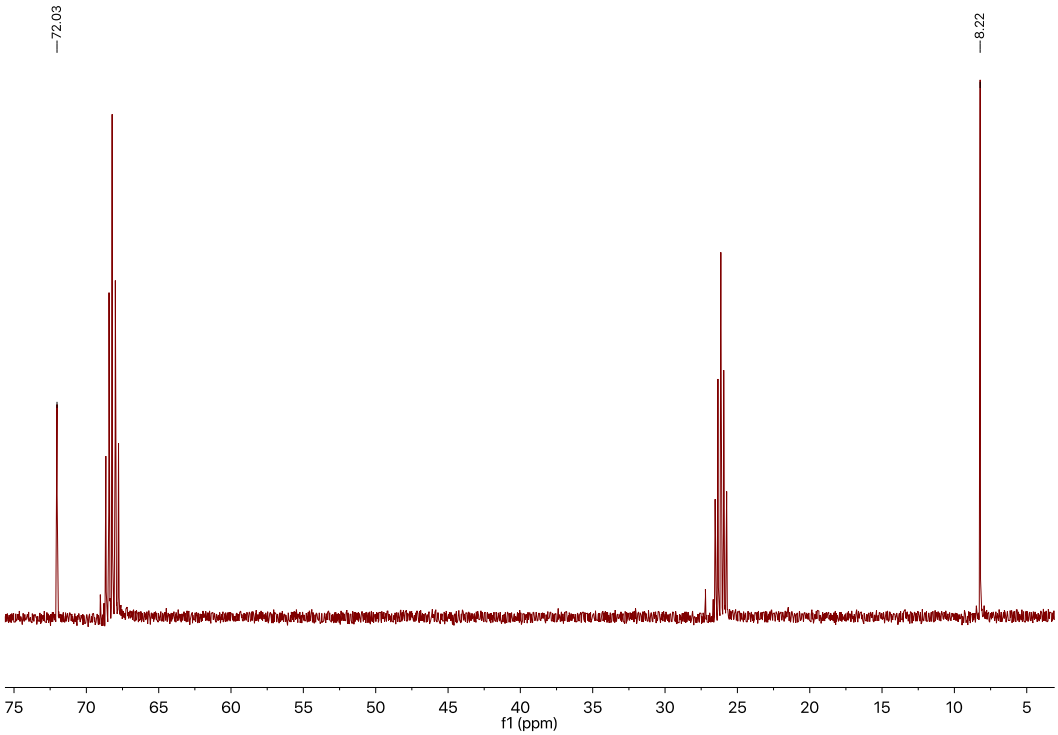

Figure A5.6. ^{13}C NMR spectrum of **[K][5.1]** in THF-d_8.

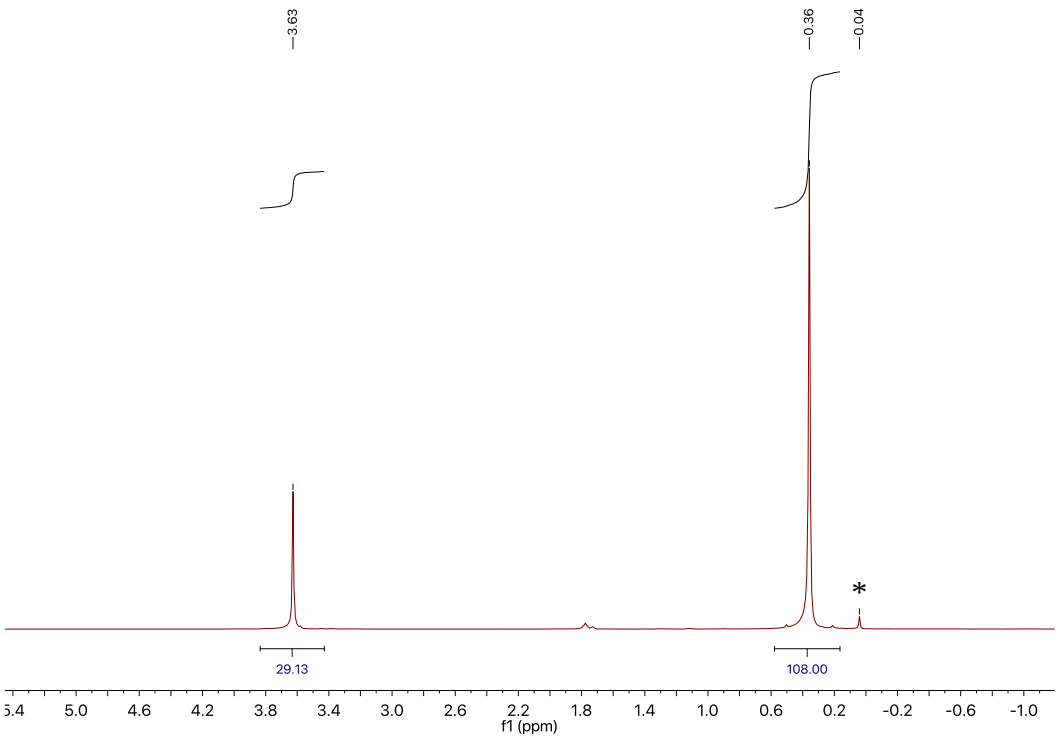

Figure A5.7. ^{1}H NMR spectrum of **[K][5.1-^{15}N]** in THF-d_8. (*) indicates the presence of $HN(SiMe_3)_2$.

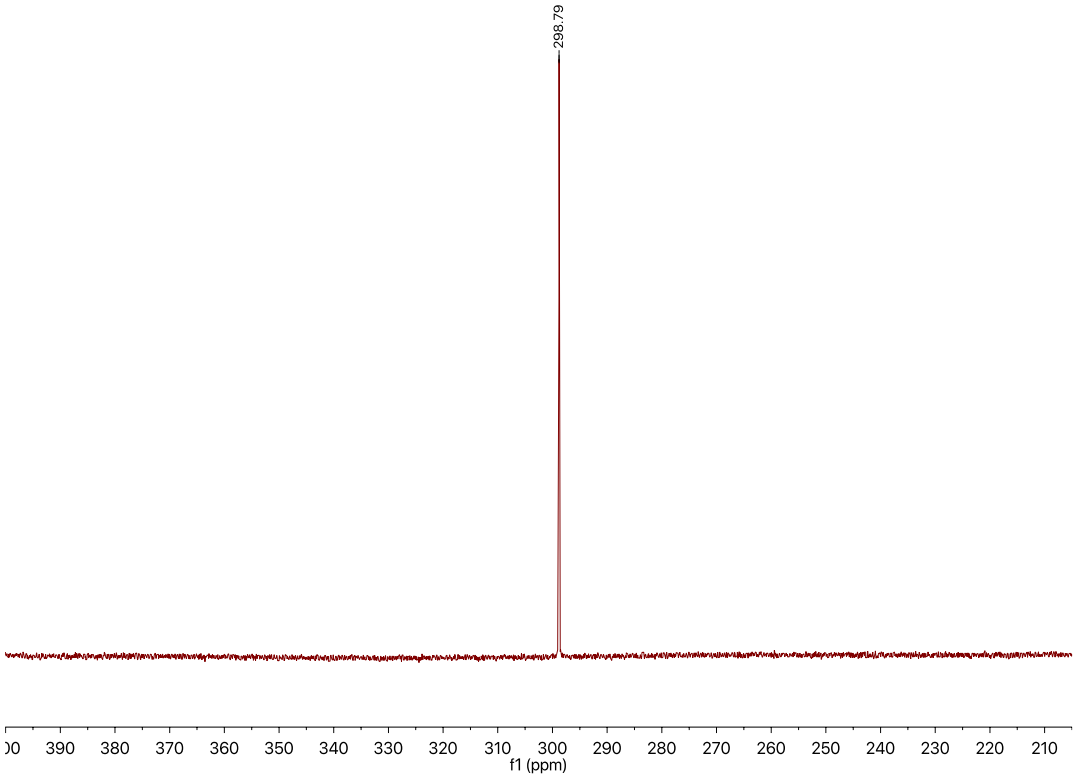

Figure A5.8. $^{15}N\{^{1}H\}$ NMR spectrum of **[K][5.1-^{15}N]** in THF-d_8.

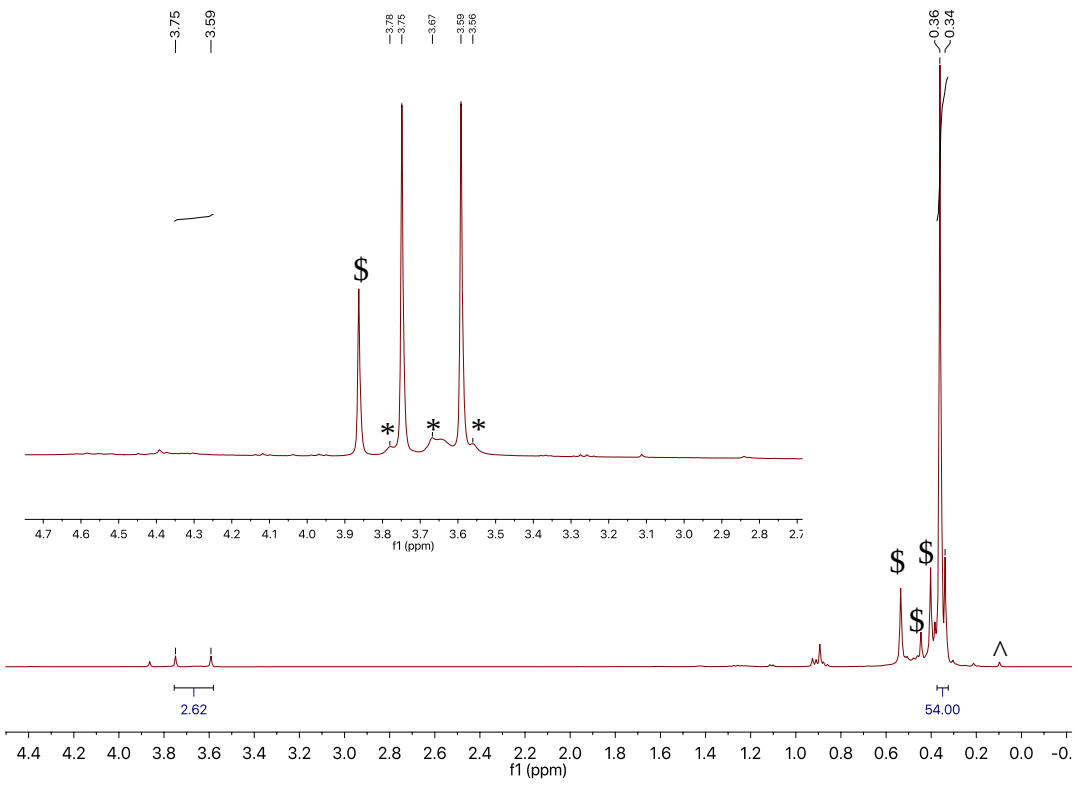

Figure A5.9. ^{1}H NMR spectrum of **5.2-^{15}N** in C_6D_6. The inset highlights the -NH_2 resonance. (*) indicates resonances assignable to a small amount of the ^{14}N isotopomer, ($) indicates the presence of unidentified products, and (^) indicates the presence of $HN(SiMe_3)_2$.

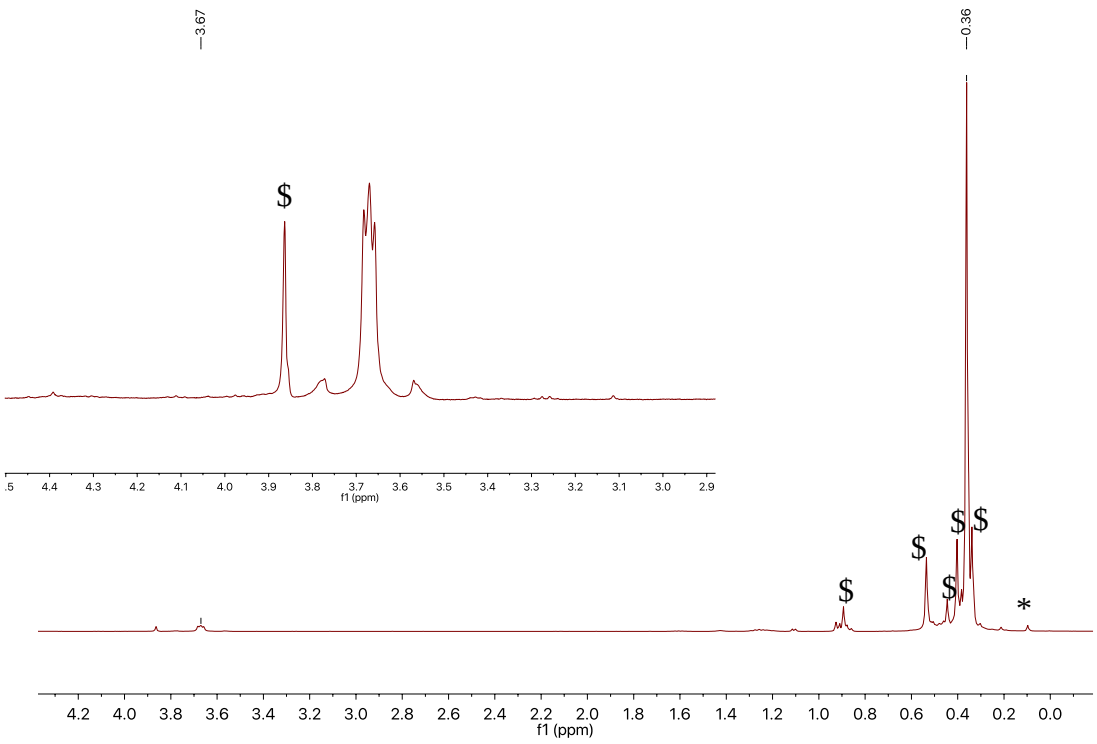

Figure A5.10. $^{1}H\{^{15}N\}$ NMR spectrum of **5.2-^{15}N** in C_6D_6. The inset highlights the -NH_2 resonance. ($) indicates the presence of unidentified products and (*) indicates the presence of $HN(SiMe_3)_2$.

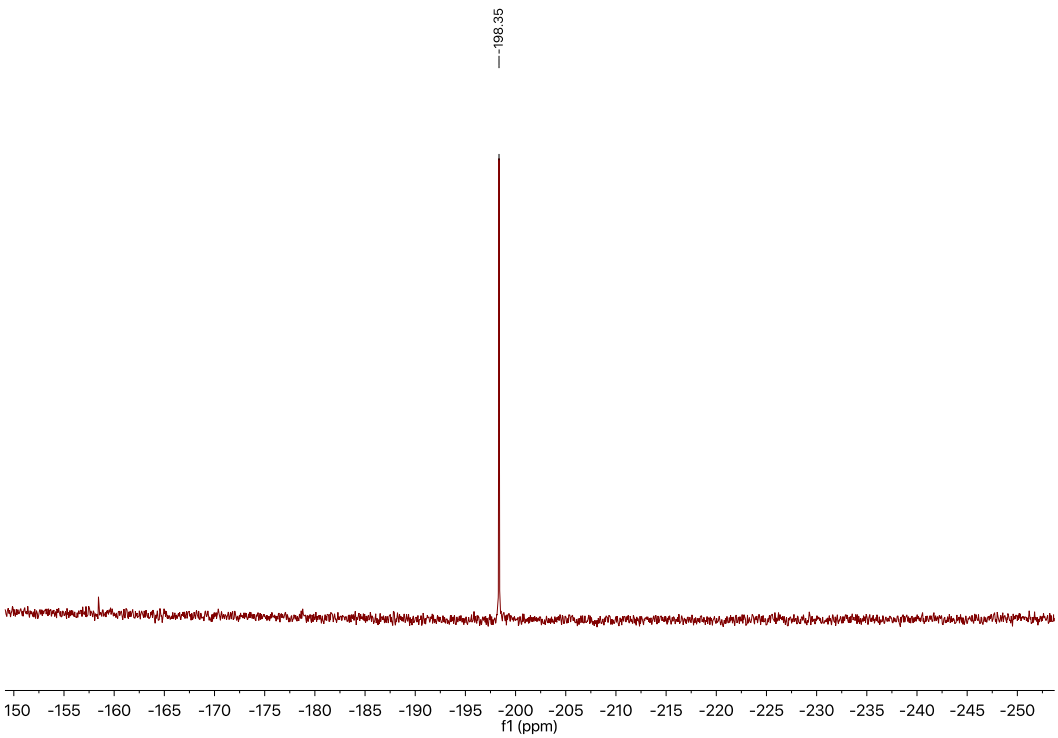

Figure A5.11. $^{15}N\{^{1}H\}$ NMR spectrum of **5.2-^{15}N i**n C_6D_6.

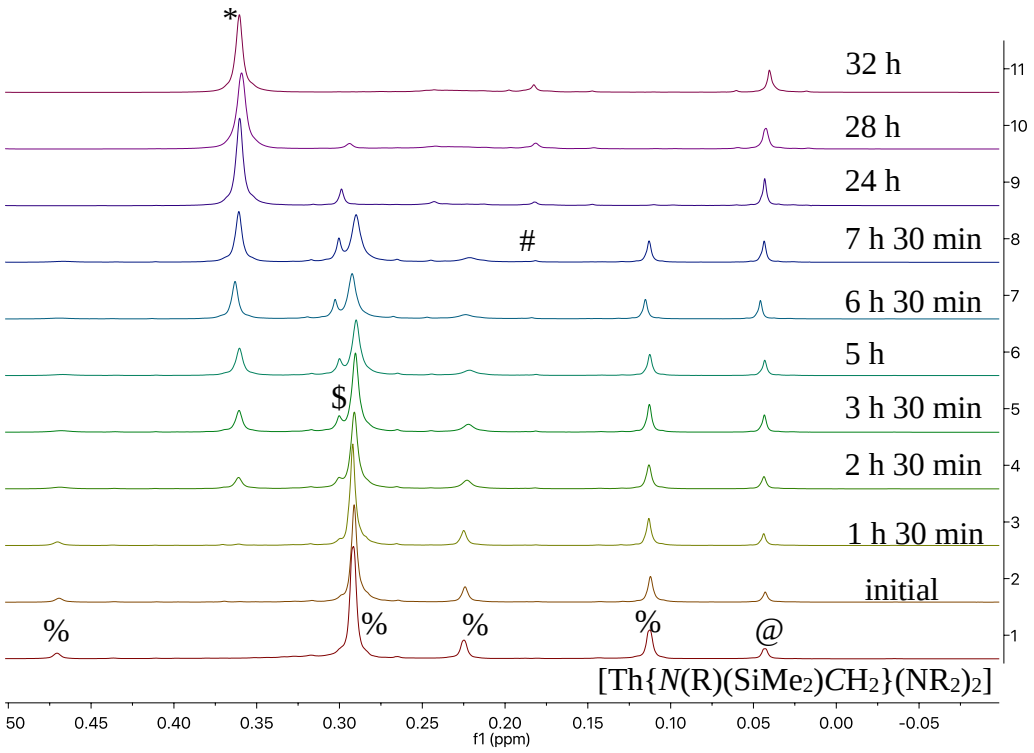

Figure A5.12. Partial *in situ* ^{1}H NMR spectrum of the reaction of [Th{*N*(R)(SiMe$_2$)*C*H$_2$}(NR$_2$)$_2$] (R = SiMe$_3$) with 1 equiv of NaNH$_2$ and 18-crown-6 in THF-d_8 over the course of 32 h. (*) indicates the presence of **[Na][5.1]**, (%) indicates the presence of [Th{*N*(R)(SiMe$_2$)*C*H$_2$}(NR$_2$)$_2$], (#) indicates the presence of [Na(THF-d_8)$_x$][Th{*N*(R)(SiMe$_2$*C*H$_2$)}$_2$(NR$_2$)], ($) indicates the presence of **5.2**, and (@) indicates the presence of HN(SiMe$_3$)$_2$.

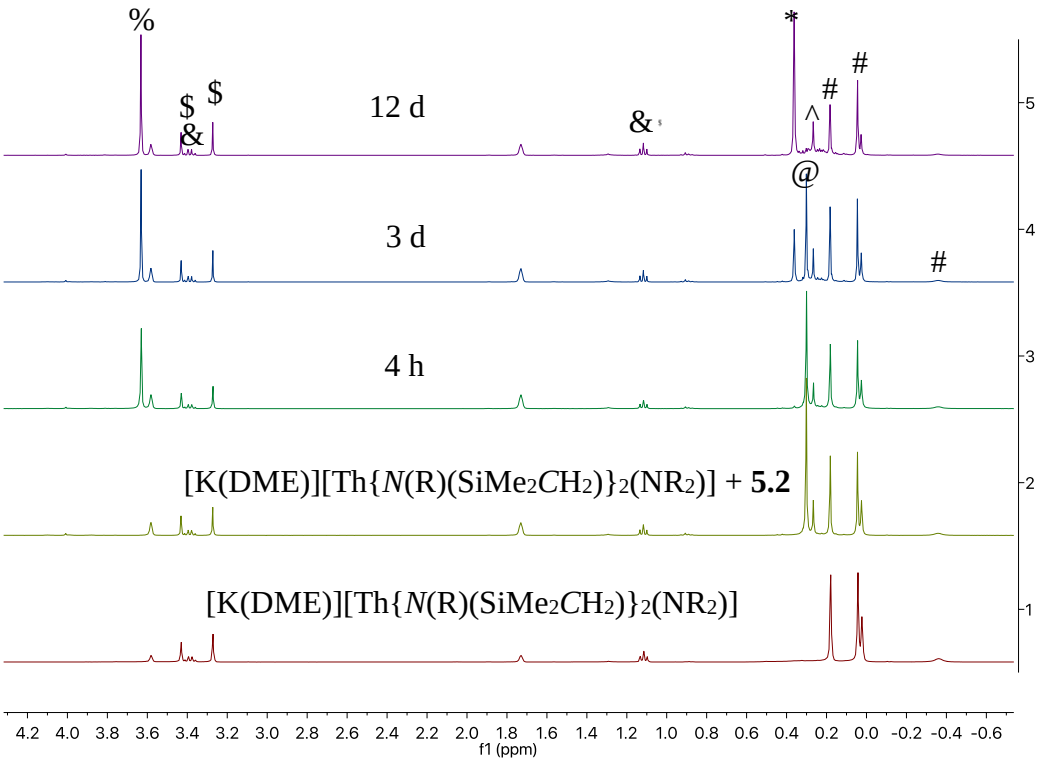

Figure A5.13. Partial *in situ* ^{1}H NMR spectrum of the reaction of [K(DME)][Th{*N*(R)(SiMe$_2$*C*H$_2$)}$_2$(NR$_2$)] (R = SiMe$_3$) with **5.2** and 18-crown-6 in THF-d_8 over 12 d. (*) indicates the presence of **[K][5.1]**, (@) indicates the presence of **5.2**, (#) indicates the presence of [K(DME)][Th{*N*(R)(SiMe$_2$*C*H$_2$)}$_2$(NR$_2$)], (%) indicates the presence of 18-crown-6, ($) indicates the presence of DME, (&) indicates the presence of Et$_2$O, and (^) indicates the presence of an unidentified product.

5.6.3 IR Spectra

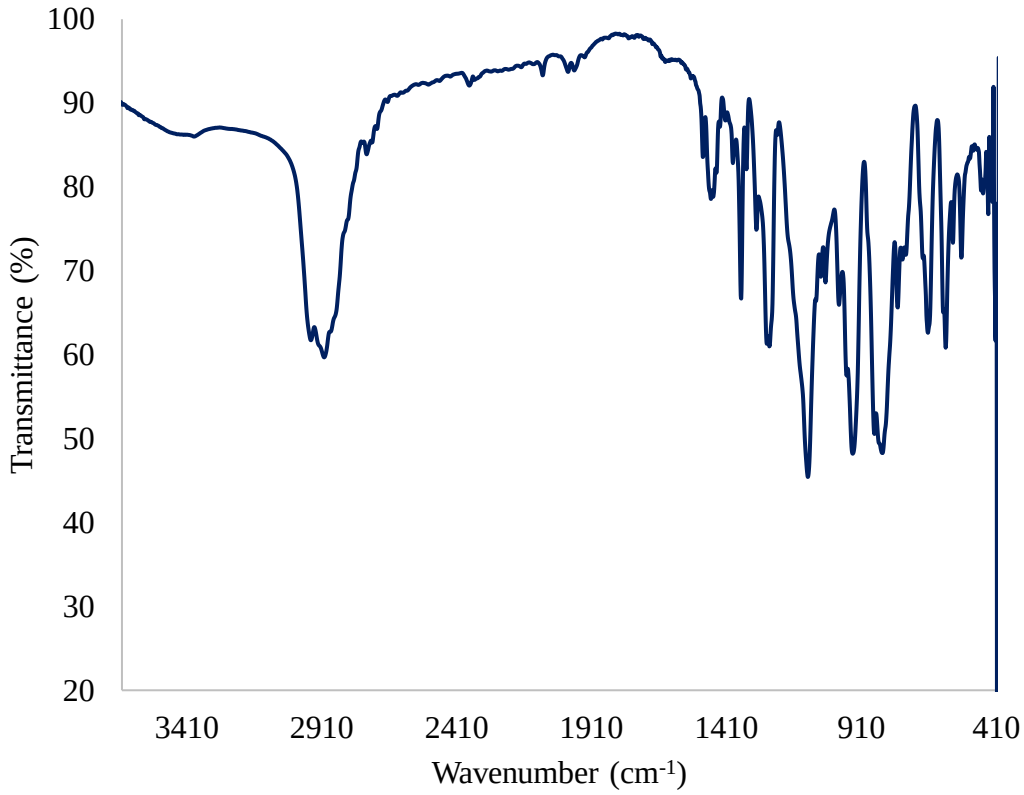

Figure A5.14. IR spectrum of **[Na][5.1]** (KBr pellet).

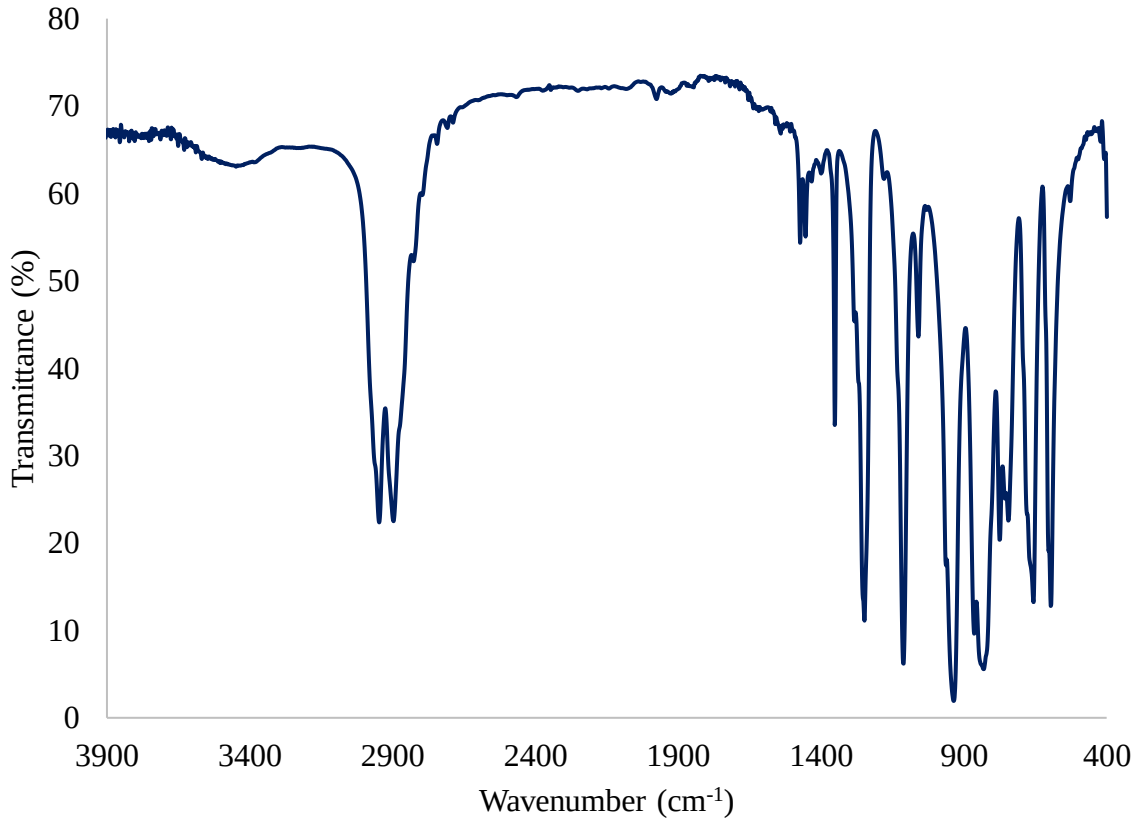

Figure A5.15. IR spectrum of **[K][5.1]** (KBr pellet).

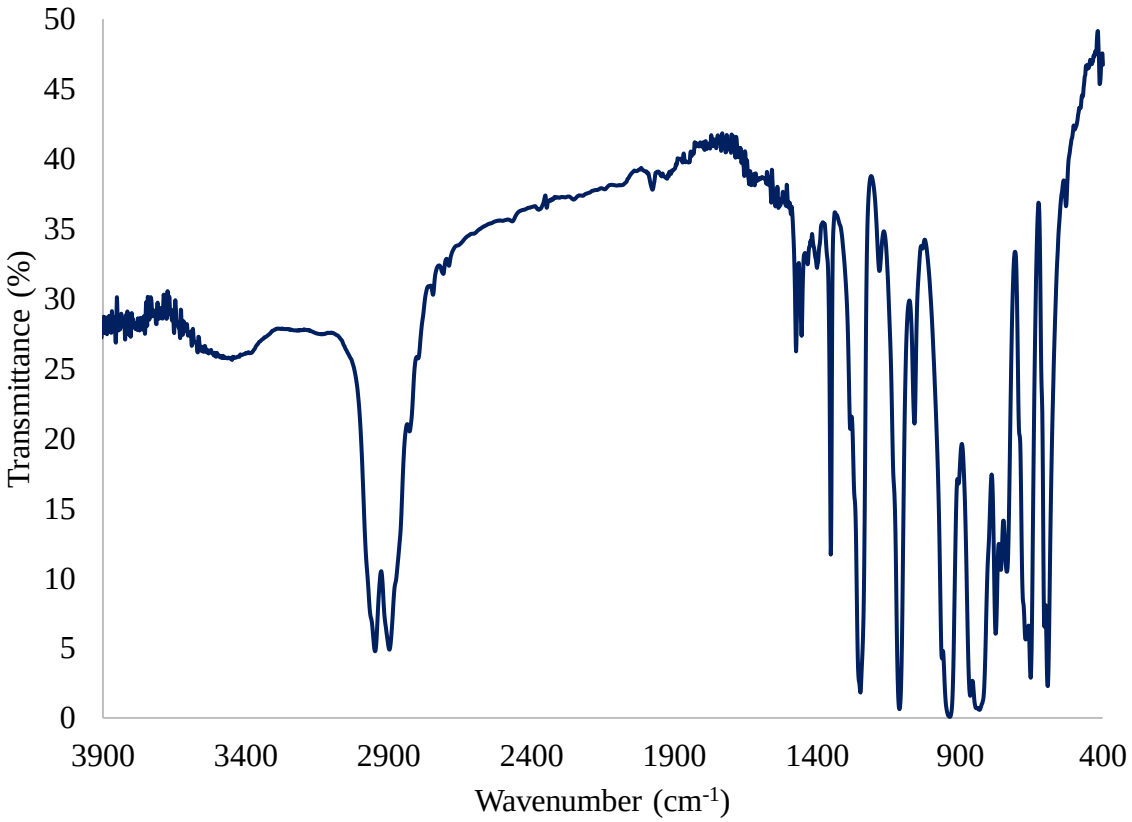

Figure A5.16. IR spectrum of **[K][5.1-^{15}N]** (KBr pellet).

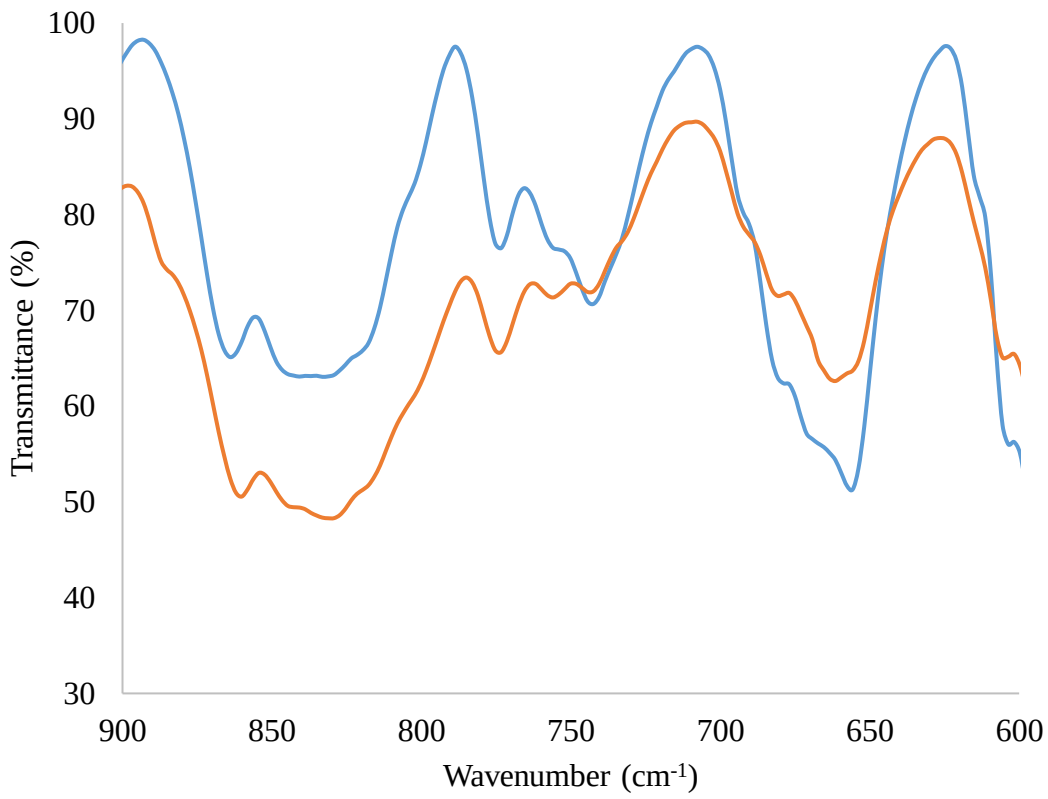

Figure A5.17. Partial IR spectrum of **[Na][5.1]** (orange) and **[K][5.1]** (blue) (KBr pellet).

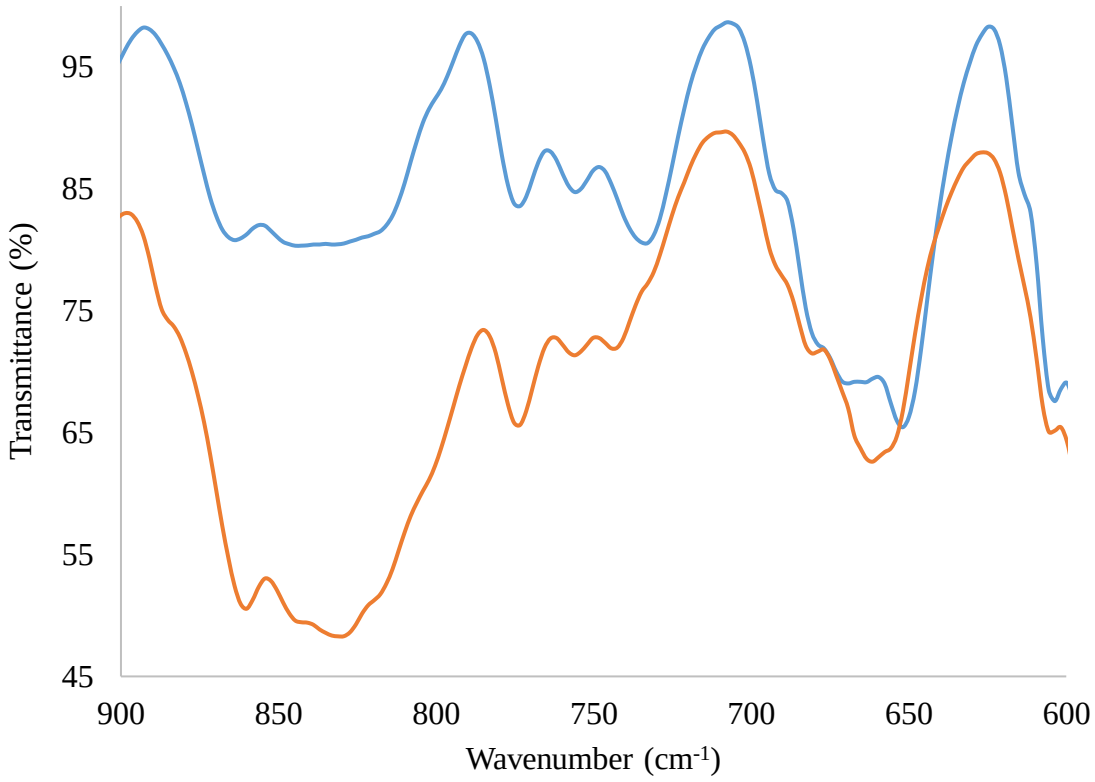

Figure A5.18. Partial IR spectra of **[Na][5.1]** (orange) and **[K][5.1-^{15}N]** (blue) (KBr pellet).

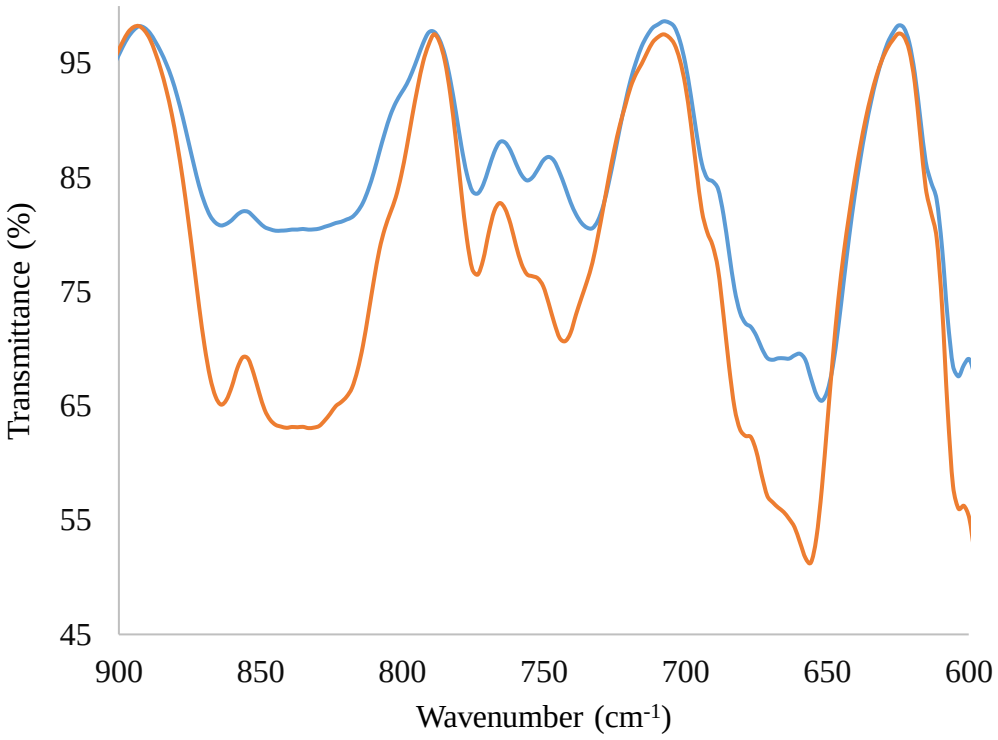

Figure A5.19. Partial IR spectra of **[K][5.1]** (orange) an**d [K][5.1-^{15}N]** (blue) (KBr pellet).

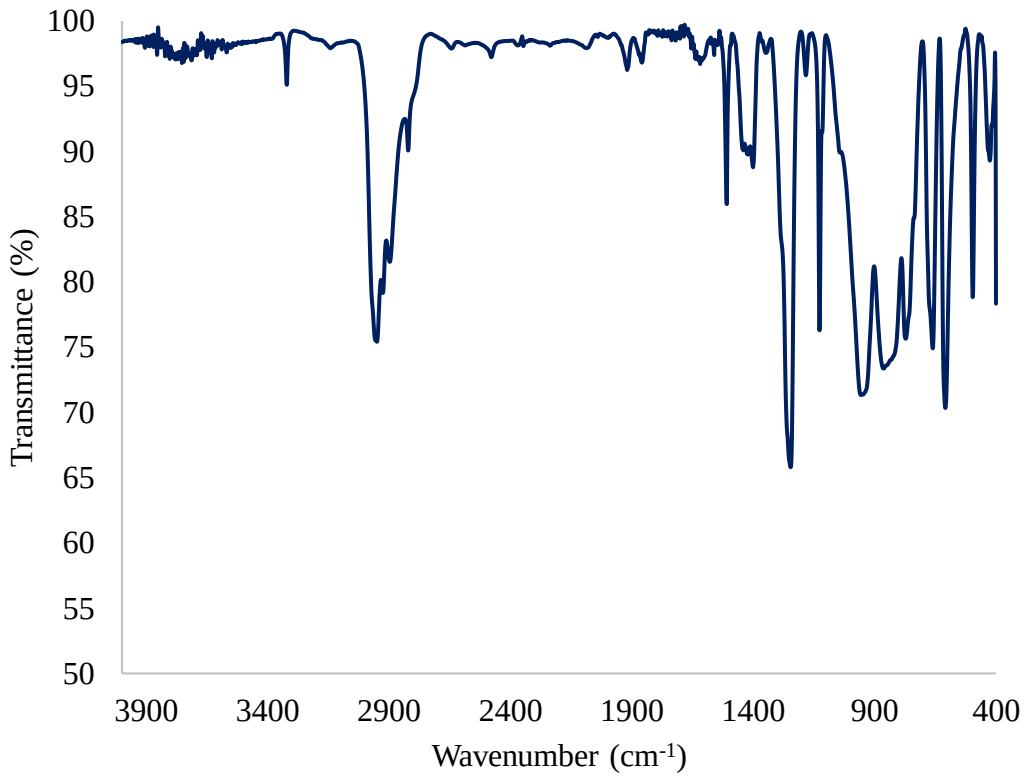

Figure A5.20. IR spectrum of **5.2** (KBr pellet).

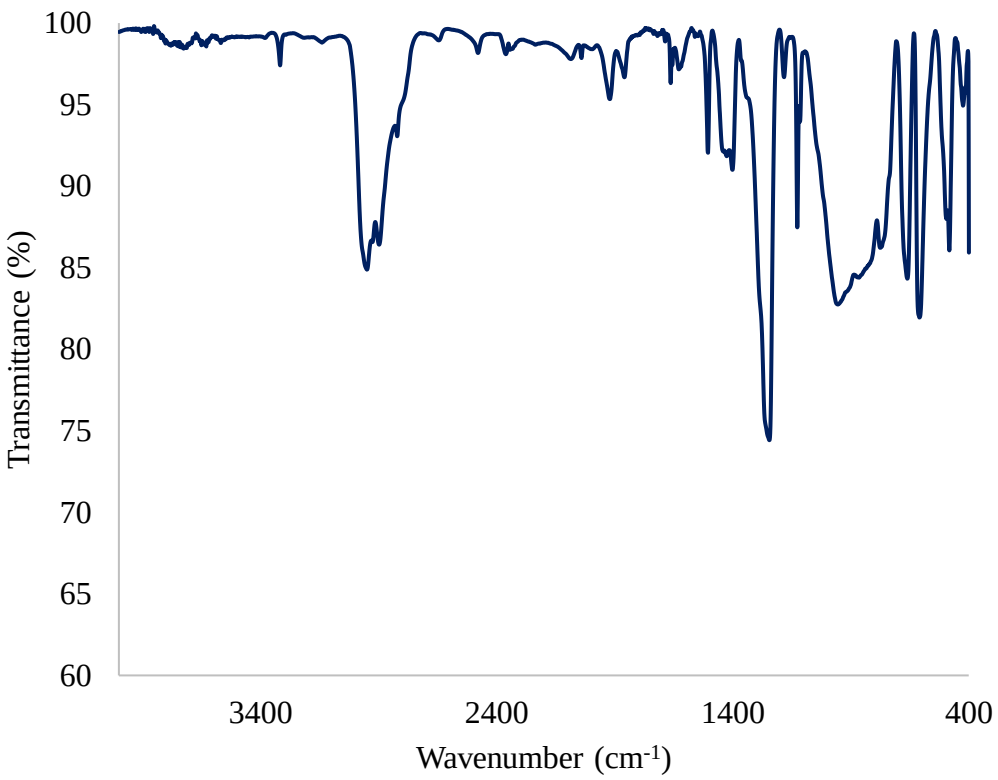

Figure A5.21. IR spectrum of **5.2-^{15}N** (KBr pellet).

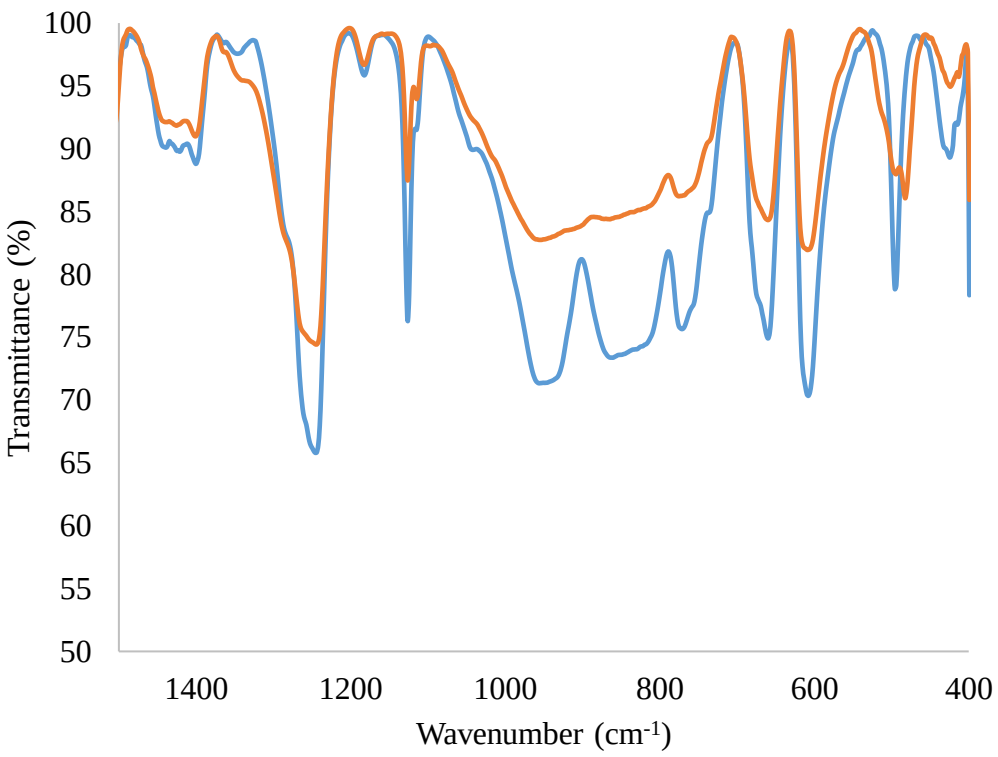

Figure A5.22. Partial IR spectra of **5.2-^{15}N** (orange) and **5.2** (blue) (KBr pellet).

5.6.4 Computational Details

The structures were fully optimized with density functional theory (DFT) using the Amsterdam Density Functional (ADF) package, version 2017.[63] The B3LYP[64-66] hybrid exchange-correlation functional was employed in conjunction with all-electron triple-ζ doubly polarized (TZ2P) basis sets for all atoms. Scalar-relativistic (SR) effects were treated with the all-electron zero-order regular approximation (ZORA) relativistic Hamiltonian.[67] An atom-pairwise correction for dispersion forces was included *via* Grimme's D3 model augmented with the Becke-Johnson (BJ) damping.[68, 69]

Nuclear shielding calculations were performed with ADF, at the DFT/ZORA-SR and DFT/spin-orbit (SO) ZORA levels. The PBE0[70, 71] and B3LYP hybrid exchange-correlation functionals were used, together with TZ2P basis sets for Th and N, and double-ζ polarized (DZP) basis sets for H, C and Si. Solvent effects were treated with the conductor-like screening model (COSMO).[72, 73] The ZORA-SO shielding calculations included the DFT exchange-correlation response.[74] The calculated nuclear shieldings (σ_{calc}, ppm) were converted to chemical shifts (δ_{calc}, ppm) relative to shielding of nitromethane (in nitromethane solvent) or ammonia (in ammonia solvent), calculated at the same level.

The equilibrium geometries obtained with ADF were subjected to Gaussian 16 (G16)[75] single-point DFT/B3LYP calculations, that used the def2-TZVP[63] basis set for N, the def2-SVP[76] basis sets for H, C and Si, and the small-core ECP60MDF pseudopotential with the associated [14s13p10d8f6g]/[6s6p5d4f3g] valence pseudo-orbital basis set for Th.[77] The results were used for natural localized molecular orbital (NLMO) analyses, performed with the NBO6 package.[78] Vibrational frequency calculations were conducted, with G16, on top of fully re-optimized geometries using the aforementioned computational details.

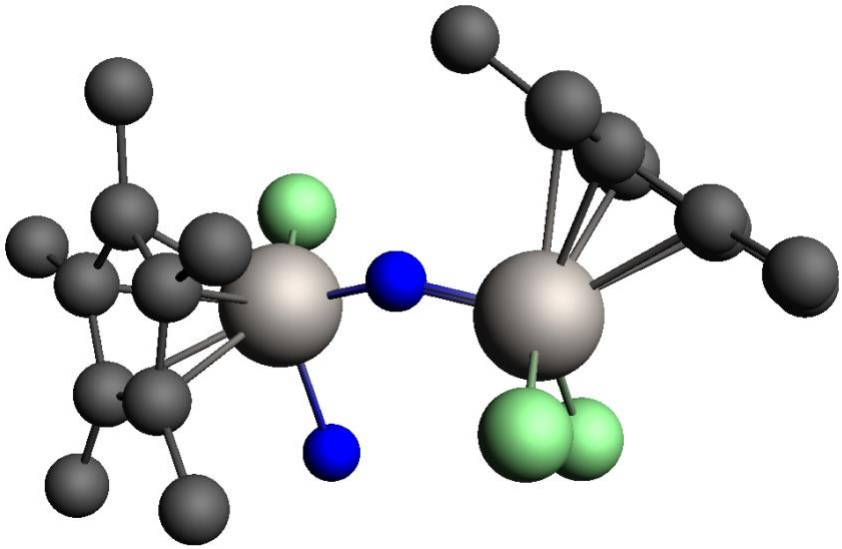

Figure A5.23. Optimized structure of [{Cp*TiCl$_2$}(μ-N){Cp*TiCl(NH$_3$)}] at the DFT/B3LYP/TZ2P level of theory (using ADF). Hydrogen atoms omitted for clarity. Color code: Ti light gray, N blue, Cl green, C dark gray. Cartesian coordinates are printed below.

Ti	-0.73149487	-0.76769287	1.45060032
Ti	1.09376293	1.14321788	-0.74062345
C	0.36391051	0.53287718	-3.96788162
Cl	-0.00729108	0.60274460	3.19290028
Cl	-0.01433096	3.11473285	-1.09450434
N	0.00000000	0.00000000	0.00000000
N	2.12891761	1.77680256	1.06844488
H	1.47565952	1.60075703	1.84295445
H	2.97718848	1.26129417	1.27603474
H	2.35685541	2.76565719	1.05574511

C	-2.71880292	-2.01671347	1.99735998
C	-2.58192621	-1.96540850	0.58001517
C	-2.72044944	-0.61310980	0.17118451
C	-2.89405901	0.17749554	1.33701156
C	-2.91493829	-0.69504050	2.46409649
H	-0.47135616	-0.10026750	-3.67353501
H	0.70802140	0.19219971	-4.94805953
H	-0.01382530	1.54772939	-4.08249809
C	2.50433304	2.81009715	-3.45263126
H	1.51224854	3.20063312	-3.67228753
H	3.03842213	2.69619191	-4.39990202
H	3.02828228	3.56459629	-2.86753098
C	4.48823386	1.80677120	-1.18988020
C	-2.73624984	-0.10761609	-1.23262717
H	-2.30432352	0.88880351	-1.29937972
H	4.28676827	2.87541224	-1.10706231
H	-2.16602567	-0.75855912	-1.89240492
C	-3.05956332	1.66379884	1.36304862
H	-2.47209407	2.14124512	0.57995742
H	-2.73865446	2.07936080	2.31631869
H	-4.10663436	1.94086077	1.21254062
C	-3.16917421	-0.29379814	3.88063009
H	-4.23824515	-0.34845130	4.10368375

H	-2.83746911	0.72395811	4.07221897
H	-2.65039658	-0.94512197	4.58223537
C	2.90647575	-0.26489057	-1.33656969
C	1.79406969	-0.63225507	-2.13233734
C	1.47398626	0.47454577	-2.96562843
C	2.43016136	1.50488664	-2.72925655
C	3.30754278	1.05325082	-1.71725310
C	3.55609305	-1.14348640	-0.31270883
H	4.20712859	-1.88039467	-0.79018961
H	2.81641500	-1.68757352	0.27418713
H	4.18114442	-0.57457959	0.37681385
C	1.11265873	-1.96028149	-2.10996684
H	5.34830131	1.69408097	-1.85483041
H	4.80194251	1.44420186	-0.21109331
H	0.09563111	-1.88753295	-2.48981648
Cl	0.51775607	-2.66894561	1.75285794
H	1.05840411	-2.36202832	-1.10043563
H	1.65189113	-2.67632271	-2.73608434
H	-3.76149525	-0.06088352	-1.60974901
C	-2.71061518	-3.25633082	2.83120728
H	-3.71300369	-3.69066770	2.88234090
H	-2.38721302	-3.05044485	3.85034810
H	-2.03936771	-4.00703275	2.41900065

C	-2.39493960	-3.14423526	-0.32033482
H	-1.89630473	-2.86153349	-1.24571874
H	-3.35991263	-3.58568136	-0.58424354
H	-1.79252025	-3.91464355	0.15723615

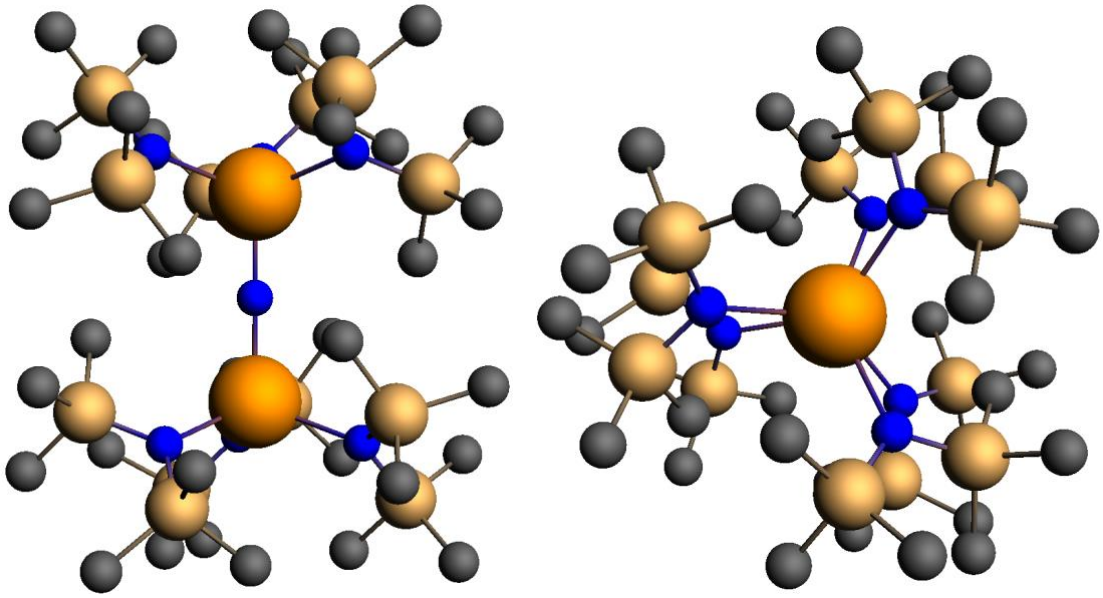

Figure A5.24. Views along the Y-axis (left) and along the Z-axis (right) of the optimized geometry of $[(R_2N)_3Th(\mu\text{-}N)Th(NR_2)_3]^-$ (R = $SiMe_3$) at the DFT/B3LYP/TZ2P level of theory (using ADF). Hydrogen atoms omitted for clarity. Color code: Th orange, N blue, Si beige, C gray. Cartesian coordinates are printed below.

C	-3.39744725	2.90662531	3.24687966
H	-4.29280930	2.68375624	2.66416894
H	-2.66330788	3.33341724	2.56512363
H	-3.65437673	3.67073877	3.98464860
C	2.48061434	4.38855580	1.71797027
H	3.05707116	3.80740233	1.00135507
H	3.12440676	4.60259331	2.57219026
H	2.22451257	5.34096852	1.25079913
C	0.06687792	4.63229118	3.49101510

H	-0.88874738	4.23388133	3.82735238
H	-0.12853462	5.58751370	2.99584088
H	0.67492363	4.83260100	4.37190190
C	-0.26767066	3.31938151	0.82632502
H	0.15515836	2.80861711	-0.03412515
H	-0.59276996	4.31203600	0.50684929
H	-1.17432199	2.77780156	1.10268500
C	2.70837477	3.19646516	5.25704869
H	2.96946862	4.13007263	4.76002613
H	3.50300966	2.96850567	5.97243476
H	1.78940854	3.35827116	5.82203123
C	4.20803994	1.49980070	3.25344874
H	4.21493168	0.64615817	2.57717172
H	4.99545348	1.34620702	3.99550142
H	4.46332597	2.38340381	2.66623998
C	2.18505812	0.27620273	5.21881162
H	1.98825433	-0.65479009	4.69324421
H	1.32404689	0.49931026	5.85035633
H	3.04481787	0.11133943	5.87241679
C	3.00854583	-1.43229765	0.83283145
H	2.35254544	-1.54036790	-0.02630812
H	4.02906562	-1.65239850	0.51161108
H	2.99868642	-0.37622285	1.10913084

C	3.97341817	-2.37465494	3.50100172
H	4.10652985	-1.34712157	3.83526019
H	4.89900131	-2.68502324	3.00816020
H	3.84062100	-2.99931931	4.38299499
C	2.55451436	-4.34476199	1.72871415
H	3.50645607	-4.60103547	1.26065669
H	1.76181028	-4.55323835	1.01332578
H	2.41808390	-5.00790866	2.58408284
C	-0.81372974	-4.38567691	3.26063239
H	-1.34373667	-4.98804062	4.00259564
H	-0.17612034	-5.05142992	2.67662389
H	-1.55357806	-3.96485583	2.58134279
C	-2.89905428	1.64193606	-0.82793081
H	-2.61141124	1.04417211	0.03225450
H	-3.66425305	2.35270387	-0.50810065
H	-2.02803389	2.23858145	-1.10550554
C	2.20067440	-0.08480501	-5.21960152
H	1.92013380	0.82452521	-4.69394289
H	1.36429739	-0.38319719	-5.85330131
H	3.04366277	0.15696528	-5.87107437
C	4.32200788	-1.13223758	-3.25339153
H	4.25593650	-0.28246533	-2.57546369
H	5.09436512	-0.91123210	-3.99422082

H	4.65064492	-1.99213466	-2.66734195
C	2.97453175	-2.94871502	-5.25942085
H	2.07293908	-3.18864267	-5.82479215
H	3.31474857	-3.85680364	-4.76289045
H	3.74680108	-2.65302777	-5.97447179
C	0.01610005	-3.32937933	-0.83135918
H	0.39324731	-2.78439316	0.02936568
H	-0.22214942	-4.34653532	-0.51245016
H	-0.93386569	-2.86802007	-1.10791093
C	2.84484488	-4.16219162	-1.72116964
H	3.37049280	-3.53545626	-1.00390954
H	3.50482767	-4.32225105	-2.57487032
H	2.66781157	-5.13257432	-1.25421965
C	-1.03828953	1.94908999	-5.21796480
H	-0.36140019	1.37287451	-5.85037614
H	-1.66832294	2.55766963	-5.87074480
H	-1.68596778	1.25251896	-4.69166044
C	-1.19262619	4.30721580	-3.24784803
H	-1.89176217	3.82343732	-2.56728363
H	-1.77430102	4.86400224	-3.98669581
H	-0.61188266	5.02339953	-2.66419705
C	1.05033396	4.05530414	-5.25911758
H	1.66985463	4.80142531	-4.76289169

H	0.40547139	4.57958794	-5.96936565
H	1.70539494	3.39576711	-5.83005741
C	2.87173034	1.68237804	-0.83693650
H	2.21238721	1.73521284	0.02478509
H	3.87181208	1.98586740	-0.51939880
H	2.94853224	0.62912790	-1.11379654
C	3.74851702	2.70539997	-3.50510713
H	3.97050306	1.69228651	-3.83603151
H	4.64430367	3.09747635	-3.01555670
H	3.55963899	3.31258780	-4.38909190
C	2.17366179	4.54789707	-1.72804061
H	1.97950766	5.19802486	-2.58217184
H	3.10252503	4.88226420	-1.26286140
H	1.36876695	4.68877643	-1.00990935
N	0.00000000	0.00000000	0.00000000
N	-2.28536006	0.16000544	2.90637995
N	1.27360889	1.90575245	2.90125991
N	1.01079346	-2.05315943	2.90602888
N	1.43336039	-1.78759380	-2.90336918
N	0.82409715	2.13643910	-2.90520269
Si	0.92663366	3.47426547	2.27016252
Si	2.52713506	1.73158670	4.07449207
Si	2.54242876	-2.54083367	2.27803946

Si	0.23025701	-3.04721698	4.08067495
Si	2.66758959	-1.50573618	-4.07600556
Si	1.22026000	-3.38050765	-2.27453513
Si	-0.04172646	3.06439274	-4.07457613
Si	2.31078718	2.74993902	-2.27957337
Th	-0.00012511	0.00093583	2.10931023
Th	0.00000000	-0.00000000	-2.10936850
C	-4.22541904	1.89317323	-3.49304779
H	-4.65808687	1.42844703	-4.37762783
H	-5.01257763	2.47051354	-3.00013286
H	-3.46044148	2.59386136	-3.82310546
C	1.40471640	-3.93945569	5.26465261
H	0.80757783	-4.51199420	5.97937331
H	2.08147907	-4.63432904	4.76868667
H	2.00559411	-3.22608642	5.83042380
C	-1.32829846	1.76889374	5.21955146
H	-1.09484697	0.91292459	5.85429780
H	-0.42206137	2.05836080	4.69360009
H	-1.61270937	2.59929688	5.87001371
C	-0.85513066	-2.01774146	5.22382380
H	-0.22879400	-1.38556260	5.85469121
H	-1.56030935	-1.37920049	4.69771000
H	-1.43082175	-2.67664041	5.87798998

Si	-3.47123895	-0.92673920	2.28167758
C	-2.74174249	-1.88827929	0.83979759
H	-2.51098669	-1.26922098	-0.02250392
H	-1.81978599	-2.40344604	1.11639387
H	-3.44002824	-2.66620262	0.52311826
C	-5.04216434	-0.04287645	1.72770236
H	-4.82925550	0.74427103	1.00761698
H	-5.73748013	-0.74460127	1.26388149
H	-5.54990960	0.40994573	2.58035396
C	-4.04090407	-2.24694857	3.50790091
H	-4.51776343	-1.81818158	4.38798119
H	-4.77016781	-2.89661106	3.01598239
H	-3.21655178	-2.87293559	3.84513003
Si	-3.54097615	0.62355572	-2.27200505
C	-5.02658959	-0.39971807	-1.72249405
H	-5.78257737	0.23456994	-1.25651555
H	-5.49085107	-0.89278508	-2.57760684
H	-4.74419386	-1.16765558	-1.00549452
Si	-2.75971818	1.33779802	4.07518258
C	-4.12125384	0.77036683	5.25914873
H	-5.06028103	0.52867549	4.76255703
H	-3.80404376	-0.10398515	5.82918616
H	-4.32066140	1.57658665	5.97010554

C	0.46305608	-4.60582733	-3.49782881
H	1.08817591	-4.75448800	-4.37698917
H	0.34666587	-5.57414151	-3.00319872
H	-0.52156249	-4.28848214	-3.83678271
N	-2.26431577	-0.35206539	-2.90227137
C	-3.13688380	-3.18278813	-3.25704574
H	-2.36864660	-3.54952049	-2.57791600
H	-4.04767317	-3.04068001	-2.67310120
H	-3.32798964	-3.96158216	-3.99947807
C	-4.03834218	-1.10680555	-5.26060918
H	-3.79633419	-0.20576536	-5.82592349
H	-4.16656783	-1.92371562	-5.97575736
H	-4.99545639	-0.94895055	-4.76485845
C	-1.17075258	-1.86451119	-5.22079919
H	-1.38464937	-2.71191344	-5.87632761
H	-1.00851511	-0.98857583	-5.85047936
H	-0.24410025	-2.08077241	-4.69529426
Si	-2.63494857	-1.56111600	-4.07676141

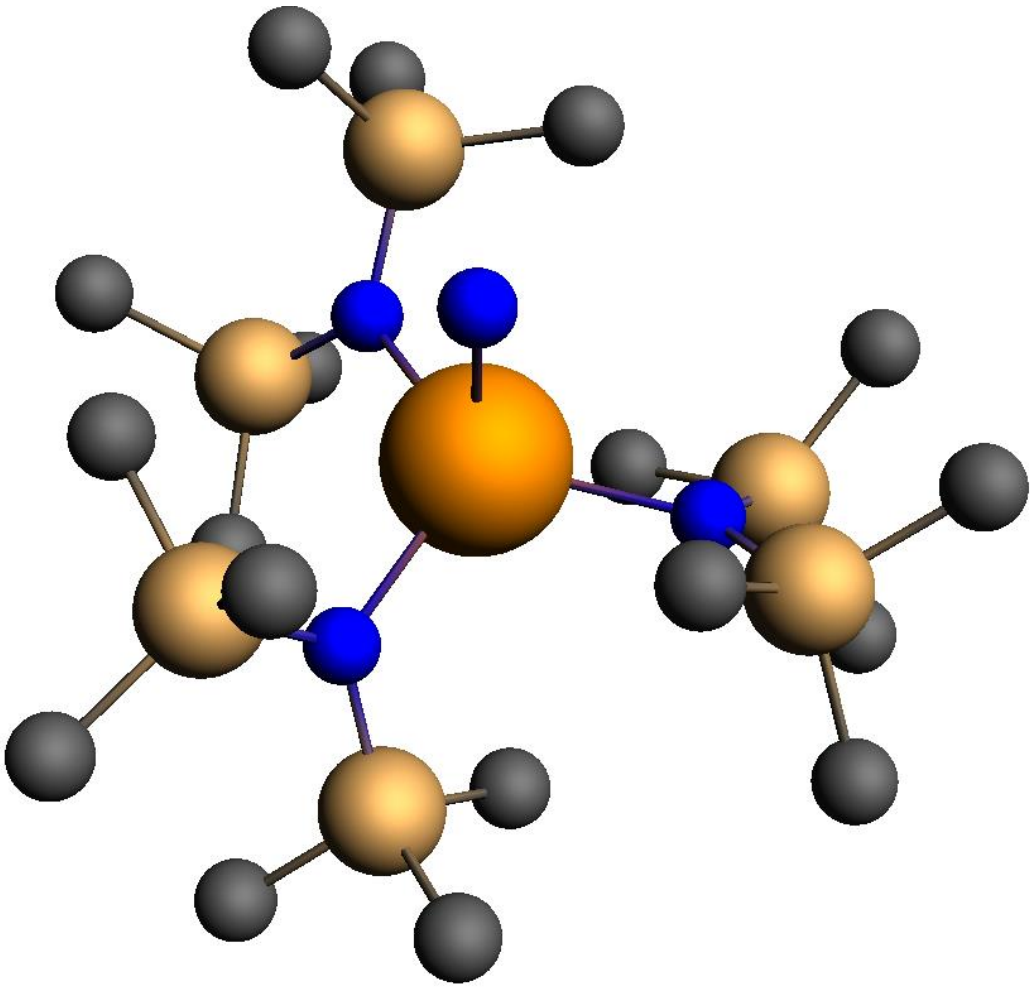

Figure A5.25. Optimized geometry of $[Th(NR_2)_3(NH_2)]$ (R = $SiMe_3$) at the DFT/B3LYP/TZ2P level of theory (using ADF). Hydrogen atoms omitted for clarity. Color code: Th orange, N blue, Si beige, C gray. Cartesian coordinates are printed below.

Si	-3.40923682	0.03406635	0.86176104
Si	1.70427757	-2.96230216	0.76361240
C	2.50736186	-4.52256301	0.08477690
N	0.84457288	2.13446981	-0.46502442
C	-0.98404181	4.50857923	-0.65391188

Th	0.00000000	0.00000000	0.00000000
N	0.00000000	0.00000000	2.25719717
C	-2.86371927	1.76711967	1.35846623
Si	-2.70977737	-1.77725729	-1.44827851
C	-3.56708913	-1.05342789	2.38918005
C	-3.80929108	-1.05148160	-2.79024498
C	-1.16544733	-2.37667679	-2.34843834
C	-3.56754911	-3.26939597	-0.69467257
N	-2.24633979	-0.61866836	-0.24844079
Si	2.61908714	-1.53243089	-1.77175930
C	-1.34737272	2.00335343	-2.37947630
C	2.60531942	-3.02054466	-2.92137236
C	2.00342689	-0.10185179	-2.84565481
C	4.39538203	-1.19166554	-1.26240718
N	1.58615983	-1.67023420	-0.39278386
C	0.94347267	3.89586971	-2.91763900
Si	2.35300542	2.63332949	0.22163594
Si	-0.07640222	3.12550463	-1.54024395
C	2.92944969	1.34168237	1.47190865
C	3.72776197	2.78568315	-1.05409284
C	-5.13784198	0.21777893	0.14436166
C	-0.03410243	-3.46127637	1.29795064
C	2.70556976	-2.44965021	2.26740104

C	2.20737092	4.27473313	1.12237380
H	-3.51720055	2.14962599	2.14585010
H	-1.84462756	1.81647820	1.74696008
H	-2.94554308	2.44730208	0.51006543
H	-5.78801984	0.67076617	0.89648942
H	-5.58019126	-0.73810855	-0.13691058
H	-5.14283872	0.86438665	-0.73359337
H	-2.61322459	-1.21138554	2.89327549
H	-3.94800037	-2.03769581	2.11199033
H	-4.25793140	-0.61906049	3.11483953
H	-0.56527295	-3.94596012	0.47772498
H	-0.64388860	-2.62647717	1.64485856
H	0.02020680	-4.17488293	2.12311032
H	2.80797537	-3.28061861	2.96881358
H	2.23023933	-1.62183414	2.79118738
H	3.70862330	-2.13448059	1.97381778
H	1.96404910	-4.92900833	-0.76789795
H	2.51149837	-5.28127240	0.87089457
H	3.54269553	-4.36140862	-0.21790852
H	1.89494275	0.84910542	-2.32732118
H	1.05440285	-0.34422569	-3.32939674
H	2.72467703	0.06129417	-3.64974103
H	3.07444529	-2.74424945	-3.86879837

H	1.58566826	-3.34145951	-3.13741550
H	3.15023543	-3.87209129	-2.51922700
H	5.04350952	-1.05718600	-2.13092075
H	4.79165216	-2.02613617	-0.68025676
H	4.46799965	-0.29697532	-0.64388632
H	-1.95725774	2.60362590	-3.05814361
H	-2.04398607	1.50502334	-1.70336302
H	-0.86666563	1.23686654	-2.99439475
H	1.63251715	4.65072849	-2.53725489
H	0.28302496	4.38790150	-3.63522989
H	1.52654166	3.14721985	-3.45484070
H	-0.28218887	5.25791409	-0.28610660
H	-1.54259086	4.13410933	0.20304530
H	-1.68481908	5.01051642	-1.32475499
H	4.65995152	3.06402048	-0.55687994
H	3.51272316	3.54539019	-1.80398669
H	3.90132193	1.84456391	-1.57528013
H	3.12768470	4.50108379	1.66511161
H	1.38593251	4.25236948	1.84025408
H	2.02344711	5.09773041	0.42994942
H	2.82691510	0.30560594	1.14183108
H	2.41784416	1.45015968	2.42797496
H	3.99476292	1.49219758	1.65944960

H	-3.35942612	-0.15196919	-3.21334838
H	-4.80054442	-0.78915429	-2.42486230
H	-3.93363999	-1.77441673	-3.59995572
H	-2.94629210	-3.72753004	0.07562480
H	-3.77769079	-4.02400030	-1.45551152
H	-4.51763286	-2.99417393	-0.23426509
H	-0.41467819	-2.82362278	-1.69988087
H	-0.68314153	-1.57841824	-2.91827224
H	-1.46212857	-3.13264697	-3.07922587
H	-0.74394599	-0.34674713	2.85028796
H	0.73501389	0.34586735	2.85995523

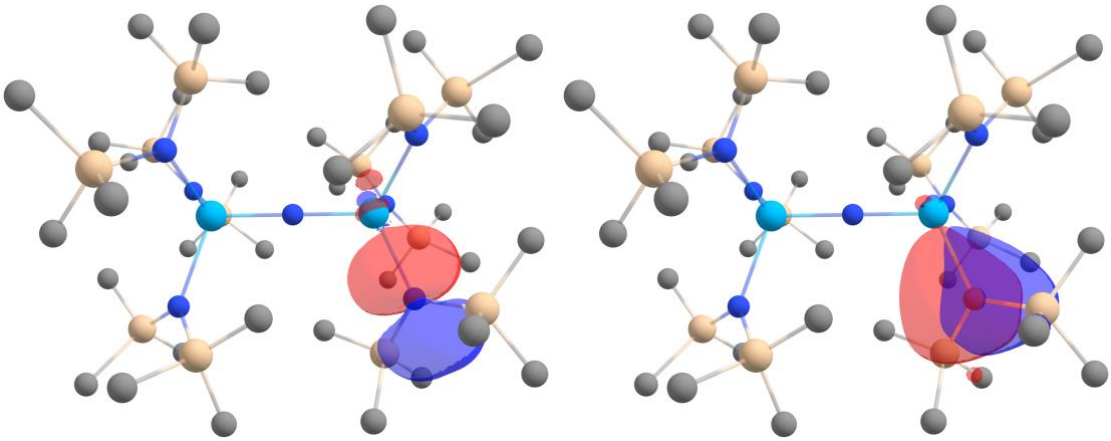

Figure A5.26. Th−$N_{silylamide}$ (σ+π) bonding NLMOs in $[(NR_2)_3Th(\mu\text{-}N)Th(NR_2)_3]^-$ (R = $SiMe_3$; isosurface plots ±0.03 au; hydrogen atoms are omitted for clarity). Color code for atoms: Th, light blue; N, blue; Si, beige; C, gray.

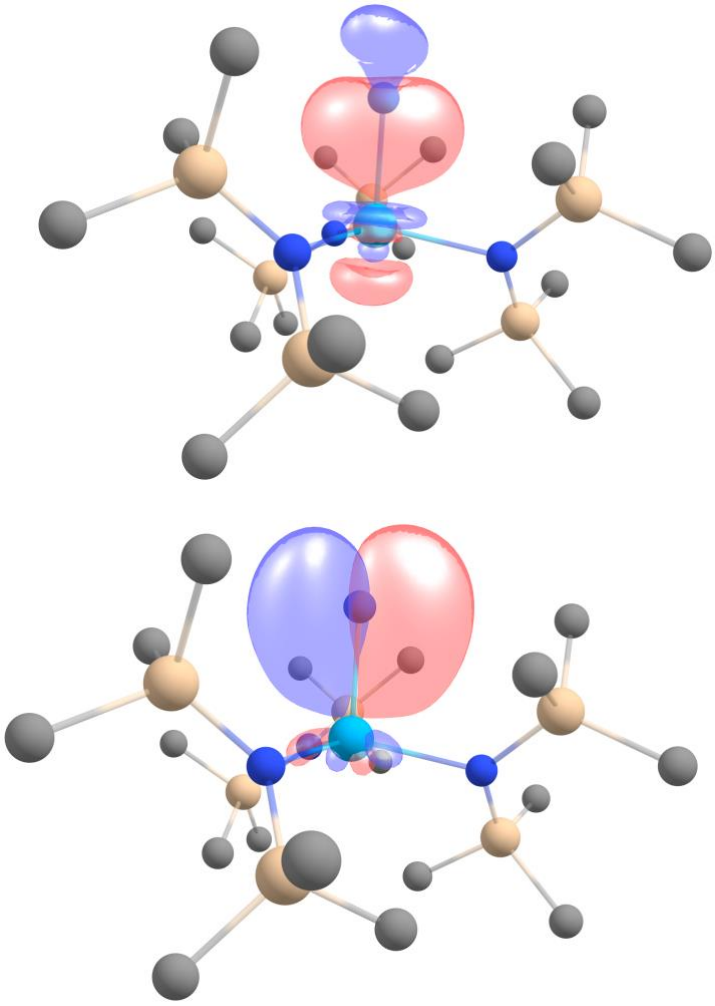

Figure A5.27. Th−N_{amide} (σ+π) bonding NLMOs in [Th$(NR_2)_3(NH_2)$] (R = $SiMe_3$; isosurface plots ±0.03 au; hydrogen atoms are omitted for clarity). Color code for atoms: Th, light blue; N, blue; Si, beige; C, gray.

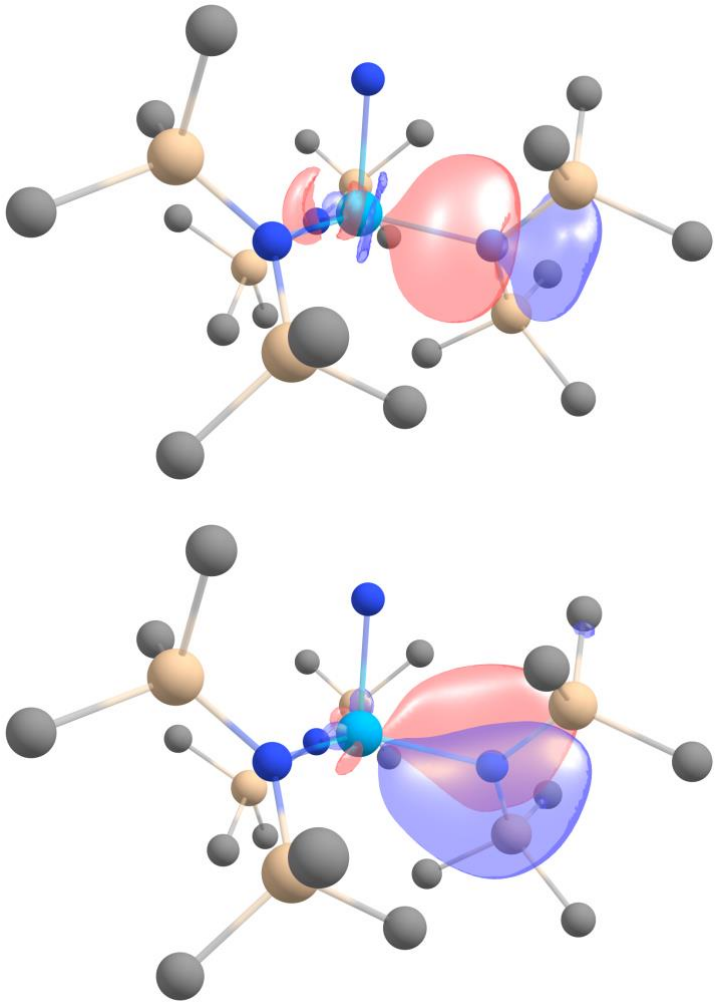

FigureA5.28. Th−$N_{silylamide}$ (σ+π) bonding NLMOs in [Th$(NR_2)_3(NH_2)$] (R = $SiMe_3$; isosurface plots ±0.03 au; hydrogen atoms are omitted for clarity). Color code for atoms: Th, light blue; N, blue; Si, beige; C, gray.

Table A5.1. % compositions of the Th-$N_{silylamide}$ Bonding NLMOs in $[(NR_2)_3Th(\mu\text{-}N)Th(NR_2)_3]^-$ and $[Th(NR_2)_3(NH_2)]$ (R = $SiMe_3$).

Complex	**Orbital**	**%N**			**%Th**					**%Si**			
		Total N	2s	2p	Total Th	7s	7p	6d	5f	Total Si	3s	3p	3d
$[Th(NR_2)_3(NH_2)]$	σ	92	31	69	6	8	6	61	25	2	0	94	6
	π	90	0	100	90	0	0	48	52	4	0	89	11
$[(NR_2)_3Th(\mu\text{-}N)Th(NR_2)_3]^-$	σ	94	15	85	4	2	12	62	24	2	7	86	7
	π	90	0	100	4	0	0	52	48	4	0	90	10

Table A5.2. Calculated Shielding and chemical shifts for DFT/B3LYP/TZ2P optimized geometries of nitromethane, [{Cp*TiCl$_2$}(μ-N){Cp*TiCl(NH$_3$)}], [(NR$_2$)$_3$Th(μ-N)Th(NR$_2$)$_3$]$^-$, and [Th(NR$_2$)$_3$(NH$_2$)] (R = SiMe$_3$).

Compound	**Method**	**σ_{calcd} (ppm)**	**δ_{calcd} (ppm)[a]**	**δ_{expt} (ppm)**
MeNO$_2$	PBE0	–159.9	-	-
	SO-PBE0	–156.2	-	-
	B3LYP	–166.7	-	-
	SO-B3LYP	–162.8	-	-
[{Cp*TiCl$_2$}(μ-N){Cp*TiCl(NH$_3$)}]	PBE0	–566.7	406.8	431.6
	SO-PBE0	–570.7	414.5	
	B3LYP	–588.5	421.8	
	SO-B3LYP	–593.3	430.5	
[(NR$_2$)$_3$Th(μ-N)Th(NR$_2$)$_3$]$^-$	PBE0	–385.9	226.0	298.8
	SO-PBE0	–461.6	305.4	
[Th(NR$_2$)$_3$(NH$_2$)]	PBE0	94.0	–253.9	–198.4
	SO-PBE0	53.5	–209.7	

[a] Referenced to nitromethane: $\delta_{calcd} = \sigma_{calcd}$ (N, nitromethane) – σ_{calcd} (N, metal complex).

Solvents were used in the calculations (COSMO model): nitromethane for MeNO$_2$, chloroform for [{Cp*TiCl$_2$}(μ-N){Cp*TiCl(NH$_3$)}], tetrahydrofuran for [(NR$_2$)$_3$Th(μ-N)Th(NR$_2$)$_3$]$^-$, and benzene for [Th(NR$_2$)$_3$(NH$_2$)].

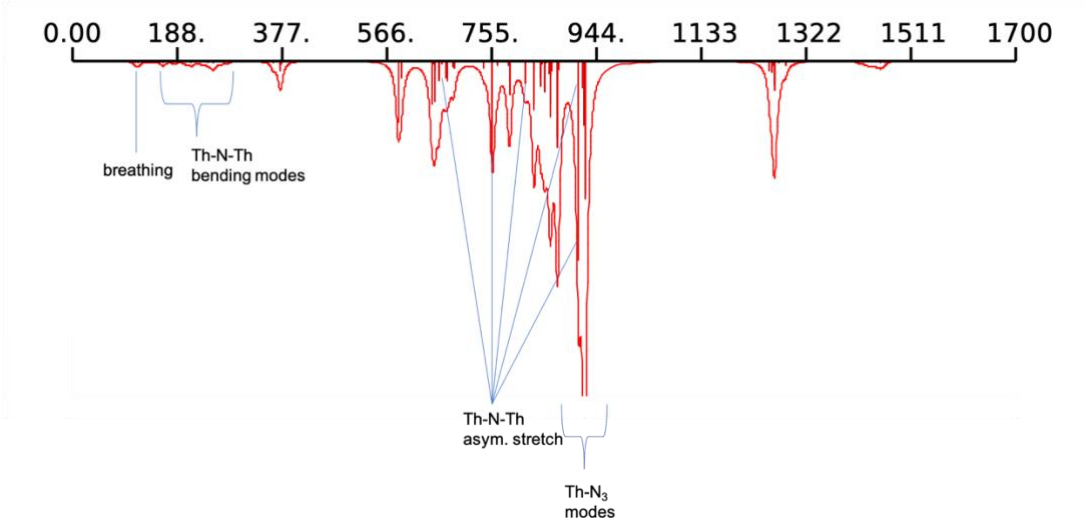

Figure A5.29. Calculated IR spectrum for **[5.1]**$^{-}$. The principal Th-N-Th asymmetric stretching mode can be observed at 758.2 cm^{-1}. However, several other modes, at 817, 913.4 and 923 cm^{-1}, also have a Th-N-Th asymmetric stretching component, but they are combined with Th-$N_{silylamide}$ modes. Moreover, modes at 588.1, 648.6, 654, 673 cm^{-1} are a combination of the Th-N-Th asymmetric stretch along with various modes of the whole molecular skeleton. There is a breathing mode at 113 cm^{-1} which is not very intense. Finally, there are Th-N-Th bending modes at 254.1, 255.2, 268 and 281.6 cm^{-1}.

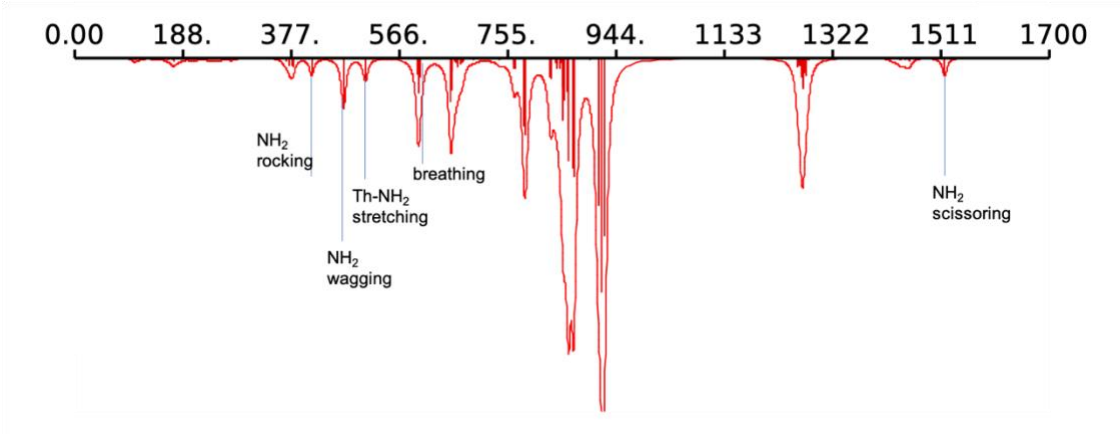

Figure A5.30. Calculated IR spectrum for **5.2**. Assignments (cm^{-1}): 414.7 (NH_2 rocking), 470.1 (NH_2 wagging), 508.4 (Th-NH_2 stretching), 613.5 (Th-N breathing), 1518.8 (NH_2 scissoring).

5.7 References

1. Hayton, T. W., Metal–ligand multiple bonding in uranium: structure and reactivity. *Dalton Trans.* **2010,** *39* (5), 1145-1158.
2. Hayton, T. W., Recent developments in actinide–ligand multiple bonding. *Chem. Commun.* **2013,** *49* (29), 2956-2973.
3. Jones, M. B.; Gaunt, A. J., Recent Developments in Synthesis and Structural Chemistry of Nonaqueous Actinide Complexes. *Chem. Rev.* **2013,** *113* (2), 1137-1198.
4. Patel, D.; Liddle, S. T., f-Element-metal bond chemistry. *Prog. Inorg. Chem.* **2012,** *32* (1), 1.
5. Liddle, S. T., The Renaissance of Non-Aqueous Uranium Chemistry. *Angew. Chem. Int. Ed.* **2015,** *54* (30), 8604-8641.
6. King, D. M.; Liddle, S. T., Progress in molecular uranium-nitride chemistry. *Coord. Chem. Rev.* **2014,** *266-267*, 2-15.
7. Korobkov, I.; Gambarotta, S.; Yap, G. P. A., A Highly Reactive Uranium Complex Supported by the Calix[4]tetrapyrrole Tetraanion Affording Dinitrogen Cleavage, Solvent Deoxygenation, and Polysilanol Depolymerization. *Angew. Chem. Int. Ed.* **2002,** *41* (18), 3433-3436.
8. Evans, W. J.; Kozimor, S. A.; Ziller, J. W., Molecular Octa-Uranium Rings with Alternating Nitride and Azide Bridges. *Science* **2005,** *309* (5742), 1835.
9. Falcone, M.; Chatelain, L.; Scopelliti, R.; Živković, I.; Mazzanti, M., Nitrogen reduction and functionalization by a multimetallic uranium nitride complex. *Nature* **2017,** *547*, 332.
10. Fortier, S.; Wu, G.; Hayton, T. W., Synthesis of a Nitrido-Substituted Analogue of the Uranyl Ion, $[N{=}U{=}O]^{+}$. *J. Am. Chem. Soc.* **2010,** *132* (20), 6888-9.
11. Fox, A. R.; Arnold, P. L.; Cummins, C. C., Uranium-Nitrogen Multiple Bonding: Isostructural Anionic, Neutral, and Cationic Uranium Nitride Complexes Featuring a Linear U=N=U Core. *J. Am. Chem. Soc.* **2010,** *132* (10), 3250-1.
12. Chatelain, L.; Scopelliti, R.; Mazzanti, M., Synthesis and Structure of Nitride-Bridged Uranium(III) Complexes. *J. Am. Chem. Soc.* **2016,** *138* (6), 1784-1787.
13. Cleaves, P. A.; Kefalidis, C. E.; Gardner, B. M.; Tuna, F.; McInnes, E. J. L.; Lewis, W.; Maron, L.; Liddle, S. T., Terminal Uranium(V/VI) Nitride Activation of Carbon Dioxide and Carbon Disulfide: Factors Governing Diverse and Well-Defined Cleavage and Redox Reactions. *Chem. Eur. J.* **2017,** *23* (12), 2950-2959.
14. Cleaves, P. A.; King, D. M.; Kefalidis, C. E.; Maron, L.; Tuna, F.; McInnes, E. J. L.; McMaster, J.; Lewis, W.; Blake, A. J.; Liddle, S. T., Two-Electron Reductive Carbonylation of Terminal Uranium(V) and Uranium(VI) Nitrides to Cyanate by Carbon Monoxide. *Angew. Chem. Int. Ed.* **2014,** *53* (39), 10412-10415.
15. Falcone, M.; Chatelain, L.; Mazzanti, M., Nucleophilic Reactivity of a Nitride-Bridged Diuranium(IV) Complex: CO_2 and CS_2 Functionalization. *Angew. Chem. Int. Ed.* **2016,** *55* (12), 4074-4078.
16. Falcone, M.; Chatelain, L.; Scopelliti, R.; Mazzanti, M., CO Cleavage and CO Functionalization under Mild Conditions by a Multimetallic CsU_2 Nitride Complex. *CHIMIA* **2017,** *71* (4), 209-212.
17. Falcone, M.; Kefalidis, C. E.; Scopelliti, R.; Maron, L.; Mazzanti, M., Facile CO Cleavage by a Multimetallic CsU_2 Nitride Complex. *Angew. Chem. Int. Ed.* **2016,** *55* (40), 12290-12294.

18. Falcone, M.; Poon, L. N.; Fadaei Tirani, F.; Mazzanti, M., Reversible Dihydrogen Activation and Hydride Transfer by a Uranium Nitride Complex. *Angew. Chem. Int. Ed.* **2018,** *57* (14), 3697-3700.
19. Hayton, T. W., An actinide milestone. *Nat. Chem.* **2013,** *5*, 451.
20. King, D. M.; Cleaves, P. A.; Wooles, A. J.; Gardner, B. M.; Chilton, N. F.; Tuna, F.; Lewis, W.; McInnes, E. J. L.; Liddle, S. T., Molecular and electronic structure of terminal and alkali metal-capped uranium(V) nitride complexes. *Nat. Commun.* **2016,** *7*, 13773.
21. King, D. M.; Tuna, F.; McInnes, E. J. L.; McMaster, J.; Lewis, W.; Blake, A. J.; Liddle, S. T., Synthesis and Structure of a Terminal Uranium Nitride Complex. *Science* **2012,** *337* (6095), 717.
22. Mullane, K. C.; Ryu, H.; Cheisson, T.; Grant, L. N.; Park, J. Y.; Manor, B. C.; Carroll, P. J.; Baik, M.-H.; Mindiola, D. J.; Schelter, E. J., C–H Bond Addition across a Transient Uranium–Nitrido Moiety and Formation of a Parent Uranium Imido Complex. *J. Am. Chem. Soc.* **2018,** *140* (36), 11335-11340.
23. Thomson, R. K.; Cantat, T.; Scott, B. L.; Morris, D. E.; Batista, E. R.; Kiplinger, J. L., Uranium azide photolysis results in C–H bond activation and provides evidence for a terminal uranium nitride. *Nat. Chem.* **2010,** *2*, 723.
24. Falcone, M.; Barluzzi, L.; Andrez, J.; Fadaei Tirani, F.; Zivkovic, I.; Fabrizio, A.; Corminboeuf, C.; Severin, K.; Mazzanti, M., The role of bridging ligands in dinitrogen reduction and functionalization by uranium multimetallic complexes. *Nat. Chem.* **2019,** *11* (2), 154-160.
25. Du, J.; King, D. M.; Chatelain, L.; Lu, E.; Tuna, F.; McInnes, E. J. L.; Wooles, A. J.; Maron, L.; Liddle, S. T., Thorium- and uranium-azide reductions: a transient dithorium-nitride *versus* isolable diuranium-nitrides. *Chem. Sci.* **2019,** *10*, 3738-3745.
26. Green, D. W.; Reedy, G. T., Identification of matrix-isolated thorium nitride and the thorium-dinitrogen complex. *J. Mol. Spectrosc.* **1979,** *74* (3), 423-434.
27. Kushto, G. P.; Souter, P. F.; Andrews, L., An infrared spectroscopic and quasirelativistic theoretical study of the coordination and activation of dinitrogen by thorium and uranium atoms. *J. Chem. Phys.* **1998,** *108* (17), 7121-7130.
28. Vlaisavljevich, B.; Andrews, L.; Wang, X.; Gong, Y.; Kushto, G. P.; Bursten, B. E., Detection and Electronic Structure of Naked Actinide Complexes: Rhombic-Ring $(AnN)_2$ Molecules Stabilized by Delocalized π-Bonding. *J. Am. Chem. Soc.* **2016,** *138* (3), 893-905.
29. Cantat, T.; Scott, B. L.; Kiplinger, J. L., Convenient access to the anhydrous thorium tetrachloride complexes $ThCl_4(DME)_2$, $ThCl_4(1,4\text{-dioxane})_2$ and $ThCl_4(THF)_{3.5}$ using commercially available and inexpensive starting materials. *Chem. Commun.* **2010,** *46* (6), 919-21.
30. Bell, N. L.; Maron, L.; Arnold, P. L., Thorium Mono- and Bis(imido) Complexes Made by Reprotonation of *cyclo*-Metalated Amides. *J. Am. Chem. Soc.* **2015,** *137* (33), 10492-5.
31. Garner, M. E.; Hohloch, S.; Maron, L.; Arnold, J., A New Supporting Ligand in Actinide Chemistry Leads to Reactive Bis(NHC)borate-Supported Thorium Complexes. *Organometallics* **2016,** *35* (17), 2915-2922.
32. Haskel, A.; Straub, T.; Eisen, M. S., Organoactinide-Catalyzed Intermolecular Hydroamination of Terminal Alkynes. *Organometallics* **1996,** *15* (18), 3773-3775.

33. Ren, W.; Zi, G.; Walter, M. D., Synthesis, Structure, and Reactivity of a Thorium Metallocene Containing a 2,2′-Bipyridyl Ligand. *Organometallics* **2012,** *31* (2), 672-679.
34. Straub, T.; Haskel, A.; Neyroud, T. G.; Kapon, M.; Botoshansky, M.; Eisen, M. S., Intermolecular Hydroamination of Terminal Alkynes Catalyzed by Organoactinide Complexes. Scope and Mechanistic Studies. *Organometallics* **2001,** *20* (24), 5017-5035.
35. Yang, P.; Zhou, E.; Hou, G.; Zi, G.; Ding, W.; Walter, M. D., Experimental and Computational Studies on the Formation of Thorium–Copper Heterobimetallics. *Chem. Eur. J.* **2016,** *22* (39), 13845-13849.
36. Zhang, C.; Yang, P.; Zhou, E.; Deng, X.; Zi, G.; Walter, M. D., Reactivity of a Lewis Base Supported Thorium Terminal Imido Metallocene toward Small Organic Molecules. *Organometallics* **2017,** *36* (23), 4525-4538.
37. Yu, X.; Xue, Z.-L., Deprotonation Reactions of Zirconium and Hafnium Amide Complexes $H_2N{-}M[N(SiMe_3)_2]_3$ and Subsequent Silyl Migration from Amide $-N(SiMe_3)_2$ to Imide =NH Ligands. *Inorg. Chem.* **2005,** *44* (5), 1505-1510.
38. Korobkov, I.; Gambarotta, S.; Yap, G. P. A., Amide from Dinitrogen by In Situ Cleavage and Partial Hydrogenation Promoted by a Transient Zero-Valent Thorium Synthon. *Angew. Chem. Int. Ed.* **2003,** *42* (40), 4958-4961.
39. Smiles, D. E.; Wu, G.; Hrobárik, P.; Hayton, T. W., Use of ^{77}Se and ^{125}Te NMR Spectroscopy to Probe Covalency of the Actinide-Chalcogen Bonding in $[Th(E_n)\{N(SiMe_3)_2\}_3]^-$ (E = Se, Te; *n* = 1, 2) and Their Oxo-Uranium(VI) Congeners. *J. Am. Chem. Soc.* **2016,** *138* (3), 814-825.
40. King, D. M.; Tuna, F.; McInnes, E. J. L.; McMaster, J.; Lewis, W.; Blake, A. J.; Liddle, S. T., Isolation and characterization of a uranium(VI)–nitride triple bond. *Nat. Chem.* **2013,** *5*, 482.
41. Zi, G.; Jia, L.; Werkema, E. L.; Walter, M. D.; Gottfriedsen, J. P.; Andersen, R. A., Preparation and Reactions of Base-Free Bis(1,2,4-tri-*tert*-butylcyclopentadienyl)uranium Oxide, Cp'_2UO. *Organometallics* **2005,** *24* (17), 4251-4264.
42. Abarca, A.; Gómez-Sal, P.; Martín, A.; Mena, M.; Poblet, J. M.; Yélamos, C., Ammonolysis of Mono(pentamethylcyclopentadienyl) Titanium(IV) Derivatives. *Inorg. Chem.* **2000,** *39* (4), 642-651.
43. Semproni, S. P.; Milsmann, C.; Chirik, P. J., Structure and Reactivity of a Hafnocene μ-Nitrido Prepared From Dinitrogen Cleavage. *Angew. Chem.* **2012,** *51* (21), 5213-6.
44. Sergentu, D.-C.; Kent, G. T.; Staun, S. L.; Yu, X.; Cho, H.; Autschbach, J.; Hayton, T. W., Probing the Electronic Structure of a Thorium Nitride Complex by Solid-State ^{15}N NMR Spectroscopy. *Inorg. Chem.* **2020,** *59* (14), 10138-10145.
45. Smiles, D. E.; Wu, G.; Kaltsoyannis, N.; Hayton, T. W., Thorium–ligand multiple bonds *via* reductive deprotection of a trityl group. *Chem. Sci.* **2015,** *6* (7), 3891-3899.
46. King, D. M.; Tuna, F.; McMaster, J.; Lewis, W.; Blake, A. J.; McInnes, E. J. L.; Liddle, S. T., Single-Molecule Magnetism in a Single-Ion Triamidoamine Uranium(V) Terminal Mono-Oxo Complex. *Angew. Chem. Int. Ed.* **2013,** *52* (18), 4921-4924.
47. Smiles, D. E.; Wu, G.; Hrobárik, P.; Hayton, T. W., Synthesis, Thermochemistry, Bonding, and ^{13}C NMR Chemical Shift Analysis of a Phosphorano-Stabilized Carbene of Thorium. *Organometallics* **2017,** *36* (23), 4519-4524.
48. Neidig, M. l. L.; Clark, D. L.; Martin, R. L., Covalency in f-element complexes. *Coord. Chem. Rev.* **2013,** *257* (2), 394-406.

49. Mullane, K. C.; Hrobárik, P.; Cheisson, T.; Manor, B. C.; Carroll, P. J.; Schelter, E. J., ^{13}C NMR Shifts as an Indicator of U–C Bond Covalency in Uranium(VI) Acetylide Complexes: An Experimental and Computational Study. *Inorg. Chem.* **2019,** *58*, 4152–4163.
50. Pedrick, E. A.; Hrobárik, P.; Seaman, L. A.; Wu, G.; Hayton, T. W., Synthesis, structure and bonding of hexaphenyl thorium(IV): observation of a non-octahedral structure. *Chem. Commun.* **2016,** *52* (4), 689-692.
51. Seaman, L. A.; Walensky, J. R.; Wu, G.; Hayton, T. W., In Pursuit of Homoleptic Actinide Alkyl Complexes. *Inorg. Chem.* **2013,** *52* (7), 3556-3564.
52. Wu, W.; Rehe, D.; Hrobárik, P.; Kornienko, A. Y.; Emge, T. J.; Brennan, J. G., Molecular Thorium Compounds with Dichalcogenide Ligands: Synthesis, Structure, ^{77}Se NMR Study, and Thermolysis. *Inorg. Chem.* **2018,** *57* (23), 14821-14833.
53. Seaman, L. A.; Hrobárik, P.; Schettini, M. F.; Fortier, S.; Kaupp, M.; Hayton, T. W., A Rare Uranyl(VI)–Alkyl Ate Complex $[Li(DME)_{1.5}]_2[UO_2(CH_2SiMe_3)_4]$ and Its Comparison with a Homoleptic Uranium(VI)–Hexaalkyl. *Angew. Chem.* **2013,** *52* (11), 3259-3263.
54. Simpson, S. J.; Turner, H. W.; Andersen, R. A., Preparation and hydrogen-deuterium exchange of alkyl and hydride bis(trimethylsilyl)amido derivatives of the actinide elements. *Inorg. Chem.* **1981,** *20* (9), 2991-2995.
55. Harris, R. K.; Becker, E. D.; Cabral de Menezes, S. M.; Goodfellow, R.; Granger, P., NMR nomenclature: nuclear spin properties and conventions for chemical shifts. IUPAC Recommendations 2001. International Union of Pure and Applied Chemistry. Physical Chemistry Division. Commission on Molecular Structure and Spectroscopy. *Magn. Reson. Chem.* **2002,** *40* (7), 489-505.
56. Harris, R. K.; Becker, E. D.; De Menezes, S. M. C.; Granger, P.; Hoffman, R. E.; Zilm, K. W., Further Conventions for NMR Shielding and Chemical Shifts (IUPAC Recommendations 2008). *Magn. Reson. Chem.* **2008,** *46* (6), 582-598.
57. *SMART* Apex II, Version 2.1ed.; Bruker AXS Inc.: Madison, WI, 2004. .
58. *SAINT Software User's Guide*, Version 7.34a ed.; Bruker AXS Inc.: Madison, WI, 2005.
59. *SADABS*, Sheldrick, G.M.; University of Göttingen, Germany: 2005.
60. *SHELXTL*, Version 6.12 ed.; Bruker AXS Inc.: Madison, WI, 2005.
61. Bénaud, O.; Berthet, J.-C.; Thuéry, P.; Ephritikhine, M., The Bis Metallacyclic Anion $[U(N\{SiMe_3\}_2)(CH_2SiMe_2N\{SiMe_3\})_2]^-$. *Inorg. Chem.* **2010,** *49* (17), 8117-8130.
62. Palumbo, C. T.; Barluzzi, L.; Scopelliti, R.; Zivkovic, I.; Fabrizio, A.; Corminboeuf, C.; Mazzanti, M., Tuning the structure, reactivity and magnetic communication of nitride-bridged uranium complexes with the ancillary ligands. *Chem. Sci.* **2019,** *10* (38), 8840-8849.
63. Baerends, E. J.; Ziegler, T.; Atkins, A. J.; Autschbach, J.; Bashford, D.; Baseggio, O.; Brces, A.; Bickelhaupt, F. M.; Bo, C.; Boerritger, P. M.; Cavallo, L.; Daul, C.; Chong, D. P.; Chulhai, D. V.; Deng, L.; Dickson, R. M.; Dieterich, J. M.; Ellis, D. E.; van Faassen, M.; Ghysels, A.; Giammona, A.; van Gisbergen, S. J. A.; Goez, A.; Gtz, A. W.; Gusarov, S.; Harris, F. E.; van den Hoek, P.; Hu, Z.; Jacob, C. R.; Jacobsen, H.; Jensen, L.; Joubert, L.; Kaminski, J. W.; van Kessel, G.; Knig, C.; Kootstra, F.; Kovalenko, A.; Krykunov, M.; van Lenthe, E.; McCormack, D. A.; Michalak, A.; Mitoraj, M.; Morton, S. M.; Neugebauer, J.; Nicu, V. P.; Noodleman, L.; Osinga, V. P.; Patchkovskii, S.; Pavanello, M.; Peeples, C. A.; Philipsen, P. H. T.; Post, D.; Pye, C. C.;

Ramanantoanina, H.; Ramos, P.; Ravenek, W.; Rodrguez, J. I.; Ros, P.; Rger, R.; Schipper, P. R. T.; Schlns, D.; van Schoot, H.; Schreckenbach, G.; Seldenthuis, J. S.; Seth, M.; Snijders, J. G.; Solà, M., ADF2017, SCM, Theoretical Chemistry, Vrije Universiteit, Amsterdam, The Netherlands.
64. Becke, A. D., Density-functional exchange-energy approximation with correct asymptotic behavior. *Phys. Rev. A* **1988,** *38* (6), 3098.
65. Lee, C.; Yang, W.; Parr, R. G., Development of the Colle-Salvetti correlation-energy formula into a functional of the electron density. *Phys. Rev. B* **1988,** *37* (2), 785.
66. Stephens, P. J.; Devlin, F. J.; Chabalowski, C. F.; Frisch, M. J., *Ab initio* Calculation of Vibrational Absorption and Circular Dichroism Spectra Using Density Functional Force Fields. *J. Phys. Chem.* **1994,** *98* (45), 11623-11627.
67. Lenthe, E. v.; Baerends, E.-J.; Snijders, J. G., Relativistic regular two-component Hamiltonians. *J. Chem. Phys.* **1993,** *99* (6), 4597-4610.
68. Grimme, S.; Antony, J.; Ehrlich, S.; Krieg, H., A consistent and accurate *ab initio* parametrization of density functional dispersion correction (DFT-D) for the 94 elements H-Pu. *J. Chem. Phys.* **2010,** *132* (15), 154104.
69. Grimme, S.; Ehrlich, S.; Goerigk, L., Effect of the damping function in dispersion corrected density functional theory. *J. Comput. Chem.* **2011,** *32* (7), 1456-1465.
70. Adamo, C.; Barone, V., Toward chemical accuracy in the computation of NMR shieldings: the PBE0 model. *Chem. Phys. Lett.* **1998,** *298* (1), 113-119.
71. Perdew, J. P.; Burke, K.; Ernzerhof, M., Generalized Gradient Approximation Made Simple. *Phys. Rev. Lett.* **1996,** *77* (18), 3865.
72. Klamt, A., Conductor-Like Screening Model for Real Solvents - A New Approach to the Quantitative Calculation of Solvation Phenomena. *J. Phys. Chem.* **1995,** *99* (7), 2224-2235.
73. Pye, C. C.; Ziegler, T., An implementation of the conductor-like screening model of solvation within the Amsterdam density functional package. *Theor. Chem. Acc.* **1999,** *101* (6), 396-408.
74. Autschbach, J., The role of the exchange-correlation response kernel and scaling corrections in relativistic density functional nuclear magnetic shielding calculations with the zeroth-order regular approximation. *Mol. Phys.* **2013,** *111* (16-17), 2544-2554.
75. Frisch, M. J.; Trucks, G. W.; Schlegel, H. B.; Scuseria, G. E.; Robb, M. A.; Cheeseman, J. R.; Scalmani, G.; Barone, V.; Petersson, G. A.; Nakatsuji, H.; Li, X.; Caricato, M.; Marenich, A. V.; Bloino, J.; Janesko, B. G.; Gomperts, R.; Mennucci, B.; Hratchian, H. P.; Ortiz, J. V.; Izmaylov, A. F.; Sonnenberg, J. L.; Williams; Ding, F.; Lipparini, F.; Egidi, F.; Goings, J.; Peng, B.; Petrone, A.; Henderson, T.; Ranasinghe, D.; Zakrzewski, V. G.; Gao, J.; Rega, N.; Zheng, G.; Liang, W.; Hada, M.; Ehara, M.; Toyota, K.; Fukuda, R.; Hasegawa, J.; Ishida, M.; Nakajima, T.; Honda, Y.; Kitao, O.; Nakai, H.; Vreven, T.; Throssell, K.; Montgomery Jr., J. A.; Peralta, J. E.; Ogliaro, F.; Bearpark, M. J.; Heyd, J. J.; Brothers, E. N.; Kudin, K. N.; Staroverov, V. N.; Keith, T. A.; Kobayashi, R.; Normand, J.; Raghavachari, K.; Rendell, A. P.; Burant, J. C.; Iyengar, S. S.; Tomasi, J.; Cossi, M.; Millam, J. M.; Klene, M.; Adamo, C.; Cammi, R.; Ochterski, J. W.; Martin, R. L.; Morokuma, K.; Farkas, O.; Foresman, J. B.; Fox, D. J. *Gaussian 16 Rev. B.01*, Wallingford, CT, 2016.

76. Weigend, F.; Ahlrichs, R., Balanced basis sets of split valence, triple zeta valence and quadruple zeta valence quality for H to Rn: Design and assessment of accuracy. *Phys Chem Chem Phys* **2005,** *7* (18), 3297-3305.
77. Weigand, A.; Cao, X.; Hangele, T.; Dolg, M., Relativistic Small-Core Pseudopotentials for Actinium, Thorium, and Protactinium. *J. Phys. Chem. A* **2014,** *118* (13), 2519-2530.
78. Glendening, E. D.; Landis, C. R.; Weinhold, F., *NBO 6.0*: Natural bond orbital analysis program. *J. Comput. Chem.* **2013,** *34* (16), 1429-1437.

Chapter 6. Synthesis and Characterization of a Rare U^{IV}/Th^{IV} Bridging Nitride and Its Oxidation to a Stable U^{V}/Th^{IV} Species

6.1 Introduction

The past decade has seen significant progress toward the synthesis of uranium nitrido complexes. Since the first molecular uranium nitride was reported by Gambarotta and co-workers in 2002,[1] they are now being reported with increasing frequency. Many bridging and terminal uranium nitrides have now been reported,[2-16] whereas the first molecular thorium nitride was only published in 2019 by our group and it remains to be the only example.[17] As actinide-ligand multiple bonds chemistry expands,[13, 18-22] new insights into electronic structure have been made and novel modes of reactivity have been revealed.[2, 6, 7, 9, 10, 23-25] For example, uranium nitrides have been shown to have a potential use in catalysis,[26, 27] a role that went unnoticed until their chemical reactivity in [2+2] cycloaddition reactions[28] and challenging C-H bond activations was reported.[29]

High-valent uranium(V) complexes are $5f^1$ systems that are recognized for their simplified crystal field description and the ability to address spin-orbit coupling in a straightforward manner,[30-32] properties that have helped deepen our fundamental understanding of actinide electronic structure, reactivity, and bonding.[33] Therefore, data from electron paramagnetic resonance (EPR) spectroscopy,[34] magnetic susceptibility (SQUID) measurements,[35] UV-vis/NIR spectroscopy, and density functional theory (DFT) calculations are easier to analyze compared to uranium complexes in the 3+ and 4+ oxidation state, which have multiple unpaired electrons.[36]

In this regard, a handful of U(V) nitrides have been synthesized (Scheme 6.1) and characterized using the techniques mentioned above to provide insight into the electronic structure of these metal-ligand multiple bonded complexes.[1, 4, 6, 8, 11, 12, 15, 16, 37] For example, Liddle and co-workers reported the formation of a U(V) terminal nitride, $[Na(12\text{-crown-}4)_2][U(N)\{N(CH_2CH_2NSi^iPr_3)_3\}]$ (^{i}Pr = $CH(CH_3)_2$), which exhibits a short U≡N bond

distance (1.825(15) Å) (Scheme 6.1, **C**).[16] DFT calculations revealed three molecular orbitals involved in the U-N interaction, consistent with a formal U-N triple bond. A natural bond order (NBO) analysis of the three molecular orbitals involved in the U-N bond revealed substantial covalency, where the σ -bond (HOMO – 1) contained 32% uranium character and the two π-bonds (HOMO – 2 and HOMO – 3) contained 27% uranium character.[16] However, this is a rare example of an isolable terminal nitride, where the majority of reported U(V) nitrides are bridging and feature mixed-valent electronic configurations, most commonly U(V)/U(IV) (Scheme 6.1, **B**, **E**, **F**),[1, 11, 12, 37] which complicates the electronic structure analysis.[33] One route that has been attempted to eliminate this complication is to isolate a U(V)/U(V) bridging nitrido (Scheme 6.1, **A**, **D**, **F**).[4, 8, 12, 15] An alternative approach could be to synthesize a hetero-bimetallic actinide bridging nitride involving uranium and thorium, in which a U(V)/Th(IV) mixed-valent species would feature similar electronic behavior as a terminal U(V) nitride. This is desirable because the diamagnetic thorium center, with no unpaired electrons, would allow for simpler interpretation of data collected by EPR spectroscopy, SQUID, UV-vis/NIR spectroscopy, and DFT.

Scheme 6.1. Previously reported uranium(V) nitrides. A, Ref. 8; B, Ref. 11; C, Ref. 16; D, Ref. 4; E, Ref. 37; F, Ref. 12.

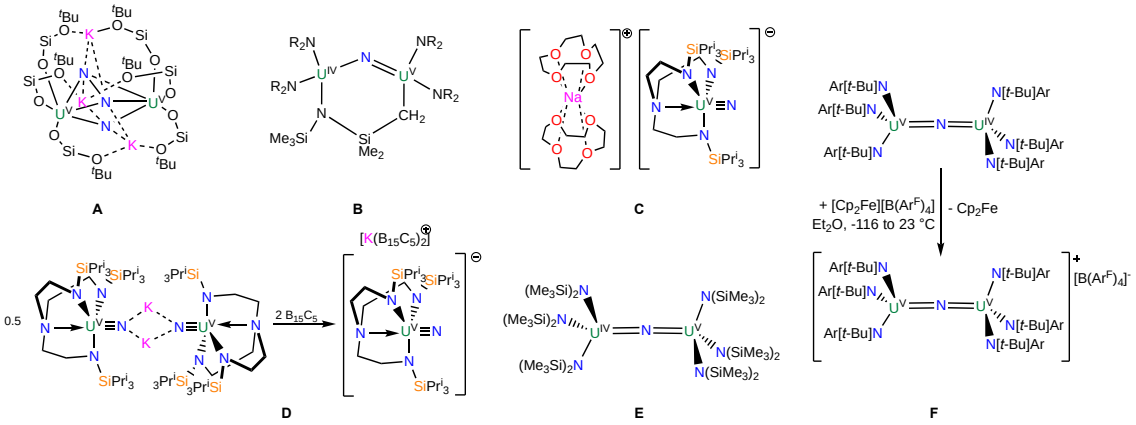

Herein, I report the synthesis of the first isolable molecular mixed actinide nitride complex, $[K(18\text{-crown-6})(THF)_2][(NR_2)_3U^{IV}(\mu\text{-}N)Th^{IV}(NR_2)_3]$ (R = $SiMe_3$), formed by reaction of the known thorium bis(metallacycle), $[K(DME)][Th\{N(R)(SiMe_2CH_2)\}_2(NR_2)]$,[38] with the new uranium parent amide complex, $[U(NR_2)_3(NH_2)]$. In addition, I explored the redox properties of the U^{IV}/Th^{IV} nitride and synthesized the mixed-valent nitride complex, $[(NR_2)_3U^{V}(\mu\text{-}N)Th^{IV}(NR_2)_3]$. I report within the electronic absorption spectroscopy, magnetometry, electronic structure calculations, and ^{15}N-isotopic labeling, which has allowed me to confirm the structural assignments and evaluate the degree of 5f covalency within the U=N=Th unit.

6.2 Results and Discussion

6.2.1 Synthesis and Characterization of $[U(NR_2)_3(NH_2)]$ (6.1)

Addition of 3 equiv of NH_3, as a 0.4 M solution in THF, to a cold (-25 °C) THF solution of the known uranium metallacycle, $[U\{N(R)(SiMe_2)CH_2\}(NR_2)_2]$ (R = $SiMe_3$),[39] results in the formation of $[U(NR_2)_3(NH_2)]$ (**6.1**), which can be isolated in 69% yield after work-up as dark brown-orange blocks (eqn (6.1)). The rate of formation of **6.1** is dependent on the amount of NH_3 added. It has been observed that the concentration listed on the reagent bottle (0.4 M) of the ammonia solution is not reliable, therefore an addition of excess NH_3 is often required to achieve complete conversion to **6.1**. Upon addition of the NH_3 solution, the reaction turns dark brown-orange, indicating the reaction is near completion, unlike the Th analogue (Chapter 5),[17] which required a small aliquot of the reaction mixture to be transferred to a new vial, dried *in vacuo*, and dissolved into benzene-d_6 for a ^1H NMR spectrum before work-up, due to the lack of color change. It should be noted that due to the lengthy crystallization period required to isolate crystalline blocks of **6.1**, the product was typically isolated as a brown

powder by drying the pentane solution *in vacuo*. Additionally, if the NH_3 solution is from a fresh bottle, it is recommended to start with 1 equiv and increase the number of equivalents as needed because too much NH_3 at 0.4 M has been shown to quickly form an insoluble dark solid.

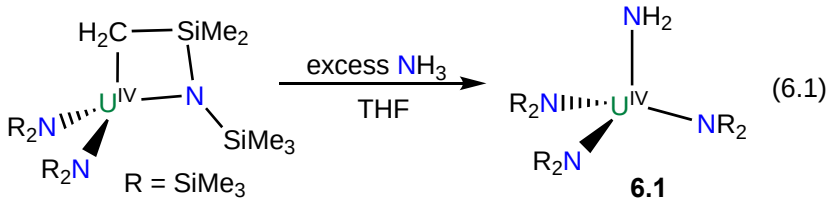

(6.1)

The ^{1}H NMR spectrum of **6.1** in benzene-d_6 features a sharp resonance at -2.95 ppm (54H), assigned to the $SiMe_3$ groups (Figure A6.1). However, the protons assignable to the -NH_2 resonance could not be definitely located in the ^{1}H NMR spectrum. For comparison, the ^{1}H NMR spectra for the uranium(IV) terminal amide complex, [U(NH_2)(Tren^{TIPS})] (Tren^{TIPS} = {N($CH_2CH_2NSi^iPr_3$)$_3$}$^{3-}$), features a singlet at -5.03 ppm assigned to the -NH_2 (2H) fragment and the ^{1}H NMR spectra for [{η^5-1,2,4-$C_5H_2{}^tBu_3$}$_2$U(NH_2)$_2$] features a peak at -34 ppm (FWHM = 27 Hz) assigned to the UN*H*$_2$ environment.[40, 41] Moreover, the J_{NH} value for the analogous Th complex was found to be 45.8 Hz[17] and the J_{NH} values for the isostructural group(IV) complexes, [M(NR_2)$_3$(NH_2)] (M = Zr, Hf), were found to be 45.6 Hz (Zr) and 46.0 Hz (Hf).[42]

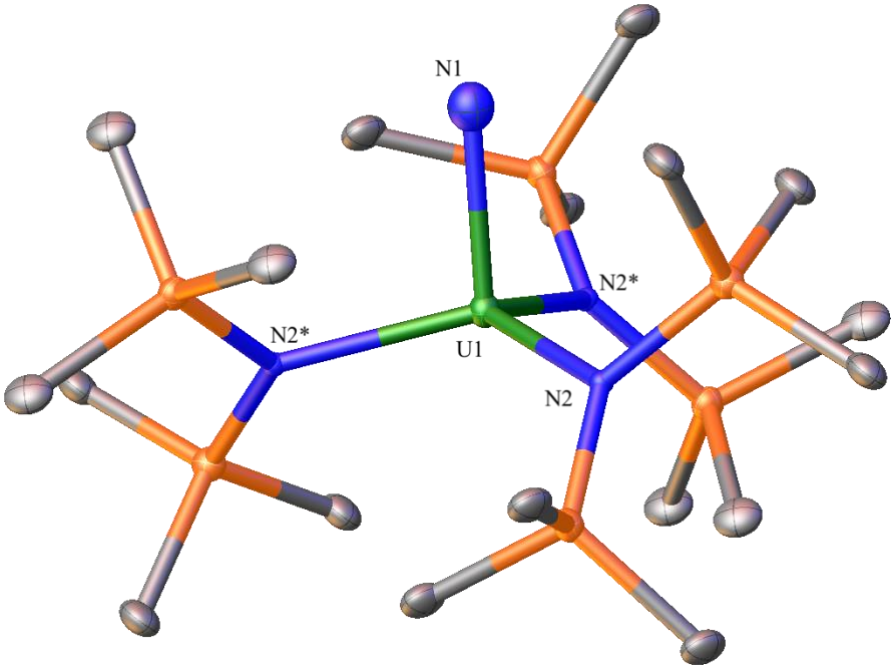

Figure 6.1. Solid-state molecular structure of **6.1**, shown with 50% probability ellipsoids. Hydrogen atoms removed for clarity. Selected bond lengths (Å) and angles (°): U1-N1 = 2.18(4), U1-N2 = 2.26(2), N1-U1-N2 = 100.5(5), N2-U1-N2* = 116.8(3).

The connectivity of complex **6.1** was verified by X-ray crystallography (Figure 6.1). Complex **6.1** crystallizes in the trigonal space group $R\bar{3}c$. In the solid-state, complex **6.1** is disordered over two positions in a 50:50 ratio, which somewhat lowers the precision of the resulting metrical parameters. It features a pseudo-tetrahedral geometry about the uranium center. Due to the large ESDs, the U-NH_2 distance (2.18(4) Å) in **6.1** is statistically identical to its U-$N_{silylamido}$ distances (2.26(2) Å).[43-45] The analogous Th complex is iso-structural to **6.1** and its Th-NH_2 and $N_{silylamido}$ distances (2.24(6) Å and 2.36(2) Å, respectively) are longer than **6.1**, which is consistent with the larger ionic radius of Th^{4+}.[17, 46] For further comparison, the uranium(IV) terminal amide complexes, [U(NH_2)($Tren^{TIPS}$)] ($Tren^{TIPS}$ = {$N(CH_2CH_2NSi^iPr_3)_3$}$^{3-}$) and [{η^5-1,2,4-$C_5H_2{}^tBu_3$}$_2$U(NH_2)$_2$], feature U-NH_2 bond lengths of 2.228(4) Å and 2.19 Å (av.), respectively.[40, 41]

Complex **6.1** is highly soluble in pentane, benzene, Et_2O, and THF. Furthermore, **6.1** is stable as a C_6D_6 solution for over 24 h with minimal signs a decomposition. In addition, the IR spectrum of **6.1** features a prominent N-H stretching mode at 3336 cm^{-1} (Figure A6.11), providing further support for its formulation. For comparison, this mode is observed at 3321 cm^{-1} for its Th analogue,[17] and 3342 cm^{-1}(Zr) and 3364 cm^{-1} (Hf) for $[M(NR_2)_3(NH_2)]$ (M = Zr, Hf).[42]

I hypothesized that the reaction of **6.1** with the known thorium bis(metallacycle), $[K(DME)][Th\{N(R)(SiMe_2CH_2)\}_2(NR_2)]$,[38] in THF with the presence of 18-crown-6, would result in formation of a mixed U(IV)/Th(IV) nitride. Specifically, the NH_2 moiety of **6.1** would protonate the two CH_2 groups of $[K(DME)][Th\{N(R)(SiMe_2CH_2)\}_2(NR_2)]$ and open up the rings of the bis(metallacycle) anion, while the lone N from **6.1** would then bridge the two metals.

6.2.2 Synthesis and Characterization of $[K(18\text{-crown-}6)(THF)_2][(NR_2)_3U^{IV}(\mu\text{-}N)Th^{IV}(NR_2)_3]$ (6.2)

The reaction of **6.1** and the known thorium bis(metallacycle) was monitored in THF-d_8 by ^{1}H NMR spectroscopy. After standing at room temperature for 4 h, reveals a new broad resonance at 9.73 ppm, which is assignable to **6.2** (Figures A6.7-A6.9). After 22 h, resonances assignable to **6.1** are completely gone, while resonances assignable to $[K(DME)][Th\{N(R)(SiMe_2CH_2)\}_2(NR_2)]$[38] and 18-crown-6 have shifted significantly. After 48 h, the resonances showed no change from 22 h, and the reaction was considered complete. Work up of the reaction mixture, followed by crystallization from THF/pentane (1:1) for 24 h at -25 °C, results in the isolation of $[K(18\text{-crown-}6)(THF)_2][(NR_2)_3U^{IV}(\mu\text{-}N)Th^{IV}(NR_2)_3]$ (**6.2**) as pale orange crystals in 56% yield. Complex **6.2** can be synthesized on large scale in THF

by stirring for 24 h at room temperature. When formed in this fashion it can be isolated in 48% yield as pale orange blocks (eqn (6.2)). A second product, $[(K(18\text{-crown-}6)_{0.5})(K(18\text{-crown-}6)_{0.5}Et_2O)][(NR_2)_2U^{IV}(\mu\text{-}N)(CH_2SiMe_2NR)Th^{IV}(NR_2)_2]$ (**6.3**), can be isolated from the reaction mixture as golden brown needles, in 34% yield (eqn (6.2)), by crystallization of the remaining solid from an Et_2O solution layered with pentane that was stored at -25 °C for two weeks (see **6.2.3** for more details).

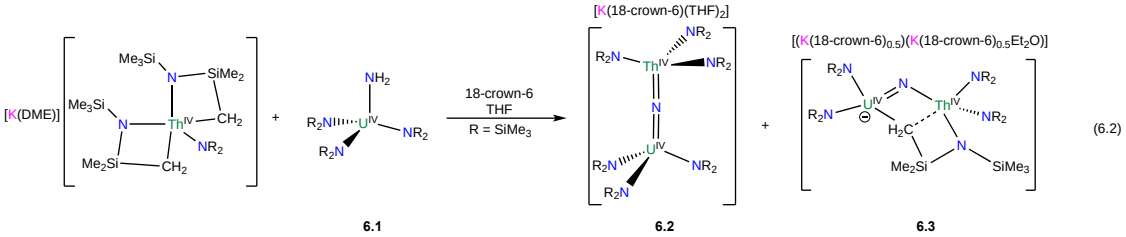

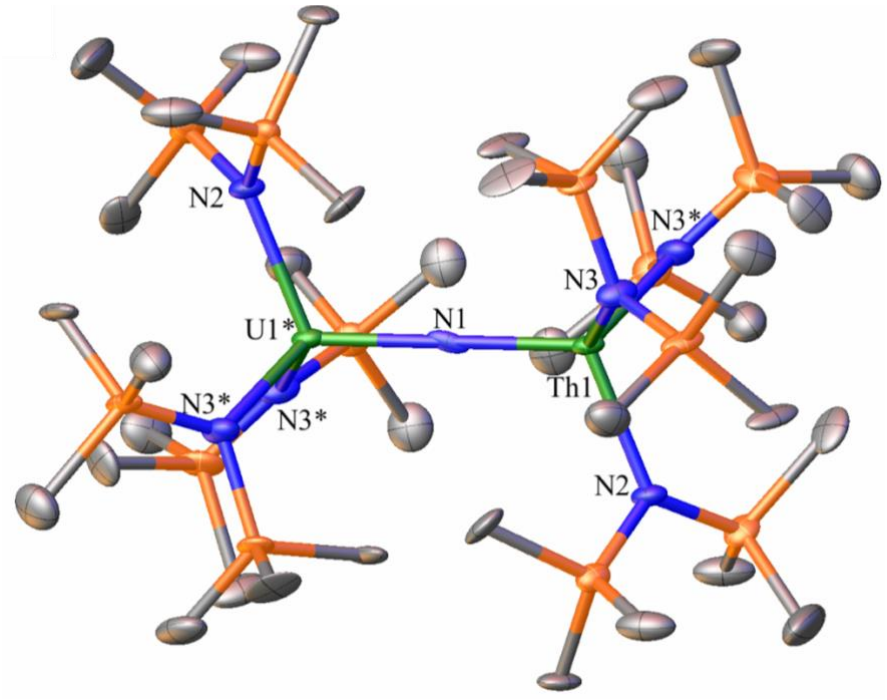

Figure 6.2. Solid-state molecular structure of **6.2** shown with 50% probability ellipsoids. $[K(18\text{-crown-}6)(THF)_2]^+$ counterion and hydrogen atoms removed for clarity.

The connectivity of complex **6.2** was verified by X-ray crystallography (Figure 6.2, Table 6.1). Complex **6.2** crystalizes in the monoclinic space group *C*2/m. In the solid-state, each Th and U center features a pseudo-tetrahedral coordination geometry. Due to the space group, the Th and U atoms are disordered over 2 positions with 50% occupancy and can be interchanged, which is noted by U* in Figure 6.2. In addition, the U*-$N_{nitride}$-Th linkage is linear (180°), while the U*/Th-$N_{nitride}$ bond lengths (U1*/Th1-N1 = 2.1037(9) Å) are much shorter than the U1*/Th1-$N_{silylamido}$ bond lengths (av. 2.389 Å), suggesting multiple bond character in the former. A $[K(18\text{-crown-6})(THF)_2]^+$ counterion is also present in the unit cell.

Complex **6.2** is the first hetero-bimetallic nitrido complex reported for the actinides and is isostructural with the previously reported nitrides, $[Na(18\text{-crown-6})(Et_2O)][(R_2N)_3Th(\mu\text{-}N)Th(NR_2)_3]$ and $[NBu_4][(R_2N)_3U(\mu\text{-}N)U(NR_2)_3]$.[2, 12, 17] Complex **6.2** features bond lengths that range in the middle of the homo-bimetallic nitrido complexes. For example, $[Na(18\text{-crown-6})(Et_2O)][(R_2N)_3Th(\mu\text{-}N)Th(NR_2)_3]$ features longer Th-$N_{nitride}$-Th distances (Th1-N1 = 2.12(3) Å; Th1-N2 = 2.13(3) Å) as well as slightly longer Th-$N_{silylamido}$ distances (av. = 2.40 Å), but a similar linear Th=N=Th linkage (176(1)°).[17] Whereas, the bridged U(IV)/U(IV) nitride, $[NBu_4][(R_2N)_3U(\mu\text{-}N)U(NR_2)_3]$,[37] features a linear U=N=U linkage (179(1)°), but shorter An-$N_{nitride}$ bond distances (2.076(5) Å, 2.083(5) Å, and 2.075(2) Å), consistent with the smaller ionic radius of uranium. Similar metric parameters are observed in $[Cs][\{U(OSi(O^tBu)_3)_3\}_2(\mu\text{-}N)]$ (U-N-U = 170.2(3)°; U1-N1 = 2.058(5) Å; U2-N1 = 2.079(5) Å).[2]

Table 6.1. Selected bond lengths (Å) and angles (deg) in complexes **6.2**, [Na(18-crown-6)(Et_2O)][$(R_2N)_3Th(\mu\text{-}N)Th(NR_2)_3$],[17] [$NBu_4$][$(R_2N)_3U(\mu\text{-}N)U(NR_2)_3$],[37] **6.4**, and [$(R_2N)_3U(\mu\text{-}N)U(NR_2)_3$].[37]

	6.2 An = Th, U	$[(R_2N)_3Th(\mu\text{-}N)Th(NR_2)_3]^-$	$[(R_2N)_3U(\mu\text{-}N)U(NR_2)_3]^-$	**6.4** An = Th, U	$[(R_2N)_3U(\mu\text{-}N)U(NR_2)_3]$
An-$N_{nitride}$	2.1037(9), 2.1037(9)	2.12(3), 2.13(3)	2.076(5), 2.083(5), 2.075(2)	2.099(12), 1.269(12)	2.080(5), 2.150(5)
An-N_{amide} (av)	2.39	2.40	2.35	2.302, 2.306	2.274(5)
An-N-An	180	176(1)	179(1)	177.9(6)	179.4(3)

The ^{1}H NMR spectrum of **6.2** in THF-d_8 should feature two different $SiMe_3$ environments due to the different metal centers. However, the spectrum features only one broad singlet at 9.73 ppm, assignable to one of the $SiMe_3$ environments, along with a sharp singlet at 3.43 ppm, assignable to the 18-crown-6 moiety (Figure 6.3).

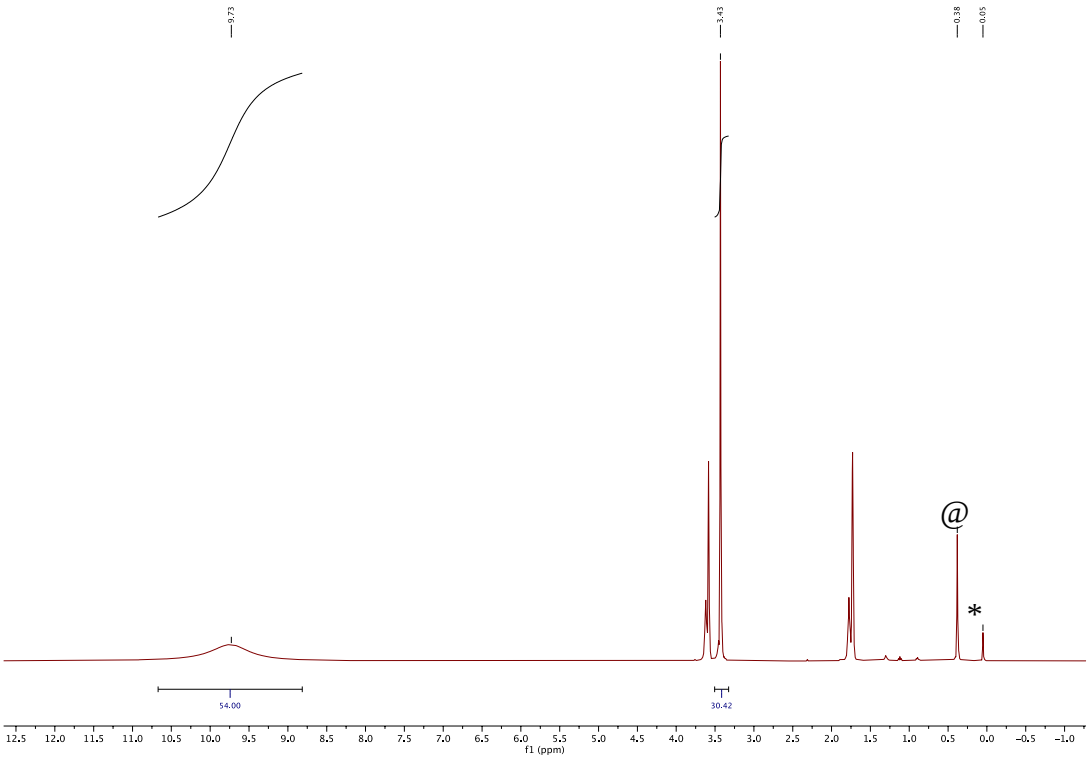

Figure 6.3. ^{1}H NMR spectrum of [K(18-crown-6)(THF)$_2$][(NR$_2$)$_3$U^{IV}(μ-N)Th^{IV}(NR$_2$)$_3$] (**6.2**) in THF-d_8. (*) indicates HN(SiMe$_3$)$_2$ and (@) indicates an unidentified peak.

Due to the single broad peak in the ^{1}H NMR spectrum, I performed Variable Temperature (VT) NMR spectroscopy to see if the two expected proton environments would appear as the temperature was decreased. As the sample was cooled from room temperature to -15 °C, two distinct resonances appear at 8.71 ppm and 13.81 ppm, in a 1:1 ratio, that have been assigned to both SiMe$_3$ environments. However, as the THF-d_8 sample of complex **6.2** was cooled past -15 °C, the ^{1}H NMR spectrum had more resonances than expected, most likely due to sample contamination with complex **6.3** (Figure A6.10).

Complex **6.2** is insoluble in pentane and benzene, but is soluble in Et$_2$O and THF. It is stable as a THF-d_8 solution at room temperature for at least 1 h, showing minimal signs of

decomposition over this time. The ultraviolet-visible (UV-vis) spectrum of **6.2** in THF features a broad absorption at 370 nm (ε = 204 M^{-1} cm^{-1}) (Figure A6.21). Finally, the IR spectrum of **6.2** features a mode at 744 cm^{-1}, which corresponds to the principal U^{IV}-N-Th^{IV} asymmetric stretch (Figure 6.4), which was later confirmed by ^{15}N labeling (see Section **6.2.5** for more details). For comparison, the principal Th-N-Th asymmetric stretch reported in $[(R_2N)_3Th(\mu\text{-}N)Th(NR_2)_3]$ (R = $SiMe_3$), was featured at 742 cm^{-1}.[17]

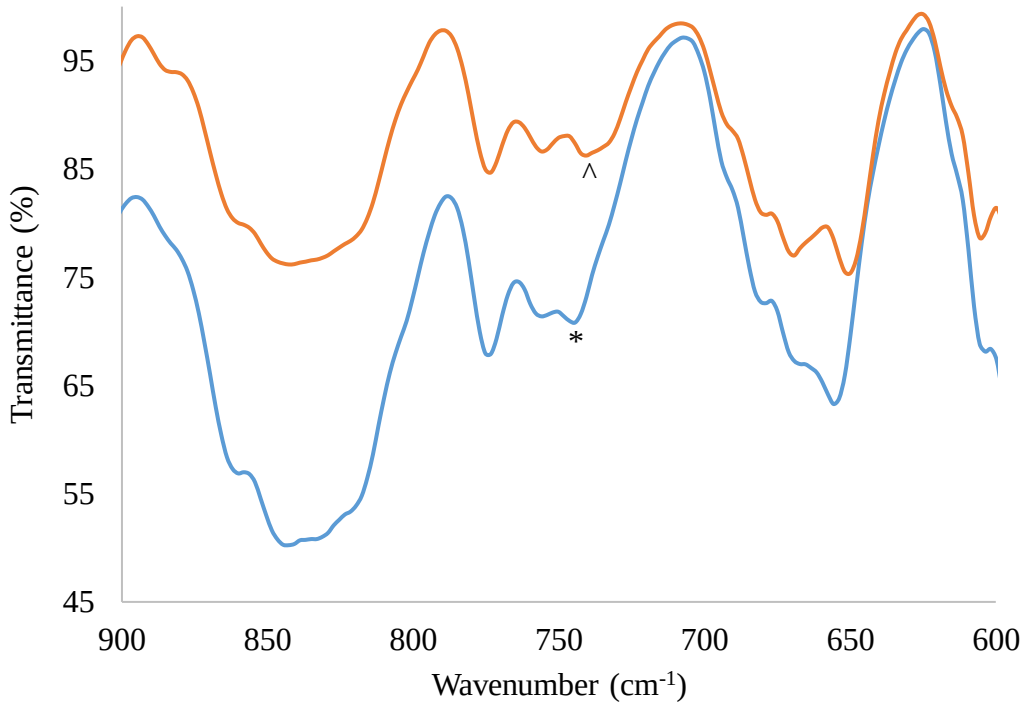

Figure 6.4. IR spectrum of $[K(18\text{-crown-6})(THF)_2][(NR_2)_3U^{IV}(\mu\text{-}N)Th^{IV}(NR_2)_3]$ (**6.2**) (blue) and $[K(18\text{-crown-6})(THF)_2][(NR_2)_3U^{IV}(\mu\text{-}^{15}N)Th^{IV}(NR_2)_3]$ (**6.2-^{15}N**) (orange) (KBr pellet). (*) denotes the ν(U-N-Th) stretch for **6.2** and (^) denotes the ν(U-N-Th) stretch for **6.2-^{15}N**.

Interestingly, the reverse reaction, whereupon the thorium parent amide, $[Th(NR_2)_3(NH_2)]$ is mixed with the known uranium bis(metallacycle), $[Na(DME)][U\{N(R)(SiMe_2CH_2)\}_2(NR_2)]$,[17, 47] in THF-$d_8$ with the presence of 18-crown-6,

does not result in a mixed U(IV)/Th(IV) nitride (eqn (6.3)). The reaction was monitored in THF-d_8 by ^{1}H NMR spectroscopy for 24 h, where the green solution showed no change in its spectra. Upon heating at 50 °C, the solution changed from green to orange, but the ^{1}H NMR spectra displayed no new resonances over 48 h of heating.

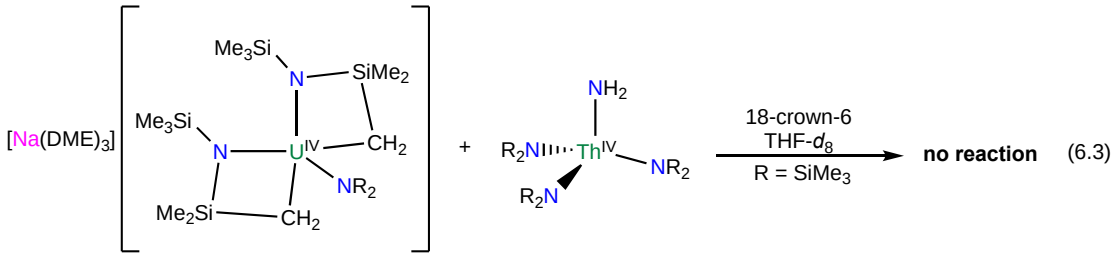

In retrospect, it is not surprising that the uranium bis(metallacycle) is a poor starting material for the nitride synthesis. For one, it has poor reactivity with acids, specifically NH_3, as was seen in Chapter 5.6.1. Moreover, it has been previously shown by Smiles and co-workers that the uranium(IV) metallacycle, [U{*N*(R)(SiMe$_2$)*C*H$_2$}(NR$_2$)$_2$], is more stable than the analogous thorium(IV) metallacycle,[48] according to protonation experiments with Ph_3PCH_2, suggesting that U-C bonds are less reactive than analogous Th-C bonds.

6.2.3 Synthesis and Characterization of [(K(18-crown-6)$_{0.5}$)(K(18-crown-6)$_{0.5}$Et$_2$O)][(NR$_2$)$_2$U^{IV}(μ-N)(*C*H$_2$SiMe$_2$*N*R)Th^{IV}(NR$_2$)$_2$] (6.3)

As mentioned in **6.2.2**, a second product, [(K(18-crown-6)$_{0.5}$)(K(18-crown-6)$_{0.5}$Et$_2$O)][(NR$_2$)$_2$U^{IV}(μ-N)(*C*H$_2$SiMe$_2$*N*R)Th^{IV}(NR$_2$)$_2$] (**6.3**), can be isolated from the reaction mixture as golden brown needles, in 34% yield (eqn (6.2)), by crystallization of the remaining solid from Et$_2$O layered with pentane that was stored at -25 °C for two weeks. It should be noted here that **6.3** is often isolated as a mixture with uranium bis(metallacycle), [K(DME)][U{*N*(R)(SiMe$_2$*C*H$_2$)}$_2$(NR$_2$)].[47] As described in **6.2.1**, if uranium metallacycle, [U{*N*(R)(SiMe$_2$)*C*H$_2$}(NR$_2$)$_2$], does not react with enough NH_3 in the THF solution, it does

not completely convert to **6.1**, leaving minor amounts of metallacycle behind in the sample of **6.1** after work up. Therefore, any unreacted uranium metallacycle that is present in the sample of **6.1** is carried through the ongoing reactions and forms uranium bis(metallacycle) from the recrystallization technique (Et_2O/pentane) to isolate **6.3**.

Complex **6.2** is formally related to **6.3** by deprotonation of a methyl group by $[NR_2]^-$, resulting in the μ-CH_2 species and free amine. Previously, this type of conversion has been seen in transition metal,[49] lanthanide,[50] and actinide systems,[11, 51-53] whereupon the $SiMe_3$ groups undergo deprotonation. For example, our group synthesized a U(IV) bridged-nitrido complex $[Na][(NR_2)_2U(\mu\text{-}N)(CH_2SiMe_2NR)U(NR_2)_2]$, which was thought to form through transient formation of $[Na][\{U(NR_2)_3\}_2(\mu\text{-}N)]$ that was unstable and resulted in the subsequent deprotonation described above.[11]

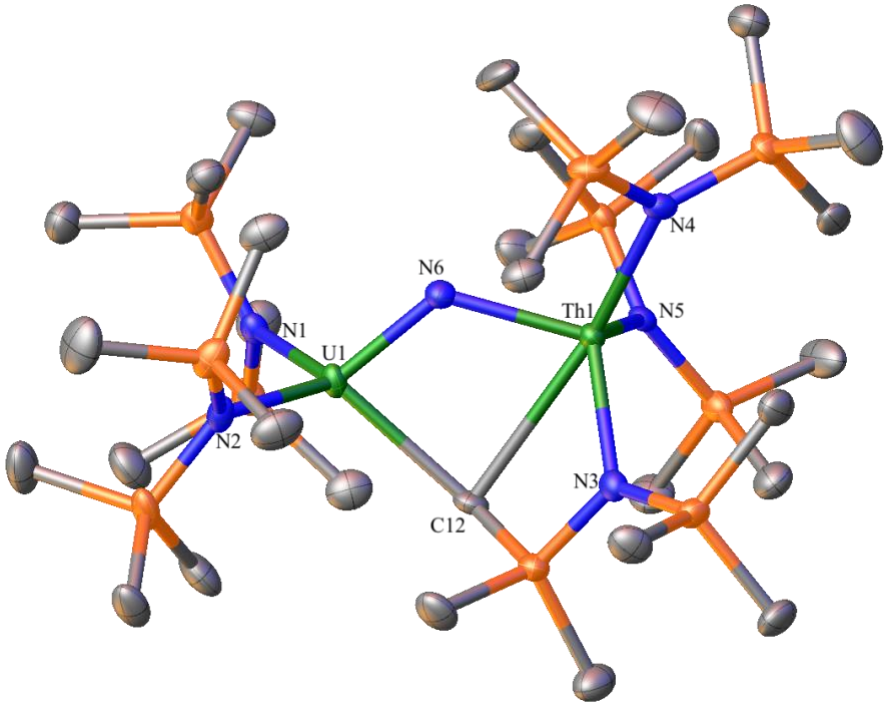

Figure 6.5. Solid-state molecular structure of **6.3** shown with 50% probability ellipsoids. $[(K(18\text{-crown-}6)_{0.5})(K(18\text{-crown-}6)_{0.5}Et_2O)]^+$ and hydrogen atoms removed

for clarity. Selected bond lengths (Å) and angles (°): U1 – N6 = 2.002(4), Th1 – N6 = 2.160(5), av. U1 – $N(SiMe_3)_2$ = 2.358, av. Th1 – $N(SiMe_3)_2$ = 2.397, U1 – C12 = 2.525(6), Th1 – C12 = 2.962(5), U1 – N6 – Th1 = 122.2(2), U1 – C12 – Th1 = 82.83(16), N – U1 – N (av) = 112.58, N – Th1 – N (av) = 109.09.

The connectivity of complex **6.3** was verified by X-ray crystallography (Figure 6.5). Complex **6.3** crystalizes in the triclinic space group *P-1*. The sold-state molecular structure of **6.3** exhibits a U-$N_{nitride}$ bond distance of 2.002(4) Å and a Th-$N_{nitride}$ bond distance of 2.160(5) Å. The An-$N_{nitride}$ bond lengths are inequivalent and suggest localized Th-N=U bonding interactions,[11, 54-56] similar to the U(IV) analogue, [Na][$(NR_2)_2$U(μ-N)(*C*H_2SiMe_2*N*R)U$(NR_2)_2$], reported by Hayton and co-workers, which reported U-$N_{nitride}$ bond distances of U1-N1 = 1.95(1) Å and U2-N1 = 2.12(1) Å.[11] This asymmetry is most likely due to the different metal ions, where uranium is more likely to form a double bond since it has accessible f-orbitals compared to thorium. The μ-CH_2 interactions in **6.3** are also inequivalent, as the U1-C12 distance (2.525(6) Å) is considerably shorter than the Th1-C12 distance (2.962(5) Å). The analogous U(IV)/U(IV) bridged-nitrido complex previously mentioned displayed similar trends with an acute U1-N1-U2 bond angle of 123.5(5)°, due to the bridging nature of the methylene group, and also featured inequivalent μ-CH_2 interactions (U1-C1 = 2.51(1) Å and U2-C1 = 2.88(1) Å).[11]

The ^{1}H NMR of **6.3** in THF-d_8 features five resonances at -9.47 ppm (36H), -5.47 ppm (6H), 3.38 ppm (24H), 6.01 ppm (9H), and 10.57 ppm (36H), assignable to the $NSiCH_3$ group, $SiMe_2CH_2$, 18-crown-6, $Me_3SiNSiMe_2CH_2$, and the other $NSiCH_3$ group, respectively (Figure 6.6). There are two resonances at 3.32 ppm (24H) and 9.55 ppm (54H) that can be assigned to 18-crown-6 and $NSiMe_3$, respectively, from small amounts of **6.2** in the sample.

Furthermore, the CH_2 resonance is not observed; it was not observed in the U(IV) analogue, $[(NR_2)_2U(\mu\text{-}N)(CH_2SiMe_2NR)U(NR_2)_2]^-$, either.[11]

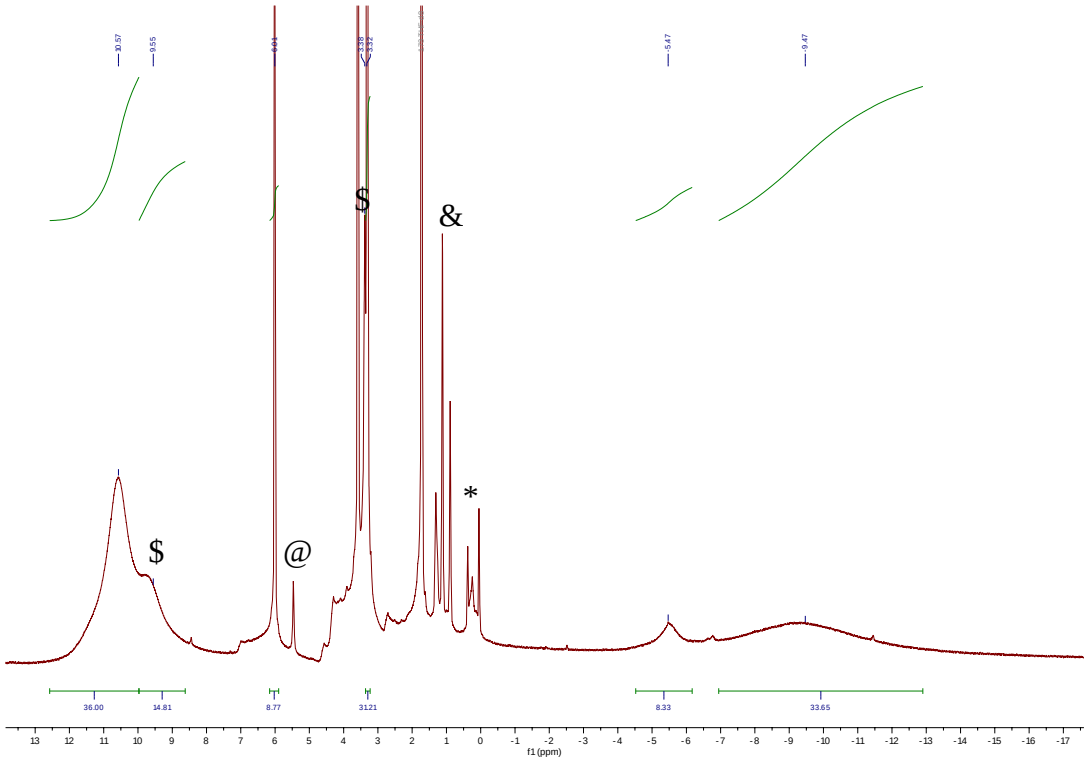

Figure 6.6. ^1H NMR spectrum of $[(K(18\text{-crown-}6)_{0.5})(K(18\text{-crown-}6)_{0.5}Et_2O)][(NR_2)_2U^{IV}(\mu\text{-}N)(CH_2SiMe_2NR)Th^{IV}(NR_2)_2]$ (**6.3**) in THF-d_8. (*) indicates $HN(SiMe_3)_2$, ($) indicates **6.2**, (&) indicates residual diethyl ether and pentane, and (@) indicates an unidentified peak.

Finally, the IR spectrum of **6.3** is found in Figure A6.16. I was unable to confidently assign a peak for the principal U^{IV}-N-Th^{IV} asymmetric stretch. Even upon ^{15}N labeling, I was still unable to confidently assign a peak (Figure A6.18)

The analogous complex that our group synthesized, the U(IV) bridged-nitrido complex $[Na][(NR_2)_2U(\mu\text{-}N)(CH_2SiMe_2NR)U(NR_2)_2]$, was able to undergo oxidation chemistry to access U(V/IV) and U(VI/IV) species. However, this oxidation chemistry is apparently not

transferable to **6.3**, and I was not able to access a U(V)/Th(IV) or U(VI)/Th(IV) species as desired. Instead, 1e$^-$ oxidation with 0.5 equiv of I_2 resulted in formation of $[U(NR_2)_3I_2][K(18\text{-crown-6})]$ in low yield, where uranium remains in the 4+ oxidation state. Moreover, reactions with the 2e$^-$ oxidants, Me_3NO and TEMPO, led to intractable material instead of the desired mixed-valent U(VI)/Th(IV) complex. I think that this redox chemistry could be hindered by the inability to access **6.3** as a pure sample; the small impurity identified as the uranium bis(metallacycle) may be interfering with the potential redox reactivity that was achieved with the analogous U(IV/IV) complex.[11]

6.2.4 Synthesis and Characterization of $[(NR_2)_3U^V(\mu\text{-}N)Th^{IV}(NR_2)_3]$ (6.4)

With complex **6.2** in hand, I attempted to oxidize the uranium center from +4 to +5, in an effort to generate a $5f^1$ complex that would be amenable to EPR spectroscopy and SQUID. Thus, addition of 0.5 equiv of I_2 in cold (-25 °C) THF, to a cold (-25 °C) THF solution of **6.2**, resulted in a color change to a dark red. Work up of the reaction mixture after 2 min, followed by crystallization from pentane/iso-octane (3:2) for 24 h at -25 °C, resulted in the isolation of $[(NR_2)_3U^V(\mu\text{-}N)Th^{IV}(NR_2)_3]$ (**6.4**) as dark brown crystalline blocks in 42% yield (eqn (6.4)).

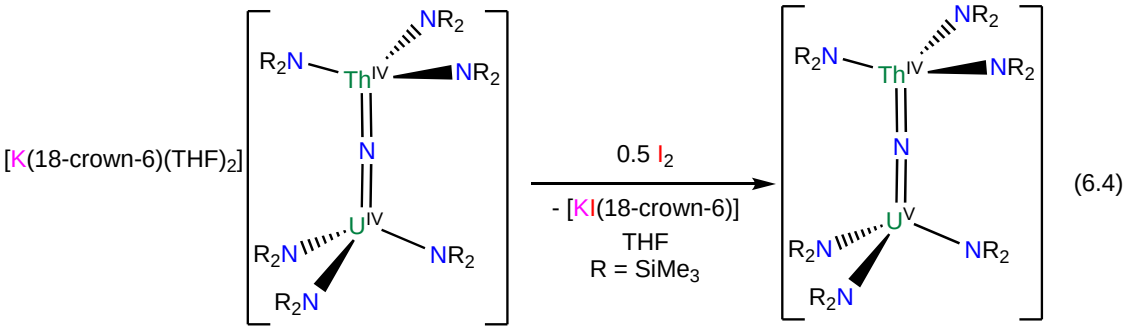

6.2 **6.4** (6.4)

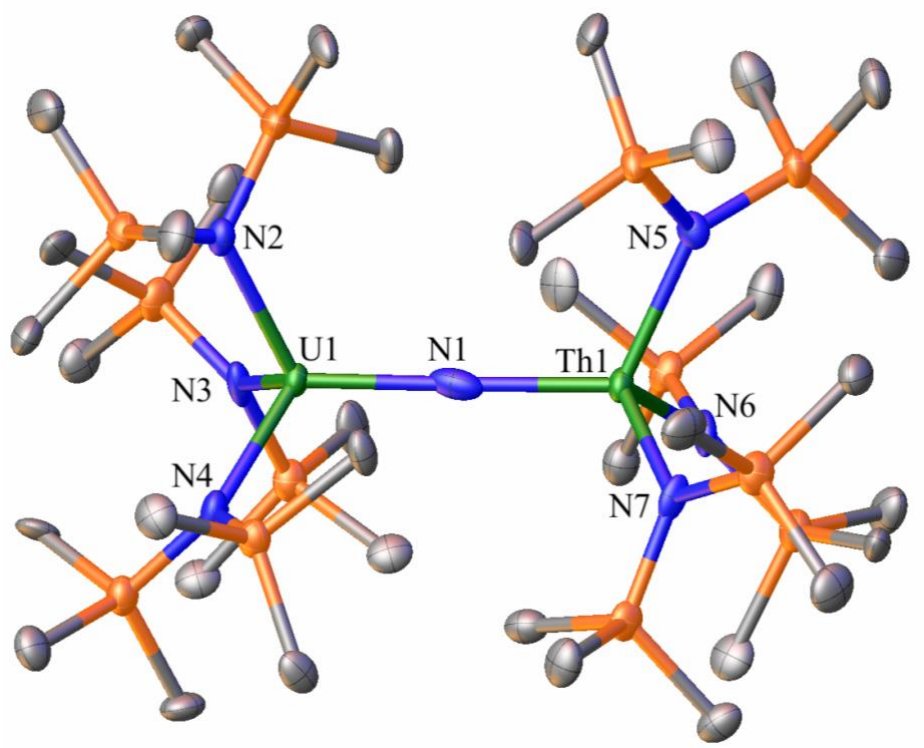

Figure 6.7. Solid-state molecular structure of **6.4**, shown with 50% probability ellipsoids. Hydrogen atoms removed for clarity.

The connectivity of complex **6.4** was verified by X-ray crystallography (Figure 6.7, Table 6.1). Complex **6.4** crystalizes in the monoclinic space group $P2_1/n$. In the solid-state, each Th and U center features a pseudo-tetrahedral coordination geometry. The disorder seen in complex **6.2** is no longer present, as revealed by the disparate An-N(nitride) bond lengths. The U-$N_{nitride}$-Th linkage remains linear (177.9(6)°). While the U1-$N_{nitride}$ bond length (U1-N1 = 2.099(12) Å) is slightly shorter than the Th1-$N_{nitride}$ bond length (Th1-N1 = 2.169(12) Å), both are much shorter than the An-$N_{silylamido}$ bond lengths (av. U-N = 2.302 Å; av. Th-N = 2.306 Å), suggesting multiple bond character in the former. Lastly, the U-$N_{nitride}$ and U-$N_{silylamido}$ bond lengths and angles contract from **6.2** to **6.4**, which supports the oxidation of U(IV) to U(V).[46]

For further comparison, [Na(18-crown-6)(Et_2O)][$(R_2N)_3Th(\mu\text{-}N)(Th(NR_2)_3$] now features shorter Th-$N_{nitride}$ distances (Th1-N1 = 2.14(2) Å; Th1-N2 = 2.11(2) Å) , but still slightly longer Th-$N_{silylamido}$ distances (av. = 2.41 Å), than those seen in **6.3**.[17] Whereas, the isostructural bridged U(IV)/U(V) nitride,[$(R_2N)_3U(\mu\text{-}N)(U(NR_2)_3$],[37] features U-N bond distances that are no longer symmetrical (2.080(5) Å and 2.150(5) Å), much like **6.4**, suggesting the presence of localized valence. Similar metric parameters are observed by Cummins and co-workers for the bridged U(IV)/U(V) nitrido complex, [{U(N(*t*Bu)Ar)$_3$}$_2$(μ-N)] (Ar = 3,5-$Me_2C_6H_3$), with U-N(nitride) bond lengths of 2.0625(2) Å and a U-N-U bond angle of 180°,[12] [{K(dme)(calix[4]tetrapyrrole)U}$_2$(μ-NK)$_2$][K(dme)$_4$], reported by Gambarotta and co-workers, with U-N(nitride) bond lengths of 2.076(6) Å and 2.099(5) Å,[1] as well as Hayton and co-workers mixed-valent U(IV/V) complex, $(NR_2)_2U(\mu\text{-}N)(CH_2SiMe_2NR)U(NR_2)_2$, which revealed U-$N_{nitride}$ bond lengths of 1.909(6) Å and 2.201(6) Å.[11] The U(V)=N bond distance is much shorter (1.909(6) Å) compared to **6.4** (2.099(12) Å), which is most likely due to the bent nature of the U-N-U bond in the former.[11]

The ^{1}H NMR spectrum of **6.4** in THF-d_8 features two broad singlets at -12.47 ppm and 4.79 ppm, assignable to the two unique $SiMe_3$ environments attached to different metal centers (Figure 6.8). The observed paramagnetic shift from 9.73 ppm (**6.2**) to 4.79 ppm (**6.4**), assigned to one of the $SiMe_3$ environments in the ^{1}H NMR spectrum, in THF-d_8, supports an oxidation reaction from a U(IV) to U(V) center, respectively.

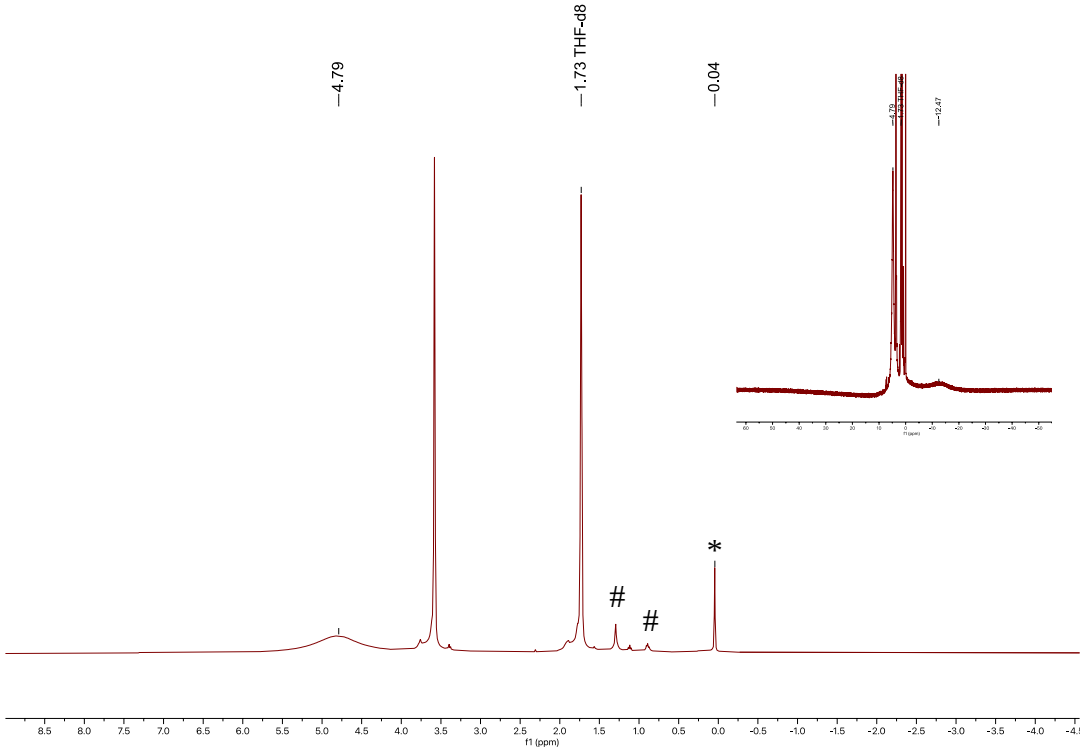

Figure 6.8. ^{1}H NMR spectrum of [$(NR_2)_3U^{V}(\mu\text{-}N)Th^{IV}(NR_2)_3$] (**6.4**) in THF-$d_8$. The inset highlights the second $SiMe_3$ resonance. (*) indicates the presence of $HN(SiMe_3)_2$ and (#) indicates the presence of pentane.

Finally, the IR spectrum of **6.4** features a mode at 725 cm^{-1}, which corresponds to the principal U^{V}-N-Th^{IV} asymmetric stretch (Figure 6.9) and was confirmed by ^{15}N labeling (see **6.2.6** for more details). Compared to **6.2** (U^{IV}-N-Th^{IV} asymmetric stretch = 744 cm^{-1}), this stretch is redshifted by 19 cm^{-1} and it is not entirely clear why it is not blue shifted, as expected.

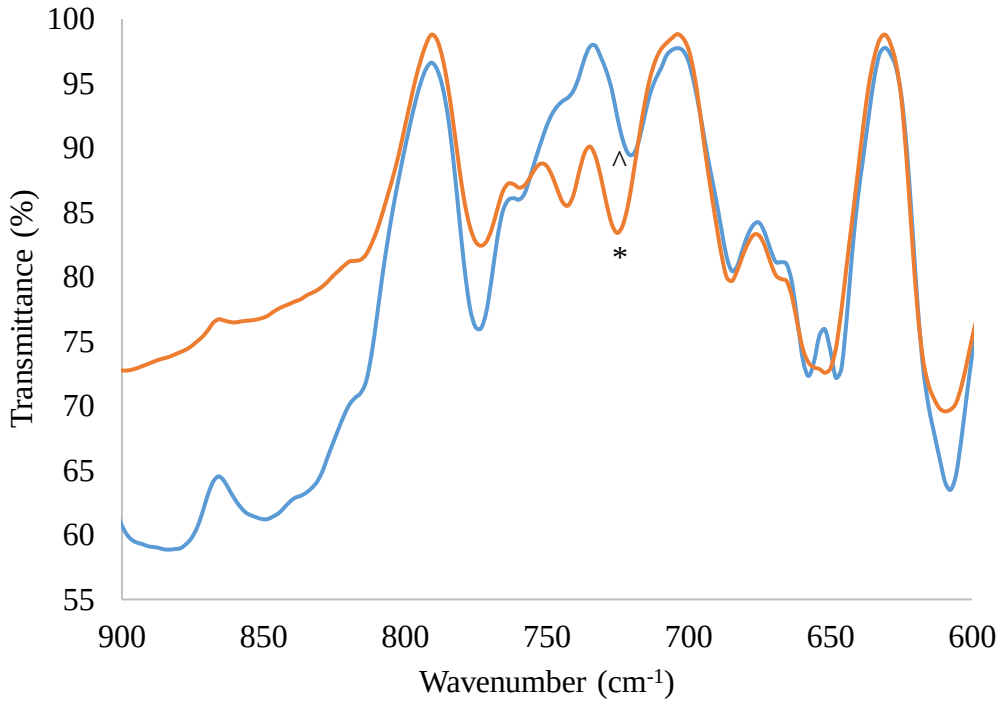

Figure 6.9. IR spectrum of $[(NR_2)_3U^V(\mu\text{-}N)Th^{IV}(NR_2)_3]$ (**6.4**) (orange) and $[(NR_2)_3U^V(\mu\text{-}^{15}N)Th^{IV}(NR_2)_3]$ (**6.4-^{15}N**) (blue) (KBr pellet). (*) denotes the ν(U-N-Th) stretch for **6.4** and (^) denotes the ν(U-N-Th) stretch for **6.4-^{15}N**.

The UV-vis/NIR electronic absorption spectrum of **6.4** (Figure 6.10) is dominated by f-f-transitions in the NIR region. Experimental results support the uranium(V) oxidation state of **6.4**, where four transitions are observed at 979 nm (ε = 83.4 L $mol^{-1}cm^{-1}$), 1221 nm (ε = 56.5 $mol^{-1}cm^{-1}$), 1410 (ε = 70.0 $mol^{-1}cm^{-1}$), and 1599 (ε = 69.2 $mol^{-1}cm^{-1}$) in a 10.44 mM THF solution. These features are assigned to Laporte forbidden 5f-5f transitions, where three 5f-5f transitions have been tentatively assigned, going from the ground state ($5f_{y(y^2-3x^2)}$, $5f_{x(x^2-3y^2)}$) to the LUMO ($5f_{xyz}$, $5f_{z(x^2-y^2)}$), LUMO+1 ($5f_{xz^2}$, $5f_{yz^2}$), and LUMO+2 ($5f_{z^3}$).

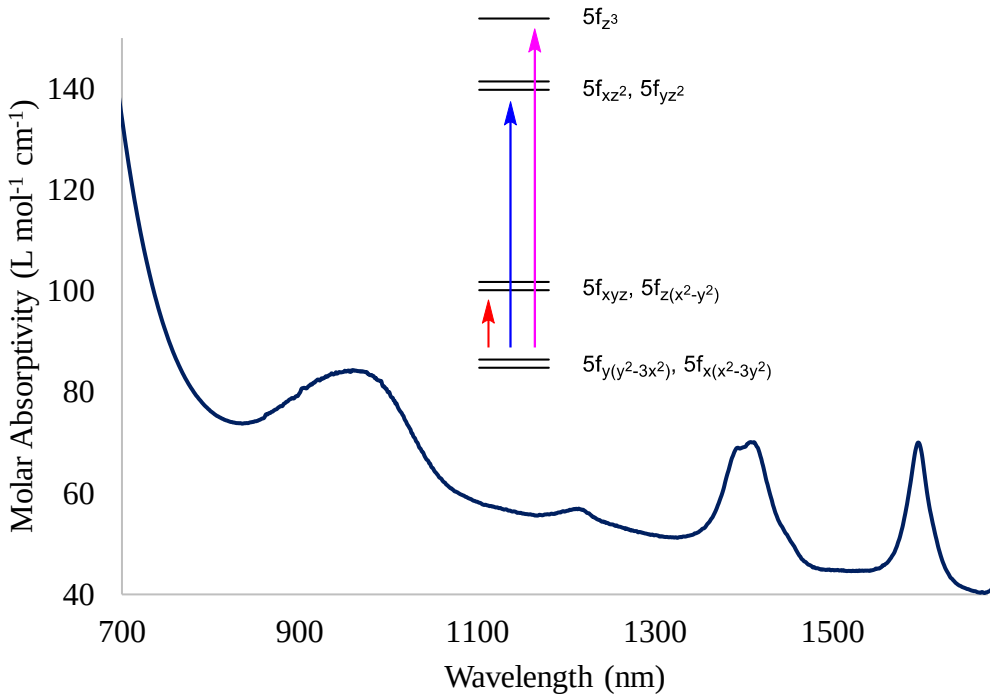

Figure 6.10. UV-vis/NIR spectrum of $[(NR_2)_3U^{V}(\mu\text{-}N)Th^{IV}(NR_2)_3]$ (**6.4**) (10.44 mM, λ_{max} 979 nm (ε = 83.4 L mol^{-1}cm^{-1}), λ_{max} 1221 nm (ε = 56.5 mol^{-1}cm^{-1}), λ_{max} 1410 (ε = 70.0 mol^{-1}cm^{-1}), λ_{max} 1599 (ε = 69.2 mol^{-1}cm^{-1})) in THF.

6.2.5 Synthesis and Characterization of $[U(NR_2)_3(^{15}NH_2)]$ (6.1-^{15}N)

Access to the ^{15}N-labeled complex of **6.1** was achieved by reaction of $[U\{N(R)(SiMe_2)CH_2\}(NR_2)_2]$[39], in THF, with 1 equiv of $^{15}NH_3$ gas, added using the Schlenk line. The reaction mixture sat for 24 h, as the solution turned a darker brown-orange color, whereupon work-up in pentane and dried *in vacuo* resulted in a dark brown-orange solid of $[U(NR_2)_3(^{15}NH_2)]$ (**6.1-^{15}N**) in 41% yield, based on the ratio of product to uranium starting material determined by the ^{1}H NMR spectrum (Figure A6.2). The ^{1}H NMR spectrum in benzene-d_6, has the same broad singlet at -2.95 ppm (54H), assignable to the $SiMe_3$ groups, as seen in **6.1**. However, the $-NH_2$ resonance is most likely masked by the presence of

[U{*N*(R)(SiMe$_2$)*C*H$_2$}(NR$_2$)$_2$][39] (Figure A6.2), which is also present in the sample. According to integrations of the ^{1}H NMR spectrum, **6.1-^{15}N** and [U{*N*(R)(SiMe$_2$)*C*H$_2$}(NR$_2$)$_2$] are present in a 1:0.5 ratio.[39] As mentioned in Section **6.2.1**, full conversion to the parent amide works best with excess NH$_3$, but if too much NH$_3$ is added it can lead to the formation of an insoluble solid. For this reason, I made sure not to add excess NH$_3$, and as a result the conversion to **6.1-^{15}N** was incomplete. Despite **6.1-^{15}N** being impure, the isolated material was used in the proceeding reactions, which worked as expected. Finally, the IR spectrum of **6.1-^{15}N** features a prominent N-H stretching mode at 3331 cm^{-1} that is redshifted by 5 cm^{-1} from that observed for **6.1** (Figure A6.12 and A6.13).

6.2.6 Synthesis and Characterization of [K(18-crown-6)(THF)$_2$][(NR$_2$)$_3$U^{IV}(μ-^{15}N)Th^{IV}(NR$_2$)$_3$] (6.2-^{15}N) and [(K(18-crown-6)$_{0.5}$)(K(18-crown-6)$_{0.5}$Et$_2$O)][(NR$_2$)$_2$U^{IV}(μ-^{15}N)(*C*H$_2$SiMe$_2$*N*R)Th^{IV}(NR$_2$)$_2$] (6.3-^{15}N)

With **6.1-^{15}N** in hand, a cold THF solution of [K(DME)][Th{*N*(R)(SiMe$_2$*C*H$_2$)}$_2$(NR$_2$)][38] and 18-crown-6 were added to a cold, stirring dark brown-orange solution of **6.1-^{15}N**. Work-up of the reaction after 24 h resulted in isolation of pale orange crystals of [K(18-crown-6)(THF)$_2$][(NR$_2$)$_3$U^{IV}(μ-^{15}N)Th^{IV}(NR$_2$)$_3$] (**6.2-^{15}N**), which grew from a THF/pentane solution stored at -25 °C for 24 h and were isolated in 45% yield. Similar to **6.2**, the ^{1}H NMR spectrum in THF-d_8 reveals two resonances at 3.45 ppm (24H) and 9.76 ppm (54H), assigned to the 18-crown-6 moiety and one of the expected two SiMe$_3$ groups, respectively (Figure A6.3). Finally, the IR spectrum of **6.2-^{15}N** features a stretch at 741 cm^{-1}, which corresponds to the U^{IV}-N-Th^{IV} asymmetric stretch (Figure 6.11) and is redshifted by 3 cm^{-1} from that observed for **6.2**. This observed shift is unusually small, but I am confident in my assignment. For

comparison, the principal Th-N-Th asymmetric stretch reported in the ^{15}N analogue of $[(R_2N)_3Th(\mu\text{-}N)Th(NR_2)_3]$, was redshifted by 7 cm^{-1} from the unlabeled complex.[17]

Similar to the synthesis of **6.3**, the supernatant of **6.2-^{15}N** was dried and extracted into diethyl ether and layered with pentane. After storage at -25 °C for 2 weeks, crystalline material of $[(K(18\text{-crown-}6)_{0.5})(K(18\text{-crown-}6)_{0.5}Et_2O)][(NR_2)_2U^{IV}(\mu\text{-}^{15}N)(CH_2SiMe_2NR)Th^{IV}(NR_2)_2]$ (**6.3-^{15}N**) was isolated in 23% yield, along with the known uranium bis(metallacycle), $[K(DME)][U\{N(R)(SiMe_2CH_2)\}_2(NR_2)]$,[47] in a 1:7 ratio, respectively. The large presence of uranium bis(metallacycle) is most likely from $[U\{N(R)(SiMe_2)CH_2\}(NR_2)_2]$[39] that remained in solution from **6.1-^{15}N** and carried through the reaction of **6.2-^{15}N**. The ^{1}H NMR spectrum of the isolated material supports the ratio of **6.3-^{15}N** to uranium bis(metallacycle) anion (Figures A6.4, A6.5).[47]

6.2.7 Synthesis and Characterization of $[(NR_2)_3U^V(\mu\text{-}^{15}N)Th^{IV}(NR_2)_3]$ (6.4-^{15}N)

Reaction of a cold, stirring THF solution of **6.2-^{15}N** with 0.5 equiv I_2 as a cold THF solution, resulted in a color change from pale orange to dark red-brown. Work-up of the reaction mixture resulted in isolation of $[(NR_2)_3U^V(\mu\text{-}^{15}N)Th^{IV}(NR_2)_3]$ (**6.4-^{15}N**) in 34% yield as dark crystalline powder. The ^{1}H NMR spectrum of **6.4-^{15}N** in THF-d_8 reveals the loss of $[K(18\text{-crown-}6)(THF)_2][I]$, where two broad resonance at -12.15 ppm and 4.78 ppm are assigned to the two unique $SiMe_3$ groups on the different metal centers (Figure A6.6). Similar to **6.4**, the resonances are too broad to determine accurate integrations. Lastly, the IR spectrum of **6.4-^{15}N** features a mode at 719 cm^{-1}, which corresponds to the principal U^V-N-Th^{IV} asymmetric stretch (Figure A6.20) and is redshifted by 6 cm^{-1} from that observed for **6.4**, providing further support for my formulation (Figure 6.9).

6.2.8 EPR Spectroscopy of 6.4

The electron paramagnetic resonance (EPR) spectrum of **6.4** (Figure 6.11) was recorded by Dr. Shamon Walker at UCSB and was obtained in quartz glass at 4 K as a powdered sample. This spectrum displays a single peak at 3.58, which is assigned to $g_{\|}$ (Figure 6.11). The other g value, which would be assignable to $g_{\perp}$, likely resides below 0.7, which is outside of the range of the spectrometer. For comparison, Liddle and co-workers report a family of uranium(V) nitride complexes, $[(Tren^{TIPS})U^{V}\{(\mu\text{-}N)(\mu\text{-}M)\}_2U^{V}(Tren^{TIPS})]$ ($Tren^{TIPS}$ = $\{N(CH_2CH_2NSi^{i}Pr_3)_3\}^{3-}$, M = Li, Na, K, Rb, Cs), which have a dominant feature at g = 3.74(9), except for when M = Li and Na.[15] Complex **6.4** features a smaller $g_{\|}$ than what is reported in these complexes.

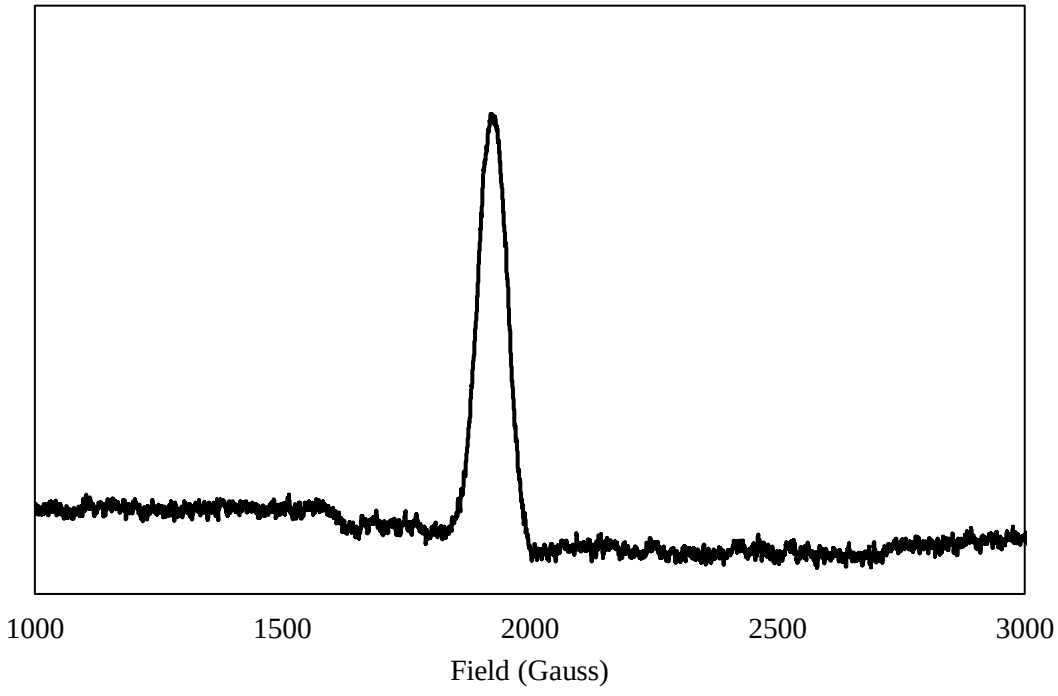

Figure 6.11. EPR spectrum of $[(NR_2)_3U^{V}(\mu\text{-}N)Th^{IV}(NR_2)_3]$ (**6.4**) at 4K.

6.2.9 SQUID Spectroscopy of 6.4

Variable-temperature superconducting quantum interference device (SQUID) magnetometry, performed by Dr. Wayne Lukens at LBNL, was done on a powdered sample of **6.4** to confirm the pentavalent assignment of the uranium center (Figure 6.12). The effective magnetic moment is 2.2 μ_B at 300 K for 4, 5, and 6 T, respectively, where μ_B is a Bohr magneton. Compared to the theoretical magnetic moment reported for uranium(V), which is 2.54 μ_B for one uranium(V) center, the magnetic moment is lower in **6.4**.[33] As the temperature decreases, the magnetic moment does too, and at 4 K, μ_{eff} = 1.44 μ_B. This trend has been observed with other U(V) compounds.[16, 57, 58] For comparison, $[OU^{V}(NR_2)_3]$, reported by Hayton and co-workers,[58] exhibits a magnetic moment of 1.59 μ_B at 300 K, which gradually decreased to 0.94 μ_B at 4 K. Similar to **6.4**, these values are also noticeably lower than the theoretical U(V) free ion value, but by a greater degree. Whereas the complex $[U(O)(tacn(OAr^{R})_3)]$ (μ_{eff} = 1.98 μ_B, R = ^{t}Bu; μ_{eff} = 1.92 μ_B, R = Ad), at room temperature, features values that are closer to what I report for **6.4**.[57] The low μ_{eff} reported for **6.4** could be due to the decrease of spin-orbit coupling that could come from covalent actinide-nitrogen interactions.[57-59]

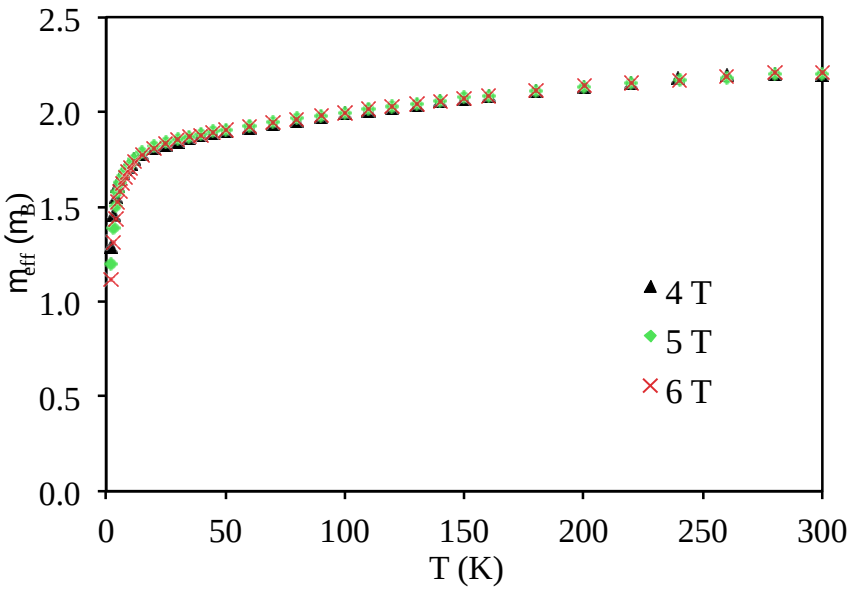

Figure 6.12. Magnetic moment of **6.4** versus temperature with ferromagnetic impurity correction.

6.3 Summary

I have synthesized and characterized a novel uranium parent amide, $[U(NR_2)_3(NH_2)]$ (**6.1**), which proved to be synthetically useful en route to the first isolable hetero-bimetallic actinide nitride complex, $[(NR_2)_3U^{IV}(\mu\text{-}N)Th^{IV}(NR_2)_3]^-$ (**6.2**), upon reaction with the known thorium bis(metallacycle)[38] and 18-crown-6. Interestingly, the reverse reaction, using the thorium parent amide and uranium bis(metallacycle),[17, 47] as an alternative route to **6.2** proved to be unsuccessful, on account of the relatively low reactivity of uranium bis(metallacycle) with acids.[48]

Furthermore, **6.2** undergoes subsequent deprotonation of a methyl group by $[NR_2]^-$ to generate the $\mu\text{-}CH_2$ moiety, $[(NR_2)_2U^{IV}(\mu\text{-}N)(CH_2SiMe_2NR)Th^{IV}(NR_2)_2]^-$ (**6.3**), isolated from the supernatant. Isostructural to the previously reported U(IV) bridged-nitrido complex, I sought to transfer the oxidation chemistry that was achieved with this reported bridged-nitrido to **6.3**, but the desired reactivity to a U(V)/Th(IV) or U(VI)/Th(IV) species proved

unsuccessful.[11] Instead, 1e$^-$ oxidation to U(V), with 0.5 equiv I_2, resulted in undesirable reactivity where [U(NR$_2$)$_3$I$_2$][K(18-crown-6)] was isolated, which features an unoxidized U(IV) center. Moreover, 2e$^-$ oxidation to U(VI), with Me$_3$NO and TEMPO, resulted in intractable material. One explanation as to why this hetero-bimetallic bridged nitrido cannot undergo the same redox chemistry that was seen with the analogous U(IV/IV) bridged-nitrido complex is because the desired oxidation is being hindered by the small impurity, uranium bis(metallacycle), that is present upon work-up of **6.3** as a by-product; a result of using isolated material of **6.1** that did not achieve complete conversion and consequently contains uranium metallacycle for the proceeding reactions. Therefore, it is of interest to improve the synthesis of **6.3** and try this desired redox chemistry again with pure material.

Gratifyingly, complex **6.2** was oxidized by 0.5 equiv of I_2 to form the novel, mixed-valent hetero-bimetallic actinide bridging nitride complex, [(NR$_2$)$_3$U^V(μ-N)Th^{IV}(NR$_2$)$_3$] (**6.4**). This complex is unique because the diamagnetic thorium(IV) center allows for an easier analysis of the bonding between the metal centers and the nitride fragment, compared to previously reported U(V/IV) nitridos.[1, 11, 12, 37] As Th has no unpaired electrons, it makes the spectroscopic data easier to interpret. This fact was shown in the analysis of the data collected using several characterization techniques, including EPR spectroscopy, which revealed a $g_{||}$ value of 3.58 and SQUID magnetometry, which featured an effective magnetic moment of 2.2 μ_B at 300 K for 4, 5, and 6 T. The UV-vis/NIR spectrum of **6.4** shows three peaks in the NIR region that have been tentatively assigned to three Laporte forbidden 5f-5f transitions. Lastly, using IR spectroscopy and ^{15}N-isotopic labeling, the structural assignment was confirmed to support my uranium(V) assignment.

This route to a hetero-bimetallic actinide nitride described within could be extended to the transuranics, helping to advance transuranic synthesis and characterization, which lags far behind that of uranium and thorium.[13, 18, 19, 21, 60] In particular, the Np bis(metallacycle) (see Chapter 7 for more details),[47] could be a useful precursor for the synthesis of a Np(IV)/An(IV) (An = Th, U) bridging nitride. Using either **6.1** or the Th analogue[17] in the presence of Np bis(metallacycle) and a complexing agent, such as 18-crown-6, the desired Np-An nitride could be isolated. This proposed reaction shows promise because complexes **6.2** and **6.3** can be isolated on small scale (20 mg), as shown *via* ^{1}H NMR spectroscopy monitoring reactions, which is necessary for the transfer of early actinide chemistry to the transuranics.[47] The isolation of this proposed transuranic nitride complex would greatly help advance non-aqueous neptunium coordination chemistry[61] and provide interesting insight into the bonding modes of a novel transuranic nitride.

6.4 Acknowledgements

This work was supported by the U.S. Department of Energy, Office of Basic Energy Sciences, Chemical Sciences, Biosciences, and Geosciences Division, under Contract DE-SC0001861. I would like to thank Shamon Walker (UCSB MRL) for his help with the EPR measurements. The MRL Shared Experimental Facilities are supported by the MRSEC Program of the NSF under Award No. DMR 1720256; a member of the NSF-funded Materials Research Facilities Network (www.mrfn.org). I would also like to thank Wayne Lukens (LBNL) for his help with the SQUID measurements and Sam in the Ménard lab (UCSB) for $^{15}NH_3$, his help with the gas addition, and willing to store my bottle of NH_3 in his glovebox freezer.

6.5 Experimental

6.5.1 General Methods

All reactions and subsequent manipulations were performed under anaerobic and anhydrous conditions under an atmosphere of nitrogen. Hexanes, Et_2O, pentane, and toluene were dried using a Vacuum Atmospheres DRI-SOLV Solvent Purification system and stored over 3Å sieves for 24 h prior to use. THF was dried by distillation from sodium/ benzophenone, and stored over 3Å sieves for 24 h prior to use. Benzene-d_6 and THF-d_8 were dried over 3Å molecular sieves for 24 h prior to use. [U{*N*(R)(SiMe$_2$)*C*H$_2$}(NR$_2$)$_2$] and [K(DME)][Th{*N*(R)(SiMe$_2$*C*H$_2$)}$_2$(NR$_2$)] were synthesized according to the previously reported procedures.[38, 39] All other reagents were purchased from commercial suppliers and used as received.

NMR spectra were recorded on an Agilent Technologies 400-MR DD2 400 MHz Spectrometer, a Varian UNITY INOVA 500 spectrometer, or a Varian Unity Inova 600 MHz spectrometer. ^{1}H NMR spectra were referenced to external tetramethylsilane (TMS) using the residual protio solvent peaks as internal standards. ^{13}C{^{1}H} NMR spectra were referenced indirectly with the ^{1}H resonance of TMS at 0.0 ppm, according to IUPAC standard,[62, 63] using the residual solvent peaks as internal standards. IR spectra were recorded on a Nicolet 6700 FT-IR spectrometer with a NXR FT Raman Module. Electronic absorption spectra were recorded on a Shimadzu UV3600 UV-NIR Spectrometer. Elemental analyses were performed by the Micro-Analytical Facility at the University of California, Berkeley.

EPR Spectroscopy: About 20 mg of a crystalline powered sample of **6.4** was finely ground using a mortar and pestle (cleaned and oven dried before use). The ground sample was transferred into a quartz tube (5 mm) and a small amount of glass wool was placed inside. The

tube was placed under vacuum for a few minutes before transferred to the glass shop, where the quartz tube was flame sealed with a propane/oxygen torch. Data was recorded on a Bruker X-band EPR EMX Plus spectrometer equipped with a Bruker dual-mode cavity (ER 4116DM) for both parallel and perpendicular modes. Equipped with an Oxford Instruments SPE62NT900 liquid helium quartz cryostat using an Oxford Instruments ITC503 temperature and gas flow controller. Parameters include microwave frequency (9.646641 GHz), microwave power (100.2 mW), and number of scans (10).

SQUID: A sample of **6.4** (18.2 mg) was sandwiched between two pieces of quartz wool (8.7 mg total) inside a 3 mm OD quartz tube and compressed with quartz rods to form a pellet. The ends of the tube were capped with septa to seal. The middle of the tube was wrapped with a Kimwipe and cooled with liquid nitrogen. One end of the tube was flame sealed with a propane/oxygen torch. The sealed end of the tube was immersed in liquid nitrogen, and the other end of the tube was flame-sealed. Data was recorded at 6 T, 5 T, 4 T, 3 T 2 T, and 1 T using a Quantum Designs MPMS magnetometer. Data were corrected for inherent diamagnetism of the compound using Pascal's constants. The data showed the presence of a ferromagnetic impurity, and the appropriate correction was applied. The correction, 2×10^{-3} emu is large relative to the magnetization of the sample at fields below 4 T. As a result, the high temperature data is not usable at low field. For this reason, only the data at 6, 5, and 4 T are used.

An additional complication is that the compound contains 2 pentane molecules of crystallization, which can be lost during drying of the compound. Based on the results, it seems likely that the pentane molecules were retained, so the results are given assuming that the sample analyzed still contains the two pentane molecules of solvation.

6.5.2 Synthesis and Characterization of [U(NR$_2$)$_3$(NH$_2$)] (R = SiMe$_3$) (6.1)

To a stirring, cold (-25 °C), orange solution of [U{*N*(R)(SiMe$_2$)*C*H$_2$}(NR$_2$)$_2$] (111.6 mg, 0.162 mmol) in THF (2 mL) was added a THF solution of NH_3 (1.17 mL, 0.468 mmol, 0.4 M). The orange reaction mixture was allowed to warm to room temperature with stirring. After 1 h, the volatiles were removed *in vacuo* to provide a dark brown-orange solid. The solid was then extracted into pentane (3 mL) and the resulting dark-brown, cloudy suspension was filtered through a Celite column supported on glass wool (0.5 × 2 cm). The filtrate was transferred to a 4 mL vial, which was placed inside a 20 mL scintillation vial and iso-octane (2 mL) was added to the outer vial. Storage of this two-vial system at -25 °C for 5 d resulted in the deposition of dark brown-orange blocks. The solid was isolated by decanting the supernatant and then dried *in vacuo* to yield **6.1** (17.0 mg). The supernatant was transferred to a new 4 mL vial, which was placed inside a 20 mL scintillation vial and iso-octane (2 mL) was added to the outer vial. Storage of this two-vial system at -25 °C for 2 d resulted in the deposition of more dark brown-orange crystalline solid (62.3 mg). Total yield: 0.0793 g, 69% yield. Anal. Calcd for $C_{18}H_{56}N_4Si_6U$: C, 29.41; H, 7.68; N, 7.62. Found: C, 29.38; H, 7.38; N, 7.24. ^{1}H NMR (400 MHz, 25 °C, C_6D_6): δ -2.95 (s, 54H, SiC*H*$_3$). IR (KBr pellet, cm^{-1}): 432 (s), 525 (s), 609 (s), 613 (s), 864 (w), 1180 (s), 1246 (s), 1402 (m), 1504 (s), 1618 (m), 1919 (m), 2949 (w), 3336 (s, ν_{NH}).

6.5.3 Synthesis and Characterization of [U(NR$_2$)$_3$(^{15}NH$_2$)] (R = SiMe$_3$) (6.1-^{15}N)

To an orange solution of [U{*N*(R)(SiMe$_2$)*C*H$_2$}(NR$_2$)$_2$] (255.3 mg, 0.3555 mmol) in THF (2 mL) was added to a 20 mL Schlenk tube fitted with a rotaflow valve. The Schlenk tube was removed from the glovebox, attached to a vacuum line, the headspace was evacuated, and

gaseous $^{15}NH_3$ (1 atm, 8 mL, 0.3555 mmol) was added to the Schlenk flask. The Schlenk tube was brought back into the gloveback, allowed to stand for 24 h, and the darker reaction mixture was transferred to a 20 mL vial. The volatiles were removed *in vacuo* to provide a dark solid. The solid was extracted into pentane (4 mL) and the resulting cloudy suspension was filtered through a Celite column supported on glass wool (0.5 × 2 cm), where upon the volatiles were removed *in vacuo* to provide a dark brown-orange solid as **6.1-^{15}N** (213.9 mg, 41% yield) in a 1:0.5 ratio with [U{*N*(R)(SiMe$_2$)*C*H$_2$}(NR$_2$)$_2$][39]. ^{1}H NMR (400 MHz, 25 °C, C_6D_6): δ -13.21 (s, 36H, N(SiMe$_3$)$_2$, metallacycle), -2.95 (s, 54H, SiC*H*$_3$, **6.1-^{15}N**), 9.74 (s, 9H, NSiMe$_3$, metallacycle), 11.41, (s, 6H, SiMe$_2$, metallacycle). IR (KBr pellet, cm^{-1}): 609 (s), 660 (m), 756 (m), 843 (w), 931 (w), 1182 (s), 1254 (s), 1400 (w), 1603 (w), 2897 (w), 2954 (w), 3331 (s, ν_{NH}).

6.5.4 Synthesis and Characterization of [K(18-crown-6)(THF)$_2$][(NR$_2$)$_3$U^{IV}(μ-N)Th^{IV}(NR$_2$)$_3$] (6.2)

To a stirring, cold (-25 °C), dark brown solution of **6.1** (90.7 mg, 0.123 mmol) in THF (2 mL) was added a cold (-25 °C), pale-yellow solution of [K(DME)][Th{*N*(R)(SiMe$_2$*C*H$_2$)}$_2$(NR$_2$)] (103 mg, 0.123 mmol) in THF (2 mL) , along with a colorless THF (2 mL) solution of 18-crown-6 (33.2 mg, 0.126 mmol). After 24 h, the solution was filtered through a Celite column supported on glass wool (0.5 × 2 cm), concentrated *in vacuo* to 2 mL, and layered with pentane (4 mL). Storage at -25 °C for 24 h resulted in the deposition of pale orange crystalline material, which was isolated by decanting the supernatant and then dried *in vacuo* to yield **6.2**. Total yield: .111 g, 48% yield. Anal. Calcd for $C_{56}H_{148}KN_7O_8Si_{12}ThU$: C, 35.51; H, 7.88; N, 5.18. Found: C, 35.64; H, 7.74; N, 5.00. ^{1}H NMR (400 MHz, 25 °C, THF-d_8): δ 3.43 (s, 24H, 18-crown-6), 9.73 (br s, 54H,

SiCH_3). UV-vis/NIR (THF, 0.5 mM, 25 °C, L $mol^{-1}cm^{-1}$): 370 nm (ε = 203.8). IR (KBr pellet, cm^{-1}): 594 (s), 656 (s), 744 (s, asym, ν_{UNTh}), 843 (w), 930 (w), 1111 (m), 1250 (m), 1352 (s), 2895 (w), 2949 (w), 3448 (w).

6.5.5 Synthesis and Characterization of [K(18-crown-6)(THF)$_2$][(NR$_2$)$_3$U^{IV}(μ-^{15}N)Th^{IV}(NR$_2$)$_3$] (6.2-^{15}N)

To a stirring, cold (-25 °C), dark brown solution of **6.1-^{15}N** (180.1 mg, 0.2450 mmol) in THF (2 mL) was added a cold (-25 °C), pale-yellow solution of [K(DME)][Th{*N*(R)(SiMe$_2$*C*H$_2$)}$_2$(NR$_2$)] (207.4 mg, 0.2468 mmol) in THF (2 mL) , along with a colorless THF (2 mL) solution of 18-crown-6 (65.2 mg, 0.2469 mmol). After 24 h, the solution was filtered through a Celite column supported on glass wool (0.5 × 2 cm), concentrated *in vacuo* to 2 mL, and layered with pentane (4 mL). Storage at -25 °C for 24 h resulted in the deposition of pale orange crystalline material, which was isolated by decanting the supernatant and then dried *in vacuo* to yield **6.2-^{15}N**. Total yield: 0.2069 g, 45% yield. ^{1}H NMR (400 MHz, 25 °C, THF-d_8): δ 3.45 (s, 24H, 18-crown-6), 9.76 (br s, 54H, SiCH_3). IR (KBr pellet, cm^{-1}): 590 (s), 648 (s), 741 (s, asym, ν_{UNTh}), 773 (w), 841 (w), 928 (w), 1111 (m), 1180 (s), 1250 (m), 1352 (s), 1452 (m), 2895 (w), 2951 (w).

6.5.6 Synthesis and Characterization of [(K(18-crown-6)$_{0.5}$)(K(18-crown-6)$_{0.5}$Et$_2$O)][(NR$_2$)$_2$U^{IV}(μ-N)(*C*H$_2$SiMe$_2$*N*R)Th^{IV}(NR$_2$)$_2$] (6.3)

The supernatant from **6.2** was dried *in vacuo* to yield a dark solid which was extracted with Et$_2$O and the resulting dark brown solution was filtered through a Celite column supported on glass wool (0.5 × 2 cm), concentrated *in vacuo* to 2 mL, and layered with pentane (4 mL). Storage at -25 °C for 2 weeks resulted in the deposition of golden brown crystalline

material, which was isolated by decanting the supernatant and then dried *in vacuo* to yield **6.3** and the known uranium bis(metallacycle), [K(DME)][U{*N*(R)(SiMe$_2$*C*H$_2$)}$_2$(NR$_2$)][47]. Total yield: .070 g, 34% yield. Anal. Calcd for $C_{46}H_{123}KN_6O_7Si_{10}ThU$: C, 33.23; H, 7.46; N, 5.06. Found: C, 32.87; H, 7.32; N, 5.04. ^{1}H NMR (400 MHz, 25 °C, THF-d_8): δ -9.47 (br s, 36H, NSi*Me$_3$*), -5.47 (br s, 6H, Si*Me$_2$*CH$_2$), 3.32 (s, 24H, 18-crown-6, **6.2**), 3.38 (s, 24H, 18-crown-6), 6.01 (s, 9H, *Me$_3$*SiNSiMe$_2$CH$_2$), 9.55 (br s, 54H, SiC*H$_3$*, **6.2**), 10.57 (br s, 36H, NSi*CH$_3$*). IR (KBr pellet, cm^{-1}): 596 (s), 663 (s), 746 (sh w), 773 (w), 837 (w), 849 (w), 1109 (m), 1250 (m), 1352 (s), 1454 (m), 2895 (w), 2900 (w).

6.5.7 Synthesis and Characterization of [(K(18-crown-6)$_{0.5}$)(K(18-crown-6)$_{0.5}$Et$_2$O)][(NR$_2$)$_2$U^{IV}(μ-^{15}N)(*C*H$_2$SiMe$_2$*N*R)Th^{IV}(NR$_2$)$_2$] (6.3-^{15}N)

The supernatant from **6.2-^{15}N** was dried *in vacuo* to yield a dark solid which was extracted with Et$_2$O and the resulting dark brown solution was filtered through a Celite column supported on glass wool (0.5 × 2 cm), concentrated *in vacuo* to 2 mL, and layered with pentane (4 mL). Storage at -25 °C for 2 weeks resulted in the deposition of golden brown crystalline material, which was isolated by decanting the supernatant and then dried *in vacuo* to yield **6.3-^{15}N** and the known uranium bis(metallacycle), [K(DME)][U{*N*(R)(SiMe$_2$*C*H$_2$)}$_2$(NR$_2$)],[47] in a 1:7 ratio, respectively. Total yield: .0932 g, 23% yield. ^{1}H NMR (400 MHz, 25 °C, THF-d_8): δ -37.32 (br s, 18H, N(SiC*H$_3$*)$_3$, bis(metallacycle)), -9.35 (br s, 36H, NSi*Me$_3$*), -6.21 (br s, 6H, Si(C*H$_3$*)$_2$, bis(metallacycle)), -5.52 (br s, 6H, Si*Me$_2$*CH$_2$), 3.08 (s, 24H, 18-crown-6), 6.10 (s, 9H, *Me$_3$*SiNSiMe$_2$CH$_2$), 9.73 (br s, 54H, SiC*H$_3$*, **6.2-^{15}N**), 10.67 (br s, 36H, NSi*CH$_3$*), 31.86 (br s, 6H, Si(C*H$_3$*)$_2$, bis(metallacycle)), 39.47 (br s, 18H, N(SiC*H$_3$*)$_3$, bis(metallacycle)). IR (KBr pellet, cm^{-1}): 582 (m), 667 (m), 717 (s), 756 (m), 833 (m), 933 (m), 962 (m), 1105 (m), 1147 (s), 1244 (s), 1352 (s), 1456 (m), 2893 (w), 2904 (w).

6.5.8 Synthesis and Characterization of $[(NR_2)_3U^{V}(\mu\text{-}N)Th^{IV}(NR_2)_3]$ (6.4)

To a stirring, cold (-25 °C), pale orange solution of **6.2** (65.6 mg, 0.0346 mmol) in THF (2 mL) was added a cold (-25 °C), bright red-orange solution of I_2 (4.80 mg, 0.0189 mmol) in THF (2 mL). After 2 min, the volatiles were removed *in vacuo* to provide a dark red-brown solid. The solid was then extracted into diethyl ether (3 mL) and the resulting dark red-brown solution was filtered through a Celite column supported on glass wool (0.5 × 2 cm). The solution was concentrated *in vacuo* and stored at -25 °C for 24 h resulted in the deposition of red-brown crystalline precipitate. The resulting material was again dried *in vacuo* and extracted into 3 mL pentane and the resulting dark red-brown solution was filtered through a Celite column supported on glass wool (0.5 × 2 cm). The filtrate was transferred to a 4 mL vial, which was placed inside a 20 mL scintillation vial and iso-octane (2 mL) was added to the outer vial. Storage of this two-vial system at -25 °C for 24 h resulted in the deposition of dark brown blocks. The crystalline solid was isolated by decanting the supernatant and then dried *in vacuo* to yield **6.4** (20.8 mg, 42% yield). Anal. Calcd for $C_{36}H_{108}N_7Si_{12}ThU \cdot C_{10}H_{24}$: C, 34.73; H, 8.36; N, 6.16. Anal. Calcd for $C_{36}H_{108}N_7Si_{12}ThU$: C, 29.89; H, 7.53; N, 6.78. Found: C, 30.11; H, 7.97; N, 6.44. ^{1}H NMR (400 MHz, 25 °C, THF-d_8): δ -12.47 (br s, 54H, SiCH_3), 4.79 (br s, 54H, SiCH_3). UV-vis/NIR (THF, 10.44 mM, 25 °C, L mol^{-1}cm^{-1}): 979 nm (ε = 83.4), 1221 (ε = 56.5), 1410 (ε = 70.0), 1599 (ε = 69.2). IR (KBr pellet, cm^{-1}): 609 (s), 654 (m), 725 (s, asym, ν_{UNTh}), 773 (s), 849 (w), 879 (w), 912 (s), 1182 (s), 1248 (m), 1401 (m), 2899 (m), 2954 (m).

6.5.9 Synthesis and Characterization of $[(NR_2)_3U^{V}(\mu\text{-}^{15}N)Th^{IV}(NR_2)_3]$ (6.4-^{15}N)

To a stirring, cold (-25 °C), pale orange solution of **6.2-^{15}N** (74.2 mg, 0.0392 mmol) in THF (2 mL) was added a cold (-25 °C), bright red-orange solution of I_2 (5.50 mg, 0.0217 mmol) in THF (2 mL). After 2 min, the volatiles were removed *in vacuo* to provide a dark red-brown solid. The solid was then extracted into diethyl ether (3 mL) and the resulting dark red-brown solution was filtered through a Celite column supported on glass wool (0.5 × 2 cm). The solution was concentrated *in vacuo* and stored at -25 °C for 24 h resulted in the deposition of red-brown crystalline precipitate. The resulting material was again dried *in vacuo* and extracted into 3 mL pentane and the resulting dark red-brown solution was filtered through a Celite column supported on glass wool (0.5 × 2 cm). The filtrate was transferred to a 4 mL vial, which was placed inside a 20 mL scintillation vial and iso-octane (2 mL) was added to the outer vial. Storage of this two-vial system at -25 °C for 24 h resulted in the deposition of dark brown blocks. The crystalline solid was isolated by decanting the supernatant and then dried *in vacuo* to yield **6.4-^{15}N** (19.0 mg, 34% yield). ^{1}H NMR (400 MHz, 25 °C, THF-d_8): δ -12.15 (br s, 54H, SiCH_3), 4.78 (s, 54H, SiCH_3). IR (KBr pellet, cm^{-1}): 607 (s), 648 (s), 690 (s), 719 (s, asym, ν_{UNTh}), 773 (s), 847 (w), 850 (w), 933 (s), 1182 (s), 1250 (s), 1404 (m), 2900 (w), 2954 (w).

6.5.10 NMR scale reaction of $[K(DME)][Th\{N(R)(SiMe_2CH_2)\}_2(NR_2)]$ with $[U(NR_2)_3(NH_2)]$ (6.1).

An NMR tube fitted with a J-Young valve was charged with a dark-brown crystalline powder of **6.1** (13.3 mg, 0.018 mmol). A pale-yellow THF-d_8 (0.5 mL) solution of $[K(DME)][Th\{N(R)(SiMe_2CH_2)\}_2(NR_2)]$[38] (15.7 mg, 0.019 mmol) was added to the NMR tube, along with a colorless THF-d_8 (0.5 mL) solution of 18-crown-6 (5.0 mg, 0.19 mmol).

The mixture turned golden-brown and a ^{1}H NMR spectrum was then recorded (Figures A6.7-A6.9). ^{1}H NMR (400 MHz, 25 °C, THF-d_8): δ -2.94 (br s, 54H, SiCH_3, **6.1**), -0.36 (br s, 54H, CH_2), 0.02 (s, 12H, N(SiCH_3)$_2$), 0.04 (s, 18H, N(SiCH_3)$_3$), 0.18 (s, 18H, N(SiCH_3)$_3$)$_2$), 3.75 (s, 24H, 18-crown-6). After 4 h, a ^{1}H NMR spectrum was re-recorded. This spectrum revealed the presence of a new broad peak assigned to **6.2**, concomitant with a decrease in the intensity of the resonances assignable to **6.1** and [K(DME)][Th{*N*(R)(SiMe$_2$*C*H$_2$)}$_2$(NR$_2$)].[38] ^{1}H NMR (400 MHz, 25 °C, THF-d_8): δ -2.94 (br s, 54H, SiCH_3, **6.1**), 0.02 (s, 12H, N(SiCH_3)$_2$), 0.04 (s, 18H, N(SiCH_3)$_3$), 0.18 (s, 18H, N(SiCH_3)$_3$)$_2$), 3.75 (s, 24H, 18-crown-6), 9.73 (br s, 54H, SiCH_3, **6.2**). After 22 h, a ^{1}H NMR spectrum was re-recorded. This spectrum revealed new sharp peaks, concomitant with the complete loss of **6.1** and decrease in the intensity of the resonances assignable [K(DME)][Th{*N*(R)(SiMe$_2$*C*H$_2$)}$_2$(NR$_2$)].[38] ^{1}H NMR (400 MHz, 25 °C, THF-d_8): δ 0.02 (s, 12H, N(SiCH_3)$_2$), 0.04 (s, 18H, N(SiCH_3)$_3$), 0.18 (s, 18H, N(SiCH_3)$_3$)$_2$), 3.75 (s, 24H, 18-crown-6), 9.73 (br s, 54H, SiCH_3, **6.2**). After 48 h, a ^{1}H NMR spectrum was re-recorded. This spectrum revealed an adjustment of peaks corresponding to [K(DME)][Th{*N*(R)(SiMe$_2$*C*H$_2$)}$_2$(NR$_2$)][38] by about 0.02 ppm and 18-crown-6. ^{1}H NMR (400 MHz, 25 °C, THF-d_8): δ 0.04 (s, 12H, N(SiCH_3)$_2$), 0.06 (s, 18H, N(SiCH_3)$_3$), 0.20 (s, 18H, N(SiCH_3)$_3$)$_2$), 3.43 (s, 24H, 18-crown-6), 9.73 (br s, 54H, SiCH_3, **6.2**). A small amount of golden powder was observed at the bottom of the NMR tube. The NMR tube was brought back into the box, where the solution was transferred to a 20 mL scintillation vial and the volatiles were removed *in vacuo* to afford a solid. The solid was then extracted into THF (2 mL) and layered with pentane (2 mL), which was stored at -25 °C for 4 d resulted in the deposition of pale orange crystals. The solid was isolated by decanting the supernatant and then dried *in vacuo* to yield **6.2** (11.7 mg, 34 % yield). The supernatant was transferred to a

new 20 mL vial and storage of this system at -25 °C for 5 d resulted in the deposition of more pale orange crystals of **6.2** (4.2 mg). Total yield: 0.0159 g, 46% yield.

6.5.11 X-ray Crystallography

Data for **6.1**, **6.2**, **6.3**, and **6.4** were collected on a Bruker KAPPA APEX II diffractometer equipped with an APEX II CCD detector using a TRIUMPH monochromator with a Mo Kα X-ray source (α = 0.71073 Å). The crystals were mounted on a cryoloop under Paratone-N oil. Complex **6.1** and **6.3** were collected at 100(2) K and complexes **6.2** and **6.4** were collected at 110(2) K, using an Oxford nitrogen gas cryostream. Data were collected using ω scans with 0.5° frame widths. Frame exposures of 10, 20, 10, and 10 seconds were used for **6.1**, **6.2**, **6.3**, and **6.4** respectively. Data collection and cell parameter determinations were conducted using the SMART program.[64] Integration of the data frames and final cell parameter refinements were performed using SAINT software.[65] Absorption corrections of the data were carried out using the multi-scan method SADABS for **6.1**-**6.4**.[66] Subsequent calculations were carried out using SHELXTL.[67] Structure determination was done using direct or Patterson methods and difference Fourier techniques. All hydrogen atom positions were idealized, and rode on the atom of attachment. Structure solution, refinement, graphics, and creation of publication materials were performed using SHELXTL or Olex2.[67-69] Further crystallographic details can be found in Tables 6.2-6.3.

Table 6.2. X-ray Crystallographic Data for **6.1**, **6.2**, and **6.3**.

	6.1	**6.2**	**6.3**
empirical formula	$C_{18}H_{56}N_4SiU$	$C_{56}H_{148}KN_7O_8Si_{12}ThU$	$C_{46}H_{123}KN_6O_7Si_{10}ThU$
crystal habit, color	Block, Brown	Block, Pale Orange	Needle, Brown
crystal size (mm)	0.2 × 0.2 × 0.15	0.2 × 0.2 × 0.15	0.25 × 0.15 × 0.1
space group	$R\bar{3}c$	$C2/m$	$P\text{-}1$
volume ($Å^3$)	4972.8(5)	4477(2)	3915.2(12)
a (Å)	18.4115(8)	23.339(7)	12.170(2)
b (Å)	18.4115(8)	17.672(5)	14.705(3)
c (Å)	16.9393(10)	11.858(3)	23.648(4)
α (deg)	90	90	83.016(3)
β (deg)	90	113.746(7)	84.664(3)
γ (deg)	120	90	68.977(2)
Z	6	2	2
formula weight (g/mol)	735.23	1894.06	1662.57
density (calculated) (Mg/m^3)	1.473	1.405	1.410
absorption coefficient (mm^{-1})	5.125	3.717	4.209
F_{000}	2208	1932	1676
total no. reflections	11002	27158	33783
unique reflections	1193	4742	16197
Final R Indices ($I > 2\sigma(I)$]	$R_1 = 0.0731$ $wR_2 = 0.1978$	$R_1 = 0.0653$ $wR_2 = 0.1680$	$R_1 = 0.0402$ $wR_2 = 0.0798$
largest diff. peak and hole ($e^- A^{-3}$)	1.200 and -2.338	1.291 and -1.980	2.411 and -2.238
GOF	1.468	1.197	0.986

Table 6.3. X-ray Crystallographic Data for **6.4**.

	6.4
empirical formula	$C_{46}H_{132}N_7Si_{12}ThU$
crystal habit, color	Block, Dark Brown
crystal size (mm)	0.2 × 0.15 × 0.1
space group	$P2_1/n$
volume (Å^3)	7396.9(6)
a (Å)	16.2396(6)
b (Å)	16.3992(8)
c (Å)	28.8104(12)
α (deg)	90
β (deg)	105.408(2)
γ (deg)	90
Z	4
formula weight (g/mol)	1590.73
density (calculated) (Mg/m^3)	1.423
absorption coefficient (mm^{-1})	4.422
F_{000}	3204
total no. reflections	32067
unique reflections	15054
Final R Indices (I >2σ(I)]	R_1 = 0.0667 wR_2 = 0.1634
largest diff. peak and hole (e$^-$ A^{-3})	5.392 and -2.357
GOF	1.071

6.6 Appendix

6.6.1 NMR Spectra

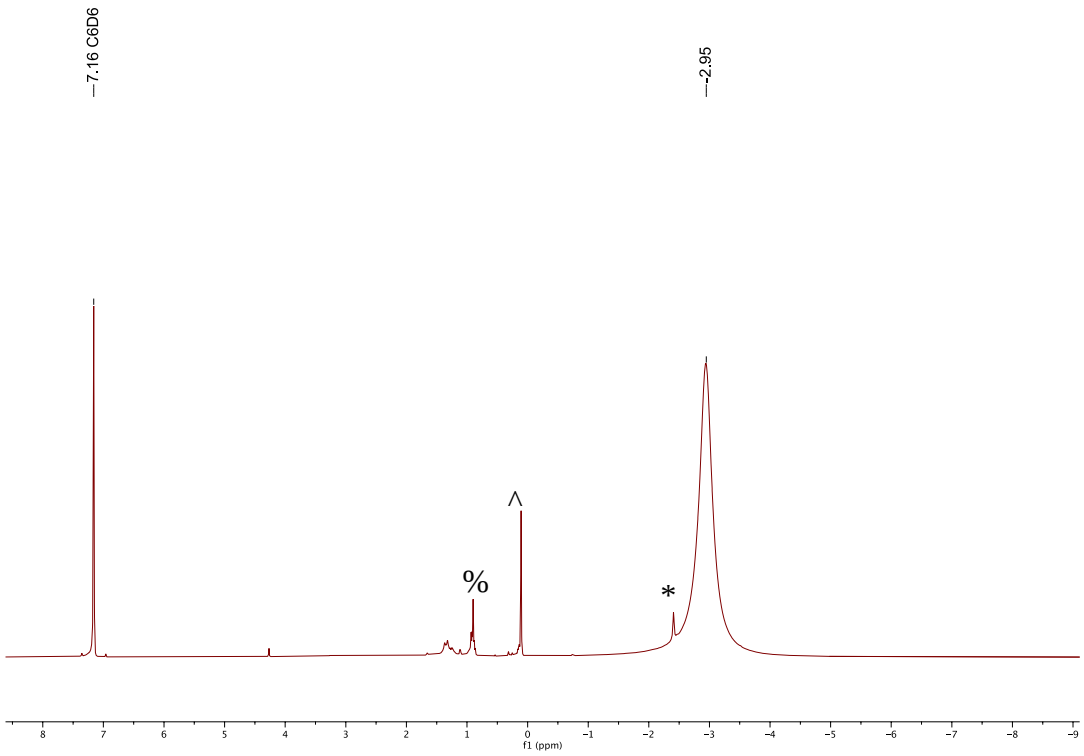

Figure A6.1. ^{1}H NMR spectrum of $[U(NR_2)_3(NH_2)]$ (**6.1**) in C_6D_6. (^) indicates $HN(SiMe_3)_2$, (%) indicates pentane, and (*) indicates an unidentified peak.

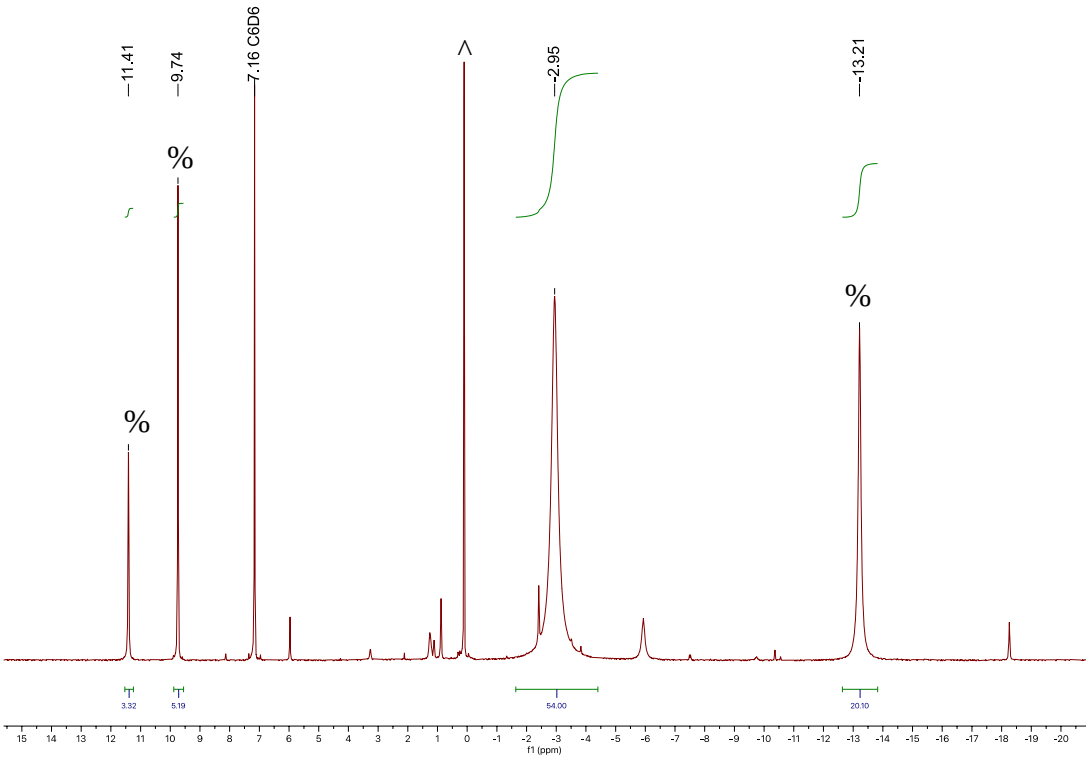

Figure A6.2. ^{1}H NMR spectrum of [U(NR$_2$)$_3$(^{15}NH$_2$)] (**6.1-^{15}N**) in C$_6$D$_6$. (%) indicates [U{*N*(R)(SiMe$_2$)*C*H$_2$}(NR$_2$)$_2$] and (^) indicates HN(SiMe$_3$)$_2$.

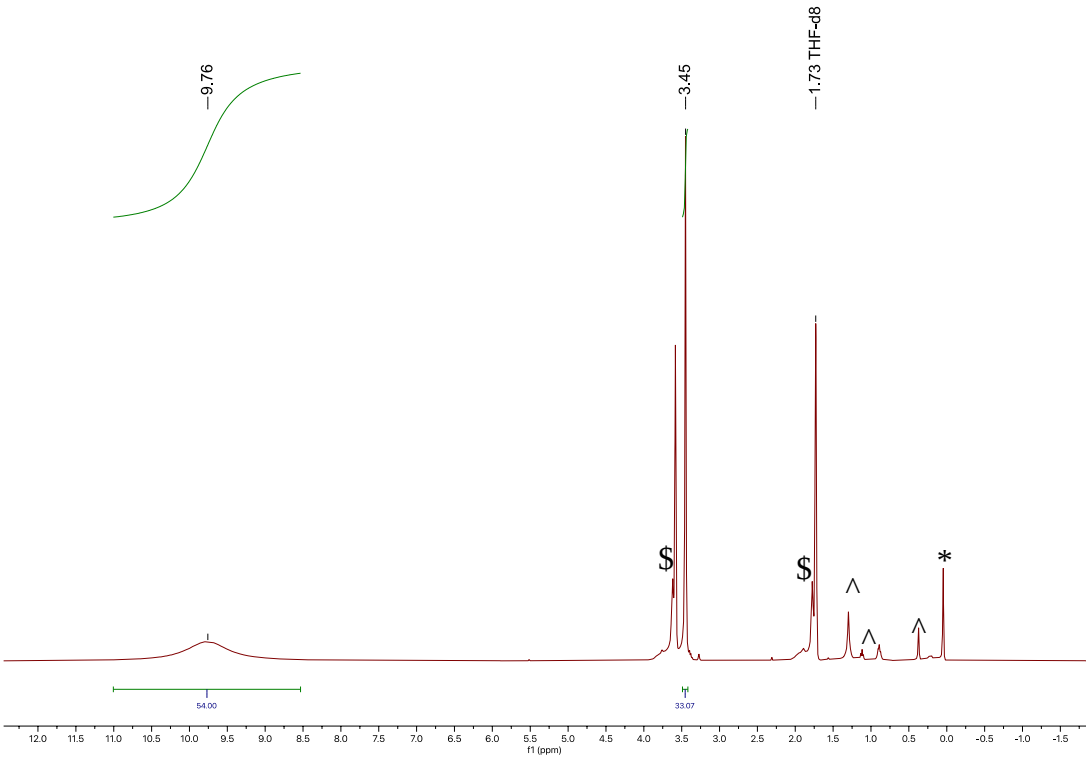

Figure A6.3. ^{1}H NMR spectrum of [K(18-crown-6)(THF)$_2$][(NR$_2$)$_3$U^{IV}(μ-^{15}N)Th^{IV}(NR$_2$)$_3$] (**6.2-^{15}N**) in THF-d_8. (*) indicates HN(SiMe$_3$)$_2$, (^) indicates pentane, and ($) indicates THF-$h_8$.

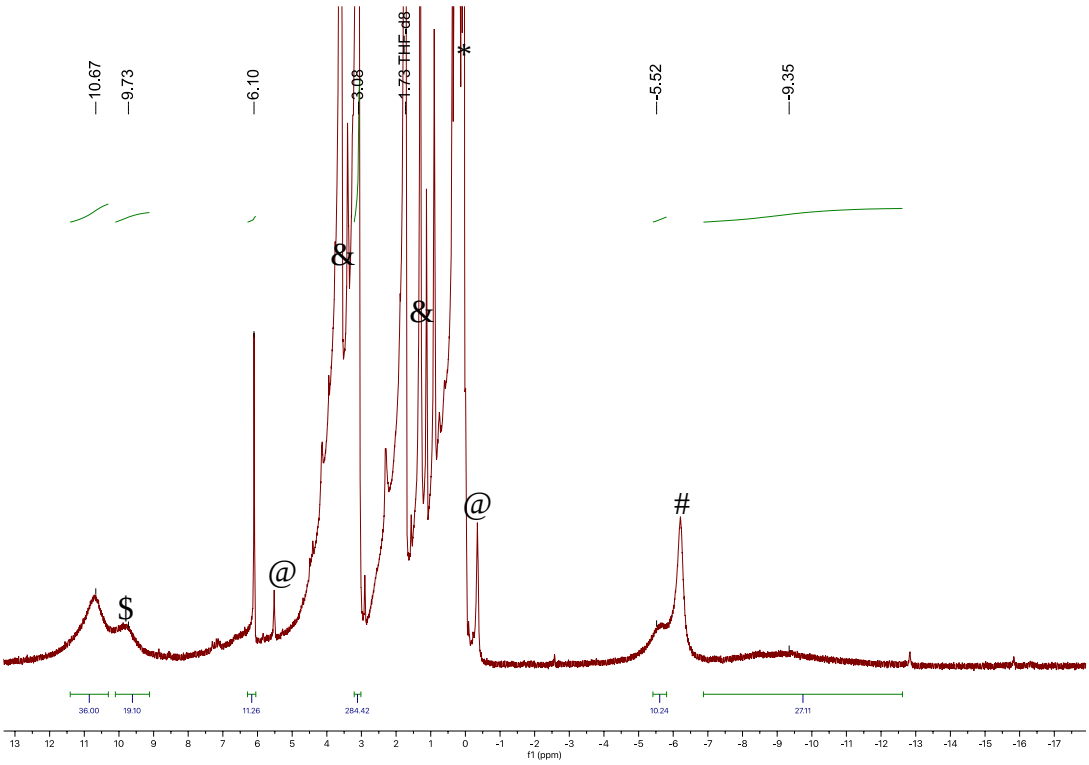

Figure A6.4. Partial ^{1}H NMR spectrum of [(K(18-crown-6)$_{0.5}$)(K(18-crown-6)$_{0.5}$Et$_2$O)][(NR$_2$)$_2$U^{IV}(μ-^{15}N)(*C*H$_2$SiMe$_2$*N*R)Th^{IV}(NR$_2$)$_2$] (**6.3-^{15}N**) in THF-d_8. (*) indicates HN(SiMe$_3$)$_2$, ($) indicates **6.2-^{15}N**, (&) indicates residual diethyl ether and pentane, (#) indicates [Na(THF)][U{*N*(R)(SiMe$_2$*C*H$_2$)}$_2$(NR$_2$)], and (@) indicates unidentified peaks.

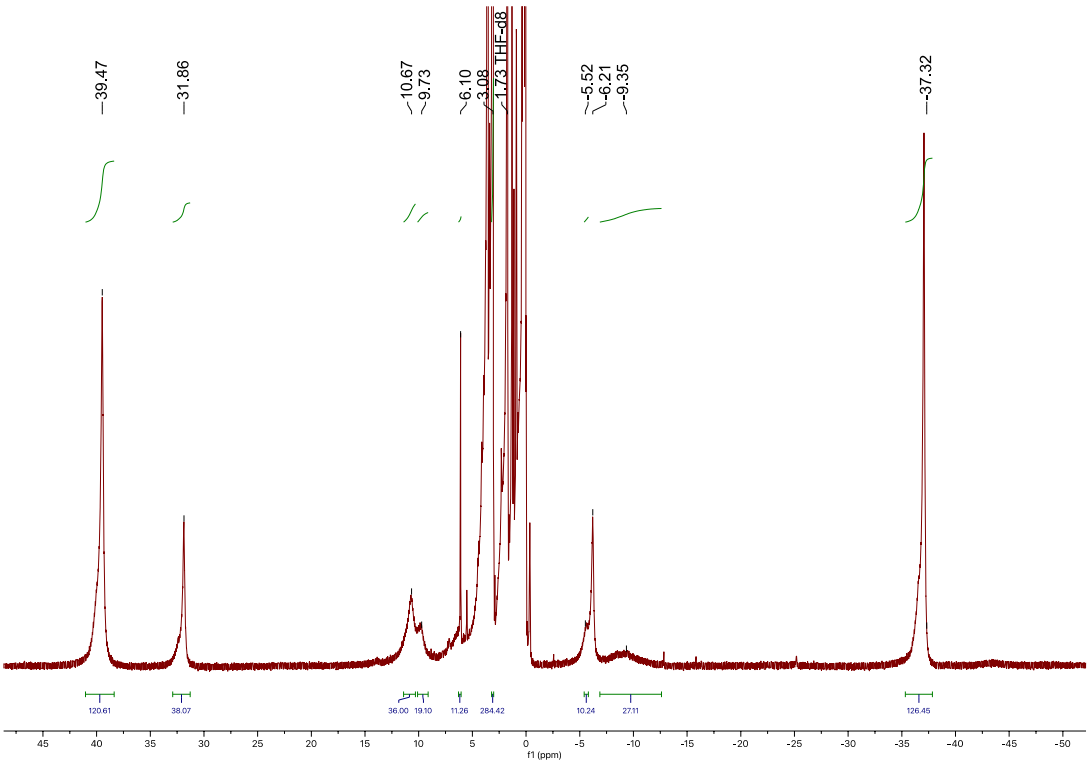

Figure A6.5. ^{1}H NMR spectrum of [(K(18-crown-6)$_{0.5}$)(K(18-crown-6)$_{0.5}$Et$_2$O)][(NR$_2$)$_2$U^{IV}(μ-^{15}N)(*C*H$_2$SiMe$_2$*N*R)Th^{IV}(NR$_2$)$_2$] (**6.3-^{15}N**) in THF-d_8.

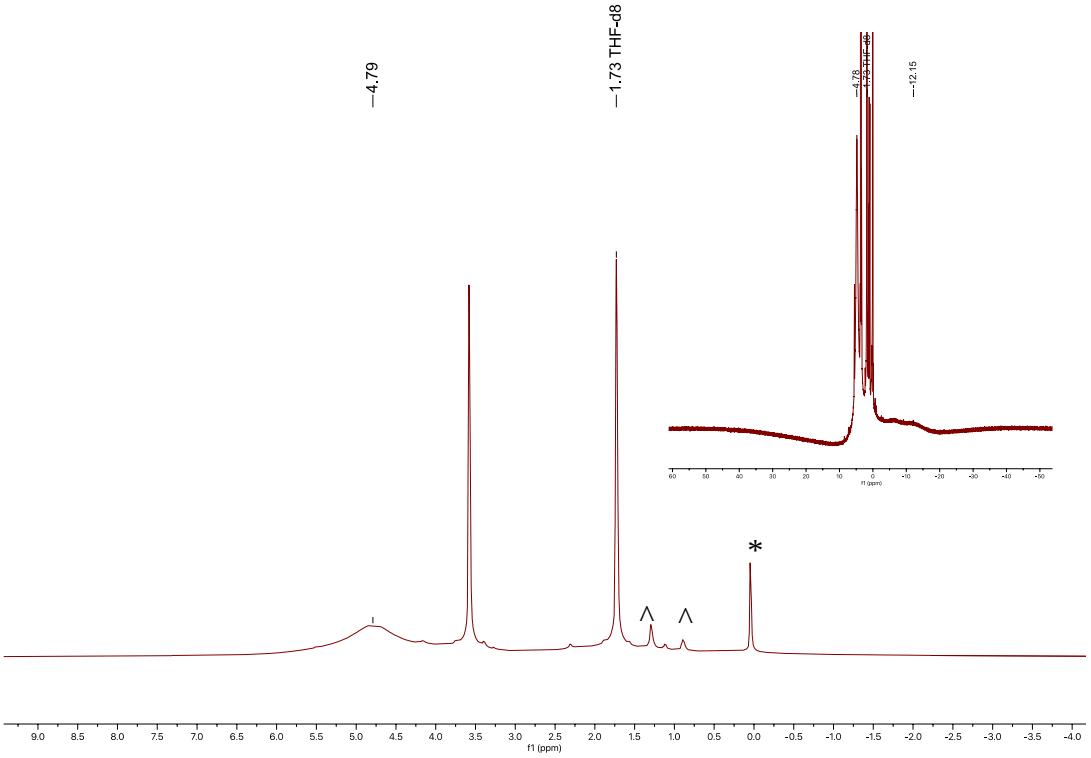

Figure A6.6. ^{1}H NMR spectrum of $[(NR_2)_3U^{V}(\mu\text{-}^{15}N)Th^{IV}(NR_2)_3]$ (**6.4-^{15}N**) in THF-d_8. The inset highlights the second $SiMe_3$ resonance. (*) indicates $HN(SiMe_3)_2$ and (^) indicates pentane.

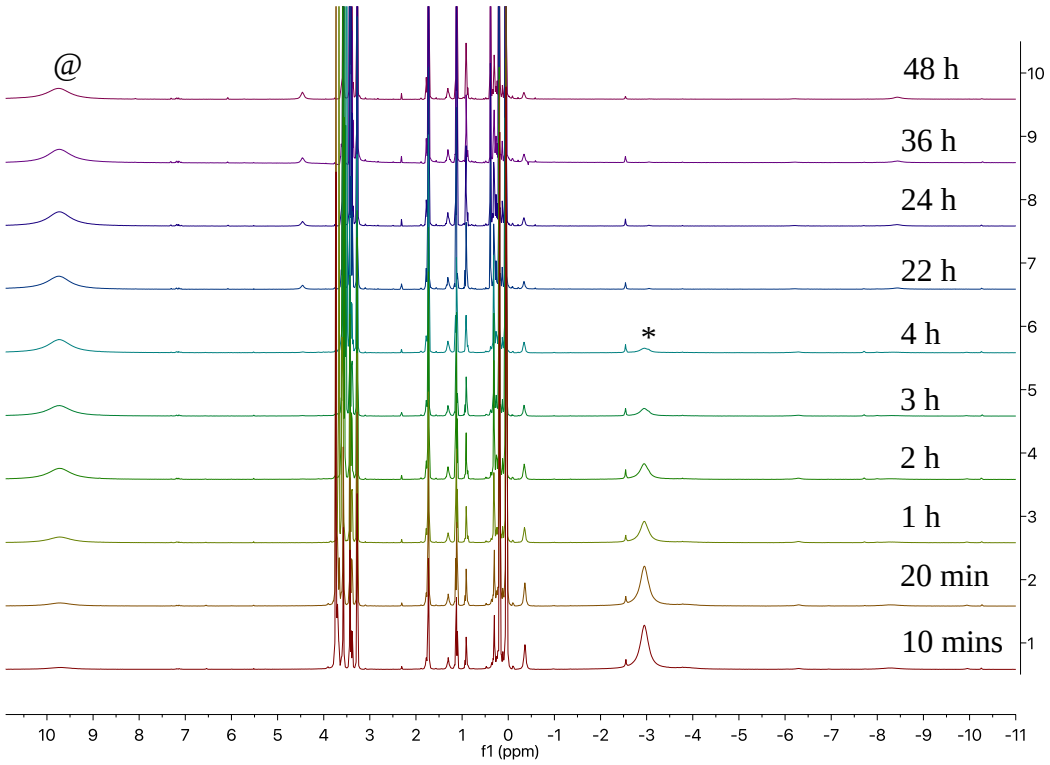

Figure A6.7. ^{1}H NMR spectrum of the reaction of **6.1** with [K(DME)][Th{*N*(R)(SiMe$_2$*C*H$_2$)}$_2$(NR$_2$)] (R = SiMe$_3$) and 18-crown-6 in THF-d_8 over the course of 48 h. (*) indicates **6.1** and (@) indicates **6.2**.

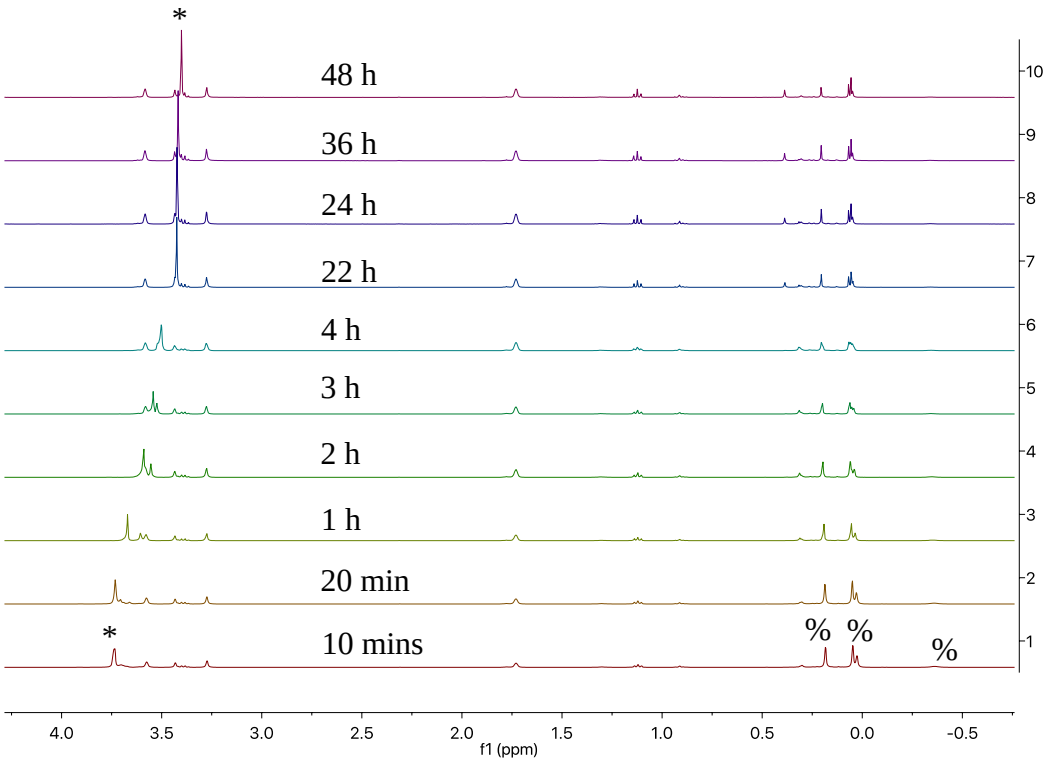

Figure A6.8. ^{1}H NMR spectrum of the reaction of **6.1** with [K(DME)][Th{*N*(R)(SiMe$_2$*C*H$_2$)}$_2$(NR$_2$)] (R = SiMe$_3$) and 18-crown-6 in THF-d_8 over the course of 48 h. (*) indicates 18-crown-6, and (%) indicates [K(DME)][Th{*N*(R)(SiMe$_2$*C*H$_2$)}$_2$(NR$_2$)].

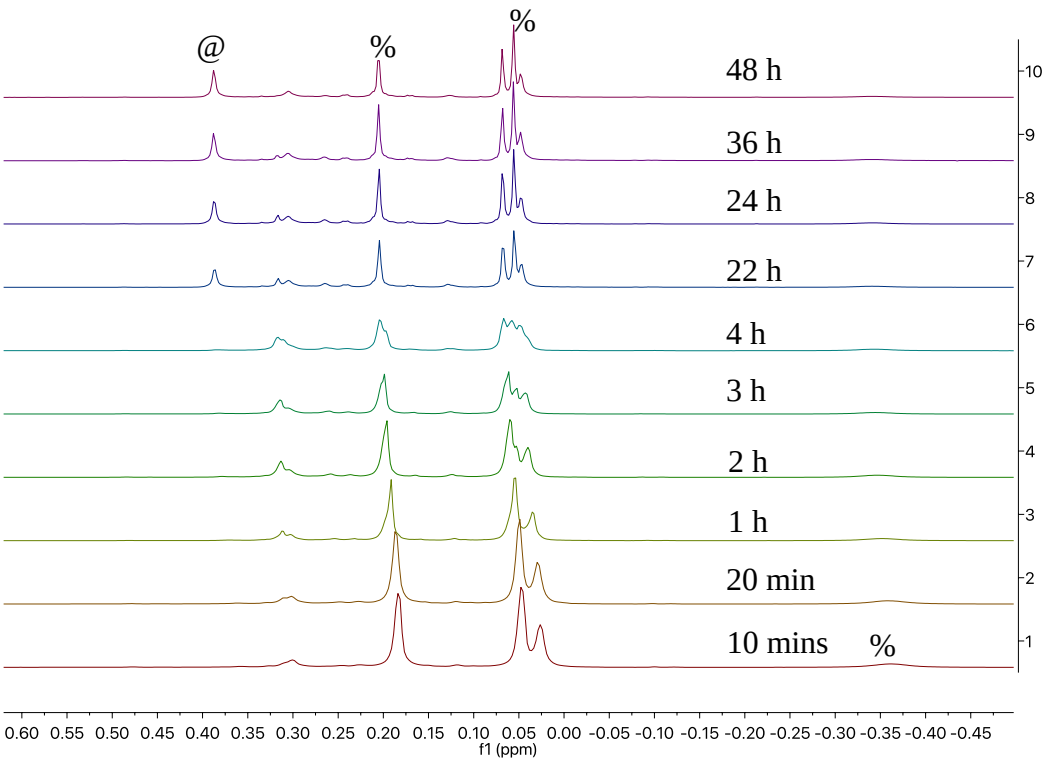

Figure A6.9. ^{1}H NMR spectrum of the reaction of **6.1** with [K(DME)][Th{*N*(R)(SiMe$_2$*C*H$_2$)}$_2$(NR$_2$)] (R = SiMe$_3$) and 18-crown-6 in THF-d_8 over the course of 48 h. (@) indicates **6.2** and (%) indicates [K(DME)][Th{*N*(R)(SiMe$_2$*C*H$_2$)}$_2$(NR$_2$)].

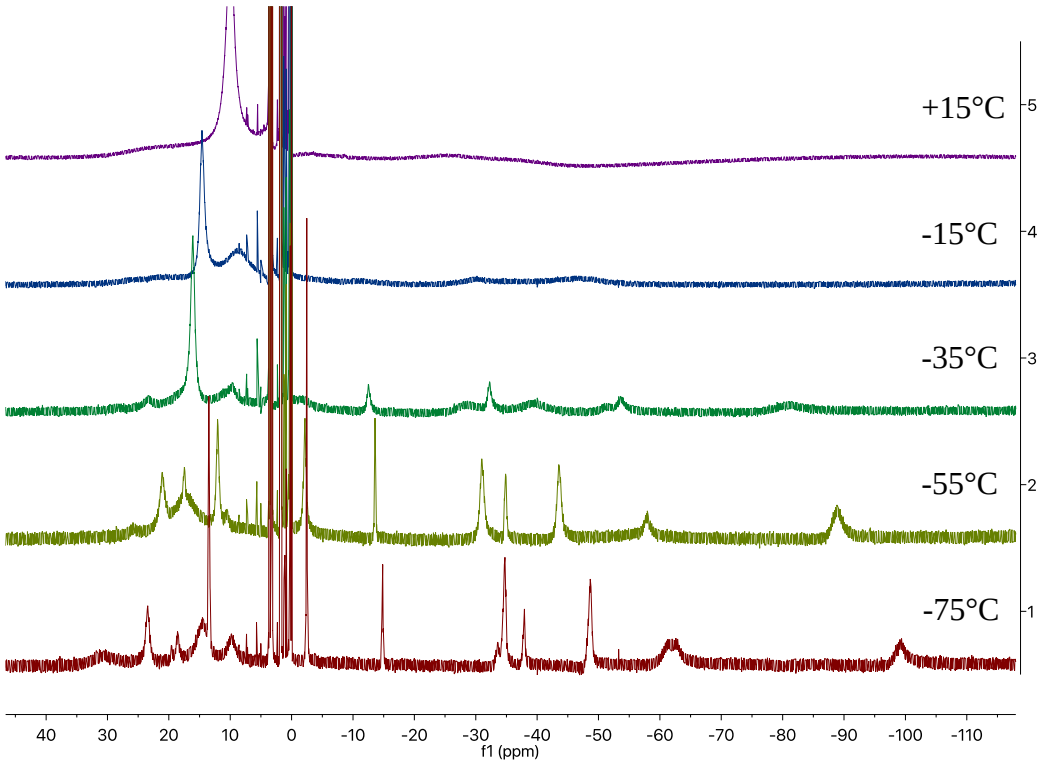

Figure A6.10. VT ^{1}H NMR spectrum of [K(18-crown-6)(THF)$_2$][(NR$_2$)$_3$U^{IV}(μ-N)Th^{IV}(NR$_2$)$_3$] (**6.2**) mixed with [(NR$_2$)$_2$U^{IV}(μ-N)(*C*H$_2$SiMe$_2$*N*R)Th^{IV}(NR$_2$)$_2$]$^-$ (**6.3**) in THF-d_8.

6.6.2 IR Spectra

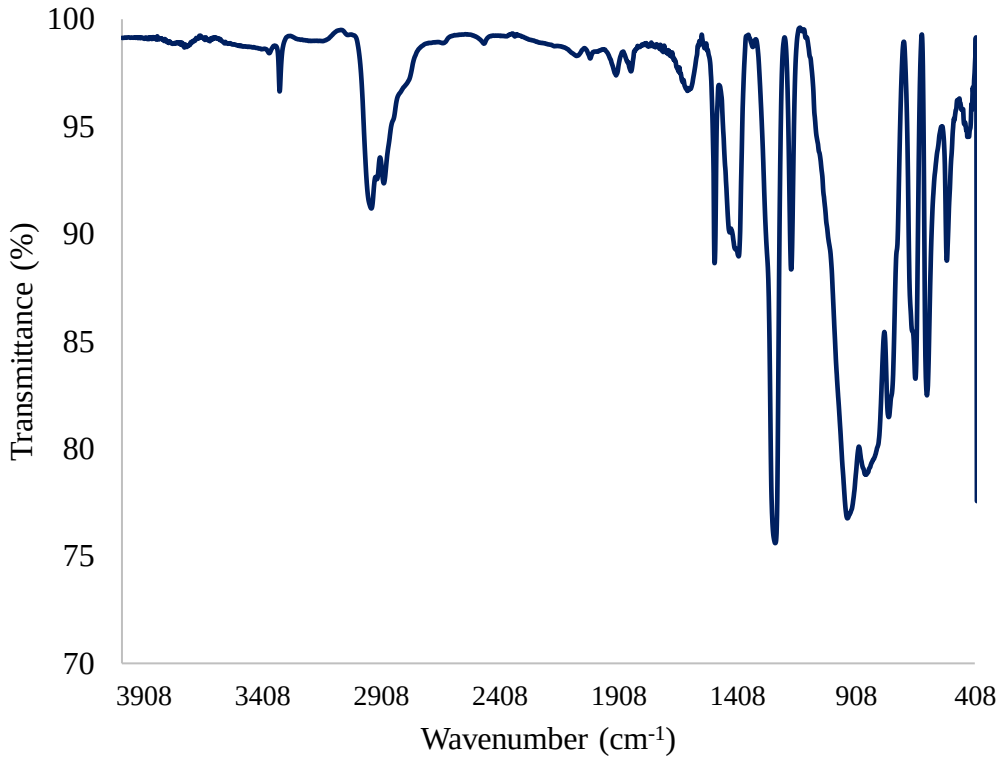

Figure A6.11. IR spectrum of $[U(NR_2)_3(NH_2)]$ (**6.1**) (KBr pellet).

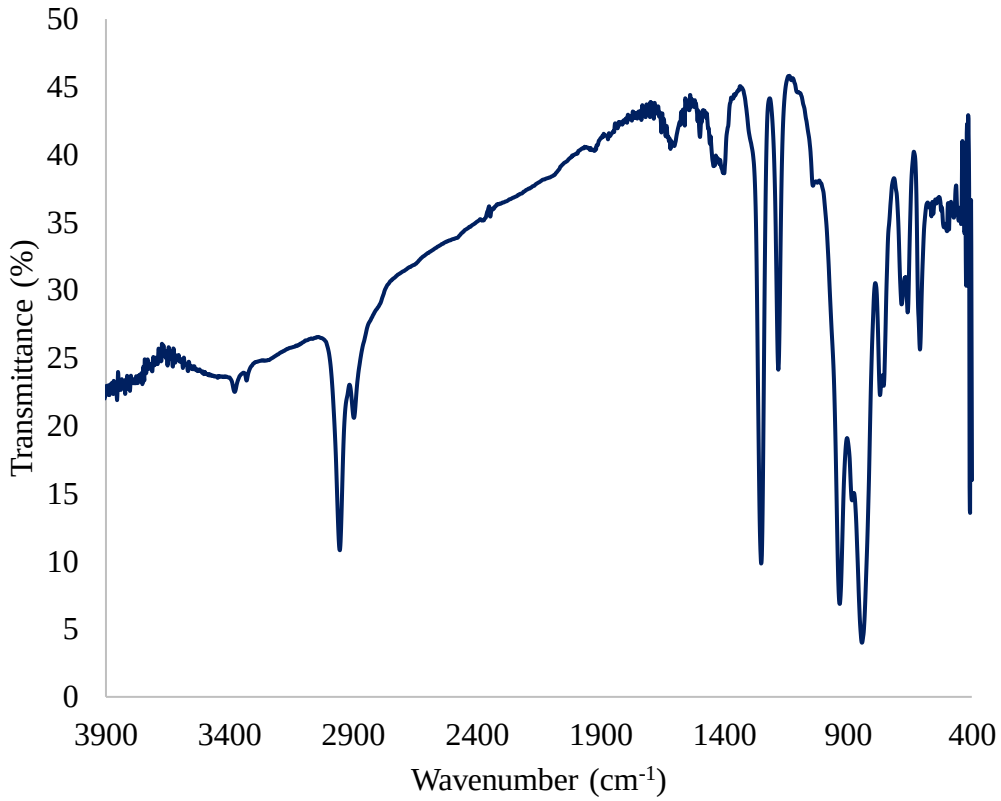

Figure A6.12. IR spectrum of $[U(NR_2)_3(^{15}NH_2)]$ (**6.1-^{15}N**) (KBr pellet).

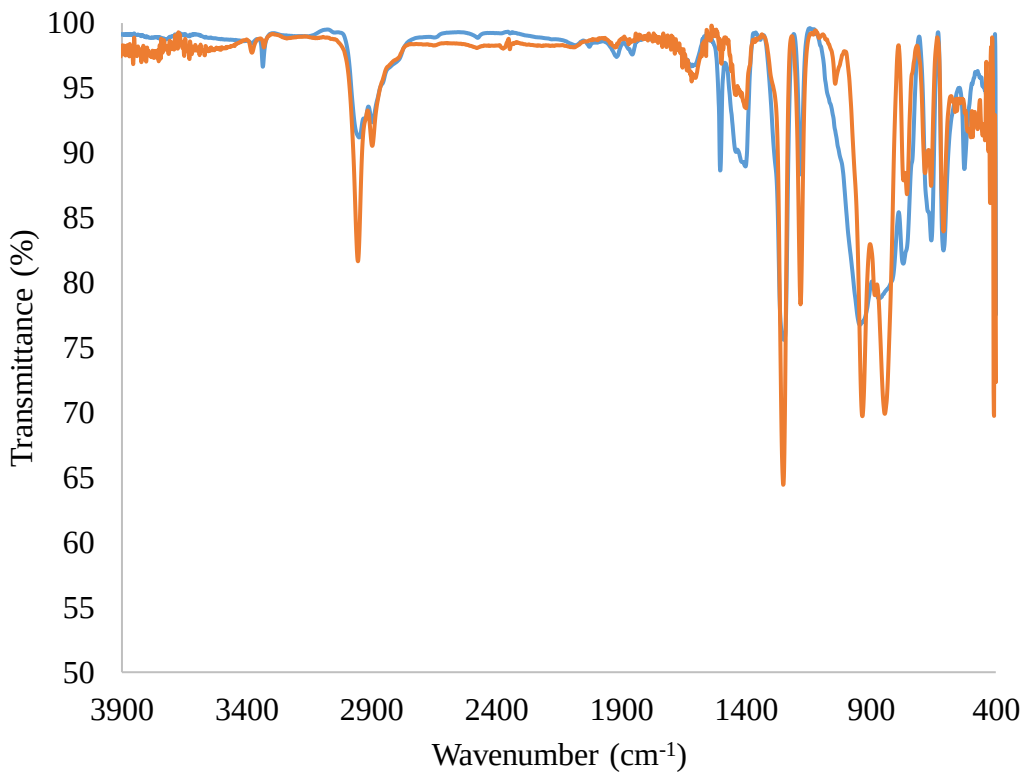

Figure A6.13. IR spectrum of $[U(NR_2)_3(NH_2)]$ (**6.1**) (blue) and $[U(NR_2)_3(^{15}NH_2)]$ (**6.1-^{15}N**) (orange) (KBr pellet).

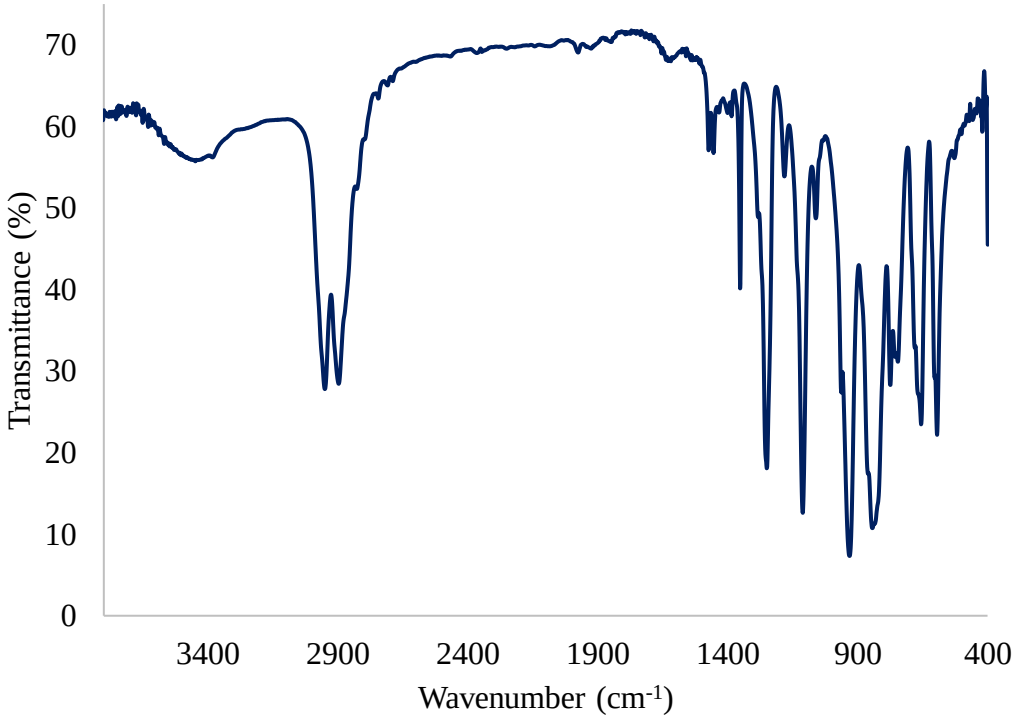

Figure 6.14. IR spectrum of $[K(18\text{-crown-6})(THF)_2][(NR_2)_3U^{IV}(\mu\text{-}N)Th^{IV}(NR_2)_3]$ (**6.2**) (KBr pellet).

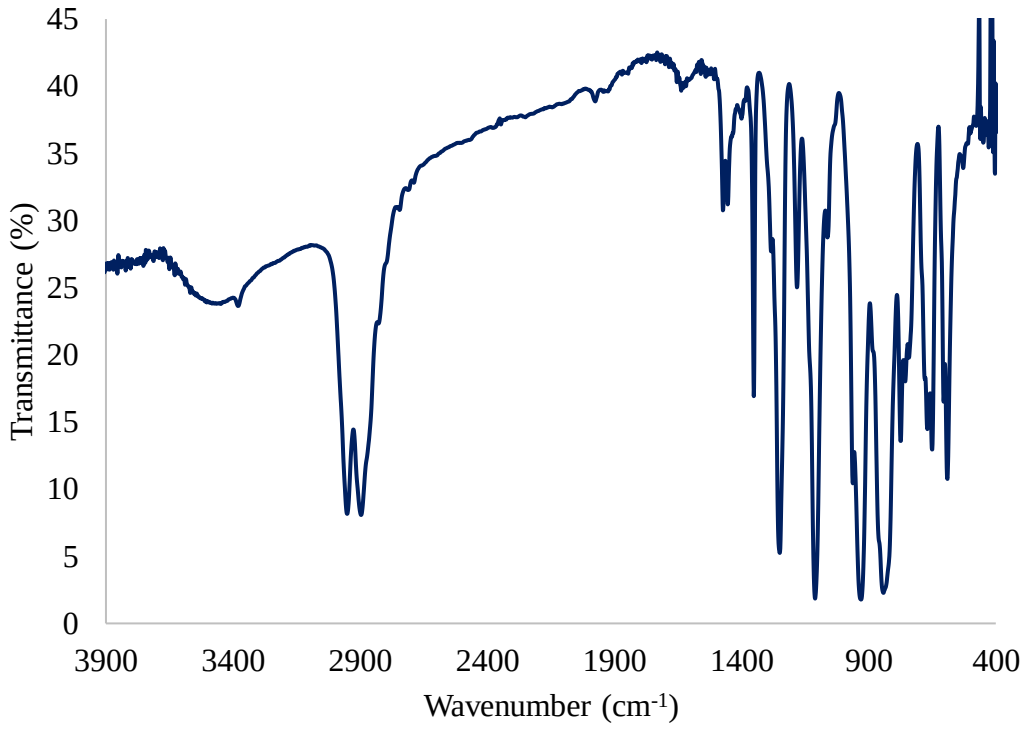

Figure A6.15. IR spectrum of $[K(18\text{-crown-6})(THF)_2][(NR_2)_3U^{IV}(\mu\text{-}^{15}N)Th^{IV}(NR_2)_3]$ (**6.2-^{15}N**) (KBr pellet).

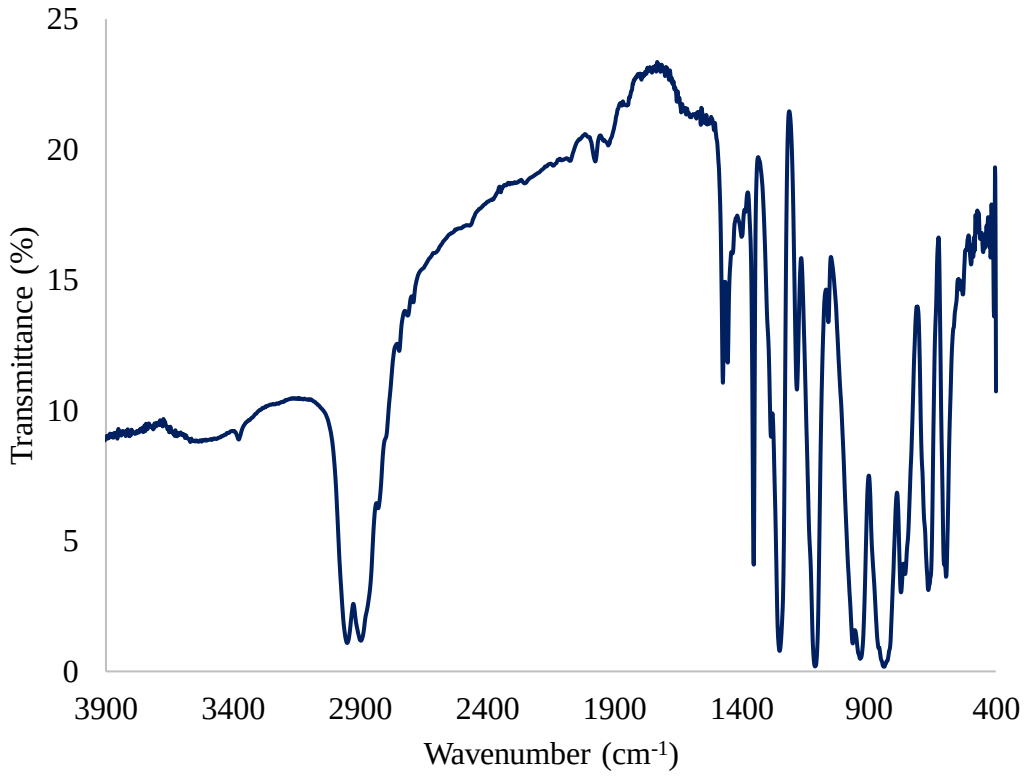

Figure A6.16. IR spectrum of [(K(18-crown-6)$_{0.5}$)(K(18-crown-6)$_{0.5}$Et$_2$O)][(NR$_2$)$_2$U^{IV}(μ-N)(*C*H$_2$SiMe$_2$*N*R)Th^{IV}(NR$_2$)$_2$] (**6.3**) (KBr pellet).

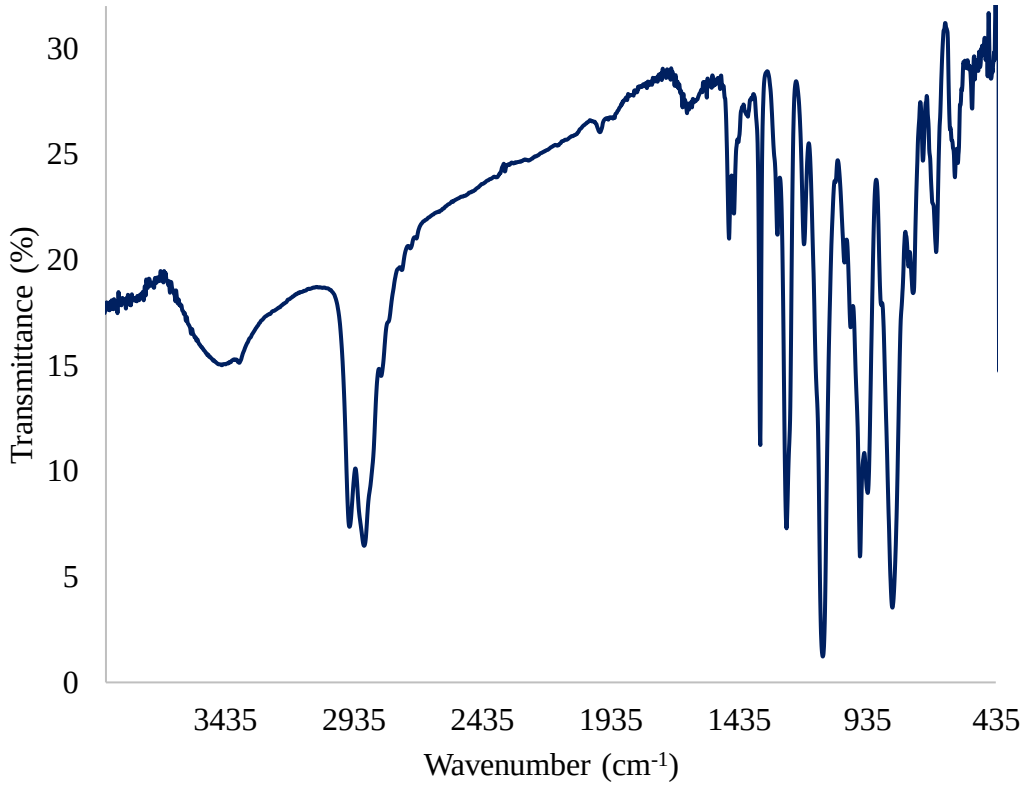

Figure A6.17. IR spectrum of [(K(18-crown-6)$_{0.5}$)(K(18-crown-6)$_{0.5}$Et$_2$O)][(NR$_2$)$_2$U^{IV}(μ-^{15}N)(*C*H$_2$SiMe$_2$*N*R)Th^{IV}(NR$_2$)$_2$] (**6.3-^{15}N**) (KBr pellet).

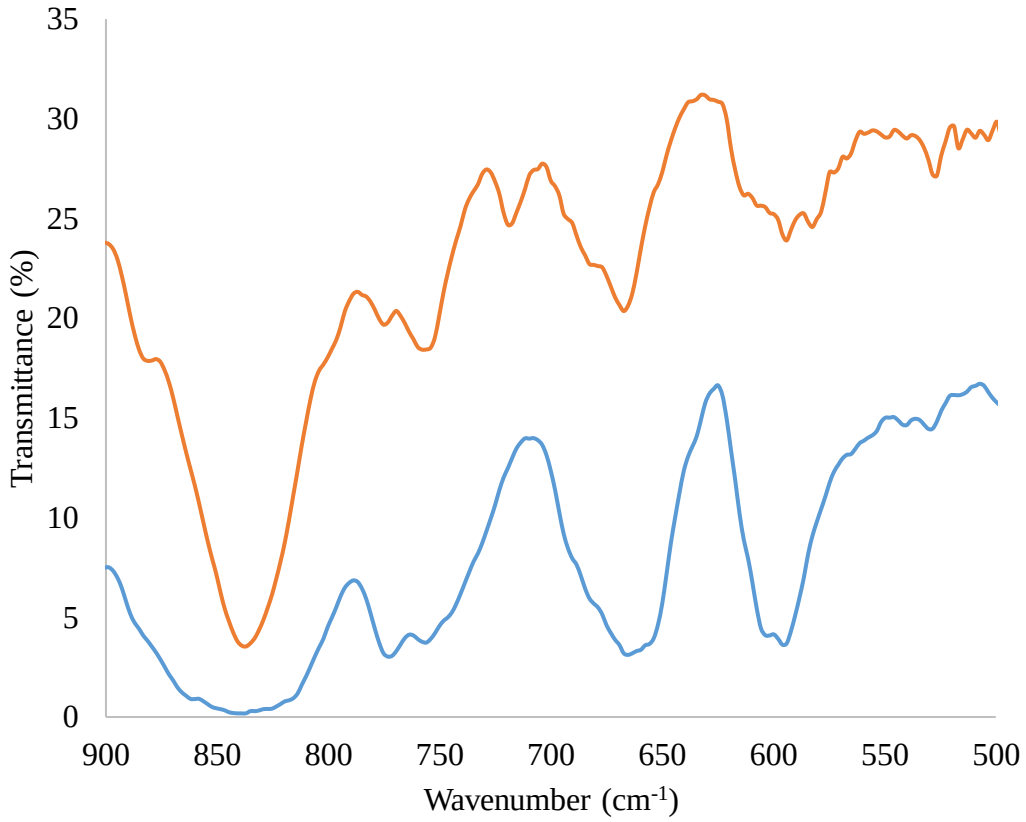

Figure A6.18. IR spectrum of [(K(18-crown-6)$_{0.5}$)(K(18-crown-6)$_{0.5}$Et$_2$O)][(NR$_2$)$_2$U^{IV}(μ-N)(*C*H$_2$SiMe$_2$*N*R)Th^{IV}(NR$_2$)$_2$] (**6.3**) (blue) and [(K(18-crown-6)$_{0.5}$)(K(18-crown-6)$_{0.5}$Et$_2$O)][(NR$_2$)$_2$U^{IV}(μ-^{15}N)(*C*H$_2$SiMe$_2$*N*R)Th^{IV}(NR$_2$)$_2$] (**6.3-^{15}N**) (orange) (KBr pellet).

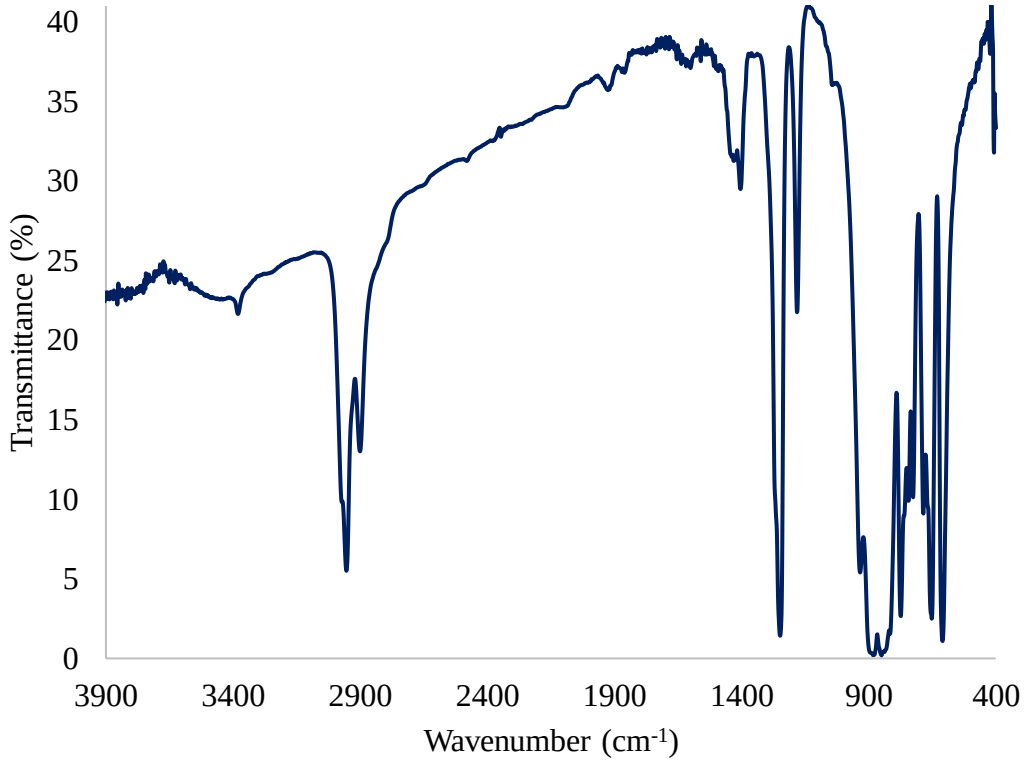

Figure 6.19. IR spectrum of $[(NR_2)_3U^{V}(\mu\text{-}N)Th^{IV}(NR_2)_3]$ (**6.4**) (KBr pellet).

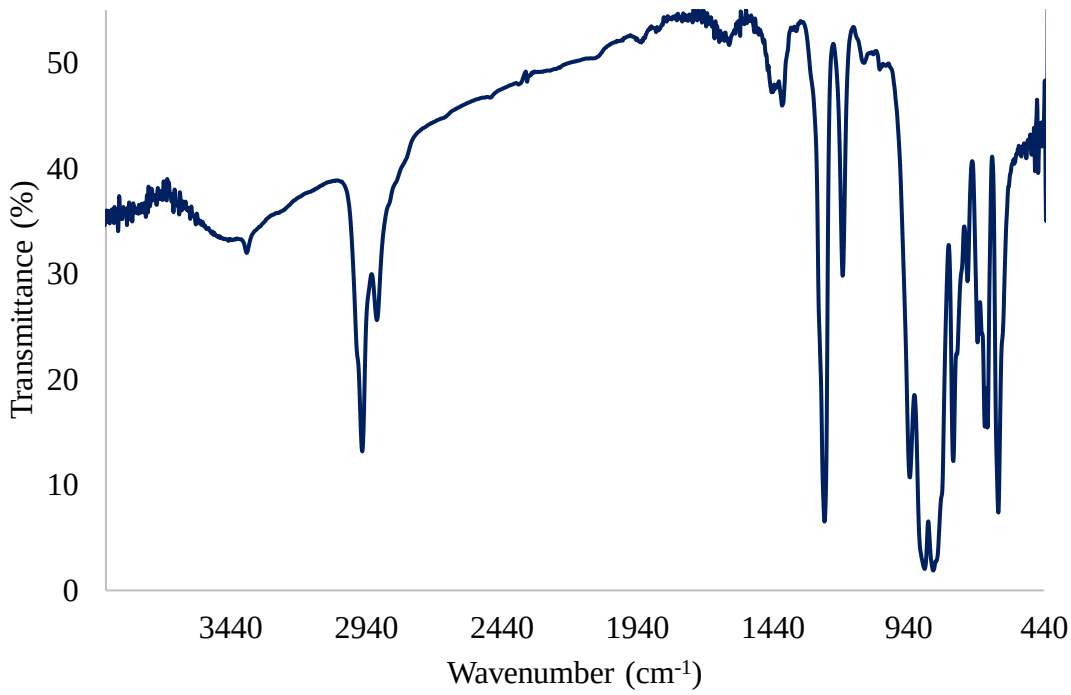

Figure A6.20. IR spectrum of $[(NR_2)_3U^{V}(\mu\text{-}^{15}N)Th^{IV}(NR_2)_3]$ (**6.4-^{15}N**) (KBr pellet).

6.6.3 UV-Vis Spectra

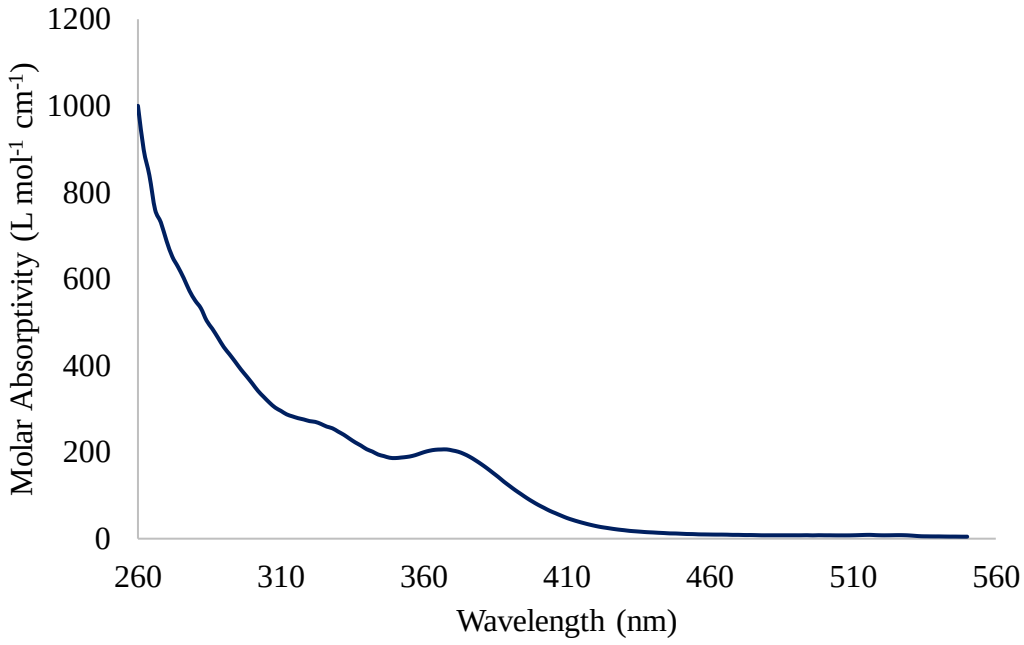

Figure A6.21. UV-vis spectrum of [K(18-crown-6)(THF)$_2$][(NR$_2$)$_3$U^{IV}(μ-N)Th^{IV}(NR$_2$)$_3$] (**6.2**) (0.5 mM, λ_{max} 370 nm (ε = 203.8 L mol^{-1}cm^{-1})) in THF.

6.6.4 SQUID Spectra

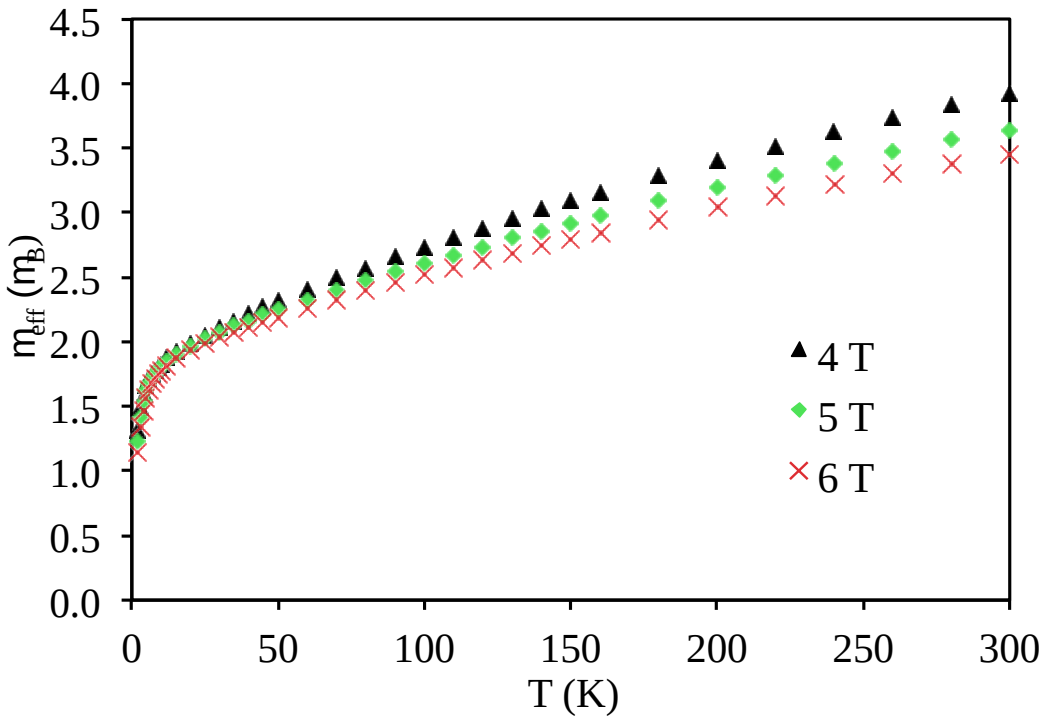

Figure A6.22. Magnetic moment of **6.4** versus temperature without correction for a ferromagnetic impurity.

As shown in Figure 6.12, the data at different fields are in good agreement once corrected for the presence of a ferromagnetic impurity. The ferromagnetic impurity is assumed to be iron, chromium, and nickel oxides from the surface of stainless steel equipment. The corrected data is shown as χT vs T in Figure A6.23. From 50 to 150 K, χT is linear in T, which indicates that a single state (the ground state) is occupied over this temperature range. The deviation from linearity above 150 K is due to excited states becoming thermally populated. The deviation from linearity below 50 K is due to magnetization of **6.4** no longer being linear in H. This is a property of the magnetization vs field curve (the magnetization is no longer in the linear region of the Brillioun function). The χT vs T curve can be fit with a linear function between 50 and 150 K to determine the value of χT extrapolated to 0 K (χT_0).

It should be noted that complex **6.4** crystallizes with 2 pentane molecules in the lattice and upon work up these pentane molecules can be lost. However, the SQUID data aligns better with results that take the pentane molecules into account. For reference, if **6.4** is assumed to have lost the pentane molecules, the magnetic susceptibility would give a smaller magnetic moment of 1.73 μ_B. Assuming $g_2 = g_3 = 0$, the value of μ_{eff} would be 1.79 μ_B, which is larger than the observed value. For this reason, **6.4** is assumed to retain its pentane of solvation.

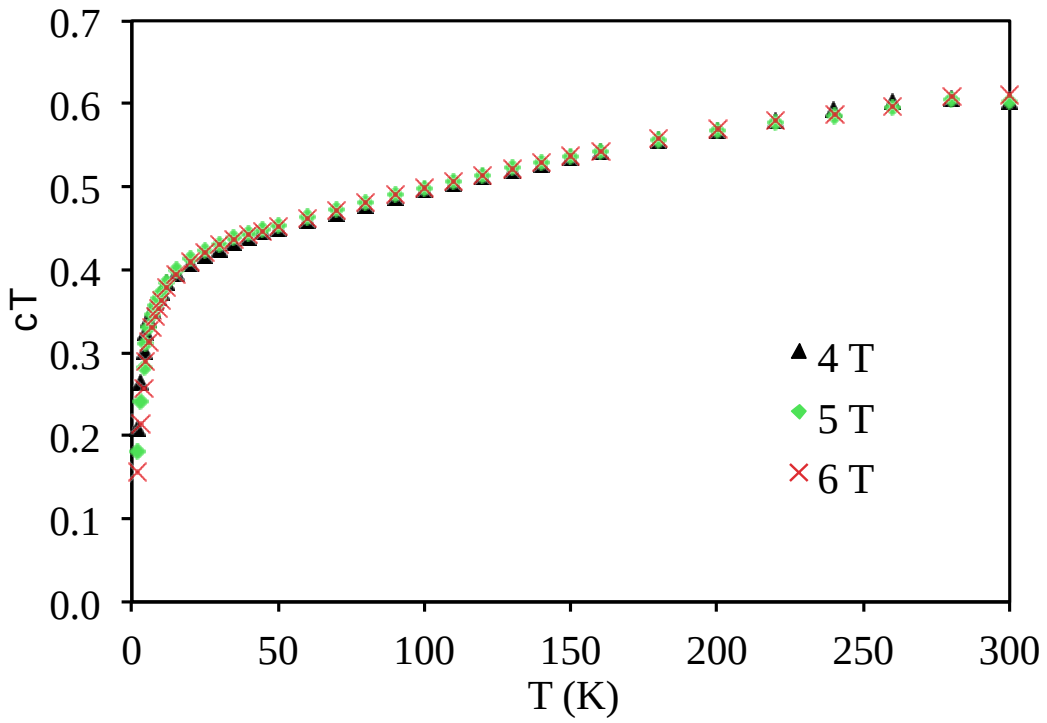

Figure A6.23. Magnetic susceptibility of **6.4** versus temperature with ferromagnetic impurity correction. The decrease in susceptibility below 50 K indicates that magnetization is no longer linear in field at these temperatures. The decrease does not reflect either a change in the electronic structure of the molecule or coupling.

6.7 References

1. Korobkov, I.; Gambarotta, S.; Yap, G. P. A., A Highly Reactive Uranium Complex Supported by the Calix[4]tetrapyrrole Tetraanion Affording Dinitrogen Cleavage, Solvent Deoxygenation, and Polysilanol Depolymerization. *Angew. Chem. Int. Ed.* **2002,** *41* (18), 3433-3436.
2. Chatelain, L.; Scopelliti, R.; Mazzanti, M., Synthesis and Structure of Nitride-Bridged Uranium(III) Complexes. *J. Am. Chem. Soc.* **2016,** *138* (6), 1784-1787.
3. Cleaves, P. A.; Kefalidis, C. E.; Gardner, B. M.; Tuna, F.; McInnes, E. J. L.; Lewis, W.; Maron, L.; Liddle, S. T., Terminal Uranium(V/VI) Nitride Activation of Carbon Dioxide and Carbon Disulfide: Factors Governing Diverse and Well-Defined Cleavage and Redox Reactions. *Chem. Eur. J.* **2017,** *23* (12), 2950-2959.
4. Cleaves, P. A.; King, D. M.; Kefalidis, C. E.; Maron, L.; Tuna, F.; McInnes, E. J. L.; McMaster, J.; Lewis, W.; Blake, A. J.; Liddle, S. T., Two-Electron Reductive Carbonylation of Terminal Uranium(V) and Uranium(VI) Nitrides to Cyanate by Carbon Monoxide. *Angew. Chem. Int. Ed.* **2014,** *53* (39), 10412-10415.
5. Evans, W. J.; Kozimor, S. A.; Ziller, J. W., Molecular Octa-Uranium Rings with Alternating Nitride and Azide Bridges. *Science* **2005,** *309* (5742), 1835.
6. Falcone, M.; Chatelain, L.; Mazzanti, M., Nucleophilic Reactivity of a Nitride-Bridged Diuranium(IV) Complex: CO_2 and CS_2 Functionalization. *Angew. Chem. Int. Ed.* **2016,** *55* (12), 4074-4078.
7. Falcone, M.; Chatelain, L.; Scopelliti, R.; Mazzanti, M., CO Cleavage and CO Functionalization under Mild Conditions by a Multimetallic CsU_2 Nitride Complex. *CHIMIA* **2017,** *71* (4), 209-212.
8. Falcone, M.; Chatelain, L.; Scopelliti, R.; Živković, I.; Mazzanti, M., Nitrogen reduction and functionalization by a multimetallic uranium nitride complex. *Nature* **2017,** *547*, 332.
9. Falcone, M.; Kefalidis, C. E.; Scopelliti, R.; Maron, L.; Mazzanti, M., Facile CO Cleavage by a Multimetallic CsU_2 Nitride Complex. *Angew. Chem. Int. Ed.* **2016,** *55* (40), 12290-12294.
10. Falcone, M.; Poon, L. N.; Fadaei Tirani, F.; Mazzanti, M., Reversible Dihydrogen Activation and Hydride Transfer by a Uranium Nitride Complex. *Angew. Chem. Int. Ed.* **2018,** *57* (14), 3697-3700.
11. Fortier, S.; Wu, G.; Hayton, T. W., Synthesis of a Nitrido-Substituted Analogue of the Uranyl Ion, $[N{=}U{=}O]^+$. *J. Am. Chem. Soc.* **2010,** *132* (20), 6888-9.
12. Fox, A. R.; Arnold, P. L.; Cummins, C. C., Uranium-Nitrogen Multiple Bonding: Isostructural Anionic, Neutral, and Cationic Uranium Nitride Complexes Featuring a Linear U=N=U Core. *J. Am. Chem. Soc.* **2010,** *132* (10), 3250-1.
13. Hayton, T. W., Recent developments in actinide–ligand multiple bonding. *Chem. Commun.* **2013,** *49* (29), 2956-2973.
14. Hayton, T. W., An actinide milestone. *Nat. Chem.* **2013,** *5*, 451.
15. King, D. M.; Cleaves, P. A.; Wooles, A. J.; Gardner, B. M.; Chilton, N. F.; Tuna, F.; Lewis, W.; McInnes, E. J. L.; Liddle, S. T., Molecular and electronic structure of terminal and alkali metal-capped uranium(V) nitride complexes. *Nat. Commun.* **2016,** *7*, 13773.

16. King, D. M.; Tuna, F.; McInnes, E. J. L.; McMaster, J.; Lewis, W.; Blake, A. J.; Liddle, S. T., Synthesis and Structure of a Terminal Uranium Nitride Complex. *Science* **2012,** *337* (6095), 717.
17. Staun, S. L.; Sergentu, D.-C.; Wu, G.; Autschbach, J.; Hayton, T. W., Use of ^{15}N NMR spectroscopy to probe covalency in a thorium nitride. *Chem. Sci.* **2019,** *10* (26), 6431-6436.
18. Hayton, T. W., Metal–ligand multiple bonding in uranium: structure and reactivity. *Dalton Trans.* **2010,** *39* (5), 1145-1158.
19. Jones, M. B.; Gaunt, A. J., Recent Developments in Synthesis and Structural Chemistry of Nonaqueous Actinide Complexes. *Chem. Rev.* **2013,** *113* (2), 1137-1198.
20. King, D. M.; Liddle, S. T., Progress in molecular uranium-nitride chemistry. *Coord. Chem. Rev.* **2014,** *266-267*, 2-15.
21. Liddle, S. T., The Renaissance of Non-Aqueous Uranium Chemistry. *Angew. Chem. Int. Ed.* **2015,** *54* (30), 8604-8641.
22. Patel, D.; Liddle, S. T., f-Element-metal bond chemistry. *Prog. Inorg. Chem.* **2012,** *32* (1), 1.
23. Falcone, M.; Barluzzi, L.; Andrez, J.; Fadaei Tirani, F.; Zivkovic, I.; Fabrizio, A.; Corminboeuf, C.; Severin, K.; Mazzanti, M., The role of bridging ligands in dinitrogen reduction and functionalization by uranium multimetallic complexes. *Nat. Chem.* **2019,** *11* (2), 154-160.
24. Mullane, K. C.; Ryu, H.; Cheisson, T.; Grant, L. N.; Park, J. Y.; Manor, B. C.; Carroll, P. J.; Baik, M.-H.; Mindiola, D. J.; Schelter, E. J., C–H Bond Addition across a Transient Uranium–Nitrido Moiety and Formation of a Parent Uranium Imido Complex. *J. Am. Chem. Soc.* **2018,** *140* (36), 11335-11340.
25. Thomson, R. K.; Cantat, T.; Scott, B. L.; Morris, D. E.; Batista, E. R.; Kiplinger, J. L., Uranium azide photolysis results in C–H bond activation and provides evidence for a terminal uranium nitride. *Nat. Chem.* **2010,** *2*, 723.
26. Fox, A. R.; Bart, S. C.; Meyer, K.; Cummins, C. C., Towards uranium catalysts. *Nature* **2008,** *455* (7211), 341-349.
27. Katz, J. J.; Morss, L. R.; Seaborg, G. T., *The Chemistry of the Actinide Elements*. 2nd ed.; 1986.
28. Mills, D. P.; Cooper, O. J.; Tuna, F.; McInnes, E. J. L.; Davies, E. S.; McMaster, J.; Moro, F.; Lewis, W.; Blake, A. J.; Liddle, S. T., *J. Am. Chem. Soc.* **2012,** *134*, 10047.
29. Thomson, R. K.; Cantat, T.; Scott, B. L.; Morris, D. E.; Batista, E. R.; Kiplinger, J. L., Uranium azide photolysis results in C–H bond activation and provides evidence for a terminal uranium nitride. *Nat. Chem.* **2010,** *2* (9), 723-729.
30. Lukens, W. W.; Edelstein, N. M.; Magnani, N.; Hayton, T. W.; Fortier, S.; Seaman, L. A., *J. Am. Chem. Soc.* **2013,** *135*, 10742.
31. Edelstein, N.; Brown, D.; Whittaker, B., Covalency effects on the ligand field splittings of octahedral 5f7 compounds. *Inorg. Chem.* **1974,** *13* (3), 563-567.
32. Burns, G.; Axe, J., Optical Properties of Ions in Crystals. *H. W., Eds.; Interscience: New York* **1967**, 53-71.
33. Graves, C. R.; Kiplinger, J. L., Pentavalent uranium chemistry—synthetic pursuit of a rare oxidation state. *Chem. Commun.* **2009,** (26), 3831-3853.
34. Liu, G.; Beitz, J. V., *Optical Spectra and Electronic Structure, The Chemistry of the Actinide and Transactinide Elements*. Morss, L. R.

Edelstein, N. M.
Fuger, J.: Springer, Berlin, 2006.
35. Edelstein, N. M.; Lander, G. H., *Magnetic Properties, The Chemistry of the Actinide and Transactinide Elements*. Morss, L. R.
Edelstein, N. M.
Fuger, J.: Springer, Berlin, 2006; p 2225-2306.
36. Kaltsoyannis, N.; Hay, P. J.; Li, J.; Blaudeau, J. P.; Burnsten, B. E., *Theoretical Studies of the Electronic Structure of Compounds of the Actinide Elements*. Morss, L. R.
Edelstein, N. M.
Fuger, J.: Springer, Berlin, 2006.
37. Palumbo, C. T.; Barluzzi, L.; Scopelliti, R.; Zivkovic, I.; Fabrizio, A.; Corminboeuf, C.; Mazzanti, M., Tuning the structure, reactivity and magnetic communication of nitride-bridged uranium complexes with the ancillary ligands. *Chem. Sci.* **2019,** *10* (38), 8840-8849.
38. Bell, N. L.; Maron, L.; Arnold, P. L., Thorium Mono- and Bis(imido) Complexes Made by Reprotonation of *cyclo*-Metalated Amides. *J. Am. Chem. Soc.* **2015,** *137* (33), 10492-10495.
39. Simpson, S. J.; Turner, H. W.; Andersen, R. A., Preparation and hydrogen-deuterium exchange of alkyl and hydride bis(trimethylsilyl)amido derivatives of the actinide elements. *Inorg. Chem.* **1981,** *20* (9), 2991-2995.
40. King, D. M.; Tuna, F.; McInnes, E. J. L.; McMaster, J.; Lewis, W.; Blake, A. J.; Liddle, S. T., Isolation and characterization of a uranium(VI)–nitride triple bond. *Nat. Chem.* **2013,** *5*, 482.
41. Zi, G.; Jia, L.; Werkema, E. L.; Walter, M. D.; Gottfriedsen, J. P.; Andersen, R. A., Preparation and Reactions of Base-Free Bis(1,2,4-tri-*tert*-butylcyclopentadienyl)uranium Oxide, Cp‘$_2$UO. *Organometallics* **2005,** *24* (17), 4251-4264.
42. Yu, X.; Xue, Z.-L., Deprotonation Reactions of Zirconium and Hafnium Amide Complexes $H_2N{-}M[N(SiMe_3)_2]_3$ and Subsequent Silyl Migration from Amide $-N(SiMe_3)_2$ to Imide =NH Ligands. *Inorg. Chem.* **2005,** *44* (5), 1505-1510.
43. Smiles, D. E.; Wu, G.; Hayton, T. W., Synthesis of Uranium–Ligand Multiple Bonds by Cleavage of a Trityl Protecting Group. *J. Am. Chem. Soc.* **2014,** *136* (1), 96-99.
44. Smiles, D. E.; Wu, G.; Hayton, T. W., Synthesis of Terminal Monochalcogenide and Dichalcogenide Complexes of Uranium Using Polychalcogenides, $[E_n]^{2-}$ (E = Te, *n* = 2; E = Se, *n* = 4), as Chalcogen Atom Transfer Reagents. *Inorg. Chem.* **2014,** *53* (19), 10240-10247.
45. Smiles, D. E.; Wu, G.; Hayton, T. W., Synthesis, Electrochemistry, and Reactivity of the Actinide Trisulfides $[K(18\text{-crown-}6)][An(\eta^3\text{-}S_3)(NR_2)_3]$ (An = U, Th; R = $SiMe_3$). *Inorg. Chem.* **2016,** *55* (18), 9150-9153.
46. Shannon, R., Acta Crystallogr., Sect. A: Cryst. Phys., Diffr., Theor. Gen. Crystallogr. **1976,** (32), 751-767.
47. Staun, S. L.; Stevens, L. M.; Smiles, D. E.; Goodwin, C. A. P.; Billow, B. S.; Scott, B. L.; Wu, G.; Tondreau, A. M.; Gaunt, A. J.; Hayton, T. W., Expanding the Nonaqueous Chemistry of Neptunium: Synthesis and Structural Characterization of $[Np(NR_2)_3Cl]$, $[Np(NR_2)_3Cl]^-$, and $[Np\{N(R)(SiMe_2CH_2)_2(NR_2)]^-$ (R = $SiMe_3$). *Inorg. Chem.* **2021,** *60* (4), 2740-2748.

48. Smiles, D. E.; Wu, G.; Hrobárik, P.; Hayton, T. W., Synthesis, Thermochemistry, Bonding, and ^{13}C NMR Chemical Shift Analysis of a Phosphorano-Stabilized Carbene of Thorium. *Organometallics* **2017,** *36* (23), 4519-4524.
49. Yu, X.; Bi, S.; Guzei, I. A.; Lin, Z.; Xue, Z.-L., Zirconium, Hafnium, and Tantalum Amide Silyl Complexes: Their Preparation and Conversion to Metallaheterocyclic Complexes via γ-Hydrogen Abstraction by Silyl Ligands. *Inorg. Chem.* **2004,** *43* (22), 7111-7119.
50. Marc, K.; Klaus, H.; Gerd, S.; Werner, M.; Stefan, F.; Gernot, F.; Kurt, D., Die Deprotonierung silylierter Amido-Komplexe von Seltenerdelementen. *Anorg. Allg. Che.* **1999,** *625* (12), 2055-2063.
51. Gardner, B. M.; McMaster, J.; Lewis, W.; Blake, A. J.; Liddle, S. T., A Crystallizable Dinuclear Tuck-In-Tuck-Over Tuck-Over Dialkyl Tren Uranium Complex and Double Dearylation of BPh_4^- To Give the BPh_2-Functionalized Metallocycle $[U\{N(CH_2CH_2NSiMe_3)_2(CH_2CH_2NSiMe_2CHBPh_2)\}(THF)]$. *J. Am. Chem. Soc.* **2009,** *131* (30), 10388-10389.
52. Graves, C. R.; Schelter, E. J.; Cantat, T.; Scott, B. L.; Kiplinger, J. L., A Mild Protocol To Generate Uranium(IV) Mixed-Ligand Metallocene Complexes using Copper(I) Iodide. *Organometallics* **2008,** *27* (20), 5371-5378.
53. Simpson, S. J.; Turner, H. W.; Andersen, R. A., Hydrogen-Deuterium Exchange: Perdeuteriohydridotris (hexamethyldisilylamido)- thorium(IV) and -uranium(IV). *J. Am. Chem. Soc.* **1979,** *101* (26), 7728-7729.
54. Evans, W. J.; Kozimor, S. A.; Ziller, J. W., Molecular octa-uranium rings with alternating nitride and azide bridges. *Science* **2005,** *309* (5742), 1835-1838.
55. Wheeler, R. A.; Hoffmann, R.; Straehle, J., Transition-metal nitrides, organic polyenes, and phosphazenes: a structural and orbital analogy. *J. Am. Chem. Soc.* **1986,** *108* (18), 5381-5387.
56. Wheeler, R. A.; Whangbo, M. H.; Hughbanks, T.; Hoffmann, R.; Burdett, J. K.; Albright, T. A., Symmetric vs. Asymmetric linear M-X-M Linkages in Molecules, Polymers, and Extended Networks. *J. Am. Chem. Soc.* **1986,** *108* (9), 2222-2236.
57. Bart, S. C.; Anthon, C.; Heinemann, F. W.; Bill, E.; Edelstein, N. M.; Meyer, K., Carbon dioxide activation with sterically pressured mid-and high-valent uranium complexes. *J. Am. Chem. Soc.* **2008,** *130* (37), 12536-12546.
58. Fortier, S.; Brown, J. L.; Kaltsoyannis, N.; Wu, G.; Hayton, T. W., Synthesis, Molecular and Electronic Structure of $U^V(O)[N(SiMe_3)_2]_3$. *Inorg. Chem.* **2012,** *51* (3), 1625-1633.
59. Castro-Rodriguez, I.; Olsen, K.; Gantzel, P.; Meyer, K., *J. Am. Chem. Soc.* **2003,** *125*, 4565.
60. Arnold, P. L.; Dutkiewicz, M. S.; Walter, O., Organometallic Neptunium Chemistry. *Chem. Rev.* **2017,** *117* (17), 11460-11475.
61. Ibers, J., Neglected neptunium. *Nature Chem.* **2010,** *2* (11), 996-996.
62. Harris, R. K.; Becker, E. D.; Cabral de Menezes, S. M.; Goodfellow, R.; Granger, P., NMR nomenclature: nuclear spin properties and conventions for chemical shifts. IUPAC Recommendations 2001. International Union of Pure and Applied Chemistry. Physical Chemistry Division. Commission on Molecular Structure and Spectroscopy. *Magn. Reson. Chem.* **2002,** *40* (7), 489-505.

63. Harris, R. K.; Becker, E. D.; De Menezes, S. M. C.; Granger, P.; Hoffman, R. E.; Zilm, K. W., Further Conventions for NMR Shielding and Chemical Shifts (IUPAC Recommendations 2008). *Magn. Reson. Chem.* **2008,** *46* (6), 582-598.
64. *SMART* Apex II, Version 5.632.; Bruker AXS, Inc.: Madison, WI, 2005.
65. *SAINT Software User's Guide*, Version 7.34a ed.; Bruker AXS Inc.: Madison, WI, 2005.
66. *SADABS*, Sheldrick, G.M.; University of Göttingen, Germany: 2005.
67. *SHELXTL*, Version 6.12 ed.; Bruker AXS Inc.: Madison, WI, 2005.
68. Olex2 1.2 (compiled 2014.06.27 svn.r2953 for OlexSys, GUI svn. r4855).
69. Dolomanov, O.; Bourhis, L.; Gildea, R.; Howard, J.; Puschmann, H., *J. Appl. Cryst* **2009,** *42*, 339-341.

Chapter 7. Expanding the Non-aqueous Chemistry of Neptunium: Synthesis and Structural Characterization of $[Np(NR_2)_3Cl]$, $[Np(NR_2)_3Cl]^-$, and $[Np\{N(R)(SiMe_2CH_2)\}_2(NR_2)]^-$ (R = $SiMe_3$)

Portions of this work were published in:

Selena L. Staun, Lauren M. Stevens, Danil E. Smiles, Conrad A. P. Goodwin, Brennan S. Billow, Brian L. Scott, Guang Wu, Aaron M. Tondreau, Andrew J. Gaunt, Trevor W. Hayton

Inorg. Chem. **2021**, *60*, 2740-2748.

7.1 Introduction

Following World War II, the public disclosure of the Manhattan project meant that plutonium attained instant name recognition and its fundamental chemical and material properties became the subject of widespread interest.[1-8] While neptunium never achieved the same level of fame,[3] it was nonetheless recognized as a critically important element because of its presence in nuclear waste streams coupled with the unique challenges associated with its redox control.[9-16] Yet, despite the central role of both Np and Pu in the nuclear fuel cycle, contemporary knowledge of their physicochemical properties has not kept pace with the recent surge of interest in Th and U chemistry,[17-21] due in part to the need for specialist radiological facilities that allow for the safe handling of these elements.[1, 3, 22] However, with the recent development of several new transuranic starting materials,[23, 24] including $AnCl_4(DME)_2$ (An = Np, Pu)[25] and $NpCl_4(THF)_3$,[26] which can be widely employed in the synthetic protocols previously developed for early actinide An(IV) chemistry, the coordination chemistry of Np and Pu has started to expand.[9, 27-29] The ability to access different oxidation states of these metals has also accelerated in the recent years.[9, 26, 27]

Guided by its well-developed chemistry in the early actinides,[30-36] we rationalized that new bis(trimethylsilyl)amide ($[N(SiMe_3)_2]^-$) complexes of the transuranics would be synthetically valuable.[37] In this regard, the first transuranic silylamide complexes were developed by Zwick and co-workers, who reported the synthesis and characterization of $[An(NR_2)_3]$ (An = Np, Pu; R =$SiMe_3$) in 1994.[38] The related U(IV) and Th(IV) metallacycles, $[An\{N(R)(SiMe_2)CH_2\}(NR_2)_2]$,[36, 39] are also accessible and have proven to be synthetically useful;[32-34, 40-46] however, their transuranic analogues are currently unknown. They would represent not only excellent starting materials, but also interesting complexes in their own right. Indeed, well-characterized alkyl complexes of the transuranics are exceptionally rare.

The majority of transuranic organometallics feature cyclopentadienyl-type ligands, such as Cp_3An (An = Np - Cf)[47-51] and $[An^{II}(1,3\text{-}(Me_3Si)_2C_5H_3)_3]^-$ (An = Np, Pu).[10, 17, 52-55] In contrast, transuranic hydrocarbyl complexes have proven harder to isolate. Notably, however, Walensky and co-workers reported the first structurally characterized Np hydrocarbyl complex, $Np[\eta^4\text{-}Me_2NC(H)C_6H_5]_3$, in 2019, with the recently developed $NpCl_4(DME)_2$ precursor facilitating its isolation.[28] These actinide alkyl complexes are of interest for their small-molecule activation reactivity,[56] their spectroscopic and magnetic properties,[57] and their ability to function as starting materials.[58]

Herein, I describe the syntheses of several new neptunium silylamide complexes, including $[Np(NR_2)_3Cl]$ (R = $SiMe_3$) and the Np(IV) organometallic, $[Np\{N(R)(SiMe_2CH_2)\}_2(NR_2)]^-$, a rare example of a transuranic hydrocarbyl complex. To make best use of a valuable resource and increase the probability of success,[55] small scale synthetic protocols were first developed for uranium, and then extended to neptunium. The new Np complexes were then compared to their U analogues to better understand the reactivity and bonding trends across the 5f-block. The redox properties of $[Np(NR_2)_3Cl]$ were also investigated.

7.2 Results and Discussion

7.2.1 Synthesis and Characterization of $[Np(NR_2)_3Cl]$ (7.1)

Reaction of 3 equiv of $NaNR_2$ (R = $SiMe_3$) with $NpCl_4(DME)_2$ in THF affords the Np(IV) silylamide complex, $[Np(NR_2)_3Cl]$ (**7.1**), which can be isolated as orange needles or blocks in 69% yield after work-up (Scheme 7.1). The ^{1}H NMR spectrum of the isolated material in benzene-d_6 features a broad resonance at -2.48 ppm, which is assignable to the $SiMe_3$ environment (Figure A7.1). In addition, complex **7.1** exhibits a solution-state effective

magnetic moment of 2.57 μ_B at 298 K in benzene-d_6, according to an Evans' method analysis. This value deviates considerably from predicted value for the $^4I_{9/2}$ ground state expected for Np^{4+} (3.62 μ_B) in the R-S coupling scheme (Figure A7.2, Table A7.1). The reason for this deviation is not readily apparent, although crystal-field effects, which are not insignificant in the actinides, could quench some of the orbital contribution to the moment.[59] The UV-vis-NIR spectrum of **7.1**, taken in THF, features a number of sharp transitions between 600-1100 nm that are tentatively assigned to the Laporte forbidden 5f→5f transitions expected for a Np(IV) ion (Figure A7.16), although the possibility of 5f→6d transitions cannot be ruled out. Additionally, there is a broad absorption in the visible region at ca. 390 nm (ε = 213 $M^{-1}cm^{-1}$). This spectrum is qualitatively similar to that observed for [Np(TREN^{TIPS})(Cl)] (TREN^{TIPS} = $\{N(CH_2CH_2NSi^iPr_3)_3\}^{3-}$; toluene solution), supporting the Np(IV) oxidation state assignment in **7.1**.[25, 27]

Scheme 7.1. Synthesis of complex **7.1**.

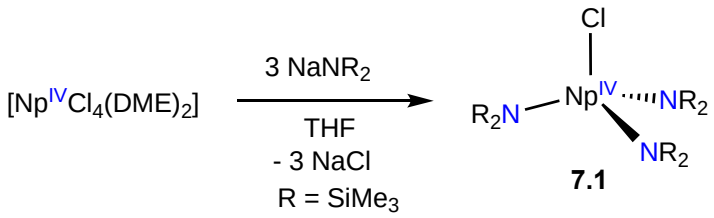

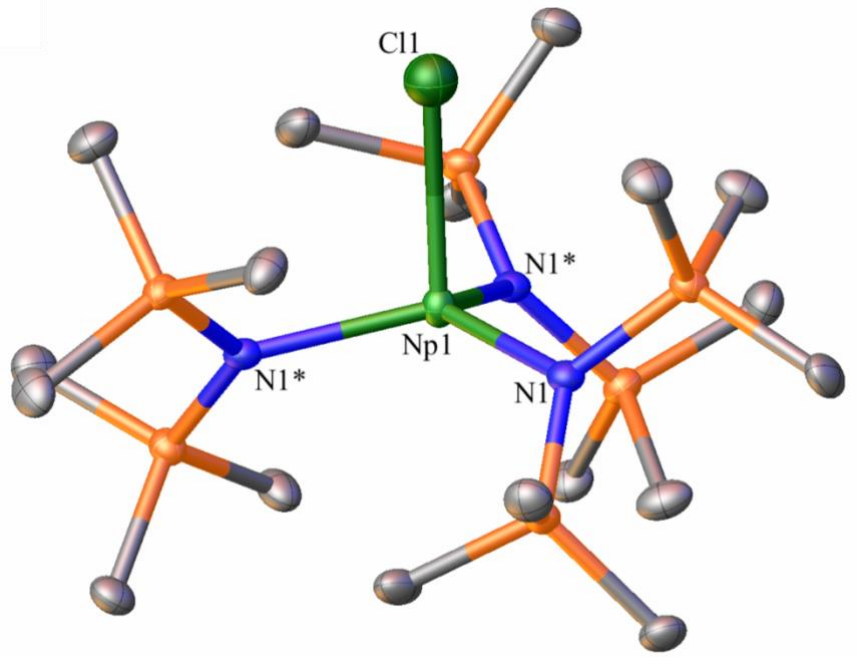

Figure 7.1. Solid-state molecular structure of $[Np(NR_2)_3Cl]$ (**7.1**) shown with 50% probability ellipsoids. Hydrogen atoms removed for clarity. Selected bond lengths (Å) and angles (°): $Np\text{-}N_{silylamido}$ = 2.221(4), Np-Cl = 2.586(3), N-Np-N = 117.37(6), N-Np-Cl = 99.43(11).

Table 7.1. Selected bond lengths (Å) and angles (°) in complexes **7.1**, **7.3**, **7.4**, $[Th(NR_2)_3Cl]$,[60] $[U(NR_2)_3Cl]$,[46] and $[Pu(NR_2)_3Cl]$.[23]

	7.1 M = Np	**7.3** M = U	**7.4** M = Np	$[Th(NR_2)_3Cl]$	$[U(NR_2)_3Cl]$	$[Pu(NR_2)_3Cl]$
M-N	2.221(4)	2.386(16) 2.403(15) 2.366(16)	2.234(7) 2.315(7) 2.342(7)	2.293(2)	2.239(2)	2.207(6)
M-Cl	2.586(3)	2.704(5)	2.813(19)	2.647(1)	2.593(2)	2.595(3)
N-M-N	117.37(6)	119.2(5) 118.2(5) 112.4(5)	115.6(3) 117.2(2) 118.0(3)	116.53(4)	116.79(4)	117.1(1)
N-M-Cl	99.43(11)	100.0(4) 101.2(4) 101.0(4)	96.14(18) 105.66(17) 98.76(16)	100.53(4)	100.44(6)	99.9(1)

The connectivity of complex **7.1** was verified by X-ray crystallography (Figure 7.1). Complex **7.1** crystallizes in the trigonal space group *R3c* and features a distorted tetrahedral geometry about the neptunium center. Its crystallographic characterization marks the completion of the silylamide series, $[An(NR_2)_3Cl]$ (An = Th, U, Np, Pu) (Table 7.1), a rare example of an actinide series with four structurally-characterized representatives. Its Np-N_{amide} distance (Np-N = 2.221(4) Å) is consistent with those reported for other Np(IV) amide complexes, which range from 2.206(2) to 2.232(2) Å.[27] In addition, the Np-N_{amide} distance is

shorter than that seen in the Th analogue (2.293(2) Å) (Table 7.1), comparable (within error) to U-N distance observed for [$U(NR_2)_3Cl$] (2.239(2) Å), and longer than the reported distances for the Pu analogue (2.207(6) Å),[23, 46, 60] consistent with the actinide contraction. The Np-Cl distance (2.586(3) Å) is comparable to those reported in the $NpCl_4(DME)_2$ starting material (av. 2.61 Å),[25] [$Np(TREN^{TIPS})Cl$] (2.6200(6) Å),[27] and $NpCl_4(THF)_3$ (av. 2.59 Å).[26] However, a comparison of this distance with those seen in [$Th(NR_2)_3Cl$], [$U(NR_2)_3Cl$], and [$Pu(NR_2)_3Cl$] (2.647(1) Å, 2.593(2) Å, and 2.595(3) Å, respectively)[23, 46, 60] does not reveal an obvious trend; although I note that these data were collected at different temperatures, ranging from 100K to 150K, which may mask any anticipated bond length changes.

The cyclic voltammogram of **7.1**, recorded in THF (1.8 mM) using [$^nPr_4N$][$BArF^{24}$] (67 mM) as the supporting electrolyte, exhibits a reversible (*vide infra*) redox event centered at $E_{1/2}$ = -1.26 V (vs. Fc/Fc^+). I have assigned this feature to a metal-centered Np(IV/III) couple (Figure 7.2). The reversibility of this feature suggests that [**7.1**]$^-$ could be isolable. Most electrochemistry measurements of transuranic complexes have been performed in aqueous media,[17, 61-63] which makes contextualization of my data more challenging. However, the cyclic voltammograms of Cp_4Np, Cp_3NpCl, and $Cp^*_2NpCl_2$, all recorded in THF, were reported by Gaudiello and co-workers in 1988.[64] Each complex featured a single redox event (Cp_4Np: $E_{1/2}$ = -1.27 V; Cp_3NpCl: $E_{1/2}$ = -1.29 V; $Cp^*_2NpCl_2$: $E_{1/2}$ = -1.38 V, vs. Fc/Fc^+), assignable to the reversible Np(IV/III) couple. These values are in good agreement with that observed for **7.1**. For further comparison, the cyclic voltammogram of [$Np(L)_2$] (H_2L = *N*,*N*′-bis[(4,4′-diethylamino)salicylidene]-1,2-phenylenediamine) features an irreversible Np(IV/III) reduction event at $E = -2.91$ V (vs. Fc/Fc^+) in DMSO. This value it much lower than the reduction potential observed for **7.1** and likely reflects the much higher coordination

number in [Np(L)$_2$].[65] I also recorded the cyclic voltammogram of the uranium analogue, [U(NR$_2$)$_3$Cl], in THF at a variety of scan rates, using [NBu$_4$][BPh$_4$] as the supporting electrolyte. Its cyclic voltammogram features an irreversible redox feature at -2.26 V (100 mV/s scan rate, vs. Fc/Fc$^+$; Figure A7.27), which I have assigned to a U(IV/III) reduction event. The substantially lower reduction potential observed for [U(NR$_2$)$_3$Cl] is consistent with established periodic trends.[66]

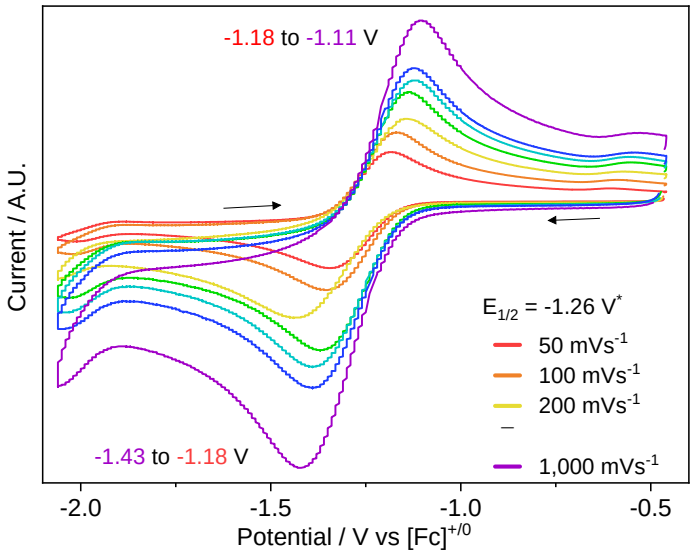

Figure 7.2. Cyclic voltammogram of [Np(NR$_2$)$_3$Cl] (**7.1**) (1.8 mM), measured in THF with 67 mM [^{n}Pr$_4$N][BArF^{24}] as supporting electrolyte. The scan at 200 mV·s^{-1} showed an anomalous cathodic peak and was not used for the $E_{1/2}$ determination.

7.2.2 Synthesis and Characterization of [K(2,2,2-cryptand)][U(NR$_2$)$_3$Cl] (7.2) and [K(DB-18-C-6)(THF)$_2$][U(NR$_2$)$_3$Cl] (7.3).

Reaction of [U(NR$_2$)$_3$Cl] with 1.5 equiv of KC$_8$ in THF, in the presence of either 2,2,2-cryptand or dibenzo-18-crown-6 (DB-18-C-6), results in a rapid color change from pale pink to dark purple. Work-up of the respective reaction mixtures, followed by crystallization from THF/hexanes, results in the isolation of [K(2,2,2-cryptand)][U(NR$_2$)$_3$Cl] (**7.2**) or [K(DB-18-

C-6)(THF)$_2$][U(NR$_2$)$_3$Cl] (**7.3**) as dark purple blocks in 70% or 74% yield, respectively (Scheme 7.2).

Scheme 7.2. Synthesis of complexes **7.2** and **7.3**.

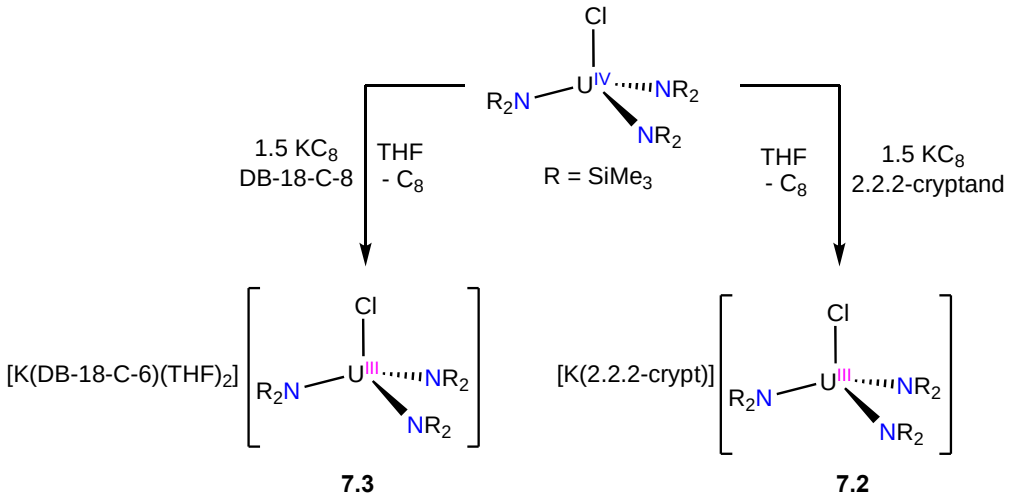

Complexes **7.2** and **7.3** crystallize in the orthorhombic and triclinic space groups $P2_12_12_1$ and *P-1*, respectively. In addition, complex **7.2** crystallizes as the THF solvate, **7.2**·THF. Both feature pseudo-tetrahedral geometries about their uranium centers (Figures 7.3 and 7.7, Table 7.3). Their U-N$_{amide}$ distances (**7.2**: av. U-N = 2.36; **7.3**: av. U-N = 2.38 Å) are consistent with those reported for other U(III) amide complexes.[30, 67] Moreover, their U-Cl distances (**7.2**: U-Cl = 2.701(3) Å; **7.3**: U-Cl = 2.704(5) Å) are consistent with those reported for other U(III)-Cl complexes.[68]

The ^{1}H NMR spectrum of **7.2** exhibits a sharp singlet at -5.57 ppm, which is assignable to the SiMe$_3$ environment, as well as broad singlets at 2.03, 3.00, and 3.03 ppm, which are assignable to the three proton environments of the 2,2,2-cryptand fragment (Figure A7.3). The ^{1}H NMR spectrum of **7.3** exhibits a sharp singlet at -5.62 ppm, which is assignable to the SiMe$_3$ environment, and four sharp singlets at 2.29, 2.98, 6.17, and 6.53 ppm, in a 2:2:1:1 ratio, which are assignable to the four unique proton environments of dibenzo-18-crown-6

fragment (Figure A7.4). Finally, the UV-vis-NIR spectra of **7.2** and **7.3**, recorded in THF (Figures A7.17 and A7.18), are broadly consistent with those observed for $UCl_3(py)_4$ (in pyridine),[68] $UCl_3(THF)_x$ (in THF),[69] $[U\{N(SiMe_2Ph)_2\}_3]$,[67] and $[U\{N(SiMe_2tBu)_2\}_3]$,[70] providing further support for the U(III) oxidation state assignment.

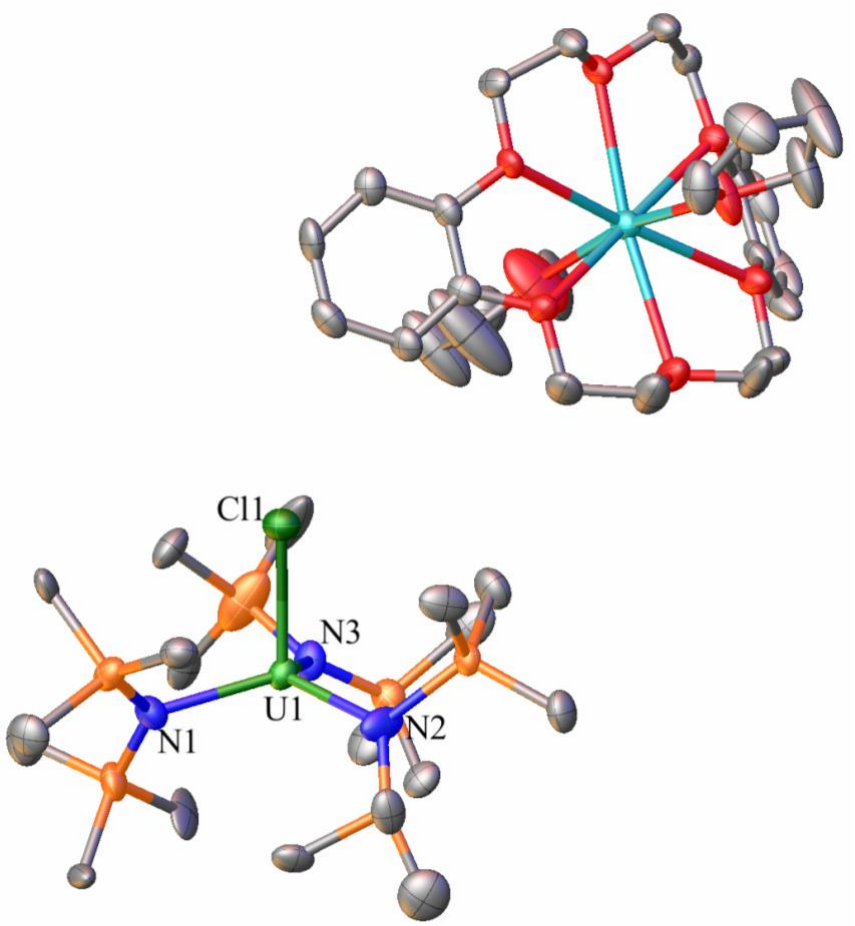

Figure 7.3. Solid-state molecular structure of $[K(DB\text{-}18\text{-}C\text{-}6)(THF)_2][U(NR_2)_3Cl]$ (**7.3**) shown with 50% probability ellipsoids. Hydrogen atoms removed for clarity. Selected bond lengths (Å) and angles (°): Np-$N_{silylamido}$ (av.) = 2.385, Np-Cl = 2.704(5), N-Np-N (av.) = 116.6, N-Np-Cl (av.) = 100.7.

7.2.3 Synthesis and Characterization of [{K(DB-18-C-6)(THF)}$_3$(μ$_3$-Cl)][Np(NR$_2$)$_3$Cl]$_2$ (7.4)

Reaction of [Np(NR$_2$)$_3$Cl] (**7.1**) with 1.5 equiv of KC$_8$ in THF, in the presence of 1 equiv of dibenzo-18-crown-6, resulted in color change from orange to golden yellow. Work-up of the reaction mixture, followed by crystallization from THF/*n*-hexane, resulted in the isolation of [{K(DB-18-C-6)(THF)}$_3$(μ$_3$-Cl)][Np(NR$_2$)$_3$Cl]$_2$ (**7.4**), the first structurally characterized Np(III) amide, as yellow needles in 63% yield (Scheme 7.3). Interestingly, the reduction of **7.1** with KC$_8$, in the presence of 2,2,2-cryptand, also resulted in a color change to yellow, however, crystalline material could not be isolated from this reaction mixture.

Scheme 7.3. Synthesis of complex **7.4**.

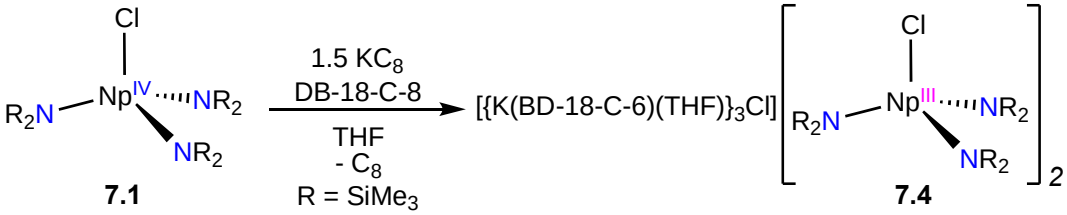

Complex **7.4** crystallizes in the monoclinic space group *I*2/a and features a pseudo-tetrahedral geometry about the neptunium center (Figure 7.4). Its Np-N$_{amide}$ distances (av. Np-N = 2.297 Å) are longer than those in **7.1** (2.221(4) Å), consistent with the larger ionic radius of Np^{3+}.[71] However, its Np-N$_{amide}$ distances are shorter than those in the uranium analogue, **7.3** (av. 2.38 Å) (Table 7.1), a consequence of the actinide contraction. Its Np-Cl distance (2.813(19) Å) is remarkably longer than that seen in **7.1** (2.586(3) Å), again consistent with the larger ionic radius of Np^{3+}.[71] The Np-Cl distance in **7.4** is also much longer than those reported for two other Np^{3+} complexes, NpCl$_3$(py)$_4$ (av. 2.7166 Å) and [(L^{Ar})NpCl] (H$_2$L^{Ar} = *trans*-calix[2]benzene[2]pyrrole) (2.6694(9) Å),[26, 72] likely on account of its anionic charge. The cation in **7.4** consists of a [μ$_3$-Cl]$^-$ anion capped by three [K(DB-18-C-6)(THF)]$^+$

fragments in a trigonal planar array. This $[\mu_3\text{-Cl}]^-$ anion could be generated by decomposition of some sacrificial $[Np(NR_2)_3Cl]^-$, but given the relatively high yield of **7.4**, I suggest that it is formed from adventitious NaCl that is still present from the original synthesis of the $[Np(NR_2)_3Cl]$ starting material. Salt inclusion has previously been noted as a problem in actinide silylamide syntheses.[60, 73]

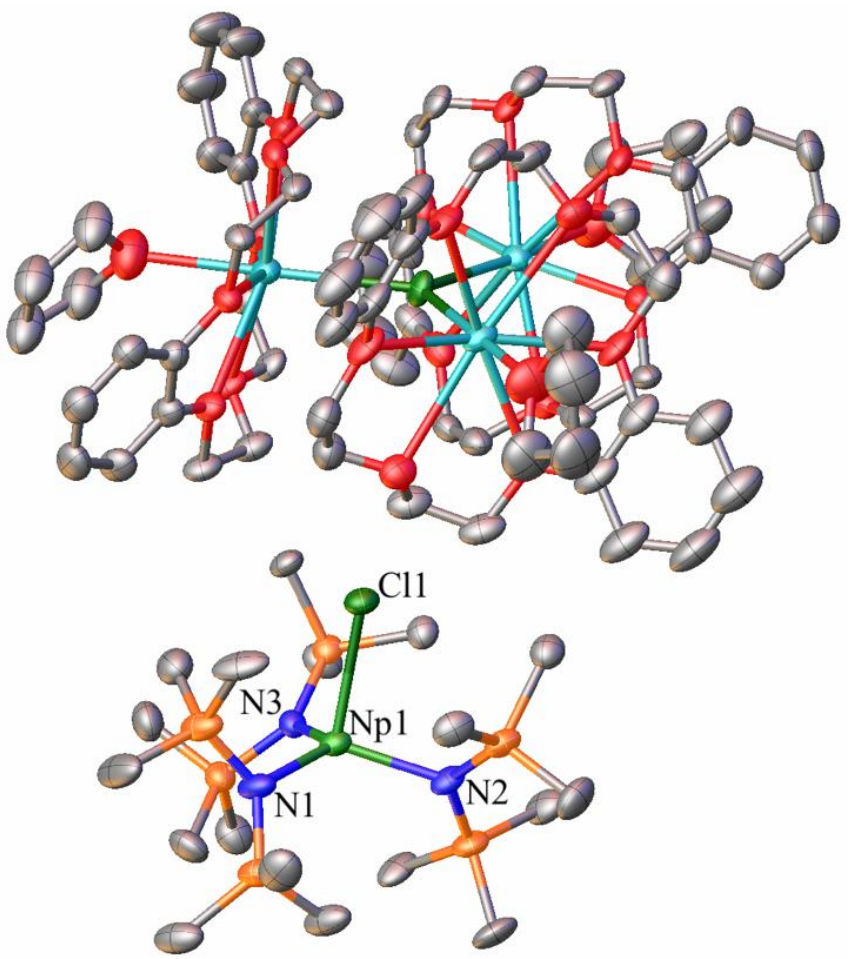

Figure 7.4. Solid-state molecular structure of $[\{K(DB\text{-}18\text{-}C\text{-}6)(THF)\}_3(\mu_3\text{-}Cl)][Np(NR_2)_3Cl]_2$ (**7.4**) shown with 50% probability ellipsoids. Hydrogen atoms removed for clarity. Selected bond lengths (Å) and angles (°): $Np\text{-}N_{silylamido}$ (av.) = 2.297, Np-Cl = 2.813(19), N-Np-N (av.) = 116.9, N-Np-Cl (av.) = 100.2.

The ^{1}H NMR spectrum of **7.4** exhibits a sharp singlet at -3.42 ppm, which is assignable to the $SiMe_3$ environment, as well as broad resonances at 4.43, 4.55, 7.00, and 7.20 ppm, which are assignable to the four unique environments of the dibenzo-18-crown-6 fragment. In addition, complex **7.4** exhibits a solution-state effective magnetic moment of 3.00 μ_B at 298 K in THF-d_8, according to an Evans' method analysis. This value deviates somewhat from the value expected for the $^{5}I_4$ ground state of Np^{3+} (2.68 μ_B) in the R-S coupling scheme (Figure A7.8, Table A7.1), but it is close to that predicted for this ion in the intermediate coupling scheme (2.88 μ_B).[74] The UV-vis-NIR spectrum of **7.4** in THF features a number of weak bands in the 600-1100 nm region (Figure 7.5), which are likely assignable to Laporte forbidden 5f→5f transitions. Similar features are observed in the NIR spectra if $NpCl_3(py)_4$ (in pyridine) and [(L^{Ar})NpCl] (in THF).[26, 72] Several, much more intense, absorptions are observed below 500 nm (above 20,000 cm^{-1}) and are likely due to 5f→6d transitions and/or ligand-to-metal charge transfer bands.

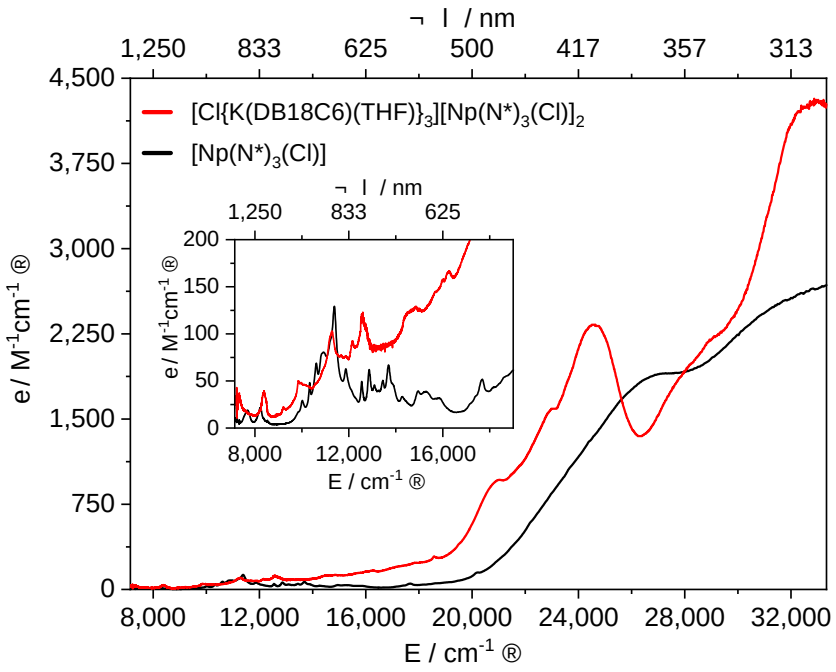

Figure 7.5. UV-vis-NIR spectra of complexes **7.1** (1 mM) and **7.4** (0.5 mM) in THF.

7.2.4 Synthesis and Characterization of [Np{*N*(R)(SiMe$_2$)*C*H$_2$}(NR$_2$)$_2$] (7.5)

A mixture of 4 equiv of NaNR$_2$ and 1 equiv of NpCl$_4$(DME)$_2$ in toluene was heated at 70° C for 4 h, whereupon the solution turned deep brown (Scheme 7.4). Work-up of this reaction mixture lead to the isolation of an orange-brown crystalline material, which contained a mixture of **7.1**, the Np(IV) bis(metallacycle), [Np{*N*(R)(SiMe$_2$*C*H$_2$)}$_2$(NR$_2$)]$^-$ (**7.8**), and another material tentatively identified as [Np{*N*(R)(SiMe$_2$)*C*H$_2$}(NR$_2$)$_2$] (**7.5**).[33] The ^{1}H NMR spectrum of this mixture in benzene-d_6 exhibited four sharp resonances 13.48, -0.99, -9.48, and -146.73 ppm, in a ratio of 6:9:36:2, respectively, corresponding to the SiMe$_2$, SiMe$_3$, N(SiMe$_3$)$_2$, and CH$_2$ environments of **7.5** (Figure A7.9). Similar values are observed for the paramagnetic uranium analogue.[36, 39] Also present in the sample is a singlet at -2.92 ppm, which is assignable to the silylamide environment of complex **7.1**, as well as singlets at -29.58, -3.89, 25.57, and 30.25 ppm (Figure A7.9), which are assignable to [Np{*N*(R)(SiMe$_2$*C*H$_2$)}$_2$(NR$_2$)]$^-$ (**7.8**). Unfortunately, I could never achieve clean conversion to **7.5**, as samples were always contaminated with complexes **7.1** and **7.8**. Additionally, preliminary experiments with the mixture revealed that the presence of even small amounts of **7.1** and [Np{*N*(R)(SiMe$_2$*C*H$_2$)}$_2$(NR$_2$)]$^-$ (**7.8**) interfered with subsequent chemistry. Thus, further attempts to develop the synthesis of **7.5** were abandoned.

Scheme 7.4. Synthesis to complex **7.5**.

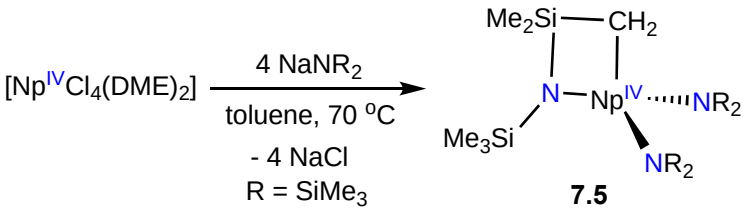

7.2.5 Synthesis and Characterization of [Na(DME)$_3$][U{*N*(R)(SiMe$_2$*C*H$_2$)}$_2$(NR$_2$)] (7.6) and [{Na(DB-18-C-6)(Et$_2$O)$_{0.5}$(κ^1-DME)$_{0.5}$}$_2$(μ-DME)][U{*N*(R)(SiMe$_2$*C*H$_2$)}$_2$(NR$_2$)]$_2$ (7.7)

Given its formation during my attempts to prepare **7.5**, I hypothesized that the Np(IV) bis(metallacycle) [Np{*N*(R)(SiMe$_2$*C*H$_2$)}$_2$(NR$_2$)]$^-$ could be targeted rationally by reaction of NpCl$_4$(DME)$_2$ with 5 equiv of NaNR$_2$. To improve my chances of success, however, I first explored the small scale (0.03 mmol) synthesis of the known U(IV) bis(metallacycle), [U{*N*(R)(SiMe$_2$*C*H$_2$)}$_2$(NR$_2$)]$^-$,[33] in a mixture of THF and DME, both with and without dibenzo-18-crown-6 as a Na$^+$ complexing agent. Work-up of the respective reaction mixtures resulted in isolation of either [Na(DME)$_3$][U{*N*(R)(SiMe$_2$*C*H$_2$)}$_2$(NR$_2$)] (**7.6**) or [{Na(DB-18-C-6)(Et$_2$O)$_{0.5}$(κ^1-DME)$_{0.5}$}$_2$(μ-DME)][U{*N*(R)(SiMe$_2$*C*H$_2$)}$_2$(NR$_2$)]$_2$ (**7.7**), which I could reproducibly isolate in 60-70% yield at these small scales (Scheme 7.5).

Scheme 7.5. Synthesis of complexes **7.6** and **7.7**.

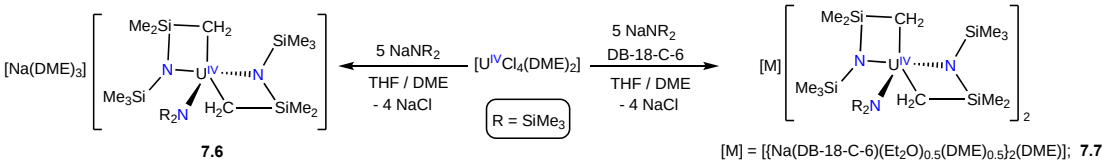

Note that while the [U{*N*(R)(SiMe$_2$*C*H$_2$)}$_2$(NR$_2$)]$^-$ fragment has been reported previously,[33] it has not been reported with either the [{Na(DB-18-C-6)(Et$_2$O)$_{0.5}$(κ^1-DME)$_{0.5}$}$_2$(μ-DME)] or [Na(DME)$_3$]$^+$ counterions. Similar to the previously reported [U{*N*(R)(SiMe$_2$*C*H$_2$)}$_2$(NR$_2$)]$^-$ complexes, the ^{1}H NMR spectrum of **7.7** in THF-d_8 exhibits two signals at 39.51 and -37.02 ppm, each integrating for 18H and assignable to the two unique SiMe$_3$ environments, two resonances at 31.93 and -6.22 ppm, each integrating for 6H and assignable to the diastereotopic SiMe$_2$ groups, and two resonances at -285.77 and -297.16 ppm, each integrating for 2H and assignable to the diastereotopic CH$_2$ hydrogens.[33]

Furthermore, sharp resonances at 6.11 and 6.43 ppm, in a 4:4 ratio, are assignable to the two aryl C-H environments of the $[\{Na(DB\text{-}18\text{-}C\text{-}6)(Et_2O)_{0.5}(\kappa^1\text{-}DME)_{0.5}\}_2(\mu\text{-}DME)]^+$ counterion.

7.2.6 Synthesis and Characterization of $[\{Na(DB\text{-}18\text{-}C\text{-}6)(Et_2O)_{0.62}(\kappa^1\text{-}DME)_{0.38}\}_2(\mu\text{-}DME)][Np\{N(R)(SiMe_2CH_2)\}_2(NR_2)]_2$ (7.8) and $[Na(DME)_3][Np\{N(R)(SiMe_2CH_2)\}_2(NR_2)]$ (7.9)

Gratifyingly, I found that these reaction conditions could be extended to Np. Thus, reaction of $NpCl_4(DME)_2$ with 5 equiv of $NaNR_2$ and 1 equiv of dibenzo-18-crown-6 in a mixture of THF and DME at room temperature afforded the Np(IV) bis(metallacycle), $[\{Na(DB\text{-}18\text{-}C\text{-}6)(Et_2O)_{0.62}(\kappa^1\text{-}DME)_{0.38}\}_2(\mu\text{-}DME)][Np\{N(R)(SiMe_2CH_2)\}_2(NR_2)]_2$ (**7.8**), as orange needles in 57% yield after work-up (Scheme 7.6).

Scheme 7.6. Synthesis of complexes **7.8** and **7.9**.

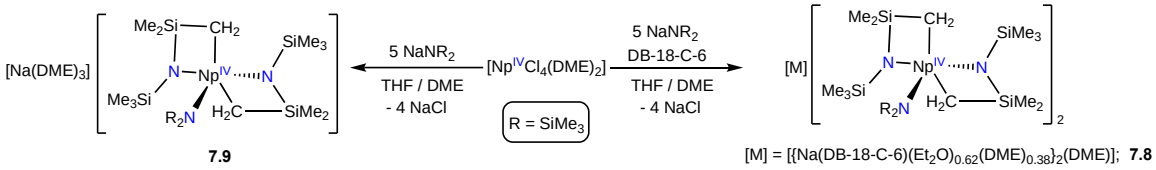

The Np analogue of **7.6**, namely, $[Na(DME)_3][Np\{N(R)(SiMe_2CH_2)\}_2(NR_2)]$ (**7.9**), could also be synthesized in comparable yields. It is isomorphous to **7.6**, but always gave poorly-diffracting crystals that could only be used to confirm connectivity (Figure 7.8). The ^{1}H NMR spectra of **7.8** and **7.9** in THF-d_8 are consistent with my proposed structure. Specifically, for **7.8** I observed resonances at 26.36 and -26.36 ppm, each integrating for 18H, which are assignable to the two unique $SiMe_3$ environments. Additionally, I observed resonances at 29.95 and -3.94 ppm, each integrating for 6H and assignable to the diastereotopic $SiMe_2$ groups. Curiously, I only observed a single peak, at -242.58 ppm, which is assignable to the

diastereotopic CH_2 hydrogens, and not two resonances as were observed for complexes **7.6** or **7.7**. However, I note that this signal is very broad, suggesting that it may consist of two overlapping resonances. Finally, I observed four resonances at 6.55, 6.36, 3.36, and 2.94 ppm, in a 1:1:2:2 ratio, which are assignable to the four unique dibenzo-18-crown-6 environments of the $[\{Na(DB\text{-}18\text{-}C\text{-}6)(Et_2O)_{0.62}(\kappa^1\text{-}DME)_{0.38}\}_2(\mu\text{-}DME)]^{2+}$ counterion. The UV-vis spectrum of **7.8** in THF features many sharp transitions between 600-1100 nm that are consistent with Laporte forbidden f→f transitions (Figure A7.20). These transitions are broadly similar to those reported for $NpCl_4(DME)_2$ (in DME), $[Np^{IV}(TREN^{TIPS})(Cl)]$ (in toluene), and complex **7.1**, supporting the 4+ oxidation state assignment for this complex.[25, 27]

Complex **7.8** is isomorphous with **7.7** and features a distorted trigonal bipyramidal geometry about the neptunium center (Figure 7.6), with $\tau_5 = 0.45$.[75] It also features a badly disordered counterion that was best modeled as $[\{Na(DB\text{-}18\text{-}C\text{-}6)(Et_2O)_{0.62}(\kappa^1\text{-}DME)_{0.38}\}_2(\mu\text{-}DME)]$. Its Np-C distances (2.440(10) and 2.454(12) Å) are in line with those in **7.7** (2.455(6) and 2.456(7) Å), but are much shorter than those of the previously reported Th analogue, $\{[K(DME)][Th\{N(R)(SiMe_2CH_2)\}_2(NR_2)]\}_\infty$ (2.562(5) and 2.576(5) Å),[32] consistent with smaller ionic radius of Np^{4+} (Table 7.2). Moreover, its Np-N distances (2.287(8), 2.279(8), and 2.341(8) Å) are comparable (within error) to the U-N distances observed in **7.7**, but are longer than those reported for other Np(IV) amide complexes, which range from 2.206(2) to 2.232(2) Å.[27] For further comparison, Walensky's Np(III) hydrocarbyl complex, $Np[\eta^4\text{-}Me_2NC(H)C_6H_5]_3$, features much longer Np-C distances (av. 2.582 Å), which can be rationalized by the larger ionic radii of Np(III) *vs*. Np(IV), as well as its higher coordination number.[28]

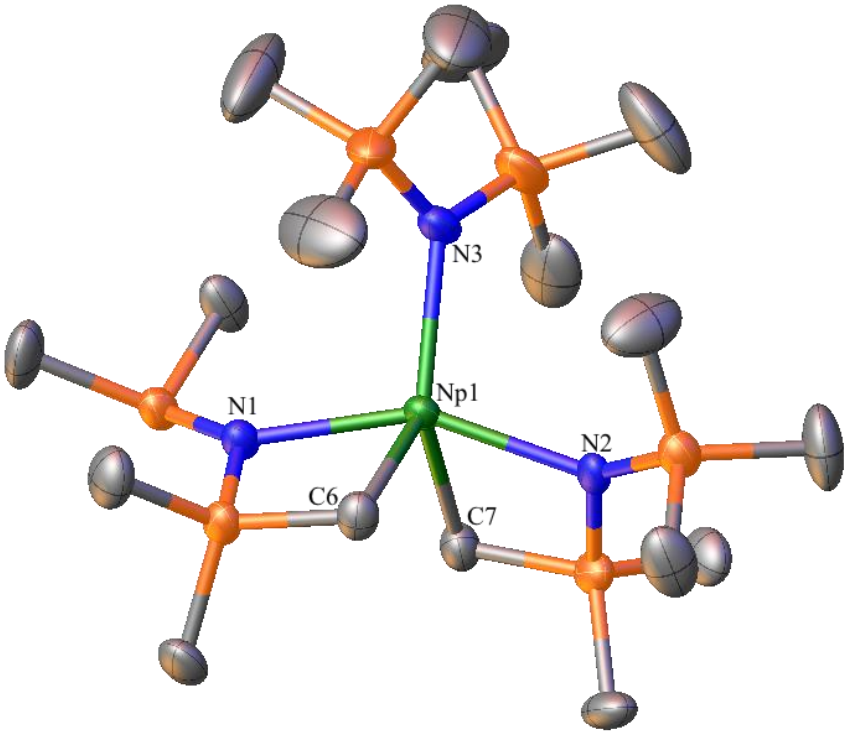

Figure 7.6. Solid-state molecular structure of [{Na(DB-18-C-6)(Et_2O)$_{0.62}$(κ^1-DME)$_{0.38}$}$_2$(μ-DME)][Np{*N*(R)($SiMe_2$*C*H_2)}$_2$(NR_2)]$_2$ (**7.8**) shown with 50% probability ellipsoids. Counterion and hydrogen atoms removed for clarity. Selected bond lengths (Å) and angles (°): Np-C (av.) = 2.447, Np-N (av.) = 2.302, N-Np-N (av.) = 120.

Table 7.2. Selected bond lengths (Å) and angles (°) in complexes **7.6**, **7.7**, **7.8**, and {[K(DME)][Th{*N*(R)(SiMe$_2$*C*H$_2$)}$_2$(NR$_2$)]}$_\infty$.[32]

	7.6 M = U	**7.7** M = U	**7.8** M = Np	{[K(DME)] [Th{*N*(R)(SiMe$_2$*C*H$_2$)}$_2$(NR$_2$)]}$_\infty$
M-C	2.474(7)	2.455(6)	2.440(10)	2.562(5)
	2.489(8)	2.456(7)	2.454(12)	2.576(5)
M-N	2.291(6)	2.278(5)	2.287(8)	2.352(3)
	2.289(7)	2.280(5)	2.279(8)	2.363(4)
	2.366(6)	2.357(5)	2.341(8)	2.381(4)
N-M-N	106.0(2)	152.29(17)	152.0(3)	138.15(14)
	151.2(2)	103.19(18)	103.5(3)	109.52(13)
	102.8(2)	104.52(18)	104.5(3)	112.14(13)

7.3 Summary

In summary, I have synthesized a series of Np silylamide complexes, including [Np(NR$_2$)$_3$Cl] (**7.1**), [Np(NR$_2$)$_3$Cl]$^-$ (**7.4**), and [Np{*N*(R)(SiMe$_2$*C*H$_2$)}$_2$(NR$_2$)]$^-$ (**7.8**), greatly expanding the scope of anhydrous Np coordination chemistry. Notably, [Np{*N*(R)(SiMe$_2$*C*H$_2$)}$_2$(NR$_2$)]$^-$ (**7.8**) is an exceptionally rare example of a structurally-characterized neptunium hydrocarbyl. These transuranic materials can be easily synthesized in good yields and should greatly help advance non-aqueous neptunium coordination chemistry, which lags markedly behind that of uranium and thorium.[1] Moving forward, I plan to employ both [Np(NR$_2$)$_3$Cl] (**7.1**) and [Np{*N*(R)(SiMe$_2$*C*H$_2$)}$_2$(NR$_2$)]$^-$ (**7.8**) as precursors to

Np oxo, imido, and nitrido complexes. Well-characterized transuranic complexes with multiple bonds, outside of the neptunyl (NpO_2^{n+}, n = 1, 2) moiety, are exceptionally rare,[9, 17, 76, 77] and my new Np silylamide complexes should be useful precursors to these materials.

7.4 Acknowledgements

This work was supported by the U.S. Department of Energy, Office of Basic Energy Sciences, Chemical Sciences, Biosciences, and Geosciences Division, under Contract DE-SC0001861 (TWH, SLS; University of California, Santa Barbara) and DE-AC52-06NA25396 (AJG; Heavy Element Chemistry program at Los Alamos). I gratefully acknowledge the support of the U.S. Department of Energy through the Los Alamos National Laboratory – Laboratory Directed Research and Development program (LANL-LDRD) Program and the G.T. Seaborg Institute. I also gratefully acknowledges the U.S. Department of Energy Office of Science and the Oak Ridge Institute for Science and Education (ORISE), through the Office of Science Graduate Student Research (SCGSR) Award.

Finally, I would like thank my mentors and peers at LANL and UCSB. Specifically, Dr. Danil Smiles (UCSB and Hayton alumni), who laid the groundwork for this project at LANL. His preliminary results and insights helped me immensely with finishing this project. Dr. Andrew Gaunt, my transuranic mentor at LANL, who provided his time and resources to help this chemistry succeed. Dr. Aaron Tondreau, my uranium mentor at LANL, who also provided his time and resources toward this chemistry. Dr. Conrad Goodwin, Dr. Lauren Stevens, and Dr. Brennan Billow, who each helped with characterization techniques.

7.5 Experimental

7.5.1 General Methods

Caution! All neptunium chemistry (using the ^{237}Np isotope) was conducted inside specialist radiological facilities designed for the safe handling and manipulation of high specific-activity α-particle emitting radionuclides. Multiple levels of containment were utilized when appropriate for safety reasons. As a consequence of the radiological hazards, it is not possible to have elemental analyses performed on compounds by a third-party micro-analytical laboratory.

All uranium reactions and subsequent manipulations were performed under anaerobic and anhydrous conditions under an atmosphere of nitrogen. All neptunium reactions were performed under anaerobic and anhydrous conditions inside a negative pressure glovebox under a high purity helium atmosphere. All solvents were purchased in anhydrous grade and dried over 3 Å or 4 Å sieves for several days before use. Benzene-d_6 and THF-d_8 were dried over 3 Å molecular sieves for 24 h prior to use. $UCl_4(DME)_2$, $NpCl_4(DME)_2$, and $U(N(SiMe_3)_2)_3Cl$ were synthesized according to the previously reported procedures.[25, 78, 79] $[^nPr_4N][BArF^{24}]$ [$BArF^{24}$ = $B(C_6H_3\text{-}3,5\text{-}CF_3)_4$] was prepared as previously described,[80] and recrystallized twice from a DCM/Et_2O/*n*-hexane solution, followed by grinding of the crystals and drying *in vacuo* (5×10^{-4} mbar) for 48 h. All other reagents were purchased from commercial suppliers and used as received.

NMR spectra at UCSB were recorded on an Agilent Technologies 400-MR DD2 400 MHz Spectrometer. NMR spectra at LANL, including ^1H (400.13 MHz), $^{13}C\{^1H\}$ (100.61 MHz), and $^{29}Si\{^1H\}$ (79.49 MHz) NMR spectra, were recorded on a Bruker Avance II spectrometer. Sample solutions were loaded into a fresh FEP NMR liner that was protected from surface

contamination with Parafilm while inside a transuranium glovebox. The liner was sealed with two PTFE plugs, brought out of the glovebox and verified to be free of surface contamination and the liner loaded into a precision thin-walled 5 mm glass NMR tube, or a J. Young tap-appended glass NMR tube. $^{29}Si\{^{1}H\}$ data was collected using the INEPT pulse sequence,[81] with d1 = 2.0 s,[82] (no significant improvement is observed with d1 = 1.0 s). Solution magnetic susceptibility was determined by the Evans method,[83] by adding several drops of C_6H_6 or THF into the outer liner and re-recording the ^{1}H NMR spectrum and comparing to the previously recorded ^{1}H NMR spectrum (this work). ^{1}H NMR spectra were referenced to external tetramethylsilane (TMS) using the residual protio solvent peaks as internal standards. $^{13}C\{^{1}H\}$ and $^{29}Si\{^{1}H\}$ NMR spectra were referenced indirectly with the ^{1}H resonance of TMS at 0.0 ppm, according to IUPAC standard,[84, 85] using the residual solvent peaks as internal standards.

Solution-phase electronic absorption spectra and solid-phase diffuse reflectance electronic absorption spectra of **7.1**, **7.2**, **7.3**, **7.4**, and **7.8** were collected in screw-capped quartz cuvettes (loaded in a transuranic drybox using parafilm during the loading procedure to wrap and protect the exterior surface of the cuvette and cap from radioactive contamination) at room temperature using a Varian Cary 6000i UV-vis-NIR spectrophotometer with an installed Internal Diffuse Reflectance Accessory. IR spectra were recorded on a Nicolet 6700 FT-IR spectrometer with a NXR FT Raman module. Elemental analyses of **7.2**, **7.3**, and **7.6** were performed by the Micro-Analytical Facility at the University of California, Berkeley.

Electrochemical experiments (Cyclic Voltammetry, CV; and Differential Pulse Voltammetry, DPV) at LANL were performed using a Bio-Logic SP50 potentiostat. A simple 3-electrode cell was used, composed of a polished Au disk electrode (7 mm^2 area), Pt wire counter electrode (1 mm thickness) and a Ag/AgCl pseudo-reference electrode made from Ag

wire (0.5 mm thickness) dipped in concentrated $FeCl_3$ to afford a surface layer of AgCl, which was then washed with deionized water and acetone, and dried *in vacuo* before use. All electrodes were freshly polished and/or prepared (pseudo-reference) prior to beginning the study. The solution was contained in a small volume (3 mL) high-recovery V-vial equipped with a small PTFE stir bar. Between each run the solution was manually agitated, and the working electrode surface wiped clean with a Kim Wipe, the solution was then allowed to settle for 10 s before beginning the next measurement. Cell resistances were <500 Ω, and the open circuit potential was checked before each measurement, ensuring ΔV/s <50 mV. All potentials are referenced to an internal $Fc^{+/0}$ redox standard. The electrochemical window of the solvent/electrolyte combination (THF, 67 mM [$^{n}Pr_4N$][$BArF^{24}$]) *versus* the pseudo-reference was assessed prior to addition of the analyte, and was found to be –2.25 V to +1.85 V (*versus* the Ag/AgCl couple in my cell), thus measurements were not performed beyond this maxima to avoid reaction with species generated from degradation of the solvent/electrolyte. Unless stated otherwise, all potentials are reported *versus* the $Fc^{+/0}$ couple.

CV experiments at UCSB were performed with a CH Instruments 600c Potentiostat, and the data were processed using CHI software (version 6.29). All experiments were performed inside the glovebox using a 20 mL glass vial as the cell. The working electrode consisted of glassy carbon (2 mm diameter), the counter electrode was a platinum wire, and a Ag/AgCl wire was used as a reference electrode. Solutions employed for CV studies were typically 1 mM in analyte and 0.1 M in [NBu_4][BPh_4]. Ferrocene was used to reference all experiments.

7.5.2 Synthesis and Characterization of [Np(NR$_2$)$_3$Cl] (7.1, R = SiMe$_3$).

To a stirring, cold (-35 °C), salmon pink solution of $NpCl_4(DME)_2$ (15.3 mg, 27.0 μmol) in THF (3 mL) was added a cold (-35 °C) pale yellow solution of $NaNR_2$ (15.8 mg, 86.0 μmol)

in THF (3 mL). The reaction mixture was allowed to warm to room temperature with stirring. After 24 h, the volatiles were removed *in vacuo* to provide a yellow-orange solid. The solid was then extracted into *n*-hexane (3 mL) and the resulting yellow-orange solution was filtered through a filter paper column. The orange filtrate was concentrated *in vacuo* to 2 mL and stored at -35 °C for 24 h, which resulted in the deposition of a mixture of orange needles and orange blocks. The solid was isolated by decanting the supernatant and then dried *in vacuo* to yield **7.1** as a orange crystalline solid (14.3 mg, 69 % yield). ^{1}H NMR (400.13 MHz, 25 °C, C_6D_6): δ -2.48 (s, 54H, SiC*H*$_3$). UV-Vis/NIR (*n*-hexane, 0.878 mM, 25 °C, L·mol^{-1}·cm^{-1}): 387 nm (ε = 1730), 600 nm (ε = 16.9), 741 nm (ε = 45.3), 840 nm (ε = 59.2), 900 nm (ε = 79.6), and 1100 nm (ε = 4.24). UV-Vis/NIR (THF, 1.01 mM, 25 °C, L·mol^{-1}·cm^{-1}): 387 nm (ε = 213), 600 nm (ε = 12.1), 741 nm (ε = 45.8), 900 nm (ε = 30.3), and 1100 nm (ε = 1.23).

7.5.3 Synthesis and Characterization of [K(2,2,2-cryptand)][U(NR$_2$)$_3$Cl] (7.2).

To [U(NR$_2$)$_3$Cl] (20.5 mg, 0.0272 mmol) was added 2,2,2-cryptand (10.7 mg, 0.0284 mmol) and THF (3 mL) to afford a pale pink solution. KC_8 (6.0 mg, 0.044 mmol) was then added as a solid. The reaction mixture quickly turned dark purple. After 5 min, the solution was filtered through a filter paper column. The filtrate were concentrated *in vacuo* to 2 mL, layered with hexanes (4 mL) and stored at -35 °C for 24 h, which resulted in the deposition of purple blocks. The solid was isolated by decanting the supernatant and then dried *in vacuo* to yield **7.2** (4.7 mg, 15% yield). The supernatant (5 mL) was transferred to a new vial and stored at -25 °C for 24 h. This resulted in the deposition of a second crop of purple crystalline solid (17.6 mg). Total yield: 0.022 g, 70% yield. Anal. Calcd for $C_{40}H_{98}ClKN_5O_7Si_6U$: C, 38.67; H, 7.95; N, 5.64. Found: C, 37.56; H, 7.81; N, 5.90. Found: C, 37.89; H, 7.77; N, 6.00. Despite multiple attempts, a satisfactory C% analysis of **7.2** was not obtained. The low carbon values

were attributed to incomplete combustion of the sample as a result of silicon carbide formation.[86] ^{1}H NMR (400.13 MHz, 25 °C, THF-d_8): δ -5.57 (s, 54H, SiC*H*$_3$), 2.03 (s, 12H, cryptand), 3.00 (s, 12H, cryptand), 3.03 (s, 12H, cryptand). UV-Vis/NIR (THF, 1.94 mM, 25 °C, L·mol^{-1}·cm^{-1}): 357 nm (ε = 1470), 500 nm (ε = 1160), 620 nm (ε = 772.0), 751 nm (ε = 60.40), 909 nm (ε = 62.30), 934 nm (ε = 66.60), 1039 nm (ε = 53.50), 1198 nm (ε = 27.70) and 1279 nm (ε = 11.00). IR (KBr pellet, cm^{-1}): 523 (s), 598 (s), 661 (m), 752 (m), 831 (m), 949 (m), 1099 (m), 1180 (m), 1257 (m), 1294 (m), 1356 (s), 1477 (m), 1630 (w), 2729 (w), 2814 (w), 2883 (w), 2954 (w), 3448 (w).

7.5.4 Synthesis and Characterization of [K(DB-18-C-6)(THF)$_2$][U(NR$_2$)$_3$Cl] (7.3).

To [U(NR$_2$)$_3$Cl] (16.4 mg, 0.0217 mmol) was added dibenzo-18-crown-6 (7.9 mg, 0.022 mmol) and THF (3 mL) to afford a pale pink solution. KC$_8$ (4.5 mg, 0.03 mmol) was then added as a solid. The reaction mixture quickly turned dark purple. After 5 min, the solution was filtered through a filter paper column. The filtrate were concentrated *in vacuo* to 2 mL, layered with hexanes (4 mL) and stored at -35 °C for 24 h, which resulted in the deposition of purple blocks. The solid was isolated by decanting the supernatant and then dried *in vacuo* to yield **7.3** (20.8 mg, 74% yield). Anal. Calcd for $C_{46}H_{94}ClKN_3O_8Si_6U$: C, 42.55; H, 7.30; N, 3.24. Found: C, 42.25; H, 6.74; N, 2.50. ^{1}H NMR (400 MHz, 25 °C, THF-d_8): δ -5.62 (s, 54H, SiC*H*$_3$), 2.29 (s, 8H, C*H*$_2$), 2.98 (s, 8H, C*H*$_2$), 6.17 (s, 4H, phenyl-*p*, C*H*), 6.53 (s, 4H, phenyl-*m*, C*H*). UV-Vis/NIR (THF, 0.505 mM, 25 °C, L·mol^{-1}·cm^{-1}): 357 nm (ε = 150), 500 nm (ε = 919), 620 nm (ε = 599), 751 nm (ε = 28.8), 909 nm (ε = 36.2), 934 nm (ε = 40.3), 1039 nm (ε = 32.1), 1198 nm (ε = 13.5), and 1279 nm (ε = 0.646). IR (KBr pellet, cm^{-1}): 607 (s), 660 (s), 690 (sh, s), 748 (s), 781 (sh, s), 825 (w), 899 (sh, w), 930 (w), 1049 (s), 1119 (s), 1188 (sh,

m), 1232 (m), 1329 (s), 1363 (s), 1392 (m), 1452 (s), 1512 (s), 1599 (s), 2563 (s), 2845 (sh, w), 2873 (w), 2931 (w), 3061 (m), 3363 (w).

7.5.5 Synthesis and Characterization of [Cl{K(DB-18-C-6)(THF)}$_3$][Np(NR$_2$)$_3$Cl]$_2$ (7.4).

To [Np(NR$_2$)$_3$Cl] (7.0 mg, 9.0 μmol) was added dibenzo-18-crown-6 (3.4 mg, 9.0 μmol) and THF (3 mL) to afford an orange solution. KC$_8$ (2.0 mg, 15 μmol) was then added as a solid. The reaction mixture quickly turned golden yellow. After 5 min, the solution was filtered through a filter paper column. The filtrate was then concentrated *in vacuo* to 2 mL, layered with *n*-hexane (4 mL) and stored at -35 °C for 24 h, which resulted in the deposition of yellow needles. The solid was isolated by decanting the supernatant and then dried *in vacuo* to yield **7.4** (8.6 mg, 63% yield). ^{1}H NMR (400.13 MHz, 25 °C, THF-d_8): δ -3.42 (s, 54H, SiC*H*$_3$), 4.43 (br s, 8H, C*H*$_2$), 4.55 (br s, 8H, C*H*$_2$), 7.00 (s, 4H, phenyl-*p*, C*H*), 7.20 (s, 4H, phenyl-*m*, C*H*). ^{13}C{^{1}H} NMR (100.61 MHz, 25 °C, C$_6$D$_6$): δ -65.50 (s, Si*C*H$_3$), 69.35 (s, *C*H$_2$), 71.03 (s, *C*H$_2$), 113.46 (s, phenyl-*m*, *C*H), 122.32 (s, phenyl-*p*, CH), 149.17 (s, phenyl-*o*, *C*H). ^{29}Si{^{1}H} NMR (79.49 MHz, 25 °C, C$_6$D$_6$): δ -194.74 (s, *Si*CH$_3$). UV-Vis/NIR (THF, 0.506 mM, 25 °C, L·mol^{-1}·cm^{-1}): 417 nm (ε = 210), 625 nm (ε = 156), 700 nm (ε = 106), 830 nm (ε = 77.0), 840 nm (ε = 75.8), 1100 nm (ε = 14.8).

7.5.6 Attempted Synthesis and Characterization of [Np{*N*(R)(SiMe$_2$)*C*H$_2$}(NR$_2$)$_2$] (7.5).

To NpCl$_4$(DME)$_2$ (19.5 mg, 34.9 μmol) was added NaNR$_2$ (26.6 mg, 145.1 μmol) and toluene (2 mL) to afford a yellow-orange solution. The resulting solution was heated at 70 °C for 4 h with stirring, whereupon the solution turned orange brown. After 4 h, the volatiles were removed *in vacuo* to provide an orange brown solid. The solid was then extracted into *n*-

hexane (3 mL) and the resulting deep brown solution was filtered through a filter paper column. The deep brown filtrate was concentrated *in vacuo* to 2 mL and stored at -35 °C for 24 h, which resulted in the deposition of orange-brown crystalline material (25 mg). The solid was isolated by decanting the supernatant and then dried *in vacuo* to yield a material that contained a mixture of **7.5**, **7.1**, and **7.8** in a 1:0.13:0.02 ratio. ^{1}H NMR (400.13 MHz, 25 °C, C_6D_6): δ -146.73 (s, 2H, C*H*$_2$, **7.5**), -29.58 (br s, 18H, N(SiC*H*$_3$)$_3$, **7.8**), -9.48 (s, 36H, N(SiMe$_3$)$_2$, **7.5**), -3.89 (s, 6H, Si(C*H*$_3$)$_2$, **7.8**), -2.92 (s, 54H, Me, **7.1**), -0.99 (s, 9H, NSiMe$_3$, **7.5**), 13.48 (s, 6H, SiMe$_2$, **7.5**), 25.57 (br s, 18H, N(SiC*H*$_3$)$_3$, **7.8**), 30.25 (br s, 6H, Si(C*H*$_3$)$_2$, **7.8**).

7.5.7 Synthesis and Characterization of [Na(DME)$_3$][U{*N*(R)(SiMe$_2$*C*H$_2$)}$_2$(NR$_2$)] (7.6).

To a stirring, cold (-35 °C), pale green solution of $UCl_4(DME)_2$ (93.0 mg, 0.166 mmol) in THF (3 mL) and DME (1 mL) was added a cold (-35 °C) pale yellow solution of $NaNR_2$ (152.2 mg, 0.8300 mmol) in THF (3 mL). The reaction mixture was allowed to warm to room temperature with stirring. After 2 h, the volatiles were removed *in vacuo* to provide a green solid. The solid was then extracted into Et_2O (3 mL) and the resulting green solution was filtered through a filter paper column. The green filtrate was concentrated *in vacuo* to 2 mL, layered with pentane (4 mL) and stored at -35 °C for 24 h, which resulted in the deposition of dark green plates. The solid was isolated by decanting the supernatant and then dried *in vacuo* to yield **7.6** as a green powder (106.5 mg, 63% yield). Anal. Calcd for $C_{30}H_{82}N_3O_6NaSi_6U$: C, 35.66; H, 8.18; N, 4.16. Found: C, 35.35; H, 8.30; N, 4.30. ^{1}H NMR (400 MHz, 25 °C, THF-*d*$_8$): δ -294.50 (br s, 2H, C*H*$_2$), -283.10 (br s, 2H, C*H*$_2$), -36.66 (br s, 18H, N(SiC*H*$_3$)$_3$), -6.09 (br s, 6H, Si(C*H*$_3$)$_2$), 3.22 (s, 18H, C*H*$_3$, DME), 3.37 (s, 12H, C*H*$_2$, DME), 31.65 (br s, 6H,

Si(CH_3)$_2$), 39.20 (br s, 18H, N(SiCH_3)$_3$). IR (KBr pellet, cm^{-1}): 582 (m), 663 (m), 837 (w), 999 (w), 1088 (m), 1097 (m), 1246 (m), 1369 (s), 1458 (m), 2827 (w), 2895 (w), 2945 (w), 3435 (w).

7.5.8 Synthesis and Characterization of [{Na(DB-18-C-6)(κ^1-DME)$_{0.5}$(Et$_2$O)$_{0.5}$}$_2$(κ^1-DME)][U{*N*(R)(SiMe$_2$*C*H$_2$)}$_2$(NR$_2$)]$_2$ (7.7).

To a stirring, cold (-35 °C), pale green solution of UCl$_4$(DME)$_2$ (19.6 mg, 0.0350 mmol) in THF (3 mL) and DME (1 mL) was added a cold (-35 °C) pale yellow solution of NaNR$_2$ (32.1 mg, 0.175 mmol) in THF (3 mL) and a cold (-35 °C) colorless suspension of dibenzo-18-crown-6 (12.6 mg, 0.0350 mmol), also in THF (3 mL). The reaction mixture was allowed to warm to room temperature with stirring. After 2 h, the volatiles were removed *in vacuo* to provide a green solid. The solid was then extracted into Et$_2$O (3 mL) and the resulting green solution was filtered through a Celite column supported on glass wool (0.5 × 2 cm). The green filtrate was concentrated *in vacuo* to 2 mL, layered with pentane (4 mL) and stored at -35 °C for 24 h, which resulted in the deposition of green plates. The solid was isolated by decanting the supernatant and then dried *in vacuo* to yield **7.7** as a green powder (36.7 mg, 85% yield). ^{1}H NMR (400 MHz, 25 °C, THF-*d*$_8$): δ -297.16 (br s, 2H, C*H*$_2$), -285.77 (br s, 2H, C*H*$_2$), -37.02 (br s, 18H, N(SiC*H*$_3$)$_3$), -6.22 (br s, 6H, Si(C*H*$_3$)$_2$), 1.14 (t, 7, 6H, C*H*$_3$, Et$_2$O), 2.53 (br s, 8H, C*H*$_2$, DB-18-C-6), 3.02 (br s, 8H, C*H*$_2$, DB-18-C-6), 3.29 (s, 4H, C*H*$_2$, DME), 3.38 (q, 7, 4H, C*H*$_2$, Et$_2$O), 3.44 (s, 6H, C*H*$_3$, DME), 6.11 (br s, 4H, meta C*H*, DB-18-C-6), 6.43 (br s, 4H, ortho C*H*, DB-18-C-6), 31.95 (br s, 6H, Si(C*H*$_3$)$_2$), 39.54 (br s, 18H, N(SiC*H*$_3$)$_3$. IR (KBr pellet, cm^{-1}): 417 (s), 582 (s), 584 (s), 606 (sh, m), 665 (s), 675 (s), 692 (s), 741 (s), 843 (m), 868 (sh, m), 935 (m), 995 (m), 1059 (s), 1130 (s), 1254 (w), 1331 (s), 1360 (s), 1394 (m), 1456 (s), 1506 (s), 1597 (s), 2582 (m), 2748 (m), 2885 (w), 2947(w), 3066 (m).

7.5.9 Synthesis and Characterization of [{Na(DB-18-C-6)(κ^1-DME)$_{0.38}$(Et_2O)$_{0.62}$}$_2$(κ^1-DME)][Np{*N*(R)($SiMe_2CH_2$)}$_2$(NR_2)]$_2$ (7.8).

To a stirring, cold (-35 °C), salmon solution of $NpCl_4(DME)_2$ (20.7 mg, 0.0370 mmol) in THF (2 mL) and DME (1 mL) was added a cold (-35 °C) pale yellow solution of $NaNR_2$ (34.1 mg, 0.186 mmol) in THF (2 mL), whereupon the reaction mixture became yellow in color. Next, a cold (-35 °C) colorless suspension of dibenzo-18-crown-6 (13.4 mg, 0.0372 mmol) in THF (2 mL) was added, whereupon the reaction mixture became deep red-brown in color. The reaction mixture was allowed to warm to room temperature with stirring for 140 min, whereupon the volatiles were removed *in vacuo* from the deep orange reaction mixture. The solid was then extracted into Et_2O (3 mL) and the resulting solution was filtered through a glass fiber plug supported in a glass pipette. The glass fiber plug was rinsed with Et_2O (0.5 mL). The deep orange filtrate was concentrated *in vacuo* to 2 mL, layered with pentane (4 mL) and stored at -35 °C for 24 h, which resulted in the deposition of orange crystals. The solid was isolated by decanting the supernatant, where it was washed with *n*-hexane (3 mL × 2) and pentane (4 mL), and dried *in vacuo* to yield **7.8** as an orange-red (micro)crystalline powder (25.8 mg, 57% yield). ^{1}H NMR (400.13 MHz, 25 °C, THF-d_8): δ -242.58 (br s, 4H, CH_2), -26.36 (br s, 18H, N(SiCH_3)$_3$), -3.94 (br s, 6H, Si(CH_3)$_2$), 1.13 (t, 6H, CH_3, Et_2O), 2.94 (br s, 8H, CH_2, DB-18-C-6), 3.28 (s, 8H, CH_2, DB-18-C-6), 3.36 (s, 4H, CH_2, DME), 3.38 (q, 4H, CH_2, Et_2O), 3.44 (s, 6H, CH_3, DME), 6.36 (s, 4H, *p*-C*H*, DB-18-C-6), 6.55 (s, 4H, *m*-C*H*, DB-18-C-6), 26.36 (br s, 18H, N(SiCH_3)$_3$), 29.95 (br s, 6H, Si(CH_3)$_2$). UV-Vis/NIR (THF, 1.07 mM, 25 °C, L·mol^{-1}·cm^{-1}): 350 (ε = 215), 615 (ε = 27.9), 740 (ε = 29.8), 745 (ε = 29.0), 800 (ε = 38.9), 830 (ε = 25.7), 880 (ε = 41.1), 1000 (ε = 74.2), 1041 (ε = 3.62).

7.5.10 Synthesis and Characterization of [{Na(DME)$_3$][Np{*N*(R)(SiMe$_2$*C*H$_2$)}$_2$(NR$_2$)] (7.9).

To a stirring, cold (-35 °C), salmon solution of $NpCl_4(DME)_2$ (16.5 mg, 0.0300 mmol) in THF (3 mL) and DME (1 mL) was added a cold (-35 °C) pale yellow solution of $NaNR_2$ (27.5 mg, 0.150 mmol) in THF (3 mL). The reaction mixture was allowed to warm to room temperature with stirring for 120 min, whereupon the volatiles were removed *in vacuo* from the deep red-orange reaction mixture. The solid was then extracted into DME (3 mL) and the resulting solution was filtered through a glass fiber plug supported in a glass pipette. The glass fiber plug was rinsed with DME (0.5 mL). The deep orange filtrate was concentrated *in vacuo* to 2 mL, layered with *n*-hexane (4 mL) and stored at -35 °C for 24 h, which resulted in the deposition of red-orange crystals. The solid was isolated by decanting the supernatant and then dried *in vacuo* to yield **7.9** as an orange-red (micro)crystalline powder (21.9 mg, 73% yield). ^{1}H NMR (400.13 MHz, 25 °C, THF-d_8): δ -25.93 (br s, 18H, N(SiC*H*$_3$)$_3$), -3.33 (br s, 12H, Si(C*H*$_3$)$_2$), 3.26 (br s, 4H, C*H*$_2$, DME), 3.41 (s, 6H, C*H*$_3$, DME), 25.75 (br s, 18H, N(SiC*H*$_3$)$_3$), 29.29 (br s, 6H, Si(C*H*$_3$)$_2$). The Np-C*H*$_2$ resonances were not observed. Crystallographic details: $C_{30}H_{82}N_3O_6NaSi_6Np$, space group = *P*2$_1$/c, a = 16.382, b = 21.4527, c = 29.2386, β = 95.425, Z = 8.

7.5.11 X-ray Crystallography

Neptunium complexes **7.1**, **7.4**, and **7.8** were coated in paratone-N oil and mounted inside a 0.5 mm capillary tube, which was sealed with hot capillary wax. The capillary was coated with a thin film of acrylic in ethyl acetate (Hard as Nails®) to provide structural integrity and additional containment. In the case of **7.1** and **7.8**, the capillary was placed on a Bruker AXS SMART APEX II charge-coupled-device diffractometer. In the case of **7.4** the capillary was

placed on a Bruker D8 Quest diffractometer with a CMOS detector. The instruments were equipped with a sealed, graphite monochromatized MoKα X-ray source (λ= 0.71073 Å). Data for **7.1**, **7.4**, and **7.8** were collected at 100(2) K, 110(2) K, and 100(2) K, respectively. Frame exposures of 20, 10, and 10 s were used for **7.1**, **7.4**, and **7.8**, respectively.

Data for **7.2**·THF were collected on a Bruker D8 Quest using a Mo Kα (α = 0.71073 Å) *Iμ*S 3.0 Microfocus source X-ray generator, while data for **7.3** and **7.6** were collected Bruker AXS SMART APEX II diffractometer, and data for **7.7** were collected on a Bruker KAPPA APEX II diffractometer equipped with an APEX II CCD detector using a TRIUMPH monochromator with a Mo Kα X-ray source (α = 0.71073 Å). The crystals were mounted on a cryoloop under Paratone-N oil. Data for **7.2**·THF, **7.3**, **7.6**, and **7.7** were collected at 100(2) K using an Oxford nitrogen gas cryostream. Data were collected using ω scans with 0.5° frame widths. Frame exposures of 45, 45, 60, and 15 s were used for **7.2**·THF, **7.3**, **7.6**, and **7.7**, respectively.

Data collection and cell parameter determinations were conducted using the SMART program.[87] Integration of the data frames and final cell parameter refinements were performed using SAINT software.[88] Absorption corrections of the data were carried out using the multi-scan method SADABS or TWINABS (for **7.2**·THF).[89] Subsequent calculations were carried out using SHELXTL[90] or the GUI Olex2 software package (for **7.6** and **7.8**).[91, 92] Structure determination was done using direct or Patterson methods and difference Fourier techniques. All hydrogen atom positions were idealized, and rode on the atom of attachment. Structure solution, refinement, graphics, and creation of publication materials were performed using SHELXTL or Olex2.[90-92] Further crystallographic details can be found in Tables 7.3 – 7.5.

For complex **7.3**, each silylamide group was found to be disordered over two positions. This disorder was modeled in a 50:50 ratio. For complexes **7.7** and **7.8**, the Na^+ cations featured one coordination site occupied by a mixture of DME and Et_2O. For **7.7**, this coordination site was modeled as a 50:50 mixture of DME and Et_2O. For **7.8**, this coordination site was modeled as a 38:62 mixture of DME and Et_2O. Hydrogen atoms were not assigned to the carbon atoms of the partial-occupancy ligands and their carbon and oxygen atoms were refined isotropically.

Complexes **7.1**-**7.8** have been deposited in the Cambridge Structural Database (**7.1**: CCDC 2046340; **7.2**: CCDC 2046341; **7.3**: CCDC 2046342; **7.4**: CCDC 2046343; **7.6**: CCDC 2046344, **7.7**: CCDC 2046345, **7.8**: CCDC 2046346).

Table 7.3. X-ray Crystallographic Data for **7.1**, **7.2**·THF, and **7.3**.

	7.1	**7.2**·THF	**7.3**
empirical formula	$C_{18}H_{54}NpN_3ClSi_6$	$C_{40}H_{98}ClKN_5O_7Si_6U$	$C_{46}H_{94}ClKN_3O_8Si_6U$
crystal habit, color	Needle, Orange	Block, Purple	Block, Purple
crystal size (mm)	0.30 × 0.15 × 0.15	0.3 × 0.25 × 0.25	0.2 × 0.1 × 0.1
space group	*R3c*	$P2_12_12_1$	*P-1*
volume ($Å^3$)	4964.8(2)	6276.9(5)	3235(2)
a (Å)	18.4197(4)	14.9548(7)	12.176(5)
b (Å)	18.4197(4)	19.2351(9)	14.837(5)
c (Å)	16.8967(4)	21.8206(10)	18.481(9)
α (deg)	90	90	86.339(5)
β (deg)	90	90	77.656(4)
γ (deg)	120	90	82.996(3)
Z	6	4	2
formula weight (g/mol)	753.64	1242.35	1298.36
density (calculated) (Mg/m^3)	1.512	1.315	1.333
absorption coefficient (mm^{-1})	3.449	2.851	2.769
F_{000}	2262	2564	1334
total no. reflections	14583	52929	28926
unique reflections	2098	11538	11598
Final R Indices (I >2σ(I)]	R_1 = 0.0218 wR_2 = 0.0514	R_1 = 0.0452 wR_2 = 0.0898	R_1 = 0.0542 wR_2 = 0.1644
largest diff. peak and hole ($e^- A^{-3}$)	1.104 and -0.448	0.913 and -1.528	1.883 and -1.519
GOF	1.063	1.075	1.051

Table 7.4. X-ray Crystallographic Data for **7.4**, **7.6**, and **7.7**.

	7.4	**7.6**	**7.7**
empirical formula	$C_{108}H_{204}Cl_3K_3N_6Np_2O_{21}Si_{12}U$	$C_{30}H_{82}N_3NaO_6Si_6U$	$C_{44}H_{91}N_3NaO_{8.5}Si_6U$
crystal habit, color	Block, Yellow	Plate, Green	Block, Green
crystal size (mm)	0.3 × 0.25 × 0.25	0.22 × 0.12 × 0.07	0.25 × 0.10 × 0.10
space group	*I2/a*	*P2₁/c*	*P-1*
volume ($Å^3$)	17082(6)	10312(7)	2966.4(18)
a (Å)	25.8708(15)	16.457(6)	11.611(4)
b (Å)	24.536(8)	21.522(8)	15.680(6)
c (Å)	27.748(4)	29.261(12)	18.861(6)
α (deg)	90	90	67.039(8)
β (deg)	104.116(10)	95.778(5)	73.060(9)
γ (deg)	90	90	73.406(8)
Z	4	8	2
formula weight (g/mol)	2957.49	2021.08	1227.75
density (calculated) (Mg/m^3)	1.150	1.302	1.375
absorption coefficient (mm^{-1})	1.463	3.330	2.911
F_{000}	6096	4144	1262
total no. reflections	57901	79172	20393
unique reflections	16048	18862	12094
Final R Indices ($I > 2\sigma(I)$]	$R_1 = 0.0720$ $wR_2 = 0.1568$	$R_1 = 0.0556$ $wR_2 = 0.1056$	$R_1 = 0.0517$ $wR_2 = 0.1013$
largest diff. peak and hole ($e^- A^{-3}$)	0.947 and -0.681	4.578 and -1.942	3.009 and -1.339
GOF	1.040	1.021	1.057

Table 7.5. X-ray Crystallographic Data for **7.8**.

	7.8
empirical formula	$C_{44.02}H_{81}N_3NaNpO_{8.38}Si_6$
crystal habit, color	Block, Orange-red
crystal size (mm)	0.25 × 0.12 × 0.09
space group	*P-1*
volume ($Å^3$)	3027.8(8)
a (Å)	11.6735(18)
b (Å)	15.842(2)
c (Å)	18.991(3)
α (deg)	66.653(2)
β (deg)	73.160(2)
γ (deg)	73.450(2)
Z	2
formula weight (g/mol)	1214.96
density (calculated) (Mg/m^3)	1.333
absorption coefficient (mm^{-1})	1.887
F_{000}	1242
total no. reflections	30887
unique reflections	11717
Final R Indices (I $>2\sigma(I)$]	$R_1 = 0.0788$ $wR_2 = 0.1960$
largest diff. peak and hole ($e^- A^{-3}$)	4.479 and -4.626
GOF	1.157

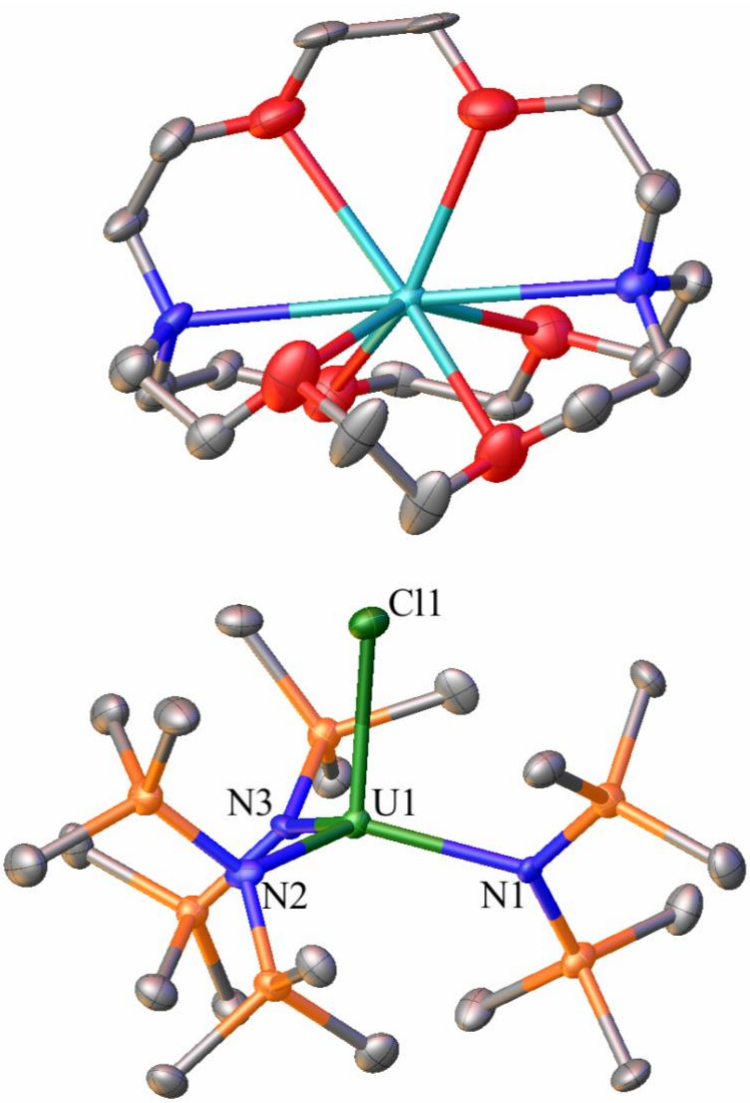

Figure 7.7. Solid-state molecular structure of **7.2**·THF shown with 50% probability ellipsoids. Hydrogen atoms removed for clarity. THF solvate removed for clarity. Selected bond lengths (Å) and angles (°): U-$N_{silylamido}$ (av.) = 2.315, U-C (av.) = 2.482, N-U-N (av.) = 120.

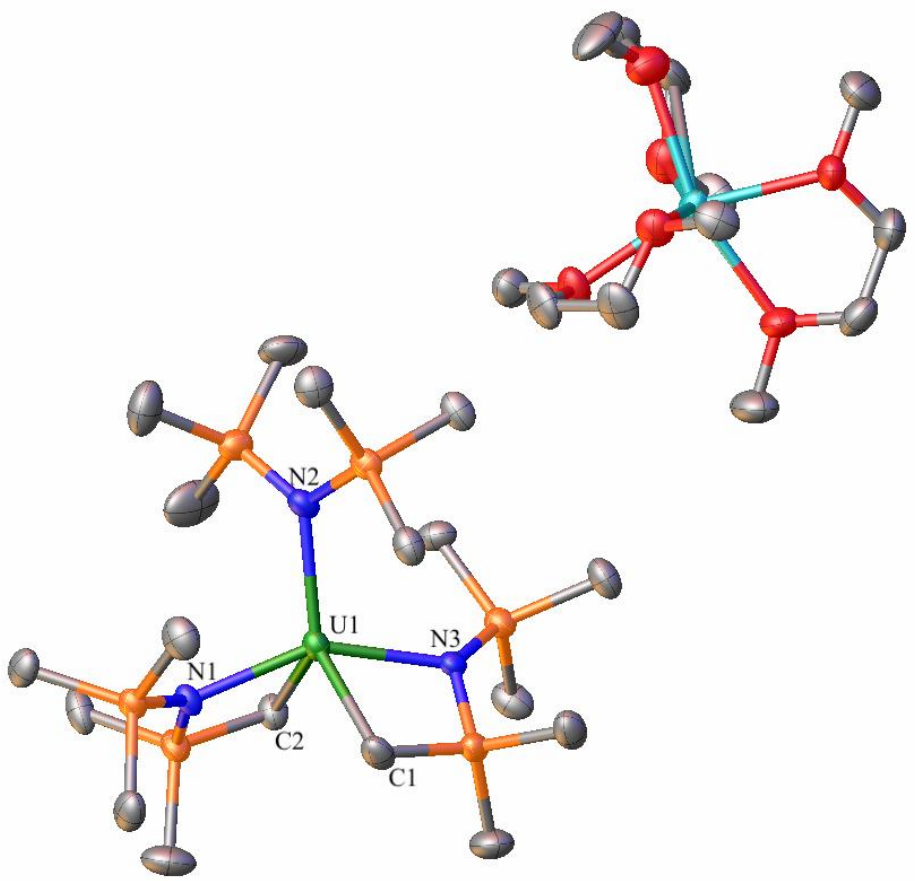

Figure 7.8. Solid-state molecular structure of **7.6** shown with 50% probability ellipsoids. Hydrogen atoms removed for clarity. Selected bond lengths (Å) and angles (°): U-$N_{silylamido}$ (av.) = 2.305, U-C (av.) = 2.455, N-U-N (av.) = 120.

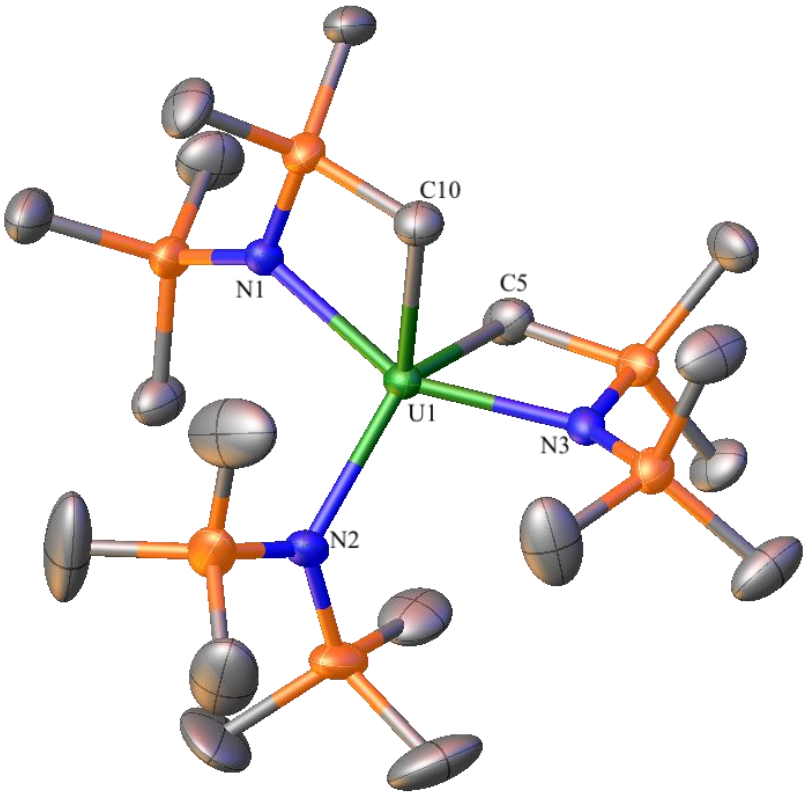

Figure 7.9. Solid-state molecular structure of **7.7** shown with 50% probability ellipsoids. Hydrogen atoms and Na^+ counterion removed for clarity. Selected bond lengths (Å) and angles (°): U-$N_{silylamido}$ (av.) = 2.305, U-C (av.) = 2.455, N-U-N (av.) = 120.

7.6 Appendix

7.6.1 NMR Spectra

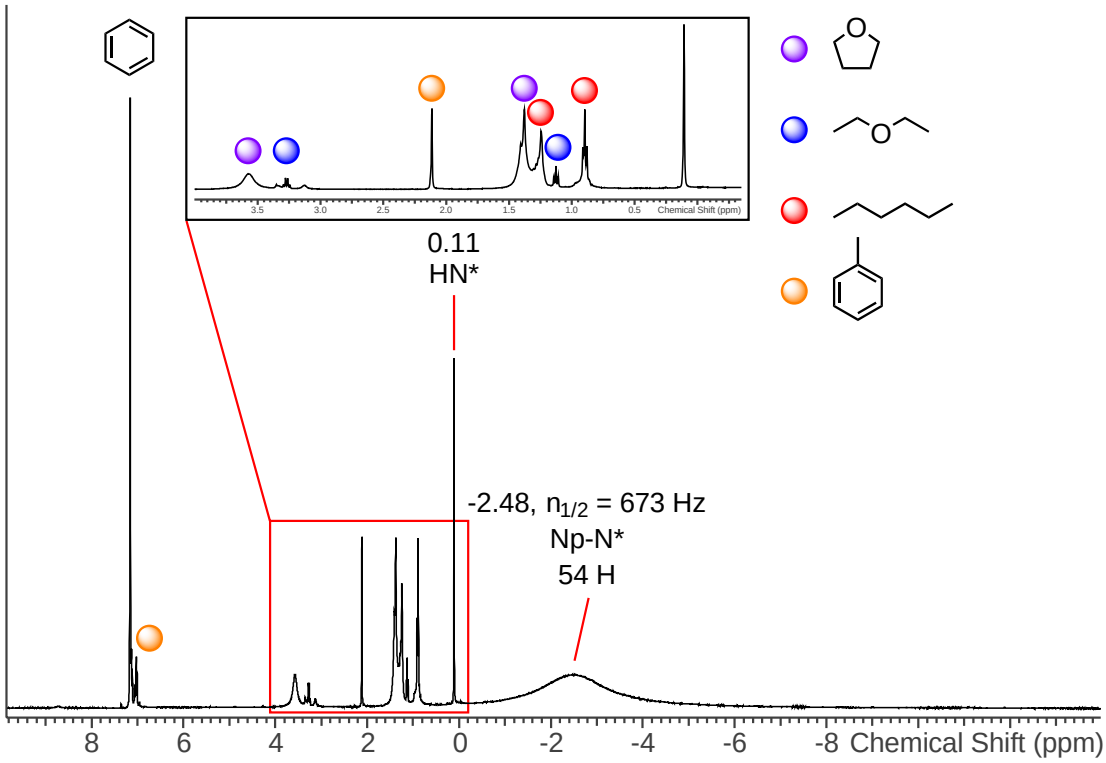

Figure A7.1. ^{1}H NMR spectrum of [Np(NR$_2$)$_3$Cl] (**7.1**) in C_6D_6. Protic solvent impurities from sample preparation are denoted.

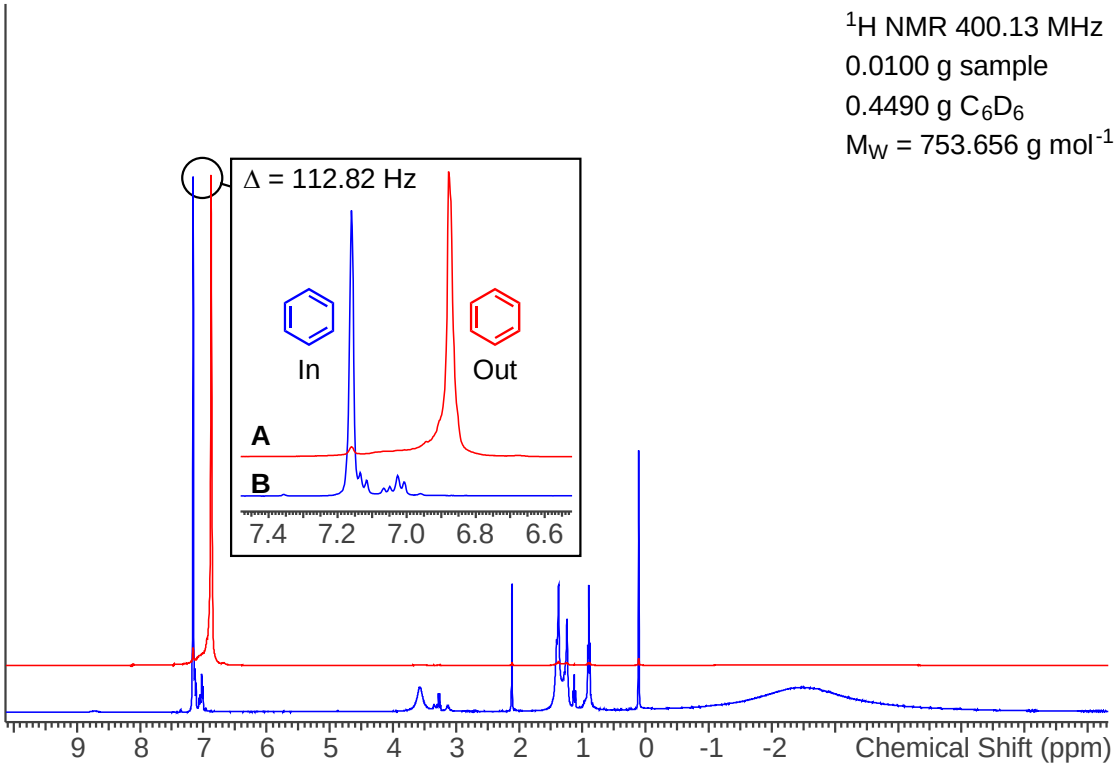

Figure A7.2. (A) shows the ^{1}H NMR spectrum of **7.1** in benzene-d_6 with several drops of protio-benzene external to the FEP liner; (B) shows the original ^{1}H NMR spectrum to show that the complex peaks overlap with those of (A). Color-coded and positioned labels in the inset denote which peaks arises from which spectrum., $\mu_{eff} = 2.57\ \mu_B\ mol^{-1}$; $\chi_M = 3.49 \times 10^{-8}\ m^3\ mol^{-1}$.

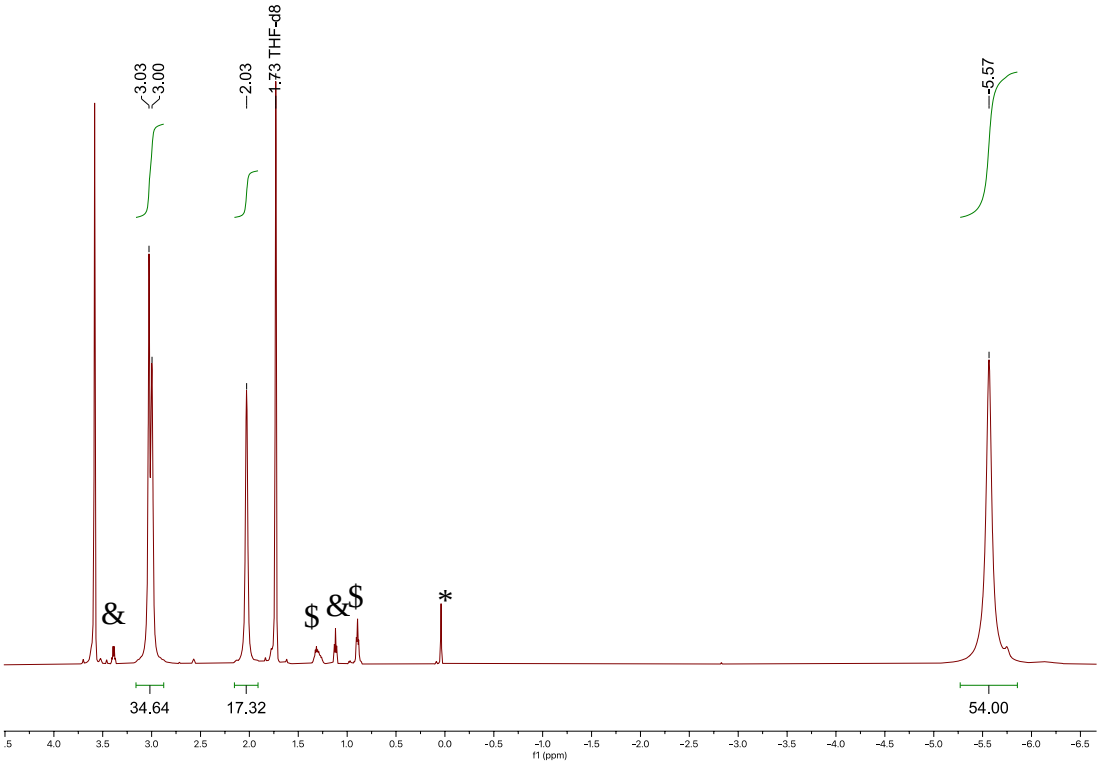

Figure A7.3. ^{1}H NMR spectrum of [K(2,2,2-cryptand)][U(NR$_2$)$_3$Cl] (**7.2**) in THF-d_8. (*) indicates resonance assignable to free HN(SiMe$_3$)$_2$, ($) indicates hexanes, and (&) indicates Et$_2$O.

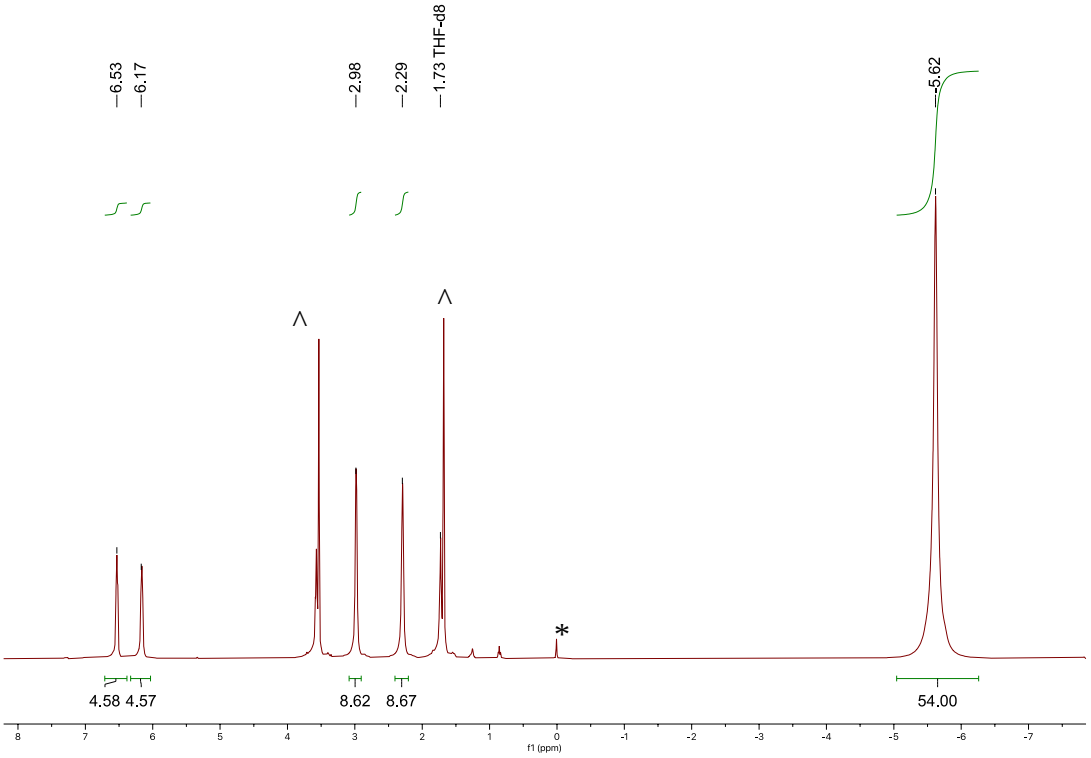

Figure A7.4. ^{1}H NMR spectrum of [K(DB-18-C-6)(THF)$_2$][U(NR$_2$)$_3$Cl] (**7.3**) in THF-d_8. (*) indicates resonance assignable to free HN(SiMe$_3$)$_2$ and (^) indicates resonances assignable to THF.

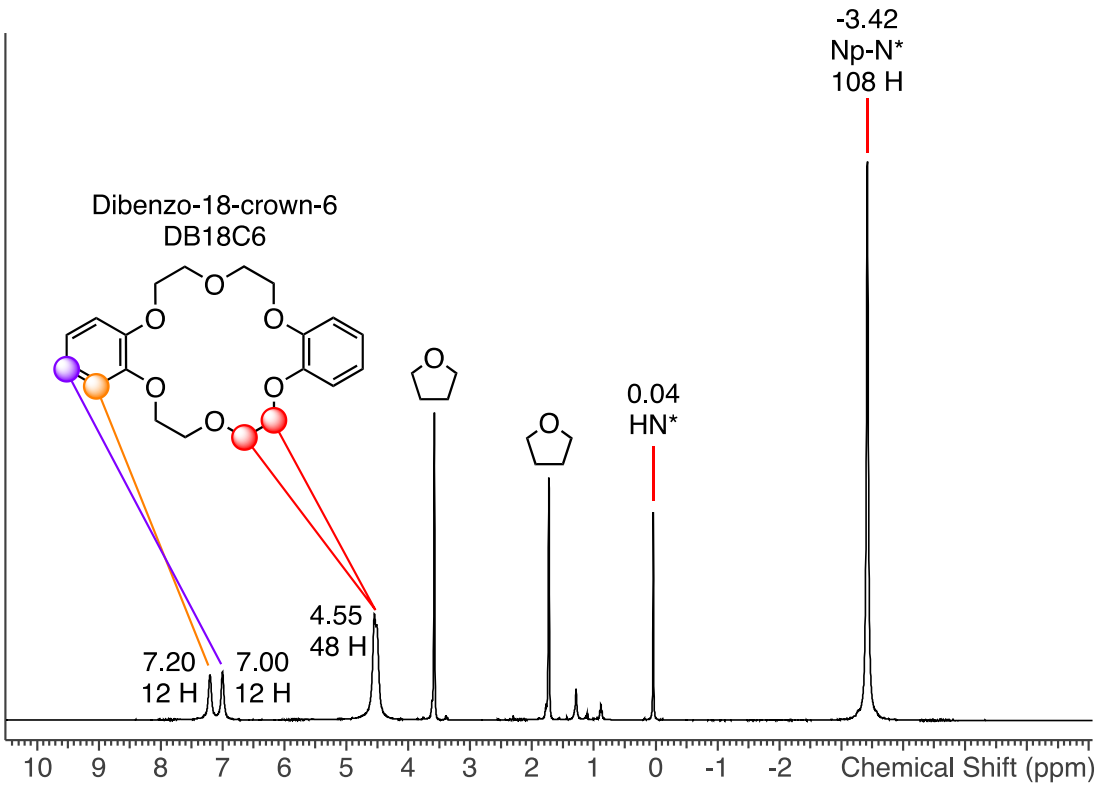

Figure A7.5. ^{1}H NMR spectrum of $[Cl\{K(DB\text{-}18\text{-}C\text{-}6)(THF)\}_3][Np(NR_2)_3Cl]_2$ (**7.4**) in THF-d_8.

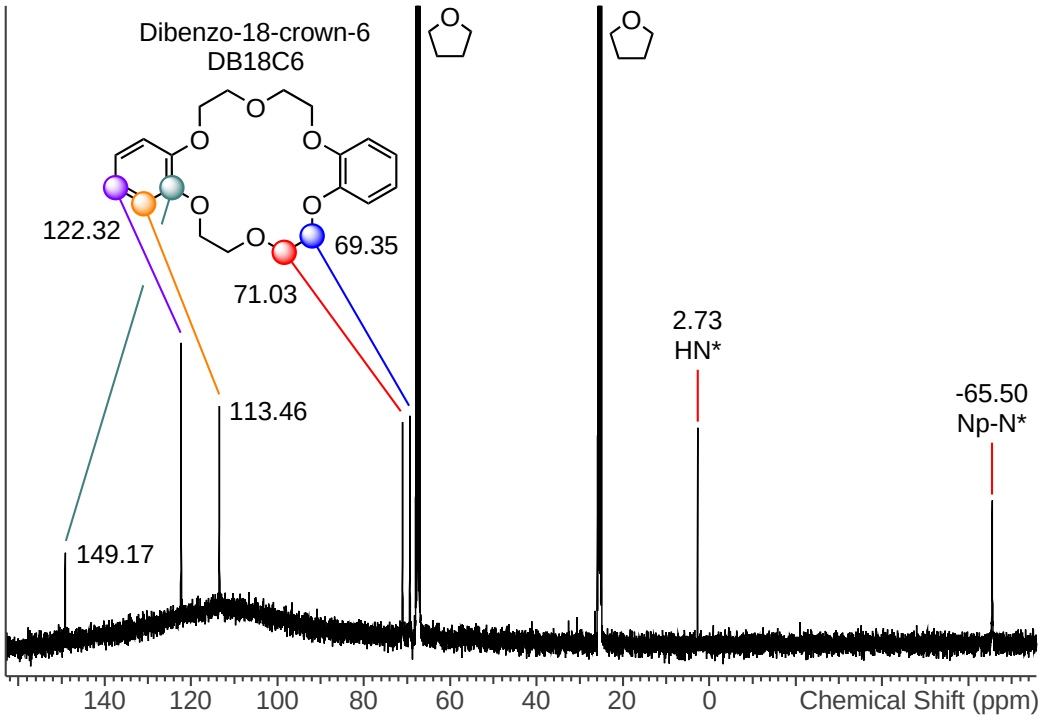

Figure A7.6. $^{13}C\{^{1}H\}$ NMR spectrum of $[Cl\{K(DB\text{-}18\text{-}C\text{-}6)(THF)\}_3][Np(NR_2)_3Cl]_2$ (**7.4**) in THF-d_8. Protic solvent impurities from sample preparation are denoted. Broad feature centered about 110 ppm is due to the FEP liner.

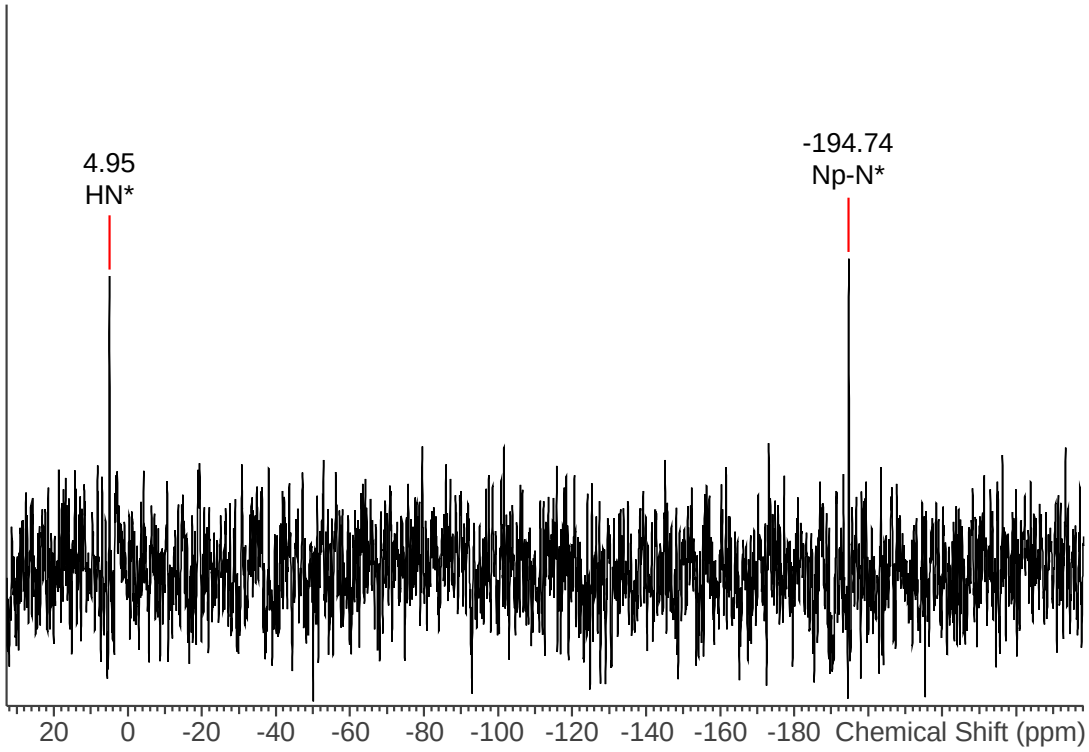

Figure A7.7. $^{29}Si\{^{1}H\}$ NMR spectrum of $[Cl\{K(DB\text{-}18\text{-}C\text{-}6)(THF)\}_3][Np(NR_2)_3Cl]_2$ (**7.4**) in THF-d_8.

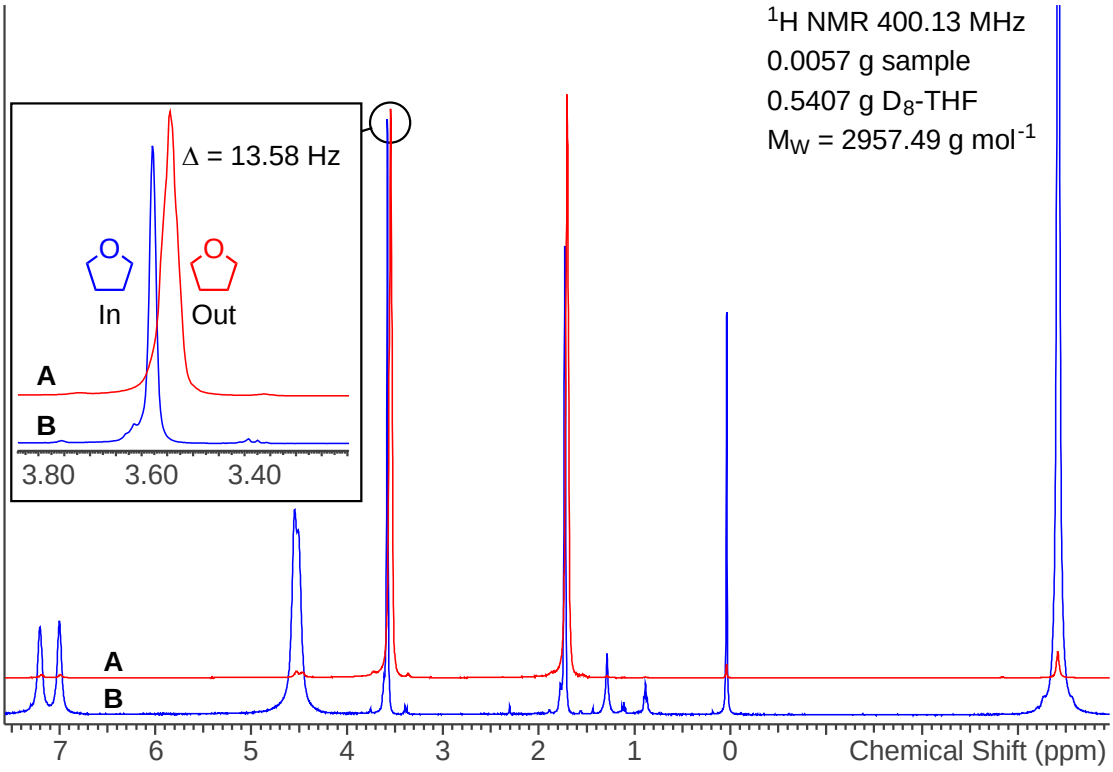

Figure A7.8. (A) shows the ^{1}H NMR spectrum of **7.4** in THF-d_8 with several drops of protio-THF external to the FEP liner; (B) shows the original ^{1}H NMR spectrum to show that the complex peaks overlap with those of (A). Color-coded and positioned labels in the inset denote which peaks arises from which spectrum. $\mu_{eff} = 3.00\,\mu_B\,mol^{-1}$; $\chi_M = 4.73 \text{ x } 10^{-8}\,m^3\,mol^{-1}$.

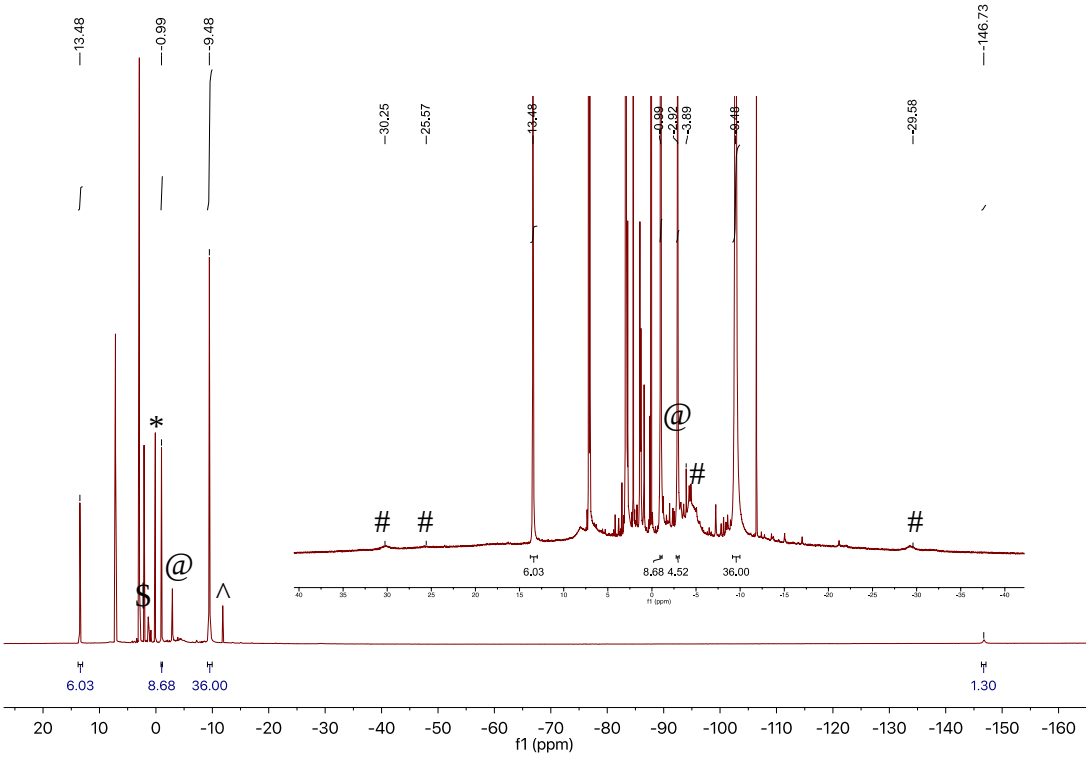

Figure A7.9. ^{1}H NMR spectrum of [Np{*N*(R)(SiMe$_2$)*C*H$_2$}(NR$_2$)$_2$] (**7.5**) in C$_6$D$_6$. The inset highlights the resonances of **7.1** and **7.8**. (@) indicates resonance assignable to **7.1**, (#) indicates resonances assignable to **7.8**, (*) indicates resonance assignable to free HN(SiMe$_3$)$_2$, ($) indicates toluene, and (^) indicates the presence of an unidentified product.

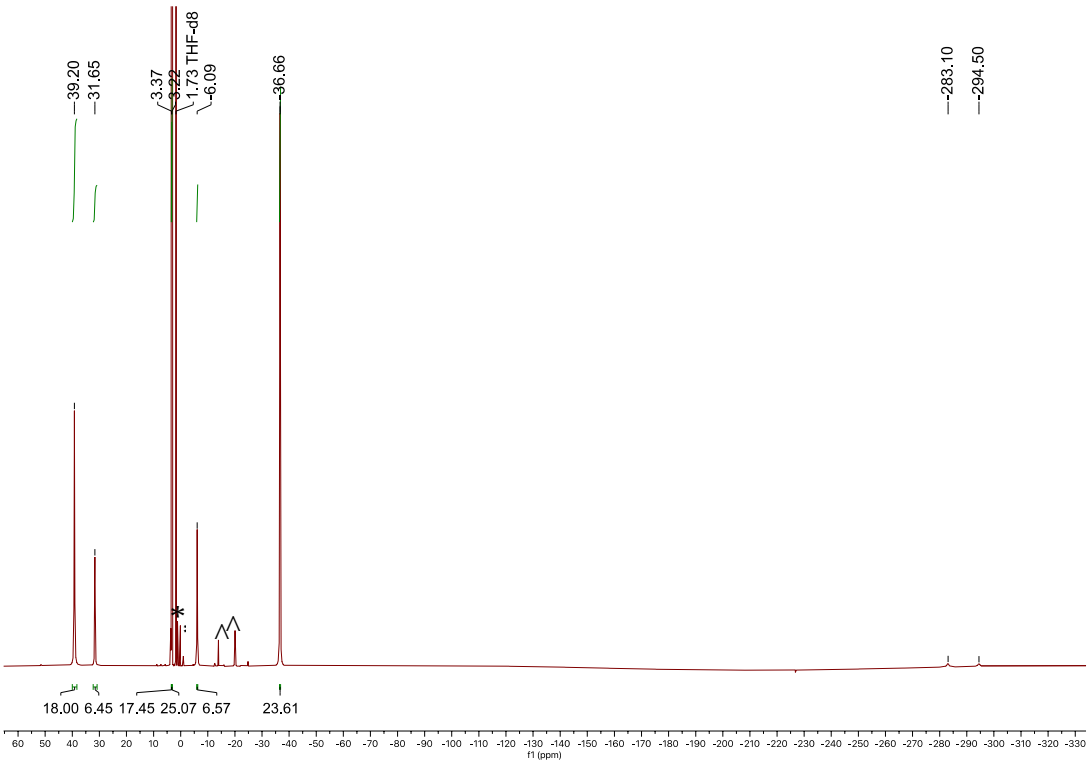

Figure A7.10. ^{1}H NMR spectrum of [Na(DME)$_3$][U{*N*(R)(SiMe$_2$*C*H$_2$)}$_2$(NR$_2$)] (**7.6**) in THF-d_8. (*) indicates the presence of Et$_2$O and pentane, and (^) indicates the presence of an unidentified product.

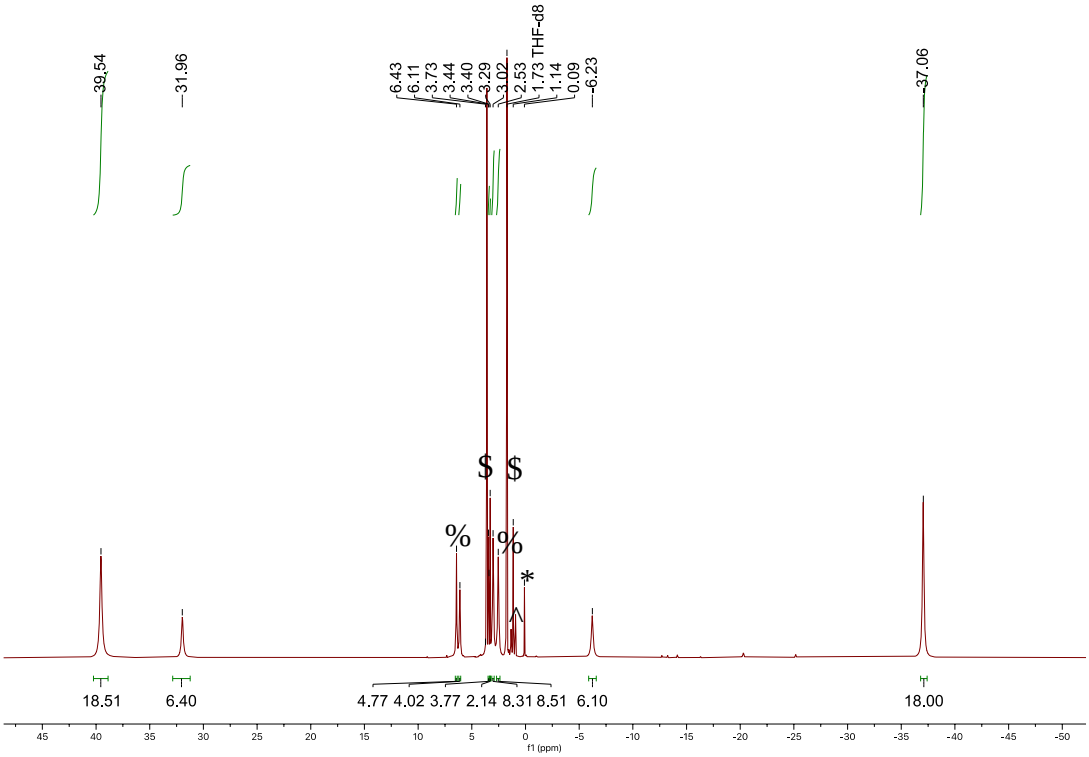

Figure A7.11. Partial ^{1}H NMR spectrum of **7.7** in THF-d_8. (*) indicates resonance assignable to free $HN(SiMe_3)_2$, ($) indicates DME, (%) indicates DB-18-C-6, and (^) indicates the presence of pentane.

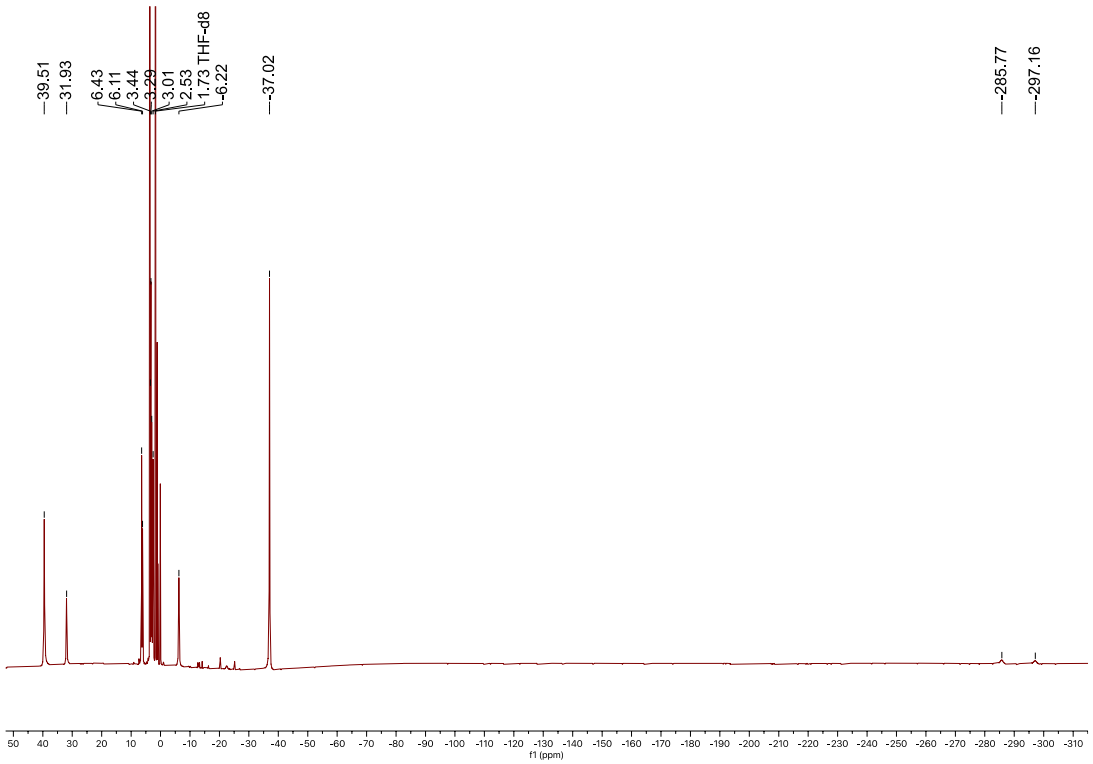

Figure A7.12. ^{1}H NMR spectrum of **7.7** in THF-d_8.

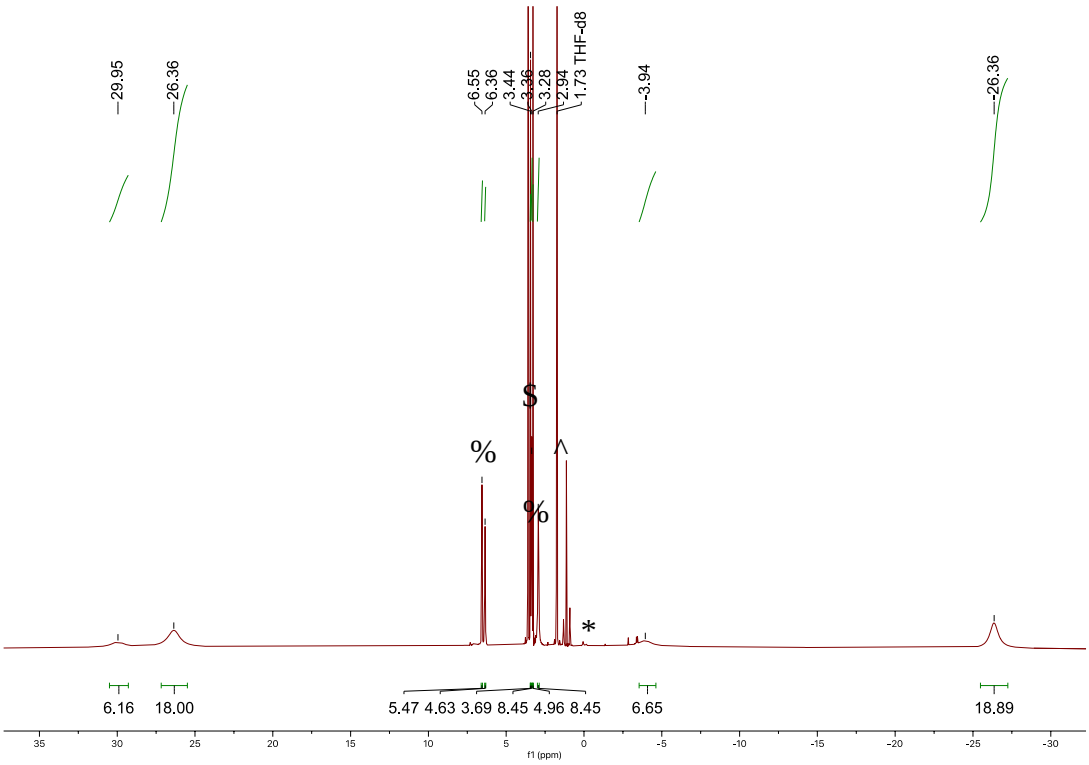

Figure A7.13. Partial ^{1}H NMR spectrum of **7.8** in THF-d_8. (*) indicates resonance assignable to free $HN(SiMe_3)_2$, ($) indicates DME, (%) indicates DB-18-C-6, and (^) indicates the presence of pentane.

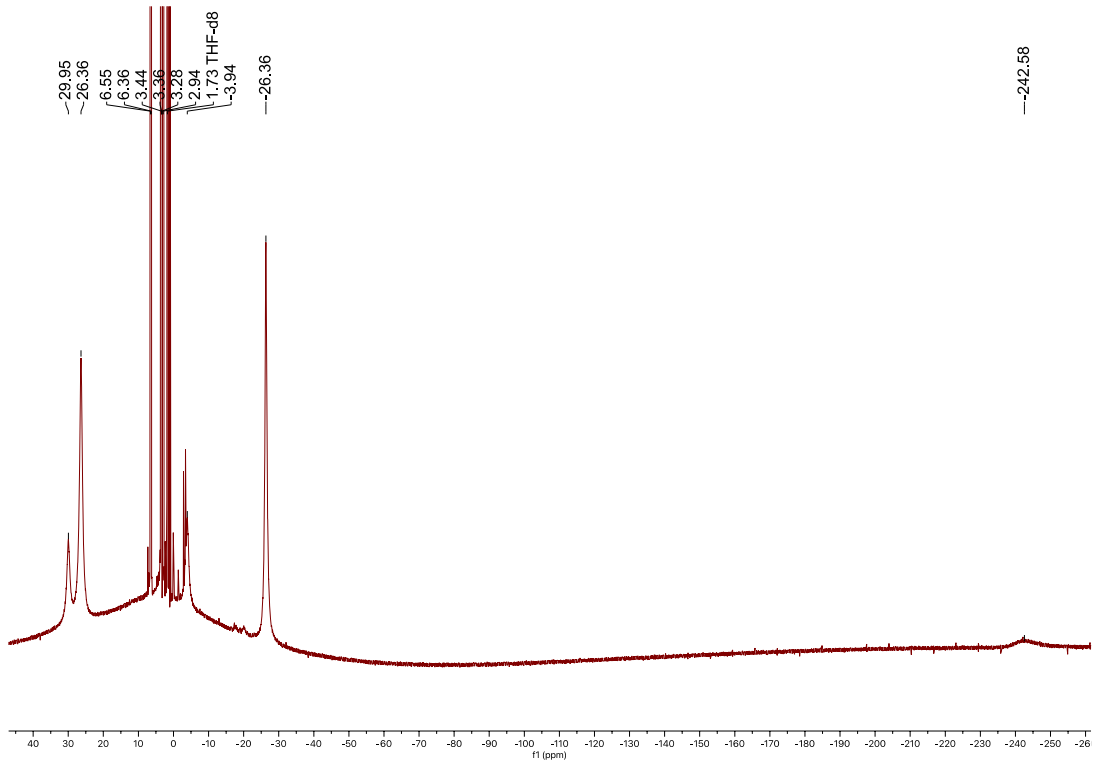

Figure A7.14. ^{1}H NMR spectrum of **7.8** in THF-d_8.

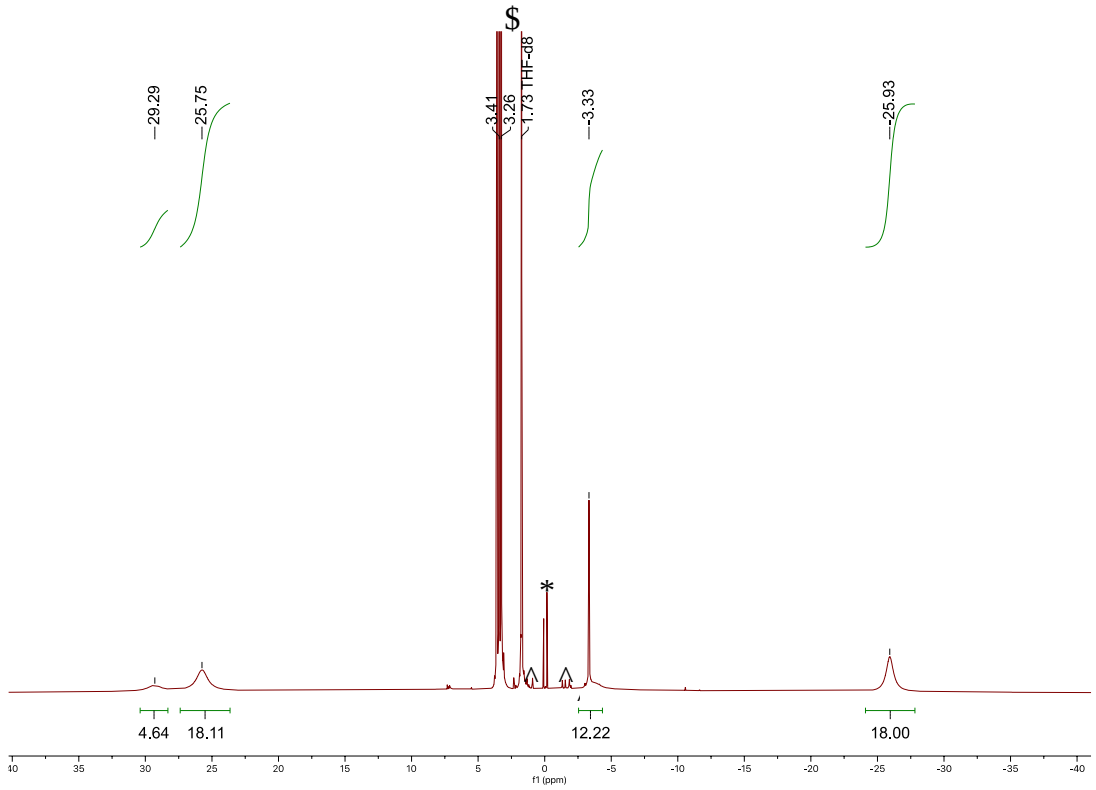

Figure A7.15. ^{1}H NMR spectrum of [Na(DME)$_3$][Np{*N*(R)(SiMe$_2$*C*H$_2$)}$_2$(NR$_2$)] (**7.9**) in THF-d_8. (*) indicates resonance assignable to free HN(SiMe$_3$)$_2$, ($) indicates resonances assignable to DME, and (^) indicates the presence of an unidentified product.

7.6.2 UV-vis Spectra

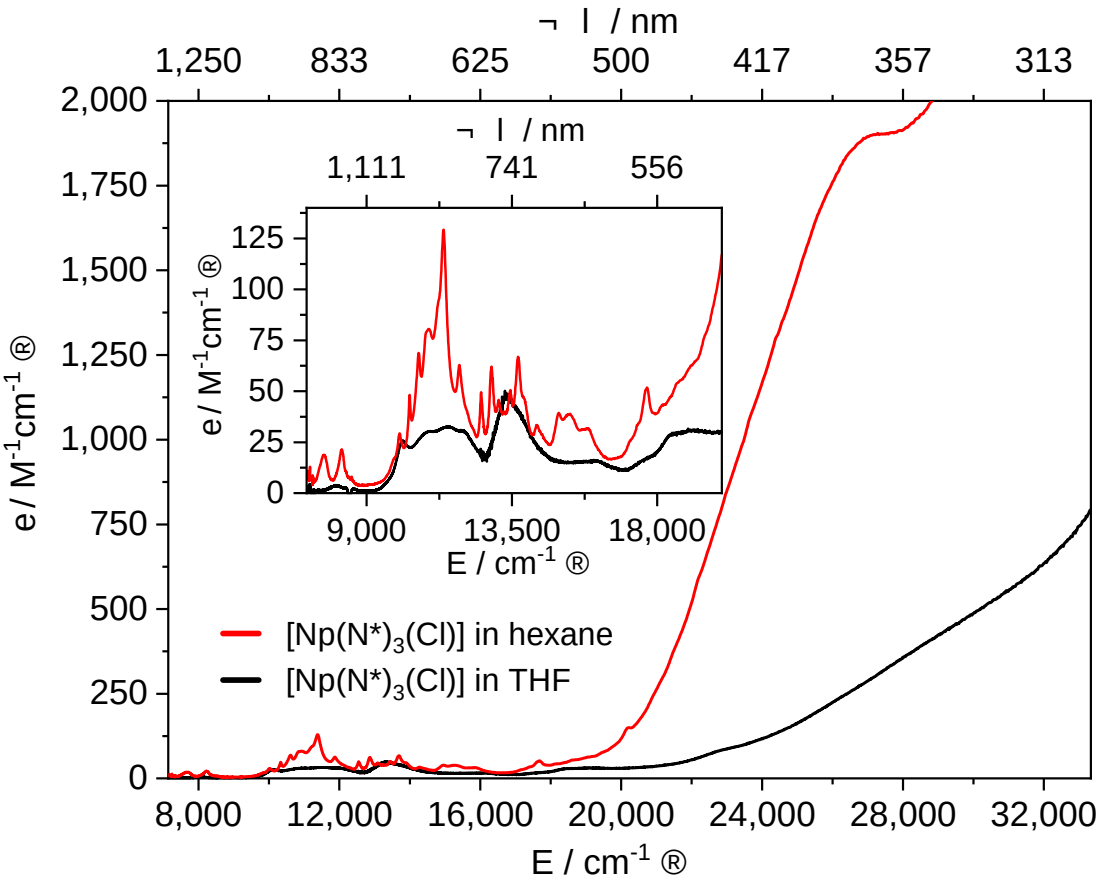

Figure A7.16. UV-vis spectrum of [Np(NR$_2$)$_3$Cl] (**7.1**) (0.878 mM solution in *n*-hexane and 1.01 mM solution in THF).

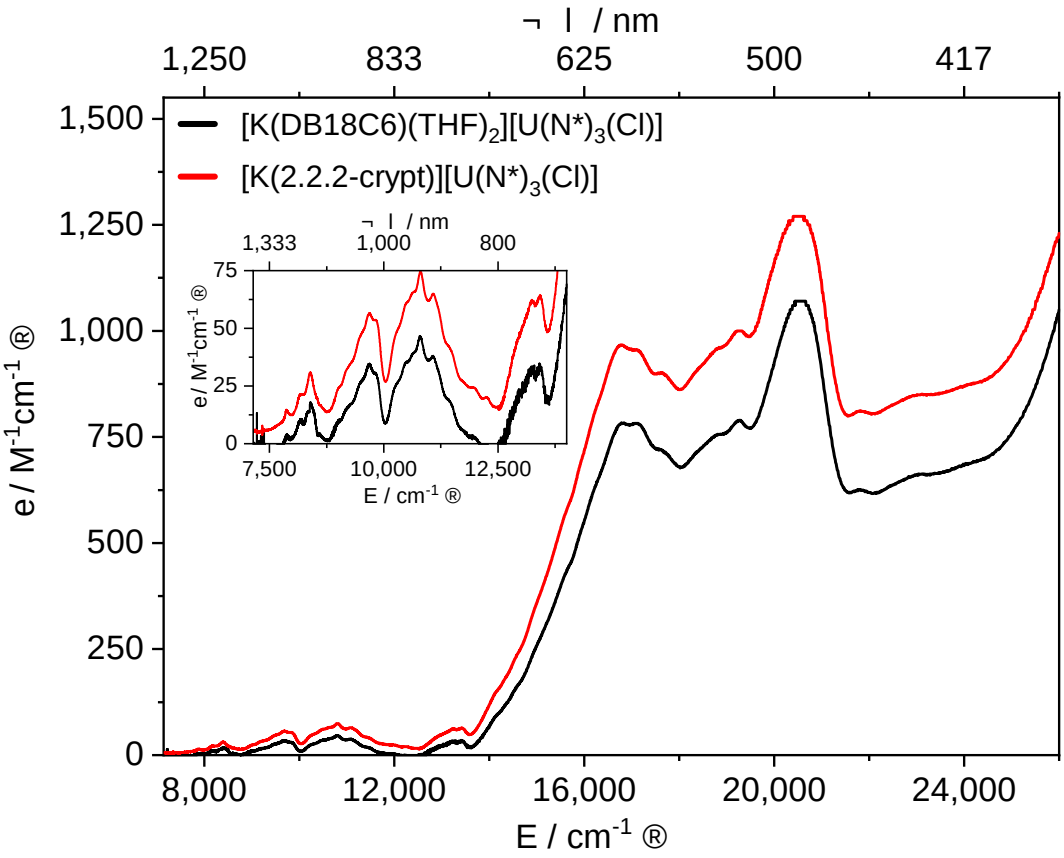

Figure A7.17. UV-vis spectra of **7.2** (1.94 mM solution in THF) and **7.3** (0.505 mM solution in THF).

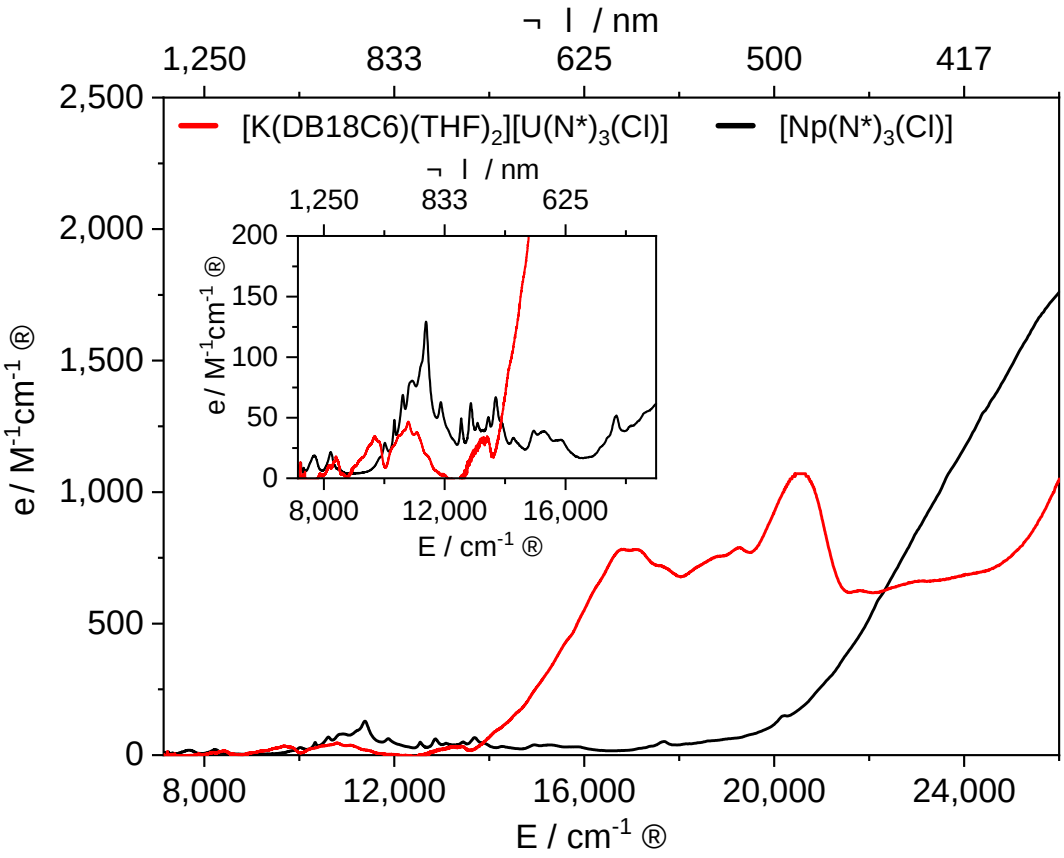

Figure A7.18. UV-vis spectra of **7.1** (1.01 mM solution in THF) and **7.3** (0.505 mM solution in THF).

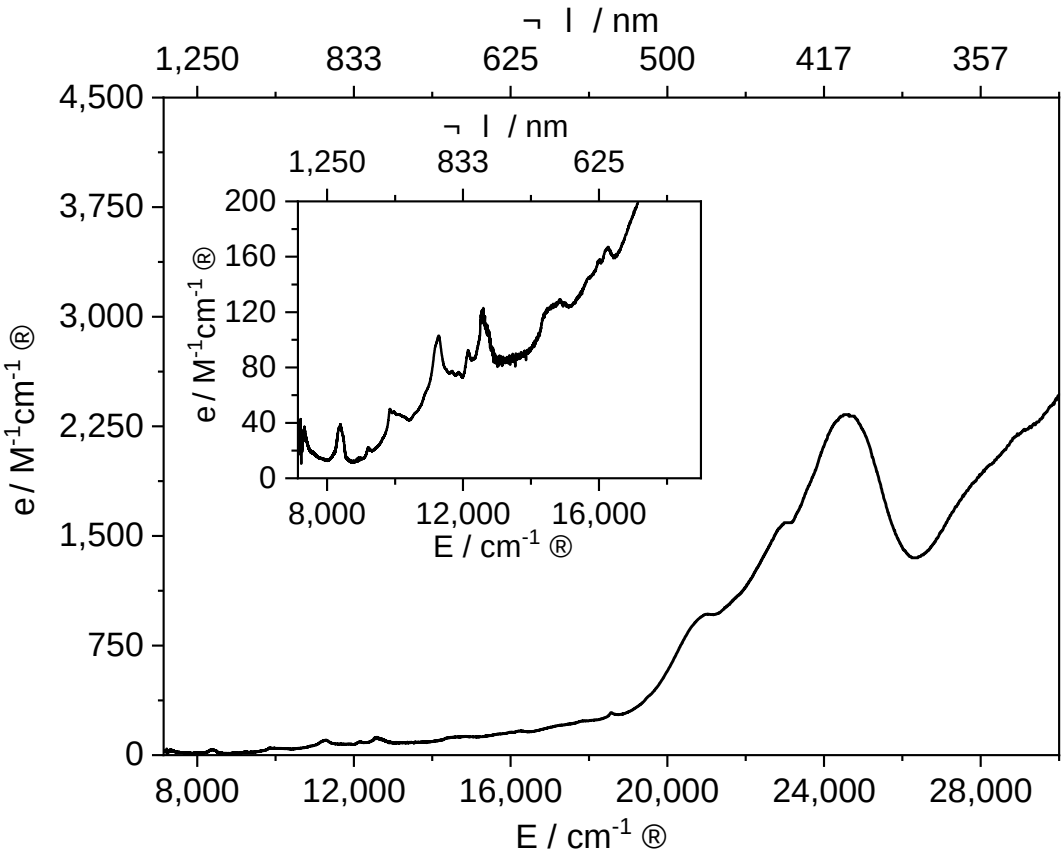

Figure A7.19. UV-vis spectrum of $[Cl\{K(DB\text{-}18\text{-}C\text{-}6)(THF)\}_3][Np(NR_2)_3Cl]_2$ (**7.4**) (0.506 mM solution in THF).

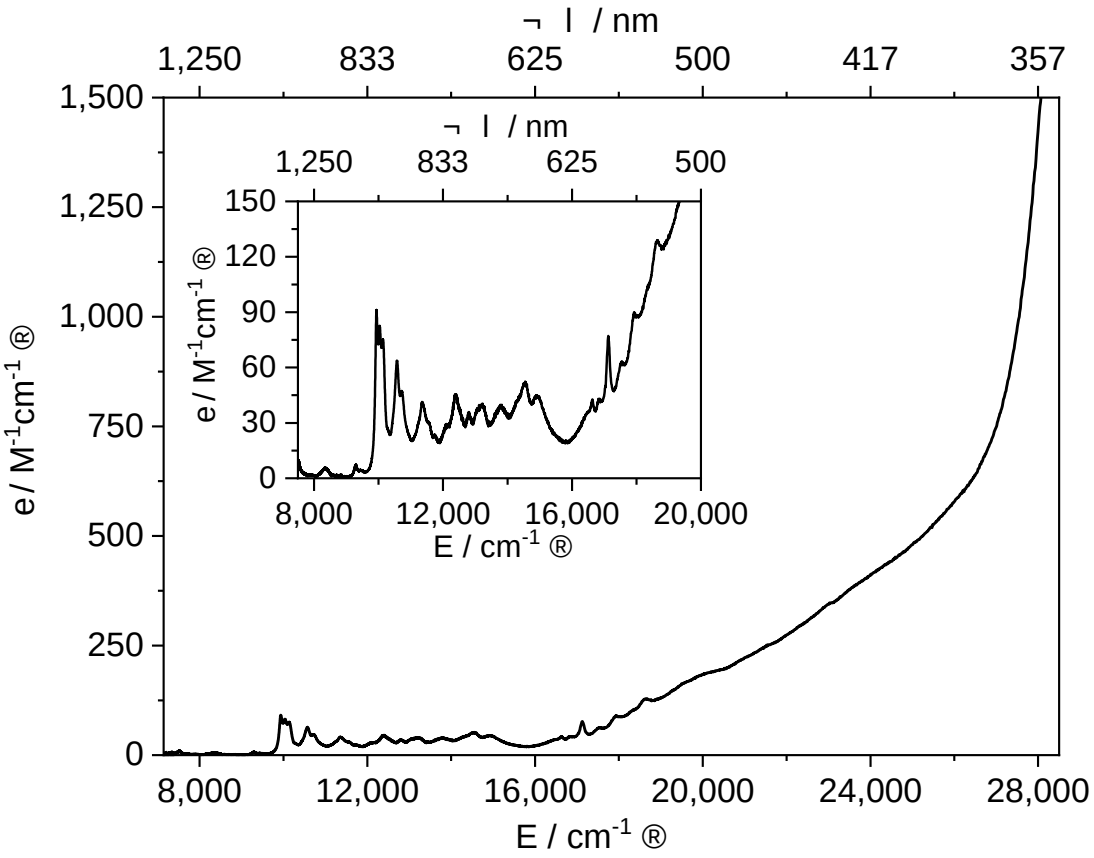

Figure A7.20. UV-vis spectrum of **7.8** (1.068 mM solution in THF).

7.6.3 IR Spectra

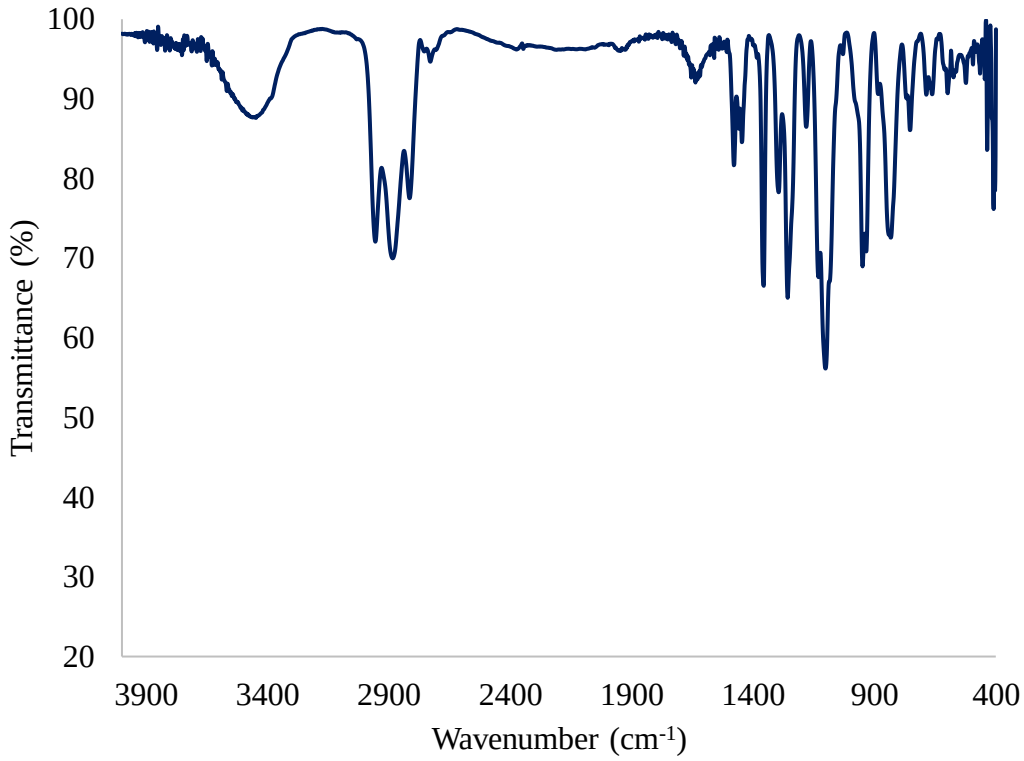

Figure A7.21. IR spectrum of **7.2** (KBr pellet).

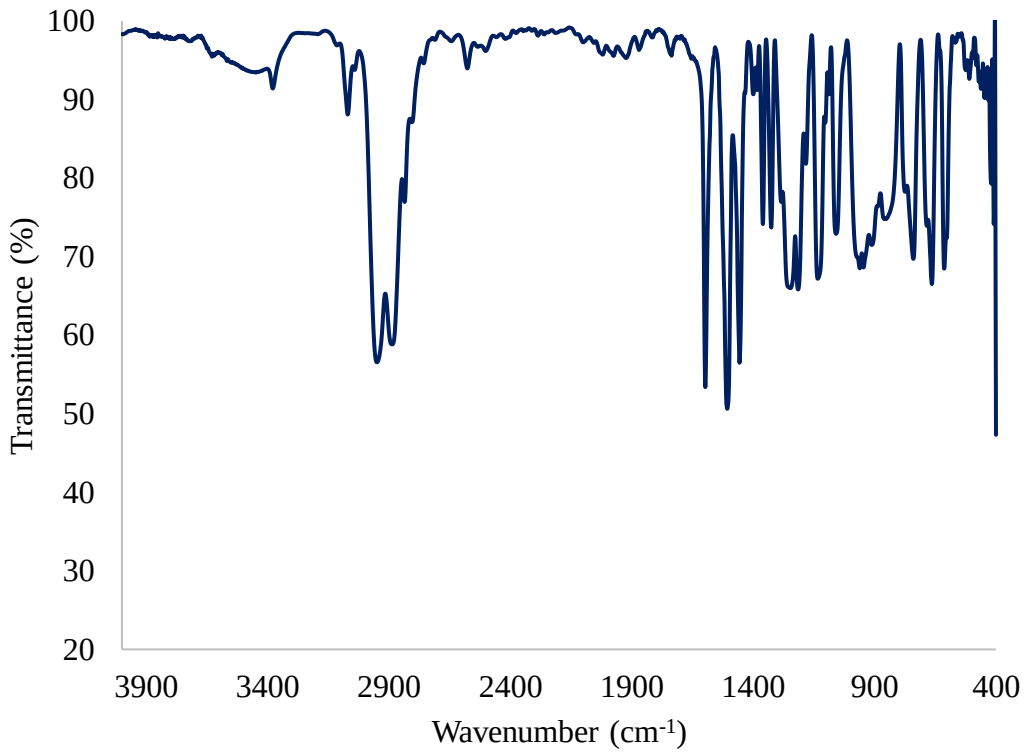

Figure A7.22. IR spectrum of **7.3 (**KBr pellet).

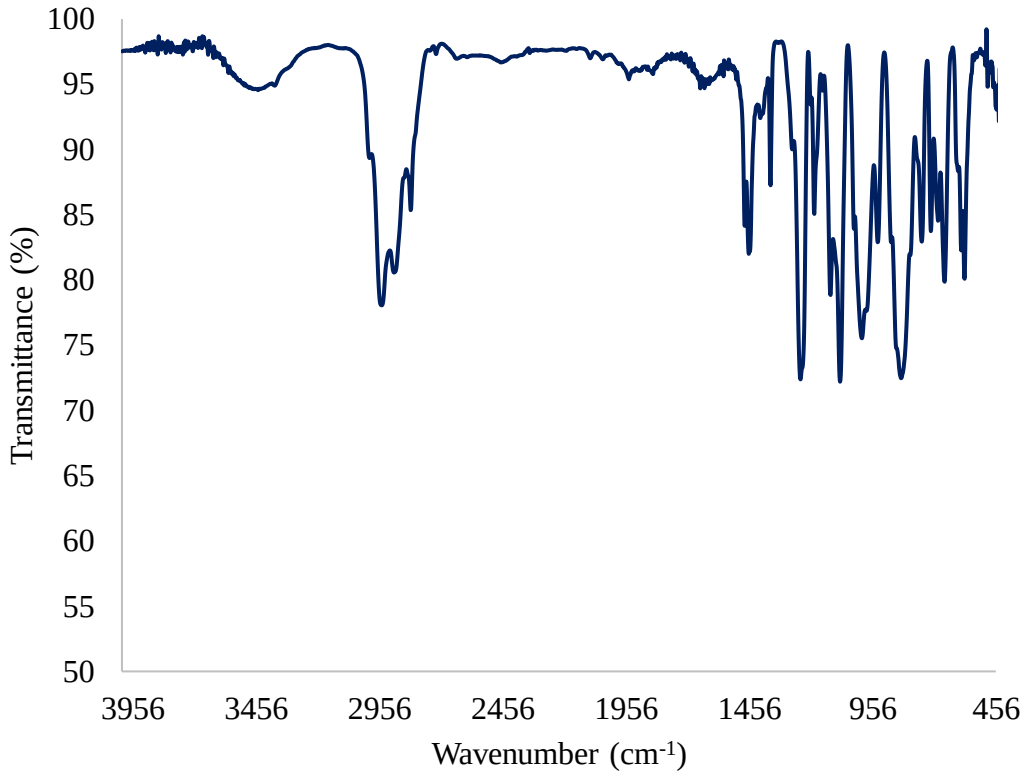

Figure A7.23. IR spectrum of **7.6** (KBr pellet).

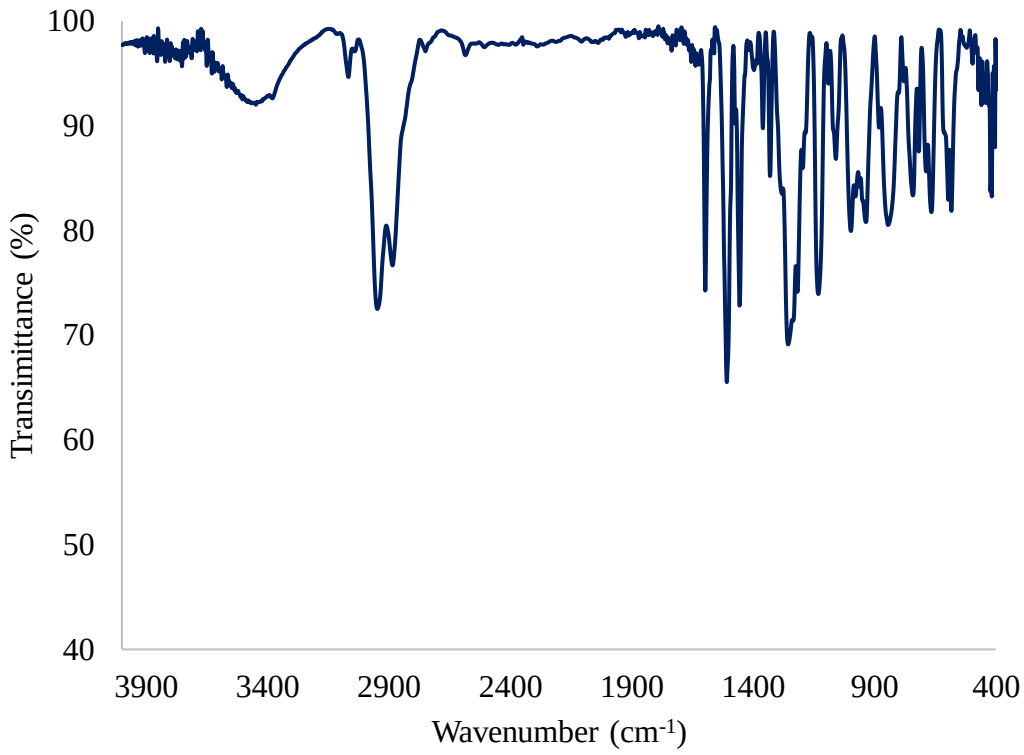

Figure A7.24. IR spectrum of **7.7** (KBr pellet).

7.6.4 Evans NMR

Table A7.1. Solution magnetic susceptibility data for **7.1** and **7.4**.

[a] Sample	μ_{eff} / B.M mol^{-1}	χ'_mT (S.I.)/ m^3 mol^{-1}	χ'_mT (c.g.s. e.m.u.)/ cm^3 mol^{-1} K	χ'_mT (S.I.)/ m^3 mol^{-1} K	mass of sample / g	mass of solvent + sample / g	M_r / g mol^{-1}	Δ peak / Hz
7.1	2.572	3.49E-08	0.827	1.04E-05	0.0100	0.4590	753.656	112.82
7.4	2.995	4.73E-08	1.121	1.41E-05	0.0057	0.5407	2957.49	13.58

[a]Spectrometer frequency 400.130 MHz. Simple diamagnetic correction of M_r / -2,000,000 applied. $\rho_{D8\text{-}THF}$ = 0.985 g mL^{-1}. ρ_{C6D6} = 0.950 g mL^{-1}.

7.6.5 Electrochemistry

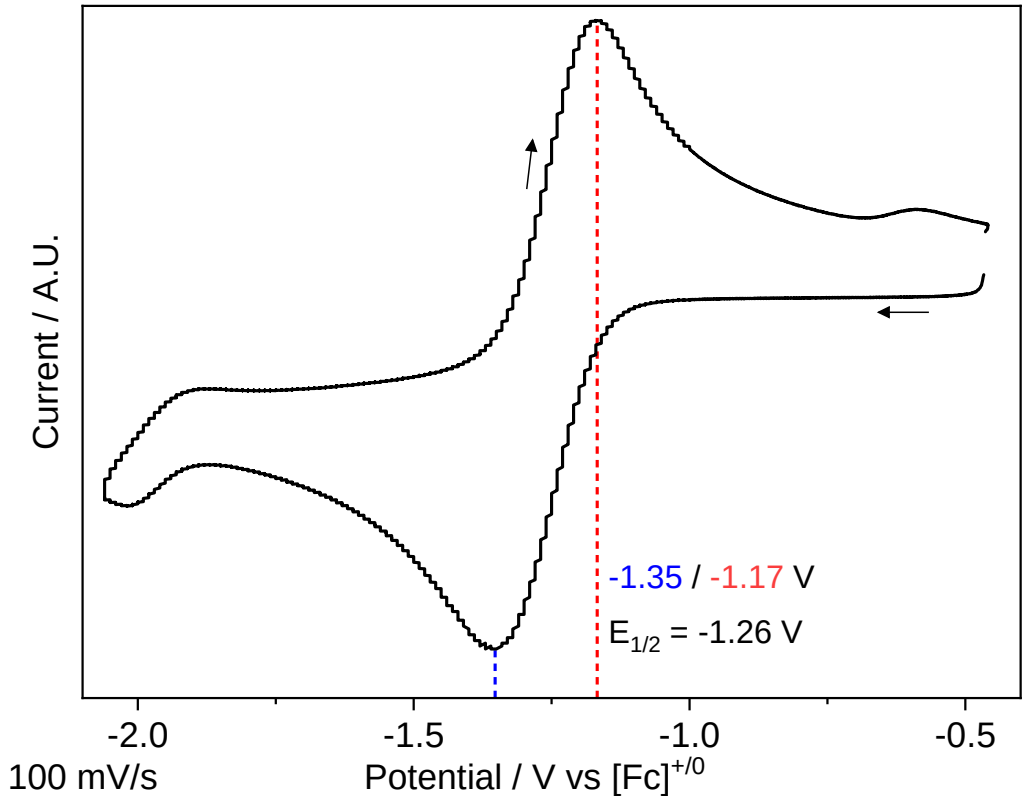

Figure A7.25. Cyclic voltammogram of **7.1** in THF (1.8 mM) supported by [^{n}Pr$_4$N][BArF^{24}] (67 mM) at 100 mV/s.

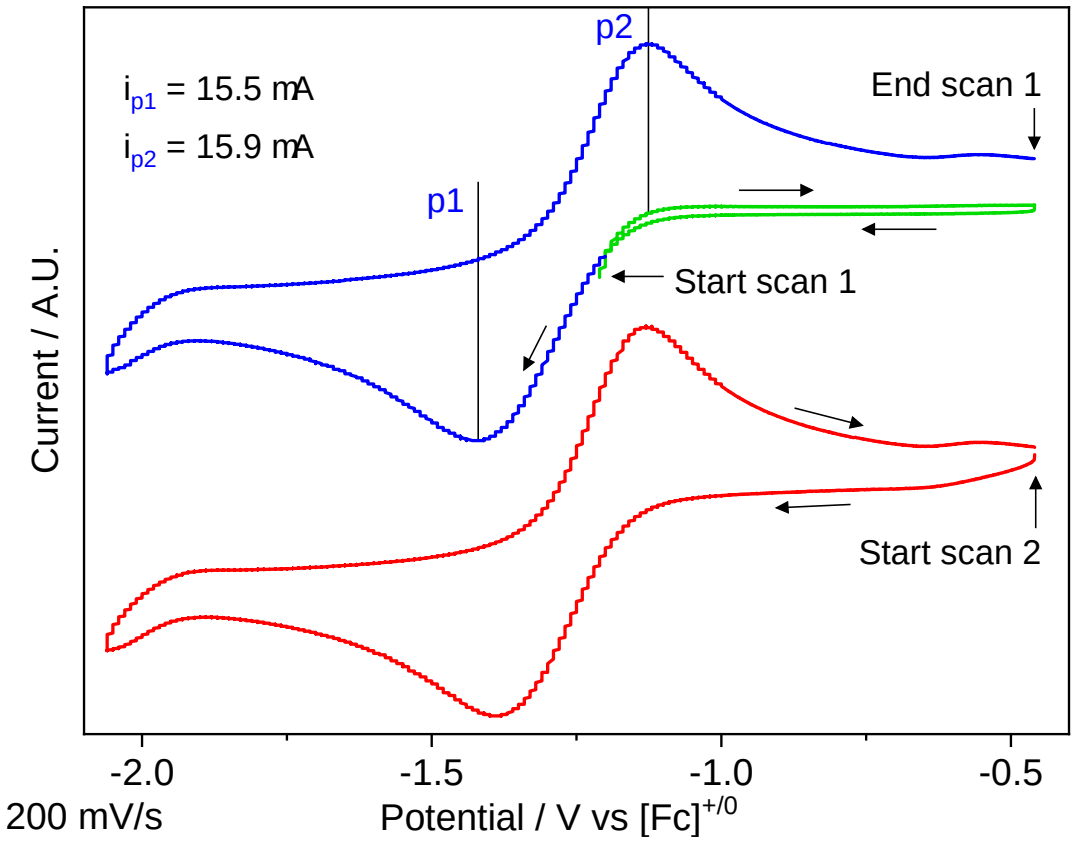

Figure A7.26. Cyclic voltammogram of **7.1** in THF (1.8 mM) supported by $[^{n}Pr_4N][BArF^{24}]$ (67 mM) at 200 mV/s, shown to assess the dependence of p2 on p1, indicative of a Np(IV/III) couple. $E_{1/2}$ for p1/p2 = –1.26 V.

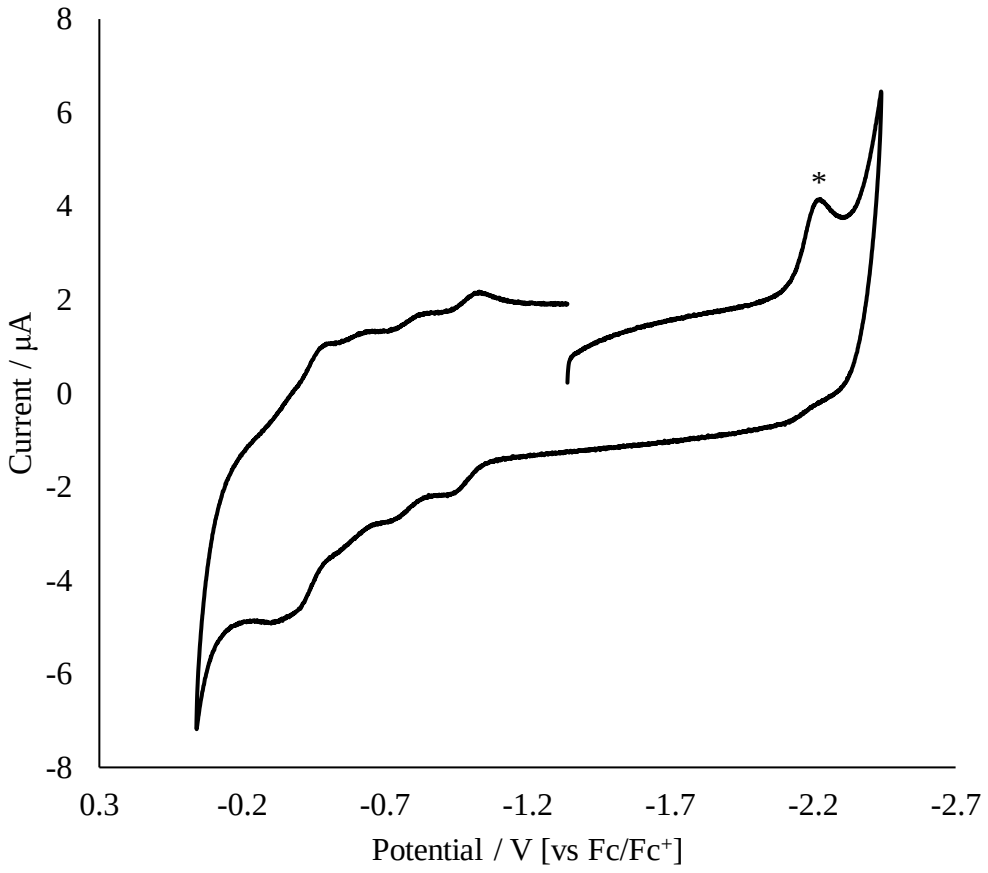

Figure A7.27. Cyclic voltammogram of $[U(NR_2)_3Cl]$ (200 mV/s scan rate, vs Fc/Fc^+). Measured in THF with 0.1 M $[NBu_4][BPh_4]$ as the supporting electrolyte. (*) is assignable to the irreversible U(IV/III) reduction feature.

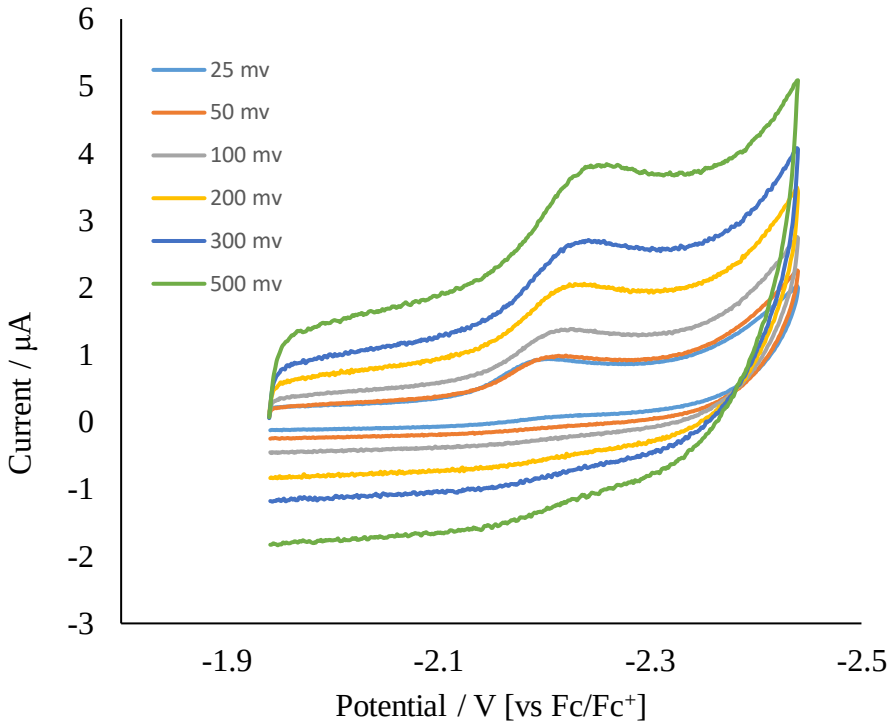

Figure A7.28. Scan-rate-dependent cyclic voltammogram of $[U(NR_2)_3)Cl]$ (vs Fc/Fc^+). Measured in THF with 0.1 M $[NBu_4][BPh_4]$ as the supporting electrolyte.

7.7 References

1. Ibers, J., Neglected neptunium. *Nature Chem.* **2010,** *2* (11), 996-996.
2. Levine, C. A.; Seaborg, G. T., The occurrence of plutonium in nature. *J. Am. Chem. Soc.* **1951,** *73* (7), 3278-3283.
3. Rhodes, R., *The making of the atomic bomb*. Simon and Schuster: 2012.
4. SEABORG, G. T., The Chemical and Radioactive Properties of the Heavy Elements. In *Modern Alchemy*, pp 20-23.
5. Seaborg, G. T., Forty Years of Plutonium Chemistry: The Beginnings. In *Plutonium Chemistry*, AMERICAN CHEMICAL SOCIETY: Vol. 216, pp 1-22.
6. Weigel, F.; Katz, J. J.; Seaborg, G. T., *Plutonium*. Chapman and Hall: United Kingdom, 1986.
7. Seaborg, G. T.; Segrè, E., *The transuranium elements*. Atomic Energy Commission: 1946.
8. Seaborg, G. T., The Transuranium Elements. *Science* **1946,** *104* (2704), 379-386.
9. Brown, J. L.; Batista, E. R.; Boncella, J. M.; Gaunt, A. J.; Reilly, S. D.; Scott, B. L.; Tomson, N. C., A Linear *trans*-Bis(imido) Neptunium(V) Actinyl Analog: $Np^{V}(NDipp)_2(^{t}Bu_2bipy)_2Cl$ (Dipp = 2,6-$^{i}Pr_2C_6H_3$). *J. Am. Chem. Soc.* **2015,** *137* (30), 9583-9586.
10. Su, J.; Windorff, C. J.; Batista, E. R.; Evans, W. J.; Gaunt, A. J.; Janicke, M. T.; Kozimor, S. A.; Scott, B. L.; Woen, D. H.; Yang, P., Identification of the Formal +2 Oxidation State of Neptunium: Synthesis and Structural Characterization of $\{Np^{II}[C_5H_3(SiMe_3)_2]_3\}^{1-}$. *J. Am. Chem. Soc.* **2018,** *140* (24), 7425-7428.
11. Schnaars, D. D.; Gaunt, A. J.; Hayton, T. W.; Jones, M. B.; Kirker, I.; Kaltsoyannis, N.; May, I.; Reilly, S. D.; Scott, B. L.; Wu, G., Bonding Trends Traversing the Tetravalent Actinide Series: Synthesis, Structural, and Computational Analysis of $An^{IV}(^{Ar}acnac)_4$ Complexes (An = Th, U, Np, Pu; ^{Ar}acnac = Ar*N*C(Ph)CHC(Ph)*O*; Ar = 3,5-$^{t}Bu_2C_6H_3$). *Inorg. Chem.* **2012,** *51* (15), 8557-8566.
12. Wigeland, R. A.; Bauer, T. H.; Fanning, T. H.; Morris, E. E., Separations and transmutation criteria to improve utilization of a geologic repository. *Nucl. Tech.* **2006,** *154* (1), 95-106.
13. Sarsfield, M. J.; Taylor, R. J.; Maher, C. J., Neptunium(V) disproportionation and cation–cation interactions in TBP/kerosene solvent. *Radiochimica Acta* **2007,** *95* (12), 677-682.
14. Seaborg, G. T.; Katz, J. J.; Morss, L. R., *The Chemistry of the Actinide Elements*. Springer: 1986; Vol. 2.
15. Taylor, R.; Denniss, I.; Wallwork, A., Neptunium control in an advanced Purex process. *Nuclear Energy* **1997,** *36* (1), 39-46.
16. Tian, G.; Xu, J.; Rao, L., Optical Absorption and Structure of a Highly Symmetrical Neptunium(V) Diamide Complex. *Angew. Chem.* **2005,** *117* (38), 6356-6359.
17. Arnold, P. L.; Dutkiewicz, M. S.; Walter, O., Organometallic Neptunium Chemistry. *Chem. Rev.* **2017,** *117* (17), 11460-11475.
18. Hayton, T. W., Metal–ligand multiple bonding in uranium: structure and reactivity. *Dalton Trans.* **2010,** *39* (5), 1145-1158.
19. Hayton, T. W., Recent developments in actinide–ligand multiple bonding. *Chem. Commun.* **2013,** *49* (29), 2956-2973.

20. Liddle, S. T., The Renaissance of Non-Aqueous Uranium Chemistry. *Angew. Chem. Int. Ed.* **2015,** *54* (30), 8604-8641.
21. Jones, M. B.; Gaunt, A. J., Recent developments in synthesis and structural chemistry of nonaqueous actinide complexes. *Chem. Rev.* **2013,** *113* (2), 1137-1198.
22. Gaunt, A. J.; Brown, J. L., *Organometallic and Nonaqueous Chemistry of Plutonium*. 2 ed.; Plutonium Handbook, 2019; Vol. 4.
23. Gaunt, A. J.; Reilly, S. D.; Enriquez, A. E.; Hayton, T. W.; Boncella, J. M.; Scott, B. L.; Neu, M. P., Low-Valent Molecular Plutonium Halide Complexes. *Inorg. Chem.* **2008,** *47* (18), 8412-8419.
24. Gaunt, A. J.; Reilly, S. D.; Hayton, T. W.; Scott, B. L.; Neu, M. P., An entry route into non-aqueous plutonyl coordination chemistry. *Chem. Commun.* **2007,** (16), 1659-1661.
25. Reilly, S. D.; Brown, J. L.; Scott, B. L.; Gaunt, A. J., Synthesis and characterization of $NpCl_4(DME)_2$ and $PuCl_4(DME)_2$ neutral transuranic An(IV) starting materials. *Dalton Trans.* **2014,** *43* (4), 1498-1501.
26. Pattenaude, S. A.; Anderson, N. H.; Bart, S. C.; Gaunt, A. J.; Scott, B. L., Non-aqueous neptunium and plutonium redox behaviour in THF – access to a rare Np(III) synthetic precursor. *Chem. Commun.* **2018,** *54* (48), 6113-6116.
27. Brown, J. L.; Gaunt, A. J.; King, D. M.; Liddle, S. T.; Reilly, S. D.; Scott, B. L.; Wooles, A. J., Neptunium and plutonium complexes with a sterically encumbered triamidoamine (TREN) scaffold. *Chem. Commun.* **2016,** *52* (31), 5428-5431.
28. Myers, A. J.; Tarlton, M. L.; Kelley, S. P.; Lukens, W. W.; Walensky, J. R., Synthesis and Utility of Neptunium(III) Hydrocarbyl Complex. *Angew. Chem. Int. Ed.* **2019,** *58* (42), 14891-14895.
29. Fichter, S.; Kaufmann, S.; Kaden, P.; Brunner, T. S.; Stumpf, T.; Roesky, P. W.; März, J., Enantiomerically Pure Tetravalent Neptunium Amidinates: Synthesis and Characterization. *Chem. Eur. J.* **2020,** *26* (41), 8867-8870.
30. Andersen, R. A., Tris((hexamethyldisilyl)amido)uranium(III): preparation and coordination chemistry. *Inorg. Chem.* **1979,** *18* (6), 1507-1509.
31. Andersen, R. A.; Zalkin, A.; Templeton, D. H., Crystal and molecular structure of hydridotris[bis(trimethylsilyl)amido]uranium(IV). *Inorg. Chem.* **1981,** *20* (2), 622-623.
32. Bell, N. L.; Maron, L.; Arnold, P. L., Thorium Mono- and Bis(imido) Complexes Made by Reprotonation of *cyclo*-Metalated Amides. *J. Am. Chem. Soc.* **2015,** *137* (33), 10492-10495.
33. Bénaud, O.; Berthet, J.-C.; Thuéry, P.; Ephritikhine, M., The Bis Metallacyclic Anion $[U(N\{SiMe_3\}_2)(CH_2SiMe_2N\{SiMe_3\})_2]^-$. *Inorg. Chem.* **2010,** *49* (17), 8117-8130.
34. Bénaud, O.; Berthet, J.-C.; Thuéry, P.; Ephritikhine, M., Iodide, Azide, and Cyanide Complexes of (*N*,*C*), (*N*,*N*), and (*N*,*O*) Metallacycles of Tetra- and Pentavalent Uranium. *Inorg. Chem.* **2011,** *50* (23), 12204-12214.
35. Simpson, S. J.; Turner, H. W.; Andersen, R. A., Hydrogen-Deuterium Exchange: Perdeuteriohydridotris (hexamethyldisilylamido)- thorium(IV) and -uranium(IV). *J. Am. Chem. Soc.* **1979,** *101* (26), 7728-7729.
36. Simpson, S. J.; Turner, H. W.; Andersen, R. A., Preparation and hydrogen-deuterium exchange of alkyl and hydride bis(trimethylsilyl)amido derivatives of the actinide elements. *Inorg. Chem.* **1981,** *20* (9), 2991-2995.

37. Goodwin, C. A. P.; Mills, D. P., Silylamides: towards a half-century of stabilising remarkable f-element chemistry. In *Organometallic Chemistry: Volume 41*, The Royal Society of Chemistry: 2017; Vol. 41, pp 123-156.
38. Avens, L. R.; Bott, S. G.; Clark, D. L.; Sattelberger, A. P.; Watkin, J. G.; Zwick, B. D., A Convenient Entry into Trivalent Actinide Chemistry: Synthesis and Characterization of $AnI_3(THF)_4$ and $An[N(SiMe_3)_2]_3$ (An = U, Np, Pu). *Inorg. Chem.* **1994,** *33* (10), 2248-2256.
39. Cantat, T.; Scott, B. L.; Kiplinger, J. L., Convenient access to the anhydrous thorium tetrachloride complexes $ThCl_4(DME)_2$, $ThCl_4(1,4\text{-dioxane})_2$ and $ThCl_4(THF)_{3.5}$ using commercially available and inexpensive starting materials. *Chem. Commun.* **2010,** *46* (6), 919-921.
40. Fortier, S.; Walensky, J. R.; Wu, G.; Hayton, T. W., Synthesis of a Phosphorano-Stabilized U(IV)-Carbene via One-Electron Oxidation of a U(III)-Ylide Adduct. *J. Am. Chem. Soc.* **2011,** *133* (18), 6894-6897.
41. Smiles, D. E.; Wu, G.; Hrobárik, P.; Hayton, T. W., Synthesis, Thermochemistry, Bonding, and ^{13}C NMR Chemical Shift Analysis of a Phosphorano-Stabilized Carbene of Thorium. *Organometallics* **2017,** *36* (23), 4519-4524.
42. Staun, S. L.; Sergentu, D.-C.; Wu, G.; Autschbach, J.; Hayton, T. W., Use of ^{15}N NMR spectroscopy to probe covalency in a thorium nitride. *Chem. Sci.* **2019,** *10* (26), 6431-6436.
43. Dormond, A.; Aaliti, A.; El Bouadili, A.; Moise, C., Reactivity of the uranium-carbon σ-bond in 'silylamido' compounds. *Inorganica Chim. Acta* **1987,** *139* (1), 171-176.
44. Dormond, A.; El Bouadili, A. A.; Moïse, C., Reactivity of the actinoid–carbon σ bond: reaction of $[(Me_3Si)_2N]_2MCH_2Si(Me)_2NSiMe_3$ with acidic hydrogen, ready C–H activation. *Chem. Commun.* **1985,** (13), 914-916.
45. Dormond, A.; Möise, C.; Elbouadili, A.; Bitar, H., Réactivité de la liaison uranium-carbone. Le métallacycle $[(Me_3Si)_2N]_2UCH_2SiMe_2NSiMe_3$ comme réactif de réactif de déplacement chimique de cétones polycycliques. *J. Organomet. Chem.* **1989,** *371* (2), 175-185.
46. Hervé, A.; Bouzidi, Y.; Berthet, J.-C.; Belkhiri, L.; Thuéry, P.; Boucekkine, A.; Ephritikhine, M., U^{III}–CN versus U^{IV}–NC Coordination in Tris(silylamide) Complexes. *Inorg. Chem.* **2015,** *54* (5), 2474-2490.
47. Baumgärtner, F.; Fischer, E.; Kanellakopulos, B.; Laubereau, P., Triscyclopentadienylplutonium. *Angew. Chem. Int. Ed.* **1965,** *4* (10), 878-878.
48. Baumgärtner, F.; Fischer, E. O.; Kanellakopulos, B.; Laubereau, P., *Angew. Chem. Int. Ed.* **1966,** *5*, 134-135.
49. Karraker, D.; Stone, J., Mössbauer and Magnetic Susceptibility Studies of Uranium(III), Uranium(IV), Neptunium(III), and Neptunium(IV) compounds with the Cyclopentadiene Ion. *Inorg. Chem.* **1972,** *11* (8), 1742-1746.
50. Laubereau, P.; Burns, J. H., Tricyclopentadienyl-curium. *Inorg. Nucl. Chem. Lett.* **1970,** *6* (1), 59-63.
51. Laubereau, P. G.; Burns, J. H., Microchemical preparation of tricyclopentadienyl compounds of berkelium, californium, and some lanthanide elements. *Inorg. Chem.* **1970,** *9* (5), 1091-1095.
52. Bohlander, R. *The Organometallic Chemistry of Neptunium*; Germany, 1986, p 180.

53. Dutkiewicz, M. S.; Apostolidis, C.; Walter, O.; Arnold, P. L., Reduction chemistry of neptunium cyclopentadienide complexes: from structure to understanding. *Chem. Sci.* **2017,** *8* (4), 2553-2561.
54. Windorff, C. J.; Chen, G. P.; Cross, J. N.; Evans, W. J.; Furche, F.; Gaunt, A. J.; Janicke, M. T.; Kozimor, S. A.; Scott, B. L., Identification of the Formal +2 Oxidation State of Plutonium: Synthesis and Characterization of $\{Pu^{II}[C_5H_3(SiMe_3)_2]_3\}^-$. *J. Am. Chem. Soc.* **2017,** *139* (11), 3970-3973.
55. Windorff, C. J.; Dumas, M. T.; Ziller, J. W.; Gaunt, A. J.; Kozimor, S. A.; Evans, W. J., Small-Scale Metal-Based Syntheses of Lanthanide Iodide, Amide, and Cyclopentadienyl Complexes as Analogues for Transuranic Reactions. *Inorg. Chem.* **2017,** *56* (19), 11981-11989.
56. Arnold, P. L., Uranium-mediated activation of small molecules. *Chem. Commun.* **2011,** *47* (32), 9005-9010.
57. Liddle, S. T.; van Slageren, J., Improving f-element single molecule magnets. *Chem. Soc. Rev.* **2015,** *44* (19), 6655-6669.
58. Johnson, S. A.; Bart, S. C., Achievements in uranium alkyl chemistry: celebrating sixty years of synthetic pursuits. *Dalton Trans.* **2015,** *44* (17), 7710-7726.
59. Edelstein, N. M.; Fuger, J.; Morss, L. R., *The chemistry of the actinide and transactinide elements*. Springer: 2006.
60. Smiles, D. E.; Wu, G.; Kaltsoyannis, N.; Hayton, T. W., Thorium–ligand multiple bonds *via* reductive deprotection of a trityl group. *Chem. Sci.* **2015,** *6* (7), 3891-3899.
61. Brown, M. A.; Paulenova, A.; Gelis, A. V., Aqueous Complexation of Thorium(IV), Uranium(IV), Neptunium(IV), Plutonium(III/IV), and Cerium(III/IV) with DTPA. *Inorg. Chem.* **2012,** *51* (14), 7741-7748.
62. Ikeda-Ohno, A.; Hennig, C.; Rossberg, A.; Funke, H.; Scheinost, A. C.; Bernhard, G.; Yaita, T., Electrochemical and Complexation Behavior of Neptunium in Aqueous Perchlorate and Nitrate Solutions. *Inorg. Chem.* **2008,** *47* (18), 8294-8305.
63. Ikeda-Ohno, A.; Tsushima, S.; Takao, K.; Rossberg, A.; Funke, H.; Scheinost, A. C.; Bernhard, G.; Yaita, T.; Hennig, C., Neptunium Carbonato Complexes in Aqueous Solution: An Electrochemical, Spectroscopic, and Quantum Chemical Study. *Inorg. Chem.* **2009,** *48* (24), 11779-11787.
64. Sonnenberger, D. C.; Gaudiello, J. G., Cyclic Voltammetric Study of Organoactinide Compounds of Uranium(IV) and Neptunium(IV). Ligand Effects on the M(IV)/M(III) couple. *Inorg. Chem.* **1988,** *27* (15), 2747-2748.
65. Klamm, B. E.; Windorff, C. J.; Celis-Barros, C.; Beltran-Leiva, M. J.; Sperling, J. M.; Albrecht-Schönzart, T. E., Exploring the Oxidation States of Neptunium with Schiff Base Coordination Complexes. *Inorg. Chem.* **2020,** *ASAP*.
66. Bratsch, S. G., Standard Electrode Potentials and Temperature Coefficients in Water at 298.15 K. *J. Phys. Chem. Ref. Data* **1989,** *18* (1), 1-21.
67. Mansell, S. M.; Perandones, B. F.; Arnold, P. L., New U^{III} and U^{IV} silylamides and an improved synthesis of $NaN(SiMe_2R)_2$ (R = Me, Ph). *J. Organometallic Chem.* **2010,** *695* (25), 2814-2821.
68. La Pierre, H. S.; Heinemann, F. W.; Meyer, K., Well-defined molecular uranium(III) chloride complexes. *Chem. Commun.* **2014,** *50* (30), 3962-3964.

69. Moody, D. C.; Odom, J. D., The chemistry of trivalent uranium: The synthesis and reaction chemistry of the tetrahydrofuran adduct of uranium trichloride, $UCl_3(THF)_x$. *J. Inorg. Nucl. Chem.* **1979,** *41* (4), 533-535.
70. Goodwin, C. A. P.; Tuna, F.; McInnes, E. J. L.; Liddle, S. T.; McMaster, J.; Vitorica-Yrezabal, I. J.; Mills, D. P., $[U^{III}\{N(SiMe_2tBu)_2\}_3]$: A Structurally Authenticated Trigonal Planar Actinide Complex. *Chem. Eur. J.* **2014,** *20* (45), 14579-14583.
71. Shannon, R., Acta Crystallogr., Sect. A: Cryst. Phys., Diffr., Theor. Gen. Crystallogr. **1976,** (32), 751-767.
72. Dutkiewicz, M. S.; Farnaby, J. H.; Apostolidis, C.; Colineau, E.; Walter, O.; Magnani, N.; Gardiner, M. G.; Love, J. B.; Kaltsoyannis, N.; Caciuffo, R.; Arnold, P. L., Organometallic neptunium(III) complexes. *Nature Chem.* **2016,** *8* (8), 797-802.
73. Fortier, S.; Brown, J. L.; Kaltsoyannis, N.; Wu, G.; Hayton, T. W., Synthesis, molecular and electronic structure of $U^V(O)[N(SiMe_3)_2]_3$. *Inorg. Chem.* **2012,** *51* (3), 1625-1633.
74. Amoretti, G., Calculation of the Stevens factors **α**, **β** and **γ** in the intermediate coupling scheme for U and Np ions with f 2, f3 and f4 configurations. *J. Phys. France* **1984,** *45* (6), 1067-1069.
75. Addison, A. W.; Rao, T. N.; Reedijk, J.; van Rijn, J.; Verschoor, G. C., Synthesis, structure, and spectroscopic properties of copper(II) compounds containing nitrogen–sulphur donor ligands; the crystal and molecular structure of aqua[1,7-bis(*N*-methylbenzimidazol-2′-yl)-2,6-dithiaheptane]copper(II) perchlorate. *Dalton Trans.* **1984,** (7), 1349-1356.
76. Arnold, P. L.; Dutkiewicz, M. S.; Zegke, M.; Walter, O.; Apostolidis, C.; Hollis, E.; Pécharman, A. F.; Magnani, N.; Griveau, J. C.; Colineau, E., Subtle Interactions and Electron Transfer between U^{III}, Np^{III}, or Pu^{III} and Uranyl Mediated by the Oxo Group. *Angew. Chem.* **2016,** *128* (41), 12989-12993.
77. Magnani, N.; Colineau, E.; Eloirdi, R.; Griveau, J. C.; Caciuffo, R.; Cornet, S. M.; May, I.; Sharrad, C. A.; Collison, D.; Winpenny, R. E. P., Superexchange Coupling and Slow Magnetic Relaxation in a Transuranium Polymetallic Complex. *Phys. Rev. Lett.* **2010,** *104* (19), 197202.
78. Schnaars, D. D.; Wu, G.; Hayton, T. W., Reactivity of UH_3 with mild oxidants. *Dalton Trans.* **2008,** (44), 6121-6126.
79. Turner, H. W.; Andersen, R. A.; Zalkin, A.; Templeton, D. H., Chloro-, methyl-, and (tetrahydroborato)tris((hexamethyldisilyl)amido)thorium(IV) and uranium(IV). Crystal structure of (tetrahydroborato)tris((hexamethyldisilyl)amido)thorium(IV). *Inorg. Chem.* **1979,** *18* (5), 1221-1224.
80. Thomson, R. K.; Scott, B. L.; Morris, D. E.; Kiplinger, J. L., Synthesis, structure, spectroscopy and redox energetics of a series of uranium(IV) mixed-ligand metallocene complexes. *C. R. Chim.* **2010,** *13* (6), 790-802.
81. Blinka, T. A.; Helmer, B. J., Spectroscopy for Silicon–29: The INEPT and DEPT Techniques. *Adv. in Organometallic Chem.* **1984**, 193.
82. Windorff, C. J.; Evans, W. J., ^{29}Si NMR spectra of silicon-containing uranium complexes. *Organometallics* **2014,** *33* (14), 3786-3791.
83. Sur, S. K., Measurement of magnetic susceptibility and magnetic moment of paramagnetic molecules in solution by high-field fourier transform NMR spectroscopy. *J. Mag. Reson.* **1989,** *82* (1), 169-173.

84. Harris, R. K.; Becker, E. D.; Cabral de Menezes, S. M.; Goodfellow, R.; Granger, P., NMR nomenclature: nuclear spin properties and conventions for chemical shifts. IUPAC Recommendations 2001. International Union of Pure and Applied Chemistry. Physical Chemistry Division. Commission on Molecular Structure and Spectroscopy. *Magn. Reson. Chem.* **2002,** *40* (7), 489-505.
85. Harris, R. K.; Becker, E. D.; De Menezes, S. M. C.; Granger, P.; Hoffman, R. E.; Zilm, K. W., Further Conventions for NMR Shielding and Chemical Shifts (IUPAC Recommendations 2008). *Magn. Reson. Chem.* **2008,** *46* (6), 582-598.
86. Cobb, P. J.; Wooles, A. J.; Liddle, S. T., A Uranium(VI)–Oxo-Imido Dimer Complex Derived from a Sterically Demanding Triamidoamine. *Inorg. Chem.* **2020,** *59* (14), 10034-10041.
87. *SMART* Apex II, Version 5.632.; Bruker AXS, Inc.: Madison, WI, 2005.
88. *SAINT Software User's Guide*, Version 7.34a ed.; Bruker AXS Inc.: Madison, WI, 2005.
89. *SADABS*, Sheldrick, G.M.; University of Göttingen, Germany: 2005.
90. *SHELXTL*, Version 6.12 ed.; Bruker AXS Inc.: Madison, WI, 2005.
91. Olex2 1.2 (compiled 2014.06.27 svn.r2953 for OlexSys, GUI svn. r4855).
92. Dolomanov, O.; Bourhis, L.; Gildea, R.; Howard, J.; Puschmann, H., *J. Appl. Cryst* **2009,** *42*, 339-341.